Transactions of the ASME

Oil and Gas-Well Casing Suspension Assemblies . . . . . *A. F. Rhodes and J. C. Wilhoit, Jr.* 225
Study of Pneumatic Processes in the Continuous Control of Motion With Compressed Air—I . . . . . *J. L. Shearer* 233
Study of Pneumatic Processes in the Continuous Control of Motion With Compressed Air—II. . . . . *J. L. Shearer* 243
Dynamic Analysis of Chemical Processes . . . . . *E. G. Holzmann* 251
Determination of System Characteristics From Normal Operating Records . . . . . *T. P. Goodman and J. B. Reswick* 259
The Chemical Deaeration of Boiler Water—The Use of Hydrazine Compounds . . *J. Leicester* 273
Controlling Iron and Copper Pickup With Neutralizing Amines *J. D. Ristroph and E. A. Yorkgitis* 287
Hydrazine as an Oxygen Scavenger—A Progress Report on Tests at Springdale Station . . . . . *M. D. Baker and V. M. Marcy* 299
Lower Flue-Gas Exit Temperatures Through Removal of the Solids Ahead of the Air Preheater . . . . . *A. J. Tigges and Hilmer Karlsson* 305
Design Aspects of an Electrostatic Precipitator for the Collection of Small Solids Ahead of the Air Heater . . . . . *H. Klemperer and J. E. Sayers* 317
Investigations Into Blade-Root Fixings of High-Temperature Steels . . . . . *W. Siegfried* 327
Factors Influencing the Notch Fatigue Strengthening of N-155 Alloy at Elevated Temperatures . . . . . *W. S. Hyler and W. F. Simmons* 339
Factors Influencing the Notch-Rupture Strength of Heat-Resistant Alloys at Elevated Temperatures . . . . . *R. L. Carlson, R. J. MacDonald, and W. F. Simmons* 349
Orifice Coefficients for Reynolds Numbers From 4 to 50,000 . . . . . *H. W. Iversen* 359
Discharge Measurements at Low Reynolds Numbers—Special Devices . . . . *A. L. Jorissen* 365
Effect of a Globe Valve in Approach Piping on Orifice-Meter Accuracy . . . . . *J. W. Murdock, C. J. Foltz, and Clarence Gregory, Jr.* 369
Flow of Saturated Boiler Water Through Knife-Edge Orifices in Series . . . *E. S. Monroe, Jr.* 373
Notes on Some Recently Published Experiments on Orifice Meters . . . . *Edgar Buckingham* 379
The Mechanism of Separation in the Louver-Type Dust Separator *J. L. Smith, Jr., and M. J. Goglia* 389
Plastic Working of Metals . . . . . *W. S. Wagner* 401
Plasticity Equations and Their Application to Working of Metals in the Work-Hardening Range . . . . . *E. G. Thomsen* 407
Plastic Metalworking . . . . . *E. V. Crane* 413
Performance Characteristics of Francis Type Pump-Turbines . . . . . *W. J. McCormack* 417
Zirconium-Fabrication Techniques and Alloy Development . . . . *C. E. Lacy and J. H. Keeler* 427
Laminar Free Convection From a Vertical Plate With Uniform Surface Heat Flux . . . . . *E. M. Sparrow and J. L. Gregg* 435
Heat Transfer to Laminar Flow in a Round Tube or Flat Conduit—The Graetz Problem Extended . . . . . *J. R. Sellars, Myron Tribus, and J. S. Klein* 441

TRANSACTIONS OF THE AMERICAN SOCIETY OF MECHANICAL ENGINEERS

VOLUME 78 FEBRUARY 1956 NUMBER 2

Transactions

of The American Society of Mechanical Engineers

Published on the tenth of every month, except March, June, September, and December

OFFICERS OF THE SOCIETY:

J. W. Barker, *President*

Joseph L. Kopf, *Treasurer* — C. E. Davies, *Secretary*

Edgar J. Kates, *Asst. Treasurer*

COMMITTEE ON PUBLICATIONS:

Otto de Lorenzi, *Chairman*

W. E. Reaser — John de S. Coutinho

Kerr Atkinson — B. G. A. Skrotzki

R. A. Cederberg, H. N. Weinberg } *Junior Advisory Members*

George A. Stetson, *Editor* — K. W. Clendenning, *Managing Editor*; J. A. North, *Asst. Managing Editor*

REGIONAL ADVISORY BOARD OF THE PUBLICATIONS COMMITTEE:

Roy L. Parsell—I
A. D. Blake—II
C. C. France—III
Francis C. Smith—IV
H. M. Cather—V
C. R. Earle—VI
M. B. Hogan—VII
Linn Helander—VIII

Published monthly by The American Society of Mechanical Engineers. Publication office at 20th and Northampton Streets, Easton, Pa. The editorial department is located at the headquarters of the Society, 29 West Thirty-Ninth Street, New York 18, N. Y. Cable address, "Dynamic," New York. Price $1.50 a copy, $12.00 annually for Transactions and the *Journal of Applied Mechanics* to members, $1.00 a copy, $6.00 annually. Add $1.50 for postage to all countries outside the United States, Canada, and Pan American Union. Changes of address must be received at Society headquarters seven weeks before they are to be effective on the mailing list. Please send old as well as new address.... By-Law: The Society shall not be responsible for statements or opinions advanced in papers or...printed in its publications (B13, Par. 4).... Entered as second-class matter March 2, 1928, at the Post Office at Easton, Pa., under the Act of August 24, 1912.... Copyrighted, 1956, by The American Society of Mechanical Engineers. Reprints from this publication may be made on condition that full credit be given the Transactions of the ASME and the author, and that date of publication be stated.

Oil and Gas-Well Casing Suspension Assemblies

By A. F. RHODES,[1] and J. C. WILHOIT, JR.,[2] HOUSTON, TEXAS

This paper provides the engineer with an analytical method for use in designing or evaluating oil and gas-well casing suspension assemblies. It develops equations for deflection and stress and confirms their results by reports of controlled experiments. The design applications of the theory are discussed and detailed consideration given to an optimum casing suspension design.

1 EFFECT ON THIN-WALLED CYLINDERS OF COMBINED LOADING FROM TENSION AND EXTERNAL SLIP COMPRESSION

Introduction

CONSIDER a thin-walled cylindrical tube loaded as shown in Fig. 1, the loading being symmetric with the axis of the tube. It is desired to determine deflection and stresses in the tube when the elastic limit is not exceeded. Owing to the short length of applied load and to the free end, this is clearly a three-dimensional problem and precludes the use of the two-dimensional plane strain Lamé equation for the stresses and deflections in a thick-walled cylinder. For a relatively small thickness-to-radius ratio, the tube is considered a thin-walled tube and the problem is one of bending of a cylindrical tube under axially symmetric loading.

The practical problem which is simulated is that of casing collapse in oil wells. The casing is hung in slips (see Fig. 2) which are "set" by the weight of the pipe itself. The assumption that this loading will give rise to the relatively uniform pressure on the casing over the slip length is made largely due to the observed uniform nature of the teeth marks made by well-designed slips on casing as made by slip manufacturers in the oil industry. The importance of a knowledge of casing deflection in the present case is evident when it is realized that equipment with an outside diameter close to the inside diameter of the casing must pass through the casing after it is hung in the slips.

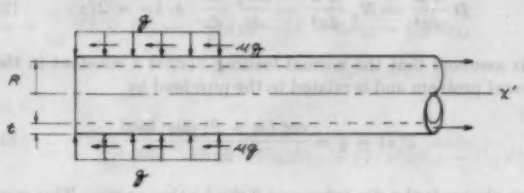

Fig. 1

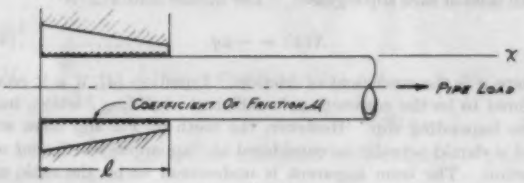

Fig. 2

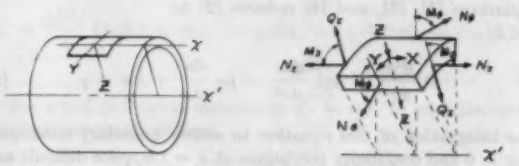

Fig. 3

Analytical Solution of the Problem

Co-Ordinate System: Notation

An element of the thin cylindrical tube showing the co-ordinate system is shown in Fig. 3. The notation to be used in Part 1 is as follows:

w = deflection of middle surface of tube in radial direction, positive inward

M_x, N_x, Q_x = bending moment per unit length about y-axis, tensile force per unit length, and shearing force per unit length, respectively, on a surface normal to x-axis

M_ϕ, N_ϕ, Q_ϕ = bending moment per unit length about x-axis, tensile force per unit length, and shearing force per unit length on surface of element parallel to axis of tube x'

X, Y, Z = body or surface forces per unit area in the three co-ordinate directions

l = length of slips

$D = Et^3/12(1 - \nu^2)$ = flexural rigidity

E = modulus of elasticity

ν = Poisson's ratio

$k = \dfrac{Et}{R^2}$ = foundation modulus

R = mean radius of casing

t = thickness of casing

α = angle of taper of slips

θ = angle of friction of slips on slip hanger

μ = coefficient of friction of inner surface of slips on casing

q = pressure between slips and casing

Symmetry about the x'-axis requires M_ϕ and N_ϕ constant

Shell Equations With Varying Tension

It is evident that in the actual loading, Fig. 3, the tensile force N_x must be zero at the surface $x = 0$ and must equal the total pipe load per unit of circumference at $x = l$. Therefore, under the slips, the tensile force N_x goes rapidly to zero. Outside the slips

---

[1] Director of Engineering, McEvoy Company. Mem. ASME.

[2] Assistant Professor of Mechanical Engineering, The Rice Institute. Assoc. Mem. ASME.

Contributed by the Petroleum Division and presented at the Petroleum-Mechanical Engineering Conference, New Orleans, La., September 25–28, 1955, of The American Society of Mechanical Engineers.

Note: Statements and opinions advanced in papers are to be understood as individual expressions of their authors and not those of the Society. Manuscript received at ASME Headquarters, August 30, 1955. Paper No. 55—PET-27.

there is a gradual decrease as x increases but for all practical purposes N_x outside the slips can be treated as constant in determining the deflection under the slips. The thin-shell equations for $x < l$ are

$$\frac{dN_x}{dx} = -X(x) \quad [1]$$

$$D\frac{d^4w}{dx^4} - N_x\frac{d^2w}{dx^2} - \frac{dN_x}{dx}\frac{dw}{dx} + kw = Z(x) \quad [2]$$

It is assumed that the normal loading $Z(x)$ is a constant in the present problem and is related to the pipe load by

$$Z(x) = q = \frac{\cot(\alpha + \theta)\ \text{pipe load}}{2\pi Rl} \quad [3]$$

Note that α is the slip taper and θ the friction angle. This relation follows from simple statics if uniform pressure is assumed on both sides of each slip segment. The surface load $X(x)$ is

$$X(x) = -\mu q \quad [4]$$

where μ is the coefficient of friction. Equation [4], if μ is considered to be the conventional coefficient of sliding friction, implies impending slip. However, the teeth on the slip have set and μ should actually be considered an "apparent" coefficient of friction. The term apparent is understood to be the ratio of surface to normal force after local yielding has occurred.[3] The friction angle θ is understood to be in the same sense. Use of Equations [1], [3], and [4] reduces [2] to

$x < l$

$$D\frac{d^4w}{dx^4} + \mu qx\frac{d^2w}{dx^2} - \mu q\frac{dw}{dx} + kw = q \quad [5]$$

The integration of this equation to satisfy boundary conditions at $x = 0$ and continuity conditions at $x = l$ is quite difficult and was not attempted for the present problem. Instead, the simplifications to be discussed were studied.

Simplified Theory Assuming Constant Tension

It is assumed that there is no axial force $X(x)$ and the full tension due to the pipe load is constant across the slips

$$\left.\begin{aligned} X(x) &= 0 \\ N_x &= T \end{aligned}\right\} \quad [6]$$

Then Equation [2] is

$$\left.\begin{aligned} &0 < x < l \\ &D\frac{d^4w}{dx^4} - T\frac{d^2w}{dx^2} + kw = q \end{aligned}\right\} \quad [7]$$

$$\left.\begin{aligned} &x > l \\ &D\frac{d^4w}{dx^4} - T\frac{d^2w}{dx^2} + kw = 0 \end{aligned}\right\} \quad [8]$$

The boundary conditions which must be satisfied are

$$\left.\begin{aligned} x = 0 \qquad & M_x = 0 \quad (a) \\ x = 0 \qquad & Q_x = Q_n + T\frac{dw}{dx} = 0 \quad (b) \\ x \to \infty \qquad & w \to 0 \quad (c) \\ x \to \infty \qquad & \frac{dw}{dx} \to 0 \quad (d) \end{aligned}\right\} \quad [9]$$

where Q_n is the normal shear acting in the plane of the section normal to the deflection line.

Equation [9b] for a free end is given in Hetenyi.[4] Making use of the analogy between the bending of thin-wall tubes and beams on an elastic foundation (see, for instance, Den Hartog[5] or Hetenyi[4]) the problem reduces itself to that shown in Fig. 4.

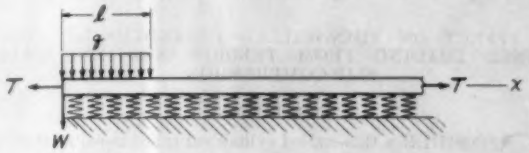

FIG. 4

The solution of Equations [7] and [8] subject to Equation [9] is accomplished by the superposition of several known solutions in Hetenyi,[4] namely, the conversion of his solution for a concentrated load on an infinite beam to that for a uniformly distributed load by integration and the use of solutions for a concentrated end moment and a concentrated end force on a semi-infinite beam. It is noted that, in all three cases, the uniform tensile load T acts. These solutions are

$$w = \frac{q\lambda^2}{2k\alpha\beta}\left\{\frac{\beta^2 - \alpha^2}{\beta^2 + \alpha^2}\left[e^{-(\alpha-\beta)x}B_{\beta x} + e^{-(\alpha-\beta)(l-x)}B_{\beta(l-x)}\right] - \frac{2\alpha\beta}{\beta^2 + \alpha^2}\left[e^{-(\alpha-\beta)x}D_{\beta x} + e^{-(\alpha-\beta)(l-x)}D_{\beta(l-x)}\right] + \frac{4\alpha\beta}{\beta^2 + \alpha^2} + \left[e^{-(\alpha-\beta)l}e^{-(\alpha-\beta)x}\frac{(\beta^2 + \alpha^2)B_{\beta l}}{\beta(3\alpha^2 - \beta^2)}(\beta D_{\beta x} - \alpha B_{\beta x})\right] - \frac{1}{\beta^2 + \alpha^2}\left[-1 + e^{-(\alpha-\beta)l}D_{\beta l} + e^{-(\alpha-\beta)l}\frac{\alpha(\alpha^2 - 3\beta^2)}{\beta(3\alpha^2 - \beta^2)}B_{\beta l}\right]e^{-(\alpha-\beta)x}\left[2\alpha\beta D_{\beta x} + (\alpha^2 - \beta^2)B_{\beta x}\right]\right\} \quad [10]$$

For $x > l$, $4\alpha\beta/\beta^2 + \alpha^2$ is dropped and the two terms containing $(l - x)$ are multiplied by (-1) and have $(x - l)$ substituted for $(l - x)$

$$\frac{dw}{dx} = \frac{q\lambda^2}{2k\alpha\beta}\left\{e^{-(\alpha-\beta)l}\left[\beta D_{\beta l} - \frac{\alpha(\alpha^2 + 5\beta^2)}{(3\alpha^2 - \beta^2)}B_{\beta l}\right]e^{-(\alpha-\beta)x}D_{\beta x} + e^{-(\alpha-\beta)l}\left[\alpha D_{\beta l} + \frac{2\alpha^4 - 3\alpha^2\beta^2 - \beta^4}{\beta(3\alpha^2 - \beta^2)}B_{\beta l}\right]e^{-(\alpha-\beta)x}B_{\beta x} - \beta e^{-(\alpha-\beta)(l-x)}D_{\beta(l-x)} - \alpha e^{-(\alpha-\beta)(l-x)}B_{\beta(l-x)}\right\} \quad [11]$$

[3] "A Study of Quasi-Frictional Forces Resulting on Serrated Clamping Elements," by E. I. Moser, unpublished Master's thesis, The Rice Institute, Houston, Texas, 1955.

[4] "Beams on Elastic Foundation," by M. Hetenyi, The University of Michigan Press, Ann Arbor, Mich., 1946.

[5] "Advanced Strength of Materials," by J. P. Den Hartog, McGraw-Hill Book Company, Inc., New York, N. Y., 1952.

For $x > l$ replace each $(l - x)$ by $(x - l)$

$$M_x = \frac{Dq\lambda^2}{2k\alpha\beta}(\beta^2 + \alpha^2)\left\{e^{-(\alpha-\beta)l}\left[D_{\beta l} + 2\frac{\alpha(\alpha^2 - 3\beta^2)}{\beta(3\alpha^2 - \beta^2)}B_{\beta l}\right]e^{-(\alpha-\beta)x}B_{\beta x} - e^{-(\alpha-\beta)l}B_{\beta l}e^{-(\alpha-\beta)x}D_{\beta x} + e^{-(\alpha-\beta)(l-x)}B_{\beta(l-x)}\right\} \quad [12]$$

For $x > l$ multiply the last term by (-1) and replace $(l - x)$ by $(x - l)$

$$Q_x = -\frac{Dq\lambda^2}{2k\alpha\beta}(\beta^2 + \alpha^2)\left\{e^{-(\alpha-\beta)l}\left[\frac{\alpha(7\beta^2 - 5\alpha^2)}{(3\alpha^2 - \beta^2)}B_{\beta l} - \beta D_{\beta l}\right]e^{-(\alpha-\beta)x}D_{\beta x} + e^{-(\alpha-\beta)l}\left[\frac{2\alpha^4 - 9\alpha^2\beta^2 + \beta^4}{\beta(3\alpha^2 - \beta^2)}B_{\beta l} + \alpha D_{\beta l}\right]e^{-(\alpha-\beta)x}B_{\beta x} + \beta e^{-(\alpha-\beta)(l-x)}D_{\beta(l-x)} - \alpha e^{-(\alpha-\beta)(l-x)}B_{\beta(l-x)}\right\} \quad [13]$$

For $x > l$ replace each $(l - x)$ by $(x - l)$. In the foregoing relations

$$\lambda^2 = \sqrt{\frac{k}{4D}} \quad [14]$$

$$\alpha = \sqrt{\lambda^2 + \frac{T}{4D}} = \lambda\sqrt{1 + \frac{\sqrt{3(1-\nu^2)}}{Et^2}TR} \quad [15]$$

$$\beta = \sqrt{\lambda^2 - \frac{T}{4D}} = \lambda\sqrt{1 - \frac{\sqrt{3(1-\nu^2)}}{Et^2}TR} \quad [16]$$

$$B_{\beta x} = e^{-\beta x}\sin\beta x \quad [17]$$

$$D_{\beta x} = e^{-\beta x}\cos\beta x \quad [18]$$

The use of the functions $B_{\beta x}$ and $D_{\beta x}$ is indicated since they are tabulated by Hetenyi.[4] The resultant stresses are

$$\left.\begin{aligned} \sigma_{x\max} &= \frac{T}{t} \pm \frac{6M_x}{t^2} && (a)\\ \sigma_{y\max} &= -\frac{Ew}{R} \pm \frac{\nu 6M_x}{t^2} + \nu\frac{T}{t} && (b)\\ \tau_{xz\max} &= \frac{3Q_x}{2t} = \frac{3}{2t}\left(Q_x + T\frac{dw}{dx}\right) && (c)\end{aligned}\right\} \quad [19]$$

where σ_x is the normal stress which gives rise to the N_x and M_x, τ_{xz} is the shear and stress giving rise to Q_x, and σ_y is the normal stress which gives rise to N_ϕ and M_ϕ.

Simplified Theory Assuming Zero Tension

In this case Equations [7] and [8] become

$$\left.\begin{aligned} &x < l\\ &D\frac{d^4w}{dx^4} + kw = q\end{aligned}\right\} \quad [20]$$

$$\left.\begin{aligned} &x > l\\ &D\frac{d^4w}{dx^4} + kw = 0\end{aligned}\right\} \quad [21]$$

This problem is given in Hetenyi[4] and the solution is

$x < l$

$$w = \frac{q}{2k}[(1 + B_{\lambda l} - C_{\lambda l})A_{\lambda x} - (1 + 2B_{\lambda l} - C_{\lambda l})B_{\lambda x} + (2 - D_{\lambda x} - D_{\lambda(l-x)})] \quad [22]$$

$x > l$

$$w = \frac{q}{2k}[(1 + B_{\lambda l} - C_{\lambda l})A_{\lambda x} - (1 + 2B_{\lambda l} - C_{\lambda l})B_{\lambda x} - D_{\lambda x} + D_{\lambda(x-l)}] \quad [23]$$

$x < l$

$$\frac{dw}{dx} = -\frac{q\lambda}{2k}[2(1 + B_{\lambda l} - C_{\lambda l})B_{\lambda x} + (1 + 2B_{\lambda l} - C_{\lambda l})C_{\lambda x} - A_{\lambda x} + A_{\lambda(l-x)}] \quad [24]$$

For $x > l$ replace $(l - x)$ by $(x - l)$

$x < l$

$$M_x = \frac{qD\lambda^2}{k}[(1 + B_{\lambda l} - C_{\lambda l})C_{\lambda x} - (1 + 2B_{\lambda l} - C_{\lambda l})D_{\lambda x} + B_{\lambda x} + B_{\lambda(l-x)}] \quad [25]$$

For $x > l$ the last term is multiplied by (-1) and $(l - x)$ is replaced by $(x - l)$

$x < l$

$$Q_x = \frac{qD\lambda^3}{k}[-2(1 + B_{\lambda l} - C_{\lambda l})D_{\lambda x} + (1 + 2B_{\lambda l} - C_{\lambda l})A_{\lambda x} + C_{\lambda x} - C_{\lambda(l-x)}] \quad [26]$$

For $x > l$, $(l - x)$ is replaced by $(x - l)$. In addition to the symbols previously defined

$$A_{\lambda x} = e^{-\lambda x}(\cos\lambda x + \sin\lambda x) \quad [27]$$

$$C_{\lambda x} = e^{-\lambda x}(\cos\lambda x - \sin\lambda x) \quad [28]$$

The use of these functions is indicated since they are tabulated in Hetenyi.[4]

It is clearly evident that for computational purposes, the solution for zero tension is very much simpler than for full tension. Furthermore, it is felt that the two solutions should bracket the "exact" solution for varying tension.

Analytical Comparison of Two Simplified Solutions

For the zero tension case $\alpha = \beta = \lambda$ and the first simplified solution reduces to the second. Reference to Equations [14] and [15] indicates that α and β differ from λ as

$$\sqrt{1 \pm \frac{\sqrt{3(1-\nu^2)}}{Et^2}TR}$$

For all the tubing considered in this paper there is little variation in t. Thus the greatest variation in the two solutions is expected with the greatest TR. As an extreme case $9^5/_8$-in. casing under a pipe load of 606,000 lb with a slip length of 6 in. was considered. The slip angle is 7 deg and a friction angle θ of 6.1 deg was used. The figure of 6.1 deg was suggested by Mills.[6] The results for pipe deflection, bending moment M_x, and shearing force Q_x are shown in Figs. 5, 6, and 7. The results clearly indicate that the zero tension solution is sufficient for this example

[6] "Factors Influencing the Load Capacity of Slip Suspension Equipment," by K. N. Mills, *The Slide Rule*, May, 1946.

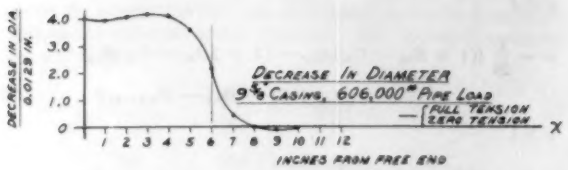

FIG. 5

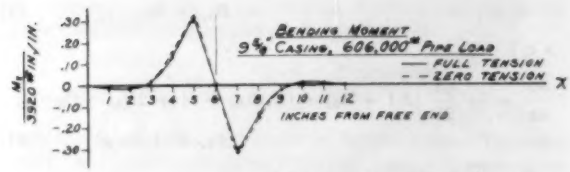

FIG. 6

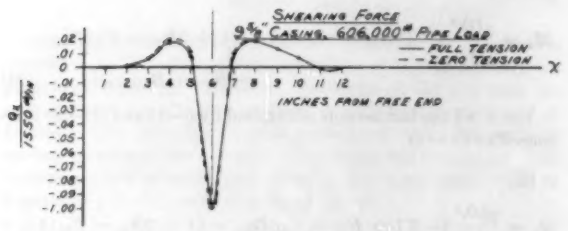

FIG. 7

and since this is one of the most extreme cases to be encountered in casing collapse, it is felt that this justifies the use of the zero solution in the determination of deflection and stresses involved in casing collapse.

It is fully realized that the foregoing does not constitute a mathematical proof of the limit of T/R for which the difference in the two simplified cases would be less than a given percentage. However, the use of the extreme case and spot checks for smaller casing indicate that, in the range considered, the zero tension case is quite sufficient.

Experimental Results

The experimental technique is shown in Fig. 8. Smooth-backed slips were used to grip 7-in. 23-lb N-80 casing, about 2¼-in. of the casing extending above the slips. The casing was loaded hydraulically and circumferential strain readings were recorded by means of eight SR-4 A-1 gages mounted on the inner surface of the casing. The location of these gages is also shown in Fig. 8.

The casing was evidently not perfectly round as some gages under the slips took on large tensile strains as the load was initially applied, changing to compressive strains as the loading increased. Thus, although the load-strain curves were linear after the first few readings up to the elastic limit, the lines did not pass through the origin. The corrections made to get a true picture of the load-strain curve are illustrated in Fig. 9 for gage 3. It should be noted that a zero reading after yield was used in Fig. 9 to determine the recorded strains. The deflection corresponding to these strains ϵ_ϕ is obtained from

$$\epsilon_\phi = -\frac{w}{R} \quad \ldots\ldots [29]$$

In attempting to compare the experimental and analytical results, it is noted that the previous solution does not account for the casing extended above slips. This is easily accomplished by the superposition shown in Fig. 10. The solution is

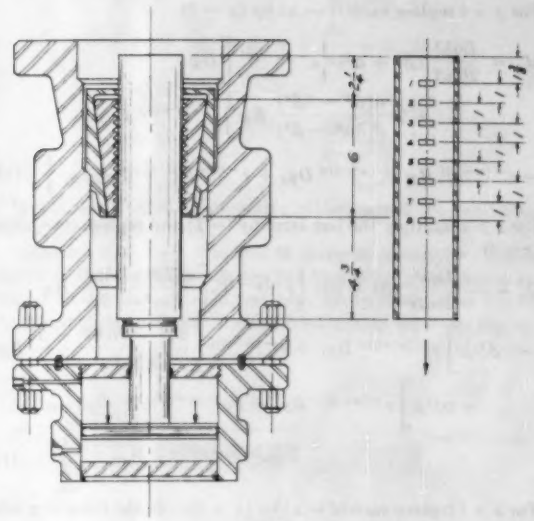

FIG. 8

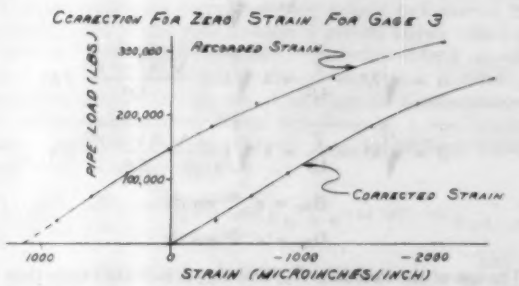

FIG. 9 CORRECTION FOR ZERO STRAIN FOR GAGE 3

$x < l$

$$w = \frac{q}{2k}\left[(B_{\lambda(l+a)} - B_{\lambda a} - C_{\lambda(l+a)} + C_{\lambda a})A_{\lambda x} - (2B_{\lambda(l+a)} - 2B_{\lambda a} - C_{\lambda(l+a)} + C_{\lambda a})B_{\lambda x} - D_{\lambda(l+a-x)} + D_{\lambda(a-x)}\right] \quad \ldots\ldots [30a]$$

$0 < x < l + a$

$$w = \frac{q}{2k}\left[(B_{\lambda(l+a)} - B_{\lambda a} - C_{\lambda(l+a)} + C_{\lambda a})A_{\lambda x} - (2B_{\lambda(l+a)} - 2B_{\lambda a} - C_{\lambda(l+a)} + C_{\lambda a})B_{\lambda x} - D_{\lambda(l+a-x)} - D_{\lambda(x-a)} + 2\right] \quad \ldots\ldots [30b]$$

$x > l + a$

$$w = \frac{q}{2k}\left[(B_{\lambda(l+a)} - B_{\lambda a} - C_{\lambda(l+a)} + C_{\lambda a})A_{\lambda x} - (2B_{\lambda(l+a)} - 2B_{\lambda a} - C_{\lambda(l+a)} + C_{\lambda a})B_{\lambda x} + D_{\lambda(x-l-a)} - D_{\lambda(x-a)}\right] \quad \ldots\ldots [30c]$$

A comparison of deflection as obtained experimentally by the strain gages and calculated by Equations [30] are shown in Fig. 11. The results show a remarkable prediction of maximum deflection but leave the assumption of uniform pressure somewhat suspect. The indication is that the pressure in this particular test was rela-

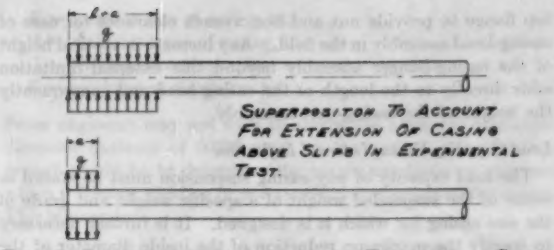

FIG. 10 SUPERPOSITION TO ACCOUNT FOR EXTENSION OF CASING ABOVE SLIPS IN EXPERIMENTAL TEST

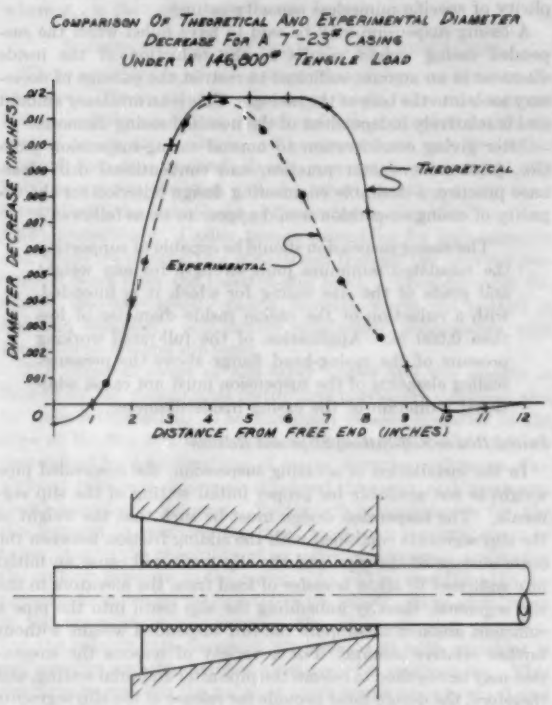

FIG. 11 COMPARISON OF THEORETICAL AND EXPERIMENTAL DIAMETER DECREASE FOR A 7 IN. 23-LB CASING UNDER A 146,800-LB TENSILE LOAD

tively uniform at the top of the slips but is considerably less at the lower end of the slips. Fig. 12 shows a comparison of measured and calculated maximum deflection against load. Figs. 11 and 12 indicate the adequacy of the theoretical solution.

Design Formulas, Discussion of Maximum Stresses

For the range of tensile load, casing diameter, and slip lengths considered in the paper, it can be shown that the maximum diameter decrease in the elastic range is approximately

$$\text{Maximum diameter decrease} = \frac{2q}{k} = \frac{\cot(\alpha+\theta)\, R \text{ pipe load}}{\pi l t E} \quad \ldots\ldots [31]$$

The maximum bending moment can be shown to be approximately

$$M_{z\max} \approx \frac{0.0485 \cot(\alpha+\theta)\, t \text{ pipe load}}{2\pi l} \quad \ldots\ldots [32]$$

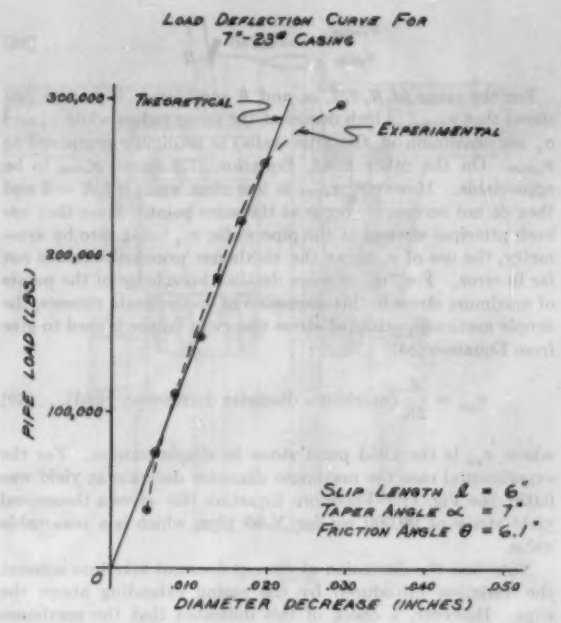

FIG. 12 LOAD DEFLECTION CURVE FOR 7 IN. 23-LB CASING

or the normal stress is

$$\sigma_{z\max} \approx \frac{\text{pipe load}}{2\pi R t}\left[1 + \frac{0.291\, R \cot(\alpha+\theta)}{l}\right] \quad \ldots\ldots [33]$$

Reference to Fig. 5 shows that this occurs, for the particular example shown, about an inch above and an inch below the bottom of the slips. The maximum tangential, or hoop, stress can be shown to be approximately

$$\sigma_{y\max} \approx \frac{E_{y\max}}{R} = \frac{(\text{pipe load})\cot(\alpha+\theta)}{2\pi l t} \quad \ldots\ldots [34]$$

This occurs at the maximum deflection somewhere near the center of the slips. The maximum shearing force can be shown to be approximately

$$Q_{z\max} \approx -0.097\sqrt{\frac{t}{R}}\,\frac{(\text{pipe load})\cot(\alpha+\theta)}{2\pi l} \quad \ldots\ldots [35]$$

or the shearing stress is

$$\tau_{xz\max} \approx -0.146\,\frac{1}{\sqrt{Rt}}\,\frac{(\text{pipe load})\cot(\alpha+\theta)}{2\pi l} \quad \ldots\ldots [36]$$

This maximum occurs at the lower end of the slip, Fig. 7.

A prediction of yield stress would actually require a consideration of combined stresses and an accurate knowledge of where the maxima occur. However, Equations [33], [34], and [36] show

$$\frac{\sigma_{z\max}}{\sigma_{y\max}} \approx \left(\frac{l}{R}\right)\left(\frac{1 + 0.291\,\frac{R}{l}\cot(\alpha+\theta)}{\cot(\alpha+\theta)}\right) = \left(\frac{l}{R}\right)\left[\tan(\alpha+\theta) + 0.291\,\frac{R}{l}\right] \quad \ldots\ldots [37]$$

$$\frac{\tau_{z\max}}{\sigma_{y\max}} \simeq -0.146\sqrt{\frac{t}{R}} \quad \ldots\ldots\ldots\ldots [38]$$

For the range of R, t, l, α, and θ considered, Equation [38] shows that $\tau_{z\max}$ (which occurs at the mean radius while σ_z and σ_y are maximum at the pipe walls) is negligible compared to $\sigma_{y\max}$. On the other hand, Equation [37] shows $\sigma_{z\max}$ to be appreciable. However, $\sigma_{z\max}$ is less than $\sigma_{y\max}$ if $l/R < 3$ and they do not necessarily occur at the same point. Since they are both principal stresses at the pipe walls, τ_{zy} being zero by symmetry, the use of $\sigma_{y\max}$ as the maximum principal stress is not far in error. For lack of more detailed knowledge of the points of maximum stress in this discussion of approximate stresses, the simple maximum principal-stress theory of failure is used to give from Equation [34]

$$\sigma_{yp} \simeq \frac{E}{2R}\,(\text{maximum diameter decrease at yield}) \ldots [39]$$

where σ_{yp} is the yield point stress in simple tension. For the experimental case the maximum diameter decrease at yield was 0.020, see Fig. 11. Therefore Equation [39] gives a theoretical yield stress of 90,000 psi for N-80 pipe, which is a reasonable value.

Note that the discussion of stresses does not take into account the variation introduced by the casing extending above the slips. However, a check of this indicated that the maximum shearing force Q_z remains approximately the same while the bending moment M_z is decreased. Therefore the previous conclusions still hold.

2 APPLICATION TO PROBLEM OF OIL-WELL CASING SUSPENSION

From the mathematical relations developed in Part 1, the engineer is now in a position to proceed with the design of an oil-well casing suspension. However, before an optimum design can be derived from the equations, it is necessary to examine more closely the operating requirements and the practical design restrictions that limit the selection of values for the design variables found in the general equations.

Statement of General Design Problem

Dimensional Restrictions

The casing suspension is only one part of the over-all well completion, and it is a primary requirement that its dimensions conform to restrictions inherent in the other completion equipment. This places a considerable limitation on the design engineer. A certain range of casing sizes is inherently associated with a fixed size of well head-flange bore. The maximum diameter of any casing suspension is limited to that which will pass through full opening blowout preventers mounted on the casing-head flange. All standard API casing heads must be full opening to the lightest weight of the largest-size casing upon which they may be mounted. The support area for the casing suspension is thus limited to the annular area between these two critical dimensions.

In deeper wells with multiple strings of casing, the vertical height of the casing nest portion of the Christmas tree assembly is of considerable concern to the operator. The casing hanger assembly (suspension and pressure packoff) is limited at the top in that it should not rise above the surrounding flange surface and is limited at the bottom in that it must not overlap the side outlet by an amount which would cause a significant flow restriction. In conventional casing-head design, the center line of the side outlet is placed far enough below the lower surface of the top flange to provide nut and box wrench clearance for ease of casing-head assembly in the field. Any increase in vertical height of the casing-hanger assembly beyond this external limitation adds directly to the length of the casing head and consequently the height of the casing-nest assembly.

Load Capacity Versus Internal Deflection

The load capacity of any casing suspension must be stated in terms of the suspended weight of a specific weight and grade of the size casing for which it is designed. It is further necessary to specify the maximum reduction of the inside diameter of the casing which is associated with the rated suspended weight. It is obvious, therefore, that any one casing suspension has a multiplicity of specific numerical capacity ratings.

A casing suspension may be said to have failed when the suspended casing weight results in the reduction of the inside diameter in an amount sufficient to restrict the passage of necessary tools into the bore of the casing. This is an arbitrary amount and is relatively independent of the nominal casing diameter.

After giving consideration to normal casing-suspension practice, joint safety-factor practice, and conventional drift-clearance practice, a desirable engineering design criterion for the capacity of casing suspension would appear to be as follows:

> The casing suspension should be capable of supporting the tabulated minimum joint strength for any weight and grade of the size casing for which it is intended, with a reduction of the casing inside diameter of less than 0.030 in. Application of the full-rated working pressure of the casing-head flange above the pressure-sealing elements of the suspension must not cause additional reduction of the casing inside diameter.

Initial Bite or Self-Setting Slips and Release

In the installation of a casing suspension, the suspended pipe weight is not available for proper initial setting of the slip segments. The suspension design must be such that the weight of the slip segments combined with the sliding friction between the outer surface of the pipe and the slip teeth will cause an initial bite sufficient to allow transfer of load from the elevators to the slip segments, thereby imbedding the slip teeth into the pipe a sufficient amount to support the full suspended weight without further relative motion. For a variety of reasons the suspension may be required to release the pipe after an initial setting, and therefore, the design must provide for release of the slip segments upon upward relative motion of the pipe to the casing head.

Separation of Pressure and Slip Loading

A casing hanger assembly consists of a casing suspension and a pressure packoff. This paper is concerned only with the casing suspension, but it is a necessary design condition that the hydraulic forces acting on the pressure-sealing elements have no detrimental effect on the suspension performance.

The Engineering Design Equations

From the conclusions of Part 1 may be set forth the two equations governing the design of oil-well casing suspensions. They are

$$\text{Max diam decrease} = \frac{\cot(\alpha + \theta)R}{\pi l t E} \times \text{pipe load}$$

$$\text{Tangential stress} = \frac{\cot(\alpha + \theta)}{2\pi l t} \times \text{pipe load}$$

where

α = taper angle, deg
θ = friction angle, deg

R = mean radius of casing, in.
t = wall thickness of casing, in.
l = slip segment length, in.
E = modulus of elasticity, psi

Some engineers may not wish to accept the arbitrary maximum diameter decrease of 0.030 used by the author. Another approach would be to determine the maximum diameter decrease which will cause yielding or permanent deformation of the casing. This is given by

$$\text{Diam decrease at casing yield point} = \frac{2R\sigma_{yp}}{E}$$

where σ_{yp} is the yield stress for the casing used.

Suspension-Design Variables and Their Limits

Three variables in a casing suspension design are open to the engineer. These are the slip taper angle, the slip segment length, and the coefficient of sliding friction associated with slip motion on its taper surface. Slip suspensions may be further divided into two general classes, one using an inserted slip bowl to support the slips and the other providing a slip taper integral with the casing head as illustrated in Fig. 13(*a*) and Fig. 13(*b*), respectively. Casing hanger assemblies for high capacity and which are designed for installation through the blowout preventers must have the inserted slip bowl. When properly designed, medium-capacity casing hangers, where the packoff is installed separately, will deliver satisfactory performance with the use of an integral slip taper.

The practical range of slip taper angles and slip lengths is limited by the dimensional restrictions previously discussed and by their interrelation. The maximum outside diameter of the slips at the top and the minimum diameter at the bottom are determined by considerations of casing diameter, minimum slip-segment thickness, minimum slip-bowl thickness, and maximum casing-head bore diameter. Further, it is undesirable for the slip segment to overhang the taper by a large amount, above or below, due to the possibility of an unbalanced couple destroying the uniform pressure on the casing. As will be seen from the design equations, either an increase in the slip length or an increase in the taper angle will increase the slip-suspension capacity. For the reasons just discussed, an increase in both variables is not possible, and the designer must accept a compromise. This compromise restricts the range of taper angles to between 5 and 9 deg and the range of slip lengths to between $3^1/_2$ and 11 in. in practically all the currently available oil-well casing suspension systems.

The third variable is the coefficient of sliding friction between the slip segment and its supporting taper. Surprisingly enough, little engineering attention has been given in the past to this factor, in spite of the obvious fact that it is the only one of the variables not subject to dimensional restrictions. The past history of casing suspension design records a number of experiments with increasing the coefficient of friction by "rough machining" of the slips and/or bowl. This method has never come into general use for two important reasons. Since the high coefficient of friction resulting from rough machining is present during the initial setting operation, considerable difficulty is experienced in getting the teeth on the face of the slip sufficiently imbedded in the casing to support the high load of the final setting without shearing or relative motion between the slips and the casing. When slips of this type are fully set under a high load, it is almost impossible to retrieve them due to the myriad ridges fully indented into the bowl taper. Despite this problem it is apparent from the design equations that even a small change in the coefficient of friction or friction angle will cause a significant increase in the load capacity of the suspension system and will require no changes in the physical dimensions.

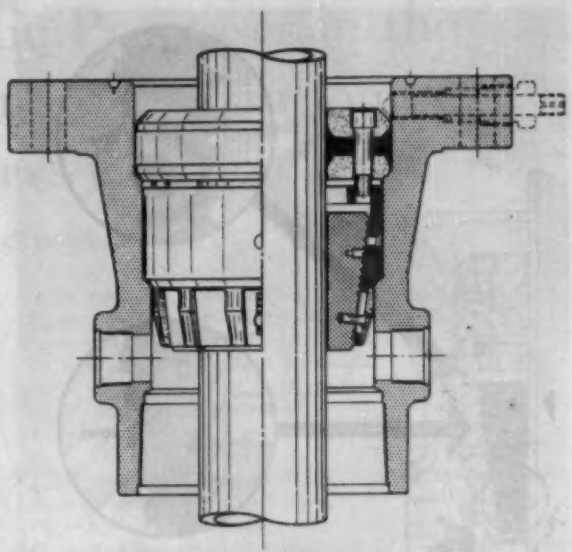

Fig. 13(*a*)

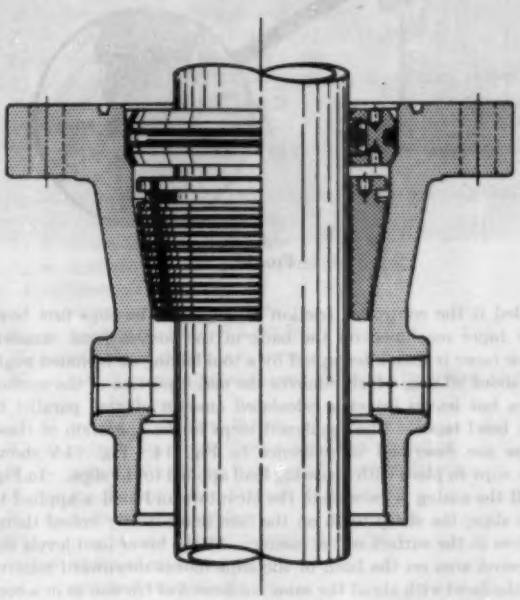

Fig. 13(*b*)

The Concept of "Controlled Friction"

In considering the use of the friction angle as a design variable, the requirements for high load capacity and good initial pipe bite are apparently irreconcilable. However, if a slip construction could be adopted which would cause an increase in the friction angle in a predictable relationship to the increase of load, this would present an attractive solution to the problem.

One such slip construction is shown in Fig. 14, and we have

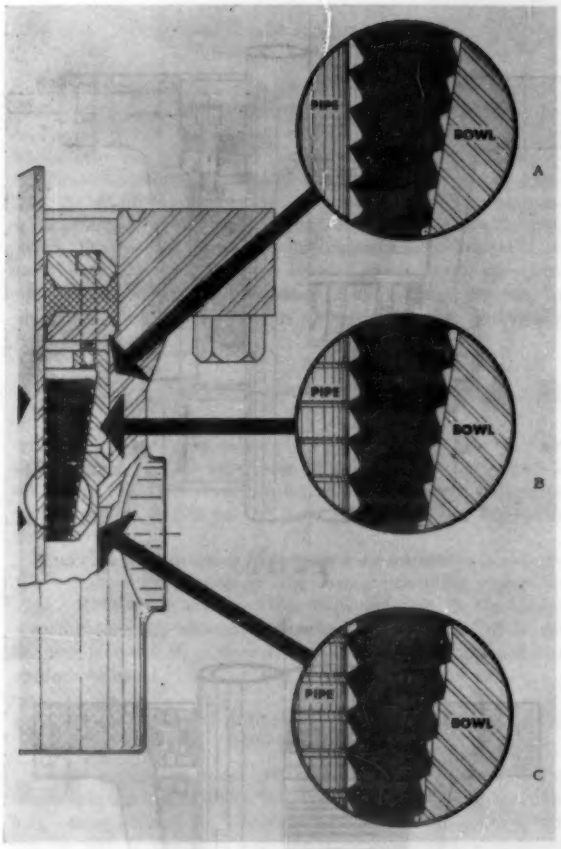

FIG. 14

called it the controlled friction principle. The slips first have the taper machined on the back in the conventional manner. This taper is then interrupted by a tool having an included angle of about 90 deg, which removes the major portion of the surface area but leaves intact a calculated amount of area parallel to the bowl taper. The significant steps in the operation of these slips are described in reference to Fig. 14. Fig. 14A shows the slips in place with no casing load applied to the slips. In Fig. 14B the casing is lowered in the elevators and load is applied to the slips; the sharp teeth on the face immediately imbed themselves in the surface of the casing. At the lower load levels the tapered area on the back of the slips moves downward relative to the bowl with about the same coefficient of friction as in a conventional slip suspension. In Fig. 14C the casing load transferred to the slip increases the normal pressure between the slip and the bowl to a point where the surface compressive stress becomes greater than the yield stress of the bowl material. At this point the lower edge of the tapered surface on the slip begins shearing a very thin layer of the bowl material. This causes a continuous increase in the apparent friction angle as the applied load rises.

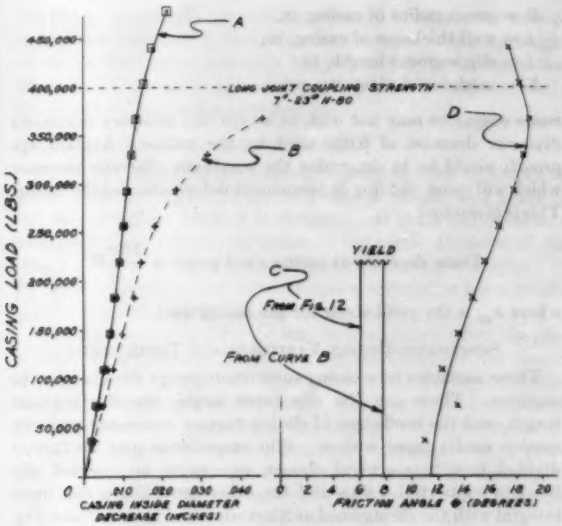

FIG. 15

The small angle with the bowl taper, made by the interrupting tool at the upper edge of the flat surface on the slip, facilitates easy release of the slip suspension in response to upward movement of the pipe relative to the casing hanger. The desired capacity can be achieved with a contact area on the back of the slip sufficient to reduce the brinelling of the bowl to a few thousandths of an inch. This allows the suspension assembly to be re-used a considerable number of times without remachining.

Fig. 15, curve A, shows the casing inside diameter decrease versus casing load with a slip suspension using controlled friction as compared to a dimensionally identical smooth back slip suspension in curve B. As can be seen from the design equations, the only factor which can account for the difference in casing collapse at the same casing load is the friction angle θ. Since curve B is a straight line in the elastic region, the friction angle is a constant and is shown as the vertical line in curve C. The friction angle used in Fig. 12 of Part 1 is also shown. Substitution of the observed casing collapse values for curve A in the design equation results in curve D. This graphically portrays the increase in friction angle with casing load due to the controlled friction structure used on the back of the slips.

Study of Pneumatic Processes in the Continuous Control of Motion With Compressed Air—I

By J. L. SHEARER,[1] CAMBRIDGE, MASS.

A pneumatic servomotor consisting of a 4-way control valve and double-acting ram is analyzed to determine the effective use of this system for continuous control of ram motion. Special emphasis is placed on studying the dynamic behavior of the fluid in the ram chambers and the pressure-flow characteristics of the control valve. Comparisons are made of the measured and theoretical characteristics of a typical control valve. The results of a simple experiment with a control valve and tank determine the validity of the ram-chamber analysis. A subsequent paper will show how the complete servomotor system, including mass load, is analyzed for its response to small changes of valve opening and to changes of external load force, and a simple electronic analog of the system is used to study means of providing adequate system damping.

Nomenclature

The following nomenclature is used in the paper:

A = ram area, sq in.
A_e = area of exhaust-orifice opening, sq in.
A_o = orifice area, sq in.
A_s = area of supply-orifice opening, sq in.
C = compressible flow coefficient, $\sqrt{\text{deg R}}$/sec
C_1 = partial derivative of weight rate of flow with respect to valve opening, lb/sec-in.
C_2 = partial derivative of weight rate of flow with respect to load pressure, sq in/sec
C_d = orifice-discharge coefficient
c_p = specific heat at constant pressure, sq in/sec²-deg R
c_v = specific heat at constant volume, sq in/sec²-deg R
D = denotes derivative with respect to time d/dt, 1/sec
d = diameter, in.
e = subscript denoting exhaust
F_l = total load force, lb
f = subscript to designate final condition
f = to indicate a functional relationship
f_v = functional relationship between valve flow W, valve opening X, and load pressure P
f_1 = function of pressure ratio
g = acceleration due to gravity, 386 in/sec²
i = subscript to designate initial condition
k = ratio of specific heats, c_p/c_v, for air: 1.4
L = load force, lb
m = load mass, lb-sec²/in.
P_a = pressure in a chamber a, psi
P_{aq} = quiescent value of P_a, ($W_a = 0$ and $x = 0$), psi
P_b = pressure in chamber b psi
P_{bq} = quiescent value of P_b, ($W_b = 0$ and $x = 0$), sq in.
P_d = downstream pressure, psi
P_e = exhaust pressure, psi
P_i = initial pressure, psi
P_q = quiescent value of P_a and P_b when they are equal, psi
P_s = pressure of gas supply, psi
P_u = upstream pressure, psi
Q_h = heat transferred to system, in-lb, 1 Btu = 9336 in-lb
R = gas constant (for air: 2.47×10^3), sq in/sec²-deg R
s = subscript denoting supply
ss = subscript denoting steady state
T_a = temperature in chamber a, deg R
T_b = temperature in chamber b, deg R
T_e = stagnation temperature upstream of exhaust orifice
T_i = initial temperature, deg R
T_l = line temperature, deg R
T_{la} = stagnation temperature of gas in the line entering chamber a, deg R
T_{lb} = stagnation temperature of gas in the line entering chamber b, deg R
T_s = temperature of supply gas
T_u = upstream stagnation temperature, deg R
t = time, sec
U = valve underlap, in.
V_a = volume of chamber a, cu in.
V_b = volume of chamber b, cu in.
V_i = initial volume at each end of ram (including lines to valve), cu in.
W = weight rate of flow, lb/sec
W_a = weight rate of flow from a end of valve, lb/sec
W_b = weight rate of flow from b end of valve, lb/sec
W_e = weight rate of flow through A_e, lb/sec
W_q = quiescent-leakage flow
W_s = weight rate of flow through A_s, lb/sec
w_e = width of exhaust port, in.
w_s = width of supply port, in.
X = valve displacement measured from center position, in.
Y = ram displacement measured from center position, in.
γ = dimensionless valve displacement
Δ = small change
ρ_a = mass density of fluid in chamber a, lb sec²/in.⁴
ρ_b = mass density of fluid in chamber b, lb sec²/in.⁴

Introduction

The flow of fluid under pressure is a widely used means of transmitting power from an energy source to the point of power utilization. Hydraulic systems have undergone a high degree of development, and they have been used effectively for the transmission and control of power in applications ranging from giant

[1] Assistant Professor of Mechanical Engineering, Massachusetts Institute of Technology. Mem. ASME.

Contributed by the Instruments and Regulators Division and presented at the Instruments and Regulators Division Conference, Ann Arbor, Mich., April 25–26, 1955, of The American Society of Mechanical Engineers.

Note: Statements and opinions advanced in papers are to be understood as individual expressions of their authors and not those of the Society. Manuscript received at ASME Headquarters, February 4 1955. Paper No. 55—IRD-4.

hydroelectric power installations to compact hydraulic servomechanisms. Compressed gases have served successfully as the working fluid in systems as diversified as air brakes and steam and gas-turbine power plants.

Except for the low-pressure (10 to 20 psig) pneumatic control systems developed for industrial process controls, compressed gases seldom have been applied to the continuous control of motion required in many servomechanisms and automatic control systems. Use has been limited mainly to simple on-off control functions in systems where mechanical stops provide the required positive positioning action. The continuous control systems developed for operation with compressed gas (usually air) as the working fluid are largely low-pressure instrument systems where speed of response is not a critical factor and the power controlled is usually a small fraction of 1 hp.

With a few possible exceptions, no rational engineering approach has been made to the problem of providing continuous pneumatic control of motion of a member having a significant mass when subjected to external load forces. Such existing systems seem to have evolved from the application of a fortunate combination of trial-and-error techniques and intuition.

The purpose of this paper is to try to gain a thorough understanding of the fundamental factors governing the performance of a valve-controlled pneumatic servomotor in the presence of external load forces in order to evolve a rational design procedure that will facilitate the design and/or evaluation of systems of this kind in a straightforward manner.

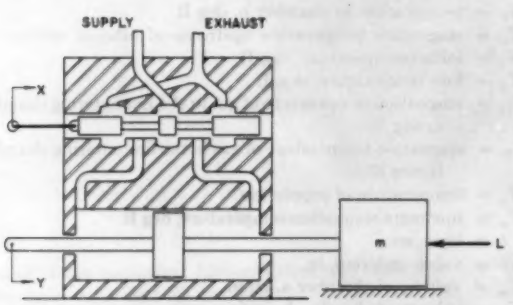

FIG. 1 VALVE-CONTROLLED PNEUMATIC SERVOMOTOR WITH LOAD

Fig. 1 shows schematically the basic system under consideration. Factors deemed to be of outstanding importance in the evaluation of this system are speed of response, degree of dynamic stability, load sensitivity, and efficiency. Practical design considerations such as the strengths of structural members, means of fastening and sealing, arrangement of components, and selection of materials are not to be dealt with here.

DYNAMIC ANALYSIS OF RAM CHAMBERS

Fig. 2 shows a valve-controlled ram schematically. The weight rate of flow of gas to chamber a is W_a, and the weight rate of flow of gas to chamber b is W_b, with stagnation temperatures designated by T_{ta} and T_{tb}, respectively. The ram chambers a and b have volumes V_a and V_b, respectively. As a first approximation, an assumption of perfect mixing in chambers a and b makes possible the use of a single pressure and a single temperature to describe the state of the fluid in each chamber. The quantities P_a and T_a then will be the pressure and temperature in chamber a, P_b and T_b the pressure and temperature in chamber b. The effective area of the ram is A, and Y is the displacement of the ram from its center position.

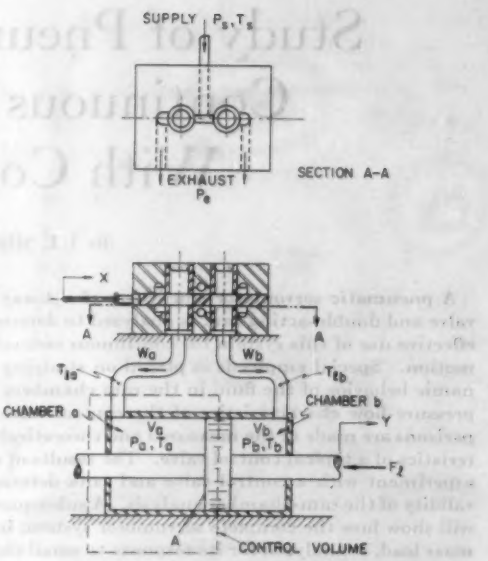

FIG. 2 SCHEMATIC CROSS SECTION OF VALVE-CONTROLLED RAM

From the continuity equation of the control volume drawn around chamber a

$$W_a = g \frac{d}{dt} (\rho_a V_a) \quad \ldots\ldots [1]$$

Since the gas used here may be considered a pure substance as long as it never starts to liquefy [1], its mass density ρ_a may be expressed in terms of its pressure P_a and its temperature T_a

$$\rho_a = f(P_a, T_a)$$

In many engineering problems (pneumatic control systems included), the perfect-gas equation may be used as the equation of state

$$\rho_a = \frac{P_a}{RT_a} \quad \ldots\ldots [2]$$

where

R = gas constant, sq in/sec^2 deg R

Equation [2] may not be used when the state of the gas approaches its liquid state. However, Equation [2] may be used with reasonable accuracy (1)[2] for air when its temperature is above 450 deg Rankine (—10 F) and its pressure is below 4000 psi.

Equations [1] and [2] may be combined to give

$$W_a = \frac{g}{R} \frac{d}{dt} \frac{P_a V_a}{T_a} \quad \ldots\ldots [3]$$

Even when the flow rate W_a and the volume V_a are known, P_a and T_a still are undetermined in Equation [3]. To determine P_a and T_a, the energy equation must be applied to the control volume

$$\frac{c_p}{g} W_a T_{ta} - P_a \frac{dV_a}{dt} + \frac{dQ_a}{dt} = \frac{d}{dt} (c_v \rho_a V_a T_a) \quad \ldots\ldots [4]$$

[2] Numbers in parentheses refer to the Bibliography at the end of the paper.

From Equation [2] for the perfect gas

$$W_a T_{la} - \frac{gP_a}{c_p}\frac{dV_a}{dt} + \frac{g}{c_p}\frac{dQ_h}{dt} = \frac{g}{kR}\frac{d}{dt}(P_a V_a) \quad [5]$$

In general, the rate of heat flow dQ_h/dt is difficult to evaluate by either analytical or experimental means. In practice, the value of dQ_h/dt lies somewhere between two possible extremes:

1 Zero, when the ram is perfectly insulated.

2 Infinity, when sufficient heat is transferred to hold T_a constant regardless of the rate at which compression or expansion effects take place in the chamber.

Even without special provisions to insulate the ram chamber, heat-transfer rate is negligible in most fast-acting systems, but it may be appreciable in slower-acting systems.

Skinner and Wagner (2) investigated the basic processes of charging and discharging constant-volume containers, experiments conducted with cylindrical tanks surrounded with still air at atmospheric conditions. Their results may be employed to estimate the significance of heat-transfer effects in this type of system. Present experience indicates that heat-transfer effects are seldom important in fast-acting pneumatic control systems.

Here an attempt will be made to evaluate servomotor performance for the two extreme cases, namely, isothermal changes and adiabatic changes in the ram chambers. These two cases bracket most engineering applications of this work. An exception would be when a strong heat or energy source is present and acts as another disturbance to the system.

Isothermal Changes

When the pressure P_a changes isothermally, T_a is constant and Equation [3] may be simplified to give

$$W_a = \frac{g}{RT_a}\frac{d}{dt}(P_a V_a) \quad [6]$$

or by integration with respect to time

$$P_a V_a = \frac{RT_a}{g}\int W_a dt + (P_a V_a)_{\text{initial}} \quad [7]$$

Similarly, for chamber b

$$W_b = \frac{g}{RT_b}\frac{d}{dt}(P_b V_b) \quad [8]$$

or

$$P_b V_b = \frac{RT_b}{g}\int W_b dt + (P_b V_b)_{\text{initial}} \quad [9]$$

When only small changes of P_a, P_b, V_a, and V_b occur from initially steady values, Equations [6] and [8] may be written as follows

$$\Delta W_a = \frac{g}{RT_a}\left(P_{ai}\frac{d\Delta V_a}{dt} + V_{ai}\frac{d\Delta P_a}{dt}\right) \quad [10]$$

$$\Delta W_b = \frac{g}{RT_b}\left(P_{bi}\frac{d\Delta V_b}{dt} + V_{bi}\frac{d\Delta P_b}{dt}\right) \quad [11]$$

where the subscript i designates the initially steady value of each variable. If the ram moves small distances near its center position and the temperatures and pressures are initially the same on both sides of the ram, the following equation may be obtained by subtracting Equation [11] from Equation [10]

$$\Delta W_a - \Delta W_b = \frac{g}{RT_i}\left[2P_i A\frac{d\Delta Y}{dt} + V_i\frac{d}{dt}(\Delta P_a - \Delta P_b)\right] \quad [12]$$

Although Equation [12] is valid only when P_a, P_b, and Y change by a small percentage of their initial values, it gives a qualitative picture of the relationship between pressures in the ram chambers, flow from the valve, and ram motion. Chamber pressure tends to vary directly with ram position but varies as the time integral of the valve flow. If a change in pressure is to result from a change in valve flow, sufficient time must elapse for this integrating action to occur before the desired pressure change can take place.

The equations just derived for small changes of all variables resemble the equations which apply to a similar hydraulic system (3). Since such hydraulic systems operate very nearly isothermally, a complete analogy exists for the two cases.

Adiabatic Changes

When the changes in each chamber occur adiabatically, both Equations [3] and [5] should be used. The term dQ_h/dt is zero, but T_a is now a variable. In most instances, the temperature T_a is of little direct interest, and in a fast system, would be very difficult to measure. Therefore, for the time being, it should be eliminated. In Equation [5] T_a does not appear directly as a variable. As long as the flow W_a remains positive, T_a can be ignored completely as well as the way it varies with time in chamber a. However, when the flow W_a is negative, the temperature T_{la} becomes T_a.

The results from a thesis investigation (1) show that in most cases the temperature T_{la} does not vary appreciably from its value when W_a is positive. Therefore Equation [5] alone describes the relationship between pressure, flow, and ram motion for each of the ram chambers.

Accordingly, the equations describing the adiabatic changes in chambers a and b are

$$W_a T_{la} - \frac{gP_a}{c_p}\frac{dV_a}{dt} = \frac{g}{kR}\frac{d}{dt}(P_a V_a) \quad [13]$$

$$W_b T_{lb} - \frac{gP_b}{c_p}\frac{dV_b}{dt} = \frac{g}{kR}\frac{d}{dt}(P_b V_b) \quad [14]$$

When all variables undergo small changes from initially steady values, the equations may be written

$$T_{la}\Delta W_a - \frac{gP_{ai}}{c_p}\frac{d\Delta V_a}{dt} = \frac{g}{kR}\left(P_{ai}\frac{d\Delta V_a}{dt} + V_{ai}\frac{d\Delta P_a}{dt}\right) \quad [15]$$

$$T_{lb}\Delta W_b - \frac{gP_{bi}}{c_p}\frac{d\Delta V_b}{dt} = \frac{g}{kR}\left(P_{bi}\frac{d\Delta V_b}{dt} + V_{bi}\frac{d\Delta P_b}{dt}\right) \quad [16]$$

In addition, if the ram moves small distances near its center position, if the pressures are initially the same on both sides of the ram, and if $T_{la} = T_{lb} = T_i$, then the following equation may be obtained by subtracting Equation [16] from Equation [15] and using $1/c_p + 1/kR \equiv 1/R$

$$(\Delta W_a - \Delta W_b) = \frac{g}{RT_i}\left[2P_i A\frac{d\Delta Y}{dt} + \frac{V_i}{k}\frac{d}{dt}(\Delta P_a - \Delta P_b)\right] \quad [17]$$

It is significant that the equations just derived for small adiabatic

changes, namely, Equations [15], [16], and [17], are very nearly like Equations [10], [11], and [12], which were derived for small isothermal changes, the only difference being the factor k that appears in the terms of the right-hand sides of Equations [15], [16], and [17]. For air which has a value for k of 1.4, the adiabatic-pressure changes are 1.4 times as large as the isothermal-pressure changes.

Control-Valve Characteristics

Experience gained in the development of fluid-power control systems indicates that a slide-type variable orifice is one of the best flow resistances to use in control valves. Although the flow characteristics are nonlinear, a variable orifice provides a means of obtaining a large change in resistance to flow with a very small valve motion. The valves shown as part of the servomotors in Figs. 1 and 2 are examples of slide-type valves, Fig. 1 showing a sliding-spool-type valve, and Fig. 2 showing a sliding-plate-type valve using the hole-slot-and-plug construction developed by Lee (4). Although the clearance spaces between the moving parts must be kept at a minimum to reduce unwanted leakage effects, the forces required to stroke such valves are relatively small, and the valves require little space.

To control the flow of fluid from a single constant-pressure source of power to the ends of a double-acting ram, four flow resistances are required, one or more of which may be variable. It is usually important to keep the flow of fluid from the power source at a minimum when the ram is not moving. Since this quiescent-leakage flow is related inversely to the values of the four resistances when the valve is in its neutral or centered position, the valve must be constructed so that the resistances are large when it is centered. Such a valve is termed a closed-center valve because the metering orifices comprising the flow resistances are very nearly closed when the valve is near its center position. Although a closed-center valve may be advantageous from other considerations, the quiescent power loss due to leakage is a very serious consideration except when the fluid power supply is overabundant or generated in such a way that it must be consumed at a high rate at all times. This quiescent leakage is doubly important when the working fluid is a compressed gas because as the gas leaks through the valve, it expands to many times its initial volume without doing any useful work, whereas a large amount of work was required to compress the gas to its initial pressure.

When quiescent-leakage flow is not a critical factor, the valve may be designed to have its orifices open when it is in the centered position. Such a valve is termed an open-center valve or underlapped valve. A 4-orifice valve of the type illustrated in Figs. 1 and 2 is called a 4-way valve.

A large-scale, two-dimensional model study of the flow of air through a single slide-type orifice has been made by Stenning (5). This work shows that there are two flow conditions possible in such a valve orifice: One with a discharge coefficient of approximately 0.8 and the other with a discharge coefficient of approximately 1.0. Either flow condition may be obtained with greater than critical pressure drop across the orifice (i.e., choked flow), but the higher coefficient is obtained more frequently at large pressure-drop conditions. Furthermore, the discharge coefficient for an orifice of this type (6) operating with hydraulic fluid is only about 0.63.

The four orifices comprising a 4-way valve may be considered as two pairs of orifices, one pair controlling the flow to or from one ram chamber, the other pair controlling the flow to or from the other ram chamber. Each pair of orifices may be considered as a 3-way valve of the type often used to control the motion of a single-acting ram. Thus a study of 3-way valve characteristics also yields information that is directly useful in the design of single-acting systems, such as that shown in Fig. 3 where A_s and

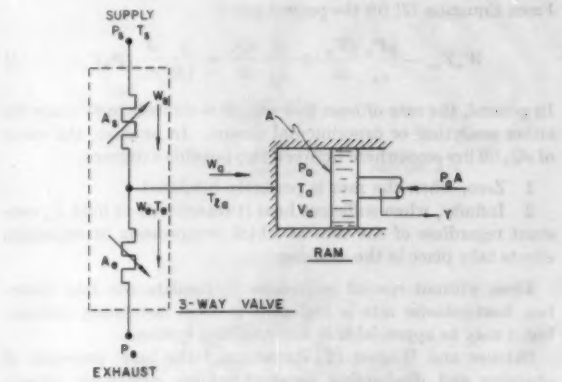

Fig. 3 Schematic Diagram of Single-Acting Ram Controlled by 3-Way Valve

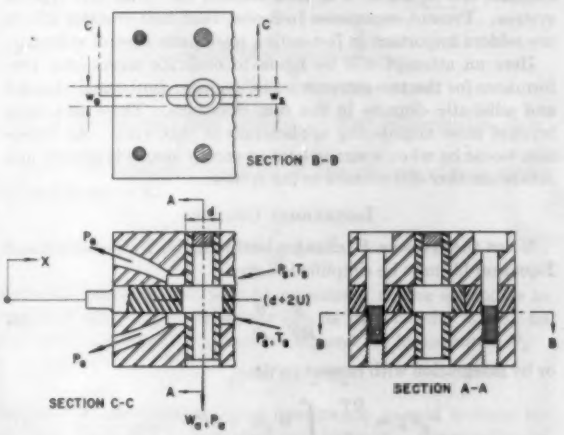

Fig. 4 Cross-Sectional Drawing of One End of 4-Way Sliding-Plate Valve

A_e designate the area of the opening of the supply and exhaust orifices and W_s and W_e are the weight rate of flow through A_s and A_e, respectively.

A sliding-plate valve of the type shown in Fig. 2 may be used to illustrate the following analysis. One end of this valve contains the two orifices that make up a 3-way valve as shown in detail in Fig. 4. The areas A_s and A_e are, respectively, $2w_s(U + X)$ and $2w_e(U - X)$ if the clearance between the valve plate and valve blocks is negligible. The quantity U, called the valve underlap, is a measure of the opening of each orifice when the valve is centered. Although valve underlap is undesirable when the quiescent-leakage flow must be kept at a minimum, it is included in this discussion for generality.

For the time being, side leakage to atmosphere in the clearance spaces is assumed to be negligible. Then the flow to the ram W_a is equal to the difference between the supply flow W_s and the exhaust flow W_e

$$W_a = W_s - W_e \quad [18]$$

Usually, the equation describing the flow of a compressible fluid through an orifice is of the form

$$W = C_d A_o f\left(P_u, T_u, \frac{P_d}{P_u}\right) \quad [19]$$

The function $f(P_u, T_u, P_d/P_u)$ can be expressed as follows (7)

$$f\left(P_u, T_u, \frac{P_d}{P_u}\right) = C\,\frac{P_u}{\sqrt{T_u}}\,f_1\left(\frac{P_d}{P_u}\right) \quad \ldots\ldots [20]$$

where

$$C = g\sqrt{\frac{k}{R\left(\frac{k+1}{2}\right)^{\frac{k+1}{k-1}}}}\left(\frac{\sqrt{\text{deg R}}}{\text{sec}}\right) \quad \ldots\ldots [21]$$

Gases such as air having a value of $k = 1.4$ then have a value of $C = 0.54\ \sqrt{\text{deg R}}/\text{sec}$. The function $f_1(P_d/P_u)$ for air is shown graphically in Fig. 5.

When the gas is air, the flow W_a then may be expressed

$$W_a = C_{da}(2w_r)(U + X)(0.54)\left(\frac{P_u}{\sqrt{T_u}}\right)f_1\left(\frac{P_a}{P_u}\right) - C_{dc}(2w_r)(U - X)(0.54)\left(\frac{P_a}{\sqrt{T_u}}\right)f_1\left(\frac{P_c}{P_a}\right) \quad \ldots\ldots [22]$$

or by collecting terms

$$W_a = \frac{1.08\,C_{da}w_rUP_u}{\sqrt{T_u}}\left[\left(1 + \frac{X}{U}\right)f_1\left(\frac{P_a}{P_u}\right) - \left(1 - \frac{X}{U}\right)\frac{C_{dc}w_cP_a}{C_{da}w_rP_u}\sqrt{\frac{T_u}{T_c}}\,f_1\left(\frac{P_c}{P_a}\right)\right] \quad \ldots\ldots [23]$$

The quiescent-leakage flow W_q is the flow through A_a and A_c when $W_a = 0$ and $X = 0$, and is given by

$$W_q = \frac{1.08\,C_{da}w_rUP_u}{\sqrt{T_u}}\,f_1\left(\frac{P_{aq}}{P_u}\right) \quad \ldots\ldots [24]$$

and an equation for W_a/W_q may be written as

$$\frac{W_a}{W_q} = \left(1 + \frac{X}{U}\right)\frac{f_1\left(\frac{P_a}{P_u}\right)}{f_1\left(\frac{P_{aq}}{P_u}\right)} - \left(1 - \frac{X}{U}\right)\frac{C_{dc}w_cP_a}{C_{da}w_rP_u}\sqrt{\frac{T_u}{T_c}}\,\frac{f_1\left(\frac{P_c}{P_a}\right)}{f_1\left(\frac{P_{aq}}{P_u}\right)} \quad \ldots\ldots [25]$$

The quantities $(1 + X/U)$ and $(1 - X/U)$ never can become negative in a real valve. When the magnitude of X/U exceeds unity, one of the orifices is closed, and either $(1 - X/U)$ or $(1 + X/U)$ is merely zero. In most applications the temperature T_c upstream of A_c may be assumed to be the same as T_u. Even when T_c does vary appreciably from T_u, the effect of this variation appears only as the square root of T_c.

The value of P_{aq} may be determined from Equation [23] by setting $W_a = X/U = 0$ and $T_c = T_u$

$$f_1\left(\frac{P_{aq}}{P_u}\right) = \frac{C_{dc}w_cP_{aq}}{C_{da}w_rP_u}\,f_1\left(\frac{P_c}{P_{aq}}\right) \quad \ldots\ldots [26]$$

When C_{da}, C_{dc}, and port widths w_c and w_r are known, Equation [26] may be solved for P_{aq} by trial and error by use of Fig. 5. The value of C_{dc}/C_{da} is usually nearly unity. The value of port-width ratio w_c/w_r is a significant design parameter because it largely determines the value of the quiescent pressure ratio P_{aq}/P_u in the ram chamber.

In a high-pressure pneumatic servomotor, $P_u \ll P_c$ or P_a and $f_1(P_c/P_{aq}) = 1$. For the special case when $C_{dc}w_c/C_{da}w_r = 1$, the value of P_{aq}/P_u is the same as the value of $f_1(P_{aq}/P_u)$. From Fig. 5, P_{aq}/P_u is approximately 0.82 for this special case, and increasing w_c/w_r results in decreasing P_{aq}/P_u.

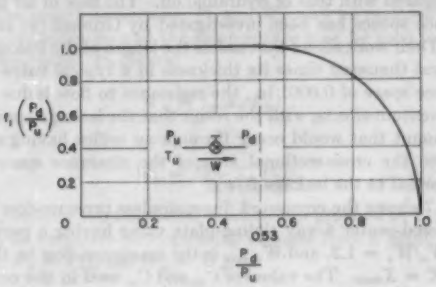

FIG. 5 GRAPHICAL REPRESENTATION OF $f_1(P_d/P_u)$

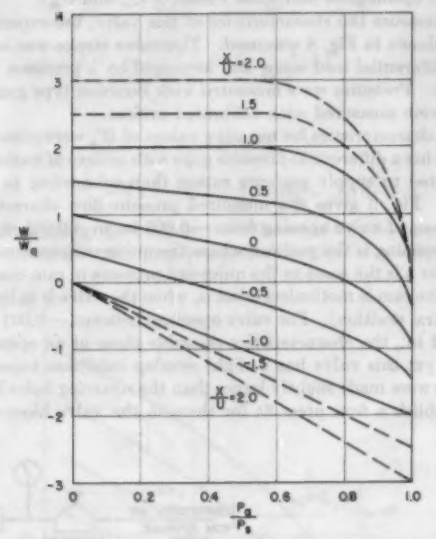

FIG. 6 THEORETICAL PRESSURE-FLOW CHARACTERISTICS OF OPEN-CENTER 3-WAY VALVE

$[C_{dc}w_c/(C_{da}w_r) = 1,\ P_u \ll P_c \text{ or } P_a,\ W_q = (1.08C_{da}w_rUP_u/\sqrt{T_u})f_1(P_{aq}/P_u).]$

Once P_{aq}/P_u is known, curves of W_a/W_q versus P_a/P_u can be plotted for various values of X/U. This can be done by systematically selecting values of P_a/P_u and X/U and solving for W_a/W_q by use of Fig. 5 or the Gas Tables (8). This has been done for the special case when $C_{dc}w_c/C_{da}w_r = 1$ and when $P_u \ll P_c$ or P_a, and the results are shown in Fig. 6. Dotted curves represent values of X greater than U. As the value of the valve underlap U approaches zero, X/U is greater than unity for even small valve displacements from center, and the solid curves tend to become an insignificant part of the valve characteristics.

Although valves can be manufactured with zero underlap or even overlap, it is impossible to manufacture valves with zero clearance between the moving parts of the valve. Effects of leakage through the clearance spaces cannot be neglected in a nominally closed-center valve operating with air. Clearance spaces at the orifices and rounding of the orifice corners in themselves do not affect seriously the value of the quiescent ram pressure since these effects are very nearly the same as valve underlap when the valve is centered. Side leakage to atmosphere, however, does

tend to lower P_{aq}. Although side leakage has not proved to be significant in hydraulic valves because of high resistance to flow of viscous liquids in capillary clearance spaces, it is very important in pneumatic valves because of the very low viscosity of air compared with that of hydraulic oil. The flow of air in small clearance spaces has been investigated by Grinnell (9) and Egli (10). Their work shows that unless the length of the leakage path is several thousand times its thickness in a typical valve with a clearance space of 0.0001 in., the resistance to flow is due mostly to momentum effects, with the result that the leakage approaches the amount that would occur through an orifice having an area equal to the cross-sectional area of the clearance spaces (i.e., area normal to the leakage flow).

Fig. 7 shows the computed dimensionless pressure-flow curves of a closed-center 4-way sliding-plate valve having a port-width ratio $W_a/W_b = 1.2$, and $W_{a\,max}$ is the maximum flow to the ram when $X = X_{max}$. The values of C_{ds} and C_{de} used in the computations were 0.89 and 0.84, respectively (the valve has to be tested at large openings to find these values of C_{ds} and C_{de}).

To measure the characteristics of this valve, the experimental setup shown in Fig. 8 was used. The valve stroke was adjusted by a differential lead screw and measured by a precision dial indicator. Pressures were measured with Bourdon type gages, and flows were measured with calibrated orifices.

The characteristics for negative values of W_a were obtained by employing a differential-pressure gage with orifices of various sizes connected to supply pressure rather than exhausting to atmosphere. Fig. 9 gives the measured pressure-flow characteristics for values of valve opening from —0.005 in. to +0.005 in. Zero valve opening is the position where the quiescent pressure in ram chamber a is the same as the quiescent pressure in ram chamber b when the ram is motionless (that is, when the valve is in its center or neutral position). For valve openings between —0.001 in. and +0.001 in., the characteristics resemble those of an open-center valve, yet this valve has a slight overlap condition because the sleeves were made slightly larger than the metering holes in order to establish a firm press fit for them in the valve blocks. The

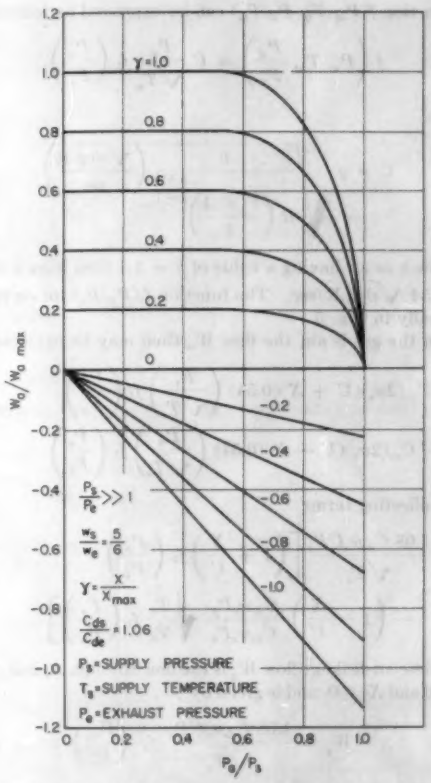

FIG. 7 COMPUTED DIMENSIONLESS PRESSURE-FLOW CURVES OF IDEAL SLIDING-PLATE VALVE (SEE FIG. 4)
$[W_{a\,max} = 0.53(P_s/\sqrt{T_s})(0.89w_aX_{max}).]$

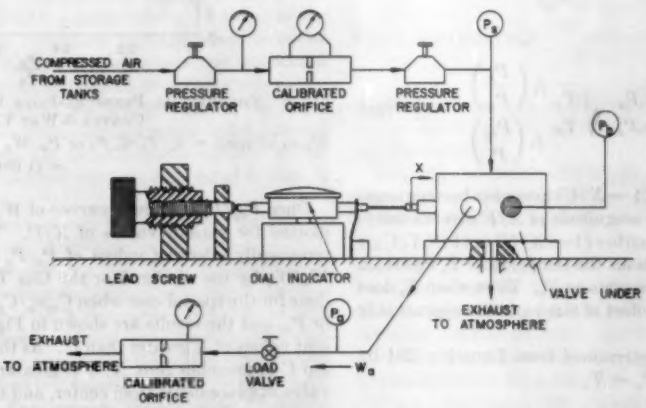

FIG. 8 SCHEMATIC DIAGRAM OF EXPERIMENTAL APPARATUS USED TO MEASURE VALVE CHARACTERISTICS

open-center effect is due to the effects of clearances and rounding of the corners at the metering orifices. The measured quiescent pressure P_{aq} is $0.66P_s$.

For larger valve openings, the characteristics approach those shown in Fig. 6 for valve positions larger than the valve underlap. The gentle slope of the left-hand portions of the measured curves for positive values of X arises largely from side-leakage flow to atmosphere through the clearance spaces. The nearly constant slope indicates that this leakage flow is very nearly proportional to P_a. The value of C_{da} was calculated by dividing the change in W_a caused by opening the valve from $X = 0.002$ in. to $X = 0.005$ in. with $P_a = 0$ by the change that would occur if the discharge coefficient for the supply orifice were 1.00. The value of C_{ds} was calculated by dividing the change in W_a caused by opening the

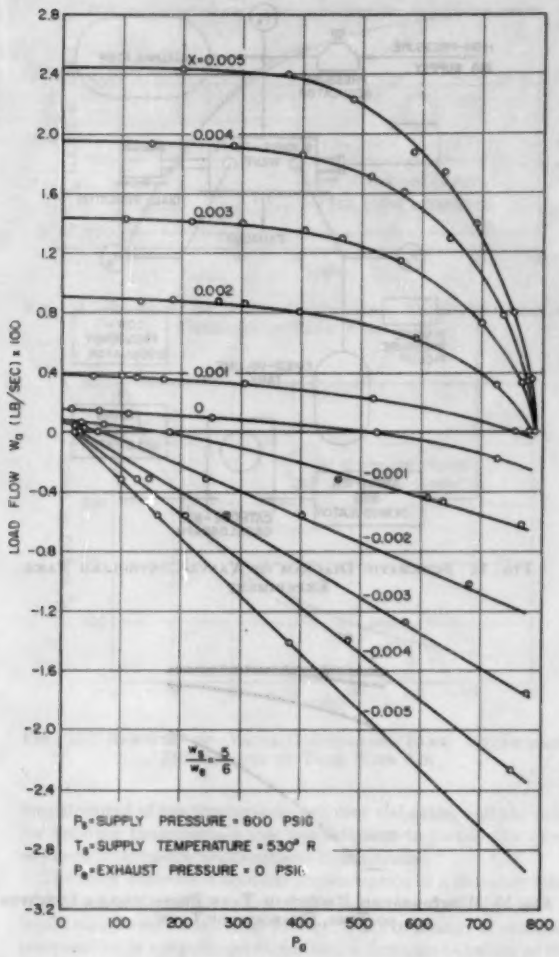

FIG. 9 MEASURED PRESSURE-FLOW CURVES OF NOMINAL CLOSED-CENTER SLIDING-PLATE VALVE (SEE FIG. 4.)

valve from $X = -0.002$ in. to $X = -0.005$ in. with $P_a = 800$ psig by the change that would occur if the discharge coefficient for the exhaust orifice were 1.00. The values of C_{d_b} and C_{d_a} were found to be 0.89 and 0.84, respectively, within the range of Stenning's measurements (5). The difference between C_{d_b} and C_{d_a} may be attributed to a stronger three-dimensional contraction effect in the exhaust orifice.

The measured curves for negative values of W_a were obtained with the temperature of the flow W_a equal to the supply temperature T_s. When the temperature of this flow is appreciably different from T_s, the flow can be expected to vary inversely as the square root of this temperature. This effect partly cancels the effect noted previously when the gas is leaving the ram chamber. There an error in the term $T_{l_a}W_a$ would be incurred whenever T_a was appreciably different from T_{l_a} as W_a changed direction from positive to negative. Since $W_a \sim \sqrt{1/T_a}$ when W_a is negative, $T_{l_a}W_a \sim \sqrt{T_a}$, and there is further justification for assuming that the temperature T_{l_a} is the same for both positive and negative values of W_a. Because the flow through the valve is very nearly adiabatic, T_{l_a} can be considered equal to T_s for all but very exceptional cases.

Since the b end of the 4-way valve is identical with the a end, characteristic curves for the b end of the valve are the same as those for the a end except that curves for positive values of X of the a end correspond to curves for negative values of X of the b end of the valve. Otherwise, P_a and W_a may be replaced by P_b and W_b, respectively, and the same curves may be used for both ends of the valve. In general

$$W_a = f_v(X, P_a) \quad [27]$$

and

$$W_b = f_v(-X, P_b) \quad [28]$$

where f_v denotes the functional relationship graphed in Fig. 9.

When all variables undergo small changes from a point where $X = X_i$, $P_a = P_{a_i}$, and $W_a = W_{a_i}$

$$\Delta W_a = \frac{\partial W_a}{\partial X}\Delta X + \frac{\partial W_a}{\partial P_a}\Delta P_a \quad [29]$$

$$\Delta W_b = \frac{\partial W_b}{\partial X}\Delta X + \frac{\partial W_b}{\partial P_b}\Delta P_b \quad [30]$$

or

$$\Delta W_a = k_{1a}\Delta X + k_{2a}\Delta P_a \quad [31]$$

$$\Delta W_b = k_{1b}\Delta X + k_{2b}\Delta P_a \quad [32]$$

Fig. 10 illustrates graphically how the values of k_{1a} and k_{2a} may be measured from a family of pressure-flow curves for a valve.

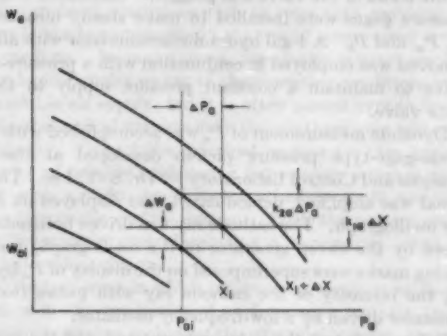

FIG. 10 GRAPHICAL DETERMINATION OF k_{1a} AND k_{2a}

The variation of W_a with X when $P_a = P_{a_q}$ is of particular interest because this shows the flow sensitivity of the valve when the ram pressure does not vary appreciably from its quiescent value. Fig. 11 is a plot of W_a versus X when $P_a = P_{a_q} = 525$ psig. The slope of this curve is k_{1a}.

Everything that has been discussed about k_{1a} and k_{2a} can be repeated for k_{1b} and k_{2b}, with care being taken to change the sign of X_i throughout; and a plot of $-W_b$ versus X when $P_b = P_{b_q} = 540$ psig would be the same as the curve of W_a versus X. The curve of W_a versus X consists of two straight-line portions of nearly the same slope with a small S-curved section near the origin where the slope is less than one third the slope of the straight portions. This region of low valve sensitivity is due in part at least to a slight overlap condition which has been discussed already. For large variations of X, the low-sensitivity region becomes negligible, and the flow W_a is very nearly linearly related to valve opening X when $P_a = P_{a_q}$. This means that a subsequent linear analysis of the complete system may allow large

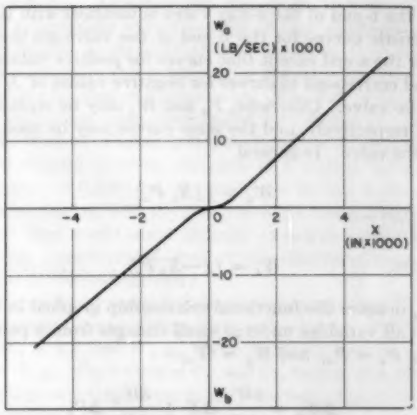

FIG. 11 PLOT OF W_a AND W_b VERSUS X WHEN $P_a = P_b = P_g = 525$ PSIG

variations of X if the variations of P_a do not exceed a few per cent of P_{ag}.

EXPERIMENTS WITH A VALVE-CONTROLLED TANK

To ascertain the validity of some of the assumptions made in the dynamic analysis of ram chambers, some simple experiments were conducted with the sliding-plate valve and $^1/_5$-gal tank arranged as shown in Fig. 12. The tank was connected by a short line to the port at the a end of the sliding-plate valve. The port at the b end of the valve was plugged. Calibrated Bourdon type pressure gages were installed to make steady measurements of P_g, P_a, and P_b. A 1-gal hydraulic accumulator with all of the oil removed was employed in conjunction with a pressure-regulating valve to maintain a constant pressure supply to the sliding-plate valve.

Dynamic measurement of P_a was accomplished with a bonded-strain-gage-type pressure pickup developed at the Dynamic Analysis and Control Laboratory by Dr. S.-Y. Lee. The pressure signal was amplified, demodulated, and displayed on a cathode-ray oscillograph. The cathode ray was driven horizontally at low speed by the sweep generator of the oscillograph, and accurate timing marks were superimposed on the display of P_a by modulating the intensity of the cathode ray with pulses from a pulse generator driven by a low-frequency oscillator.

Before each test the valve was centered, and the pressure and temperature in the fixed-volume tank were allowed to reach steady values. Then the valve plate was suddenly displaced to a new position and held there for the duration of the test. The display of P_a on the face of the cathode-ray oscillograph was recorded photographically, and the initial and final values of P_a were read from the Bourdon type gages to provide a means of calibrating the photographic records. Valve-plate displacement was measured with a dial indicator. Both charging and discharging tests were made. Fig. 13 reproduces one of the photographic records made during charging of the tank.

To evaluate the analytical work in the dynamic analysis of ram chambers, enlargements were made of the photographic records and compared with the results computed by performing a step-by-step numerical integration of Equation [13] together with the measured pressure-flow characteristics, Fig. 9, of the valve. Figs. 14 and 15 graph the measured and calculated responses of P_a as a function of time for charging and discharging of the tank. The excellent agreement between measurements and calculations during the early part of the responses lends strong support to the assumptions made in the analysis for adiabatic changes. After 3

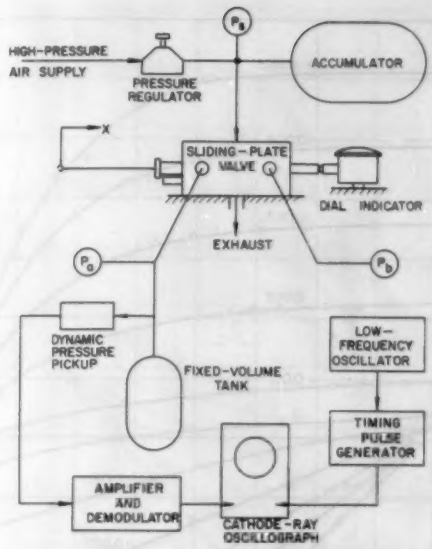

FIG. 12 SCHEMATIC DIAGRAM OF VALVE-CONTROLLED TANK EXPERIMENT

FIG. 13 PHOTOGRAPHIC RECORD OF TANK PRESSURE AS A FUNCTION OF TIME, CHARGING OF TANK

sec, the divergence of the measured response from the calculated response begins to become noticeable, presumably because of the effects of heat transfer. Yet, the correspondence between measured and calculated results during the later periods is still good enough for most engineering work. According to the results of the work by Skinner and Wagner (2), the effects of heat transfer up to this time should be negligible.

On the other hand, the results of the discharging tests also lend support to the assumption that the temperature of the gas leaving the tank after tank pressure has fallen may be taken as equal to the initial temperature in the tank because the calculations were made on this basis. This apparent paradox exists because the time rate of change of temperature in the tank is of much greater significance than the effects of changes in the value of temperature itself on the flow through the valve. The situation is analogous to that existing in the pressurization of liquids where the rate of change of fluid density is of much greater significance than changes in the value of density itself (3).

No attempt was made to make dynamic measurements of temperature in the tank because of practical considerations. If careful measurements were to be made of gas temperature in the tank, measurements at many places in the tank would be required during charging because there is no direct evidence that perfect mixing occurs. The known methods of making sufficiently rapid

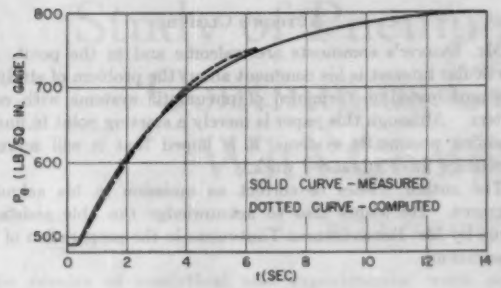

FIG. 14 RESULTS OF VALVE-CONTROLLED TANK EXPERIMENT, CHARGING OF TANK WITH AIR

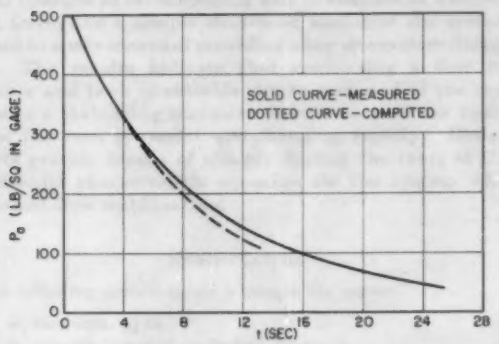

FIG. 15 RESULTS OF VALVE-CONTROLLED TANK EXPERIMENT, DISCHARGING OF TANK WITH AIR

measurement of gas temperature are very elaborate, and the need for knowing temperatures was not sufficient to justify the effort required to measure temperatures dynamically.

The main differences between pressurization of a chamber filled with a gas and pressurization of the same chamber filled with a liquid may be summarized as follows: Rate of change of chamber temperature is a significant factor in the dynamic behavior of the gas system. In a liquid system, pressurizaton of the liquid results in negligible rate of change of temperature and negligible change in temperature itself.

CONCLUSIONS

The experiments with a valve-controlled tank show that the basic equations which were derived to describe the pneumatic processes in the servomotor are in good agreement with experimental results. A subsequent paper will show how the complete servomotor system driving a mass load then is analyzed for its response to small changes of valve opening and to changes of external load force, and a simple electronic analog of the system is used to study means of providing adequate system damping.

ACKNOWLEDGMENT

The work described in this paper was supported in part by the Bureau of Ordnance, U. S. Navy Department, under Contract No. NOrd 11799 with the Division of Industrial Cooperation, Massachusetts Institute of Technology. The author is particularly indebted to members of the staff of the Dynamic Analysis and Control Laboratory for their invaluable assistance and counsel.

BIBLIOGRAPHY

1 "Continuous Control of Motion With Compressed Air," by J. L. Shearer, M.I.T., Department of Mechanical Engineering, ScD thesis, Cambridge, Mass., 1954.

2 "A Study of the Processes of Charging and Discharging Constant Volume Tanks With Air," by C. K. Skinner and F. D. Wagner, M.I.T., Department of Mechanical Engineering, SB thesis, Cambridge, Mass., 1954.

3 "Dynamic Characteristics of Valve-Controlled Servomotors," by J. L. Shearer, Trans. ASME, vol. 76, 1954, pp. 895–903.

4 "Contributions to Hydraulic Control—6, New Valve Configurations for High-Performance Hydraulic and Pneumatic Systems," by S.-Y. Lee, Trans. ASME, vol. 76, 1954, pp. 905–910.

5 "An Experimental Study of Two-Dimensional Gas Flow Through Valve-Type Orifices," by A. H. Stenning, ASME Paper No. 54—A-45, presented at the Annual Meeting of the ASME, New York, N. Y., November 28–December 3, 1954.

6 "Contributions to Hydraulic Control—1, Steady-State Axial Forces on Control-Valve Pistons," by S.-Y. Lee and J. F. Blackburn, Trans. ASME, vol. 74, 1952, pp. 1005–1009.

7 "Compressible Fluid Flow," by A. H. Shapiro, Ronald Press Co., New York N, Y., 1953, pp. 73–93.

8 "Gas Tables," by J. H. Keenan and J. Kaye, John Wiley & Sons, Inc., New York, N. Y., 1948 (revised edition), pp. 139–142.

9 "A Study of Pressurized Air Bearing Design, Steady Loading—No Rotation," by S. K. Grinnell, M.I.T., Department of Mechanical Engineering, SM thesis, Cambridge, Mass., 1954.

10 "The Leakage of Gases Through Narrow Channels," by A. Egli, *Journal of Applied Mechanics*, Trans. ASME, vol. 59, 1937, p. A-63.

Discussion

C. J. DEAVERS.[3] The author is to be commended for his well-written and timely paper on pneumatic control.

The increasing demand for control systems which must function under unusual conditions such as very high ambient temperatures is placing emphasis on the use of compressed air as a control medium. In many cases, pneumatic control would be the most logical choice owing to the operating conditions as well as an available air supply, but it is often passed over in favor of hydraulic or electrical systems even though these may add weight or complexity. One of the principal reasons for this neglect is the scarcity of reliable engineering information which a project engineer with a tight development schedule could use in designing a pneumatic control system. With the present state of the art, pneumatic control re nains a runner-up; often considered but seldom chosen.

There are two areas in which information seems to be lacking. The first is in the mechanics of performing a realistic analysis of a pneumatic system including the effects of leakage, elasticity, and friction load on the output of the servomotor. Many of the assumptions commonly made in the analysis of a hydraulic system obviously are not valid as the author points out in his paper. There are numerous gaps in our knowledge which make it difficult to put a system on a computer with any assurance that the computer system represents a reasonable physical system. A typical example is our lack of information on the effects of distributed resistance and capacity in a pneumatic circuit and how it can be handled in a computer study. This will be corrected only by combined programs of analysis and test such as that described in this paper.

The second broad unknown area is in component design. The rules of thumb which have been developed for hydraulic-component design do not hold for pneumatics. As the author points out, the effects of side leakage become significant in a pneumatic valve since a 0.0001-in. clearance space no longer can be considered a viscous-flow path except for L/h ratios on the order of several thousand. Dirt and icing problems which are

[3] Supervisor, Engineering, General Engineering Laboratory, General Electric Company, Schenectady, N. Y. Assoc. Mem. ASME.

either nonexistent or easily overcome in hydraulic components are very real factors in the design of a pneumatic control. Such differences in the basic design concepts between hydraulics and pneumatics mean that a new set of rules must be developed for the design of pneumatic components. In most cases this may mean discarding many of the more or less standardized components which are to be used with compressed air.

It is the writer's belief that such work as the author describes in this paper is a significant contribution. It is hoped that similar advancement can be made in component-design techniques so that pneumatics can achieve its rightful place as a control medium.

Author's Closure

Mr. Deaver's comments are welcome and to the point. Of particular interest is his comment about the problem of studying the anticipated performance of pneumatic systems with computers. Although this paper is merely a starting point in understanding pneumatic systems, it is hoped that it will serve to encourage more advanced work.

The author wishes to correct an omission in his acknowledgment. He wishes also to acknowledge the able assistance given by Mr. Bonaventuras Tautvaisas in the preparation of the illustrations.

Study of Pneumatic Processes in the Continuous Control of Motion With Compressed Air—II[1]

By J. L. SHEARER,[2] CAMBRIDGE, MASS.

The results of analytical and experimental work reported in Part I (Paper No. 55—IRD-4) are employed in the analysis of a valve, ram, and mass-load system. This complete servomotor system is analyzed for its response to small changes of valve opening and to changes of external load force, and a simple electronic analog of the system is used to study means of providing adequate system damping. The results indicate that connecting a flow resistance and tank of suitable size to each end of the ram permits a stabilizing transient flow to each of the tanks when the ram pressures are changing rapidly. Design charts provide means of quickly finding the roots of the third-order characteristic equation for the system with transient-flow stabilization.

Nomenclature

The following nomenclature is used in the paper:

- A = ram area, sq in.
- b = viscous-damping coefficient, lb-sec/in.
- C_1 = partial derivative of weight rate of flow with respect to valve opening, lb/sec-in.
- C_2 = partial derivative of weight rate of flow with respect to load pressure, sq in/sec.
- C_c = capillary resistance coefficient, in^5/lb-sec
- D = denotes derivative with respect to time d/dt, 1/sec
- F_l = total load force, lb
- f = to indicate a functional relationship
- f_a = functional relationship between τ_{l_1}, τ_{l_2}, π_s, and π_v
- f_b = functional relationship between ω_{n_s}, τ_{l_2}, π_s, and π_v
- f_ζ = functional relationship for ζ_s
- f_τ = functional relationship for τ_1/τ_{l_2}
- f_ω = functional relationship for $\omega_{n_s}\tau_{l_2}$
- f_1 = function of pressure ratio
- g = acceleration due to gravity, 386 in/sec^2
- i = subscript to designate initial condition
- k = ratio of specific heats, c_p/c_v, for air: 1.4
- k_1 = coefficient denoting no-load flow sensitivity, sq in/sec
- k_2 = coefficient denoting loss of flow per unit load pressure, in^5/lb-sec
- k_2' = transient-pressure-feedback coefficient, in^5/lb-sec
- k_3 = coefficient denoting fluid compliance, in^6/lb
- k_{1a} = same as C_1
- k_{1b} = same as C_1
- k_{2a} = same as C_2
- k_{2b} = same as C_2
- L = external load force, lb
- L_c = capillary passage length, in.
- m = load mass, lb-sec^2/in.
- P_a = pressure in chamber a, psi
- P_b = pressure in chamber b, psi
- P_i = initial pressure, psi
- P_q = quiescent value of P_a and P_b when they are equal, psi
- P_s = pressure of gas supply, psi
- P_{ta} = pressure in tank at a end of ram, psi
- P_{tb} = pressure in tank at b end of ram, psi
- R = gas constant (for air: 2.47×10^5), sq in/sec^2 deg R
- s = subscript denoting supply
- ss = subscript denoting steady state
- T_l = line temperature, deg R
- T_{la} = stagnation temperature of gas in line entering chamber a, deg R
- T_{lb} = stagnation temperature of gas in line entering chamber b, deg R
- T_s = temperature of supply gas, deg F
- t = time, sec
- t_c = capillary passage thickness, in.
- V_a = volume of chamber a, cu in.
- V_b = volume of chamber b, cu in.
- V_i = initial volume at each end of ram (including lines to valve), cu in.
- V_t = tank volume (when $V_{ta} = V_{tb}$), cu in.
- V_{ta} = tank volume at a end of ram, cu in.
- V_{tb} = tank volume at b end of ram, cu in.
- W = weight rate of flow, lb/sec
- W_a = weight rate of flow from a end of valve, lb/sec
- W_b = weight rate of flow from b end of valve, lb/sec
- W_t = transient flow, lb/sec
- W_{ta} = weight rate of flow to tank at a end of ram, lb/sec
- W_{tb} = weight rate of flow to tank at b end of ram, lb/sec
- w_c = capillary passage width, in.
- X = valve displacement measured from center position, in.
- Y = ram displacement measured from center position, in.
- α = analog time scale
- ζ_s = servomotor damping ratio
- Δ = small change
- μ = absolute viscosity, lb-sec/sq in.
- π_s = dimensionless parameter $2A^2V_i/(kmC_c^2P_i)$
- π_v = tank volume ratio V_t/V_i
- ρ_a = mass density of fluid in chamber a, lb sec^2/in.^{4}
- ρ_b = mass density of fluid in chamber b, lb sec^2/in.^{4}
- Σ_1 = flow summation
- Σ_2 = force summation
- τ = transient-pressure-feedback time constant, sec
- τ_i = integrating time constant, $V_i/(kC_cP_i)$, sec
- τ_1 = servomotor time constant, sec

[1] This paper, a continuation of a paper (Paper 55—IRD-4) having the same title, presents a summary of some of the work reported in the following thesis: "Continuous Control of Motion With Compressed Air," by J. L. Shearer, ScD thesis, Massachusetts Institute of Technology, Cambridge, Mass., 1954.

[2] Assistant Professor of Mechanical Engineering, Massachusetts Institute of Technology. Mem. ASME.

Contributed by the Instruments and Regulators Division and presented at the joint ASME Instruments and Regulators Division-ISA Conference, Los Angeles, Calif., September 12–16, 1955.

Note: Statements and opinions advanced in papers are to be understood as individual expressions of their authors and not those of the Society. Manuscript received at ASME Headquarters, July 21, 1955. Paper No. 55—IRD-10.

τ_2 = servomotor time constant, sec
τ_3 = servomotor time constant, sec
ω_{ns} = servomotor undamped natural frequency, rad/sec

Introduction

The purpose of this paper is to try to gain a thorough understanding of the fundamental factors governing the performance of a valve-controlled pneumatic servomotor with a mass load in the presence of external load forces in order to evolve a rational design procedure that will facilitate the design and/or evaluation of systems of this kind in a straightforward manner.

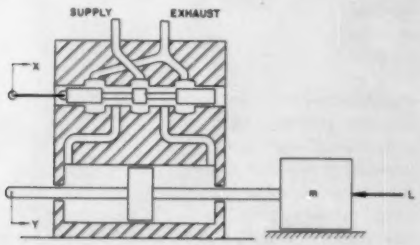

Fig. 1 Valve-Controlled Pneumatic Servomotor With Load

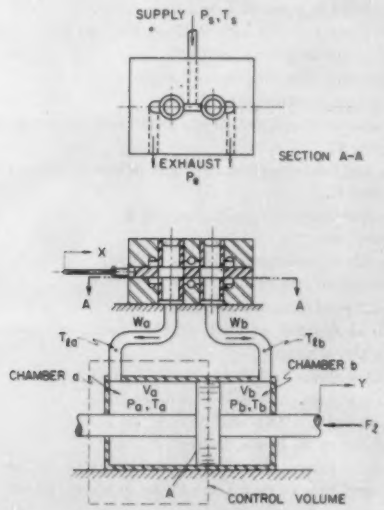

Fig. 2 Schematic Cross Section of Valve-Controlled Ram

Figs. 1 and 2 show schematically the basic system under consideration. Factors deemed to be of outstanding importance in the evaluation of this system are speed of response, degree of dynamic stability, load sensitivity, and efficiency. Practical design considerations such as the strengths of structural members, means of fastening and sealing, arrangement of components, and selection of materials are not to be dealt with here.

Analysis of Valve, Ram, and Load System

To perform a simple mathematical analysis, a number of simplifying assumptions may be made about the valve, ram, and load system. Justification for or refutation of the following assumptions can come only from experience with real systems or detailed analyses of systems of this kind:

1 Supply pressure P_s is constant.
2 Supply temperature T_s is constant.
3 Heat transfer between working gas and its environment is negligible.
4 The working gas obeys the perfect-gas law: $p = \rho RT$.
5 Temperature of the gas flowing between the valve and the ram is at all times equal to supply temperature T_s.
6 The ram moves only small distances from its center position.
7 Ram pressures P_a and P_b vary by only small amounts from an initial steady value P_i.
8 Control-valve constants k_{1a} and k_{1b} are equal and do not vary with valve opening.
9 Control-valve constants k_{2a} and k_{2b} are equal and do not vary with valve opening.
10 Valve opening does not exceed its maximum design value.
11 Passages connecting valve and ram are very short and offer negligible resistance to flow.
12 Friction forces on the ram are viscous (no dry friction).
13 External load force L is sufficiently small to make assumption 7 possible.

A small change is defined as one that is small enough to provide a given degree of accuracy in the equation where this change may appear. From Part I,[1] Equations [16], [17], and [18], which were developed for the case when the ram moves only small distances from its center position, may be used to illustrate this definition of small. When Equations [16], [17], and [18] are repeated for convenience, with T_i substituted for T_{1i}, T_{2i}, and T_{3i}

$$T_s \Delta W_a - \frac{g P_{ai}}{c_p} \frac{d\Delta V_a}{dt} = \frac{g}{kR}\left(P_{ai} \frac{d\Delta V_a}{dt} + V_{ai} \frac{d\Delta P_a}{dt}\right) \quad [1]$$

$$T_s \Delta W_b - \frac{g P_{bi}}{c_p} \frac{d\Delta V_b}{dt} = \frac{g}{kR}\left(P_{bi} \frac{d\Delta V_b}{dt} + V_{bi} \frac{d\Delta P_b}{dt}\right) \quad [2]$$

$$(\Delta W_a - \Delta W_b) = \frac{g}{RT_s}\left[2P_i A \frac{d\Delta Y}{dt} + \frac{V_i}{k} \frac{d}{dt}(\Delta P_a - \Delta P_b)\right] \quad [3]$$

The quantities V_{ai}, P_{ai}, V_{bi}, P_{bi}, V_i, and P_i may be employed as constant coefficients only as long as V_a, P_a, V_b, and P_b do not vary appreciably from their initial steady-state values. Much mathematical simplification results from use of the initial values of these variables as constant coefficients; that is, using the initial values facilitates combination of Equations [1] and [2] into a single equation. The error involved in using the initial value of V_a, for example, in Equation [1] is proportional to the change in V_a from its initial value, with the result that if V_a changes by 5 per cent of its initial value, the coefficient V_a will be in error by approximately 5 per cent after the change of V_a has occurred, and the computation probably will be in error by no more than 2.5 per cent. The same reasoning holds for variation of P_a because the coefficient gP_a will be in error by the same amount that P_a departs from P_{ai}. Since most of the engineering measurements possible may be in error by at least 2 per cent, changes of variables from initial values can be considered to be small if the computations based on coefficients using initial values are not in error by more than 2 or 3 per cent.

Although a given system may undergo large changes during operation, usually it may be expected to reach a steady-state condition at some time. The way in which it finally reaches steady state is usually of primary concern in the design of control systems. As a system finally reaches a steady-state condition, its variables change by very small amounts from their final values. Thus, when these final values are taken as the initial values of an analysis based on small changes of all variables, the analysis will

give a reasonably accurate description of the performance of the system as it reaches steady state.

To have a completely symmetrical system, and thus to be able to combine Equations [1] and [2] into Equation [3], the initial steady values of P_a and P_b must be equal, a condition possible only when the initial value of L is zero. The analysis will hold for small changes of L consistent with the allowable changes of P_a and P_b. At the same time, initially steady equal values of P_a and P_b are possible only when the control valve is centered ($X = 0$). Then each of its 3-way valves is operating with identical pressure, flow, and opening conditions. If, in the pressure-flow curves, the changes in P_a, P_b, and X are sufficiently small, the constants k_{1a} and k_{1b} are equal, and the constants k_{2a} and k_{2b} are equal. Here a small change of X must be a change that is a small percentage of its maximum value rather than of its initial value. The flows W_a and W_b may be expressed in terms of small changes as

$$\Delta W_a = C_1\Delta X - C_2\Delta P_a \quad \ldots\ldots [4]$$

$$\Delta W_b = -C_1\Delta X - C_2\Delta P_b \quad \ldots\ldots [5]$$

where C_1 is the value of k_{1a} and k_{1b} and C_2 is the value of k_{2a} and k_{2b}. Equation [5] may be subtracted from [4] to give

$$\Delta W_a - \Delta W_b = 2C_1\Delta X - C_2(\Delta P_a - \Delta P_b) \quad \ldots\ldots [6]$$

Equation [3] gives

$$\Delta W_a - \Delta W_b = \frac{gV_i}{kRT_s}\frac{d}{dt}(\Delta P_a - \Delta P_b) + \frac{2gP_iA}{RT_s}\frac{d}{dt}(\Delta Y) \quad \ldots\ldots [7]$$

Subtracting Equation [7] from [6] yields

$$\left(\frac{gV_i}{kRT_s}D + C_2\right)(\Delta P_a - \Delta P_b) = 2C_1\Delta X - \frac{2gP_iA}{RT_s}D\Delta Y \quad \ldots [8]$$

where D denotes the derivative with respect to time. Equation [8] may be rearranged to give

$$AD\Delta Y = k_1\Delta X - (k_2 + k_3D)(\Delta P_a - \Delta P_b) \quad \ldots\ldots [9]$$

where

$$k_1 = \frac{C_1RT_s}{gP_i} \ldots \frac{\text{sq in.}}{\text{sec}} \ldots \text{(no-load valve-flow sensitivity)} \ldots [10]$$

$$k_2 = \frac{C_2RT_s}{2gP_i} \ldots \frac{\text{in.}^5}{\text{lb-sec}} \ldots \begin{matrix}\text{(loss of valve flow per unit}\\ \text{load pressure)}\end{matrix} \quad \ldots\ldots [11]$$

$$k_3 = \frac{V_i}{2kP_i} \ldots \frac{\text{in.}^3}{\text{lb}} \ldots \text{(fluid compliance)} \quad \ldots\ldots [12]$$

Equation [9] is identical in form to the equation used in describing the behavior of a valve-controlled hydraulic servomotor.[3] A pneumatic system undergoing small changes behaves much like the corresponding hydraulic system except that the effective bulk modulus of compressed gas is equal to k times its pressure, whereas the bulk modulus of hydraulic fluid is very nearly independent of its pressure.

For the mechanical part of the system consisting of the ram and the mass plus viscous-damping load, an analysis of the forces acting on this part of the system yields

$$A(\Delta P_a - \Delta P_b) = mD^2\Delta Y + bD\Delta Y + \Delta L \quad \ldots\ldots [13]$$

[3] "Dynamic Characteristics of Valve-Controlled Servomotors," by J. L. Shearer, Trans. ASME, vol. 76, 1954, pp. 895–903.

Combining Equations [9] and [13] produces the second-order differential equation

$$\left[\left(\frac{k_3m}{k_2b + A^2}\right)D^2 + \left(\frac{k_3m + k_3b}{k_2b + A^2}\right)D + 1\right]D\Delta Y = \frac{k_1A\Delta X - (k_2 + k_3D)\Delta L}{k_2b + A^2} \quad \ldots\ldots [14]$$

Equation [14] is identical with the differential equation that may be derived for a similar hydraulic system, and is discussed in some detail in an earlier paper.[3] The degree of system damping is determined by the value of the viscous-damping coefficient b and/or the coefficient k_2.

The steady-state load sensitivity of a system of this kind is an important factor in many applications. The steady-state equation relating ram velocity $D\Delta Y$ to valve stroke ΔX and external load ΔL is

$$(D\Delta Y)_{ss} = \frac{k_1A(\Delta X)_{ss} - k_2(\Delta L)_{ss}}{k_2b + A^2} \quad \ldots\ldots [15]$$

Only when k_2 is zero is zero steady-state load sensitivity possible. Otherwise, in holding a steady velocity, a readjustment in $(\Delta X)_{ss}$ must be made to counteract load changes.

Since large steady loads may be imposed on such a system, its sensitivity to steady loads should be minimized. Thus quiescent power-drain limitations and load-sensitivity requirements often necessitate the use of a closed-center valve. Allowing leakage to by-pass the ram, in order to gain damping, also leads to steady-state load sensitivity and to dissipation of power during periods of steady loading because the same pressure difference across the ram, which is required to hold the load, causes a steady flow of gas through the by-pass resistance.

The presence of viscous damping does not make the system sensitive to steady external load but does tend to reduce the velocity attainable per unit valve stroke, as demonstrated in Equation [15]. Viscous damping on the ram also may dissipate a great deal of power when the ram is moving at high velocity.

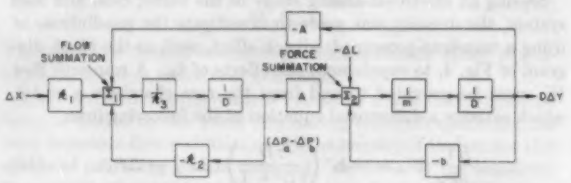

FIG. 3 BLOCK-DIAGRAM REPRESENTATION OF THE DIFFERENTIAL EQUATIONS DERIVED FROM A LINEARIZED ANALYSIS OF VALVE, RAM, AND MASS-LOAD SYSTEM

The block diagram of Fig. 3 may be constructed by performing the summations Σ_1 and Σ_2 required to satisfy Equations [13] and [14]. Since the differential operator D denotes differentiation with respect to time, $1/D$ is used to denote integration with respect to time.

As shown previously,[3] the degree of damping of a system with given values of ram area A, fluid compliance k_3, and mass load m is determined by the values of k_2 and b present in the system. Fig. 4 is an analog block diagram of the servomotor system. The coefficients k_2 and b serve as the feedback paths of two small minor loops of the system. Thus system stability seems to be related directly to the degree with which these respective minor loops are controlled by negative feedback. This suggests that other, perhaps artificial, means may be employed to close these loops to gain system stability. For instance, it might be possible to measure $(\Delta P_a - \Delta P_b)$ and to provide a feedback control sys-

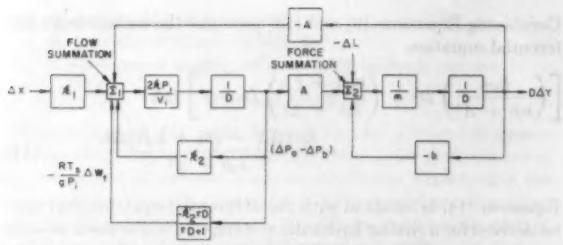

FIG. 4 ANALOG BLOCK DIAGRAM BASED ON LINEARIZED ANALYSIS AND SHOWING EFFECT OF TRANSIENT-PRESSURE FEEDBACK

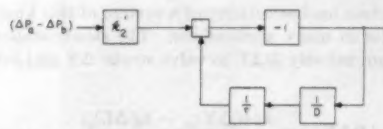

FIG. 5 ARRANGEMENT OF ANALOG-COMPUTER COMPONENTS TO SIMULATE: $W_t = -k_2'[\tau D/(\tau D + 1)](\Delta P_a - \Delta P_b)$

tem that would tend to decrease valve displacement by an amount proportional to $(\Delta P_a - \Delta P_b)$. In addition to practical difficulties involved in providing this pressure feedback, the load sensitivity of the system would increase with increasing pressure feedback just as it does with increasing k_2. Similarly, an artificial feedback scheme might be employed to simulate the effects of b but would result in excessive dissipation of power at high ram velocities.

Another possibility, investigated by Dinerstein,[4] is to measure ram velocity and employ feedback-compensation techniques around the whole system in order to stabilize it. Practical limitations due to the complexity and expense of this scheme tend to nullify some of the theoretical advantages. Nevertheless, sufficient stability can be gained by this means without increasing the steady-state load sensitivity or power dissipation at high ram velocity.

During an electronic-analog study of the valve, ram, and load system, the decision was made to investigate the possibilities of using a transient-pressure-feedback effect, such as the block diagram of Fig. 4, to supplement the effects of k_2. A transient flow W_t must be provided to and from the ram chambers a and b, which satisfies a differential equation of the following form

$$\frac{RT_s}{gP_i} W_t = -k_2' \left(\frac{\tau D}{\tau D + 1} \right) (\Delta P_a - \Delta P_b) \ldots\ldots [16]$$

The transfer characteristic $-k_2'\tau D/(\tau D + 1)$ represents the dynamic behavior of many physical systems, and it is easily instrumented with the arrangement of analog-computer components shown in Fig. 5.

This feedback effect occurs only when $(\Delta P_a - \Delta P_b)$ is time variant. When $(\Delta P_a - \Delta P_b)$ reaches a steady value, $W_t = 0$. Therefore it may be called a transient-pressure-feedback effect.

A preliminary study made on a Philbrick electronic-analog computer indicated that this scheme would insure system stability if sufficiently large values of the time constant τ could be provided. Obviously, when $\tau = \infty$, simple pressure feedback exists. The analog study indicated, however, that extremely large values of τ would not be required and that the value of k_2' necessary to attain a given degree of stability would be nearly the same as the value of k_2 that would be required otherwise.

[4] "The Development of a Valve-Controlled Pneumatic Servomechanism," by J. Dinerstein, SM thesis, Department of Electrical Engineering, Massachusetts Institute of Technology, Cambridge, Mass., 1954.

At this point, some thought was given to the means of accomplishing the transient-pressure-feedback scheme in a simple, effective manner. Several arrangements requiring elaborate control and instrumentation techniques were discarded when the desired effect seemed obtainable by employing auxiliary tanks and flow resistances, as shown in Fig. 6. Such a scheme looks promising because flows to and from tanks a and b do occur through the flow resistances during periods when P_a and P_b are changing, yet the tank pressures P_{ta} and P_{tb} must approach P_a and P_b when P_a and P_b reach steady values, and the flows W_{ta} and W_{tb} approach zero as $(P_a - P_{ta})$ and $(P_b - P_{tb})$ approach zero. In order to ascertain the values of resistances and tank sizes required, the system must be analyzed with this added complexity. As in earlier portions of this section, greatest emphasis will be given to the linearized analysis.

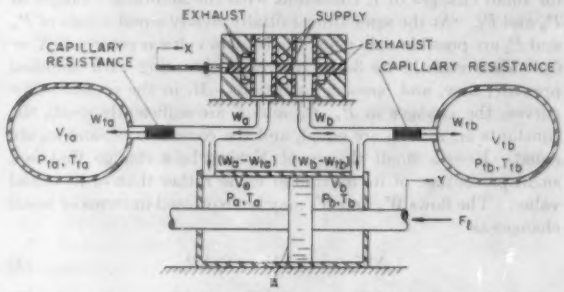

FIG. 6 SCHEMATIC DIAGRAM SHOWING ARRANGEMENT OF TANKS AND FLOW RESISTANCES TO PROVIDE SYSTEM DAMPING

Capillary flow resistances have been chosen because their characteristics are more nearly linear than orifices. Momentum effects of fluid flow in the capillary passages and heat transfer to the fluid passing through the resistances are assumed to be negligible. The equation for the flow of a compressible fluid in capillary passages[5] may be applied to each of the two flow resistances

$$W_{ta} = \frac{gw_c t_c^3}{24\mu RT_s L_c} (P_a^2 - P_{ta}^2) \ldots\ldots [17]$$

and

$$W_{tb} = \frac{gw_c t_c^3}{24\mu RT_s L_c} (P_b^2 - P_{tb}^2) \ldots\ldots [18]$$

where

w_c = capillary passage width, in.
t_c = capillary passage thickness, in.
L_c = capillary passage length, in.

For simplicity, a capillary flow coefficient is defined as

$$C_c = w_c t_c^3/12\mu L_c$$

hence

$$W_{ta} = \frac{gC_c}{2RT_s} (P_a^2 - P_{ta}^2) \ldots\ldots [19]$$

and

$$W_{tb} = \frac{gC_c}{2RT_s} (P_b^2 - P_{tb}^2) \ldots\ldots [20]$$

and if only small changes occur from the initially steady conditions existing when $P_a = P_b = P_{ta} = P_{tb} = P_i$

[5] "Notes on Fluid Power Control," summer session, Department of Mechanical Engineering, Massachusetts Institute of Technology Cambridge, Mass., section A, 1953 (unpublished).

$$\Delta W_{ta} = \frac{gC_cP_i}{RT_s}(\Delta P_a - \Delta P_{ta}) \quad [21]$$

and

$$\Delta W_{tb} = \frac{gC_cP_i}{RT_s}(\Delta P_b - \Delta P_{tb}) \quad [22]$$

The energy equations for identical tanks may be written

$$W_{ta} = \frac{gV_t}{kRT_s}\frac{dP_{ta}}{dt} \quad [23]$$

and

$$W_{tb} = \frac{gV_t}{kRT_s}\frac{dP_{tb}}{dt} \quad [24]$$

or in terms of small changes

$$\Delta W_{ta} = \frac{gV_t}{kRT_s}\frac{d}{dt}(\Delta P_{ta}) \quad [25]$$

$$\Delta W_{tb} = \frac{gV_t}{kRT_s}\frac{d}{dt}(\Delta P_{tb}) \quad [26]$$

Combining Equations [21] with [25], and [22] with [26] gives

$$\Delta W_{ta} = \frac{gV_t}{kRT_s}\frac{d}{dt}\left(\frac{-RT_s}{gC_cP_i}\Delta W_{ta} + \Delta P_a\right) \quad [27]$$

and

$$\Delta W_{tb} = \frac{gV_t}{kRT_s}\frac{d}{dt}\left(\frac{-RT_s}{gC_cP_i}\Delta W_{tb} + \Delta P_b\right) \quad [28]$$

Collecting terms yields

$$\frac{V_t}{kC_cP_i}\frac{d(\Delta W_{ta})}{dt} + \Delta W_{ta} = \frac{gV_t}{kRT_s}\frac{d}{dt}(\Delta P_a) \quad [29]$$

and

$$\frac{V_t}{kC_cP_i}\frac{d(\Delta W_{tb})}{dt} + \Delta W_{tb} = \frac{gV_t}{kRT_s}\frac{d}{dt}(\Delta P_b) \quad [30]$$

Thus Equations [29] and [30] are of the desired form given by Equation [16].

The net flows to chambers a and b are $(\Delta W_a - \Delta W_{ta})$ and $(\Delta W_b - \Delta W_{tb})$, respectively. The energy equations may be applied again to chambers a and b

$$\Delta W_a - \Delta W_{ta} - \frac{gP_iA}{RT_s}\frac{d}{dt}(\Delta Y) = \frac{gV_i}{kRT_s}\frac{d}{dt}(\Delta P_a) \quad [31]$$

and

$$\Delta W_b - \Delta W_{tb} + \frac{gP_iA}{RT_s}\frac{d}{dt}(\Delta Y) = \frac{gV_i}{kRT_s}\frac{d}{dt}(\Delta P_b) \quad [32]$$

Solution of Equations [29] and [30] for ΔW_{ta} and ΔW_{tb} gives

$$\Delta W_{ta} = \frac{\frac{gV_t}{kRT_s}D(\Delta P_a)}{\frac{V_t}{kC_cP_i}D + 1} \quad [33]$$

and

$$\Delta W_{tb} = \frac{\frac{gV_t}{kRT_s}D(\Delta P_b)}{\frac{V_t}{kC_cP_i}D + 1} \quad [34]$$

Combination of Equations [31] and [33] and Equations [32] and [34] gives

$$\Delta W_a - \frac{\frac{gV_t}{kRT_s}D(\Delta P_a)}{\frac{V_t}{kC_cP_i}D + 1} - \frac{gP_iA}{RT_s}D(\Delta Y) = \frac{gV_i}{kRT_s}D(\Delta P_a) \quad [35]$$

$$\Delta W_b - \frac{\frac{gV_t}{kRT_s}D(\Delta P_b)}{\frac{V_t}{kC_cP_i}D + 1} + \frac{gP_iA}{RT_s}D(\Delta Y) = \frac{gV_i}{kRT_s}D(\Delta P_b) \quad [36]$$

Subtracting Equation [36] from Equation [35] gives

$$(\Delta W_a - \Delta W_b) - \frac{\frac{gV_t}{kRT_s}D(\Delta P_a - \Delta P_b)}{\frac{V_t}{kC_cP_i}D + 1} - \frac{2gP_iA}{RT_s}D(\Delta Y) = \frac{gV_i}{kRT_s}D(\Delta P_a - \Delta P_b) \quad [37]$$

Since from Equation [6]

$$(\Delta W_a - \Delta W_b) = 2C_1\Delta X - C_2(\Delta P_a - \Delta P_b)$$

substitution for $(\Delta W_a - \Delta W_b)$ and division through by $2gP_i/RT_s$ gives

$$k_1\Delta X - k_2(\Delta P_a - \Delta P_b) - k_2'\frac{\tau D(\Delta P_a - \Delta P_b)}{\tau D + 1} - AD(\Delta Y) = k_3D(\Delta P_a - \Delta P_b) \quad [38]$$

where

$$k_2' = \frac{C_c}{2}, \quad \frac{\text{in.}^5}{\text{lb-sec}} \quad [39]$$

$$\tau = \frac{V_t}{kC_cP_i}, \quad \text{sec} \quad [40]$$

Therefore the desired transient-pressure-feedback effect is provided by the flow resistances and tanks.

Since the stabilization really is caused by a flow that is diverted from, or added to, the valve flow during transient operation, the term transient-flow stabilization will be employed to describe this means of providing system damping. Addition of the transient-flow stabilization to the system requires a third-order differential equation to describe the system. This equation is obtained by combining Equations [38] and [13]

$$k_1\Delta X - \left(k_2 + k_2'\frac{\tau D}{\tau D + 1} + k_3D\right)\left[\left(\frac{m}{A}D + \frac{b}{A}\right)D(\Delta Y) + \frac{\Delta L}{A}\right] = AD(\Delta Y) \quad [41]$$

Since a closed-center valve is employed in this investigation and no by-pass leakage is expected past the ram, k_2 is negligible. At the same time, minimizing the viscous-damping coefficient b to avoid loss of power at high ram velocities would be advantageous. Setting k_2 and b equal to zero gives a somewhat simpler equation relating $D(\Delta Y)$ to ΔX and ΔL

$$\left\{[k_2'\tau D + k_3D(\tau D + 1)]\frac{mD}{A} + A(\tau D + 1)\right\}D(\Delta Y) = k_1(\tau D + 1)\Delta X - [k_2'\tau D + k_3D(\tau D + 1)]\frac{\Delta L}{A} \quad [42]$$

Equation [42] may be written more simply if the following parameters are used

$$\pi_v = \frac{V_i}{V_t} \text{ (dimensionless)} \quad [43]$$

$$\tau_i = \pi_v \tau = \frac{V_i}{kC_c P_i} \text{ (sec)} \quad [44]$$

$$\pi_s = \frac{A^2 V_i^2 \tau^2}{k_3 m V_i^2} = \frac{2A^2 V_i}{k m C_c^2 P_i} \text{ (dimensionless)} \quad [45]$$

The resulting relationship is

$$[(\tau_i D)^3 + (1 + \pi_v)(\tau_i D)^2 + \pi_s \tau_i D + \pi_s \pi_v] D\Delta Y = \frac{k_1}{A} \pi_s \pi_v \left(\frac{\tau_i}{\pi_v} D + 1\right) \Delta X - \frac{\tau_i^3}{m(\pi_v + 1)} \left(\frac{\tau_i D}{\pi_v + 1} + 1\right) D\Delta L \quad [46]$$

For convenience, Equation [10] is repeated in computing k_1

$$k_1 = \frac{C_1 R T_s}{g P_i}, \frac{\text{sq in.}}{\text{sec}} \quad [10]$$

Equation [46] is a useful equation for this system because it is in dimensionless form and can be applied readily to design work. Before application, however, the relationship of the roots of the characteristic equation to the dimensionless parameters of the system must be found. The characteristic equation is

$$[(\tau_i D)^3 + (1 + \pi_v)(\tau_i D)^2 + \pi_s \tau_i D + \pi_s \pi_v] D\Delta Y = 0 \quad [47]$$

It will have three roots; one of which is real and the other two may be real or complex. When the system is underdamped, the other two roots will be complex, and the following identity may be used

$$(\tau_i D)^3 + (1 + \pi_v)(\tau_i D)^2 + \pi_s \tau_i D + \pi_s \pi_v \equiv \pi_s \pi_v (\tau_1 D + 1) \left[\left(\frac{1}{\omega_{ns}}\right)^2 D^2 + \frac{2\zeta_s}{\omega_{ns}} D + 1\right] \quad [48]$$

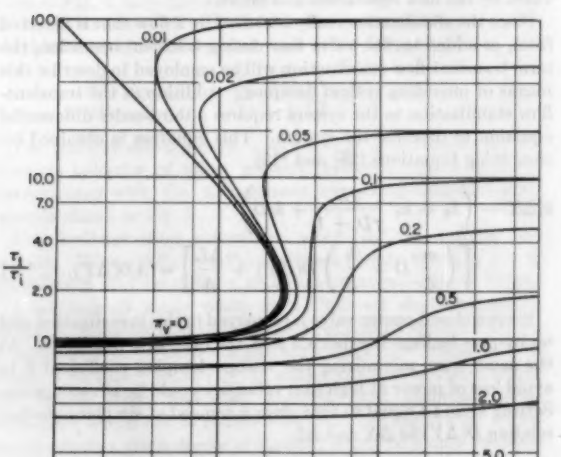

FIG. 7 GRAPHICAL REPRESENTATION OF $\tau_1/\tau_i = f_\tau(\pi_v, \pi_s)$

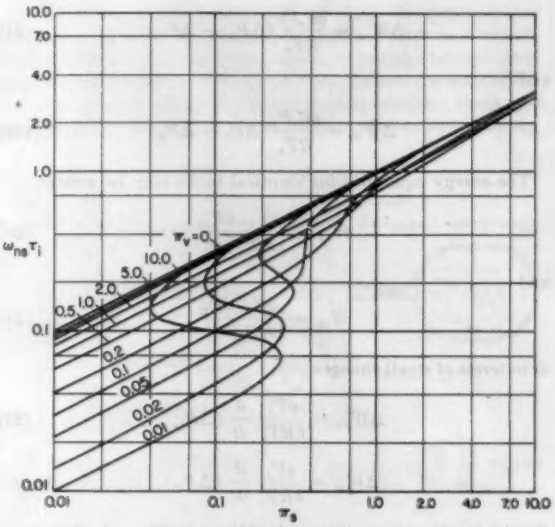

FIG. 8 GRAPHICAL REPRESENTATION OF $\omega_{ns}\tau_i = f_\omega(\pi_v, \pi_s)$

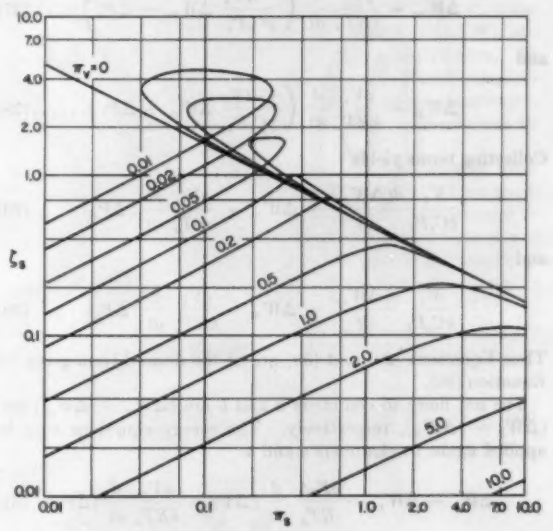

FIG. 9 GRAPHICAL REPRESENTATION OF $\zeta_s = f_\zeta(\pi_v, \pi_s)$

The use of dimensional analysis is helpful in determining how the quantities τ_1, ω_{ns}, and ζ_s are related to the quantities τ_i, π_v, and π_s. In general

$$\tau_1 = f_a(\tau_i, \pi_v, \pi_s) \quad [49]$$

or

$$\frac{\tau_1}{\tau_i} = f_\tau(\pi_v, \pi_s) \quad [50]$$

and

$$\omega_{ns} = f_b(\tau_i, \pi_v, \pi_s) \quad [51]$$

or

$$\omega_{ns}\tau_i = f_\omega(\pi_v, \pi_s) \quad [52]$$

and

$$\zeta_s = f_5(\pi_v, \pi_s) \quad [53]$$

The functional relationships shown symbolically by Equations [50], [52], and [53] may be obtained mathematically by systematically solving for the roots of the characteristic equation in terms of π_v, π_s, and τ_i. The results of such a procedure are given in graphical form in Figs. 7, 8, and 9, which show the functional relationships given by Equations [50], [52], and [53], respectively. These graphs, together with Equation [46], are the key to gaining an understanding of the dynamic characteristics of the valve, ram, and load system with transient-flow stabilization.

When the system is overdamped, the characteristic equation has three real roots, and the following identity may be used

$$(\tau_i D)^3 + (1 + \pi_s)(\tau_i D)^2 + \pi_s \tau_i D + \pi_s \pi_v \equiv \pi_s \pi_v (\tau_1 D + 1)(\tau_2 D + 1)(\tau_3 D + 1) \quad [54]$$

It can be shown by dimensional analysis that the time constants τ_1, τ_2, and τ_3 are each functions of π_v, π_s, and τ_3. When the characteristic equation is solved systematically for τ_1, τ_2, and τ_3, they coincide with the three values of τ_1 that exist in some regions of Fig. 7. Thus Fig. 7 may be used to obtain all three of the real roots of the characteristic equation when the system is overdamped. The actual roots, incidentally, are the reciprocals of the time constants τ_1, τ_2, and τ_3.

Although there are numerous ways in which the curves may be used in practical design work, one useful procedure is to specify a desired damping ratio ζ_s, select the smallest value of tank volume ratio π_v that makes such a damping ratio possible, and read from Fig. 9 the necessary value of π_s. Once this has been done, the values of the various physical parameters making up π_s often can be juggled to evolve a satisfactory design. In many cases, it is desirable to obtain the fastest response consistent with space and power limitations. The values of all of the system time constants are closely related to the values of τ_i and π_s. The dynamic terms on the right-hand side of Equation [46] must be included when assessing the speed of response of the system. As in most design problems, trial-and-error techniques may be combined with the analytical results presented here to work out a system design.

Since this system is potentially useful for the continuous control of position, velocity, or acceleration, there are many possible considerations which may enter into its practical application.

The electronic-analog computer has proved to be a valuable tool in the design process. The rather simple block diagram for the simulation of Equation [46] is shown in Fig. 10. This diagram

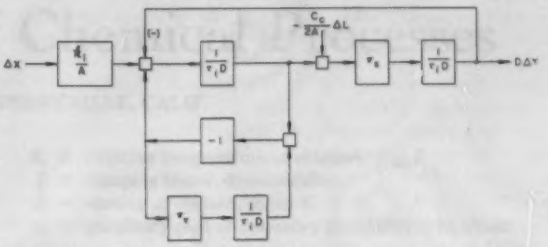

FIG. 10 BLOCK DIAGRAM FOR ANALOG SIMULATION OF EQUATION [46]

serves to emphasize the pervading influence of τ_i on system speed of response. Since

$$\tau_i = \frac{V_i}{(kC_c P_i)}$$

the volume of fluid under compression in the ram V_i must be kept small, and the largest practical value of P_i must be used. On the other hand, the largest possible value of π_s may be advantageous to gain speed of response. Since

$$\pi_s = \frac{2A^2 V_i}{kmC_c^2 P_i}$$

then when the values of m and P_i are set by other considerations it is possible that using a large ram area may be justified even though this would increase V_i and thence τ_i.

CONCLUSIONS

A fundamental study of the pneumatic process in a system used for the continuous control of motion with compressed air shows how linearized equations may be used to analyze the system. The use of analog block diagrams and an electronic-analog computer made possible a simple means of attaining system damping with very little steady-state load sensitivity and viscous-friction power loss.

ACKNOWLEDGMENT

The work described in this paper was supported in part by the Bureau of Ordnance, U. S. Navy Department, under Contract No. Nord 11799, with the Division of Industrial Cooperation, Massachusetts Institute of Technology. The author is particularly indebted to members of the staff of the Dynamic Analysis and Control Laboratory for their invaluable assistance and counsel.

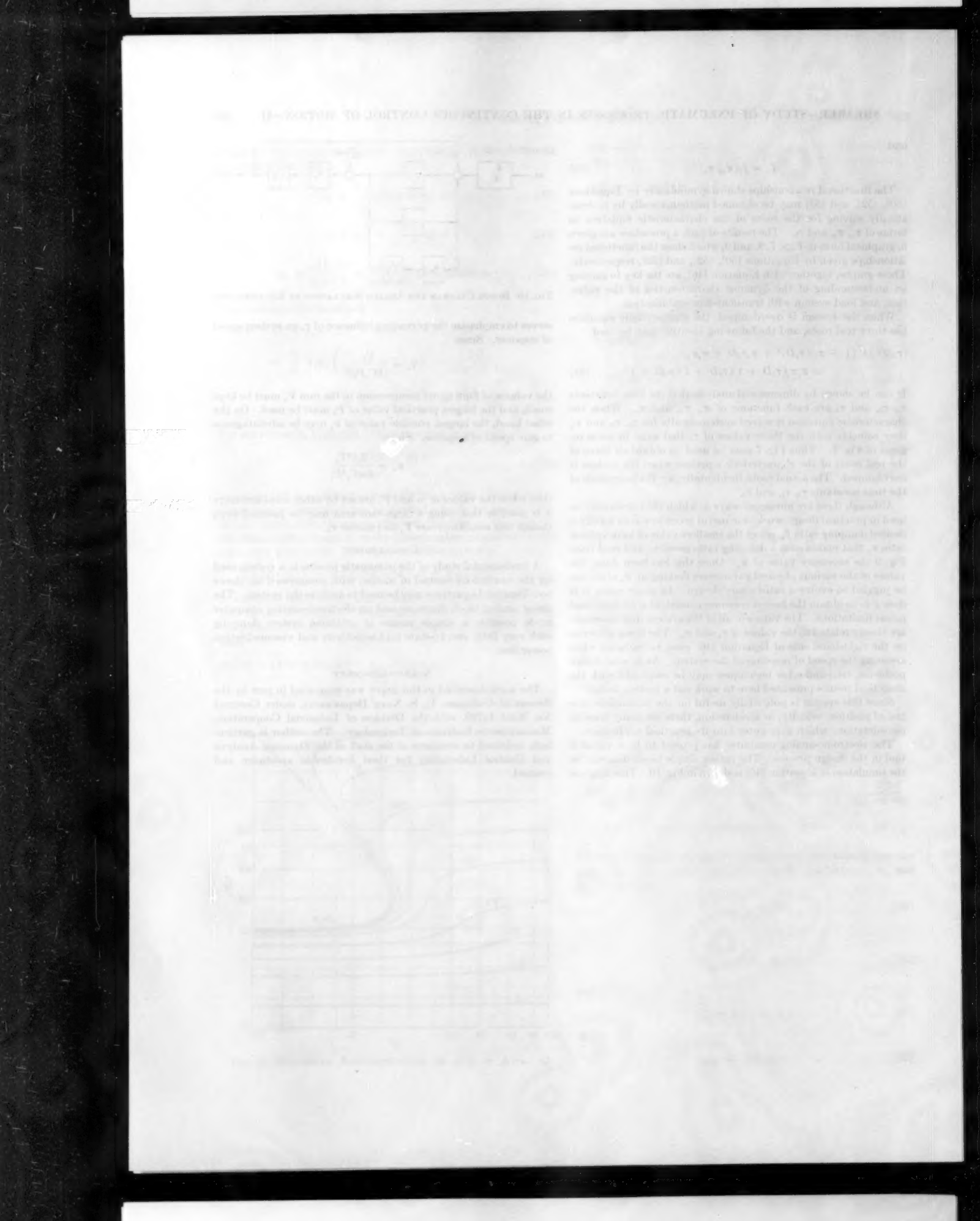

Dynamic Analysis of Chemical Processes

By E. G. HOLZMANN,[1] EMERYVILLE, CALIF.

The dynamic characteristics of a process must be known in order to predict stability of control. Necessary dynamic equations are formulated from considerations of heat balance and mass balance. The derivation of linear transfer functions for an exemplary catalytic reaction process is discussed in detail.

Nomenclature

The following nomenclature is used in the paper:

A = effective heat-transfer area of one tube, sq ft
A_L = free liquid surface area in reactor, sq ft
a = reset factor, dimensionless
C = effective heat capacity of one tube, Btu/deg F
c = specific heat of liquid coolant, Btu/lb-deg F
$G_c(s)$ = temperature controller transfer function, lb/min-deg F
$G_f(s)$ = flow controller transfer function, ft-min/lb
$G_L(s)$ = level controller transfer function, lb/min-ft
$G_r(s)$ = reaction-process transfer function, deg F-min/lb
$H(s)$ = temperature control closed-loop transfer function, dimensionless
ΔH = latent heat of vaporization, Btu/lb
h_k, h_L = enthalpy of liquid coolant at temperatures θ_k, θ_L, Btu/lb-deg F
h_v = enthalpy of saturated coolant vapor, Btu/lb-deg F
K_c = gain factor of temperature controller and valve, lb/min-deg F
K_f = gain factor of flow controller, ft-min/lb
K_L = gain factor of level controller and valve, lb/min-ft
K_r = gain factor of reaction, dimensionless
K_1 = gain factor, dimensionless
K_2 = gain factor, dimensionless
K_3 = gain factor, deg F-min/lb
K_4 = gain factor, deg F-min/lb
L = coolant level in reactor, ft
M = effective mass of liquid coolant in reactor, lb
m_L = flow rate of recycle coolant, lb/min
m_v = flow rate of vapor leaving reactor, lb/min
N = number of tubes in reactor, dimensionless
q = rate of heat dissipation from one tube, Btu/min
q_g = rate of heat generation in one tube, Btu/min
s = complex frequency parameter, radian/min
T = time constant of cooling system, min
T_c = reset time constant, min
T_r = time constant of reaction, min
t = time, min
U = effective heat-transfer coefficient, Btu/min-deg F-sq ft
α = coefficient of temperature dependence of reaction, deg F^{-1}
θ_k = effective temperature of coolant in reactor, deg F
θ_L = temperature of recycle coolant, deg F
θ_r = effective temperature of reaction, deg F
ξ = damping factor, dimensionless
ρ = density of coolant, lb/cu ft
ω = imaginary part of frequency parameter s, rad/min

Time-average values are designated by subscript 0.

Introduction

In the design of a new chemical plant certain questions arise to which past experience does not always give adequate answers. For example, what provisions must be made to insure stable control of a particular reaction? Can a critical temperature be held constant when ambient conditions change? All too often the final answer to such questions is not found until trouble arises during start-up of a new plant.

Dynamic analysis offers a way to resolve some of these baffling questions in the design stage. As a result one may anticipate trouble and reduce costly down time. Compared with the cost of delayed plant start-up, the effort required to predict difficulties and to eliminate them in the design stage is small indeed.

The paper discusses the dynamic point of view as applied to chemical plants. To illustrate the methods currently used in analysis, attention is focused on the study of a typical example, a continuous catalytic reaction.

Scope and Limitations

The problem of studying the dynamic characteristics of a chemical process arises in connection with the design and evaluation of suitable controls. To understand the scope and the limitations of dynamic analysis, we distinguish between two broad aspects of control.

Control by Set Point

First, there is static control. The chemical engineer working on a new process computes certain operating conditions. He aims to combine high quality, yield, and conversion with low initial and operating costs. The conditions thus specified are forced upon the process through the action of valves. A valve may be turned directly by hand or adjusted indirectly through the set point of a controller. In either case the control action imposes static conditions on the process to insure profitable plant operation. This might be called control by set point.

Control by Regulation

Dynamic analysis deals with a different aspect of control. It attempts to describe the behavior of a system subjected to forces that disturb its static equilibrium. In terms of the chemical plant, dynamic analysis is concerned with stability and control by regulation.

Stability. Having decided on the most desirable operating conditions, the process engineer needs to know if the plant can be controlled to operate in a stable manner under those conditions. Dynamic analysis usually provides a unique answer to the question of stability. The answer is based on data such as are used in the mechanical design of a plant and in the calculation of equilibrium conditions.

Regulation. When stability of a controlled reaction is assured, a second question often needs to be answered. Changes of weather, variations of feed quality, of steam or water pressure, and many other causes may impose disturbances on a process.

---

[1] Shell Development Company.

Contributed by the Instruments and Regulators Division and presented at the Instruments and Regulators Division Conference, Ann Arbor, Mich., April 25–26, 1955, of The American Society of Mechanical Engineers.

Note: Statements and opinions advanced in papers are to be understood as individual expressions of their authors and not those of the Society. Manuscript received at ASME Headquarters, February 17, 1955. Paper No. 55—IRD-5.

In some processes product quality depends critically on temperature of reaction. Often the dynamic properties of the reaction are subject to change. In such cases the effect of disturbances on normal operation may need to be estimated. This is called the problem of regulation. It is more difficult than the problem of stability, and one can only indicate the response to certain assumed standard disturbances. Dynamic analysis does, however, provide a basis on which to assess the relative merits of alternative control schemes. Also, the calculation may show that normal disturbances will have negligible effect on the reaction and the product. An answer of this kind is often all that is required.

A systematic approach to the problems of dynamic analysis has several advantages. It helps one to separate important detail from dynamically trivial effects. It also permits rapid review when earlier assumptions must be modified because of design changes. Last, but not least, a clear-cut procedure is more easily understood by other members of a team working on a common project. The remainder of this paper aims to present such an approach, with step-by-step illustrations taken from a typical example.

Outline of Method of Analysis

Three distinct steps are involved in making a design study of the stability and regulation of a controlled chemical process. First, one has to determine the dynamic properties of the process and of the controllers, valves, and measuring devices to be used in controlling the process. These properties are commonly expressed in terms of so-called transfer functions. Knowing the component transfer functions, the second step is to calculate the transfer function around each control loop and to find the range of control settings for which the system will be stable. Finally, one assumes that each loop is closed and that the controllers are adjusted in accordance with accepted criteria. The system response to load changes or to other disturbances is then computed as a check on performance. This last step will indicate, for example, how the controlled temperature would respond to changes in feedstream temperature.

When standard commercial control devices are used in a plant, their dynamic properties are often known from previous tests in the laboratory or in the field. Quite often, therefore, only the reaction dynamics of a new chemical plant need to be analyzed in detail.

The paper will develop transfer functions and a dynamic block diagram for the example process. Differential equations are derived from basic physical principles. To show the analogy between the actual process and its abstract dynamic model, we will introduce the concept of a functional block diagram. The results are presented in the form of frequency-response curves for the open-loop and closed-loop control system.

Description of Illustrative Example

Fig. 1 shows the basic layout of a temperature-control system for a continuous catalytic-reaction process. The reactants enter the reactor at the top. The exothermic reaction takes place in a number of parallel tubes which are packed with catalyst, the product stream emerging at the bottom. The heat of the reaction vaporizes liquid coolant which circulates around the reactor tubes. The boiling point depends on the pressure and on the composition of the coolant. If the composition remained constant, pressure control would be suitable. With a coolant of variable composition, temperature control is indicated. In our example, the temperature controller (TC) actuates a valve in the coolant vapor line. Vaporized coolant is condensed and recycled into the reactor under the control of a level controller (LC).

When the vapor control valve opens, the pressure in the reactor shell drops. The boiling mass of coolant in the reactor will swell due to the increased evaporation rate. With a fixed set point, the level controller would then throttle the flow of the liquid recycle and thus deplete the coolant inventory of the reactor. To counteract this undesirable tendency, the set point of the level controller is reset from the output of a flow controller (FC). The flow controller thus relates coolant level to vapor flow rate.

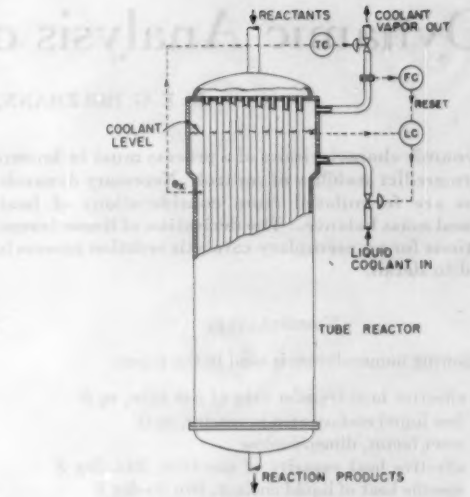

Fig. 1 Schematic Diagram of Process and Control System

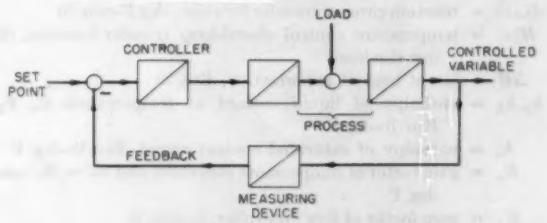

Fig. 2 Simple Functional Block Diagram

Functional Block Diagram

Dynamic analysis requires that the physical system outlined in Fig. 1 be reduced to a mathematical model. This is conveniently accomplished in two stages.

The first step leads to a topological picture of the model, called the functional block diagram. Fig. 2 is such a diagram for a system in which a single process variable is being controlled. The process is subject to external disturbances, briefly called loads. The relationships between process and control variables are shown schematically as boxes. Each box represents a transfer mechanism, that is, the physical or chemical mechanism which gives rise to the interaction of the variables.

In the second step of the analysis, the transfer mechanisms are characterized by dynamic transfer functions, as we will see later.

Example

Fig. 3 illustrates the construction of a functional block diagram for the catalytic reactor control system of Fig. 1. The ultimately controlled variable is a good starting point. In the example, it is the reaction temperature. Next, we find the variables upon which reaction temperature depends. They include the feed variables (composition, temperature, flow rate) which are independently controlled by means not shown in Fig. 1. If they are well regu-

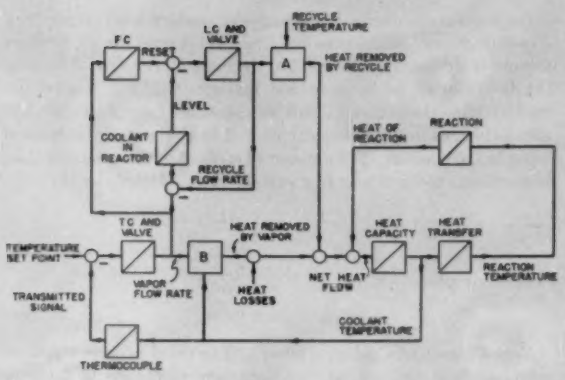

FIG. 3 FUNCTIONAL BLOCK DIAGRAM

lated, as will be assumed here, then only the effect of coolant temperature on the reaction temperature needs to be further considered. A block labeled "heat transfer" in Fig. 3 indicates this interaction.

The coolant temperature itself depends on the net rate of heat entering the reactor. The temperature rises and falls because of the finite heat capacity of the reactor. The corresponding block in Fig. 3 is, therefore, tagged "heat capacity."

Summing. The net rate of heat flow is the sum of several components. The exothermic reaction generates heat. Heat is removed by evaporation of coolant, by losses to the atmosphere, and by the liquid recycle which enters at a temperature below that of the reactor content. These heat variables are entered into the block diagram at summing points indicated by small circles.

Functions of Several Variables. Some process variables depend on two or more other variables in a nonlinear manner. For example, the heat removed from the reactor by the liquid recycle is a function both of the recycle flow rate and of the temperature. Similarly, the heat removed by evaporation depends on the coolant temperature in the reactor and on the vapor flow rate. Blocks A and B in Fig. 3 stand for the respective nonlinear relationships.

Combined Transfer Mechanisms. Two or more cascaded transfer mechanisms may often be combined to simplify the functional block diagram. For instance, a single block in Fig. 3 includes both the level controller (LC) and the recycle control valve. The temperature controller and vapor control valve are similarly combined.

MATHEMATICAL RELATIONSHIPS

Construction of the functional block diagram is the first stage in arriving at a mathematical model of the process. Next, the so-called transfer mechanisms must be described by transfer functions based on theoretical analysis and test data.

Controllers and Valves

Transfer functions of standard control apparatus are usually known with sufficient accuracy from tests in earlier applications or in the control laboratory. For instance, experience indicates that valve dynamics can be represented approximately by first-order time lags. Nonlinear effects due to valve characteristic, dead space, and hysteresis can often be neglected when considering the over-all problem of plant stability and regulation.

In the example chosen here for illustration, the frequency response of the transducers and controllers will be assumed high compared with that of the respective valves. The following time constants are used:

Vapor control valve, $T_v = 0.1$ min
Recycle control valve, $T_L = 0.5$ min

Process

We must now find the transfer functions for the process. The method proposed here is to write down differential equations for heat balance and mass balance of portions of the plant. If the boundaries are chosen with care, the equations will give dynamic relationships between the process variables of interest. After linearizing equations, their Laplace transforms are easily reduced to a form that shows the desired transfer functions.

In the example, we are mainly concerned with three process variables, namely, the reaction and coolant temperatures, and the coolant flow rate in the vapor line from the reactor. Three equations are required for finding the frequency (or time) response of these variables to sinusoidal (or transient) changes imposed upon the process-control system.

Heat Balance of Reaction. The first of the equations is derived from the condition of energy balance in a single tube of the reactor. Fig. 4 gives an oversimplified picture of the heat exchange between a reactor tube and the surrounding coolant. A first-order differential equation describes the heat-balance condition for the system shown

$$C\frac{d\theta_r}{dt} = q_s - q \qquad [1]$$

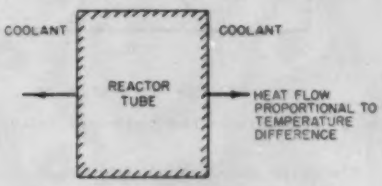

FIG. 4 HEAT BALANCE OF REACTION

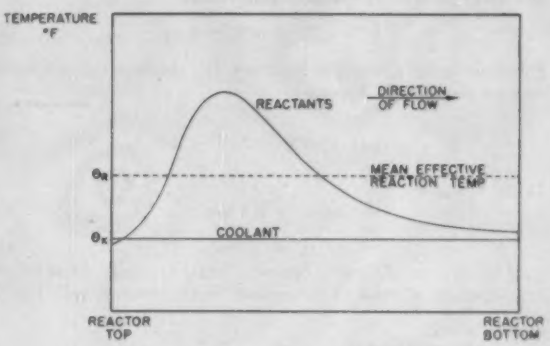

FIG. 5 TEMPERATURE PROFILE OF REACTOR

The rate of heat transfer from the tube to the surrounding coolant is

$$q = AU(\theta_r - \theta_k) \qquad [2]$$

The reaction temperature θ_r in the foregoing equations represents a mean effective temperature.

Actually, each tube will have an axial temperature profile as shown in Fig. 5. The profile arises because the reaction changes the composition of the stream passing down each tube. The rate of reaction depends on composition. Therefore less heat is generated in the lower portion of the reactor where fresh reactants are

relatively scarce. Because of differences in catalyst activity, different tubes may have different temperature profiles. The temperature at selected points in the tubes is therefore an unreliable measure of the total reaction rate. It is for this reason that control is effected from thermocouples placed in the coolant rather than in the reactor tubes.

The relation between temperature and reaction rate must be established empirically, in the present state of the art. Fig. 6 pictures such a relation obtained from a number of pilot-plant

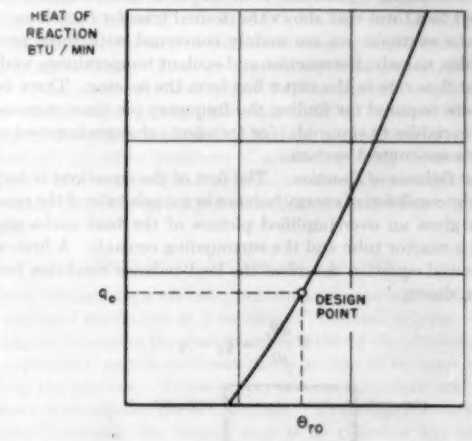

FIG. 6 TEMPERATURE DEPENDENCE OF REACTION

test runs. The curve indicates that small changes of reaction temperature are accompanied by nearly proportional changes of reaction heat. The rate of heat generation can thus be described as a linear function of reaction temperature

$$q_g = q_0[1 + \alpha(\theta_r - \theta_{r0})] \quad [3]$$

Substituting for q_g and q in Equation [1], the heat-balance equation for the reaction becomes

$$C\frac{d\theta_r}{dt} = q_0[1 + \alpha(\theta_r - \theta_{r0})] - AU(\theta_r - \theta_k) \quad [4]$$

In the example

$$\alpha q_0/C = 0.5 \text{ min}^{-1} \quad [4a]$$

$$AU/C = 1.5 \text{ min}^{-1} \quad [4b]$$

Mass Balance of Cooling System. Next, we apply the principle of continuity of mass to the coolant in the reactor shell, Fig. 7.

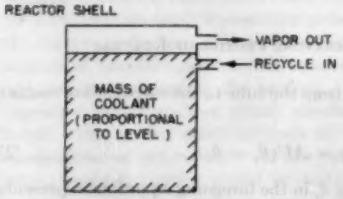

FIG. 7 MASS BALANCE OF COOLING SYSTEM

The equation is again first order. It simply states that the rate of change of coolant inside the reactor equals the difference between the vapor and the recycle liquid flow rates

$$\frac{dM}{dt} = m_L - m_v \quad [5]$$

The level controller senses changes of coolant level rather than of coolant mass. Unfortunately, the level is sensitive to pressure because the density of the coolant depends on the rate of boiling. The behavior could be described mathematically if it were desired to refine the analysis. But for the sake of simplicity, we will ignore changes in liquid density as well as changes of the mass of vapor in the reactor. The amount of coolant in the reactor is then proportional to level and free surface area. It follows that

$$\frac{dM}{dt} = A_L\rho\frac{dL}{dt} \quad [6]$$

In the example

$$A_L\rho = 2500 \text{ lb/ft} \quad [6a]$$

Heat Balance of Cooling System. The third process equation expresses heat balance at the boundary of the coolant in the

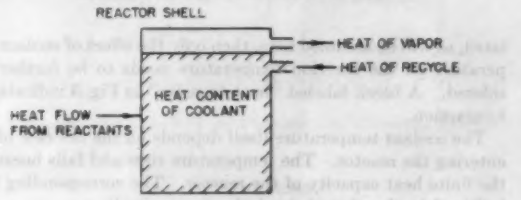

FIG. 8 HEAT BALANCE OF COOLING SYSTEM

reactor, Fig. 8. Since heat carried by a fluid stream depends both on flow rate and on enthalpy, the resulting differential equation does not have constant coefficients

$$\frac{d(h_k M)}{dt} = Nq + h_L m_L - h_v m_v \quad [7]$$

The relation between enthalpy and temperature is

$$\left.\begin{aligned} h_k &= c\theta_k \\ h_L &= c\theta_L \\ h_v &= c\theta_k + \Delta H \end{aligned}\right\} \quad [8]$$

Subtituting for q, h_k, h_L, and h_v in Equation [7] we obtain

$$c\frac{d(\theta_k M)}{dt} = NAU(\theta_r - \theta_k) + c\theta_L m_L - (c\theta_k + \Delta H)m_v \quad [9]$$

In our example

$$\frac{NAU}{cm_{v0}} = 15 \quad [9a]$$

$$\frac{\Delta H}{cm_{v0}} = 0.12 \text{ deg F-min/lb} \quad [9b]$$

$$\frac{M_0}{m_{v0}} = 11 \text{ min} \quad [9c]$$

and

$$\frac{\theta_{L0} - \theta_{L0}}{m_{v0}} = 0.011 \text{ deg F-min/lb} \quad [9d]$$

Linearization. A peculiarity of process-control systems helps us to linearise Equation [9]. Most chemical processes normally operate with fixed set points. Deviations from average temperatures and flow rates are small except during start-up. We may, therefore, consider each temperature as composed of a fixed average value and a relatively small variable part. Similarly, each

flow rate has a small variable component superimposed on a much larger fixed average flow. In multiplying temperature and flow rate, we can then disregard the product of the two small variable portions as a second-order small quantity. This method of quasi-linearization is used in the next part of the analysis.

Process Transfer Functions

Steady-State Equation

The desired transfer functions of the process will be derived from Equations [4], [5], and [9]. First, we write down the steady-state form of each equation. The variables are replaced by their time-average values. All derivatives vanish. Thus we have

$$0 = q_0 - AU(\theta_{r0} - \theta_{k0}) \quad [10]$$

$$0 = m_{L0} - m_{v0} \quad [11]$$

$$0 = NAU(\theta_{r0} - \theta_{k0}) + c\theta_{L0}m_{L0} - (c\theta_{k0} + \Delta H)m_{v0} \quad [12]$$

Incremental Equation

By subtracting the steady-state from each of the original differential equations, we obtain a new set of differential equations. These we may call incremental heat and mass-balance equations

$$C\frac{d\theta_r(t)}{dt} = q_0\alpha\theta_r(t) - AU[\theta_r(t) - \theta_k(t)] \quad [13]$$

$$\frac{dM(t)}{dt} = m_L(t) - m_v(t) \quad [14]$$

$$cM_0\frac{d\theta_k(t)}{dt} + c\theta_{k0}\frac{dM(t)}{dt} = NAU\,[\theta_r(t) - \theta_k(t)] + cm_{L0}\theta_L(t) + c\theta_{L0}m_L(t) - cm_{v0}\theta_k(t) - c\theta_{k0}m_v(t) - \Delta Hm_v(t) \quad [15]$$

The new variables in the foregoing equations represent small changes from steady-state average values. Products of any two variables have been omitted in order to linearize the equations.

Laplace Transform Equation

Each one of the incremental variables has a zero average value. Before taking Laplace transforms, we may therefore assume that the initial value is also zero. The transformed Equations [13], [14], and [15] read

$$Cs\theta_r(s) = [q_0\alpha - AU]\theta_r(s) + AU\theta_k(s) \quad [16]$$

$$sM(s) = A_L\rho_0 L(s) = m_L(s) - m_v(s) \quad [17]$$

$$[cM_0 s + cm_{v0} + NAU]\theta_k(s) = NAU\,\theta_r(s) + cm_{L0}\theta_L(s) - c[\theta_{k0} - \theta_{L0}]m_L(s) - \Delta Hm_v(s) \quad [18]$$

Equation [18] is derived after substituting for $M(s)$ from Equation [17].

Normalized Transform Equation

Finally, we normalize the equations so that the transform of each response function has unity coefficient

$$\theta_r(s) = \frac{K_r}{T_r s + 1}\,\theta_k(s) \quad [19]$$

$$L(s) = \frac{1}{A_L\rho s}[m_L(s) - m_v(s)] \quad [20]$$

$$\theta_k(s) = \frac{1}{Ts + 1}[K_1\theta_r(s) + K_2\theta_L(s) + K_3 m_v(s) + K_4 m_L(s)] \quad [21]$$

where

$$T_r = \frac{C}{AU - \alpha q_0} = 1 \text{ min} \quad [19a]$$

$$K_r = \frac{AU}{AU - \alpha q_0} = 1.5 \quad [19b]$$

$$T = \frac{cM_0}{cm_{v0} + NAU} = 0.7 \text{ min} \quad [21a]$$

$$K_1 = \frac{NAU}{cm_{v0} + NAU} = 0.94 \quad [21b]$$

$$K_2 = \frac{cm_{L0}}{cm_{v0} + NAU} = 0.063 \quad [21c]$$

$$K_3 = \frac{-\Delta H}{cm_{v0} + NAU} = -7.5 \times 10^{-3} \text{ deg F-min/lb} \quad [21d]$$

$$K_4 = \frac{-c[\theta_{k0} - \theta_{L0}]}{cm_{v0} + NAU} = -0.7 \times 10^{-3} \text{ deg F-min/lb} \quad [21e]$$

The coefficients of the transformed forcing functions on the right-hand side of Equations [19], [20], and [21] are the desired transfer functions. The normalized transform equations, therefore, place the transfer functions clearly in evidence.

Dynamic Block Diagram

The analytical transfer functions just derived may now be combined with the empirical transfer functions of the control apparatus. Together they form a linear dynamic model of the process and control system, Fig. 9.

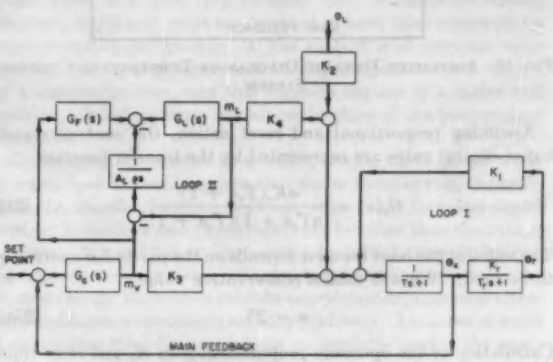

Fig. 9 Linearized Dynamic Block Diagram

If we compare Fig. 9 with the functional block diagram of Fig. 3, we find that the nonlinear blocks A and B have been replaced by linear coefficients K_1, K_3 and K_2, K_4, respectively. We also notice certain differences in the topology of the two diagrams. These apparent differences could be minimized by redrawing the functional block diagram in the light of the deeper insight gained from the analysis. But such corrections would defeat the purpose of the illustration. They would obscure the fact that the functional diagram is a useful auxiliary, rather than an essential step, in the development of the mathematical model.

The calculation of transfer functions does not depend on the functional block diagram. The diagram merely aids in relating the dynamic block diagram to the physical picture of plant and process. The functional block diagram can also serve to display the steady-state values of temperatures, flow rates, and other variables. It thus complements the dynamic block diagram.

Stability

The system of Fig. 9 is stable if the main feedback loop is stable. The subsidiary loops I and II must first be solved. The exothermic reaction (loop I) becomes

$$G_r(s) = \frac{\theta_k(s)}{m_r(s)} = \frac{K_3(T_r s + 1)}{(T_r s + 1)(Ts + 1) - K_1 K_r} \quad [22]$$

$$= \frac{-0.0075(s + 1)}{(s + 1)(0.7s + 1) - 1.41}$$

$$= \frac{-0.0183(s + 1)}{(0.38s + 1)(4.5s - 1)}$$

Loop Response With Manual Level Control

If we assume for the moment that the recycle liquid flow is on manual rather than automatic control, the block diagram reduces to that of Fig. 10. The open-loop transfer function of the temperature control system is $G_c(s)G_r(s)$. Its frequency response depends on the dynamic characteristics $G_c(s)$ of the controller as well as on those of the process.

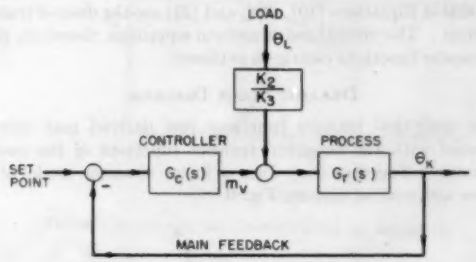

Fig. 10 Simplified Dynamic Diagram of Temperature Control System

Assuming proportional and reset action, the controller and vapor control valve are represented by the transfer function

$$G_c(s) = \frac{aK_c(T_c s + 1)}{(aT_c s + 1)(T_v s + 1)} \quad [23]$$

The value of the reset factor a depends on the particular controller to be used. We will take a conservative value

$$a = 25 \quad [23a]$$

Calculation of the optimum proportional gain K_c and reset time constant T_c is outside the scope of this paper. If we take

$$K_c = 1 \text{ lb/min-deg F} \quad [23b]$$

$$T_c = 10 \text{ min} \quad [23c]$$

the controller transfer function becomes

$$G_c(s) = \frac{25(10s + 1)}{(2500s + 1)(0.1s + 1)} \quad [24]$$

Fig. 11 shows the frequency-response curves of the open-loop temperature-control system with proportional-plus-reset (a = 25) and purely proportional (a = 1) control. By adding rate action, one could reduce the phase lag and attenuation between 10 and 100 rad/min. This would probably speed up recovery following a transient upset; but rate action is not needed for stability. The system has ample phase margin.

Flow Controller

The flow controller (FC) is adjusted to compensate for swelling

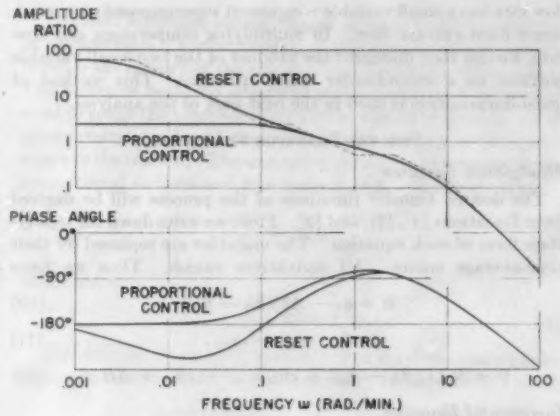

Fig. 11 Open-Loop Frequency Response

due to changes of pressure in the reactor shell. Under normal operating conditions, changes in level are nearly proportional to changes of vapor-flow rate. The constant of proportionality is

$$K_f = 0.001 \text{ ft-min/lb} \quad [25]$$

The proportional gain of the flow controller will be assumed to equal this value.

Loop Response With Automatic Level Control

Taking into account the effect of the level control loop (loop II in Fig. 9), we obtain the dynamic response of liquid flow rate $m_L(s)$ to small changes of vapor flow rate $m_v(s)$

$$\frac{m_L(s)}{m_v(s)} = G_f(s)G_L(s) + \frac{G_L(s)}{A_L\rho s + G_L(s)} \quad [26]$$

$$= K_f K_L + \frac{K_L}{A_L\rho s(T_L s + 1) + K_L} \quad [26a]$$

$$= \frac{(1.25s^2 + 2.5s + 0.001K_L + 1)K_L}{1250s^2 + 2500s + K_L} \quad [26b]$$

If the level controller is adjusted so that the level control loop is underdamped with a damping factor ξ = 0.5, then

$$K_L = 5000 \text{ lb/min-ft} \quad [27]$$

and

$$\frac{m_L(s)}{m_v(s)} = \frac{1.25s^2 + 2.5s + 6}{0.25s^2 + 0.5s + 1} \quad [28]$$

Owing to the action of automatic level control, the coefficient K_2 in Fig. 9 is modified by a factor

$$1 + \frac{K_4 m_L(s)}{K_2 m_v(s)} \begin{cases} = 1.6 \text{ at low frequencies} \\ = 1.5 \text{ at high frequencies} \end{cases} \quad [29]$$

Cascade flow-level control contributes very little phase shift to the dynamic response of the temperature-control system. We conclude therefore that the stability of the temperature control loop will not be affected by switching from manual to automatic level control provided the proportional gain of the temperature controller is reduced by a factor of 1.5.

Regulation

When the controllers have been adjusted to give stable control, the effect of outside disturbances can be estimated.

For instance, a change of recycle temperature in the example process may upset the heat balance in the reactor. The response to a unit change of temperature can be estimated from the open-loop and closed-loop transfer functions found in preceding steps of the analysis. Thus the effect of recycle temperature on coolant temperature in the reactor is

$$\frac{\theta_c(s)}{\theta_L(s)} = \frac{K_3 G_r(s)}{K_3[G_c(s)G_r(s) + 1]} \quad [30]$$

$$= K_2 H(s)/K_3 G_r(s) \quad [30a]$$

$$= 0.34 H(s) \frac{(2500s + 1)(0.1s + 1)}{(10s + 1)} \quad [30b]$$

where

$$H(s) = \frac{G_c(s)G_r(s)}{G_c(s)G_r(s) + 1} \quad [30c]$$

is the closed-loop transfer function of the main control loop with unity feedback.

The resulting frequency-response curves are shown in Fig. 12.

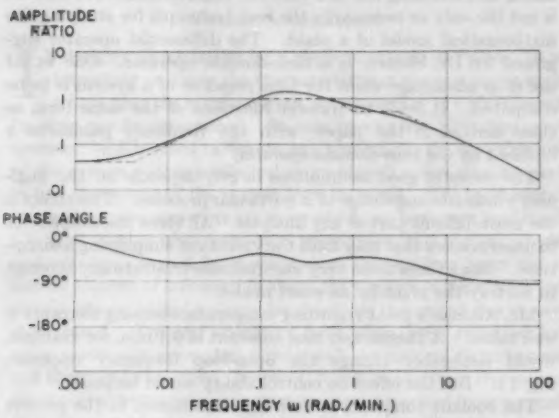

FIG. 12 CLOSED-LOOP FREQUENCY RESPONSE TO LOAD DISTURBANCES

The curves indicate that the process would be quite sensitive to disturbances in the frequency range from about 0.06 to 6 rad/min (periods from 1 min to 100 min per cycle).

CONCLUSIONS

The chief aim of dynamic analysis is to predict if stable control of a process is possible. When necessary, design changes can sometimes be suggested to improve stability.

In some processes, product quality or safety of operation requires holding a variable, usually temperature, at a fixed value. In such cases, dynamic analysis can help to estimate the response to disturbances forced upon the process. The calculations may indicate that the process environment should be controlled to minimize interference with normal operation.

The mathematical model is the basis for solving dynamic problems during the design of a new plant. To study the model process, one may combine analytical and graphical techniques adapted from servomechanism theory. For problems where nonlinearities must be taken into account one could employ an analog or digital differential analyzer.

As in all computer applications, so also in dynamic analysis the chief difficulty is to bridge the gap between the reality of the problem and its abstract formulation. The prototype process must be reduced to a dynamic model. The functional block diagram can serve as a useful intermediate step in arriving at the dynamic block diagram. Heat-balance and mass-balance equations for selected portions of the process yield the desired mathematical relationships.

The paper illustrates the method of analysis by reference to a continuous reaction process. A number of simplifying assumptions have been made, some of which could be justified in a more rigorous analysis of the problem. Although no practical results are available to support the conclusions reached in the working of the numerial example, the treatment presented is believed to be adequate for predicting the stability of a chemical process under normal operating conditions.

Discussion

A. R. AIKMAN.[2] In the plant examined by the author, control of the process itself (catalytic reaction) is accomplished by control of the environment of the reactor tubes. Fig. 5 shows that the tubes are sufficiently long that the reactants have nearly arrived at thermal equilibrium with their surroundings at the reactor bottom. It is appreciated that the author may have chosen this limiting case to illustrate his treatment with greater clarity, but it may be emphasized that in many process reactors the control of environment alone is not sufficient to maintain control of the reaction.

The author has chosen to neglect the time constants of the transducers (of level flow and temperature) by comparison with the valve time constants; this may be justified in practice for some level and flow transducers, but temperature-sensing elements, in general, must be expected to have time constants an order of magnitude greater. If the coolant is of constant composition, its vapor pressure and boiling temperature are related by a unique function, and this suggests the use of a faster and more economical pressure transducer in place of the temperature transducer.

Considering the reactor as a boiler, analogous to power-plant or waste-heat boilers, suggests that under some operating conditions the transfer function between, say, vapor flow and liquid level, or liquid flow and vapor flow, may be other than the author suggests. It is well known that, especially in high-pressure boilers, the immediate consequence of increasing steam flow is to raise the apparent level; the system exhibits nonminimum phase characteristics and raises very difficult stability problems. A number of ways of minimizing this effect have been successfully used in the past, such as controlling level by manipulation of coolant flow, and controlling pressure by resetting the set point of a vapor flow controller; or by manipulating the coolant flow as a function of level, coolant flow, and vapor flow.

Although, as the author states no practical results are available, it would be of quite exceptional interest if such results were to be made available at some later date, for only in this way can the present gap between theory and practice be bridged. The author has performed a service to control engineering by emphasizing that static analysis is no longer a sufficient basis for the design of economical, operable process plant, and that it must be supplemented by dynamic analysis.

SIDNEY LEES.[3] The paper is well organized and co-ordinates several of the factors which enter into a study of the dynamic properties of chemical processes. It is disturbing to see a lack of

[2] Schlumberger Instrument Company, Ridgefield, Conn.

[3] Assistant Professor, Aeronautical Engineering, Massachusetts Institute of Technology, Cambridge, Mass.

reference to preceeding work in this area. The relationships set down by the author surely have not been discovered by him.

It was the writer's impression on first reading, that the paper is a summary of current information. However, during the oral discussion when the paper was presented it was declared that a comprehensive statement of the several parameters contributing to the dynamic characteristics of chemical process plants has never been set down. If this is so, the author is to be commended for filling a most lamentable gap.

The author emphasizes the use of Laplace transform techniques in the solution of linear differential equations with constant coefficients. It does not appear to be a vital part of his presentation. Other well-known mathematical techniques exist for treating equations of this type. This point is noted because there is a widespread impression that the Laplace transformation is essential in the study of complex systems. In order to apply Laplace transforms, the author asserts that the equations are linear. However, linearization of mathematical relationships of physical processes requires care and justification.

The most useful part of the paper to the writer is the development of functional diagrams like Figs. 2 and 3. The paper concentrates on mathematical models without taking into account the limitations due to uncertainties, range, and nonlinearities.

J. L. Shearer.[4] One of the major contributions of this paper is the systematic approach that is made toward forming a symbolic picture of a complex physical system. Simplified mathematical relationships are deftly presented while schematic and block diagrams are employed effectively to create a clear conception of the many system variables and how they interact dynamically. There may be some questions in specific instances about the validity of some of the author's simplifying assumptions. For instance, it may not often be possible to neglect such things as nonlinear valve characteristics, dead space, or hysteresis in the control system, changes in liquid density, and changes in mass of vapor in the reactor. Yet the main parts of the picture have been painted and it is necessary to have these main parts to work with in deciding later on whether the simplifying assumptions are valid or not.

No direct benefit seems to be derived from employing the Laplace transformations—the differential equations that the author has derived speak for themselves. When the results of a study are to be presented in terms of frequency-response characteristics it is usually easier and better to simply transform to the frequency domain without getting involved with complicated transformations and tricky initial conditions. By using a transfer characteristic employing a differential operator to express the relationship between system variables it is possible to use simple block diagrams and work with the untransformed system variables in just the same way that the author builds up block diagrams based on Laplacian transfer functions and the Laplace transforms of the system variables. On the other hand, if the Laplace transformation is to be used to determine a transient response to a given disturbance or set of initial conditions, it is better to transform the simpler basic equations in which the initial conditions are usually easiest to evaluate.

It would be interesting to see the results of subsequent work that the author is undoubtedly doing, especially with regard to problems involved in starting up this process and getting it to the conditions where linearized analyses hold.

[4] Assistant Professor of Mechanical Engineering, Massachusetts Institute of Technology, Cambridge, Mass. Mem. ASME.

Author's Closure

The author wishes to express his appreciation of the understanding remarks contributed by Mr. Aikman, Dr. Lees, and Dr. Shearer. Dr. Shearer beautifully sums up the author's aims in writing the paper.

The author is grateful to Dr. Lees and Dr. Shearer for recognizing and stressing the fact that the Laplace transform method is not the only or necessarily the best technique for studying the mathematical model of a plant. The differential operator suggested by Dr. Shearer is a time-domain operator. One would use it to advantage when the time response of a system is to be computed. It leads to transfer functions of the same form as those derived in the paper, with the frequency parameter s replaced by the time-domain operator.

The choice of good assumptions largely depends on the engineer's intimate knowledge of a particular problem. This choice is the most difficult part of any analysis. All three discussers refer to uncertainties that may limit the validity of simplifying assumptions. Sometimes these very uncertainties frustrate any attempt to portray the plant by an exact model.

Mr. Aikman's point regarding temperature-sensing elements is well taken. A thermowell time constant of 0.1 min, for example, would noticeably change the open-loop frequency response, Fig. 11. But the effect on controllability would be small.

The coolant composition varies, as mentioned in the process description on page 252. If it were constant, Mr. Aikman's pressure controller would be preferred to the temperature controller used in the example.

Dr. Lees refers to an apparent gap in the literature on dynamics of chemical processes. It is indeed surprising that the literature in this field has grown so slowly. The lack of progress is probably more apparent than real. The author refrained from giving references because all the relationships set down in the paper are well known.

Determination of System Characteristics From Normal Operating Records

By T. P. GOODMAN[1] and J. B. RESWICK,[2] CAMBRIDGE, MASS.

Some new techniques are presented for experimentally determining the dynamical characteristics of linear systems. These techniques are based on analysis of random variations in the operating variables during the normal course of operation of the system. Particular attention is paid to the effects of uncorrelated variations (noise) on the methods. The use of the "delay-line synthesizer" as a device for discovering system characterizations is presented. Results obtained for the determination of a transfer operator for a human being engaged in tracking a target are presented as an example of the effectiveness of the random-data-analysis approach.

Transfer Operators

IN designing a controller for a physical system or "plant," it is important to know the characteristics of the system, in such a form that the system output corresponding to a given input function can be determined. In this paper, the term "transfer operator" will be used to denote any symbolical characterization of the system (either analytical or graphical) which may be used to find the output of the system from its input. The most useful forms of transfer operators are those which can be determined from a limited number of experimental measurements of system inputs and outputs. Stated in another way, the problem is to use a limited amount of information about the outputs of the system for certain inputs, to find a means for obtaining the output due to any other input. Transfer operators have often been obtained by using artificially generated inputs such as sudden disturbances and sinusoidal variations; however, it will be shown in this paper that equivalent transfer operators can be determined from normal operating records of system inputs and outputs, without interrupting the performance of the system and without subjecting it to any unusual disturbances.

This paper deals only with linear systems; i.e., systems which have the property that the output resulting from the sum of two or more inputs is equal to the sum of the outputs due to each input acting alone. Hence the transfer operator for a linear system depends only on the characteristics of the system itself, and not on the form or magnitude of the system inputs. Such a characterization is not possible for nonlinear systems, but in practice, the characteristics of nonlinear systems can often be represented with sufficient accuracy for useful engineering results by linear approximations.

Since a transfer operator depends only on the characteristics of the system itself, all valid transfer operators for a given system must be equivalent representations of the system. Of the many possible forms of transfer operators, the following three are in common use:

1 The *differential operator*, $H(D)$, which is merely an abbreviated way of writing the differential equation of the system.

2 The *frequency-response*, $H(j\omega)$, which gives the attenuation and phase shift of the system in response to sinusoidal inputs.

3 The *impulse-response* or *weighting-function*, $h(t)$, giving the system output, as a function of time, when the input is a *unit impulse* as defined later.

The equivalence of these three transfer operators may be shown through the use of Fourier and Laplace transforms (1).[3]

The aim of this paper is to present some ideas which derive mainly from considerations of the impulse-response form of transfer operator. For this reason the following discussion will begin by presenting a limited and rather descriptive exposition of the concepts of "convolution" and "correlation." The implications of these methods will be compared with those of more conventional approaches in later paragraphs.

Convolution

An impulse may be thought of as the limiting case of a large pulse disturbance of very short duration. Thus the pulse shown in Fig. 1(a), with height $1/\Delta t$ and duration Δt, becomes an impulse as $\Delta t \to 0$. The strength of an impulse is defined as the area under the curve of pulse height versus time, and a unit impulse is one for which this area is equal to unity in a given set of units. Fig. 1(a) shows schematically a unit impulse as input to a typical control system, and Fig. 1(b) shows the corresponding output. While an impulse, strictly speaking, is only the limiting case of the pulse shown in Fig. 1(a) as $\Delta t \to 0$, an input with small but finite Δt and unit area gives an output which in practice is almost identical to the response from a true unit impulse.

For any linear system, the impulse response $h(t)$ is defined as the response of the system to a unit impulse starting at time $t = 0$. Since a unit impulse is the first derivative of a unit step, the impulse response of a system is the first derivative of its response to a unit step. It is evident that if the impulse response is known, the response of the system to an impulse of any other strength can be found by simple proportions, and the response to an impulse at any other time can be found simply by shifting the time scale. For computational purposes, $h(t)$ can be represented conveniently as a time (or number-in-time) sequence of rectangular areas, each equal in width to a time interval T sufficiently small so that the essential character of the response is retained. Thus the impulse response of Fig. 1(b) may be represented as in Fig. 1(c), and may be written in sequence form as

$$h(t) \cong \left[\frac{T}{2}\,h(0),\ Th(T),\ Th(2T),\ \ldots,\ Th(kT)\right]$$

$$\cong [h_0,\ h_1,\ h_2,\ \ldots,\ h_k] \quad [1]$$

The impulse response of any stable system becomes arbitrarily close to zero after a finite length of time; hence $h(t)$ for a stable system can always be approximated by a finite sequence of this form. In this sequence, the general term h_n is equal to T times

---

[1] Assistant Professor of Mechanical Engineering, Massachusetts Institute of Technology. Assoc. Mem. ASME.

[2] Assistant Professor of Mechanical Engineering, Massachusetts Institute of Technology. Mem. ASME.

Contributed by the Instruments and Regulators Division and presented at the Instruments and Regulators Division Conference, Ann Arbor, Mich., April 25–26, 1955, of The American Society of Mechanical Engineers.

Note: Statements and opinions advanced in papers are to be understood as individual expressions of their authors and not those of the Society. Manuscript received at ASME Headquarters, February 5, 1955. Paper No. 55—IRD-1.

[3] Numbers in parentheses refer to the Bibliography at the end of the paper.

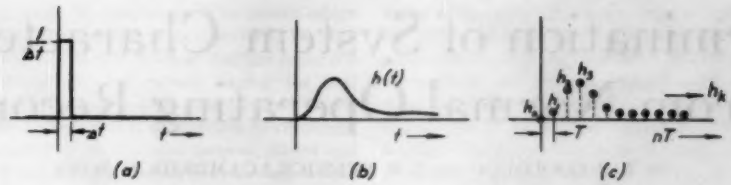

FIG. 1 TIME-SEQUENCE REPRESENTATION OF IMPULSE RESPONSE

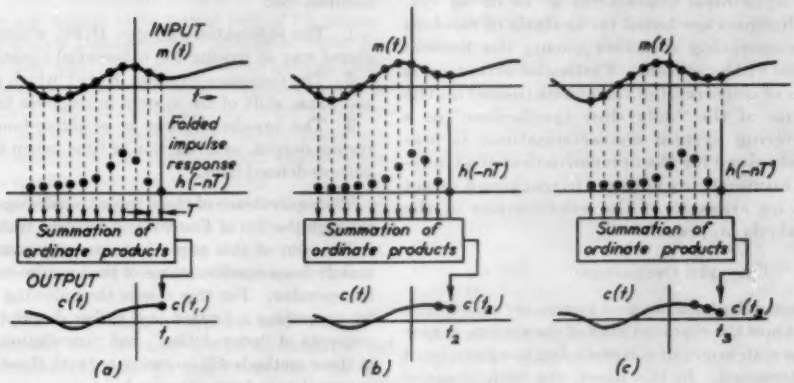

(a) Computation of output at t_1
(b) Computation of output at t_2
(c) Computation of output at t_3

FIG. 2 CONVOLUTION IN THE TIME DOMAIN

the response at time $(t + nT)$ to a unit impulse applied at time t.

To determine the response of the system to an arbitrary input $m(t)$, we may approximate $m(t)$ by a sequence of unit impulses, separated in time by the interval T, and each equal in strength to T times the corresponding ordinate of $m(t)$. Accordingly, the response $c(t)$ can be written in series form as the sum of the responses at time t due to individual past values of $m(t)$. Thus

$$c(t) = \sum_{n=0}^{k} h_n m(t - nT) = h_0 m(t) + h_1 m(t - nT) + h_2 m(t - 2T) + \ldots + h_k m(t - kT) \ldots [2]$$

so that, in particular

$$c(t_1) = \sum_{n=0}^{k} h_n m(t_1 - nT) = h_0 m(t_1) + h_1 m(t_1 - T) + h_2 m(t_1 - 2T) + \ldots + h_k m(t_1 - kT) \ldots [2a]$$

$$c(t_2) = \sum_{n=0}^{k} h_n m(t_2 - nT) = h_0 m(t_2) + h_1 m(t_2 - T) + h_2 m(t_2 - 2T) + \ldots + h_k m(t_2 - kT) \ldots [2b]$$

. . . . . .

$$c(t_i) = \sum_{n=0}^{k} h_n m(t_i - nT) = h_0 m(t_i) + h_1 m(t_i - T) + h_2 m(t_i - 2T) + \ldots + h_k m(t_i - kT) \ldots [2e]$$

In the process of computing $c(t)$ by this means, the impulse response is plotted backwards or "folded back" on the input (as shown in Fig. 2). For this reason the process is known as "folding" or convolution. Since the output at time t is essentially a weighted sum of past input values, the impulse response when used in convolution is often called a "weighting function."

Equation [2] can be made exact by letting $T \to 0$ and $k \to \infty$; it then becomes an integral known as the folding or convolution integral (1). Since the ideas to be presented in this paper do not depend on continuous representations, most equations which follow will be written only in series form.

The way in which the process of Equation [2] works may be further illustrated by considering a unit step input, Fig. 3. The coefficients of Equation [2] are seen to be the incremental heights in the approximated step response, so that the actual response will be produced when the input $m(t)$ is made a step. Since the operation represented by Equation [2] is entirely linear, it must produce the correct response $c(t)$ for any input $m(t)$.

It is significant that while the time-sequence form of the impulse response is defined in terms of discrete points in time, both the input and output are defined continuously. Fig. 2 indicates this, for no restriction is placed on the interval between t_1 and t_2, for which times the computation is illustrated.

Actual computational schemes based on these ideas have been proposed by many investigators including Tustin (2), Lewis (3), and Paynter (4). In most of these schemes the input and output, as well as the weighting function, are expressed as number sequences. Suitable interpolation functions are often added to allow solutions which are continuous in time.

Another interpretation of the convolution process is indicated by the block diagram in Fig. 4. Here the present value and past history of the input $m(t)$ are indicated as stored in a lumped delay line. This delay line is tapped at each of the lumped delay outputs where the value of each delayed input is multiplied by an appropriate constant (h_n) and then summed to produce the output $c(t)$. The process indicated in Fig. 4 is exactly that described in Equation [2] and indicated in Fig. 2. Not only is the block diagram of Fig. 4 useful for visualisation, but it also provides the basis for the actual design of an electronic-analog computing device called the "delay-line synthesizer." The use of this device in discovering weighting functions is described in the following.

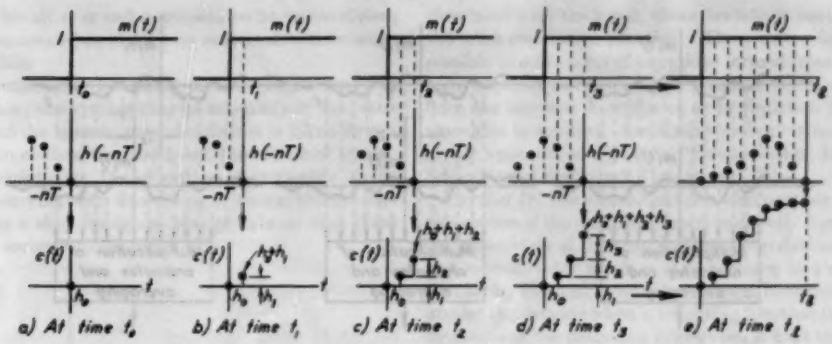

FIG. 3 DETERMINATION OF STEP RESPONSE USING WEIGHTING FUNCTION
(Incremental heights in approximated step response are seen to be the constants in Equation [2].)

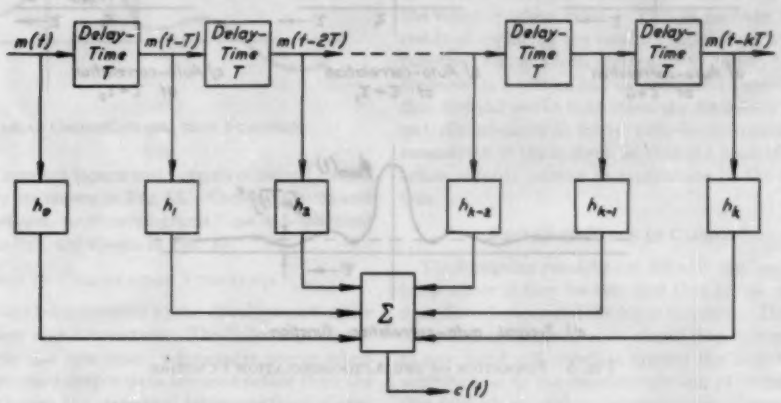

FIG. 4 BLOCK DIAGRAM OF CONVOLUTION

INVERSE CONVOLUTION

Discovery of Weighting Functions. A transfer operator for a linear system may be determined experimentally by subjecting the system to an artificially generated input disturbance such as an impulse, a step, or a series of sinusoids. But often it is not feasible to interrupt the operation of a process. A promising approach is that offered by the possibility of obtaining a weighting function from the randomly varying data recorded during actual operation.

While it is theoretically possible to obtain transfer operators directly from normal operating records, it will be shown how the process of obtaining weighting functions is greatly facilitated by the use of statistical correlation techniques (9). Theoretically, the frequency response could be obtained directly by performing a Fourier analysis of the sections of input and output records, but in practice it is difficult to analyze a section of records by Fourier methods because of the effects of noise and the spurious frequency components introduced at the cutoff points. Similarly, direct analysis to determine a weighting function is difficult because the output record is affected by inputs prior to the section of records under consideration. Thus, if an input is designated by a time sequence (m_0, m_1, $m_2 \ldots m_n$) and an output by its time sequence (c_0, c_1, c_2, $c_3 \ldots c_n$) it is possible to form a set of equations of the form of Equations [2*a*, *b* . . . . *l*]. Theoretically, it should be possible to solve such a set of equations for the unknown (h_0, h_1, $h_2 \ldots h_k$) which defines the weighting function. As indicated by Lewis (3), however, only the most accurate data in conjunction with rather simple transfer operators yield equations which are amenable to stable solutions. The presence of noise in data adds significantly to the difficulties in this process. These difficulties are largely eliminated when statistical correlations of data are used, rather than the data themselves. It will be shown that the correlation curves are related to each other in the same way as the original input and output records, but are devoid of certain spurious effects and have a more favorable shape. The result is a set of equations which is similar to Equation [2*a*, *b* . . . *l*] but is considerably more amenable to solution.

The statistical functions used in the present study are the autocorrelation of the system input and the cross correlation between input and output. By means of correlations, the essential information from a long record of random data is obtained in condensed form. The statistical approach assumes that the random variations in input are statistically stationary, that is, that their statistical properties do not change with time. This approach is useful not only when this assumption is strictly true, but also when the statistical properties of the system are changing much more slowly than its instantaneous random properties.

The autocorrelation of the input $m(t)$ is defined as the average value of the product of any two values of $m(t)$ separated by the time interval τ. Fig. 5 shows how the autocorrelation is determined at various time intervals. Using the symbol $\phi_{mm}(\tau)$ to denote autocorrelation, and a bar to denote averaging, we may write this definition as

$$\phi_{mm}(\tau) = \overline{m(t)m(t+\tau)}$$

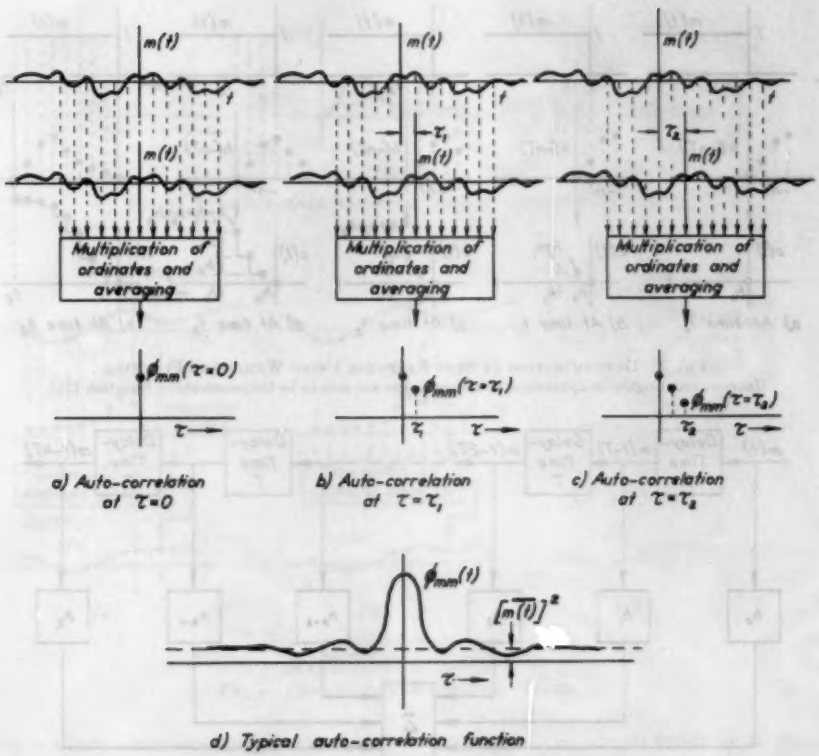

FIG. 5 FORMATION OF THE AUTOCORRELATION FUNCTION

Writing

$$m(t) = \overline{m(t)} + m'(t)$$

so that $m'(t)$ denotes the variation of $m(t)$ about its mean value, we may write

$$m(t+\tau) = \overline{m(t)} + m'(t+\tau)$$

since the assumption that $m(t)$ is statistically stationary makes $\overline{m(t+\tau)}$ equal to $\overline{m(t)}$. Substituting

$$\phi_{mm}(\tau) = [\overline{m(t)}]^2 + \overline{m'(t)m'(t+\tau)}$$

since by definition

$$\overline{m'(t)} = \overline{m'(t+\tau)} = 0$$

Evidently $[\overline{m(t)}]^2$ is a d-c component of $\phi_{mm}(\tau)$ which we may remove without losing any essential information; therefore we consider

$$\phi'_{mm}(\tau) = \phi_{mm}(\tau) - [\overline{m(t)}]^2 = \overline{m'(t)m'(t+\tau)}$$

When the time interval τ is zero, we have

$$\phi_{mm}(0) = [\overline{m'(t)}]^2 = \text{mean-square value of } m'(t)$$

For a nonzero time interval τ, the magnitude of $\phi'_{mm}(\tau)$ is a measure of how closely one could predict $m'(t+\tau)$ from a knowledge of $m'(t)$. For small τ, if $m(t)$ is changing slowly, $m'(t+\tau)$ remains in the vicinity of $m'(t)$, and $\phi'_{mm}(\tau)$ is nearly equal to $\phi'_{mm}(0)$, which is its maximum possible value. For larger τ, or if $m'(t)$ is changing more rapidly, $\phi'_{mm}(\tau)$ will be smaller. If τ becomes infinite, then $m'(t+\tau)$ cannot be predicted at al from a knowledge of $m'(t)$, and for any $m'(t)$, $m'(t+\tau)$ is as likely to have a given negative value as it is to have the corresponding positive value, so that $\phi'_{mm}(\tau)$ must approach zero as $\tau \to \infty$. Thus $\phi'_{mm}(\tau)$ is a curve which has a peak at $\tau = 0$ and becomes asymptotic to the horizontal axis as $\tau \to \pm\infty$. If $m'(t)$ is composed primarily of low-frequency fluctuations, the peak is wider than if $m'(t)$ has primarily high-frequency fluctuations. If $m'(t)$ contains all frequencies equally ("white noise"), then there is no connection between the value of $m'(t)$ at one instant and its value at any other instant, and $\phi_{mm}(\tau)$ becomes an impulse. Because of the assumption that $m'(t)$ is statistically stationary

$$\phi'_{mm}(-\tau) = \overline{m'(t)m'(t-\tau)} = \overline{m'(t+\tau)m'(t)} = \phi'_{mm}(\tau)$$

Hence the curve of $\phi'_{mm}(\tau)$ is symmetrical about the vertical axis.

The cross correlation of the input $m(t)$ with the output $c(t)$ is defined as the average value of the product of the value of $m(t)$ at any given time with the value of $c(t)$ at a time τ seconds later. The process of forming the cross correlation is similar to that shown in Fig. 5, except that the lower curve is now the output $c(t)$. The cross-correlation function which results is no longer symmetrical about the $\tau = 0$ axis. Fig. 6 shows a typical cross-correlation curve. Using the symbol $\phi_{mc}(\tau)$ for cross correlation, we may write this definition as

$$\phi_{mc}(\tau) = \overline{m(t)c(t+\tau)}$$

As in the case of autocorrelation, we may remove the d-c component so that

$$\phi'_{mc}(\tau) = \phi_{mc}(\tau) - \overline{m(t)}\ \overline{c(t)} = \overline{m'(t)c'(t+\tau)}$$

If $\phi'_{mc}(\tau) = 0$ for all τ, m and c are said to be uncorrelated; this is ordinarily the case when there is no causal relation between two random variables.

For statistically stationary functions, these average values will not change with time; the average may be taken at any time during the operation of the system, provided that it is taken over a long enough section of data to smooth out the effects of instantaneous random variations. If the statistical properties of the inputs are slowly varying with time, then of course the average must be taken over a *short* enough section of data so that these variations are not covered up.

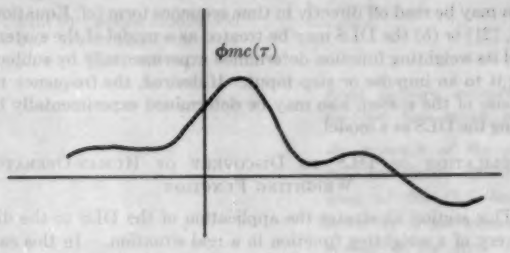

FIG. 6 A TYPICAL CROSS-CORRELATION FUNCTION

Typical sections of random inputs and outputs obtained from a human-operator study are shown in Fig. 11. Curves of auto and cross-correlation functions, or "correlograms," as the physical plots are sometimes called, are shown in Fig. 12.

APPLICATION OF CORRELATION FUNCTIONS

The foregoing text has been devoted to the development of the concepts of convolution and correlation. The following discussion will show in particular how many advantages accrue when the correlations of input and output data are used rather than the data themselves. Although the statistical interpretations of correlations are significant, it is not necessary here to understand any more than the definitions of the functions. Their use in this discussion is justified mainly by the results which follow.

Of fundamental importance is the fact that the correlation functions in τ are related by a weighting function in τ which is identical to the weighting function in t which relates the actual input-output data. This may be shown in the following where Equation [2] is repeated

$$c(t) = \sum_{n=0}^{k} h_n m(t - nT) \quad \ldots\ldots\ldots\ldots\ldots\ldots [2]$$

Correlation functions of each side of Equation [2] may be formed by correlating each side with the input $m(t)$. Since correlation is a linear operation, Equation [3] is valid by superposition

$$\overline{m(t)c(t+\tau)} = \sum_{n=0}^{k} h_n \overline{m(t)m(t+\tau-nT)}$$

$$\phi_{mc}(\tau) = \sum_{n=0}^{k} h_n \phi_{mm}(\tau - nT) \quad \ldots\ldots\ldots\ldots [3]$$

Equation [3] shows that $\phi_{mc}(\tau)$ is related to $\phi_{mm}(\tau)$ by the same transfer operator, h_n, as are $c(t)$ and $m(t)$. That t is replaced by τ in the process is not important since each would be measured in the same units.

Having established that the correlation functions may be used in place of the actual data, the advantages of so doing will be considered. When the system output data contain deviations (noise) which are not caused by the input and are therefore not correlated with the input, these deviations contribute nothing to the cross-correlation function. Thus, where noise makes it impossible to solve a set of equations formed from the original data as in Equations [2*a*, *b* . . . *l*], a similar set of equations formed from the correlation ordinates as in Equation [3] is much more amenable to solution. Levinson lucidly illustrates this technique in his appendix to Wiener's "Extrapolation, Interpolation, and Smoothing of Stationary Time Series" (5).

Paynter (6) has shown that it is also possible to obtain certain parameters of the weighting function directly from the corresponding parameters of the auto and cross correlations.

A second factor which is of importance in a solution of Equation [3] by classical means (e.g., matrix inversion) but which is of utmost importance when a weighting function is to be discovered by means of the delay-line synthesizer is that the autocorrelation $\phi'_{mm}(t)$ always exhibits a central peak, and approaches zero in both the plus and minus time directions, Fig. 5. In fact, as mentioned before, the autocorrelation becomes an impulse when the input is white noise. This is perhaps the most significant result of replacing the random input data by its autocorrelation function, for, in effect, one is able to "apply" a near pulselike disturbance to a system and determine its noise-free response. Thus this method works best when the frequency spectrum of the input disturbances is fairly wide in comparison to the frequency bandwidth of the system, so that the peak of the input autocorrelation is fairly narrow in comparison to the time lags of the system.

EFFECT OF NOISE IN CLOSED-LOOP SYSTEMS

The foregoing remarks are directly applicable in open-loop systems where it may be assumed that no correlation between random disturbances and the input can exist. However, when a feedback loop is involved as in closed-loop systems, noise introduced at any point will circulate around the loop and actually make a contribution to the cross correlation of output with input. It is this fact which makes determination of transfer operators using frequency-spectrum analysis extremely difficult, if not impossible. This problem appears in the representation of correlations as functions of time, but fortunately in a different way, for it can be shown that because of the causal paths in closed-loop systems, the effect of noise on the cross-correlation function is confined almost solely to the region of negative τ. This is indicated in Fig. 7. Equation [3] is applicable even for closed-loop systems if it is restricted to apply only in a region to the right of $\tau = 0$ in the correlogram. Actually, the effect of noise can extend a short distance A into the positive τ-region, and it is not easy to define exactly where Equation [3] becomes valid. However, this distance usually may be approximated and then checked in the light of final results. A complete discussion of the effect of noise in closed-loop systems appears in Appendix 1.

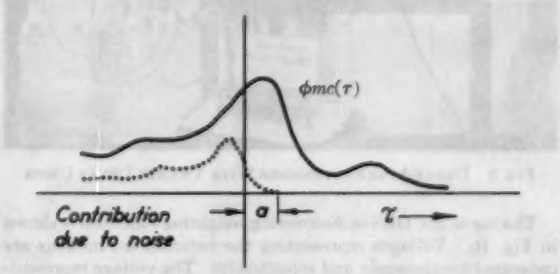

FIG. 7 EFFECT OF NOISE ON CROSS CORRELATION IN A CLOSED-LOOP SYSTEM

Use of Delay-Line Synthesizer in Weighting-Function Determination

A new analog computing device called the delay-line synthesizer (DLS) (7) has proved to be very effective in "solving" for the best linear weighting function to relate a given pair of correlations, or correlograms. The delay-line synthesizer (DLS) operates on voltages in precisely the manner indicated by Equation [2]. This operation is indicated in the block diagram shown previously in Fig. 4. In the actual DLS, interpolation is introduced by using lumped delays which are not "perfect," so that the reponse to a pulse at the input of the delay line appears at certain of the tapped points as indicated in Fig. 8. (If the delay were perfect, the responses would merely be sharp impulses delayed in time.) A photograph of the DLS developed at the Dynamic Analysis and Control Laboratory of M.I.T. appears in Fig. 9.

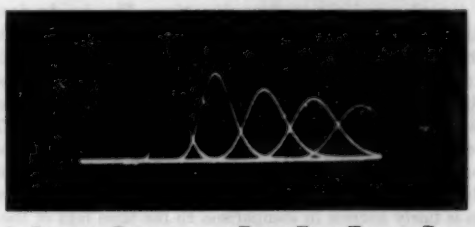

Fig. 8 Impulse Response at First Five Tapped Points of Delay Line

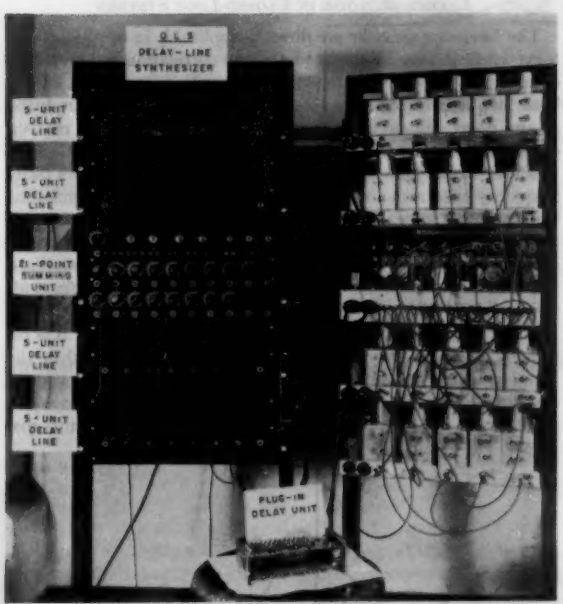

Fig. 9 Delay-Line Synthesizer With Twenty Delay Units

The use of the DLS in discovering weighting functions is shown in Fig. 10. Voltages representing the correlation functions are generated continuously and repetitively. The voltage representing the autocorrelation is introduced into the DLS, while the output of the DLS is compared with the voltage representing the cross correlation. The very significant factor in the operation is that each knob has a strong effect at a certain point in time on a repetitively displayed difference function. This results from the fact that the DLS is performing convolution on an input which has a characteristic peak. This peak, as has been shown previously, becomes more nearly an impulse as the actual input data become more nearly white noise. The process of convergence or error reduction is made rapid and straightforward by the localized-in-time effect of the DLS knob adjustments.

Another factor of great importance in the success of this technique is that the error reduction is being done by a human being who can continuously exercise judgment as to the validity of his error criterion. Thus he can arrive at a best answer independent of any formal criterion. When the DLS coefficients have been adjusted to an optimum solution, the weighting function may be determined in one of two ways: Either (*a*) the weighting function may be read off directly in time sequence form (cf. Equations [1], [2]) or (*b*) the DLS may be treated as a model of the system, and its weighting function determined experimentally by subjecting it to an impulse or step input. If desired, the frequency response of the system also may be determined experimentally by using the DLS as a model.

Application of DLS to Discovery of Human-Operator Weighting Function

This section illustrates the application of the DLS to the discovery of a weighting function in a real situation. In this case the transfer operator to be discovered is that which represents a human being when engaged in tracking a target. Random techniques are particularly significant in such studies, for tests on human beings must completely preclude the possibility of prediction based on learning. The use of frequency analysis is not possible for the reason that a person will quickly recognize the consistency in the input.

Interest in the human-operator problem was stimulated by Prof. Arnold Tustin of the University of Birmingham, England, who suggested the application of the delay-line synthesizer to the study of some tracking records which he had brought with him from England. His experimental setup from which data were obtained consisted of a movable handle unit whose output was integrated once and then made to position a mechanical pointer. A second pointer, located next to the handle-driven pointer, was given an input motion consisting of a number of sinusoidal components of a nature sufficiently involved to prevent anticipation by an operator. The operator, upon noticing an error or difference between the two pointers, was required to move the handle in such a way as to reduce this error to a minimum value. In doing this he moved his whole forearm from the elbow. Three quantities were recorded, namely, velocity of the handle, error, and handle position. A portion of this record is reproduced in Fig. 11. The operator responsible for this record had received about 8 hr of training and had reached a plateau of learning at which his average error was $^1/_8$ of its beginning value.

In addition to this record obtained at the University of Birmingham, Professor Tustin supplied a plot of the autocorrelation and cross-correlation functions which are shown in Fig. 12. A block diagram of the experimental setup used appears in Fig. 13, which is drawn in terms of a velocity output. The possibility of random variations or noise entering into the records is included. This noise is shown as adding to the handle motion. The possibility of the noise being acted upon by some sort of filter or dynamics and therefore becoming "colored" is indicated in the figure. The randomness may be visualized as originating within the body but away from the hand and, therefore, being acted upon by the arm dynamics before adding to the handle motion. The effect of this noise is felt around the entire loop, thus rendering the system impossible to analyze by Fourier methods.

The weighting function is determined by means of a DLS. A portion of the autocorrelation curve is synthesized by a function generator. The early part of this curve is not synthesized

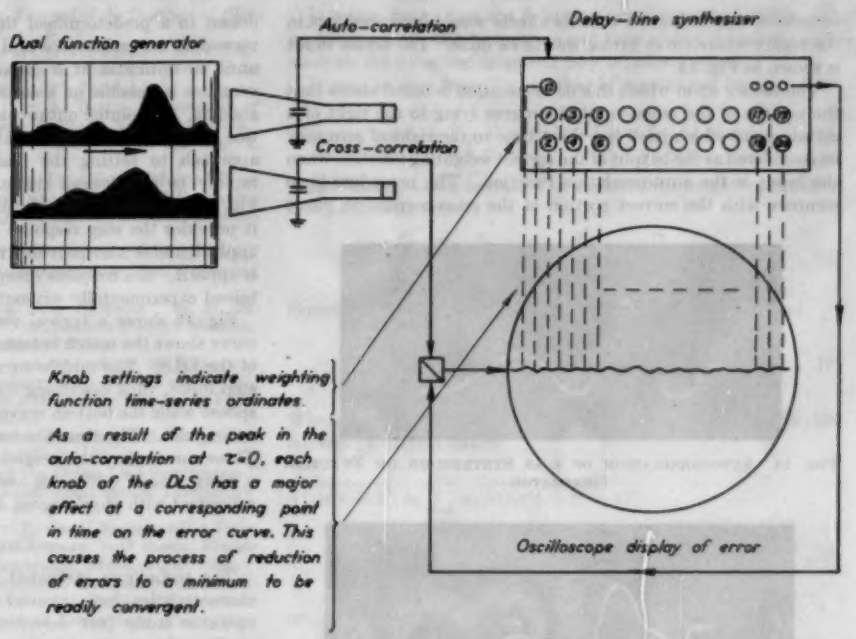
Dual function generator
Auto-correlation
Delay-line synthesizer
Cross-correlation
Knob settings indicate weighting function time-series ordinates.
As a result of the peak in the auto-correlation at τ=0, each knob of the DLS has a major effect at a corresponding point in time on the error curve. This causes the process of reduction of errors to a minimum to be readily convergent.
Oscilloscope display of error

FIG. 10 BLOCK SCHEMATIC OF WEIGHTING-FUNCTION DISCOVERY

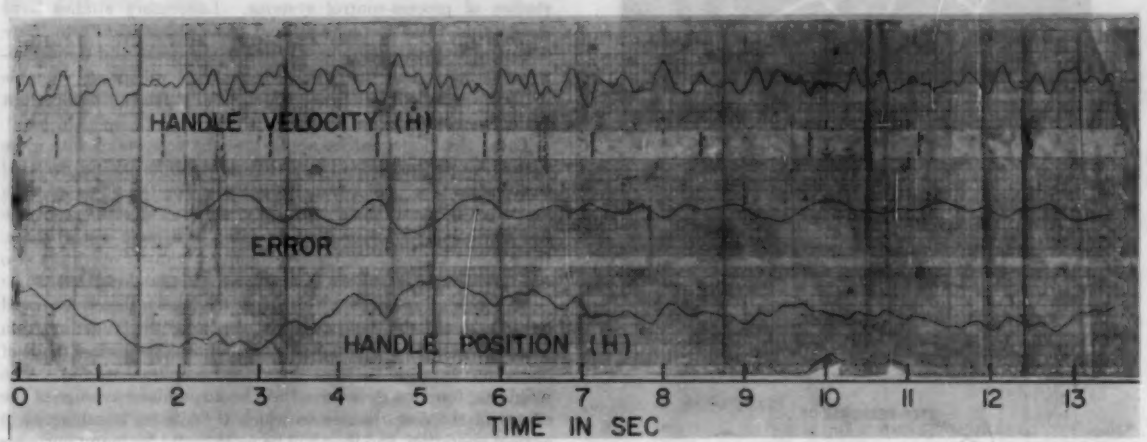

FIG. 11 TRACKING RECORD OBTAINED AT UNIVERSITY OF BIRMINGHAM

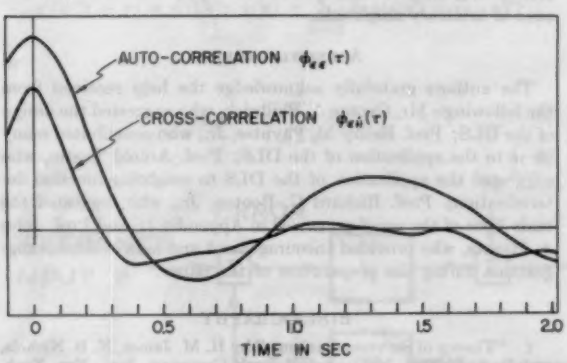

FIG. 12 AUTO AND CROSS CORRELATIONS OF INPUT ERROR AND HANDLE VELOCITY OBTAINED AT UNIVERSITY OF BIRMINGHAM

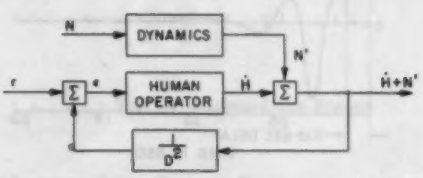

FIG. 13 BLOCK DIAGRAM OF EXPERIMENTAL SETUP FOR TRACKING RECORDS

because it was estimated that its effects would have died out in the region where curve fitting was to be done. The actual input is shown in Fig. 14.

The theory upon which this determination is based states that the portion of the cross-correlation curve lying to the right of a certain point which itself is a short time to the right of zero may be considered as the output of the correct weighting function when the input is the autocorrelation function. The procedure is to compare with the correct portion of the cross-correlation curve

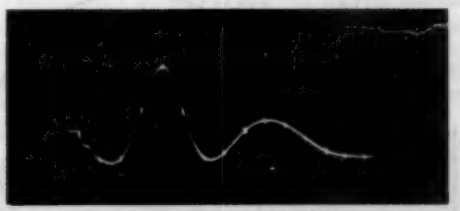

FIG. 14 AUTOCORRELATION OF ϵ AS SYNTHESIZED ON FUNCTION GENERATOR

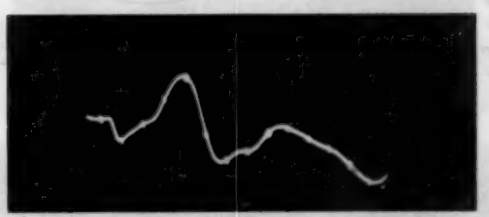

FIG. 15 CROSS-CORRELATION CURVE OBTAINED FROM DLS

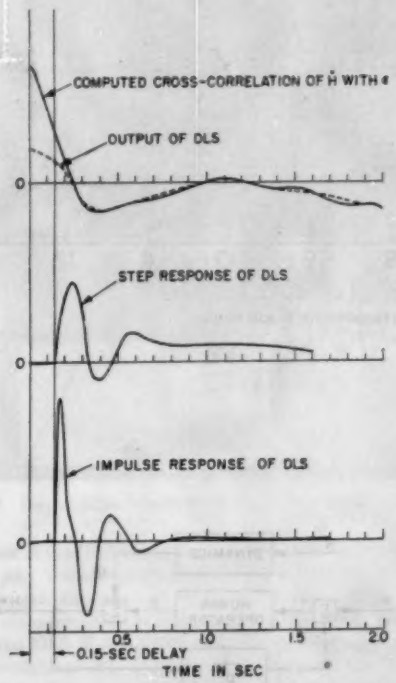

FIG. 16 RESULTS OF A TYPICAL TEST, SHOWING AGREEMENT BETWEEN CROSS CORRELATIONS COMPUTED AND OBTAINED FROM THE DLS

drawn to a predetermined time scale the output of a DLS as viewed on an oscilloscope and to adjust the settings of the DLS until an optimum fit is obtained. With the DLS, rapid convergence is possible on a sequence of dial settings which gives a good fit. As pointed out previously, the form of the autocorrelation curve with its high central peak permits a simple, systematic approach to setting the dials so that the output converges rapidly to the desired shape. An actual output is shown in Fig. 15. An advantage of using the DLS is that once adjusted, it provides the step response immediately when a step input is applied, and it also provides the impulse response when a pulse is applied. If a frequency response is desired, it also may be obtained experimentally without difficulty.

Fig. 16 shows a typical result of the experiments. The top curve shows the match between the desired curve and the output of the DLS. The middle curve is the response of the DLS to a step input, thus describing the weighting function as a step response while the bottom curve shows the response of the DLS to an impulse. The time abscissa has been presented in true time. These curves show the weighting function which is obtained when a delay time of 0.15 sec is assumed. This value of delay time is consistent with physiological data.

CONCLUSION

The techniques presented here for determination of system characteristics have proved their usefulness in the human-operator study just described, and are now being applied in studies of process-control systems. Laboratory studies have shown that these techniques yield transfer operators which are comparable to those obtained from step-response and frequency-response measurements. These techniques will prove valuable in a wide range of problems in which it is not feasible to interrupt the normal operation of a system.

These techniques can be applied readily to systems with more than one input, provided that the various inputs are uncorrelated with each other. The transfer operator for the effect of each input can be determined separately, since all inputs except the one which is of interest can be treated as system disturbances. By a recent extension of these techniques, transfer operators also can be obtained when the inputs are mutually correlated (8).

Although all remarks in this paper have been directed toward linear systems, the determination of a weighting function from data obtained from a nonlinear system during its normal mode of operation appears to have important implications (8). The weighting function determined will be a combined average of the effects of the disturbances to which the system is subjected in normal operation, and thus will be more useful for many purposes than a weighting function based on a single pulse or step disturbance of arbitrary amplitude.

ACKNOWLEDGMENTS

The authors gratefully acknowledge the help received from the following: Mr. George A. Philbrick, who suggested the design of the DLS; Prof. Henry M. Paynter, Jr., who contributed many ideas to the application of the DLS; Prof. Arnold Tustin, who suggested the application of the DLS to weighting-function determination; Prof. Richard C. Booton, Jr., who suggested the main lines of the proof presented in Appendix 1; and Prof. John A. Hrones, who provided encouragement and many valuable suggestions during the preparation of the paper.

BIBLIOGRAPHY

1 "Theory of Servomechanisms," by H. M. James, N. B. Nichols, and R. S. Phillips, McGraw-Hill Book Company, Inc., New York, N. Y., 1947, chapter 2.

2 "A Method of Analyzing the Behavior of Linear Systems in

Terms of Time Series," by A. Tustin, *Journal of the Institute of Electrical Engineers*, vol. 94, 1947, Pt II-A, n1, p. 130.

"A Method of Analysing the Effect of Certain Kinds of Nonlinearity in Closed-Cycle Control Systems," by A. Tustin, *Journal of the Institute of Electrical Engineers*, vol. 94, 1947, Pt II-A, n1.

"Automatic and Manual Control," by A. Tustin, Proceedings of the Cranfield Conference—1951, Academic Press, New York, N. Y., 1952. See papers by Jones, Smith, Brown, Sartorius, Oldenbourg, and Oppelt.

3 "Waveform Computations by the Time-Series Method," by N. W. Lewis, Proceedings of the Institution of Electrical Engineers, part 3, *Radio and Communication Engineering*, vol. 99, n61, September, 1952.

4 "Methods and Results From MIT Studies in Unsteady Flow," by H. M. Paynter, *Journal of the Boston Society of Civil Engineers*, vol. 39, n2, April, 1952.

"Practical Computation of Closed Loop Systems," by H. M. Paynter, talk given before the AIEE, Northeastern District Meeting, session of Industrial Process Control, May, 1953.

5 "Extrapolation, Interpolation, and Smoothing of Stationary Time Series," by N. Wiener, Technology Press, New York, N. Y., 1950. (See Appendix B, "The Wiener RMS Error Criterion in Filter Design and Prediction," by N. Levinson.)

6 "On an Analogy Between Stochastic Processes and Certain Dynamic Systems," by H. M. Paynter (forthcoming).

7 "The Design and Application of the Delay Line Synthesizer," by J. B. Reswick, ScD thesis, Massachusetts Institute of Technology, Cambridge, Mass., June, 1954.

8 "Experimental Determination of System Characteristics From Correlation Measurements," by T. P. Goodman, ScD thesis, Massachusetts Institute of Technology, Cambridge, Mass., June, 1955.

9 "Application of Statistical Methods to Communication Problems," by Y. W. Lee, Technical Report No. 181, Research Laboratory of Electronics, Massachusetts Institute of Technology, Cambridge, Mass., September 1, 1950.

Appendix 1

Effect of Noise in Closed-Loop Systems

Consider the rather simple situation indicated in Fig. 17. Here the effects of random disturbances N are taken as added into the output c of a plant which is under automatic control. Inspection of Fig. 17 gives

$$c'(t) = N(t) + c(t) \quad [4]$$

which may be interpreted in terms of convolution in series form by the following equation, where $h(t)$ is a weighting function

$$c'(t) = N(t) + \sum_{n=0}^{k} h_n \epsilon(t - nT) \quad [5]$$

Each term of Equation [5] may be correlated with the input t

$$\overline{\epsilon(t)c'(t+\tau)} = \overline{\epsilon(t)N(t+\tau)} + \sum_{n=0}^{k} h_n \overline{\epsilon(t)\epsilon(t+\tau-nT)}$$

or

$$\phi_{\epsilon c'}(\tau) = \phi_{\epsilon N}(\tau) + \sum_{n=0}^{k} h_n \phi_{\epsilon\epsilon}(\tau - nT) \quad [6]$$

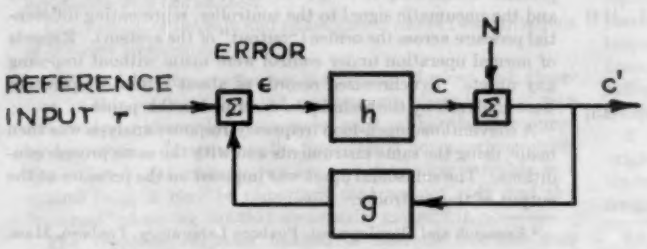

Fig. 17 Closed-Loop System

It is significant that the following proof is made possible only by using convolution techniques and their ability to include in an analysis the direction or causal flow of information.

It may be seen from Fig. 17 that in operational form

$$\epsilon(t) = \left[\frac{1}{1+hg}\right] r(t) - \left[\frac{g}{1+hg}\right] N(t) \quad [7]$$

Let the bracketed operators be replaced by weighting-function designations as follows

$$\left[\frac{1}{1+hg}\right] \equiv a(t) \quad \left[\frac{g}{1+hg}\right] \equiv b(t) \quad [8]$$

Equation [7] may be now written in terms of time series as

$$\epsilon(t) = \sum_{l=0}^{k_1} a_l r(t - lT) - \sum_{m=0}^{k_2} b_m N(t - mT) \quad [9]$$

When each term of Equation [9] is correlated with the noise, the following equation results

$$\overline{N(t)\epsilon(t+\tau)} = \sum_{l=0}^{k_1} a_l \overline{N(t)r(t+\tau-lT)} - \sum_{m=0}^{k_2} b_m \overline{N(t)N(t+\tau-mT)}$$

or

$$\phi_{N\epsilon} = \sum_{l=0}^{k_1} a_l \phi_{Nr}(\tau - lT) - \sum_{m=0}^{k_2} b_m \phi_{NN}(\tau - mT) \quad [10]$$

Since there is assumed to be no correlation between the noise and the reference variable $r(t)$, $\phi_{Nr} = 0$, and the following equation results

$$\phi_{N\epsilon}(\tau) = -\sum_{m=0}^{k_2} b_m \phi_{NN}(\tau - mT) \quad [11]$$

The right-hand side of Equation [11] is seen to be the convolution of the autocorrelation of the noise with the "backward" weighting function $b(t)$ of the closed loop. If the noise is white, ϕ_{NN} is an impulse in τ. $\phi_{N\epsilon}$ would then appear as an impulse response as in Fig. 18. When $N(t)$ is not white, its autocorrelation becomes less like an impulse and Equation [11] might be interpreted as in Fig. 19. The "response" $\phi_{N\epsilon}(\tau)$ is seen to begin a short distance (in time) A to the left of $\tau = 0$.

Returning to Equation [6], it is seen that the noise correlation appears as $\phi_{\epsilon N}$ and not $\phi_{N\epsilon}$. Equation [12] may be derived similarly to Equation [11]

$$\phi_{\epsilon N} = -\sum_{n=0}^{k_2} b_m \phi_{NN}(\tau + mT) \quad [12]$$

Equation [12] describes an "impulse" response identical to that of Equation [11] with the exception that it is "swung around" into

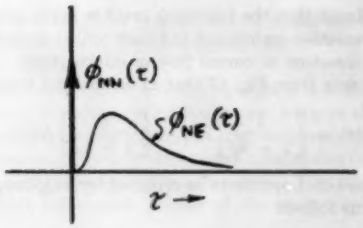

FIG. 18 INTERPRETATION OF EQUATION [11] FOR $N(t)$ WHITE

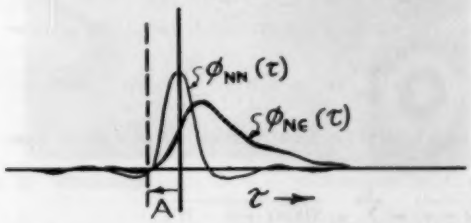

FIG. 19 INTERPRETATION OF EQUATION [11] FOR $N(t)$ NOT WHITE

the negative side of the axis. Thus the mirror image of Fig. 19, as shown in Fig. 20, applies to Equation [12]. Returning again to Equation [6], it is now seen that the effect of $\phi_{eN}(\tau)$ is confined mainly to the region of negative τ in the $\phi_{ec'}$ correlogram, extending only a distance A to the right of $\tau = 0$. The components of Equation [6] may then be pictured as in Fig. 21. In the region to the right in Fig. 21, Equation [6] reduces to

$$\phi_{ec'}(\tau) = \sum_{n=0}^{k} h_n \phi_{ec}(\tau - nT) \quad \ldots\ldots\ldots\ldots [13]$$

which is identical in form to Equation [3], and thus readily susceptible to analysis by DLS methods.

The a priori determination of the distance A probably is not possible, but intuition may provide an effective working assumption. Any given assumption may be checked once a form of $h(t)$ is discovered.

Appendix 2

CALCULATION OF CORRELATIONS

Of the various possible devices for computing auto and cross correlations, the most convenient has been found to be an automatic digital computer. This is primarily because of the diverse forms in which data are continuously recorded. A large number of closely spaced ordinates of $m(t)$ and $c(t)$ are recorded; then the correlations may be computed in the following form

$$\phi_{mm}(nT) = \overline{m_i m_{n+i}} \approx \frac{1}{N+1} [m_0 m_n + m_1 m_{n+1} + m_2 m_{n+2} + \ldots + m_N m_{n+N}] \ldots [14]$$

$$\phi_{mc}(nT) = \overline{m_i c_{n+i}} \approx \frac{1}{N+1} [m_0 c_n + m_1 c_{n+1} + m_2 c_{n+2} + \ldots + m_N c_{n+N}] \ldots [15]$$

where

$m_0, m_1, m_2, \ldots, m_{N+n}$ = successive ordinates of $m(t)$
$c_0, c_1, c_2, \ldots, c_{N+n}$ = successive ordinates of $c(t)$
$n = 0, 1, 2, 3, \ldots$

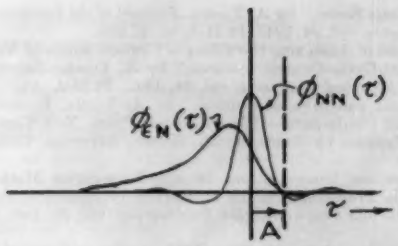

FIG. 20 INTERPRETATION OF EQUATION [12] FOR $N(t)$ NOT WHITE

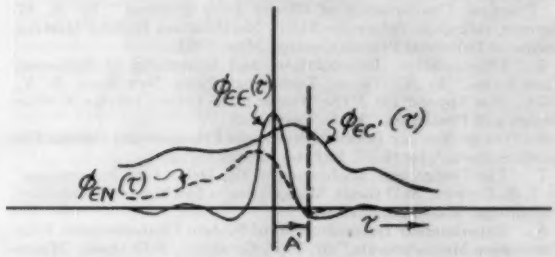

FIG. 21 INTERPRETATION OF EQUATION [6] SHOWING EFFECT OF NOISE ON $\phi_{ec'}(\tau)$

These operations can be performed readily on standard computing machines.

Since Equation [3] was derived by performing identical operations on the left and right sides of Equation [2], Equation [3] is valid only if auto and cross correlations are both computed in exactly the same way.

If $m(t)$ is statistically stationary and if N is large, then $\phi_{mm}(\tau)$ is symmetrical about the vertical axis, so that $\phi_{mm}(-nT) = \phi_{mm}(nT)$. If $m(t)$ is not statistically stationary, or if N is not large, Equation [3] is still valid, but $\phi_{mm}(\tau)$ may no longer be exactly symmetrical about the vertical axis.

Discussion

A. R. CATHERON[4] and B. D. HAINSWORTH.[4] We have tried the method of analysis proposed in this paper on an actual flow process, and we are encouraged by the results of the test.

The test process—physically located in the Research Laboratory of the writers' company—is a 2-in. water-flow line, 140 ft in length, supplied from a head tank under controlled air pressure and discharging submerged in a sump. The test flow rate was about 70 gpm. A standard proportional-plus-reset pneumatic controller controls the rate of flow, as measured by a pneumatic dry differential-pressure transmitter. The rate of flow also was measured by a magnetic flowmeter. The setup is shown diagrammatically in Fig. 22.

For these tests a multichannel, high-speed recorder showed the pressure at the output of the controller ("input" to the system) and the pneumatic signal to the controller, representing differential pressure across the orifice ("output" of the system). Records of normal operation under control were made without imposing any upsets. Synchronized records of about 2 min of operation were analyzed by the techniques described in this paper.

A conventional open-loop frequency-response analysis was then made, using the same instruments and with the same process conditions. The sinusoidal upset was imposed on the pressure at the output of the controller.

[4] Research and Development, Foxboro Laboratory, Foxboro, Mass.

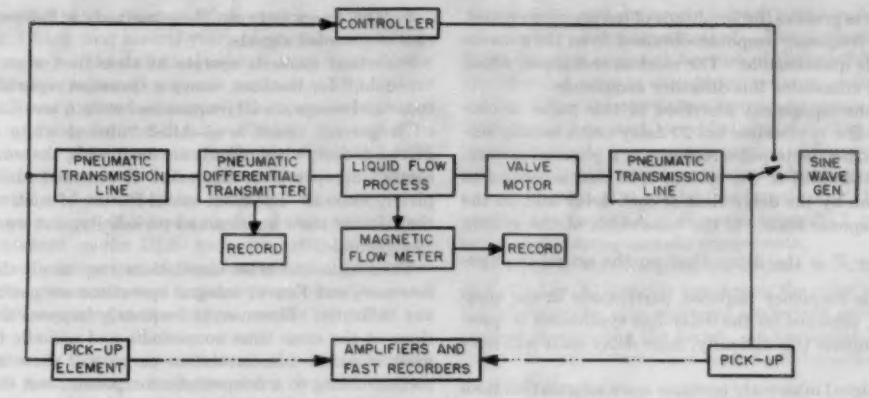

FIG. 22 TEST SETUP FOR STUDYING FLOW PROCESSES

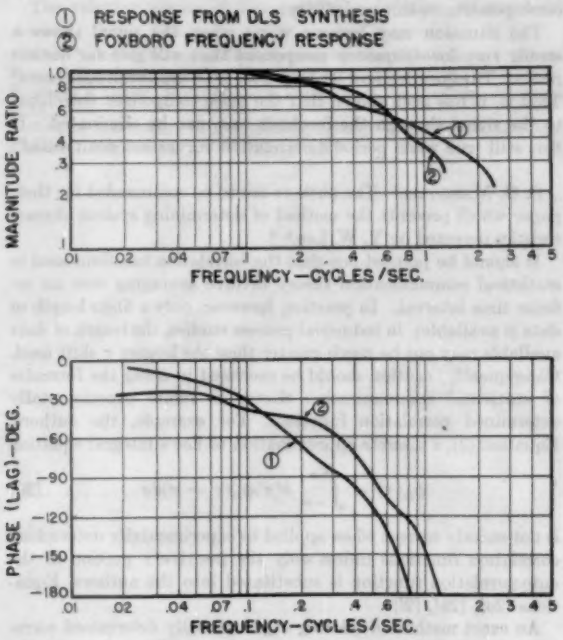

FIG. 23 FOXBORO LABORATORY FLOW SYSTEM

The curves of the Bode diagram, Fig. 23, show how the two methods describe the response of the system.

We accepted the frequency-response data as the standard for comparison because of our several years of successful, practical experience with the method.

Comparison of the gain and phase curves shows two limitations of the new techniques:

1 The delay-line synthesizer is a "linear" device; and, therefore, in this service it does not measure any phase lag that does not disappear at very low frequencies, such as phase lag introduced by hysteresis. In some applications this is not a serious objection. But if, for example, we are trying to locate trouble in a control loop, it may be important that we not only find this "residual" phase lag but that we actually measure it.

The frequency-response method of analysis tolerates nonlinearity in the system sufficiently so that the curves are directly useful in industrial work. The DLS method, on the other hand, eliminates dead time and other nonlinearity in the processing of the data. We feel that the main problem of putting this method to industrial use is the development of compensations for nonlinearities in the system under study.

2 The synthesized response curve is not reliable at high frequencies. In this test the gain curve did not show enough attenuation, and the phase lag appeared to be too great at frequencies above 0.6 cycle per sec, less than two octaves above the "break" frequency.

We hope that both these limitations are imposed by the present equipment, and that they are not limitations of the method.

The technique is certainly very promising, particularly in that the data can be obtained without subjecting the process under test to any artificial disturbances.

We do not feel that this technique is ready yet for universal unconfirmed use because the observed differences from the frequency-response data are greater than would be acceptable if appearing in consecutive frequency-response runs, but the potential value of the method seems so great as to justify a great deal of effort to develop the method still further.

C. M. CHANG.[5] The application of statistical analysis, which originates in electric communication theory, to the problem of determining system characteristics seems to be of great practical importance. Experimental results obtained so far as described in the paper are very promising in spite of the fact that the capabilities of the equipments used were limited.

Several points seem to be worth mentioning in connection with the technique.

1 The present technique yields a linear system function when in fact the system under consideration may be nonlinear. A linear representation is hence forced upon a nonlinear system. While previous experience with the conventional technique of measuring frequency response sometimes enables one to estimate the nonlinearity in the system with the conventional data obtained, sufficient experience has to be accumulated in using the random technique to do likewise.

2 In the conventional frequency-response technique, noise originating in the signal, in the system, or at any point in the transmission line often obscures the meaning of the data. At high frequencies, when the signal is greatly attenuated, the noise

[5] Sylvania Electric Products, Inc., Woburn, Mass.

amplitude may be as great as the amplitude of the proper response. In such cases the frequency response obtained from the conventional technique is questionable. The random technique, which works with noise, eliminates this difficulty completely.

3 So far as the equipment described in this paper is concerned, the delay-line synthesizer has 20 delay units, usually sufficient to characterize the impulse response of a physical system. The maximum bandwidth of the system is limited according to Shannon's criterion by the delay time of each delay unit on the actual impulse-response scale. If the bandwidth of the system exceeds $\frac{1}{2T'}$, where T is the delay time on the actual impulse-response scale, the frequency response, particularly in the high-frequency region, obtained on the delay-line synthesizer is questionable. To eliminate this difficulty, more delay units will have to be used.

4 A random signal inherently contains more information than a sinusoidal signal. The problem is how to get the information out. The correlation technique described in this paper uses part of the information in a random signal. It is of interest to consider the possibility of how more of the information contained can be analyzed.

J. M. Loeb.[6] The writer will comment on two quotations given by the author during his verbal presentation.

1 "Extrapolation, Interpolation, and Smoothing of Stationary Time Series," by N. Wiener (reference 5 of the paper). Equation [3] of the paper must be written

$$\phi_{mc}(\tau) = \int_0^\infty h(\theta)\phi_{mm}(\tau - \theta)d\theta \quad [16]$$

where $h(\theta)$ is the continuous weighting function not yet "quantized." This equation must be derived from

$$c(t) = \int_0^\infty h(\theta)m(t - \theta)d\theta \quad [17]$$

and

$$\phi_{mc}(\tau) = \lim_{T \to \infty} \frac{1}{T} \int_{-T}^{+T} m(t + \tau)\, c(t)dt \quad [18]$$

Equation [18] herewith will result from substitution of $c(t)$ drawn from Equation [17] into Equation [18]. We need to perform a permutation between the two operations, integrate from 0 to ∞, and take the limit for $T \to \infty$ of the expression

$$\frac{1}{T} \int_{-T}^{+T} \cdots$$

where the integral itself does not converge when $T \to \infty$. This cannot be derived from ordinary rules related to uniform convergence, but N. Wiener states in the quoted book that such a permutation is allowed under very wide conditions that always are fulfilled in practical problems.

2 In the report by Professor Lee (reference 9 of the paper) Equation [16] of this discussion is established, and Professor Lee indicates another means of "deconvolving" this equation, that consists in performing an integral Fourier transform on each member. One gets

$$H^*(\omega) = \frac{S_{mc}(\omega)}{S_{mm}(\omega)} \quad [19]$$

where $H^*(\omega)$ is the conjugate transfer function of the unknown network, S_{mc} the spectral repartition of ϕ_{mc}, and S_{mm} the spectral power density of the input function—so the transfer function can be calculated without any trial-and-error operation.

[6] Schlumberger Instrument Company, Ridgefield, Conn.

3 The choice between these methods will depend on the nature of recorded signals.

Statistical methods operate at their best when the signal is "random," for instance, obeys a Gaussian repartition in amplitudes and comprises all frequencies between zero and a given cut-off frequency. Such is so-called "filtered white noise." As a matter of fact, when records are dealt with, the word random becomes improper since the value of recorded function is completely known. The most useful feature of such records is that they do not show any marked periodicity, and we will call them "nonperiodic."

Their auto and cross correlations very nicely die out when τ increases, and Fourier integral operations are performed without any difficulty. However, it frequently happens that the signals show at the same time nonperiodic and periodic features. The most common autocorrelation curve will show a strong peak corresponding to a nonperiodic component, but the smooth die-out of filtered white noise is replaced by a periodic tail that goes on to infinity without any further amplitude decay. On such signals, the Fourier integral will fail to converge for the frequency corresponding to this periodicity.

The situation may become worse when the signal shows a strong very low-frequency component that will give far distant peaks. The question now is: How does DLS behave in such cases? That is, it has been shown that the noise component correlated to the signal through the feedback loop can be eliminated. Is this still true when periodic correlation curves are dealt with?

S. G. Margolis.[7] The authors are to be commended for their paper which presents the method of determining system characteristics invented by Y. W. Lee.[8, 9]

It should be pointed out that the correlation functions used in statistical communication theory involve averaging over an infinite time interval. In practice, however, only a finite length of data is available; in industrial process studies, the length of data available may not be much greater than the largest τ shift used. Consequently, caution should be exercised in using the formulas of statistical communication theory to relate experimentally determined correlation functions. For example, the authors' Equation [3], a discrete approximation to Lee's integral equation

$$\phi_{io}(\tau) = \int_{-\infty}^{\infty} h(\sigma)\phi_{ii}(\tau - \sigma)d\sigma \quad [20]$$

is not strictly correct when applied to experimentally determined correlation functions unless only the positive τ portion of the autocorrelation function is substituted into the authors' Equations [2a], [2b], [2].

An exact method of relating experimentally determined correlation functions is presented in a recent report,[10] together with the outline of a method for finding the impulse response directly from a cross-correlation function without inverse convolution. It is felt that the necessity for inverse convolution is the only weakness of the present method; in all other respects the authors' enthusiasm for the statistical method seems entirely justified.

Authors' Closure

The authors greatly appreciate the interest of Messrs. Catheron and Hainsworth and the co-operation of the Foxboro Company in

[7] Research Laboratory of Electronics, Massachusetts Institute of Technology, Cambridge, Mass.

[8] See authors' Bibliography (reference 9).

[9] "Correlation Functions and Communication Applications," by Y. W. Lee and J. B. Wiesner, *Electronics*, June, 1950, pp. 86–92.

[10] "Measurement of Industrial Process Behavior," by S. G. Margolis, Quarterly Progress Report, Research Laboratory of Electronics, Massachusetts Institute of Technology, Cambridge, Mass., April 15, 1955, p. 42.

applying the method of this paper to a flow process. The authors agree with Mr. Chang that several years of practical experience may be necessary to put the statistical method on an equal footing with the traditional frequency-response methods. The authors feel that Mr. Chang's other comments—which are based on his experience in applying the method described in the paper[11]—are also well taken. In connection with Mr. Chang's fourth point, Tustin[12] has suggested that nonlinearities in the system could be detected and identified by using the original system input record as the input to a linear model of the system (such as might be obtained on the DLS) and comparing the original system output with the output of the linear model. The difference between the two outputs then contains the information about the system which is present in the original records but not in the linear model.

Mr. Loeb raises an interesting mathematical point in his first comment. The mathematical background for the method presented in the paper, which was necessarily treated only briefly in the paper itself, is developed more fully in reference (8) of the paper.

The relative merits of the correlation-function approach of Equation [3] and the spectral-density approach of Equation [19] are currently being investigated. The authors favor the correlation-function approach because of the possibility of eliminating the effects of noise in closed-loop systems, as discussed in Appendix 1. When the correlation functions contain periodicities, the DLS can still be used, provided that function-generating equipment is available to generate a portion of the correlation functions which is at least two to three times the duration of the significantly nonzero portion of the weighting functions. The effects of noise can still be eliminated, as shown in Appendix 1, unless the noise itself contains strong periodic components.

In reply to Mr. Margolis, the authors feel that while the work of Y. W. Lee (9) is highly significant, the other references cited in the bibliography also represent important contributions to the method presented in the paper. In particular, it is felt that the delay-line synthesizer (7) is basic to the practical application of the method.

Equation [3] applies to both positive and negative values of τ, since no restriction was placed on the sign of τ in its derivation.

Mr. Margolis' method for finding the impulse response from the cross-correlation function requires the use of electrical or numerical filters which reduce the amount of significant information contained in the input and output data. The authors feel that the process of inverse convolution, as accomplished by the DLS, is not a weakness of their method but rather one of its strongest features.

---

[11] "A New Technique of Determining System Characteristics From Normal Random Operating Records," by C. M. Chang, Mechanical Engineer's Thesis, Massachusetts Institute of Technology, January, 1955.

[12] "The Mechanism of Economic Systems," by A. Tustin, London, England, Heinemann, 1955 (Appendix).

The Chemical Deaeration of Boiler Water—The Use of Hydrazine Compounds

By J. LEICESTER,[1] DORSET, ENGLAND

The preliminary stages in an experimental study of the reaction rates of the hydrazine-oxygen system are described. The work is continuing along four main lines, a bench-scale study of the mechanism of and the factors influencing the reaction, an investigation of reaction rates in a static autoclave system, study of reaction rates in a pilot-plant high-pressure boiler, and a series of full-scale boiler trials. The simple reaction between hydrazine and oxygen has been shown to be far more complex than was at first thought to be the case, and perhaps the most important conclusion is that even in dilute solutions this can proceed as a surface reaction. The experiments serve to indicate that in the present state of our knowledge, it would not appear possible to predict the efficiency of the reaction for a universal boiler application and that, to achieve the desired result, some form of reaction catalyst may have to be developed.

Introduction

DURING the past year increasing attention has been directed toward the manufacture, on a commercial scale, of hydrazine hydrate and other salts of hydrazine such as dihydrazine phosphate. These materials, relatively new to the field of water treatment, provide a method for the chemical deaeration of feedwater which offers considerable attraction to the boiler user. Unlike sodium sulphite, the hydrazine compounds have the important property of not increasing the total dissolved solids in the boiler water, or of introducing solids which may decompose in the boiler with the formation of volatile acid products. The reaction of hydrazine hydrate or hydrazine with oxygen is shown in the following equations

$$N_2H_4 \cdot H_2O + O_2 = 3H_2O + N_2$$

$$N_2H_4 + O_2 = 2H_2O + N_2$$

from which can be observed the ideal nature of the reaction products.

Under the temperature and pressure conditions prevailing in a boiler, it is likely that decomposition of excess hydrazine hydrate will occur. It is essential therefore that the reaction with dissolved oxygen should be completed before the feedwater enters the boiler and that the excess unreacted hydrazine in the boiler water should be kept to a minimum. The decomposition products formed are ammonia and nitrogen according to the following equation

$$3N_2H_4 = 4NH_3 + N_2$$

The decomposition of residual hydrazine in the boiler water, in most cases, will result in the formation of ammonia which will then be present throughout the stream and condensate system. Providing the condensate or feedwater has a low dissolved-oxygen content, the danger of ammonia attack on nonferrous metals is not likely to be serious. However, should the permissible safe limit be very low for dissolved oxygen, then it is even more essential to insure that the hydrazine/oxygen reaction is complete under all boiler operating conditions. Providing the excess hydrazine in the boiler water is controlled to prevent any undue rise in ammonia content of the steam, this reaction could provide a means of insuring a suitable alkaline pH condition throughout the steam and condensate system. Correspondingly, this would reduce the danger of corrosion of iron or steel by aggressive carbonic acid.

The possible advantages and disadvantages of the use of hydrazine hydrate or phosphate will be apparent from these brief introductory remarks. It is the purpose of the present paper to examine some of these factors in more detail and to assess the magnitude of the problem. Experiments on a laboratory scale designed to investigate the oxygen/hydrazine reaction will be summarized, followed by a description of the work in progress in the Admiralty Materials Laboratory using a pilot-plant high-pressure boiler. Finally, it is hoped to correlate this work by comparing the results of full-scale boiler trials at present in progress throughout Great Britain. The completed paper it is hoped will shed some light on what at first sight appears to be a fairly simple application of this new material, but which after much reflection has been found to be a relatively complex problem.

Laboratory and Small-Scale Experimental Work

Most of the published information dealing with the use of hydrazine compounds for the deaeration of water has been obtained during the course of full-scale practical boiler trials. These data in many cases have proved to be very conflicting. To attempt an understanding of the true mechanism of the hydrazine/oxygen reaction it is essential that a fundamental study of the kinetics of the system should be undertaken.

Experimental Studies at University of Birmingham, England. Much is being done toward fulfilling the need for such information and, in particular, reference is made to a program of research in progress in the Chemical Engineering Department of the University. (This work is being undertaken in collaboration with Messrs. Fisons & Co. Ltd., the manufacturers of hydrazine in Great Britain.) Here at Birmingham, Mr. C. Moreland is studying the kinetics of the system hydrazine/water/dissolved oxygen, with particular reference to the effects of hydrazine concentration, temperature, and pH value of the water. Also under investigation is the effect on reaction rate of metal catalysts, either in the form of a suspension or present as a solid surface. A complete account of this work, together with the results obtained, will form the subject of an independent paper to be published in the near future.

It would appear from the early stages of this work that the rate of reaction between hydrazine and oxygen in cold distilled water is much slower than is generally understood. There is also some evidence to indicate that if the water and hydrazine are in a very pure state the reaction may be nonexistent. The reaction

[1] Head of Chemical Engineering Division, Admiralty Materials Laboratory, Holton Heath.

Contributed by the Boiler Feedwater Research Division and presented at the Annual Meeting, New York, N. Y., November 28–December 3, 1954, of The American Society of Mechanical Engineers.

Note: Statements and opinions advanced in papers are to be understood as individual expressions of their authors and not those of the Society. Manuscript received at ASME Headquarters, August 11, 1954. Paper No. 54—A-123

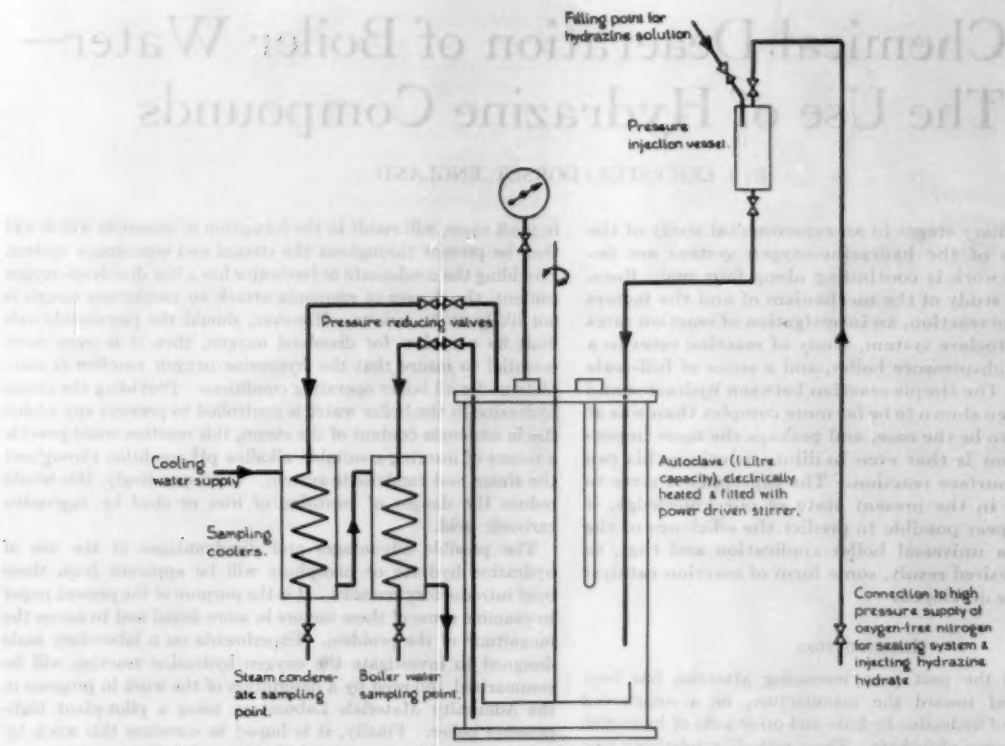
Filling point for hydrazine solution
Pressure injection vessel
Pressure reducing valves
Cooling water supply
Sampling coolers
Autoclave (1 Litre capacity), electrically heated & fitted with power driven stirrer.
Connection to high pressure supply of oxygen-free nitrogen for sealing system & injecting hydrazine hydrate
Steam condensate sampling point
Boiler water sampling point

FIG. 1 DETAILS OF EXPERIMENTAL AUTOCLAVE UNIT USED AT BRITISH LAUNDERERS' RESEARCH ASSOCIATION

rates are increased considerably by such effects as increased temperature, alkalinity of the water, and the presence of certain metal catalysts. Some preliminary rate measurements, using similar quantities of dihydrazine phosphate, have shown this compound to be apparently equal to hydrazine hydrate. Perhaps the most important conclusion from these initial experiments at Birmingham is that even in dilute solutions and at low temperatures the hydrazine/oxygen reaction can proceed as a surface reaction.

It is the author's opinion that oxide films, forming on the surface of a solid or on suspended particles in the solution, may provide the necessary step for the hydrazine reaction. These phenomena have been observed repeatedly throughout our experimental work, and they will be referred to later in the present paper. They also provide the only satisfactory explanation for many of the conflicting results obtained during full-scale practical boiler trials.

Laboratory Studies by British Launderers' Research Association, London. An independent series of small-scale laboratory experiments is being carried out for the Admiralty in the Laboratories of the foregoing research association. Here, using a stainless-steel autoclave, the kinetics of the system hydrazine/oxygen/water are being studied. The program is designed to investigate both "idle boiler" and "steaming conditions," and data are being obtained for hydrazine-hydrate concentrations of theoretical, 100 and 200 per cent excess and for similar concentrations of the compound dihydrazine phosphate. The range of autoclave pressures chosen for these experiments is 500, 750, and 1000 psig. Later in this program, it also is intended to examine the effect on reaction rates of the addition of metal catalysts to the water, either in the form of a suspension, in solution in the water, or present as a solid-metal surface.

Setup of Equipment. A diagrammatic sketch of the autoclave and ancillary equipment used for these experiments is shown in Fig. 1. The experimental technique used is to fill the autoclave with previously deaerated water while keeping a positive nitrogen sealing pressure on all the vessels. Heat is then applied and the pressure in the autoclave raised to the desired working level. Before commencing the addition of the hydrazine hydrate a sample of water is tested to establish a final value for the dissolved-oxygen content. The required volume of hydrazine hydrate is run into the injection bomb which is then pressurized up to about 2000 psig with oxygen-free nitrogen.

At the commencement of an experiment the stirrer in the autoclave is started and the hydrazine in the injection vessel is shot into the autoclave. Samples of water and steam are taken after approximately 2 min and subsequently every 10 min over a total period of about 1 hr. The water samples are then analyzed for unreacted hydrazine and the steam-condensate samples for unreacted hydrazine and ammonia.

In view of the difficulty of accurate oxygen determinations on the small sample volume available from the autoclave, and also the possible presence of excess unreacted hydrazine, it was decided to follow the course of any reaction by determining the residual amounts of unreacted hydrazine in the solution.

The analytical procedure for the determination of hydrazine was by the method of Pasea and Petit[2] using p-dimethyl amino benzaldehyde. Dissolved oxygen in the untreated water was determined by the method of Ovenston and Watson[3] while

[2] "The Detection and Estimation of Hydrazine," by M. Pasea and A. Petit, Bull. Soc. Chim. of France, 1947, pp. 1022–1023.

[3] "Spectrophotometric Determination of Small Amounts of Oxygen in Waters," by T. C. J. Ovenston and J. H. E. Watson, *The Analyst*, vol. 79, 1954, pp. 383–387.

ammonia in the presence of hydrazine was determined by buffering the solution to pH value of 7.0, titrating with 0.01N iodine, using starch solution as an indicator, followed by the addition of Nessler reagent, and completing the estimation in the normal manner. The estimation of dissolved oxygen in the presence of unreacted hydrazine was carried out by first destroying any hydrazine in the sample with an excess of standard iodine solution and then completing the oxygen determination as described previously.[3]

Results to Date. At the time of writing the present paper this experimental program at the British Launderers' Research Association is still in progress. Experiments so far have examined the reaction rate of hydrazine hydrate in cold solutions using hydrazine concentrations of theoretical 100 and 200 per cent excess; this work continues with an examination of similar concentrations of dihydrazine phosphate. The general trend of the results obtained is summarized in Fig. 2. It should be noted that throughout the series of rate measurements in cold solutions, reaction times for the hydrazine hydrate are relatively fast. At the first 2-min sampling period up to 70 per cent of the hydrazine had been used up in the reaction with the dissolved oxygen. These results differ considerably from the reaction rates measured during the experiments at Birmingham University where, in cold distilled water adjusted to pH 9.5 by the addition of trisodium phosphate, only about 35 per cent of the hydrazine had reacted with the dissolved oxygen after approximately 20 hr. The significant difference between these results and the Birmingham data would appear to be due to the effect of the metal catalyzing a surface reaction, whereas at Birmingham the rate measurements were all determined in glass apparatus. A part explanation for the very rapid reaction times also may be that, in the autoclave, metal-surface area is much greater per unit volume of water than in the case of the pilot-plant or full-scale boiler trials.

A similar series of experiments have been completed at 1000 psig autoclave pressure, and measurements have again shown that the reaction is essentially complete in 2 min. In one set of experiments, approximately 50 per cent of the hydrazine had reacted in 3 min. This left a 30 per cent residual hydrazine content in the water, 50 per cent of the hydrazine having decomposed with the formation of ammonia, and the remainder had reacted with all the oxygen present.

Because of a fault in the equipment, unfortunately it has not been possible to complete the full series of experiments for the present paper and this work is continuing. The general trend of the results obtained to date is summarized in Fig. 3.

Pilot-Plant Boiler Experiments at the Admiralty Materials Laboratory

Following logically from the measurement of reaction rates in a noncirculating system such as the autoclave, it was obvious that considerable differences might be expected in a boiler system where there would be circulation of thin films of boiler water over the highly rated heat-transfer surface. It was therefore decided to repeat these earlier trials in our pilot-plant high-pressure boiler and, in addition, attempt an over-all material balance for the boiler and feedwater system.

The oil-fired single-tube boiler used for these experiments has natural circulation with water speeds of 1.5 to 2.0 fps through the heated tube. For the present series of trials the boiler was operated at 500 psig pressure with a heat-release rating in the combustion chamber of approximately 85,000 Btu/sq ft of tube surface per hr. A general view of this boiler is given in Fig. 4, and a diagrammatic sketch, showing the various sampling points used during the trials, is given in Fig. 5. These trials are still continuing and the use of hydrazine hydrate and dihydrazine phosphate will be examined over a range of pressures up to as high as 1500

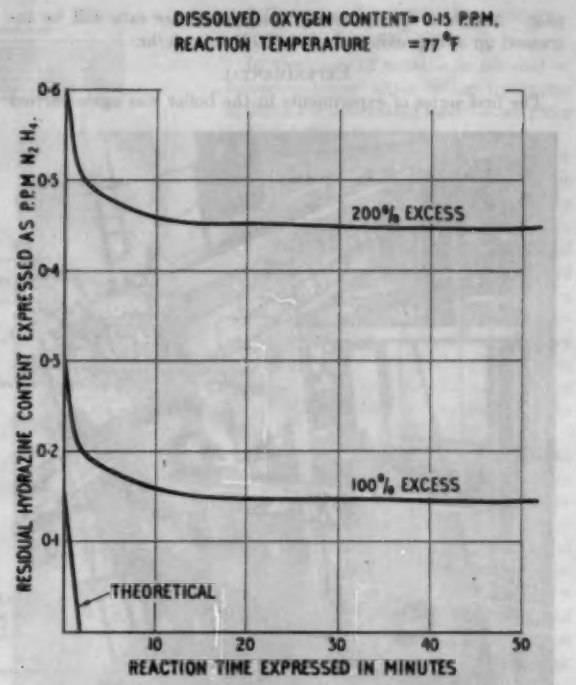

Fig. 2 Reaction Rates of Hydrazine and Oxygen Under Idle Boiler Conditions—General Trend of Results Obtained Using Autoclave Unit

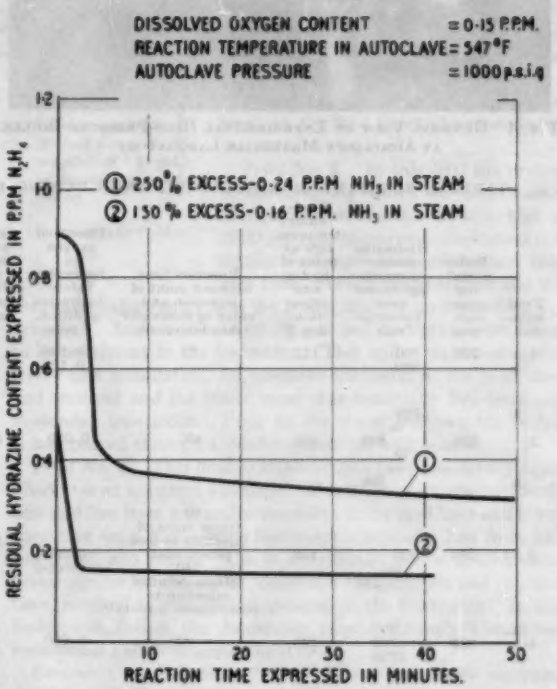

Fig. 3 Reaction Rates of Hydrazine and Oxygen Under Steaming Conditions—General Trend of Results Obtained Using Autoclave Unit

psig. Also later in the series, the heat-release rate will be increased up to approximately 200,000 Btu/sq ft/hr.

Experimental

The first series of experiments in the boiler was again carried out under "idle" conditions for comparison with the previously mentioned small-scale experiments. The general trend of the results obtained at 77 F is summarized in Fig. 6. A slower reaction time is shown than for those measured in the autoclave, but they are still considerably in excess of the rates measured at Birmingham. The slower reaction rates are also partly due to insufficient mixing of the hydrazine-hydrate solution with the bulk of the water in the boiler. These measurements are to be repeated after the equipment has been modified to give more efficient stirring.

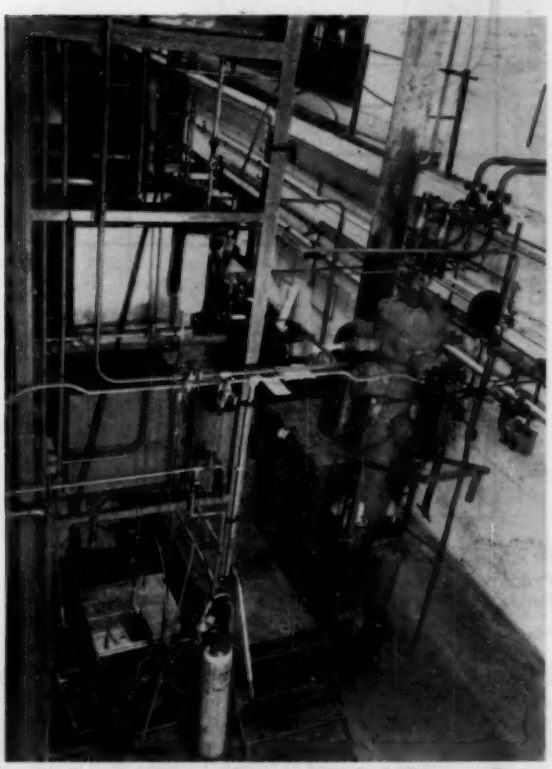

Fig. 4 General View of Experimental High-Pressure Boiler at Admiralty Materials Laboratory

Before commencing the rate measurements under steaming conditions, the boiler circuit was first conditioned for a period by steaming on feedwater to which approximately 300 per cent excess hydrazine had been added. This conditioning was carried on until it was found possible to maintain a residual hydrazine content of about 0.04 ppm in the boiler water. It was apparent that during this initial period of hydrazine addition, considerable reaction was occurring between the hydrazine and any ferric oxide on the metal surfaces of the boiler. Sampling points in the boiler circuit were so arranged that it would be possible, at any selected time interval, to obtain an approximate material balance for the system. These sampling positions are shown in Fig. 5 and comprise point (A) immediately after the feed pump, point (B) connected to the bottom blowdown cock of the boiler gage glass, and point (C) in the steam line from the boiler drum to the condenser. Samples from points (A) and (B) were analyzed for residual hydrazine content, and selected samples were checked for dissolved-oxygen content. Samples taken from point (C) were analyzed for hydrazine carry-over and for ammonia.

Three concentrations of hydrazine hydrate were again examined, theoretical 100 and 200 per cent excess. Temperature of the feedwater at the point of injection was approximately 190 F and the contact time between this point and the entry of the water to the boiler was approximately 2 min. Results so far obtained have shown that, with hydrazine hydrate added to the feedwater in quantities up to 200 per cent excess of theoretical, very little of the dissolved oxygen was removed from the feedwater prior to its entering the boiler. Reaction with oxygen did, however, take place in the boiler and, providing the residual hydrazine in the

TABLE 1 SUMMARY OF RESULTS OBTAINED DURING FULL-SCALE BOILER TRIALS USING HYDRAZINE HYDRATE

Trial number	Boiler operating pressure, psig	Hydrazine dosage (percentage excess over theoretical)	Feedwater temperature at point of hydrazine injection, deg F	Reaction time between point of injection and entry of feedwater into boiler, sec	Dissolved oxygen in feedwater before hydrazine addition, ppm	Dissolved oxygen in feedwater after hydrazine addition, ppm	Normal ammonia content of steam or condensate before hydrazine addition, ppm	Ammonia content of steam after hydrazine addition, ppm	Excess unreacted hydrazine present in boiler water, ppm	Comments
1 a	200	160	122	75	0.100	0.05	0.14	0.14	0.25	Base exchange softened water supply small amount of solids in suspension.
1 b		300			0.120	0.08		0.20	to 0.30	
2 a	350	700 to 800	190	80	0.050	0.006	0.30	0.90 (after 5 days steaming)	No data	Feed lines and heaters known to be coated internally with ferric oxide. Boiler water contained appreciable quantity of this material in suspension.
2 b		150 to 200						0.30		
3	420	200 to 250	150	50 (from point of injection to feed-pump inlet) 240 (from point of injection to economizer outlet)	0.200 (average)	0.100 0.030	0.20	0.80	0.20 to 0.40	Feed lines and economiser relatively free from ferric oxide. Feed water very good, less than 60 ppm dissolved solids. No ferric oxide in suspension.
4 a	625	200	284	82	0.030	0.028	0.04	0.40	0.10	Very little ferric oxide occurs at any point in system. Feedwater free from ferric oxide in suspension.
4 b		1100				0.028		0.48	0.40	
4 c		3700				0.014		0.64	1.25	
5	650	300	280	80	0.021	0.020	No data	Excessive formation of ammonia reported	No data	Little ferric oxide in system and feedwater free from suspended ferric oxide.

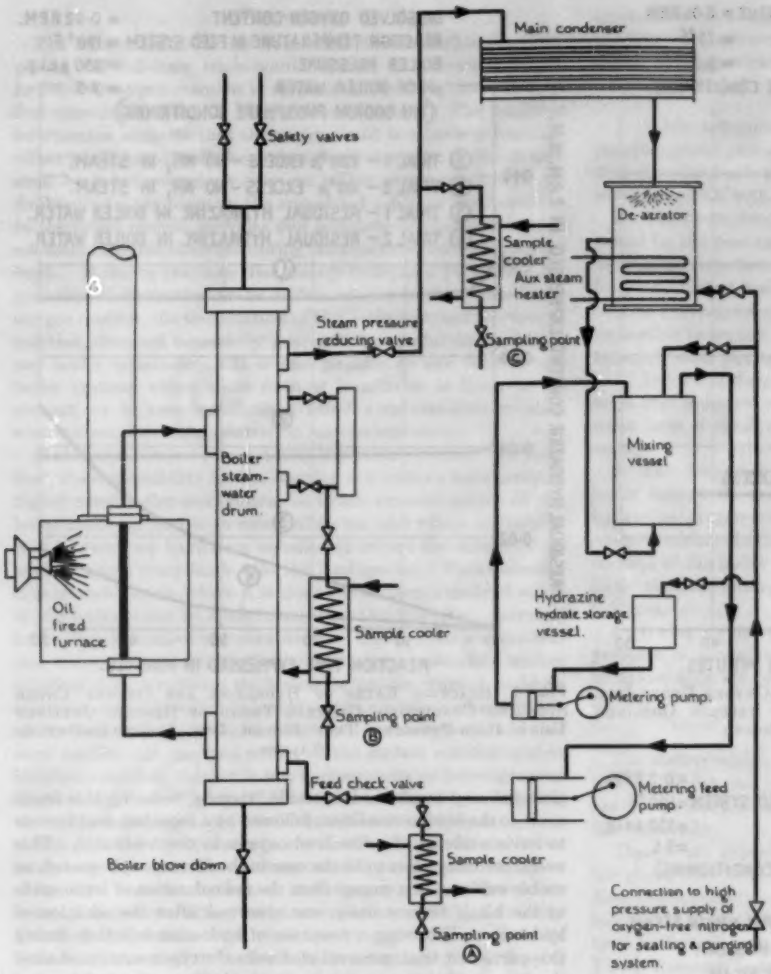

FIG. 5 DETAILS OF EXPERIMENTAL HIGH-PRESSURE BOILER CIRCUIT AT ADMIRALTY MATERIALS LABORATORY

boiler water did not exceed 0.20 ppm, no ammonia was detected in the steam and condensate samples.

To enable comparison with the autoclave experiments, a further series of trials was carried out with feedwater of up to 0.2 ppm dissolved-oxygen content. In these experiments, the amount of dissolved oxygen removed from the feedwater, prior to entering the boiler, gave evidence of an increased reaction rate. This change of rate in the presence of increased oxygen and hydrazine is obviously due to the effect of mass action. Owing to the increased quantity of hydrazine used in these trials, it was found that, with 200 per cent excess in the feedwater, residual hydrazine in the boiler water rose to as high as 0.50 ppm. In this particular case, an ammonia content of 0.08 ppm was detected in the condensate. From the present experiments it would appear that a residual hydrazine content of 0.25 to 0.30 ppm can be tolerated in boiler water before decomposition to ammonia occurs.

This latter fact is not typical of the full-scale trial experiences and requires a more detailed examination. It may be due to reactions taking place on oxide surfaces in the boiler. The general trend of the data so far obtained is summarized in Figs. 7 and 8.

A GENERAL SURVEY OF FULL-SCALE BOILER TRIALS

In the past 12 months, a number of full-scale boiler trials using hydrazine hydrate for deaeration have taken place in Great Britain.

The results of these trials have been most interesting, but at the same time they provide results which differ widely in their degree of successful deaeration. An attempt will be made to survey and correlate the information available and it is hoped to show that there may be a logical reason for certain of these apparent anomalies. To enable a relative assessment of the various trials, the range of operating conditions and the results obtained are summarized in Table 1.

It is evident from these results that in certain cases the use of hydrazine has given perfect deaeration, while in other cases, very often under similar boiler conditions, little or no oxygen removal has been recorded. A more detailed study has been made of three of the particular trials reported in Table 1 and it is thought that a logical explanation for the apparent anomalous results can be given.

Trial No. 2. Neglecting for the moment the decomposition of a high excess of hydrazine to give ammonia in the steam, this trial indicates that excellent deaeration has resulted from the use of hydrazine hydrate. The boiler used was fairly old and there was known to be a considerable amount of iron-oxide deposit in the feed line and suspended in the boiler water.

Trial No. 4. In this trial the reverse of the foregoing results was experienced. With hydrazine contents up to as high as 3700 per cent excess over theoretical and similar feedwater temperature and contact time between the hydrazine and the feedwater before entry into the boiler, little or no deaeration was achieved. In fact, dissolved oxygen and hydrazine were found to be coexistent in the feedwater. This boiler plant was a relatively new installation, no excessive corrosion in the feed lines had occurred and the boiler water was essentially free from any suspended iron oxide. Prior to the water entering the boiler, it had passed through a nonferrous-metal feed heater.

Trial No. 3. This final example chosen from the survey again illustrates an apparent anomaly. The boiler plant was relatively new and free from any undue corrosion in the feed lines and it was operating on a high-purity feedwater essentially free from any suspended iron oxides. Use of a moderate excess of hydrazine, under similar conditions of feedwater temperature and reaction time, resulted in excellent deaeration of the feedwater. In this boiler installation the feedwater passed through a cast-iron economizer before entering the boiler.

Comments on Full-Scale Trials. The major factor emerging from these results is the apparent dependence of the hydrazine/oxygen reaction on a surface phenomenon. It would appear that the initial reaction mechanism might well be between the hydra-

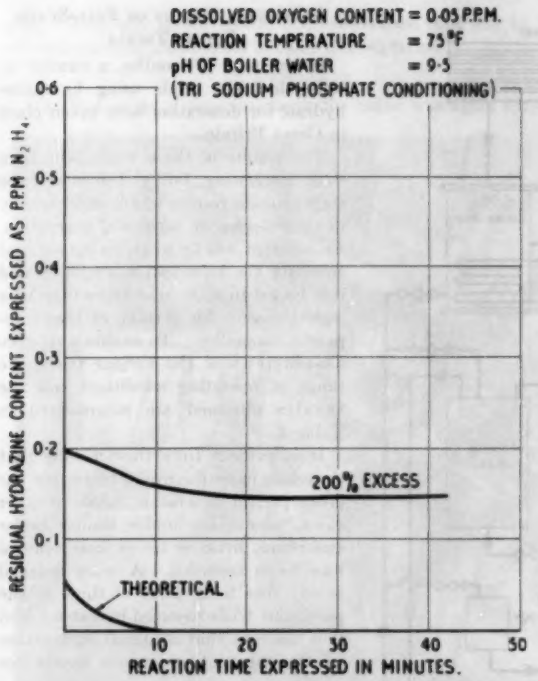

FIG. 6 REACTION RATES OF HYDRAZINE AND OXYGEN UNDER IDLE BOILER CONDITIONS—GENERAL TREND OF RESULTS OBTAINED USING HIGH-PRESSURE TEST BOILER

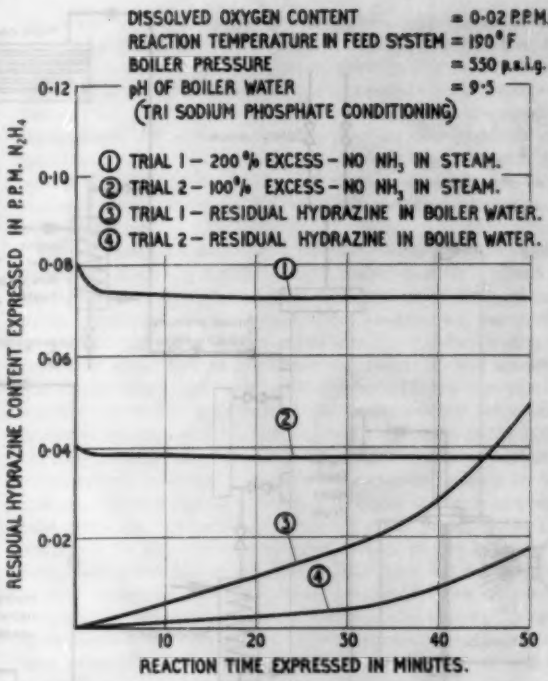
DISSOLVED OXYGEN CONTENT = 0·02 P.P.M.
REACTION TEMPERATURE IN FEED SYSTEM = 190°F
BOILER PRESSURE = 550 p.s.i.g.
pH OF BOILER WATER = 9·5
(TRI SODIUM PHOSPHATE CONDITIONING)
① TRIAL 1 – 200% EXCESS – NO NH_3 IN STEAM.
② TRIAL 2 – 100% EXCESS – NO NH_3 IN STEAM.
③ TRIAL 1 – RESIDUAL HYDRAZINE IN BOILER WATER.
④ TRIAL 2 – RESIDUAL HYDRAZINE IN BOILER WATER.
RESIDUAL HYDRAZINE CONTENT EXPRESSED IN P.P.M. N_2H_4
0·12
0·10
0·08
0·06
0·04
0·02
10
20
30
40
50
REACTION TIME EXPRESSED IN MINUTES.

FIG. 7 REACTION RATES OF HYDRAZINE AND OXYGEN UNDER STEAMING CONDITIONS—GENERAL TREND OF RESULTS OBTAINED USING HIGH-PRESSURE TEST BOILER; LOW DISSOLVED-OXYGEN VALUES

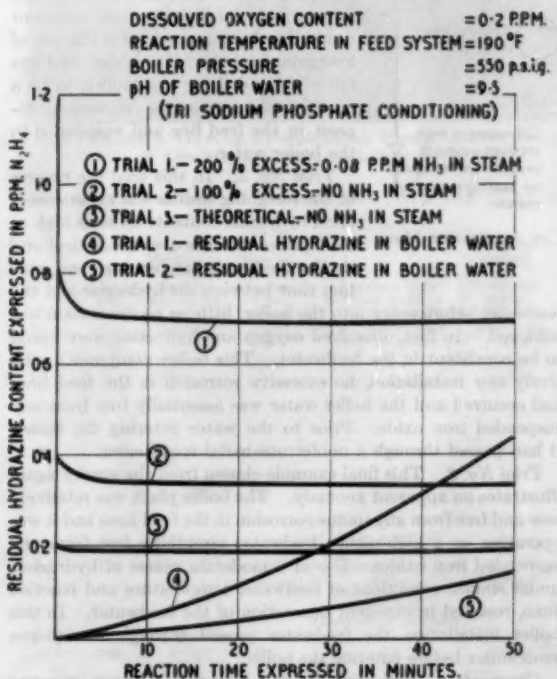
DISSOLVED OXYGEN CONTENT = 0·2 P.P.M.
REACTION TEMPERATURE IN FEED SYSTEM = 190°F
BOILER PRESSURE = 550 p.s.i.g.
pH OF BOILER WATER = 9·5
(TRI SODIUM PHOSPHATE CONDITIONING)
① TRIAL 1 – 200% EXCESS – 0·08 P.P.M NH_3 IN STEAM
② TRIAL 2 – 100% EXCESS – NO NH_3 IN STEAM
③ TRIAL 3 – THEORETICAL – NO NH_3 IN STEAM
④ TRIAL 1 – RESIDUAL HYDRAZINE IN BOILER WATER
⑤ TRIAL 2 – RESIDUAL HYDRAZINE IN BOILER WATER
RESIDUAL HYDRAZINE CONTENT EXPRESSED IN P.P.M. N_2H_4
1·2
1·0
0·8
0·6
0·4
0·2
10
20
30
40
50
REACTION TIME EXPRESSED IN MINUTES.

FIG. 8 REACTION RATES OF HYDRAZINE AND OXYGEN UNDER STEAMING CONDITIONS—GENERAL TREND OF RESULTS OBTAINED USING HIGH-PRESSURE TEST BOILER; HIGH DISSOLVED-OXYGEN VALUES

zine and any available iron oxide, thereby reducing this ferric oxide to the ferrous condition, followed by a reoxidation of ferrous to ferric oxide by the dissolved oxygen in the feedwater. This would certainly seem to be the case in the first example quoted, as visible evidence of a change from the red coloration of ferric oxide to the black ferrous oxide was observed after the addition of hydrazine. Following a cessation of hydrazine injection during this particular trial, removal of dissolved oxygen continued until the ferrous oxide in suspension in the boiler water had become fully oxidized to the original ferric condition. This example provides a typical case where the presence of a suspension of iron oxide in the feedwater may provide a large oxide surface area to catalyze the hydrazine reaction.

In the second example, where, independent of the amount of hydrazine added, little or no reaction with the oxygen occurred, excess hydrazine entered the boiler and decomposition to ammonia and nitrogen took place. In this boiler, the feedwater was free from suspended iron oxide and, in addition, the feed heater was constructed from nonferrous materials. Therefore there would be little or no opportunity for the existence of surface oxide films in this portion of the plant and, although similar feedwater temperatures and reaction times were available, the tendency would be to limit any surface reactions.

In the final example quoted, an entirely different set of conditions is apparent. The feedwater is essentially free from suspended iron oxide, but in this case there is an opportunity for the feedwater to come into contact with a relatively large surface area of cast iron. Results achieved under these particular conditions are excellent and the majority of the dissolved oxygen is removed from the feedwater. In this instance, it would appear fair to assume that iron-oxide surface films are available in the economizer to enable the reaction to proceed efficiently.

Discussion

The information obtained as a result of the small-scale, pilot-plant, and full-scale trials would appear to indicate that the hydrazine/oxygen reaction in dilute solutions may not be, as at first considered, a simple homogeneous reaction. The available information suggests that the major event is a surface reaction, either wholly or partially homogeneous in character or that it may even be a heterogeneous reaction. This reaction, that is undoubtedly taking place on the suspended solids or solid surfaces in the boiler circuit, provides one adequate explanation for the anomalous results observed during the experimental and practical work. If this be the case, then merely fixing as a parameter the quantity of hydrazine to be added on the basis of dissolved-oxygen content, the temperature of the feedwater, and the time of reaction, does not necessarily guarantee successful deaeration in any boiler installation. It is also possible to say that in old boiler systems where some form of iron oxide is likely to be present, or in new installations fitted with cast-iron or steel economizers, successful deaeration may be expected.

Such facts, however, do not help the boiler operator who may have the responsibility for the running of a modern high-pressure highly rated boiler installation, in which extreme purity of the boiler make-up feed is an essential factor, and where nonferrous feed heaters may have been installed to reduce the danger of introducing iron compounds into the feed system. Paradoxically, it is in such plants, where it is desirable to keep dissolved solids in the boiler water to a minimum, that the attractive claims of hydrazine deaeration are paramount. The key to a successful and universal use of hydrazine will be a more complete understanding of the kinetics of the hydrazine/oxygen reaction in dilute solutions, a field in which valuable results are expected as a result of the work in progress at Birmingham University. Should this work confirm the essential nature of the surface reaction and in addition establish whether it is a homogeneous or heterogeneous mechanism, then methods will have to be developed for catalyzing the hydrazine/oxygen reaction in the external feed system.

The problem of the decomposition of hydrazine in the boiler has been left to the end as this very much depends upon the degree of reaction between hydrazine and oxygen prior to the water entering the boiler. The pilot-plant experiments at the Admiralty Materials Laboratory have shown that, providing the residual hydrazine content of the boiler water is not greater than 0.2 ppm, little or no decomposition of hydrazine occurs. The point at which thermal decomposition commences varies considerably with the quantity of iron oxide present in the boiler or feedwater system. With an excess of iron oxide present throughout the boiler system, the hydrazine reaction proceeds normally, even when a large excess of hydrazine has been added to the feedwater. The reverse, however, is the case in a clean boiler with little or no iron oxide in the feedwater, all the hydrazine added to the feedwater passing into the boiler where it immediately decomposes to form ammonia and nitrogen.

Whatever degree of efficiency is achieved in the hydrazine/oxygen reaction, it would seem that any practical treatment will require excess hydrazine dosage over the theoretical to cover any unexpected rise in the dissolved-oxygen content of the feedwater. In such cases, it is probable that a proportion of uncombined hydrazine will pass into the boiler and decompose and it therefore appears that one may have to accept the presence of 0.3 to 0.5 ppm of ammonia in the steam and condensate lines. The quantity of ammonia that can be tolerated in the boiler system will greatly affect the degree of accuracy required for the hydrazine addition. The development of suitable injection and metering equipment obviously will be required for this purpose. The presence of ammonia alone is not necessarily harmful, as it is known to provide a convenient method of pH control for boiler feedwater. What must, however, be considered is the effect of this ammonia in conjunction with oxygen and carbon dioxide, and the possible corrosion of nonferrous metals in the system.

Conclusions

1 While acknowledging that hydrazine hydrate or dihydrazine phosphate provides an ideal chemical method for the deaeration of boiler feedwater, the fact must be faced that their successful reaction with dissolved oxygen is by no means universal.

2 The hydrazine/oxygen reaction in dilute solutions, such as would be the case in boiler feedwater systems, would appear to be a surface reaction. The mechanism of this reaction is not yet fully established but there is some evidence to indicate that it may be heterogeneous. In the light of this knowledge, it appears impossible to predict that hydrazine will work satisfactorily in all types of boiler plants.

3 In view of the possible surface-reaction mechanism, it would seem that to insure complete reaction with the dissolved oxygen, some form of catalyst unit in the feedwater supply will be necessary.

4 The decomposition of excess hydrazine to ammonia in the boiler water is necessarily bound up with the completeness of the hydrazine/oxygen reaction and the degree of reaction occurring at oxide surfaces in the system. Providing the residual hydrazine content of the boiler water does not rise above 0.2 ppm, it is unlikely that the ammonia in the steam will be greater than 0.3 to 0.5 ppm.

5 Owing to the danger of nonferrous-metal corrosion in the presence of excessive amounts of ammonia, it will be necessary to devise accurate metering equipment for the dosage of hydrazine.

Acknowledgments

The author wishes to thank the British Admiralty for permission to publish the present paper. The views proposed therein are the author's own responsibility and not necessarily those of the Admiralty.

Thanks are expressed to Dr. Ellis and Mr. Moreland of Birmingham University and to Mr. Wagg of the British Launderers' Research Association, for their contribution to the theoretical and laboratory work. For the valuable information relating to practical boiler trials, it is desired to thank Mr. Vero of Messrs. Fisons Research Laboratories, Mr. Spencer of Messrs. Whiffen & Son Limited, Mr. Webb of Babcock and Wilcock Limited, Mr. Hamer of the Alkali Division, Imperial Chemical Industries, Limited, and Mr. Howes of the British Electricity Authority.

Discussion

R. C. Adams.[4] We are grateful to the author for reporting to us on British progress in the use and control of hydrazine as an oxygen scavenger. The simple reaction of hydrazine with oxygen to yield completely harmless products is so appealing that it is exasperating to attempt to use hydrazine and then find either no reaction or that the hydrazine decomposes ineffectively. What we all wish to know is how to put hydrazine to work.

Our studies of the subject add little information to that which the author has provided. They show that hydrazine is quite stable in water solution at temperatures up to 175 F. At room temperature hydrazine and oxygen can coexist in solution apparently indefinitely. These experiments in glass show that heat or some other stimulant is required to initiate reaction.

---

[4] Superintendent, Chemical Engineering Laboratory, United States Naval Engineering Experiment Station, Annapolis, Md.

Note: The opinions expressed are those of the writer and are not necessarily those of the Engineering Experiment Station or of the Navy Department.

When we come to the more varied systems of feed lines and boilers, the situation is quite different. Here we have a hydrazine which is all too ready to become something else. It will destroy itself in scavenging oxygen, if the oxygen is properly served. But if there is no oxygen, the hydrazine will destroy itself any way, yielding ammonia. Since there are cheaper sources of ammonia for adjustment of condensate pH than that derived from hydrazine, it behooves the operator to channel hydrazine into the job of oxygen scavenging, a job for which theoretically it appears to be ideally suited. The means to this end will be found by such studies of reaction conditions and kinetics as the author, his compatriots, and other investigators now are conducting.

Despite the room-temperature stability of hydrazine, it has been suggested for corrosion protection in idle boilers, particularly for protection of superheaters. This would seem to be a good idea because the modern superheater tends to be increasingly inaccessible and difficult to drain or wash out. A protective material which could be drained, or even boiled out, without leaving a solid residue sounds ideal. Preliminary laboratory tests indicate that this is feasible, although fairly high concentrations of hydrazine would be required. We have tried only two concentrations, namely, 30 ppm and 300 ppm. The lower concentration was ineffective but 300 ppm of hydrazine prevented rusting and weight loss of steel coupons during exposure for 30 days.

One minor criticism of an otherwise excellent paper is that such graphs as Fig. 4 through 8, are more convincing if actual data points are shown in addition to the smooth curves. The number of such points and their closeness to the curves support the fact that the curves represent more than inspiration on the part of investigators.

S. K. Adkins.[5] The author certainly has contributed important data on hydrazine and its reactions as an oxygen scavenger in boiler feedwater. We applaud the work he and his associates have reported and the planned investigation yet to be completed.

As stated in the paper, hydrazine compounds are most exciting, from a practical operating standpoint, to operators of high-pressure, high-temperature, high heat-transfer-release, low make-up steam-generating systems. Since dissolved solids are not increased by its use, it is particularly attractive for use in modern units that use feedwater of high purity in spray-type steam-temperature controls. Also as stated in the paper, it is important to remove or react all oxygen before the feedwater enters the boiler. In view of the strong evidence presented that hydrazine does not always react with a predictable speed, it is important that it be introduced immediately after the deaerator or hot well, when the hot well also incorporates deaeration. Until more is known about accelerating or "catalyzing" the reaction, this will insure maximum allowable reaction time.

The indicated role of iron or iron oxides in the reaction are extremely interesting. Since surface area of the iron or iron oxides appears to be a major item, it would be very interesting to know if a large surface area of any type, particularly nonmetallic, would have any desirable effect. If so, the possibility of speeding the reaction without the addition of a soluble catalyst might be accomplished and the dissolved-solids advantage of hydrazine compounds retained. With some of the tube failures that have occurred due to excessive iron oxide still vivid in our minds, many will continue to eliminate them whenever possible. In this connection, preliminary indications from one moderate-pressure plant in the United States are that hydrazine may actually assist in reducing the quantity of iron oxides present in the boiler. We may hope, therefore, that advancing knowledge may reveal some equilibrium between iron oxides and hydrazine that will permit removal of oxygen and, at the same time, limit the quantity of iron oxides in the system.

Those concerned with the fundamental studies of the iron reaction and its relation to this subject may be interested in a paper by Messrs. Gothburg, Kehmna, and Johnson.[6] This paper discussed observations of the ferrous-ferric relationships and the apparent effect on deposition at various points in the system when the oxidation rate could be controlled within rather narrow limits. The actual problem in the plant experiences described was ferrous and ferric-oxide deposits on feed-pump impellers. Some relation may exist between the fundamentals considered by these authors and the observations by the present author.

One important factor of great interest is that of analytical control. It is fully realized that development of analytical-control procedures was not a part of the ambitious program undertaken by the author and his colleagues. It is important, however, that a relatively simple, reliable, analytical method be available if widespread application of hydrazine compounds is to be entirely successful. While the problem of precise micro-analytical work is not great in large, well-equipped, high-pressure central stations, a great many plants are neither staffed nor equipped with the precise analyses indicated by the very low residuals mentioned. Fractional parts per million, 0.1 to 0.3 ppm, are shown as maximums allowable before excessive ammonia is introduced by decomposition. We sincerely hope that techniques will be simplified as the general knowledge of hydrazine and its compounds advances.

Another practical aspect that usually concerns operators when a relatively new chemical is introduced is handling and storage. Hydrazine does have some objectionable characteristics which must be recognized, but relatively simple precautions make it no more difficult to handle and store than other treatment chemicals. The ability of the manufacturers to produce several hydrazine compounds, no doubt, will result in further developments to reduce the minor objections that may arise.

The work presented has pointed out some important problems. The challenge is clear, and the apparent advantages of hydrazine will stimulate further research that will solve the difficulties and permit the use of a material that seems particularly helpful as pressures and temperatures in steam operation advance upward.

T. J. Finnegan.[7] Hydrazine has been aggressively promoted during the past year or two as an oxygen scavenger. A certain type of boiler operator is especially receptive to its charms. This is the operator of the high-pressure, high-capacity utility boiler who has reduced his make-up to a small fraction of a per cent and who uses very pure water for the purpose. Good boiler-water conditions are achieved with a minute amount of added chemical so that the total solid content is so low that carry-over troubles are minimized and little or no blowdown is required except perhaps during start-ups.

When a boiler of this class has trouble it is generally associated with iron oxide and a little research and much speculation have ensued regarding the origin and effect of this iron oxide and how it can be controlled to form a thin continuous protective film instead of a bulky mass surrounding or overlying actual or potential pits.

Oxygen may be a factor. Grabowski has explained some curious cases of boiler corrosion by the presence of unsuspected oxygen and, in our own experience using an oxygen recorder, we

[5] Director, Technical Service, Boiler Feedwater, National Aluminate Corporation, Chicago, Ill. Mem. ASME.

[6] "A Preliminary Investigation of Iron-Oxide Deposition in Boiler Feedwater Systems," ASME Paper No. 53—SA-19.

[7] Chemical Engineer, Engineering Department, Niagara Mohawk Power Corporation, Buffalo, N. Y. Mem. ASME.

have found evidence of oxygen on start-ups and low loads, although the full steady-load oxygen content of the water is regularly zero.

The obvious precaution is the use of an oxygen scavenger but the usual scavenger, sodium sulphite, would increase the boiler-water solids and make continuous or at least very frequent blowdown necessary, and it may also decompose to form the objectionable gases, hydrogen sulphide and sulphur dioxide. Consequently, sulphite is not very attractive to those of us who operate with the delicately adjusted water conditions just described, especially since, on the whole, very satisfactory operation is being obtained without it.

However, hydrazine is something different. Here is a material which leaves no solid residue and upon oxidation forms only harmless water and nitrogen. Here is a substance which will permit those who would ordinarily use no scavenger but, knowing that a small amount of oxygen may get into the boiler and perhaps be harmful, would like to obtain the security of such an agent without risking the objectionable effects of sulphite.

Into this paean of joy the author has injected a sour note. He says, if the writer may make a brief paraphrase of his comments, that hydrazine is indeed a reducing agent with the ultimate products nitrogen and water in the presence of oxygen, but before we eagerly accept it as the ideal oxygen scavenger we should consider the mechanism of its oxidation; that is, the chemists should study its chemistry. His investigation of this chemical problem suggests that hydrazine needs a higher oxide of iron than the Fe_3O_4 with which we are so familiar in order to effect its oxidation in water. He suggests that, in the very clean condensate-fed boilers the writer mentions, hydrazine may be of no value.

He did not reach this conclusion by theorizing. He made an experimental study begun in the laboratory, continued through the pilot plant to full-scale boiler operation. He has done what should be done more often in the field of power-station chemistry in that he has performed some chemical research on what is essentially a chemical problem. Too often we apply new treatments directly to the plant in what our medical friends would call clinical studies without first defining the fundamental reaction of the process.

The author's conclusions may have to be modified eventually. The physical chemists may not be satisfied with the thermodynamics of his postulated reactions but even if his conclusions are changed completely, he must be commended for his fundamental approach to this highly important problem.

It is appropriate to remind ourselves that this and other papers on water treatment at meetings of the Society are contributed by the Joint Research Committee on Boiler Feedwater Studies as one of its two important functions; the other is the sponsorship of research projects.

As a group composed of representatives of the leading technical associations which are concerned with boiler feedwater and related subjects, it furnishes a single organization through which the several associations can co-operate for research. Its personnel is drawn from the utilities, consultants, the chemical manufacturers, the boiler and turbine manufacturers, the railroads, and the water works operators. It is especially qualified to sponsor fundamental research. It is, therefore, desirable that those who are influenced by such papers bear in mind that we not only need more basic studies of power-station chemistry but also that we have a thriving organization which is in a position to sponsor it.

C. Jacklin.[8] The author is to be congratulated for his courage in attacking the complex problem of determining the reactions which occur when hydrazine is used as an oxygen scavenger in boiler feedwater. The information he has presented and the results of work in progress should aid materially in clarifying the advantages and limitations of hydrazine for use in boilers.

In the first part of the paper the author mentions that ammonia resulting from the decomposition of excess hydrazine could provide a means of insuring a suitable alkaline pH condition throughout the steam and condensate system. It would reduce the danger of corrosion of iron or steel by aggressive carbonic acid. A word of caution should be inserted here. Ammonia is effective in reducing corrosion of iron and steel in steam and condensate systems, but it has a serious defect. It does not afford protection in zones where initial condensation occurs. Certain volatile alkaline organic materials have the advantage of giving protection in these zones as well as the other parts of the system.

The author's observation that hydrazine did not react completely with oxygen in the feed line of a pilot-plant boiler coincides very closely with results obtained in our laboratory in an experimental boiler unit.[9] Numerous tests were made in our unit to determine if hydrazine would be effective as an oxygen scavenger at 1500 psi. With about 0.1 ppm of dissolved oxygen in the feedwater, a hydrazine excess of 200 to 300 per cent of theoretical was not sufficient to eliminate oxygen corrosion on the boiler heating surfaces. With higher excesses, oxygen corrosion was prevented but ammonia formation increased to about 0.4 ppm. At 1500 psi the excess hydrazine detected in the boiler water was less than 0.1 ppm, even though the amount in the feedwater was as high as 2 ppm. The amount of residual hydrazine which can be maintained in the boiler water appears to decrease as the pressure increases.

Some recent tests with the same experimental boiler connected to a dissolved-hydrogen recorder indicate that hydrogen is also one of the decomposition products of hydrazine at 1500 psi. The addition of 0.5 ppm of hydrazine to the feedwater caused an increase of 6 ppb (parts per billion) of dissolved hydrogen in the steam. This corresponds to about 10 per cent of the hydrogen added as hydrazine.

This observation may only increase the complexity of the problem, but it may account for slight shifts in hydrogen evolution observed when hydrazine is used in plants which have hydrogen recorders.

V. M. Marcy[10] Prior to the presentation of this program on the use of hydrazine in boiler-water treatment, it had been presumed that hydrazine completely removed dissolved oxygen from feedwaters. The slowness of reaction between oxygen and hydrazine has been of concern to us for about three years. We are indebted to the author for his data which showed the reaction to be nil in some cases before the feedwater reaches the boiler. Of course, reaction may be hastened when the water reaches boiler temperature and pressure. However, it always should be remembered that when reaction is sluggish, considerable unconsumed oxygen can be volatilized with the steam from the drum.

Lack of published data on the speed or completeness of reaction between oxygen and hydrazine arises largely because of the uncertainties in the determination of dissolved oxygen when minute quantities are involved. Many of the trials run with hydrazine have been in plants having very efficient deaerating heaters. When a feedwater contains less than 0.005 ppm O_2, it is difficult to determine with any degree of certainty if hydrazine is or is not effective in removing oxygen.

The author's hypothesis of iron oxide acting as a catalyst for

[8] Director of Engineering Research, National Aluminate Corporation, Chicago, Ill.

[9] "Experimental Studies of Boiler Scales at 2500 psi," by J. A. Holmes and C. Jacklin, Proceedings of the Eleventh Annual Water Conference, Engineers Society of Western Pennsylvania, Pittsburgh, Pa., 1950.

[10] Hall Laboratories, Inc., Pittsburgh, Pa.

the reaction is quite interesting. His observation on the color change of the iron oxide, suspended in the boiler water after start of hydrazine treatment, could indicate that suspended materials in the water play a part in the reaction. However, we would suspect that ferric oxide would be reduced to magnetite or hydrated magnetite, not to ferrous iron oxide. If oxides are good catalysts, reaction in the boiler would be accelerated due to the large surface of oxide film coating the boiler drum and tubes.

The possible catalyzing effects of other materials should not be overlooked. For example, copper salts, even in minute concentrations, are good catalysts for the room-temperature reaction between oxygen and hydrazine. It would be interesting to know if oxygen removal in Trial 5 of the author's Table 1 would be greater if a small amount of copper sulphate were added to the feedwater along with the hydrazine.

Decomposition of hydrazine to form ammonia can occur even when the boiler water contains much less than the 0.2 ppm N_2H_4 specified in the paper. The extent of decomposition does not depend alone on concentration. As shown in the paper by Baker and Marcy, temperature of the boiler water or steam is also quite important.

We have not found it necessary to destroy hydrazine in water samples prior to analyzing for dissolved oxygen. Our tests indicate that hydrazine does not interfere in the Modified Schwartz-Gurney or ASTM Referee Methods.

PIERO STURLA.[11] The purpose of this discussion is to make further additions to this already complete and very interesting paper, by outlining the results obtained in the Emilia Power Plant of the Edison Company, Milano, Italy, after substituting the treatment by sodium sulphite with the treatment by hydrazine hydrate.

Concerning the possibility of the use of hydrazine as a reducing agent, Societa Edison received the first information regarding its practical use during the conference which was held in March, 1953, at Brussels, Belgium, by the Water Commission of Unipede (Union Internationale des Producteurs et Distributeurs d'Energie Electrique). It was on this occasion that Mr. Werner of Vereinigung Industrielle Kraftswirtschaft and Mr. H. Kohle of Grosskraftwerk Mannheim, confirmed the use of hydrazine by introduction into the feedwater system in a solution ranging from 2 per cent to 5 per cent. The ratio between oxygen and hydrazine being maintained at 1 to 1.5.

Hydrazine hydrate was used in place of sulphite because of the corrosion by SO_2.

During another conversation with Mr. Werner in Leverkusen, more detailed information was obtained.

The use of hydrazine hydrate in the Leverkusen Power Station of the Bayer Company was decided on for the following reasons:

1 By using hydrazine, the total amount of solids in the boiler does not increase. Nitrogen produced by the reaction of oxygen and hydrazine is simply removed by the condenser ejector or by the deaerator and, at any rate, it has no dangerous effect upon the system.

In the specific case, these considerations were most important because the temperature of the superheated steam reached 1070 F, the pressure 2260 psig, and the make-up approximately 100 per cent.

2 Hydrazine produces ammonia when the temperature exceeds 212 F, which is not dangerous to the system inasmuch as the increased pH, if controlled, may produce favorable results in the reduction of iron and copper pickup.

Of significance is the fact that it was possible to improve the speed of reaction between oxygen and hydrazine at ambient temperature by adding an activated carbon filter as a catalyst. Thus it was possible to control the reaction so that proportionally hydrazine and oxygen combined in the ratio of 1 to 1. The volume of the activated carbon filter used was 28 cu ft which was sufficient for a flow of 440 gpm. The filter, therefore, absorbed excess oxygen which could later react with the hydrazine residual in the boiler.

Another advantage of the filter was the removal of any traces of iron and copper in suspension.

Only four months ago it was possible to obtain in Italy the necessary amount of hydrazine to start conversion to the hydrazine treatment. This was effected as follows:

1 No filter was installed in order to simplify the system and also because the hydrazine would be fed after the boiler feed pump at which location the temperature is adequate to guarantee the rapid elimination of the residual oxygen.

2 For control, the hydrazine solution was added continuously in a ratio of 1:1.5 to the quantity of oxygen present.

3 The residual of hydrazine was controlled in the following three ways:

(*a*) Direct titration by picryl chloride (colorimetric analysis by Mr. Zimmerman).

(*b*) Control the reducing condition of the system by "dead-stop end point."

(*c*) Control the feeding of hydrazine by analyzing very accurately the ammonia content. Since there is no natural ammonia present in the water at the Emilia Plant, the ammonia found is produced only by the decomposition of hydrazine.

The results of the treatment were very satisfactory. Starting from a ratio of oxygen-hydrazine 1:1.5 (the theoretical one being 1:1), it was later reduced to 1:1.2 and even under these conditions the reducing action in the cycle was maintained while the pH increased to 8.8 to 9.1 in the condensate due to the presence of 0.1 ppm of ammonia in the absence of CO_2.

Incidentally, it was found that the best method to control the hydrazine feed was to analyze very carefully the residual ammonia in the condensate and either increase or reduce the quantity of hydrazine fed accordingly.

In addition to the favorable results mentioned, we also noted the following possible disadvantages to this method of oxygen scavenging, which are being studied at our plant:

1 The effect of hydrazine on the protective iron-oxide film.

2 The possibility of too rapid dissociation of a substantial amount of the hydrazine with subsequent lack of protection to the system.

3 The possibility that dissociation may result not only in ammonia, which can be controlled, but also in other objectionable volatile sustances such as NO, NO_2, and NO_3.

Items 1 and 2 were illustrated by the author. As for the third item, the Societa Edison still believes that the production of nitrous oxide is possible, especially at high pressure and temperature in the presence of metallic particles which act as catalysts. It is for this reason that it was decided, as soon as possible, to make a very thorough study of the gas emanating from the condenser ejector. This study will be made with the improved instruments such as the infrared spectrophotometer because of the presence of heavy molecules.

AUTHOR'S CLOSURE

In the intervening period between the submission of the paper in August, 1954, and the presentation at the Annual Meeting in New York, December, 1954, considerable advance was made in the work using the pilot-plant high-pressure boiler. For

[11] Societa Edison, Milano, Italy.

completeness, these results are recorded in the present closure, together with the author's comments on the discussion.

There have been five main developments in connection with this work:

1 To examine in more detail the relationship between hydrazine concentration in the feedwater, residual hydrazine in the boiler water, and ammonia content in the steam condensate.

2 A more detailed study of the amount of oxygen removed for a given excess of hydrazine added to the feed. This has been made with high and low initial oxygen values in the feedwater.

3 A study of the effect of feedwater temperature on the rate and amount of oxygen removal.

4 The effect of a catalyst, such as activated charcoal, on the rate and amount of oxygen removal.

5 The development of solid compounds offering increased reaction rate and more favorable handling and storage properties.

Work carried out under item 1 is summarized in Figs. 9 and 10, herewith. These graphs show the results of some 40 boiler trials and illustrate clearly the fixed relationship between the three variables.

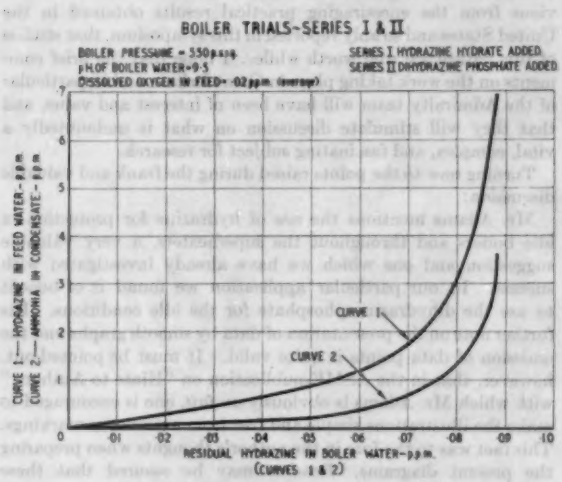
BOILER TRIALS-SERIES I & II
BOILER PRESSURE = 550 p.s.i.g.
pH OF BOILER WATER=9·5
DISSOLVED OXYGEN IN FEED=·02 p.p.m. (average)
SERIES I HYDRAZINE HYDRATE ADDED.
SERIES II DIHYDRAZINE PHOSPHATE ADDED.
CURVE 1 — HYDRAZINE IN FEED WATER — p.p.m.
CURVE 2 — AMMONIA IN CONDENSATE — p.p.m.
CURVE 1.
CURVE 2.
RESIDUAL HYDRAZINE IN BOILER WATER—p.p.m.
(CURVES 1 & 2)

Fig. 9 Hydrazine–Residual Hydrazine–Ammonia Relationships at Low Initial Oxygen Values

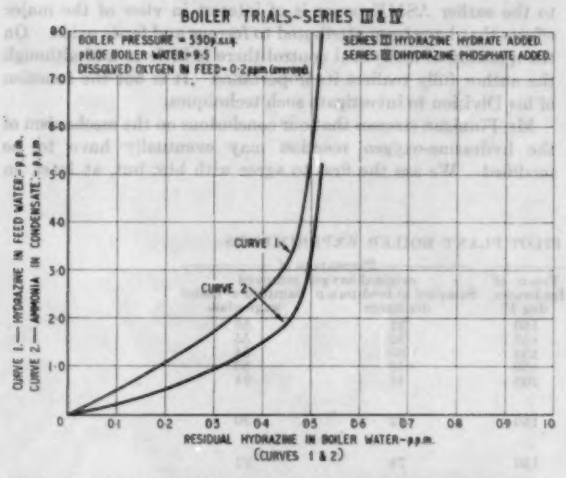
BOILER TRIALS-SERIES III & IV
BOILER PRESSURE = 550 p.s.i.g.
pH OF BOILER WATER=9·5
DISSOLVED OXYGEN IN FEED=0·2 p.p.m. (average)
SERIES III HYDRAZINE HYDRATE ADDED.
SERIES IV DIHYDRAZINE PHOSPHATE ADDED.
CURVE 1 — HYDRAZINE IN FEED WATER — p.p.m.
CURVE 2 — AMMONIA IN CONDENSATE — p.p.m.
CURVE 1.
CURVE 2.
RESIDUAL HYDRAZINE IN BOILER WATER—p.p.m.
(CURVES 1 & 2)

Fig. 10 Hydrazine–Residual Hydrazine–Ammonia Relationships at High Initial Oxygen Values

The second phase of the work studied in more detail the amount of oxygen removed for a given excess of hydrazine and the results obtained are summarized in Figs. 11 and 12. The increase in percentage removal with increasing oxygen content is as would be expected from the law of mass action. The reaction temperature in the feedwater was approximately 150 F and in no case

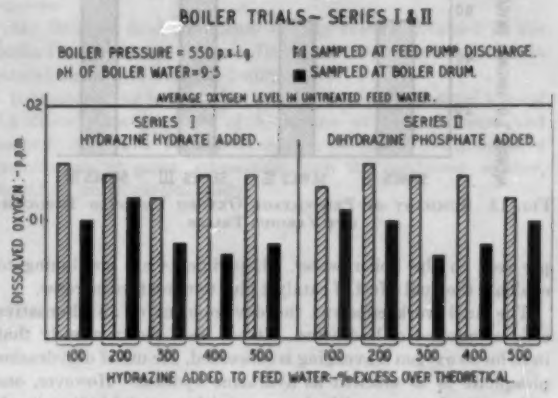
BOILER TRIALS- SERIES I & II
BOILER PRESSURE = 550 p.s.i.g.
pH OF BOILER WATER=9·5
SAMPLED AT FEED PUMP DISCHARGE.
SAMPLED AT BOILER DRUM.
AVERAGE OXYGEN LEVEL IN UNTREATED FEED WATER.
·02
·01
SERIES I
HYDRAZINE HYDRATE ADDED.
SERIES II
DIHYDRAZINE PHOSPHATE ADDED.
DISSOLVED OXYGEN - p.p.m.
100 200 300 400 500 100 200 300 400 500
HYDRAZINE ADDED TO FEED WATER-% EXCESS OVER THEORETICAL

Fig. 11 Summarized Results of Oxygen Removed With Variations in Excess Hydrazine Used at Low Initial Oxygen Values

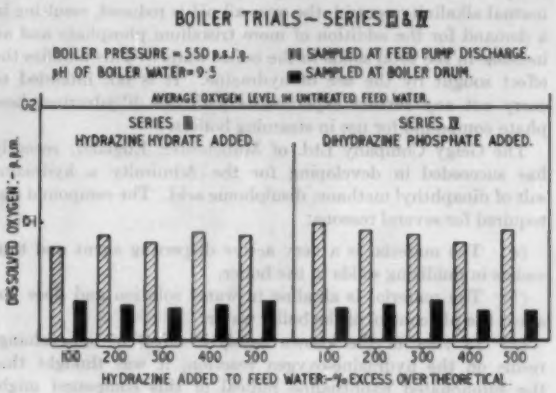
BOILER TRIALS- SERIES III & IV
BOILER PRESSURE = 550 p.s.i.g.
pH OF BOILER WATER=9·5
SAMPLED AT FEED PUMP DISCHARGE.
SAMPLED AT BOILER DRUM.
AVERAGE OXYGEN LEVEL IN UNTREATED FEED WATER.
·02
·01
SERIES III
HYDRAZINE HYDRATE ADDED.
SERIES IV
DIHYDRAZINE PHOSPHATE ADDED.
DISSOLVED OXYGEN - p.p.m.
100 200 300 400 500 100 200 300 400 500
HYDRAZINE ADDED TO FEED WATER-% EXCESS OVER THEORETICAL

Fig. 12 Summarized Results of Oxygen Removed With Variations in Excess Hydrazine Used at High Initial Oxygen Values

was the reaction complete. Finally, Fig. 13 summarizes the percentage of the original oxygen removed throughout these two series of trials.

In the third series of experiments, an attempt was made to determine the effect of feedwater temperature on the rate and degree of reaction. Quoting one typical experiment using hydrazine hydrate and a feed temperature of 203 F (an increase of 86 deg F), the amount of oxygen removed by the time the water reached the feed-pump sampling point had risen from about 60 to 81 per cent and in the boiler water from 85 to 94 per cent.

The fourth series of experiments was carried out to investigate the effect of a catalyst on the reaction rate. In these trials, hydrazine hydrate was again used with an activated charcoal catalyst. Considering the use of low-temperature feedwater at 150 F, the amount of oxygen removed is increased from 60 to 72 per cent at the feed-pump sampling point, and from 85 to 89

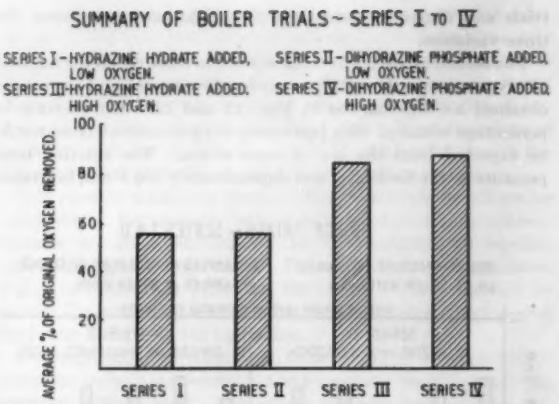
SUMMARY OF BOILER TRIALS ~ SERIES I TO IV
SERIES I - HYDRAZINE HYDRATE ADDED, LOW OXYGEN.
SERIES II - DIHYDRAZINE PHOSPHATE ADDED, LOW OXYGEN.
SERIES III - HYDRAZINE HYDRATE ADDED, HIGH OXYGEN.
SERIES IV - DIHYDRAZINE PHOSPHATE ADDED, HIGH OXYGEN.
AVERAGE % OF ORIGINAL OXYGEN REMOVED.
100
80
60
40
20
SERIES I
SERIES II
SERIES III
SERIES IV

FIG. 13 SUMMARY OF PERCENTAGE OXYGEN REMOVED THROUGHOUT VARIOUS TRIALS

per cent in the boiler water. Experiments are continuing to evaluate the dual effect of catalyst plus temperature increase.

The final work concerns the development of an alternative solid compound of hydrazine. It has been shown already that in so far as oxygen scavenging is concerned, the use of dihydrazine phosphate is as efficient as hydrazine hydrate. However, one serious disadvantage with the use of this material is that it adversely affects the pH of the boiler water. Being a more acid compound than the trisodium phosphate added to the boiler for normal alkalinity control, the over-all pH is reduced, resulting in a demand for the addition of more trisodium phosphate and an increase in the total solids in the boiler water. This nullifies the effect sought by the use of hydrazine. It is not intended to carry out any further experiments with the dihydrazine-phosphate compound for use in steaming boilers.

The Geigy Company Ltd. of Manchester, England, recently has succeeded in developing for the Admiralty a hydrazine salt of dinaphthyl methane, disulphonic acid. The compound was required for several reasons:

(*a*) The material is a very active dispersing agent and thus assists in fluidizing solids in the boiler.

(*b*) The material is alkaline in water solution and does not affect the pH control of the boiler water.

(*c*) In view of the known catalytic effect of ion-exchange resins on the hydrazine-oxygen reaction, it was thought that the sulphonated naphthaline radical of this compound might assist the reaction.

(*d*) The material contained approximately 11 to 15 per cent available hydrazine and was in the form of a dry, free-flowing, inert powder, very suitable for handling and stowage under shipboard conditions. The powder also was immediately soluble in cold water and hence presented no difficulty when preparing a diluted solution.

Initial tests with this compound showed excellent promise and a series of trials have been carried out with feedwater temperatures of 150 and 203 F. At the lower temperature and adding sufficient compound to give an excess hydrazine concentration of 200 to 300 per cent over theoretical; the amount of oxygen removed at the feed pump (compared with straight hydrazine hydrate and no catalyst) is increased from 60 to 80 per cent, and in the boiler water from 86 to 91 per cent. At the higher feed temperature of 203 F, the oxygen removed at the feed-pump discharge showed an increase from 81 to 86 per cent and in the boiler water from 94 to 96 per cent. Table 2 of this closure summarizes the results of these later trials and shows how the percentage removal of oxygen has steadily increased.

It is along this very promising line that our work proceeds and it may well be that as our knowledge of the kinetics of the hydrazine-oxygen reaction increases, so we shall find even more efficient means of promoting this desirable reaction. It is obvious from the encouraging practical results obtained in the United States and so ably reported in this symposium, that studies of this nature are well worth while. I hope that the brief comments on the work taking place in Great Britain and in particular of the Admiralty team will have been of interest and value, and that they will stimulate discussion on what is undoubtedly a vital, complex, and fascinating subject for research.

Turning now to the points raised during the frank and valuable discussion:

Mr. Adams mentions the use of hydrazine for protection in idle boilers and throughout the superheaters, a very valuable suggestion and one which we have already investigated with success. In our particular application we found it of benefit to use the dihydrazine phosphate for the idle conditions. His further note on the presentation of data by smooth graphs and the omission of data points is quite valid. It must be pointed out, however, that in the ASME publication on "Hints to Authors," with which Mr. Adams is obviously *au fait*, one is encouraged to make the illustrations simple and free from extraneous markings. This fact was to the fore in the author's thoughts when preparing the present diagrams. Readers may be assured that these graphs represent the average of some 40 boiler trials.

The points raised by Mr. Adkins have been answered in the author's summary of the more recent work. His reference to the earlier ASME paper is of interest in view of the major effects that have been attributed to ferrous and ferric oxide. On the question of analytical control there is little to add although the author fully realizes its importance. It is not the function of his Division to investigate such techniques.

Mr. Finnigan stresses that our conclusions on the mechanism of the hydrazine-oxygen reaction may eventually have to be modified. We are the first to agree with him but, at least, in

TABLE 2 SUMMARIZED RESULTS OF PILOT-PLANT BOILER EXPERIMENTS

	Conditions of trial			Percentage of original oxygen removed	
Trial series no.	Oxygen scavenger used	Oxygen in feedwater, ppm	Temp of feedwater, deg F	Sampled at feed-pump discharge	Sampled at boiler gage glass
I	Hydrazine hydrate	0.02	150	31	55
II	Dihydrazine phosphate	0.02	150	32	55
III	Hydrazine hydrate	0.20	150	60	84
IV	Dihydrazine phosphate	0.20	150	58	86
V	Hydrazine hydrate	0.20	203	81	94
VI	Hydrazine hydrate plus an activated charcoal catalyst	0.20	150	72	90
VII	Hydrazine salt of dinaphthyl methane, disulphonic acid	0.20	150	78	92
VIII	Hydrazine salt of dinaphthyl methane, disulphonic acid	0.20	203	86	96

the course of modification we shall have learned a lot more about the reaction. In a like manner, we feel no remorse at having introduced the so-called "sour note" into the halcyon picture of the use of hydrazine. It would seem from the results of our own British survey and also from the many similar statements of American experience, that this fact should have been recognized much earlier.

Mr. Jacklin's experience with hydrazine treatments in his experimental boiler unit is very interesting. This work parallels closely our own pilot-plant experiments and it will be interesting to note whether or not our later experiments at 1500 psi confirm the difficulties of maintaining the residual hydrazine content in the boiler water. The present trend of our experiments up to 1000 psi agree with this statement. With regard to the observation about the breakdown of hydrazine at 1500 psi, giving rise to hydrogen, this is very interesting and it is a point that we must follow up during our experiments.

Mr. Marcy indicates that, in his opinion, the mechanism of reduction of ferric oxide is more likely to produce magnetite or hydrated magnetite in preference to ferrous oxide. The author is inclined to agree with him on this point and our later program is scheduled to investigate in more detail this reduction mechanism. With regard to his comments on the catalyzing effect of copper sulphate, undoubtedly the speed of this reaction would have been increased if the latter material had been present. However, from our experiments with various catalysts, activated charcoal has been found to be far superior for this purpose.

Mr. Sturla's final comments on the results obtained in the Imilia Power Plant at Milano, Italy, are very stimulating and, in general, agree well with our findings.

It is interesting to note that again attention is directed toward the dissociation products of hydrazine at high pressure and temperature. The results from this proposed comprehensive examination of gases, emanating from the condenser ejector, should be worth careful study.

Controlling Iron and Copper Pickup With Neutralizing Amines

By J. D. RISTROPH[1] and E. A. YORKGITIS[2]

Cyclohexylamine and morpholine were fed to minimize pickup of iron and copper by controlling pH in the steam-feedwater cycle of a high-pressure, reheat, controlled-circulation boiler. During treatment with either amine, average iron and copper concentrations throughout the system were less than 0.01 ppm. Sampling methods and analytical techniques using improved indicators for iron and copper are described, and the effect of sample acidification is discussed.

Introduction

THE costly and troublesome effects of dissolution and redeposition of iron and copper in central-power stations have been the object of much investigation in recent years. Boiler-tube failures can be caused by corrosion products carried from the condensate-feedwater cycle (1, 2, 3*b*).[3] These deposits also reduce the efficiency of condensers and heaters (4), pumps (3*f*, 3*g*), meters (3*g*), and valves.

In central stations where effective deaeration and scavengers keep oxygen concentration at a minimum, iron and copper pickup, in general, is greater at lower pH values. Two types of inhibitors can be used to minimize this corrosion: A volatile, alkaline substance to raise the pH or a volatile, filming substance to lay down a protective film which separates the metal from the aggressive condensate. The filming amine inhibitors will not be discussed in this paper.

The neutralizing amines, cyclohexylamine and morpholine, have been widely used in recent years to increase pH of the steam-feedwater cycle in central-power stations. Several papers have been written on amine treatment in specific plants (2 to 6). It is the purpose of this paper to present data secured under duplicate operating conditions with these two amines in the steam-feedwater cycle in a high-pressure, reheat, controlled-circulation boiler.

Earlier Amine Treatment at Chesterfield Station

Chesterfield Station has two boilers, Nos. 1 and 2, operating at 900 psig and 900 F and one controlled-circulation unit, No. 3, operating at 1500 psig with initial and reheat steam temperatures of 1000 F. Each boiler supplies a separate turbine. No. 3 boiler is rated at 750,000 lb per hr, No. 3 turbine at 90,000 kw with a peak of 110,000 kw. Either evaporated or demineralized make-up can be used for the two lower-pressure boilers while the make-up for the high-pressure unit is condensate from either of the other units. Details of the station are discussed by Armacost (7) and also by Crossan and Ryan (8).

In June, 1952, the continuous feed of cyclohexylamine was begun to the two lower-pressure boilers. This amine was added also to the controlled-circulation boiler, No. 3 unit, at the start of operation in November, 1952. The results of this treatment after three months of operation were discussed by Ristroph (3*f*). It was reported that the No. 3 unit was clean when opened after several months of operation. Vacuum cleaning of drum and internals produced only 5 lb of deposit, and it was thought possible that part of even that small amount resulted from exposure of boiler metal to atmosphere during the initial chemical cleaning of the boiler. A small amount of extraneous material in the preboiler system, which was not chemically cleaned prior to operation but merely flushed out, may also have contributed to the deposit.

Preliminary investigation (3*f*) on the effect of pH on Fe and Cu pickup during cyclohexylamine treatment on No. 3 unit after three months of operation serves as background for the present discussion. Table 1 shows average Fe and Cu concentrations at several plant locations when the pH was held at 8.5 to 8.7 in the hot-well condensate and again, when the pH was held at 8.9 to 9.1 in the hot-well condensate. The data show that the difference of 0.4 in pH value is important to iron and copper pickup in the No. 3 unit. The iron and copper analyses were made by the orthophenanthroline and oxamide (ASTM tentative) methods, respectively.

Program for Comparison of Morpholine and Cyclohexylamine

Comparison of morpholine and cyclohexylamine was made on No. 3 unit at Chesterfield Station. Each amine, in turn, was fed continuously to the deaerator outlet to hold a pH close to 9 in the hot-well condensate and, after a period of stabilization, comparative data on iron and copper pickup were obtained. The sampling points are noted in the following and also in Fig. 1, the heat-balance diagram for the system:

1 Superheater steam outlet.
2 Hot-well pump discharge.
3 19th stage-heater outlet.
4 Discharge of 17 and 19th stage-heater drip pump.
5 17th stage-heater outlet.
6 14th stage deaerating heater outlet.
7 Economizer inlet.
8 Make-up.
9 Drains from after condenser of air ejector.

Fe, Cu, pH, and NH_3 determinations were run on all samples except the after-condenser drains, on which only pH and NH_3 were determined. During each run, O_2 determinations were made on hot well and 14th stage-heater samples. Continuous analyzing and recording meters also gave records of pH and O_2 content of the steam-feedwater cycle.

Treatment and operating conditions were the same during the addition of each amine. The amine was pumped through a separate chemical feeding system to the outlet of the 14th stage heater. Approximately 0.05 ppm of sulphite based on feedwater was pumped continuously as a spray above the water level in the

---

[1] Chief Chemist, Virginia Electric and Power Company, Richmond, Va.

[2] Research Engineer, Hall Laboratories, Inc., Pittsburgh, Pa.

[3] Numbers in parentheses refer to the Bibliography at the end of the paper.

Contributed by the Joint Research Committee on Boiler Feedwater Studies and presented at the Annual Meeting, New York, N. Y., November 28–December 3, 1954, of The American Society of Mechanical Engineers.

Note: Statements and opinions advanced in papers are to be understood as individual expressions of their authors and not those of the Society. Manuscript received at ASME Headquarters, December 1, 1954. Paper No. 54—A-262.

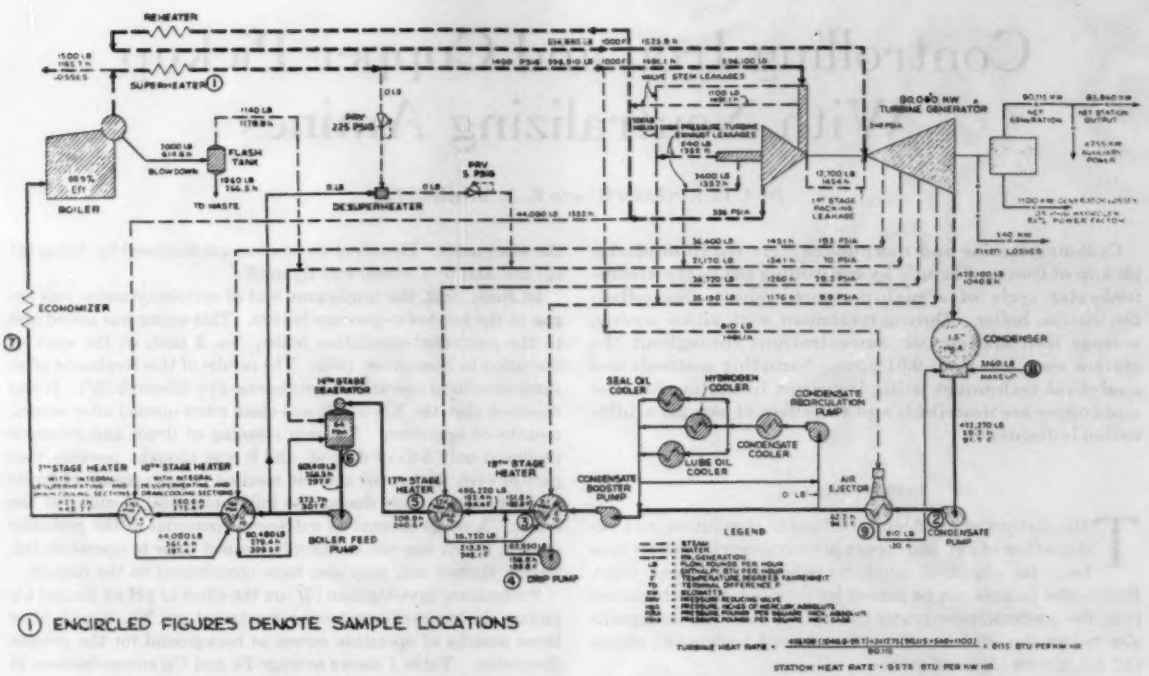

FIG. 1 HEAT BALANCE OF CHESTERFIELD STATION UNIT NO. 3

TABLE 1 Fe AND Cu CONCENTRATIONS AT TWO DIFFERENT pH LEVELS

Sample	Hot well		Inlet 17th stage heater		Inlet deaerator		Inlet economizer	
pH at hot well..	8.5–8.7	8.9–9.1	8.5–8.7	8.9–9.1	8.5–8.7	8.9–9.1	8.5–8.7	8.9–9.1
Ppm total Fe...	0.006	0.004	0.045	0.026	0.000	0.033	0.006	0.004
Ppm total Cu...	0.006	0.005	0.049	0.041	0.019	0.006	0.007	0.004

hot well to maintain 2 to 3 ppm in the boiler water. Boiler water pH was controlled with caustic soda at 10.5 to 11.0, and phosphate residual in the boiler water was 3 to 5 ppm. The free alkalinity was maintained at 25 to 40 ppm sodium hydroxide (NaOH). Condensate from No. 2 unit provided the make-up. Drains from the inner condenser of the air ejector were returned to the condenser, but the drains from the after condenser were wasted; this has always been the practice in No. 3 unit.

The schedule of treatments and testing is as follows:

1 Morpholine treatment, February 1 to March 9, 1954; nine analytical runs, March 4 to March 9.

2 Annual inspection, March 10 to April 4, 1954.

3 Cyclohexylamine treatment, April 4, 1954, to present; nine analytical runs May 3 to 5, 1954.

Runs 4 and 5 with morpholine were conducted at low load, but a low-load run with cyclohexylamine was not possible. Testing was terminated on May 5, because of impending outage of No. 2 unit for annual inspection. This outage would have necessitated the use of condensate from No. 1 unit as make-up for No. 3 unit. A change in source of make-up was not considered desirable during comparative evaluations of the two amines.

Sampling and Analytical Procedures

All sampling was done through stainless-steel lines with Inconel cooling coils and stainless-steel valves. The steam was taken through an ASTM sampling nozzle while all other samples were taken through lines tapped flush into the system. To avoid errors from disturbances all samples were kept flowing continuously at the same velocity for several weeks prior to the test period and during the entire test period.

pH measurements were made with a glass-electrode pH meter utilizing a continuous-flow cell. The meter manufacturer states measurements can be made within ±0.03 pH unit. Inasmuch as pH varies with temperature and test samples ranged between 17 and 31 C, all readings were corrected to a reference temperature of 25 C (77 F) so the data could be compared. The variation of pH with temperature in the system studied was determined by taking a series of readings on individual condensate samples at controlled temperatures over a range from 15 to 35 C. As can be seen from Fig. 2 the correction with cyclohexylamine in the system was ±0.037 pH unit per deg C; with morpholine the variation was ±0.025 pH unit per deg C. For temperatures above 25 C add the value of the correction and subtract for temperatures below 25 C.

Ammonia was determined by direct Nesslerization on 50-ml aliquots using sealed liquid standards. Oxygen determinations were made with the Schwartz and Gurney B Method and "train" sampling. Analyzing and recording meters also gave a check on O_2 content.

Because of the very low concentrations of iron and copper in the system, improved indicators were used, the need for acidification of samples was determined, and special care was used in the analytical techniques.

Newly developed analytical methods for iron and copper (*3i*, 9, 10, 11) employ the indicators bathophenanthroline and neocuproine, respectively. The sampling and analytical procedures for these determinations are discussed fully in the Appendix. Using Klett-Summerson electrophotometers, reading increments of 4.84 and 1.27 represent 0.001 ppm Fe and 0.001 ppm Cu, respec-

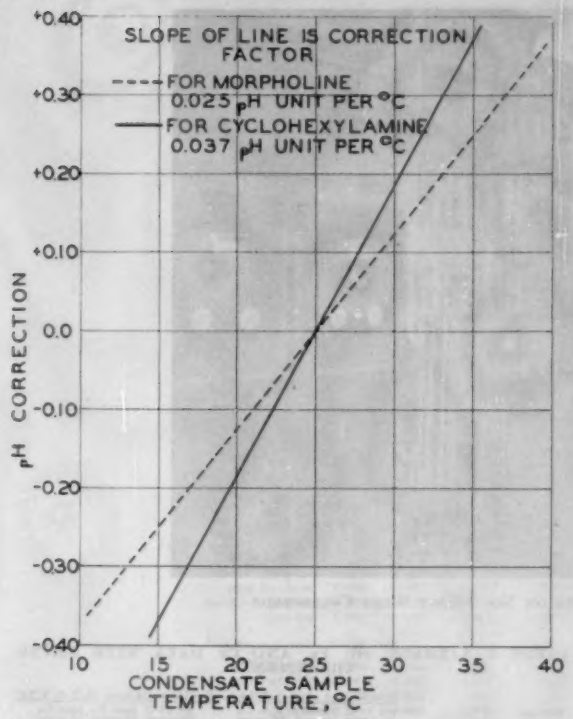

FIG. 2 CHANGE IN pH OF CONDENSATE SAMPLES CONTAINING CYCLOHEXYLAMINE AND MORPHOLINE WITH TEMPERATURE

tively. During the testing periods the Fe reagent blank, including HCl, represented 0.002 ppm Fe, while the Cu reagent blank represented less than 0.004 ppm Cu.

Checking on the necessity of acidifying samples was considered important because of the possibility that part of the iron and copper in the flowing samples was in the form of insoluble oxides or that such oxides would form in contact with air. If oxides were not then converted to a soluble form by the analytical reagents, erroneously low results would be obtained. To obviate this, it would be necessary to acidify the samples and possibly to digest them so as to solubilize any oxides still present. On the other hand, if acidification were not necessary it should be avoided because of possible iron contamination from glassware contacted by the acid and acidified samples, as well as from the acid itself.

To evaluate the three different techniques for iron utilizing, respectively, no acid, acidification, and acidification with digestion, a number of preliminary determinations were made. In each instance a separate blank on deionized water was determined to permit calculation of results. Table 2 lists comparative data taken over a period of several hours.

The necessity for acidification is clearly shown from these data. It is further indicated that digestion of acidified samples might be necessary. There was no apparent evidence that boiling was necessary for complete solubilization of iron in samples from this particular steam-feedwater cycle. Because of possible greater iron contamination from glassware arising from higher temperature in the boiling procedure, it was decided to digest the samples at 60 C (140 F) rather than boil them. As a further check on these procedures a number of the analytical runs were made in duplicate and triplicate as follows:

1 Morpholine Runs 1 and 2 were made with unacidified and acidified samples.

TABLE 2 DATA ON THE NEED FOR ACIDIFICATION OF SAMPLES AND ON THE TYPE OF DIGESTION FOR Fe DETERMINATIONS

	ppm Fe			
Sample	Not Acidified	Acidified	Acidified & Digested 1/2 Hour at 60° C	Acidified & Digested by Boiling 3 Minutes
Steam	0.002	0.003	0.003	0.003
Deaerator Outlet	0.001	0.005	0.006	0.005
Steam	0.000	0.000	0.000	0.000
Economizer Inlet	0.001	0.002	0.002	0.002
Deaerator Outlet	0.001	0.003	0.004	0.003
Hotwell	0.000	0.002	0.002	0.003

TABLE 3 COMPARISON OF AVERAGE Fe VALUES FOR UNACIDIFIED AND ACIDIFIED SAMPLES

Runs 1-3 with morpholine

	ppm Fe	
Sample Point	Not Acidified	Acidified
Superheater Outlet	0.002	0.004
Hotwell Pump	0.003	0.007
19th Stage Heater Outlet	0.003	0.006
17-19th Stage Heater Drip Pump	0.004	0.006
17th Stage Heater Outlet	0.004	0.006
14th Stage Heater Outlet	0.003	0.006
Economizer Inlet	0.003	0.005
Makeup	0.003	0.006

TABLE 4 COMPARISON OF AVERAGE Fe VALUES FOR ACIDIFIED UNDIGESTED SAMPLES, AND ACIDIFIED DIGESTED SAMPLES

Runs 3-9 with morpholine

	ppm Fe	
Sample Point	Acidified Only	Acidified and Digested
Superheater Outlet	0.005	0.005
Hotwell Pump	0.006	0.006
19th Stage Heater Outlet	0.006	0.007
17-19th Stage Heater Drip Pump	0.007	0.007
17th Stage Heater Outlet	0.006	0.007
14th Stage Heater Outlet	0.006	0.007
Economizer Inlet	0.005	0.006
Makeup	0.008	0.007

2 Morpholine Run 3 was made all three ways.

3 Morpholine Runs 4 to 9 were made with acidification and acidification with digestion of samples.

4 Cyclohexylamine Run 1 was made with unacidified and acidified digested samples.

Table 3 compares the average Fe values obtained with acidified and unacidified samples (Runs 1 to 3 with morpholine) and Table 4 compares the average Fe values for acidified undigested samples and acidified digested samples (Runs 3 to 9 with morpholine).

It is readily apparent that all of the iron is not detectable in the unacidified samples. Although a comparison of Fe data for the undigested and digested samples indicated there was negligible difference in these values, it was decided to obtain the rest of the data by digesting the samples to avoid any possibility of negative error.

Checks on several samples showed there was no difference in Cu readings made on unacidified and acidified samples.

To minimize possible errors in Fe and Cu readings due to elapsed time, glassware contamination, or change in meter accuracy, the following was done in addition to adhering to other accepted analytical techniques:

1 Separate Klett-Summerson electrophotometers were used for Fe and Cu determinations.

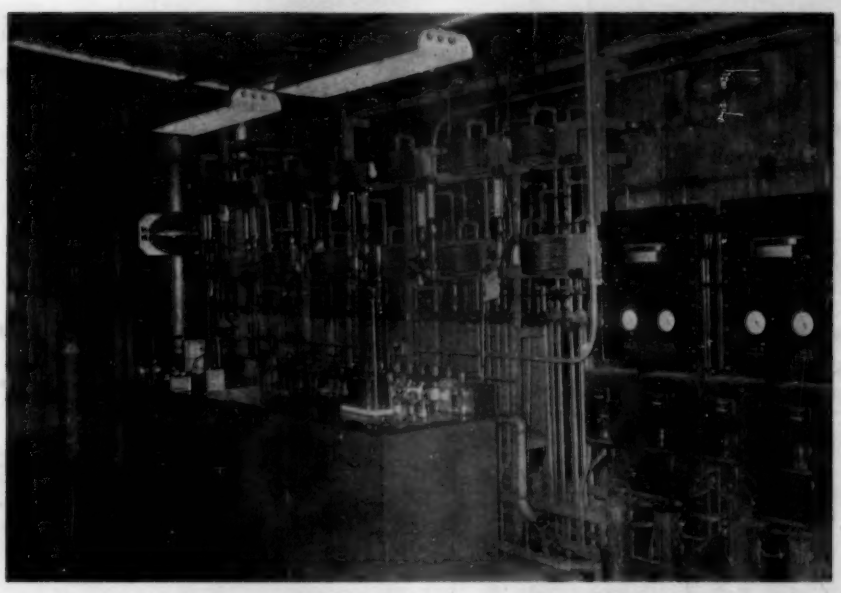

FIG. 3 MAIN WORK AREA WHERE DATA ON NO. 3 UNIT WERE COLLECTED

2 Separate sets of separatory funnels were employed for Fe and Cu determinations.

3 All glassware was used for only one step in the analysis.

4 The Erlenmeyer sampling flasks and separatory funnels were washed with a phosphate detergent and then checked for contamination by making blank runs with deionized water.

5 Sampling flasks and separatory funnels were kept closed between runs.

6 The meters were checked with the reference solution (see Appendix) before and after each set of readings and at other times when any question arose.

Bearing in mind all the factors, the individual Fe and Cu data reported herein are considered correct to ±0.002 ppm while the averages are considered correct to ±0.001 ppm. Duplicate determinations on samples always checked within 0.001 ppm.

Fig. 3 is a photograph of the main work area where the data were collected. This is not the plant laboratory but is the centralized sampling location for unit No. 3. This facility is regularly used by operating personnel who make routine control analyses of the boiler water every 4 hr for alkalinity, sulphite, and phosphate. This work is in addition to that performed by the chemical personnel of the plant.

RESULTS

Table 5 lists the averages of pH, Fe, and Cu values obtained during the principal periods of testing with cyclohexylamine and morpholine in the system. Tables 6 and 7, which are in the Appendix, give the complete data for each run.

The data show that either cyclohexylamine or morpholine, used to maintain condensate pH in the range of 9.0 to 9.1, does a very good job of keeping iron and copper pickup at a minimum. Although it is not known what the iron and copper pickup would be without treatment to raise pH, earlier data (*3f*) secured shortly after the unit was placed in operation and reproduced in Table 1 of this paper showed appreciably greater pickup at a pH level only 0.4 of a unit lower.

Within the accuracy of the meter, the pH was practically constant throughout the system with both amines except in the after-condenser drains. The data obtained do show less constancy for cyclohexylamine after the 17th stage heater. In passing through the 14th stage deaerating heater, the pH during cyclohexylamine addition dropped from 9.09 to 9.01. This would seem to indicate a loss of cyclohexylamine in passing through the deaerator. Then between the 14th stage heater and the economiser the pH went from 9.01 back up to 9.12. Here some slight increase is possible since the amine is fed between these sample points. However, contrary to what might be expected there was no comparable increase at this point during morpholine addition to the same place. Any relatively greater loss of cyclohexylamine from the deaerator apparently was offset by a greater loss of morpholine in blowdown since daily feed rates to maintain pH were comparable, 260 grams (300 ml) for cyclohexylamine and 300 grams (300 ml) for morpholine. Berk and Nigon (11) similarly point out differences in losses from open heaters and blowdown when using cyclohexylamine and morpholine in low-pressure steam systems. It should be noted that initial feed rate of morpholine is substantially higher than that of cyclohexyl-

TABLE 5 AVERAGE pH, Fe, AND Cu DATA WITH AMINE TREATMENTS

Sample	Morpholine (3/4-3/9/54) pH 25°C	ppm Fe	ppm Cu	Cyclohexylamine (3/3-5/5/54) pH 25°C	ppm Fe	ppm Cu
Steam	9.06	0.005	0.001	9.04	0.003	0.001
Hotwell	9.06	0.006	0.005	9.04	0.005	0.003
19th Stage Heater	9.05	0.007	0.006	9.09	0.007	0.003
17-19th Stage Drips	9.07	0.007	0.005	9.08	0.006	0.004
17th Stage Heater	9.06	0.007	0.004	9.09	0.006	0.009
14th Stage Deaerator	9.07	0.007	0.002	9.01	0.005	0.004
Economizer Inlet*	9.07	0.005	0.002	9.12	0.005	0.004
Makeup	8.99	0.009	0.001	9.00	0.009	0.003
After-Condenser Drains	9.69	(NH_3 = 7.2 ppm)		9.54	(NH_3 = 3.3 ppm)	

*Data for Runs 7 and 8 are not included in the averages for the Economizer Inlet since a different, little-used sampling line had to be used for those two runs.

Zero O_2 was found by the Schwartz and Gurney B Method at the hotwell and deaerator outlet on all runs.

Zero NH_3 was found by direct Nesslerization on all samples except the after-condenser drains for all runs.

TABLE 6 MORPHOLINE DATA

Runs were made from March 4 to March 9, 1954.
Zero O_2 was found by the Schwartz and Gurney B method at the hot-well and deaerator outlet on all runs.
Zero NH_3 was found by direct Nesslerization for all samples except the after-condenser drains on all runs.

Sample	Steam	Hotwell	19th Stage Heater Outlet	17-19th Stage Heater Drips	17th Stage Heater Outlet	14th Stage Heater Outlet	Economizer Inlet	Makeup	After-Condenser Drains
Run No. 1 (Load - 106,000 kw)									
pH 25°C	9.11	9.11	9.12	9.04	9.13	9.12	9.11	9.01	9.70
ppm Fe-No Acid	0.002	0.003	0.003	0.005	0.004	0.003	0.002	0.002	
Acid	0.003	0.004	0.004	0.006	0.005	0.006	0.006	0.007	NH_3 =
ppm Cu	0.000	0.004	0.006	0.002	0.003	0.002	0.002	0.001	9.0 ppm
Run No. 2 (Load - 106,000 kw)									
pH 25°C	9.08	9.10	9.06	9.06	9.08	9.10	9.08	9.00	9.63
ppm Fe-No Acid	0.002	0.002	0.003	0.003	0.004	0.003	0.003	0.003	
Acid	0.003	0.004	0.008	0.005	0.006	0.007	0.004	0.006	NH_3 =
ppm Cu	0.000	0.003	0.004	0.003	0.004	0.002	0.001	0.001	8.4 ppm
Run No. 3 (Load - 106,000 kw)									
pH 25°C	9.08	9.09	9.12	9.05	9.11	9.10	9.06	8.98	9.71
ppm Fe-No Acid	0.003	0.004	0.004	0.005	0.004	0.004	0.004	0.004	
Acid	0.006	0.010	0.007	0.007	0.007	0.006	0.006	0.008	NH_3 =
Acid + Digestion	0.007	0.007	0.007	0.007	0.007	0.007	0.005	0.008	8.0 ppm
ppm Cu	0.000	0.004	0.004	0.003	0.002	0.001	0.001	0.001	
Run No. 4 (Load - 60,000 kw)*									
pH 25°C	9.07	9.04	9.08	9.05	9.06	9.05	9.08	8.95	9.65
ppm Fe-Acid	0.004	0.004	0.005	0.007	0.004	0.005	0.004	0.008	
Acid + Digestion	0.004	0.006	0.007	0.007	0.005	0.006	0.005	0.009	NH_3 =
ppm Cu	0.000	0.004	0.005	0.008	0.005	0.001	0.001	0.001	6.0 ppm
Run No. 5 (Load - 60,000 kw)*									
pH 25°C	9.05	9.06	9.03	9.13	9.06	9.07	9.08	8.94	9.55
ppm Fe-Acid	0.003	0.003	0.005	0.006	0.005	0.004	0.004	0.006	
Acid + Digestion	0.004	0.004	0.006	0.008	0.006	0.005	0.005	0.008	NH_3 =
ppm Cu	0.002	0.006	0.009	0.011	0.004	0.002	0.002	0.002	5.6 ppm
Run No. 6 (Load - 90,000 kw)									
pH 25°C	9.02	9.01	9.03	9.00	9.05	9.07	9.06	8.98	9.73
ppm Fe-Acid	0.004	0.005	0.005	0.006	0.005	0.006	0.005	0.006	
Acid + Digestion	0.002	0.003	0.005	0.005	0.004	0.004	0.003	0.006	NH_3 =
ppm Cu	0.001	0.004	0.005	0.003	0.004	0.001	0.002	0.002	5.4 ppm
Run No. 7 (Load - 105,000 kw)									
pH 25°C	9.07	9.06	9.06	9.09	9.07	9.06	9.09**	8.98	9.67
ppm Fe-Acid	0.003	0.004	0.004	0.004	0.005	0.006	0.007**	0.006	
Acid + Digestion	0.007	0.008	0.006	0.006	0.007	0.008	0.008**	0.012	NH_3 =
ppm Cu	0.001	0.005	0.007	0.003	0.005	0.004	0.002**	0.002	6.0 ppm
Run No. 8 (Load - 105,000 kw)									
pH 25°C	9.05	9.06	9.03	9.10	9.03	9.06	9.07**	9.05	9.75
ppm Fe-Acid	0.006	0.008	0.008	0.008	0.008	0.009	0.010**	0.010	
Acid + Digestion	0.006	0.008	0.009	0.009	0.008	0.010	0.011**	0.010	NH_3 =
ppm Cu	0.001	0.006	0.006	0.005	0.004	0.006	0.004**	0.001	8.4 ppm
Run No. 9 (Load - 105,000 kw)									
pH 25°C	9.07	9.05	9.03	9.07	9.02	9.05	9.08	9.08	9.70
ppm Fe-Acid	0.007	0.008	0.007	0.010	0.009	0.008	0.006	0.010	
Acid + Digestion	0.006	0.008	0.007	0.009	0.009	0.008	0.008	0.009	NH_3 =
ppm Cu	0.000	0.005	0.006	0.004	0.004	0.002	0.006	0.001	8.0 ppm

*Low load continuously maintained starting 9 hours before Run No. 4 and continuing through Run No. 5 except for a few minutes when the load went to 90,000 kw 40 minutes before Run No. 4.
**Different, little-used economizer sampling point used for Runs 7 and 8.

amine because to obtain a pH of 9.0 to 9.1 in low CO_2 condensate, morpholine concentration has to be about twice as great as the cyclohexylamine concentration.

Iron and copper pickup was practically the same with both morpholine and cyclohexylamine. The concentrations are small and therefore the differences between results with the two amines are small. This can perhaps be better realized by noting that 0.001 ppm of Fe or Cu in the feedwater represents only about 5 or 6 lb of material entering the boiler in a year with the 5 to 6 billion pounds of water.

Fluctuations in Fe and Cu data between consecutive runs generally were greater than the average differences obtained with the two amines. This is especially true with the Fe concentrations. As an illustration of this fluctuation, iron values in Table 5 for the steam show 0.005 ppm with morpholine and 0.002 ppm with cyclohexylamine. However, two subsequent sets of data by Chesterfield personnel during cyclohexylamine addition showed Fe readings of 0.004 and 0.005 ppm without increases at the other locations.

In general, the copper concentrations were also the same with both amines. The greatest contrast existed at the outlet of the 17th stage heater where with morpholine Cu was 0.004 ppm and with cyclohexylamine it was 0.009 ppm. If we compare these small quantities to the concentrations in the outlet of the preceding 19th stage heater (0.006 ppm with morpholine and 0.003 ppm with cyclohexylamine), it is indicated that in the 17th stage heater 0.002 ppm was deposited during morpholine addition and 0.006 ppm was picked up during cyclohexylamine addition. With equal logic we can say the data indicate a deposition in the 14th stage heater of 0.002 ppm Cu with morpholine and 0.005 ppm Cu with cyclohexylamine.

Operation at low load on Runs 4 and 5 during morpholine treatment did not change the pickup of iron and copper. A low load testing period was not possible during cyclohexylamine treatment.

No ammonia was detected in the steam or condensate at any time during amine treatment using direct Nesslerization. However, there was a small amount which concentrated in the after-condenser drains and thus left the system. This ammonia in the

TABLE 7 CYCLOHEXYLAMINE DATA

Runs were made from May 3 to May 5, 1954.
Zero O_2 was found by the Schwartz and Gurney B method at the hot-well and deaerator outlet on all runs.
Zero NH_3 was found by direct Nesslerization for all samples except the after-condenser drains on all runs.

Sample	Steam	Hotwell	19th Stage Heater Outlet	17-19th Stage Heater Drips	17th Stage Heater Outlet	14th Stage Heater Outlet	Economizer Inlet	Makeup	After-Condenser Drains
Run No. 1 (Load - 105,000 kw)									
pH 25°C	9.06	9.04	9.14	9.12	9.12	9.03	9.14	9.05	9.46
ppm Fe-No Acid	0.003	0.005	0.005	0.005	0.005	0.007	0.003	0.004	
Acid + Digestion	0.006	0.008	0.010	0.009	0.014	0.013	0.009	0.011	NH_3 =
ppm Cu	0.001	0.003	0.005	0.006	0.011	0.007	0.008	0.003	2.0 ppm
Run No. 2 (Load - 110,000 kw)									
pH 25°C	9.06	9.07	9.09	9.16	9.12	8.93	9.11	9.00	9.60
ppm Fe*	0.003	0.009	0.009	0.005	0.010	0.006	0.009	0.007	NH_3 =
ppm Cu	0.000	0.003	0.003	0.004	0.008	0.004	0.008	0.000	4.0 ppm
Run No. 3 (Load - 110,000 kw)									
pH 25°C	9.10	9.08	9.12	9.13	9.11	9.07	9.21	9.05	9.63
ppm Fe*	0.003	0.006	0.010	0.007	0.007	0.008	0.006	0.009	NH_3 =
ppm Cu	0.000	0.002	0.002	0.003	0.012	0.002	0.005	0.008	3.0 ppm
Run No. 4 (Load - 104,000 kw)									
pH 25°C	9.05	9.03	9.06	9.06	9.06	9.02	9.11	8.94	9.56
ppm Fe*	0.002	0.006	0.007	0.007	0.004	0.007	0.004	0.019	NH_3 =
ppm Cu	0.001	0.003	0.004	0.005	0.009	0.003	0.004	0.007	3.0 ppm
Run No. 5 (Load - 104,000 kw)									
pH 25°C	9.06	9.02	9.12	9.08	9.11	9.01	9.12	8.94	9.50
ppm Fe*	0.004	0.004	0.007	0.005	0.007	0.008	0.004	0.009	NH_3 =
ppm Cu	0.000	0.002	0.002	0.002	0.007	0.002	0.002	0.001	3.0 ppm
Run No. 6 (Load - 106,000 kw)									
pH 25°C	9.09	9.04	9.07	9.10	9.11	9.01	9.02	9.02	9.57
ppm Fe*	0.001	0.003	0.004	0.004	0.002	0.004	0.003	0.007	NH_3 =
ppm Cu	0.001	0.003	0.003	0.004	0.008	0.002	0.002	0.001	3.5 ppm
Run No. 7 (Load - 95,000 kw)									
pH 25°C	9.01	9.02	9.05	9.04	9.06	8.99	9.04	9.00	9.56
ppm Fe*	0.001	0.004	0.006	0.006	0.003	0.002	0.003	0.007	NH_3 =
ppm Cu	0.001	0.003	0.003	0.004	0.008	0.002	0.002	0.002	3.5 ppm
Run No. 8 (Load - 94,000 kw)									
pH 25°C	9.02	9.02	9.05	9.04	9.06	9.02	9.11	9.00	9.56
ppm Fe*	0.001	0.003	0.004	0.005	0.003	0.005	0.003	0.007	NH_3 =
ppm Cu	0.001	0.002	0.004	0.004	0.009	0.002	0.003	0.002	3.5 ppm
Run No. 9 (Load - 100,000 kw)									
pH 25°C	8.94	9.03	9.05	9.05	9.05	9.03	9.10	9.04	9.52
ppm Fe*	0.001	0.003	0.005	0.004	0.003	0.004	0.003	0.007	NH_3 =
ppm Cu	0.002	0.002	0.003	0.004	0.007	0.001	0.002	0.001	3.5 ppm

*All Fe values for Runs 2-9 were determined on samples which were acidified and digested.

drains ranged from 5.4 to 9.0 ppm with morpholine and 2.0 to 4.0 ppm with cyclohexylamine. Since some of this NH_3 was probably the result of breakdown of amine, the difference during the two treatments might seem to corroborate the report by Jacklin (12) that morpholine addition results in more ammonia from breakdown than does cyclohexylamine addition. The difference could be due largely to the fact that morpholine concentration is about twice that of cyclohexylamine to maintain the cycle at a pH of 9.0 to 9.1. The flow of air-ejector after-condenser drains was found to be 435 lb per hr at a steam load of 715,000 lb per hr. Therefore the average ammonia in the after-condenser drains represented 0.004 ppm NH_3 in the steam with morpholine feed and 0.002 ppm NH_3 with cyclohexylamine. It is important to realize these figures include not only ammonia resulting from any breakdown of amine but also any ammonia appearing in the system naturally.

The boiler was found to be clean during the annual inspection, which occurred after the morpholine and before cyclohexylamine treatments. Ristroph (3*f*) reported it was clean also at the previous inspection following cyclohexylamine treatment.

The effect of the excellent oxygen removal from the system cannot be evaluated exactly, but it certainly is important. A trace difference in oxygen concentration could be of major importance, and might be the reason for fluctuations that do occur in the Fe and Cu data. Although spot checks on the hot-well condensate with the Schwartz and Gurney B Method showed zero, the recording meter indicated a range of 0.000 to 0.003 ppm.

The results presented were obtained under normal operating conditions for the No. 3 unit at Chesterfield Station. Identical Fe and Cu results would not necessarily be obtained in another central-power station. We must reiterate that this is a reheat cycle with very low moisture content in the last stages of the turbine. Thus the possibility of corrosion-erosion attack in the region of initial steam condensation is reduced. It has been reported by Bigger, et al. (3*c*), Straub (3*e*), and Archibald, et al. (6) that low pH of the initial condensate can be a factor in such turbine wastage. The same investigators reported further that the pH of condensate in the turbine depends on the solubility relationships in the steam and condensate of H_2S, SO_2, or CO_2 and/or of substances used to elevate pH of the cycle. No evidence of corrosion-erosion attack has been found in No. 3 unit, nor in units Nos. 1 and 2, which have comparable feedwater treatment but which do not operate with a reheat cycle. Fe and Cu values for the cycles of Nos. 1 and 2 closely approximate the values found in No. 3 cycle.

Conclusions

With either morpholine or cyclohexylamine fed to maintain a condensate pH of 9.0 to 9.1, Fe and Cu concentrations in No. 3 unit of Chesterfield Station are kept at very low values—less than

0.01 ppm throughout the steam-condensate-feedwater cycle. Attainment of these desirably low levels may be due in part to rigid control over other factors influencing the pickup of metals in the steam-feedwater cycle. Oxygen contamination is probably the most important of these other factors.

Good sampling facilities and analytical procedures are essential in obtaining reliable data. Of particular importance are the continuous flow of samples, solubilization of Fe and Cu in the sample, and the use of sensitive indicators such as bathophenanthroline and neocuproine in the determinations of these metallic contaminants.

Feed requirements for maintenance of pH are approximately the same in the cycle under study with either morpholine or cyclohexylamine. Build-up of ammonia in the system because of breakdown of either amine is negligible. However, part of the small amount of ammonia discarded with the after-condenser drains represents possible breakdown of the amines.

Acknowledgments

The authors wish to record their appreciation of the courteous co-operation given them during the test work and writing of the paper by personnel of Virginia Electric and Power Company and Hall Laboratories, Inc., especially by the following:

Mr. T. E. Crossan, System Superintendent of Production for Virginia Electric and Power Company.

Mr. F. H. Spies, Superintendent of Chesterfield Station.

Mr. C. D. Moore, Assistant Efficiency Engineer of Chesterfield Station.

Mr. G. B. Miller, Chemist for Chesterfield Station, for his participation in collecting the data.

Mr. R. R. Christian, Research Engineer with Hall Laboratories, Inc., for his participation in collecting the data.

Mr. V. M. Marcy of Hall Laboratories, Inc., for his advice on the various analytical procedures.

In addition, the authors wish to acknowledge the advice of Mr. R. F. Andres, Chief Chemical Engineer for The Dayton Power & Light Company, concerning the methods of analysis for Fe and Cu.

BIBLIOGRAPHY

1 "Causes and Prevention of Iron Oxide in Boilers," by S. T. Powell, L. G. von Lossberg, and J. K. Rummel, Proceedings Midwest Power Conference, vol. 12, 1950, pp. 133–144.

2 "Reduction of Condensate-Line Corrosion," by Scott Jensen and E. R. Lang, Trans. ASME, vol. 76, 1954, pp. 245–249.

3 "Panel Discussion on Corrosion and Deposits in Condensate and Feedwater Systems," Proceedings Fourteenth Annual Water Conference, Pittsburgh, Pa., sponsored by Engineers Society of Western Pennsylvania, October, 1953, pp. 81–118.

(*a*) "Factors Influencing Metal Loss in Condensate and Feedwater Systems," by S. K. Adkins, National Aluminate Corporation, Chicago, Ill., p. 81.

(*b*) "Iron and Copper Deposits in Boilers," by R. C. Ulmer, Engineering Department, Combustion Engineering-Superheater, Inc., New York, N. Y., p. 83.

(*c*) "Corrosion in the Moisture Region of Large Steam Turbines," by T. W. Bigger, J. F. Quinlan, and C. C. Carson, General Electric Company, Schenectady, N. Y., p. 85.

(*d*) "Effect of Sulphite Treatment of Boiler Water on Condensate pH," by F. L. Archibald, Supervising Engineer, Boston Edison Company, Boston, Mass., p. 89.

(*e*) "Comparison of Ammonia, Amines, and Hydrazine in Reducing Metal Pickup in the Condensate and Feedwater Systems of Closed Cycle Steam Power Plants," by F. G. Straub, Res. Prof. Chemical Engineering, University of Illinois, Urbana, Ill., p. 90.

(*f*) "The Use of Cyclohexylamine for pH Control of Condensate and Feedwater," by J. D. Ristroph, Virginia Electric and Power Company, Richmond, Va., p. 94.

(*g*) "Experiences With Ammonia and Cyclohexylamine at the Springdale and Mitchell Power Stations," by E. L. Jacobs and W. L. Thompson, West Penn Power Co., Pittsburgh, Pa., p. 100.

(*h*) "Precautions in the Use of Ammonia and Amines," by E. A. Yorkgitis, Hall Laboratories, Inc., Pittsburgh, Pa., p. 103.

(*i*) "Analytical Methods for pH, Iron, and Copper," by R. F. Andres, The Dayton Power & Light Company, Dayton, Ohio, p. 106.

4 "Accurate pH Control Eliminates Corrosion," by M. L. Crater, *Power*, vol. 16, October, 1952, p. 78.

5 "Contamination of Condensate by Heat-Exchanger-Tube Alloys," by J. D. Ristroph and E. B. Powell, Trans. ASME, vol. 75, 1953, pp. 729–745.

6 "Prevention of Metal Losses in the Wet Steam Areas of Steam Turbines," by F. L. Archibald, J. W. Pursell, Jr., and F. G. Straub, Proceedings American Power Conference, vol. 15, 1953, pp. 579–587.

7 "The Controlled-Circulation Boiler," by W. H. Armacost, Trans. ASME, vol. 76, 1954, pp. 715–725.

8 "Controlled-Circulation at Chesterfield," by T. E. Crossan and W. F. Ryan, Trans. ASME, vol. 76, 1954, pp. 727–734.

9 "The Colorimetric Determination of Iron in Raw and Treated Municipal Water Supplies by Use of 4:7-Diphenyl-1:10-Phenanthroline," by G. F. Smith, W. H. McCurdy, Jr., and Harvey Diehl, *The Analyst*, vol. 77, August, 1952, pp. 418–422.

10 "2,9-Dimethyl-1,10-Phenanthroline, New Specific in Spectrophotometric Determination of Copper," by G. F. Smith and W. H. McCurdy, Jr., *Analytical Chemistry*, vol. 24, February, 1952, pp. 371–373.

11 "Amine Volatility and Alkalinity in Relation to Corrosion Control in Steam Heating Systems," by A. A. Berk and J. Nigon, U. S. Dept. of Interior, Bureau of Mines Technical Paper 714, 1948.

12 "Experimental Boiler Studies of the Breakdown of Amines," by C. Jacklin, ASME Annual Meeting, December, 1953.

Appendix

Sampling and Analytical Procedure for Iron and Copper Determination at the Chesterfield Station

The analytical procedures used in this work are adaptations of the methods developed by G. F. Smith (9, 10). The bathophenanthroline and neocuproine indicators employed are much more sensitive than those commonly used in the industry.

The iron and copper tests are quite specific and free from interference. However, techniques had to be developed to eliminate errors which are apparent when using these highly sensitive indicators, but which are not evident when employing less sensitive ones such as orthophenanthroline for Fe and carbamate for Cu. Among factors affecting the accuracy of the analyses we can list sampling techniques, cleanliness, and "passivity" of the glassware, standardization of time intervals, and temperature for color development, and proper adjustment of sample pH.

Sampling turned out to be one of the most critical variables. Our work, as well as unpublished data of others, has shown that changes in the rate of flow in a sample line will seriously affect the iron and copper values found even several hours after the change is made. It is thought that this phenomenon is caused by the dislodging of iron and copper oxides in the sample lines by changes in the rate of flow. In the reported tests the sample lines were permitted to flow continuously at a constant rate beginning several weeks prior to actual sampling.

Various aspects of sample acidification were investigated as indicated in the text. It was noted that low iron values were found when no acidification was used. This was undoubtedly due to the presence of relatively insoluble iron oxides either already present in the condensate or formed through contact with the air during sampling. However, and we believe more nearly correct, greater values were obtained when the samples were acidified and digested.

In addition to the normal procedure for cleaning glassware, it was found necessary to passivate the surface of the new pyrex glassware used to prevent pickup of iron from the surface of the glass. Under normal cleansing procedures, extremely high readings in iron values were found on analysis of standard solutions in the range of 0 to 0.05 ppm. This was especially true with acidified samples and even more pronounced with acidified digested samples.

The problem of inadequate cleaning was overcome by allowing the pyrex glassware to soak for several hours in hydrochloric acid solution (1:4) and then thoroughly cleaning with a phosphate detergent. The glassware was further cleaned and checked by successive extractions with reagents used in the analyses. Reproducibility of results was on the order of 0.001 ppm when tests were run on glassware cleaned in the foregoing manner.

It was found essential that time and temperature variables be rigidly controlled. It was also found necessary in the Fe determination that the pH of the solution at the color development stage be approximately 4.0 for proper color development. In the Cu determination the pH at the color development stage is not as critical; it was around 5.5 with the procedure used.

Detailed procedures for the two tests are listed in the following. It is important for reasons of safety that the work be conducted in a well-ventilated area away from open flames.

Total Iron

1 Place 5 ml of hydrochloric-acid solution (1:4) in a properly cleaned Erlenmeyer flask calibrated with a mark at 500 ml. Collect the sample with a clean tube extending to the bottom of the flask, with the flask tilted initially so the sample will be collected under the acid in the flask. Fill with sample to the 500-ml mark. Agitate the sample. If a copper test is to be made, save a 200-ml aliquot for this determination. Measure another 200-ml aliquot and return it to the drained flask.

2 Within 15 min of sampling, digest the sample for 30 min at 60 C. Cool to the temperature at which the calibration curve was determined.

3 Transfer the cooled digested sample to a 250-ml separatory funnel, rinsing the flask into the funnel with 10 ml of iron-free demineralized water.

4 Add 4-ml hydroxylamine-hydrochloride solution and mix.

5 Add 8 ml of sodium-acetate solution and mix.

6 Add 2 ml of bathophenanthroline solution. Shake the funnel vigorously for exactly 1 min.

7 Immediately add 25 ml of isoamyl alcohol. Again, shake the funnel vigorously for exactly 1 min.

8 Allow to stand exactly 5 min for separation of the alcoholic and aqueous layers.

9 Drain off the aqueous layer and discard.

10 Add 10-ml isopropyl alcohol and shake the funnel exactly 30 sec.

11 Wipe the inside of the separatory funnel stem dry with lint-free tissue and flush by draining a small amount of alcoholic layer.

12 Drain the alcoholic solution into a 40-mm rectangular cuvette and measure per cent transmittance with a suitable photometer. For the testing reported in this paper an industrial model Klett-Summerson photometer was used with a KS-52 (green) filter. Use as a reference solution 25 ml of isoamyl alcohol mixed with 10 ml of isopropyl alcohol.

13 Correct the sample reading by subtracting the reagent blank. Obtain ppm Fe by multiplying the corrected reading by the calibration factor which is found in the manner discussed below.

The calibration curve is established by treating standard iron solutions as in the foregoing procedure. The standards are prepared by mixing suitable volumes of standard iron solutions with iron-free demineralized water. Since a straight line is obtained by plotting meter readings versus ppm Fe in the range 0 to 0.05 ppm Fe, a calibration factor can be used. Based on the slope of the line, the factor is 0.000207 for the particular instrument used.

Total Copper

1 A portion of the acidified sample obtained for iron, or another obtained in a similar manner, is used as the sample.

2 Transfer 200 ml of sample to a specially cleaned 250-ml separatory funnel within 15 min of sampling.

3 Add 1-ml hydroxylamine-hydrochloride solution and mix.

4 Add 10-ml sodium-acetate solution and mix.

5 Add 2-ml neocuproine solution and shake the funnel exactly 1 min.

6 Add 25-ml isoamyl alcohol and shake the funnel again exactly 1 min.

7 Allow to stand 5 min for separation of the alcohol and aqueous layers.

8 Drain off the aqueous layer and discard.

9 Add 10-ml isopropyl alcohol and shake the funnel exactly 30 sec.

10 Dry the inside of the separatory funnel stem with lint-free tissue and flush by draining a small amount of alcoholic layer.

11 Drain into a 40-mm rectangular cuvette and read per cent transmittance with a suitable photometer. For this work an industrial model Klett-Summerson photometer was used with a KS-44 (blue) filter. Use as a reference solution 25 ml of isoamyl alcohol and 10 ml of isopropyl alcohol.

12 Correct the sample reading by subtracting the reagent blank. Obtain ppm Cu by multiplying the corrected reading by the calibration factor which is found in the manner discussed below.

The calibration curve is established by treating standard copper solutions as in the foregoing procedure. The standards are prepared by mixing suitable volumes of standard copper solutions with copper-free demineralized water. A straight line is obtained by plotting meter readings versus ppm Cu in the range 0 to 0.05 ppm Cu. Based on the slope of the line, the calibration factor is 0.000787 for the particular instrument used.

Reagents

All reagents should be free of the metals to be determined. Hydroxylamine-hydrochloride and sodium-acetate solutions may be purified by using the bathophenanthroline indicator for iron and neocuproine indicator for copper.

Iron Reagents

1 Bathophenanthroline—0.0025M. Dissolve 0.0835 g in 100 ml of iron-free isopropyl alcohol.

2 Hydroxylamine hydrochloride—10 per cent solution.

3 Sodium-acetate solution—10 per cent solution.

4 Isoamyl alcohol—reagent grade.

5 Isopropyl alcohol—iron free.

6 Iron-free water—deionized water.

Copper Reagents

1 Neocuproine—dissolve 0.10 g in 50 ml of isopropyl alcohol. Dilute solution to 100 ml with copper-free deionized water.

2 Hydroxylamine hydrochloride—20 per cent solution.

3 Sodium acetate—20 per cent solution.

4 Isoamyl alcohol—reagent grade.

5 Isopropyl alcohol—iron free.

6 Copper-free water—deionized water.

Discussion

H. A. Grabowski.[4] The authors have presented data which compare the relative merits of two neutralizing amines in curbing the corrosion of copper and iron surfaces of preboiler equipment that are in contact with a pure grade of water. Extreme care was taken in selecting the procedures of sampling and analysis to insure an accurate evaluation of the factors under investigation. The testing procedure is a superior one and should serve as a ref-

[4] Research Engineer, Research Department, Combustion Engineering, Inc., New York, N. Y. Mem. ASME.

erence for future investigations of corrosion problems in a feedwater system.

In discussing the relative merits of the two amines, there may be a tendency to overlook the value of the sampling techniques which have been utilized in procuring the data for this paper. The authors have shown that it is necessary to obtain a sample under an acid solution and to digest that sample in acid in order to obtain a true value of iron content in the water. If sampling under acid is not utilized the corrosion products of iron found in the feedwater tend to form oxides which have a low solubility in acid. These materials also tend to precipitate on the surface of the sample bottle. Values recorded by the latter sampling method are low and tend to give a false impression of being free from corrosion products. Sampling under acid, followed by digestion, was used by the writer in a number of feedwater surveys. In one case the oxygen content of the feedwater was about 0.5 ppm and the pH of the water was not controlled by the use of amines or ammonia. The iron content of the water generally recorded was about 0.01 ppm. When the sampling was completed under an acid solution, the iron content of the water varied between 0.05 and 0.10 ppm.

Even with the use of the best analysis techniques it is not always possible to determine the true corrosion tendency of a system high in oxygen and low in pH. The oxygen tends to react with the corrosion products to form oxides which can precipitate on the heater surfaces. Changing flow conditions tend to loosen these oxides and a turbid sample, high in iron and copper oxides, is obtained. Testing such a system generally results in the detection of small quantities of corrosion products. In one survey the gage glasses were heavily coated with oxides and yet the iron content was about 0.02 ppm. When the pH of the feedwater was adjusted to a value of about 9.0 and the oxygen content was reduced to 0.01 ppm, the glasses cleared up and the samples were only slightly turbid after a variation in water flow. The foregoing items were recognized by the authors and consideration was given to the effect of air on the corrosion products in the sample.

The relative merits of neutralizing amines and ammonia have been discussed at length at various technical sessions. Mr. J. D. Ristroph[6] has presented evidence that ammonia and cyclohexylamine provide an equal measure of protection to iron and copper surfaces when a pH value of 9.0, due to these chemicals, was maintained in the feedwater. The data in this paper indicate that morpholine and cyclohexylamine also provide a similar corrosion protection when a pH value of 9.0 to 9.1 is maintained in the feedwater. These observations are similar to those made by the writer in the analysis of the feedwater-corrosion problem in a large number of utility systems. The protection of the iron and copper surfaces is obtained by adjusting the pH value to about 9.0 in the feedwater system. Similar rates of corrosion were found when the pH control was adjusted to maintain either 2 ppm of cyclohexylamine, 4 ppm of morpholine, or 0.3 ppm of ammonia in the water. The decision as to the chemical chosen to provide the protection is made on the basis of stability at high temperatures, ease of control, the location of the areas of metal surface that require pH control, and the cost of the item.

The concentration of morpholine at the various sample points was not included in this paper. Laboratory experiments have shown that, at about 1600 psi, there would be about 3.3 ppm of morpholine in the boiler water when there is 4.0 ppm in the steam. It would be interesting to compare the daily requirements of sulphite and phosphate in respect to the morpholine requirement. All these items should be removed by blowdown in about the same ratio. The actual feed of morpholine used at Chesterfield is low in comparison to other installations. It would be interesting to obtain a determination of the concentration of this material in the water.

Morpholine has been shown by others to protect the wet stages of a turbine. It would be interesting to collect data on the protection afforded to this region by cyclohexylamine.

R. F. Andres.[6] This paper presents precise analytical data to support the general observation that iron and copper pickup from feedwater systems can be minimized by maintaining pH values in the range of 8.9 to 9.1. From the data presented, it is apparent that either cyclohexylamine or morpholine produced excellent results in this system yielding iron and copper values in the feedwater of less than 0.01 ppm. It may be of interest that comparable low values for iron and copper pickup are being obtained in one of our stations using ammonia instead of amines.

The data presented in Table 1 from a previous paper shows iron and copper concentrations about 5 to 10 times higher than indicated in the data reported in this paper for feedwater sampled from practically identical points in the system at or near the deaerator while maintaining pH values of 8.9 to 9.1 in both cases. Perhaps the authors can explain this seemingly wide divergence in results under apparently similar operating conditions. The data in Table 1 also indicate a sizable reduction in iron and copper pickup when the pH value is raised 0.4 unit from 8.6 to 9.0. In our experience, using ammonia for pH elevation, we have not been able to detect any appreciable change in copper or iron pickup over the pH range of 8.7 to 9.1. The values for copper and iron over this pH range are less than 0.01 ppm.

The importance of dissolved oxygen on copper and iron pickup in feedwater systems is emphasized throughout the paper and sodium sulphite is added to scavenge residual traces of oxygen which might be present. We have been able to obtain values for copper and iron pickup in the same range as this paper, depending on mechanical deaeration, which produces water essentially oxygen-free by the Schwartz and Gurney B Method, without adding a chemical treatment for oxygen removal.

The methods of analyses and sampling procedures outlined in this paper seem quite complete and it is to be hoped that other companies will use this information to precisely evaluate their particular feedwater systems. The reference to the possibility of pickup of iron from glassware during analysis, particularly during the boiling or digestion stage with acid, seems feasible. Perhaps the use of polyethylene sample containers for collection and digestion of the acidified water samples might solve this problem. Since these analytical methods are based on measurement of the color developed in a solvent extractant, the sensitivity of the methods could be increased by using only 5 ml of solvent and utilizing the test-tube adapter available for the Klett-Summerson colorimeter.

The authors are to be congratulated for an informative and comprehensive paper which may serve as a guide to others faced with the problem of excessive copper and iron pickup in their feedwater systems.

L. D. Schultz.[7] In reviewing this very well-prepared paper, the writer has been especially impressed by the exceptionally low results reported for iron and copper in the feedwater at Chesterfield Station. The following comment relates mainly to this information and the test procedures by which the results were obtained.

As indicated by the authors, obtaining a representative sample

[5] Reference (3*f*) of the Bibliography of the paper.

[6] Chief Chemical Engineer, The Dayton Power and Light Co., Dayton, Ohio.

[7] Chief Chemical Engineer, Industrial Chemical Cleaning Service Co., Long Beach, Calif.

is of paramount importance. In view of the established tendency of iron and copper to plate or drop out on sample lines, and the possible pickup of iron and copper oxides by changes in sample flow rates, it seems to the writer that sample lines as short as possible would be preferable to those extended to central test stations. Of course these tendencies are overcome, in part, by flushing the sample lines at constant-flow rates for extended periods, as the authors have reported.

The authors infer that iron is leached from the pyrex glassware and/or is adsorbed on the glass surface from the samples. According to Corning Glass Works,[8] the loss in weight of pyrex-brand glass is 0.000002 gram per sq cm in redistilled water for 48 hr at 80 C, and 0.000002 gram per sq cm in 5 per cent hydrochloric acid for 72 hr. Assuming the loss of glass is proportional to time, rough calculations will show that the amount of glass lost to the sample is on the order of 0.01 to 0.02 ppm per hr, based on a 500-ml sample. With iron present in trace quantities in pyrex, this represents a negligible amount of iron, especially when compared to other sources of error.

It would seem that any significant amount of iron pickup due to glassware comes from iron adsorbed on the glassware surfaces from previous samples. If this is true, low results may be obtained by short-time digestion at low temperatures, since iron that has plated out will not contribute to the final result.

It would be of interest to know if the glassware is cleaned by the acid-soaking procedure before every sample, or is this necessary for new glassware only? Or does the glass reach equilibrium with the sample if not cleaned each time?

In a method proposed by J. K. Rummel, the copper sample is digested with nitric acid as well as hydrochloric acid, since he found exceptionally low results due to insoluble copper not dissolved by hydrochloric acid alone. It is thought that this is a well-known procedure for dissolving copper by first oxidizing it with nitric acid. It would be of interest to know if the authors have tried this modification of the method, and if they determined the effect of acidification and digestion on copper.

In the same method for copper, Mr. Rummel extracts the color developed with diethanolamine[9] with n-hexyl alcohol. This same extractant, n-hexyl alcohol, has been used in place of isoamyl alcohol for the iron procedure using an ethanol solution of bathophenanthroline.[10] Mr. G. F. Smith states that the ferrous complex is more completely removed by one extraction with n-hexyl alcohol than by a similar treatment with isoamyl alcohol, and that it is probably due to the fact that n-hexyl alcohol is the least water-soluble alcohol of the group.[9] In this case the addition of isopropyl alcohol seems an unnecessary dilution of the extracted color. It would be of interest to learn the use of the isopropyl alcohol in the authors' procedure. It is thought it may be required to dissolve water that would otherwise make the extract cloudy and is useful only incidentally in cleaning the separatory funnel.

The writer wonders if the success reported by the authors (and previously reported by Mr. Ristroph) in reducing iron and copper pickup is due entirely to the increase of pH from 8.6 to 9.0. We have seen one report from a central test station where the increase in pH from 8.4 to approximately 9.0 with morpholine had no noticeable effect on iron and copper pickup. Our own experience at one of our stations indicates that increasing the pH above 8.5 with cyclohexylamine does not appreciably reduce the iron and copper pickup. We are now, at this same station, starting a morpholine test program. Although we have not yet increased the pH above 8.7, there has been no reduction in iron and copper pickup. Before the test is completed, however, we plan to raise the pH to 9.0 and observe the effect on iron and copper. Perhaps the effect of dissolved oxygen and/or other dissolved gases has a greater influence on corrosion than an increase in pH from 8.5 to 9.0. This could explain why the authors find much less iron and copper than others, when holding the pH at 9.0.

[8] Catalog No. LP 34, p. 7, Corning Glass Works, Corning, N. Y.
[9] *Analytical Chemistry*, vol. 20, 1948, pp. 722–724.
[10] *The Analyst*, vol. 77, pp. 418–422, 1952.

Authors' Closure

The authors sincerely thank the discussers for their comments. The discussions, which are based primarily on plant experience, represent pertinent contributions to this paper. There is no disagreement among the authors and discussers concerning the widely accepted practice now of elevating the condensate pH in central stations to a value above 8 and around 9.

The discussions do, however, point up the fact that no two plants are exactly the same. Thus the iron and copper pickup does not vary with pH in quite the same way in every plant. Mr. Schultz reports that one of the Southern California Edison plants gained nothing by increasing the pH of the condensate above 8.5. Mr. Andres reports that in his company's plant experience there is no appreciable change in copper or iron pickup over the pH range of 8.7 to 9.1. Jacobs and Thompson[11] reported data for Springdale Station which suggest that there is a definite break in iron pickup around a pH of 8.6 or 8.7. Ristroph[12] reported that at Bremo Station there was a significant drop in iron pickup above a pH of about 8.6.

With good sampling facilities and the available analytical methods each plant can determine the practical minimum condensate pH which should be maintained for minimum iron and copper pickup in that system. Some plants such as cited by Mr. Schultz may not require a condensate pH above 8.5 and may not need pH even that high. However, the authors recommend that in the absence of specific plant data a condensate pH of 8.8 to 9.0 be maintained.

Mr. Grabowski's discussion of the need for collecting condensate and feedwater samples under acid and digesting them for iron and copper determinations presents valuable views on a subject whose importance cannot be overemphasized.

We do not know what the morpholine concentrations were at various points in the system nor how much was lost with blowdown. If the figures mentioned by Mr. Grabowski are assumed to apply to No. 3 Unit at Chesterfield Station, the average daily blowdown of 75,000 lb removed about 115 ml of the 300-ml feed of morpholine.

Referring to Mr. Andres' observation that earlier data for Chesterfield Station were at variance with the newest iron and copper data, the earlier data may have been high because the piping had been in use only several months and was merely flushed out and not chemically cleaned prior to use. Complete chemical and mechanical stabilization had not yet been attained. We have found that polyethylene sample containers are practical as suggested by Mr. Andres.

In the work reported, relatively large volumes of solvent were used to minimize percentage error caused by volume fluctuations brought about by evaporation and solubility of alcohol in water. Good sensitivity was obtained by using an optical depth of 40 mm. When using the test-tube adapter, the optical depth is 13 mm. Since sensitivity is inversely proportional to the volume of the solvents and directly proportioned to the optical depth, use of 5 ml of solvent and the test-tube adapter would approximately double the sensitivity over that attained in the work reported but accuracy would possibly be reduced because of operational difficulties with small volumes of solvents.

[11] Reference (3*g*) of the Bibliography of the paper.
[12] Reference (3*f*) of the Bibliography of the paper.

With reference to Mr. Schultz's comments on the leaching of pyrex glassware, from our experience it would seem iron is selectively leached.

Iron does not plate out on container walls when properly collected under acid as was done in the reported work. With both new and old containers, soaking by acid was followed by a tendency for iron to be leached from the glassware.

We agree that nitric acid would dissolve any insoluble copper corrosion products more completely than hydrochloric acid. However, since in the preliminary work at the plant the same results were obtained with and without preacidification with hydrochloric acid, it is believed that all the copper was present in the sample in soluble form.

Mr. G. F. Smith[13] indicates that both iso-amyl and n-hexyl alcohol are suitable. The distribution coefficient of the ferrous complex between the alcohol and water is on the order of 1600 to 1 for iso-amyl and 3400 to 1 for n-hexyl. While this shows that the latter more effectively removes the ferrous complex, the difference in such a high range of ratios is not of practical importance. A more practical consideration is that the odor of n-hexyl alcohol is more objectionable than that of iso-amyl alcohol.

In the paper it is pointed out that oxygen concentration can be very important as suggested by Mr. Schultz. Oxygen concentration and pH are always the two main factors in condensate corrosion. Perhaps at each low level of oxygen there is a definite pH above which there is no practical gain.

[13] Reference (9) of the Bibliography of the paper.

Hydrazine as an Oxygen Scavenger—A Progress Report on Tests at Springdale Station

By M. D. BAKER[1] and V. M. MARCY[2]

Hydrazine has been fed on a trial basis to a 1350-psi boiler at Springdale Station of West Penn Power Company since April, 1954. Preliminary observations on the use of this chemical for removing oxygen are given in the paper.

THE field study reported in the paper was undertaken because few technical facts seemed to be available to support the rather vague and differing opinions which have been expressed concerning the use of hydrazine as an oxygen scavenger. Information has been obtained on the behavior of hydrazine, but still more data will be needed to define the utility of this substance. Accordingly, the present paper is designated a progress report.

Ever since the No. 77 boiler at Springdale Station of West Penn Power Company was first placed on the line in 1946, potassium sulphite has been used as an oxygen scavenger. This B&W 800,000-lb per hr boiler has a drum pressure of 1350 psi and a superheated steam temperature of 930 F. The boiler and its turbine comprise a separate unit well suited for carrying out studies independently of the rest of the station.

Potassium Sulphite

The history of potassium-sulphite treatment and control of condensate pH for this boiler, given in detail in papers by Hankison, Baker, and associates (1, 2),[3] will be reviewed here briefly. It was discovered early that, with shot feed of sulphite to the boiler, some breakdown of the chemical was indicated by discharge of hydrogen sulphide at the air ejector of the main condenser. Potassium hydroxide, formed as a product of the breakdown, produced at times a highly alkaline boiler water. A possible reaction for the decomposition of sulphite can be written as follows

$$4K_2SO_3 + H_2O \rightarrow 3K_2SO_4 + 2KOH + H_2S$$

Sulphide in the steam and hydroxide in the boiler water gradually decreased when the feed of potassium sulphite was changed from intermittent to continuous. With continuous feed it was feasible to maintain lower sulphite residuals in the boiler water. However, production of sulphide and possibly of sulphur dioxide was not entirely eliminated. As a result, the pH of the condensate was as low as 6.0 during certain periods of the year when ammonia naturally present in the make-up water was low. Cyclohexylamine treatment was begun in 1951 to raise the pH of the condensate to 8.8. Ammonium chloride was tried for the same purpose in 1952. Both materials were effective in decreasing the amount of iron oxide in the system, but cyclohexylamine afforded greater protection and was easier to control (2).

Hydrazine

Hydrazine ($NH_2.NH_2$ or N_2H_4) is an alkaline, water-white, clear liquid which volatilizes readily at high temperatures. It was first used as an oxygen scavenger in boiler-water treatment in Germany following World War II (3, 4, 5, 6). The primary products of the reaction between hydrazine and oxygen are water and nitrogen, harmless materials which do not increase solids in the boiler water (7, 8). The reaction is

$$N_2H_4 + O_2 \rightarrow N_2 + 2H_2O$$

To consume 1 lb of oxygen, only 1 lb of hydrazine is required, as compared to 8 lb of sodium sulphite or 10 lb of potassium sulphite.

Although the foregoing reaction is desired, side reactions also are involved. Most important of these involves the production of ammonia, possibly according to the equation

$$3N_2H_4 \rightarrow N_2 + 4NH_3$$

Presence of such alkaline materials as ammonia and hydrazine in the condensate would raise its pH, not lower it as in the case with sulphite treatment. Considered only as a volatile alkali, hydrazine is, however, very expensive. Based on comparative oxygen-consuming power, hydrazine is several times as costly as sodium sulphite but about the same as potassium sulphite. Of course, cost becomes a less important consideration when only a minute amount is needed to react with traces of dissolved oxygen in the effluent from an efficient deaerator.

Feeding, Sampling, and Analysis

The trial with hydrazine was started on April 1, 1954, during a period when ammonia in the make-up water was low. Prior to that, cyclohexylamine had been discontinued in December, 1953, during a period of high natural ammonia in the system. A feed solution was prepared daily by adding a known volume of a 22½ per cent N_2H_4 solution to 30 gal of condensate in a covered stainless-steel drum in which potassium hydroxide and potassium pyrophosphate were previously dissolved. The solution was fed continuously to the inlet of the economizer over a 24-hr period. Condensate at a temperature of about 140 F was used for preparing the solution since cold water was not available at this location. Even though the condensate was hot, loss of hydrazine was only a few per cent after standing 24 hr in the feed tank.

During the test, water samples were collected from the following points:

1 Boiler water from blowdown line in drum.
2 Boiler water from front wall tube No. 119.
3 Saturated steam from drum.
4 Condensate from discharge of the condensate pump.

---

[1] Chief Chemist, West Penn Power Company, Springdale, Pa.

[2] Research Engineer, Hall Laboratories, Inc., Pittsburgh, Pa.

[3] Numbers in parentheses refer to the Bibliography at the end of the paper.

Contributed by the Joint Research Committee on Boiler Feedwater Studies and presented at the Annual Meeting, New York, N. Y., November 28–December 3, 1954, of The American Society of Mechanical Engineers.

Note: Statements and opinions advanced in papers are to be understood as individual expressions of their authors and not those of the Society. Manuscript received at ASME Headquarters, November 17, 1954. Paper No. 54—A-261.

5 Feedwater at discharge of booster pump after the deaerator and before the closed heaters.

6 Air-ejector drains from after-condenser.

Samples were tested for hydrazine, iron, copper, ammonia, pH, and conductivity (see the appendix for a discussion of the tests employed, particularly the hydrazine method).

Results of the Investigation

With few exceptions, daily tests were run for most of the constituents measured. Averages for one-half-month intervals for a number of constituents are summarized in Table 1 and some are plotted in Fig. 1. With the exception of hydrazine, practically cal methods introduced shortly before hydrazine treatment was begun. The increase in pH was mainly the result of ammonia formed through decomposition of the excess hydrazine. The average level of ammonia in the condensate increased from 0.045 ppm during the second half of March when no hydrazine was being fed to 0.31 ppm during the first half of April when hydrazine was added continuously. The increase in conductivity of the undegassed condensed steam found after the start of hydrazine treatment shows the influence primarily of increased ammonia concentration on this measurement. Results of tests on the feedwater show a trend similar to the condensate analyses, but to a lesser degree.

TABLE 1 SUMMARY OF RESULTS DURING THE TRIAL WITH HYDRAZINE AT SPRINGDALE

Average of analyses for half-month periods	Condensate pH	Condensate NH_3 (ppm)	Condensate Fe (ppm)	Condensate Cu (ppm)	Condensate Conductivity (micromhos/cm)	Feedwater pH	Feedwater Fe(ppm)	Feedwater Cu(ppm)	Air-ejector drains NH_3(ppm)	Boiler water N_2H_4 in drum (ppm)	Boiler water N_2H_4 in 119 tube (ppm)
March 1–15 Sulphite fed to boiler	8.3	0.015	0.04	0.02	0.8	8.8	0.09	0.045	0.29	0	0
March 16–31 After sulphite was stopped	8.8	0.045	0.018	0.005	0.8	8.8	0.075	0.005	0.33	0	0
April 1–15 After start of hydrazine feed	9.1	0.31	0.005	<0.002	3.0	9.1	0.041	0.003	1.2	0.020	0.035
April 16–30 Hydrazine continued during and after this period	9.1	0.38	0.004	<0.002	3.5	9.05	0.038	0.002	2.9	0.026	0.036
May 1–15[a]	8.8	0.15	0.010	0.002	2.0	8.8	0.042	0.008	0.6	0.008	0.015
May 15–31	9.05	0.38	0.008	0.002	3.9	8.95	0.025	0.004	2.8	0.010	0.021
June 1–15	9.0	0.34	0.010	<0.002	4.1	9.0	0.040	<0.002	3.5	0.007	0.020
June 16–30	8.85	0.29	0.005	<0.002	4.4	8.8	0.030	0.005	4.6	0.014	0.034
July 1–15	8.9	0.28	0.006	0.002	4.2	8.85	0.012	0.005	9.3	0.010	0.019
July 16–31	9.0	0.27	0.005	<0.002	4.5	9.0	0.012	0.007	8.0	0.014	0.022
August 1–15	...	...	...	...	...	...	...	...	...	0.019	0.019
August 16–31	...	...	...	...	...	...	...	...	...	0.021	0.020

[a] Pump used for feeding hydrazine was inoperative on May 4, 5, and 6 and the boiler was off the line on May 7, 8, and 9.

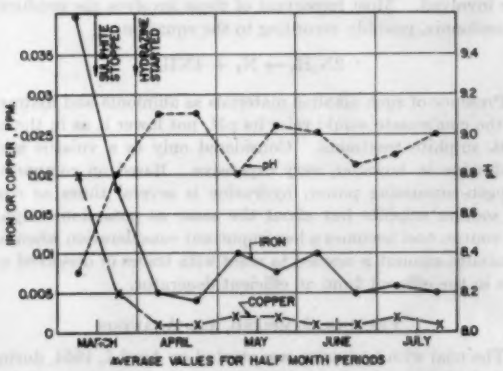

Fig. 1 Change in Iron and Copper Content of Condensate With Change in pH

all individual values for the half-month periods were within ±25 per cent of the average. Values for hydrazine in the boiler water varied from 0 to 0.060 ppm, depending on feed of the material and effectiveness of oxygen removal by the deaerating heater. Hydrazine was found in the boiler water the first day it was fed to the system.

During the first half of March, 1954, with sulphite treatment, the pH of the condensate was fairly low and iron and copper were at high levels. When sulphite addition was stopped on March 15, pH rose somewhat and iron and copper decreased. The rise in pH was probably due more to elimination of acid-forming breakdown products from sulphite than to increase in ammonia. During hydrazine treatment, pH rose further and iron and copper dropped to low levels. Part of the apparent decrease in iron and possibly also in copper was due to the use of more sensitive analyti-

When ammonia in the condensate increased, a similar increase, but magnified, was noted for ammonia in the air-ejector drains. At one stage, pH of the main condensate stream rose to 9.3. To obviate possible corrosion of nonferrous alloys, the highly alkaline after-condenser drains were discarded.

After the first month of hydrazine treatment, average feed of hydrazine was 8.5 lb per month, expressed as pure N_2H_4, with a monthly average of 510 million pounds of feedwater. This feed is sufficient to consume 0.017 ppm of dissolved oxygen in the feedwater. To determine how much hydrazine was being used up as an oxygen scavenger and how much merely decomposed in the boiler, it would have been desirable to determine exactly the weight of dissolved oxygen entering the boiler during a month's interval. This was not possible, however, since there was no continuous analysis of the minute quantities involved. Some analyses were made for dissolved oxygen in the feedwater, with results averaging less than 0.005 ppm O_2. Loss of sulphite reserve at certain times in the past has indicated, however, that the oxygen content of the feedwater was considerably higher than 0.005 ppm. Loss of scavenger reserve in the boiler water was even more frequent with hydrazine. During the first five months of the trial period, no hydrazine was found in the boiler water from the drum on 13 occasions. The hydrazine reserve was presumably used up by oxygen entering the boiler water as a result of less efficient functioning of the deaerating heater during periods of reduced load. The small reserve of hydrazine is more quickly depleted than the higher reserve of sulphite formerly maintained.

What effect would a large excess of hydrazine have on the system? To answer this question, hydrazine was temporarily discontinued for several days; then a large excess was added. Results of this test are listed in Table 2 and in part are shown in Fig. 2. When 0.47 lb of hydrazine was being added over a 24-hr period, hydrazine in the boiler water from the drum was 0.025 ppm.

TABLE 2 EFFECT OF FEEDING LARGE EXCESSES OF HYDRAZINE TO SYSTEM

Time of sampling	Pounds of N_2H_4 fed during 24-hr interval[a]	N_2H_4 found in boiler water, ppm: Drum sample	N_2H_4 found in boiler water, ppm: 119 tube sample	NH_3 in condensate, ppm	NH_3 in air-ejector drains, ppm
4/23, 9:00 a.m.		0.020	0.020	0.32	1.8
	0.47				
4/24, 9:00 a.m.		0.025	...	...	...
	0				
4/25, 9:00 a.m.		0.025	...	...	...
	0				
4/26, 9:00 a.m.		0.005	0.020	0.30	...
	1.41				
4/26, 2:00 p.m.		...	0.050	0.45	4.0
4/27, 9:00 a.m.		0.035	0.050	0.50	4.0
	1.41				
4/27, 2:00 p.m.		0.050	0.050	...	...
4/28, 9:00 a.m.		0.055	0.060	0.50	5.0
	0.23				
4/29, 9:00 a.m.		0.025	0.030	0.34	3.4
	0.47				
4/30, 9:00 a.m.		0.020	0.020	0.28	2.0

[a] Feed of hydrazine started at 9:00 a.m.

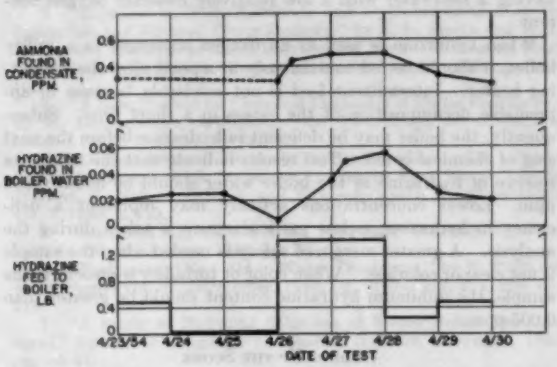

FIG. 2 AMMONIA IN THE CONDENSATE AND HYDRAZINE IN THE BOILER WATER AS A FUNCTION OF HYDRAZINE FEED

When the continuous feed of hydrazine was increased threefold, that is, to 1.41 lb per 24 hr, hydrazine in the boiler water rose only to a maximum of 0.055 ppm. Assuming no change in the amount of oxygen entering the boiler and no decomposition, a progressive increase to about 10 ppm would have been attained by the end of the second day. Results indicate that no such reserves can be maintained. Only a small part of the hydrazine could have been consumed by the oxygen entering the boiler with the feedwater. A small amount of that volatilized with the steam presumably would be lost in the system. Much of the excess must, however, have been decomposed, forming ammonia.

Some checks for hydrazine in the saturated steam and condensate were made during the course of the investigation. Hydrazine in the saturated steam averaged 0.009 ppm with individual values ranging from 0 to 0.020 ppm. Hydrazine in the condensate averaged 0.004 ppm with individual values ranging from 0 to 0.009 ppm. Hydrazine in the saturated steam was always at a higher level than hydrazine in the condensate, with indications that about a third of the material fed to the boiler decomposed in the superheater on being raised to a temperature of 930 F or, in minor part, was lost from the condenser.

Hydrazine in the condensate might seem to be of some advantage in minimizing oxygen corrosion in the condensate return lines and preboiler equipment. Even in the presence of a catalyst, however, the rate of reaction between hydrazine and oxygen is quite low at ordinary temperatures, as indicated in Table 3. The pH of the condensate would increase slightly due to volatilization of alkaline hydrazine with the steam. However, the effect

TABLE 3 OXIDATION OF HYDRAZINE IN PRESENCE AND ABSENCE OF A CATALYST

(Sample, originally containing 8 ppm dissolved oxygen, was allowed to stand in an uncovered beaker at room temperature. The pH of all samples was about 8.1.)

Test no.	—Chemicals in deionized water, ppm— N_2H_4	Catalyst	Residual hydrazine in sol. after 45 min, ppm
1	7.9	none	7.0
2	7.9	0.1 Cu^{++} (added as $CuSO_4 \cdot 5H_2O$)	2.1
3	7.9	0.5 Cu^{++}	0.9
4	7.9	0.1 Mn^{++} (added as $MnSO_4 \cdot H_2O$)	6.9
5	7.9	0.5 Mn^{++}	5.8

of the small amount found would be slight compared to that of the much larger amounts of ammonia formed during the tests.

The total solids content of the boiler water with hydrazine treatment in No. 77 unit at Springdale was about half that with sulphite treatment, under the standard operating procedure of blowing down when the silica content exceeds 3 ppm. For example, the average total solids content of the boiler water with sulphite treatment in August, 1953, was 485 ppm; with hydrazine treatment in June, 1954, it was only 220 ppm. Silica in the feedwater was relatively constant for the whole period. About 50 per cent of the total weight of chemicals fed to the boiler in 1953, exclusive of cyclohexylamine, was sulphite.

The causticity of the boiler water showed less fluctuation during hydrazine treatment than it did with sulphite treatment. Hydroxide content of the water varied from 10 to 20 ppm when sulphite was used as an oxygen scavenger whereas the variation was only 14 to 19 ppm during the hydrazine trial. Hydrazine in the concentrations present in the boiler water has virtually no effect on its causticity. On the other hand, sulphite may decompose slightly to form caustic in the boiler water and this will be variable depending on the concentration of sulphite.

The boiler has been taken off the line for inspection twice since the hydrazine trial was started. No signs of corrosion were detected either at earlier inspections during sulphite treatment or at those five weeks and five months after the start of hydrazine treatment. During boiler inspections since 1951, estimates of the amount of loose deposit found in the two ends of the drum have been made. These values are listed in Table 4. The drastic

TABLE 4 ESTIMATED WEIGHT OF DEPOSIT IN ENDS OF BOILER DRUM

Inspection period	Pounds of deposit found	Remarks
September, 1951	40	No prior treatment to raise pH of condensate
September, 1952	20	Cyclohexylamine and ammonium salts used at intervals before outage
September, 1953	10	Cyclohexylamine and ammonium salts used at intervals before outage
May, 1954	<1	Cyclohexylamine used until December, 1953. No special treatment, but some naturally occurring ammonia in the make-up until April, 1954. Five weeks with hydrazine treatment
September, 1954	<1	Hydrazine used exclusively

reduction in the weight of these deposits, which are mainly magnetic iron oxide and copper, is believed to be principally the result of elevation of pH of the condensate by various means: Neutralizing amines, ammonia derived from the make-up water, ammonia added as a salt, or ammonia formed by decomposition of hydrazine.

In the past, when the boiler was first started up after it had been drained, maintenance of reserve sulphite in the boiler water was virtually impossible until extra caustic was added to raise the pH of the water to 10.5. In contrast, hydrazine was found in the boiler water as soon as the boiler was placed in operation.

Hydrazine Tests in Low-Pressure Boilers

It was thought that feeding hydrazine to low-pressure boilers might provide valuable information on the reaction between hydrazine and dissolved oxygen at low temperatures. Hydrazine was slug-fed to feedwater lines a few feet from the drums of two boilers using undeaerated make-up water. One unit was a 115-psi HRT boiler and the other a 120-psi, two-drum, bent-tube boiler. Neither installation was located at Springdale. Results of the two tests were quite similar. Data in Table 5 relating to the 115-psi boiler indicate that high residuals of hydrazine can be

TABLE 5 TRIAL WITH HYDRAZINE IN A 115-PSI BOILER

(0.65 lb of N_2H_4 slug-fed at 9:00 A.M.)

Sampling time	Analysis of Samples (ppm) N_2H_4 in boiler water	N_2H_4 in condensate	O_2 in condensate
9:45 a.m.	3.5	...	...
10:15 a.m.	...	0.6	0.025
10:50 a.m.	14.4	0.85	0.025
11:45 a.m.	13.0	0.85	0.020
1:30 p.m.	10.4	0.90	...

maintained at this pressure and that 5 to 10 per cent of the amount present in the boiler water volatilized with the steam. Most of the condensate was returned in this case. However, the hydrazine volatilized with the steam is lost from that portion of the condensate not returned. Data on decomposition could not easily be obtained because the high concentration of hydrazine in the steam interfered in the ammonia test.

An indication of a slow rate of reaction between hydrazine and oxygen in the steam at elevated temperature is seen from the analysis of the condensate. Although the steam temperature was about 345 F, both hydrazine and small amounts of dissolved oxygen were found to exist together in the condensed-steam sample. This is not attributable to analytical difficulty since, as noted in the Appendix, hydrazine in the concentrations present does not interfere in the dissolved-oxygen test employed. When similar tests were run on these boilers with sulphite added, the same amount of oxygen was found in the steam. Apparently, deaeration was occurring as the feedwater entered the drum and some of the oxygen in the feedwater was volatilized before it reacted with the scavenger in the boiler water. Presumably, at least part of the oxygen reacted with hydrazine in the boiler during the tests because the oxygen in the steam increased after feed of the oxygen scavenger was discontinued.

Precautions in Handling Hydrazine

Hydrazine is available in the substantially pure liquid form and in solutions of various concentrations. Because weak solutions are less hazardous to handle, a $22^1/_2$ per cent N_2H_4 solution was used in the test. Since information on properties of weaker solutions is meager, for the time being it would be advisable to follow the listed precautions for the more concentrated solutions (9). Hydrazine should be stored in a cool place to prevent possible fires or explosions from the vapors. The feed solution should be prepared by adding hydrazine to a stainless-steel tank filled with water. Never use rusty containers since hydrazine may react violently with iron oxides. Avoid inhaling the sharp, irritating vapors. Use rubber gloves, goggles, mask, or other protective equipment to prevent solution or vapors coming into contact with the skin. Dilute any spillage immediately with water. Wash skin with soap immediately after flushing with large quantities of water. With some individuals dermatitis can result through contact of even very weak solutions or vapor with the skin.

General Remarks

Some plants do not feed an oxygen scavenger to their excellently degassed feedwater and have not encountered difficulty with corrosion. Many plants are using sulphite and will continue to use this scavenger with satisfactory results. Sulphite has several advantages over hydrazine. In general, larger reserves of sulphite than of hydrazine can be maintained in a high-pressure boiler; hence sulphite is better able to take care of feedwaters having a variable oxygen content. Sulphite reacts faster with oxygen than hydrazine does. Sulphite may decompose partially to produce acid-forming materials in the condensate; however, neutralizing amines and ammonium salts are quite effective in combating corrosive effects of small amounts of sulphide and sulphur dioxide (10, 11). In some cases, filming amines also will prove advantageous in controlling possible corrosion from sulphur compounds in condensate-feedwater systems. Hydrazine will find proponents since it does not add solids to the boiler water and since it produces an alkaline reaction in the condensate. The inability to maintain substantial reserves of hydrazine in a high-pressure boiler may limit its use to plants having a feedwater with a low relatively constant oxygen content.

When hydrazine is used as an oxygen scavenger in a utility boiler, it should be fed continuously at a point after the deaerating heater. Intermittent feed is not advisable because of appreciable decomposition of the excess in a short time. Subsequently, the boiler may be deficient in hydrazine before the next slug of chemical is fed. Test results indicate that the minimum reserve of hydrazine in the boiler water should be about 0.005 ppm. Lower concentrations actually may represent a deficiency in hydrazine, unless particular care is taken during the analysis. A greater margin of safety is needed when the sample is not clear or colorless. When color or turbidity is present in the sample, the minimum hydrazine content should be greater than 0.005 ppm.

Adding Up the Score

1 Hydrazine reacts only slowly with dissolved oxygen at ordinary temperatures. Hydrazine in saturated steam at 345 F also reacts slowly with oxygen.

2 In a boiler at 1350 psi, excess hydrazine decomposes so rapidly that it is not possible to maintain more than a few hundredths of a part per million in the boiler water.

3 When hydrazine decomposes in a boiler at 1350 psi, one end-product is ammonia. Indications are that decomposition is substantial in a superheater with maximum temperature of 930 F.

4 The rate of decomposition in a boiler at 115 psi is relatively low since it is possible to maintain a reserve of at least several parts per million of hydrazine in the boiler water.

5 At 115 psi, the steam carries from 5 to 10 per cent as much hydrazine as is present in the boiler water; volatilization is greater at 1350 psi.

6 Hydrazine does not add to the dissolved solids in a boiler water.

7 Caution should be exercised in handling hydrazine solutions even though it is possible that dilution removes part of the danger.

8 When hydrazine is used as an oxygen scavenger, the pH of the condensate will be increased, since ammonia resulting from its decomposition will be carried with the steam. The increase in pH from the hydrazine volatilized with the steam in the case of the 1350-psi boiler is small compared to the increase from ammonia produced by decomposition.

9 Pickup of iron and copper by condensate at a pH not exceeding 9.2 was kept to no more than 0.015 ppm of Fe and 0.003 ppm of Cu while hydrazine was fed to a 1350-psi boiler.

10 Compared on the basis of cost of removing a unit of oxy-

gen, hydrazine is currently several times as expensive as sodium sulphite and about as expensive as potassium sulphite.

11 The basic problem in the use of hydrazine in a high-pressure plant is to proportion the hydrazine to the oxygen in the feedwater so that the latter will be removed without appreciable waste of hydrazine by decomposition of any excess reaching the boiler.

Acknowledgments

The authors wish to express their appreciation to Mr. E. L. Jacobs, now of Ohio Valley Electric Company and formerly of West Penn Power Company; to Mr. W. L. Thompson and Mr. J. B. Haas of West Penn Power Company; and to Mr. J. A. Platte of Hall Laboratories, Inc., for their help in collecting the data.

BIBLIOGRAPHY

1 "Sulphite and Silica in Boiler Water at Springdale," by L. E. Hankison and M. D. Baker, Trans. ASME, vol. 72, 1950, pp. 505–509.

2 "Experiences With Ammonia and Cyclohexylamine at the Springdale and Mitchell Power Stations," by E. L. Jacobs and W. L. Thompson, Proceedings of the 14th Annual Water Conference, Engineers' Society of Western Pennsylvania, Oct. 19–21, 1953, pp. 100–102.

3 "A New Method for Chemical Degassing of Boiler Feedwater," by M. Zimmermann, *Mitteilungen der Vereinigung der Grosskesselbesitzer*, vol. 2, 1948, pp. 70–73.

4 "Degasification of Waters to Hinder Corrosion. III. Oxidation of Hydrazine With Molecular Oxygen in Pure Water," by K. Wickert, K. Nolten, J. Kroll, and E. Ipach, *Archiv für Metallkunde*, vol. 3, 1949, p. 113.

5 "European Experiences With Feedwater Treatments," *Combustion*, vol. 21, August, 1949, pp. 48–49.

6 "Hydrazine: New Aid to Water Treatment," by E. R. Woodward, *Power*, vol. 97, November, 1953, pp. 91–93, 212, 214, 216, and 218.

7 "A Study of Reducing Solutions at Steam Boiler Temperatures," by H. D. Ongman, *Combustion*, vol. 24, February, 1953, pp. 40–44.

8 "Experience With the Use of Hydrazine as an Oxygen Scavenger in High Pressure Boilers," by E. C. Fiss, Proceedings of the American Power Conference, vol. 16, March 24–26, 1954, pp. 651–654.

9 "Properties, Production, and Uses of Hydrazine," by J. E. Troyan, *Industrial and Engineering Chemistry*, vol. 45, 1953, pp. 2608–2612.

10 "Prevention of Metal Losses in the Wet Steam Areas of Steam Turbines," by F. L. Archibald, J. W. Pursell, Jr., and F. G. Straub, Proceedings of the American Power Conference, vol. 15, March 25–27, 1953, pp. 579–587.

11 "Controlling Iron and Copper Pickup With Neutralising Amines," by J. D. Ristroph and E. A. Yorkgitis, published in this issue, pp. 287–297.

12 "Amperometric Analyzer," by J. F. Haller (to Mathieson Chemical Corporation), U. S. Patent 2,651,612, September 8, 1953.

13 "A Spectrophotometric Method for the Determination of Hydrazine," by G. W. Watt and J. D. Chrisp, *Analytical Chemistry*, vol. 24, 1952, pp. 2006–2008.

14 "Standard Methods for the Examination of Water and Sewage," American Public Health Association, New York, N. Y., ninth edition, 1946, pp. 52–53.

15 Ibid., pp. 47–49.

16 "Technique in the Determination of Dissolved Oxygen," by T. H. Daugherty, Proceedings of the American Society for Testing Materials, vol. 37, part 2, 1937, pp. 615–633.

17 "Manual on Industrial Water," American Society for Testing Materials, Philadelphia, Pa., 1953, ASTM, Special Technical Publication No. 148, pp. 213–218.

Appendix

Notes on the Analytical Procedures Used at Springdale

Hydrazine. Three methods used for the analysis of hydrazine in water have been the iodometric titration (6, 8), amperometric analyzer (12), and the colorimetric test (13). The colorimetric test was selected since it is specific for hydrazine and is quite sensitive. The other two methods measure total reducing power of the sample, which could include other substances than hydrazine.

The colorimetric test was run by adding a freshly drawn, clear sample to the mark of a 100-ml volumetric flask. Five ml of indicator solution was then added to the sample and the flask was shaken for mixing. After allowing 30 min for color development, the solution was measured in a Fisher electrophotometer using distilled water similarly treated with indicator as the reference solution. When measurements were made in 50-mm cells with a 425-B filter, the concentration of hydrazine in ppm was obtained by multiplying Scale A (a log scale) by the factor 0.0025. The indicator was prepared by dissolving 1.00 gram p-dimethylaminobenzaldehyde in 50-ml isopropanol and adding 10-ml concentrated hydrochloric acid (specific gravity 1.19) to the solution. A few thousandths of a ppm of N_2H_4 can be detected by this method. The sample should be substantially clear and nearly colorless; however, compensation can be made for slight turbidity or for slight color in samples. Loss of hydrazine through sample contact with air is negligible if the sampling container is completely filled and the test is run soon after the sample is drawn.

Iron and Copper. Two different methods were used in testing for these constituents. Until several days before the start of hydrazine feed to the boiler water on April 1, 1954, iron was determined by the o-phenanthroline method (14) and copper by the carbamate method (15). Results reported later were obtained by the highly sensitive and unusually specific bathophenanthroline method for iron and neocuproine method for copper. Even as low as one to two thousandths of a ppm of iron or copper can be detected with the newer tests. Recently, in checking for iron in a number of samples by the two methods, it was found that results by the bathophenanthroline method were somewhat lower than those by the o-phenanthroline method, particularly when minute concentrations were present. The accuracy of the o-phenanthroline method was poor when less than 0.05 ppm was present.

Procedures for the bathophenanthroline method for iron and neocuproine method for copper are given in the paper by Ristroph and Yorkgitis (11). Samples for these tests were taken from undisturbed lines which were allowed to flow constantly. For each test 750 ml was drawn into a specially cleaned polyethylene bottle containing 2 ml of concentrated hydrochloric acid and then the sample was digested in the bottle at 70 to 80 C for at least 1 hr in order to dissolve any precipitated oxides.

Ammonia. The direct Nesslerization method was employed on condensed steam and feedwater samples. Hydrazine in concentration of 0.01 ppm produced ammonia results which were 10 per cent too high when the ammonia content was 0.25 ppm. Higher concentrations produced highly inaccurate results. However, since hydrazine values were less than 0.01 ppm in the samples tested, ammonia results were not affected.

Dissolved Oxygen. Measurement for this constituent was made by the Daugherty modification of the Schwartz and Gurney Method B (16). Results showed that as much as 1.0 ppm N_2H_4 produced negligible interference in this test. Neither did hydrazine interfere in the ASTM Referee Method for dissolved oxygen (17).

pH. A battery-type Beckman pH meter was used with a flow-cell arrangement. Stray currents made readings with a line-operated instrument erratic.

Discussion

F. E. Clarke.[4] Our service trials and analytical studies of

[4] Chemical Engineering Laboratory, U. S. Naval Engineering Experiment Station, Annapolis, Md.

Note: The opinions expressed are those of the discusser and are not necessarily those of the Engineering Experiment Station or of the Navy Department.

hydrazine paralleled those of the authors, except that the boiler used had a capacity of 10,000 lb and was operated at 700 psi and 25,000 to 75,000 lb of steam per hr. In continuous feed tests, hydrazine hydrate was diluted to approximately 10,000 ppm and added to the discharge of the main feedwater pump, 75 ft ahead of the economizer. The rate was adjusted to yield either 0.05 or 0.2 ppm of hydrazine in the feedwater, which averaged 0.01-ppm dissolved oxygen. On several occasions slugs of hydrazine were added directly to the steam drum to yield instantaneous boiler-water concentrations of about 3-ppm hydrazine.

At the 0.05-ppm feed rate, dissolved oxygen was absent at the economizer outlet, the boiler-water hydrazine reached equilibrium at about 0.05 ppm, and no increase in ammonia or conductivity occurred in the steam. The 0.2-ppm feed rate yielded a boiler-water equilibrium of about 0.5-ppm hydrazine. It increased steam conductivity from 1.5 to 4 micromhos and the ammonia content of the steam by about 0.2 ppm. No hydrazine could be found in the steam. The 3-ppm slugs of hydrazine in the boiler water decomposed uniformly to the equilibrium level of 0.5 ppm over a 5-hr period. The steam conductivity and ammonia showed corresponding surges and gradual declines.

These findings agree with those of the authors except for the higher boiler-water concentrations from both continuous and slug feed. These differences undoubtedly resulted from the differences in boiler characteristics and operating conditions.

Authors' Closure

Mr. Clarke's observations on a medium-pressure boiler constitute a valuable addition to the authors' paper on the behavior of hydrazine in low and high-pressure boilers.

Mr. Clarke's feeds of 0.05 and 0.2-ppm hydrazine represent five and twenty times the amount required to react with the 0.01-ppm dissolved oxygen in the feedwater. Only a small portion of the excess was found to have concentrated in the boiler water. Decomposition of hydrazine is therefore indicated. We would expect some of the excess to be volatilized with the steam. None was found in the condensed steam; however, if any were present it would only be there to the extent of 0.01 ppm or less.

Lower Flue-Gas Exit Temperatures Through Removal of the Solids Ahead of the Air Preheater

By A. J. TIGGES[1] and HILMER KARLSSON[2]

The paper is a philosophical discussion of flue gases and stresses the important part played by the "extreme fine" solids in the flue gas. These fines are considered one of the major causes of problems with low-temperature surfaces of the boiler system, cause visible smoke, and are believed to contribute to the dangers of "smog." Methods for removing fines in a high-temperature zone are discussed. Results are given from experimental work for removal of fines at high temperature and high velocity with high collecting efficiency.

Introduction

SMOKE and its problems are old and much discussed subjects and there has been a great deal of excellent work done both in technical investigations and in field applications. It is not the attempt of this paper to review or cover the vast scope of work done in this field by others.

It is important to point out how and where the subject matter of this paper fits into this field of endeavor and to offer some possible contribution. It is hoped that this presentation will stimulate thinking and more activity in this direction.

It is interesting to review just how the program described was evolved. Toward the end of World War II and directly thereafter a great deal of effort was being expended toward increasing over-all boiler efficiency by reducing gas exit temperatures without affecting high availability.

Reviewing the excellent work done by others, it was indicated that a very definite pattern of dew points with respect to different types of fuel and methods of burning existed; therefore this was not pursued. Many people here and abroad were consulted to learn the probable main influences causing deposits and corrosion. It was hoped that some basic philosophy could be set up before detailed research should be initiated. The U. S. Bureau of Mines, through John F. Barkley, was of very great assistance in directing the thinking toward a basic philosophy. There were many others who also made substantial contributions.

This work on the basic concept brought to light a rather interesting phenonenon: Briefly, identifying three major factors all of which must be present at the same time to cause troubles from deposits.

It was found that to have tenacious deposits form, which at the same time were highly corrosive, the fuel essentially must contain sulphur compounds. At the present stage of the art the sulphur compounds cannot economically be removed from the fuel and therefore have to be contended with. The deposits from the sulphur-free fuels can be handled with reasonable effectiveness and ease and with only mild oxidation of the metal.

Another element that must be present for forming tenacious deposits and corrosion is water vapor. This is always present in all boiler flue gases and it cannot be removed before it causes trouble.

Still another item necessary to cause depositions is fly ash, and particularly the very finely divided particles of fly ash. This was the only item left that had a possibility of economic removal, with the end result of reducing air-preheater deposits and possibly corrosion. Of course, the removal of the solids has to be done before they become wet and adhesive; that is, they should be in a dry state.

Therefore the efforts were directed to this end.

Philosophical Discussion of Flue Gases

What Is a Flue Gas?

Although flue gas is one of the most common products handled in the power industry, it is seldom considered in its total components. As an aid in visualizing this, tables have been prepared showing the constituents of flue gas, both chemical and solids, generated from burning high and low-sulphur coals, and high and low-sulphur oils. With respect to the physical element, fly ash, only the major components are mentioned. Typical analyses of deposits from products of combustion on cold-end surfaces are shown in a U. S. Bureau of Mines Report of Investigations No. 4996, by J. F. Barkley, et al. (1).[3]

Chemical Composition. Table 1, column 1, gives the estimated analyses of gases and solids per 1,000,000 lb of flue gas for a Midwestern coal of 4.14 sulphur content, burned in pulverized form.

Column 2 gives information for an Eastern coal having a sulphur content of only 1.15 per cent, burned in pulverized form.

These columns are based on 75 per cent of the ash in the coal being carried by the gas stream through the boiler, 20 per cent excess air prevailing at the air-preheater inlet, and 60 per cent relative humidity of the combustion air.

Column 3 gives information for Central Illinois coal of 4.65 per cent sulphur, fired in a cyclone-type burner. It has been estimated that about 7 per cent of the ash is carried by the gas stream through the boiler, 10 per cent excess air prevails at the air-preheater inlet, and relative humidity of the combustion air is 60 per cent.

Columns 4 and 5 give similar information for oil fuels of 2.41 and 0.4 per cent sulphur, respectively, both having an ash content of 0.1 per cent. These two columns are based on 80 per cent of the ash being carried by the gas stream through the boiler, 20 per cent excess air at the air-preheater inlet, and 60 per cent relative humidity of the combustion air.

---

[1] Consultant, Jackson & Moreland, Boston, Mass. Mem. ASME.
[2] Technical Manager, The Air Preheater Corporation, Wellsville, N. Y. Fellow ASME.

Contributed by the Research Committee on Corrosion and Deposits from Combustion Gases and presented at a joint session of the Research Committee on Corrosion and Deposits from Combustion Gases and Power Division at the Annual Meeting, New York, N. Y., November 28–December 3, 1954, of The American Society of Mechanical Engineers.

Note: Statements and opinions advanced in papers are to be understood as individual expressions of their authors and not those of the Society. Manuscript received at ASME Headquarters, October 27, 1954. Paper No. 54—A-247.

[3] Numbers in parentheses refer to the Bibliography at the end of the paper.

Data on Solids. An interesting observation from the tables is the great variation in quantity of solids carried by the gas streams. However, in the study of the composition of products of combustion, and before considering the effect of this composition on the operation of the boiler system, the form and size ranges in which the solids exist should be considered. For that purpose, Tables 2, 3, and 4 have been prepared showing the expectable approximate dimension range of the solids carried.

While the particles over 5 microns in size can readily be sized with good accuracy by a number of accepted methods, the finer ones are very difficult if not impossible to size. This difficulty can be overcome if the known larger sizes are plotted on Hazen log X probability co-ordinates. Using the logarithmic co-ordinate as the ordinate to represent particle size in microns and the special probability co-ordinate as the abscissa to represent per cent less than size indicated, the plot comes out as a straight line. Fig. 1 is such a plot for the three dusts shown in Tables 2, 3, and 4. This method has been developed by Mr. P. F. Best of Thermix and a check with the percentages given in the tables will show reasonable agreement with the straight lines.

The term "micron" is used for expressing the size of the particles of solids. A micron is 0.001 mm, or approximately 0.0025 in. The significance of the smallness of the measure is better visualized by comparing this with known objects. For instance, the thickness of a human hair is approximately 0.002 in. or 50 microns.

By referring to Table 2 giving data on fly ash obtained from pulverized-coal firing, it will be noted that of the number of particles in the fly ash 78 per cent are below 1 micron, while by weight these portions of the fly ash constitute only $^1/_2$ per cent of the total.

Table 3 shows similar data for coal fired in a cyclone burner and it will be noted that an even greater percentage of the number of particles falls in the range of one micron and below.

Table 4 gives computed probable dimensional data on solids in flue gas predicated on preceding tables.

For convenience, the following size classifications have been selected:

Extreme fines: 0.01 to 1.0 micron

$$\left(\text{approx } \frac{1}{2{,}500{,}000} \text{ to } \frac{1}{25{,}000} \text{ in.}\right)$$

Medium fines: 1.0 to 20 microns

$$\left(\text{approx } \frac{1}{25{,}000} \text{ to } \frac{1}{1250} \text{ in.}\right)$$

Large particles: 20 to 200 microns:

$$\left(\text{approx } \frac{1}{1250} \text{ to } \frac{1}{125} \text{ in.}\right)$$

From Tables 2 to 4 the following will be noted:

1 In oil firing, only extreme fines should be considered. No table for gas firing is provided.

2 With coal fired in a cyclone furnace it is expected that medium fines and extreme fines should be considered.

3 With conventional pulverized-coal firing, large, medium, and extreme fines should be considered.

4 With stoker firing, more large particles are present than with pulverized-coal firing. Amounts of medium and extreme fines depend on the type of coal fired and type of stoker used. Stoker firing is not tabulated.

Experience from boiler operation shows that particles in the size range of approximately 10 microns and down are responsible for causing visibility of the stack discharge as well as creating problems with the low-temperature surfaces of the boiler system in the form of deposits and corrosion in the presence of sulphurous gases and sulphur compounds.

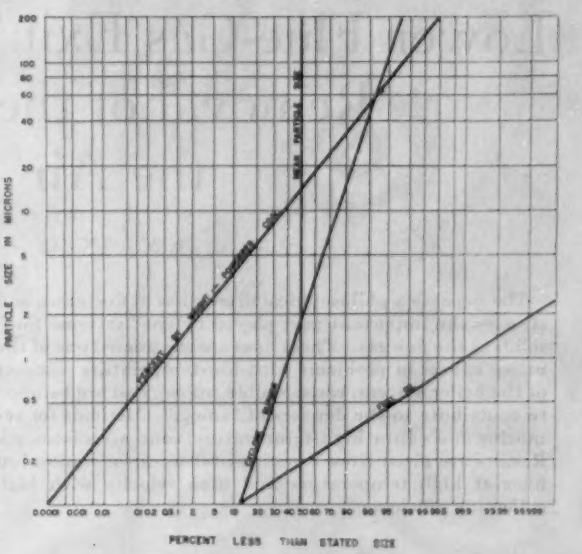

FIG. 1 SIZE CONSIST PROBABILITY CHART

It is known that the fly ash is hygroscopic and has the ability of absorbing water vapors and gases at relatively high temperatures. This is particularly pronounced in case of the fines. Operation with high-sulphur fuel oil indicates this phenonenon can occur at temperatures over 350 F.

Factors Limiting Gas Exit Temperature and Boiler Efficiency

In order to permit operating at high boiler efficiency and maintain high availability, it is necessary to keep the cold-end surfaces of the boiler system sufficiently free from deposits to maintain load.

The basic cause of deposits is the presence of sulphurous vapors, water vapor, and fly ash in the flue gas. With any one of these deleted the cold-end surfaces could be run at lower temperatures without serious deposits.

Increased sulphur content in the flue gas raises the dew point, and it is not the purpose to discuss this subject.

Water vapor in the flue gas is the big factor causing the sulphur compounds to act on the metal and fly ash to make a pasty, adhesive, corrosive material. No flue gas is free of water vapor and it cannot be eliminated.

The amount of fine fly ash in the gas stream and its composition has a proportionate bearing on the rate at which the deposits build up on the low temperature surfaces.

A great deal of research has been done along these lines by Dr. Henry Fraser Johnstone of the University of Illinois, and is reported in a bulletin of the Engineering Experiment Station (2). Furthermore, Messrs. Robertson and Gurney of Gulf States Utilities, in Baton Rouge, La., show that the presence of extremely fine fly ash in the flue-gas stream increased the dew-point temperature considerably. These experiments seem to indicate an increase in the order of around 75 deg F above that which would exist in a clean flue gas.

A review of the work by Peter Hodson (3) has shown that the presence of extreme fines in the flue gas increases materially the dew-point temperature.

TABLE 1 FLUE-GAS COMPOSITIONS (APPROX)

(Based on 650 F temperature at air-preheater inlet.)

Column		1	2	3	4	5
Fuel		Midwestern Bit. Coal	Eastern Bit. Coal	Cent. Illinois Bit. Coal "Kinkaid"	High Sulphur Fuel Oil	Low Sulphur Fuel Oil
Firing		Pulverized	Pulverized	Cyclone Burner	-	-
Excess Air		20%	20%	10%	20%	20%
ANALYSIS OF FUEL						
Moisture	H_2O	3.87%	2.82%	15.00%	0.16%	-
Carbon	C	60.21	77.60	52.00	84.94	83.90%
Hydrogen	H_2	4.52	4.88	3.85	10.95	12.70
Oxygen	O_2	7.51	4.15	8.70	1.25	1.20
Nitrogen	N_2	1.59	1.81	0.80	0.19	0.40
Sulphur	S	4.14	1.15	4.65	2.41	0.10
Ash		18.16	7.59	15.00	0.10	1.70
TOTAL		100.00	100.00	100.00	100.00	100.00
GASES per million pounds of products of combustion with 60% relative humidity combustion air.						
Carbon Dioxide	CO_2	195,160#	209,380#	185,840#	132,500#	172,600#
Sulphur Dioxide	SO_2	14,570	1,730	9,200	5,500	400
Oxygen	O_2	34,690	36,015	161,410	36,400	36,400
Nitrogen	N_2	688,355	715,715	593,740	718,650	725,900
Water Vapor	H_2O	52,925	32,560	48,960	56,100	64,100
TOTAL GASES		985,700#	995,400#	999,150#	999,150#	999,400#
SOLIDS per million pounds of flue gas.						
Sulphur Compounds		500#	100#	35#	300#	50#
Carbon		900	300	45	500	500
Fly Ash Remaining		12,900	4,200	770	50	50
TOTAL SOLIDS		14,300#	4,600#	850#	850#	600#
TOTAL PRODUCTS OF COMBUSTION		1,000,000#	1,000,000#	1,000,000#	1,000,000#	1,000,000#
		Total solids shown based on approx. 75% of Ash content in fuel and the use of circular type burners and dry bottom furnace.			Total solids will vary with furnace design and conditions.	

TABLE 2 DIMENSION RANGE OF FLY ASH—PULVERIZED COAL

Size, microns less than	Cumulative % by weight	Cumulative % by number	Cumulative % by surface area
200	99.5	99.999999+	99.991
100	97.5	99.99998+	99.873
80	95.5	99.99994	99.677
60	92.5	99.9998	99.301
40	84.5	99.9985	97.804
20	64.0	99.923	94.869
10	37.0	99.75	78.909
5	16.0	98.73	54.409
2	3.0	92.83	21.629
1	0.5	78.25	6.849
0.5	0.065	57.10	1.834
0.2	0.0025	29.75	0.302
0.1	0.0001	16.15	0.164

TABLE 3 DIMENSION RANGE OF FLY ASH—CYCLONE BURNER

Size, microns less than	Cumulative % by weight	Cumulative % by number	Cumulative % by surface area
200	97	99.9999999+	99.998
100	95	99.9999999+	99.993
80	93.5	99.9999999+	99.987
60	92	99.9999999+	99.98
40	89.5	99.9999992	99.96
20	83	99.999991	99.83
10	75	99.99991	99.60
5	65	99.998	99.21
2	50	99.98	97.66
1	39	99.80	94.99
0.5	28	99.8	89.7
0.2	17	98.9	78.6
0.1	11	93.1	65.0

TABLE 4 COMPUTED PROBABLE DIMENSIONAL DATA ON SOLIDS IN FLUE GAS

Fuel	Grains per lb flue gas	Number of particles per lb flue gas	Surface area of particles per lb flue gas, sq in.	—Per cent by Weight— Carbon	Sulphur Compounds
Pulverized Midwest bit.	99.4	307×10^9	3450	6.3	3.5
Pulverized Eastern bit.	32.2	100×10^9	1120	6.5	2.2
Central Ill. bit. coal, cyclone burner	5.95	335×10^{12}	5670	5.3	4.1
High-sulphur fuel oil	5.95	374×10^{12}	11120	58.8	35.3
Low-sulphur fuel oil	4.20	264×10^{12}	7850	83.0	8.3

NOTES: Specific gravity of fly ash in all cases 2.0.

Data pertaining to solids in flue gas from fuel oil based on: 99.9% less than 1 micron; 95% less than 0.5 micron; 50% less than 0.2 micron.

Stack Nuisances

The definition of stack nuisances can be varied depending upon the discharge as well as the locale. Three different categories of nuisance are used for this discussion, namely, (*a*) blackness of discharge, (*b*) deposit of fly ash in the neighborhood or in distant areas, (*c*) air pollution by dust and fumes which are strongly sulphur bearing.

The solids in the stack discharge known as smoke have an adverse psychological effect on the neighbors. There are many laws in settled communities governing the permissible degree of smoke blackness and dust loading.

The discoloration is due essentially to the "extreme fine particles," which are difficult to remove completely.

The fly ash may range in size from 200 microns down to less than 1 micron. The larger particles bother the immediate neighborhood.

The very fine particles travel long distances and take a longer time to settle and become a nuisance. In areas where there are heavy fogs or dews these extreme fines are damaging when containing sulphur compounds.

Air pollution due to fumes, without the presence of fines, has not been investigated by the authors.

Relative Merits of Removing Fine Solids

The removal of all solids at any temperature would eliminate atmospheric pollution due to dust. In other respects, however, the temperature at point of removal is significant.

The different temperature zones used are defined as follows:

High-temperature zone.....approx 450 to 900 F
Low-temperature zone.....approx 400 F and below

The following pros and cons for removal of the solids in a high or low-temperature zone, respectively, are presented for consideration:

1 In the high-temperature zone all the solids carried are dry and almost chemically inactive from a corrosive standpoint.

2 Removal of all the solids in a high-temperature zone prevents deposit build-up on the low-temperature surfaces.

3 In the low-temperature zone the solid particles become moist and are then, in the presence of sulphurous gases, adhesive and chemically very active.

4 Removal of all the solids in the low-temperature zone after the heating surface has no beneficial effect on the life or the availability of the plant.

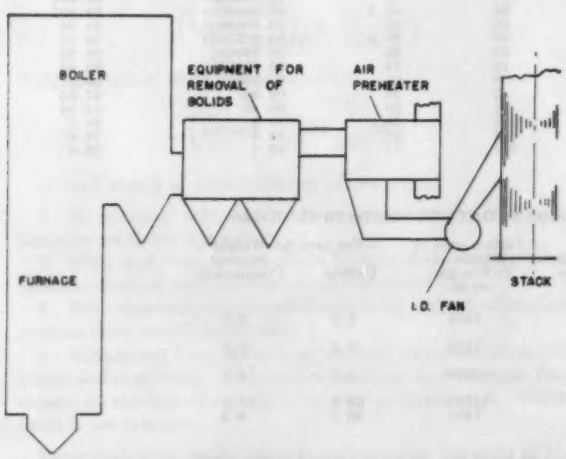

FIG. 2 TYPICAL SYSTEM SCHEMATIC

5 Even when no sulphur compounds are present in the flue gas, removal of the fines in the high-temperature zone results in ease of handling the collected material due to its dryness.

Conclusion Regarding Flue Gases

It has been noted that water vapor, sulphurous gases, and solids containing sulphur compounds adversely affect low-temperature surfaces and limit the gas exit temperature at which the boiler system can be operated. At present no practical method is known whereby the sulphurous gases and the water vapor can be removed in the high-temperature zone. The solids, which include the mineral-sulphur compounds, are the only products that can be removed. If these are removed at temperatures where they are dry, then deposits on the low-temperature surfaces are eliminated and a clear stack discharge obtained. It is also possible the elimination of solids may reduce the rate of corrosion.

A system is shown in Fig. 2 where equipment for removal of the solids has been placed ahead of the low-temperature surface.

METHODS OF REMOVING SOLIDS FROM FLUE GASES IN A HIGH-TEMPERATURE ZONE

Range of Different Methods

The various schemes in Fig. 3 are some of the probable methods of successfully removing solids from flue gases in the high-temperature zone before the cold end of the boiler system. These methods may, or may not, be similar to those now used in the low-temperature zone. Removal of the fines in the high-temperature zone

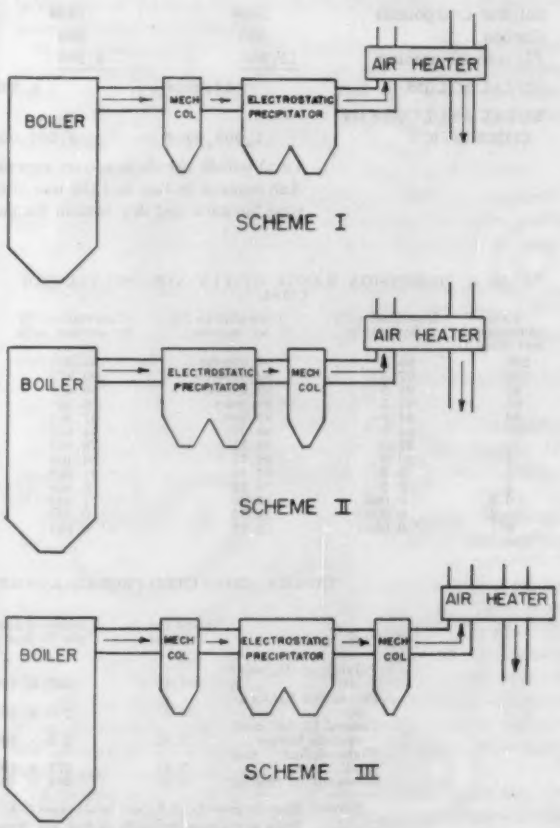

FIG. 3 POSSIBLE COLLECTOR AND PRECIPITATOR APPLICATIONS

ahead of the low-temperature surfaces eliminates possible fouling of collectors and protects the low-temperature surfaces.

Scheme I is an arrangement whereby a mechanical collector is placed ahead of the electrostatic precipitator. This would be useful where the percentage of large particles in the flue gas is high.

Scheme II is an arrangement in which the electrostatic precipitator is placed ahead of the mechanical collector. This type of arrangement is indicated where there are mostly fine particles, and where agglomerated fines are generated in the electrostatic precipitator to be picked up by the mechanical collector.

Scheme III is used where the ultimate in collection is required. Where several fuels are used, such as powdered coal, oil, and gas, either simultaneously or independently, this scheme would be indicated. Mechanical collector, electrostatic precipitator, and then another mechanical collector are used. Coarse particles would be removed by the first mechanical collector. Fines would be removed in the electrostatic, and agglomerated fines would be picked up by the trailing mechanical.

All these are possible combinations, and a selection must be developed for each specific project.

Review of Experimental Work

Waltham Experimental Plant. In early 1946, development work was initiated for removal of "extreme fines" from a flue-gas stream in a high-temperature zone. It was determined that electrostatic equipment would best serve this purpose. It further was indicated that a continuous cleaning of the collecting surfaces was essential in order to maintain high collecting efficiency.

A joint development project was set up between The Air Preheater Corporation and the Raytheon Manufacturing Company.

The first step in the program was to design suitable prototype equipment to carry out the desired results, and to determine experimentally the possible effectiveness of such an arrangement.

This prototype equipment was built and installed at the Raytheon Manufacturing Company's plant in Waltham, Mass., during the summer of 1946. Fig. 4 shows the housing structure containing the equipment and the block diagram, Fig. 5, shows the essential equipment and its schematic arrangement.

It was desired that this equipment should remove efficiently the extreme fines, largely of carbon, at high temperatures, high velocity, and high efficiency. In order to provide these conditions smoke from an oil burner taking insufficient air to provide excess carbon in the fly ash was used. To maintain temperatures at desired levels, an auxiliary gas-fired burner was used.

Referring to Fig. 4, the stack to the left indicates the type of smoke that was generated; this stack served as the by-pass for the precipitator. The stack to the right shows clear operation. A pipe was used to focus the attention on the effluent, with a white board behind the stack to give adequate background to determine small amounts of ash haze.

Efficiency tests were run according to the modified standard blackness test as set up by the U. S. Bureau of Standards. The results of these tests are shown in the simplified curve in Fig. 6. For velocities of 50-fps efficiencies varied from a maximum of about 95 per cent at 650 F to 90 per cent at 400 F and 85 per cent at 900 F.

This test proved the necessity for continuous removal of the collected material to maintain high collecting efficiency. The best collecting efficiency was at a temperature of about 650 F.

Hell Gate Station Experimental Plant. The results obtained at Waltham were discussed with Consolidated Edison Company of New York, and arrangements made for their participation in the testing of a 2000-cfm prototype unit on Boiler 12 at their Hell Gate Station. This testing program started in August, 1949, and

Fig. 4 Experimental Plant at Waltham

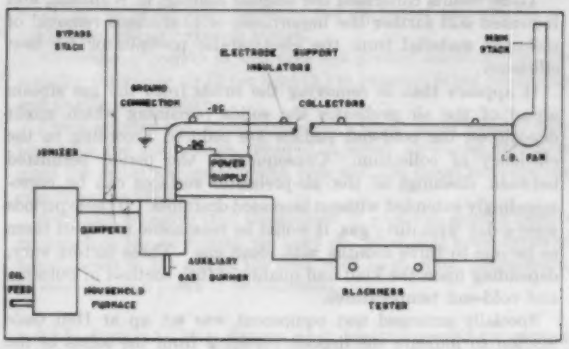

Fig. 5 Test Apparatus at Waltham

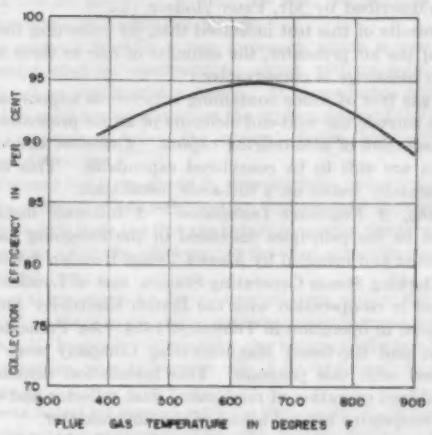

Fig. 6 Results From Test at Waltham

continued until January, 1952. Tests were run with pulverized coal, oil, and gas firing, and combinations thereof. Tests indicated that a mechanical collector ahead of the electrostatic was needed. A life test was run over a continuous period of 3300 hr.

The ASME Standard Weight Test Method did not indicate true values of the extreme fines. Work was done on the appli-

cation of the discoloration or blackness test to this particular installation. A multiple spot-testing instrument was developed, as described in a paper by Dr. Hans Klemperer and Mr. T. D. Price (4).

The discoloration instrument showed a somewhat higher efficiency of the electrostatic unit than obtained from the weight test. The reason is that while the total number of extreme fines is a large quantity, their weight is practically negligible.

With oil firing it was impractical to use the weight method for determining collection efficiency and therefore the discoloration instrument was used. Collection efficiencies as high as 98 per cent at temperatures of about 650 F and flue-gas velocities through the units of about 40 fps were measured.

On pulverized-fuel firing using the ASME weight method of testing, the combined efficiency of the mechanical collector and electrostatic precipitator was over 98 per cent at temperatures of about 650 F and about 40-fps gas velocity through the electrostatic precipitator. Under these conditions the discoloration or blackness test indicated an efficiency of about 97 per cent for the electrostatic precipitator alone.

These results confirmed the original findings in Waltham, and indicated still further the importance of continuous removal of collected material from the electrostatic precipitator for best efficiency.

It appears that in removing the solids from the gas stream ahead of the air preheater the solids remaining which might deposit on the cold-end surface are reduced according to the efficiency of collection. Consequently, the period permitted between cleanings of the air-preheater surfaces can be correspondingly extended without increased draft loss. If these periods were a day with dirty gas, it would be reasonable to expect them to be one to three months with clean gas. These factors vary, depending upon the kind and quality of fuel, method of burning, and cold-end temperatures.

Specially arranged test equipment was set up at Hell Gate Station to indicate the deposit resulting from the solids in the flue gas as against clean flue gas. The equipment consisted of glass-tube condensers cooled with water. This testing arrangement is described by Mr. Peter Hodson (3).

The results of this test indicated that, by collecting the solids ahead of the air preheater, the estimate of one to three months between cleanings is conservative.

Flue gas free of solids containing sulphurous vapors can continue to corrode the cold-end elements of an air preheater owing to condensation of acid-bearing vapors. Therefore the cold-end elements are still to be considered expendable. This is being experimentally tested on a full-scale installation.

Barking, A Full-Scale Installation. A full-scale installation designed to the principles discussed in the foregoing has been constructed and installed by Messrs. James Howden & Co., Ltd., in the Barking Steam Generating Station, east of London. This was done in co-operation with the British Electricity Authority and placed in operation in February, 1954. Air Preheater Corporation and Raytheon Manufacturing Company were closely associated with this program. This installation demonstrates the combined operation of mechanical dust collector and electrostatic precipitator located ahead of the air preheater.

This unit is installed on a pulverized-coal-fired boiler capable of generating 160,000 lb per hr of steam. This plant is described in a paper by Dr. Hans Klemperer and Mr. J. E. Sayers (5). This installation provides for obtaining data for evaluating the rate of accumulation of deposits and rate of corrosion of the air-preheater surface.

Conclusion

The work described seems to indicate that there are real possibilities toward a definite improvement in some of these very vexing problems of flue gases, namely, atmospheric pollution by dust, air-preheater deposits, and corrosion.

Further, the possibility of operating the air preheater at lower-gas exit temperatures with clean flue gases provides increased fuel economy offsetting possible higher cost of removing the solids in the high-temperature zone.

It is hoped that forces will be joined to encourage this program further.

BIBLIOGRAPHY

1 "Corrosion and Deposits in Regenerative Air Preheaters," by J. F. Barkley, et al., U. S. Bureau of Mines. Report of Investigations 4996, August, 1953.

2 "The Corrosion of Power Plant Equipment by Flue Gases," by Henry F. Johnstone, University of Illinois Engineering Experiment Station, Urbana, Ill., Bulletin No. 228, June, 1931.

3 "Influence of Fine Particles on Corrosion of Economizer and Air-Preheater Surfaces by Flue Gases," by Peter Hodson, Trans. ASME, vol. 77, 1955, pp. 279–286.

4 "Evaluation of the Multiple Spot Discoloration Tester for Flue Gas Applications," by Hans Klemperer and T. D. Price, presented at Air Pollution Control Association Meeting, May 3–5, 1954.

5 "Design Aspects of an Electrostatic Precipitator for the Collection of Small Solids Ahead of the Air Heater," by Hans Klemperer and J. E. Sayers, published in this issue, pp. 317–326.

6 "Prediction of Dust Size," by P. F. Best, "THERMIX," Data 3-TTC-1.

7 "Cyclone Furnace Boilers," by G. W. Kessler, Proceedings of the American Power Conference, vol. 16, 1954, pp. 78–90.

8 "Current Trends in Fly Ash Recovery," by Richard O'Mara, *Combustion*, vol. 21, April, 1950, pp. 38–43.

10 "Clouds and Smokes," by W. E. Gibbs, J. & A. Churchill, London, England, 1924.

11 "Micromeritica," by J. M. Dalla Valle, Pitman Publishing Corporation, New York, N. Y., second edition, 1948.

Discussion

J. F. Barkley.[4] The authors are to be commended for their thought-stimulating paper. They have summarized in a relatively short paper a wealth of study, surmising, and experimental work over a period of some 10 years in their pioneering on a different attack on the problem of corrosion and deposits from combustion gases. The writer has had the opportunity of studying the full-scale experimental equipment mentioned in the paper installed recently at Barking Power Station near London, and was impressed with the general layout of the testing equipment; it is refreshingly orderly and provides testing apparatus that should give thorough and satisfactory findings. Within a year or two we shall hear comprehensive results of this testing which will be of much interest. Speaking as chairman of the Research Committee sponsoring this paper, we are very pleased to have this excellent contribution.

O. F. Campbell.[5] This paper offers some very interesting data that may be useful in many fields other than boiler operations. Also it presents another fundamental approach to the operation of boilers at higher efficiency by the removal of solid material before an air preheater which can operate at lower temperature because of the removal of the solids.

In so far as removal of solids ahead of an air preheater when burning fuel oil or gas is concerned, it appears that it is not necessary to do so. It is noted from the paper that the carbon content of the flue gases when burning heavy fuel oil amounts to approximately 500 ppm. This quantity appears entirely too high and it would probably be cheaper to pay more attention to the com-

[4] Chief Coal Technologist, Bureau of Mines, U. S. Department of the Interior, Washington, D. C. Fellow ASME.

[5] Combustion Engineer, Sinclair Refining Company, E. Chicago, Ind. Fellow ASME.

bustion of the fuel oil and eliminate the carbon content of the exit flue gases by better combustion. If this is done the writer does not feel that it is necessary to install dust collectors preceding an air preheater when burning heavy fuel oil.

MARTIN FRISCH.[6] This paper, and the companion paper by H. Klemperer and J. E. Sayers,[7] suggest possibilities for further improving steam-generator efficiencies by several per cent.

The authors deserve great credit for the boldness of their original idea that, if an appropriate method of continuously cleaning an electrostatic precipitator could be devised, it might be possible, without impairing efficiency, to increase gas velocities from five to ten times the values now customary. Inasmuch as the authors planned to accomplish this at temperatures approximately two to three times those to which precipitators are usually subjected, their daring seems even greater because they recognized full well that the use of higher gas temperatures introduces an additional obstacle to efficient dust collection, namely, a higher gas viscosity. Nevertheless, the performance of several large-scale test installations, reported by the authors, definitely appears to confirm their expectations. For, at gas velocities of from 40 to 50 fps, and at temperatures of from 650 to 700 F, through their precipitator, powdered-coal fly-ash collection efficiencies were realized which are customarily obtained in conventional precipitators operating with gas at 300 F, at velocities of only about 5 fps. This demonstration could prove extremely important if the authors are also correct in their belief that air-preheater fouling and corrosion at the cold end will be greatly inhibited by removing most of the fine ash from the gas ahead of the air heater. Then it should be possible, as they hope, to justify installation of much larger air preheaters than heretofore used, and which would prove capable of cooling the products of combustion to temperatures as low as 250, or even 200 F. At present, outage-promoting air-heater corrosion and fouling, anticipated with over-efficient air heaters, tends to deter users from installing units capable of cooling the products of combustion to such low values.

The writer is inclined to agree with the authors that, under certain conditions, the presence of fine fly ash in the gases tends to raise the dew point, and that if the other factors tending to promote corrosion coexist, corrosion might be expected to proceed more rapidly than if the fly ash were absent. However, some lurking doubts remain in view of the fact that air heaters used in pulverized-fuel-fired installations corrode and foul less rapidly than air heaters used with stoker-fired and oil-fired installations, under analogous conditions. In fact, the trend toward the use of special powdered additives to inhibit corrosion in the colder regions of stoker and oil-fired boilers was sparked by the realization that cold-end corrosion was far less serious in pulverized-fuel-fired units. While the effects of attempts to inject pulverized-fuel fly ash, and other additives, into oil-fired furnaces for the purpose of inhibiting cold-end corrosion have not always proved beneficial, a sufficient number of successes have been achieved to warrant further trials. Therefore it does appear that the case for substantially eliminating fine fly ash from the gas delivered to the air heater needs as conclusive demonstration by the authors as they achieved in demonstrating that high electrostatic precipitator dust recovery rates are possible at elevated gas temperatures and high velocities.

The authors are to be congratulated for their fine presentation of unusually important and significant experimental work. This could lead to improvements in steam-generator efficiencies and, possibly also, to reductions in precipitator first costs. It would be interesting to know what precipitator size and cost reductions might be expected to result from the velocity increases found possible.

[6] Vice-President, Charge of Engineering, Foster Wheeler Corporation, New York, N. Y. Fellow ASME.

[7] Authors' reference (5).

W. B. GURNEY.[8] This paper on removal of flue-gas solids is a very interesting one. Our tests appear to be in agreement that the solids in the flue gas can be dry at temperatures above 450 F. Glass and steel rods inserted in our flue-gas stream showed no deposit accumulation in the zone 500 to 1000 F. Below 450 F iron-sulphate and carbon particles containing strong sulphuric acid deposited on the rods.

We are uncertain, however, that the dew point of the gas itself was raised during periods of unclean flue gas. It appears that the dew point of the gas phase may have been normal for its SO_3 content whereas the surfaces of the soot contained strong sulphuric acid.

It was quite obvious, however, that a soot-free flue gas resulted in much less air-heater metal corrosion than a sooty flue gas. The flue gas in this case contained iron which originated from refinery acid-sludge fuel. Some of this iron as iron sulphate stuck to the lime-coated metal of the air heater and greatly retarded the rate of corrosion attack.

Air-heater corrosion in this case was greatly minimized by increasing the excess air (5 per cent O_2) to improve firing conditions and to eliminate smoke.

Firing refinery gas, which contained a much lower sulphur content than the acid sludge, resulted in severe air-heater corrosion until the metal was coated with lime and the metal temperature was raised to 225 F.

Although we agree that elimination of soot will greatly reduce corrosion in the air heater, we have observed that some types of constituents in the ash in the fuel, such as calcium, magnesium, or even iron can prove to be beneficial.

S. I. JUHASZ.[9] It is known that low-temperature corrosion and deposit can be eliminated by either decreasing the dew point of the flue gas or increasing the wall temperature in the cold end of the air preheater so that the wall temperature is above the dew point by a sufficient margin.

The authors describe a new approach which is based on the suggestion that no condensation occurs without solid particles which act as condensation nuclei. It is suggested that the removal of solid particles enables the cooling down of the flue gases to a temperature below the present design level without increased difficulties.

Reference has been made in discussion to unfavorable experience in decreasing low-temperature deposits and corrosion by removing solids from the flue gas before it reaches the air preheater. In the case cited the efficiency of the dust remover was well below 98 per cent.

Thus there seems to be a contradiction about the effect of "solids" in the flue gas upon low-temperature corrosion and deposits. If, however, we consider the complex effects of the flue-dust particles, the ambiguity might be explained to a certain extent.

It was found by several workers, first by H. F. Johnstone and later by those connected with the British Boiler Availability Committee, that the sulphur content of a fuel burned in pulverized form causes less trouble than if it were burned on a stoker. The beneficial result is generally attributed to the larger amount of flue dust. According to the British workers this is due to several partial effects as follows:

[8] Supt. of Results, Gulf States Utilities Company, Beaumont, Texas. Mem. ASME.

[9] Executive Editor, Southwest Research Institute, San Antonio, Texas. Mem. ASME.

(*a*) The presence of flue dust makes the formation of atomic oxygen more difficult and thus diminishes the combustion rate of SO_2 to SO_3.

(*b*) The flue dust adsorbs the SO_3 already formed.

(*c*) The flue dust neutralizes chemically the SO_3 which has already been formed, in the event the flue-dust particles consist partly of reducing metallic oxides.

The extent of all these effects is doubtless strongly influenced by the quantity and size distribution of flue-dust particles. Until the saturation point is reached the effects described are doubtless increased by increased quantity of dust.

On the other hand, the effect of fine dust upon condensation is adverse; i.e. less fine dust is less harmful from the point of view of condensation. If the flue-dust concentration in these fines (0–5μ) were the only, or the dominating, factor influencing the extent of the difficulties, the difference between oil and pulverized-coal firing could be explained. Oil firing, which produces a very small concentration of extremely fine particles, usually causes more deposit and corrosion than pulverized-coal firing when both fuels have the same sulphur percentage. More detailed comparative experiments (with and without fine dust removal) with oil-fired boilers would be very informative.

Under normal conditions only minor difficulties occur with pulverized-fuel boilers. The importance of the suggestion lies, however, in the aspect that if lower exit-gas temperature could be used the boiler efficiency could be increased. It should be borne in mind that cooling the flue gas below the dew point without condensation means an unstable thermodynamic system which limits this additional cooling.

The authors are to be commended on their unorthodox suggestion and the writer is looking forward to the experimental results which will be obtained in the British Power Plant using the method described.

P. H. Koch.[10] The problems of fouling and corrosion of low gas-temperature portions of air heaters have been with us for a long time, and are becoming more acute with increasing efficiencies and the lowering of fuel quality. Considerable effort has been and is being given to understanding and overcoming these problems by various approaches such as cleaning methods, corrosion-resistant material and coatings, additives, design of heaters, etc. The authors have added another approach, the removal of solids ahead of the air heater, for consideration.

Our experience with the removal of solids ahead of the air preheater has not been very successful from the standpoint of preventing air-preheater fouling and corrosion. Actually, on several jobs, the fouling of the preheater was more severe than on similar jobs with no solids removal before the preheater. Of course, the efficiency of solids removal on these units was a lot less than the 98 per cent the authors have in mind. However, even with 98 per cent collection efficiency, the amount of very fine solids entering the preheater is still considerable from the standpoint of fouling of preheater surface. Based on our experience, and the fact that very fine solids will enter the preheater, we question the fouling advantage accruing from solids removal ahead of the preheater by high-efficiency collection.

In regard to alleviating corrosion by the removal of solids from the flue gas ahead of the preheater, the published works of the British investigators Kear, Whittingham, Corbet, and Flint show that smokes of carbon, silica, metal oxides, and even PC fly ash greatly reduce the dew point and SO_3 content of flue gases in both laboratory experiments and in the tests of several full-sized boilers. Our experience is not defined in quantitative terms as well as the British work. However, our field work on additives shows that if a proper selection of dusts is made, say, MgO and dolomite, these dusts will appreciably reduce the dew point and SO_3 content of the flue gases. Therefore it appears that, in some instances, removal of solids ahead of the preheater could increase the amount of corrosion. Incidentally, some coals have built-in additives of basic materials which either tie up part of the SO_3 present in the flue gases or neutralize the sulphuric acid condensing on the surface, thereby preventing corrosion and, although we do not have definite proof, we believe that may be occurring on some cyclone-furnace boilers burning Central Illinois coal.

Our experience does not indicate that the very fine solids in flue gases are mainly responsible for the cold-end corrosion. We have long observed that the main bulk of air-heater-tube deposits consists principally of fly ash in a matrix of alkali and iron sulphate with some free sulphuric acid. The fly ash in the deposits has about the same proportion of fine and coarse particles as does the parent fly ash. We also have found that so-called nonreactive or inert materials like kaolin do not affect the dew point, SO_3 content, or the corrosiveness of the gases—even though they have about 10 to 15 times the specific surface of the fly ash—and we have no particular difficulties with air-heater corrosion on the cyclone-furnace boiler where the fly ash is much finer than with other types of firing.

An additional item for consideration, other than the effect on fouling and corrosion of the preheater, is the increased cost of the solids-removal equipment when it is placed ahead of the preheater (resulting from the higher gas temperatures and volume). Insulation costs will also increase, not only because of the higher gas temperature, but also because any heat loss will require lower gas temperature leaving the preheater for the same efficiency. Air infiltration, due to the collecting equipment, also will require lower exit-gas temperatures. Lower exit-gas temperatures means lower metal temperatures and more costly heaters.

The best evaluation, of course, will be obtained by comparing the actual job performance of two identical units in the same plant with one unit having solids-removal equipment ahead of, and the other after, the air preheater. Consequently, the full-scale installation at the Barking Steam Station in England should give us very valuable data.

Benjamin Linsky.[11] This stimulating paper gives the proper type of emphasis to the increased community desire for cleaner looking air and reduced dust deposition, both adversely affected by fine fly ash.

The unmeasured effects of fine fly ash and sulphurous compounds corroding and otherwise deteriorating property is not yet generally a target except by specialists in air pollution or corrosion.

The, as yet, unmeasured effects of fine fly ash and sulphurous compounds on health, acute or chronic, is receiving increasing discussion in communities, although it is receiving very little research effort, so far as the writer knows.

The reduction in the emission of fine fly ash would reduce the number of condensation nuclei and resulting haze.

It is probably stating the obvious to point out that if the fine fly ash can be removed to a greater degree it would permit the development of sulphur-compound removal systems that would be less complex and less costly if, and when, such removal becomes a community necessity.

E. B. Powell.[12] We are greatly indebted to the authors for

[10] The Babcock & Wilcox Company, New York, N. Y.

[11] Chief, Smoke Abatement Bureau, City of Detroit, Detroit, Mich.

[12] Consulting Engineer, Stone & Webster Engineering Corporation, Boston, Mass. Fellow ASME.

presenting the problem of the steam-boiler flue-gas air heater as interestingly and in such comprehensive summary, as well as for their research results and their valuable suggestions. Experience has clearly shown the importance of the combustion-product solids deposit as a factor in the corrosion of the heater surface when the gas is sulphur-bearing. The corrosion from the hygroscopic property of the solids is also, in a considerable degree, promoted by their insulating action in depressing the surface temperature.

The authors have labored with commendable success in improvement of intermittent cleaning of the surface of the flue-gas air heater. Their work on that phase of the problem has been a real boon to a large section of the steam-generating industry. Effectively minimizing the flue-gas solids content before lowering the gas temperature within too close range of the dew point is a highly logical next step. However, the gain in continuity and relinbility of service and in thermal economy must not be too badly offset by the rise in first cost and maintenance charges occasioned by complexities and by the higher temperature to which the solids-removal equipment will be subjected. It would seem that in many locations public health and esthetic considerations, and even the dictates of over-all economy, will soon require an equal degree of freedom from solids in the finally discharged waste gas. Perhaps the new solids removal equipment mentioned by the authors as developed in collaboration with Raytheon Manufacturing Company will have solved the problems imposed heretofore by separation of extremely fine solids in high-temperature flue gas.

The descriptions given of the experimental work at the Waltham plant of Raytheon Manufacturing Company and at Hell Gate Station of Consolidated Edison Company of New York are of very practical interest, as is also, and quite emphatically, the information that full-scale application of the design principles used in this experimental work has been adopted by Messrs. James Howden Company, Ltd., and installed by them at Barking Station in southeast London. The effectiveness reported for the experimental equipment is indeed commendable. Service results from Barking Station will be keenly awaited, as the latter should bring in the factors of size and time beyond those determined from the experimental work described by the present authors, and even from the tests at Barking Station forecast by Messrs. Klemperer and Sayers in an accompanying supplemental paper.[7]

The effect of gas-temperature rise on the collection efficiency of the experimental solids precipitator at the Raytheon plant at Waltham, giving a maximum around 650 F, as shown by Fig. 6 of the paper, is very interesting. Results of any checks which the present authors may have made in application of the Deutsch formula, or H. J. White's, or others, in evaluating the opposing influences exerted by gas temperature on electrostatic-collection efficiency should be of constructive aid in analysis of future design.[13] The very gratifying preliminary test result reported by Messrs. Klemperer and Sayers would encourage confidence in the Deutsch formula for general performance. It would also be of interest to know the basis of the authors' estimate of particle surface area given in Tables 2, 3, and 4.

E. M. Powell.[14] It must be recognized by all who have heard or read this presentation that the solution presented here represents a completely new and promising approach to the solution of a most troublesome operating condition.

[13] "Electrostatic Precipitators for Electric Generating Stations," by H. J. White, Power Apparatus and Systems, April, 1953, published by the American Institute of Electrical Engineers.

[14] Assistant Chief Engineer, Combustion Engineering, Inc., New York, N. Y. Mem. ASME.

Steadily rising fuel costs have resulted in an intensive drive toward higher cycle efficiencies as evidenced by the trend toward higher steam pressures and temperatures with the use of one or two stages of reheat. For instance, two installations are now being designed to operate above the critical pressures of steam with temperatures beyond anything used before. On the other hand, progress toward higher boiler efficiency using lower exit-gas temperatures has been slow by comparison. The obstacles have been reduced availability because of air-heater and dust-collector plugging and high maintenance costs from corrosion.

The idea of removing solids from the gases before they enter the air heater is not new. There are several units in operation with mechanical collectors located in this manner. Operating experience on these units, however, has not produced the results hoped for. While in some cases there may have been some improvement, it has not been a substantial one. In others more harm than good may result. The design principles which must be adhered to with a conventional electrostatic precipitator have prevented its location in a zone of high gas temperature. Test results presented here with this new design approach indicate the ultimate success of such an innovation.

Apparently the over-all collection efficiency from the standpoint of stack emission will be at least as good as can be obtained with a standard combination of mechanical and electrical dust collectors. While this is a notable achievement the objective of those responsible for this development went beyond that to making higher efficiencies possible without sacrifice to availability and maintenance cost.

Possibly the removal of fine material, as well as the coarse material, will completely change performance achieved in previous attempts at this solution to the problem of plugging and corrosion. There is considerable evidence to support such an hypothesis. For instance, experience indicates that most severe corrosion is accompanied by heavy deposit.

It is certain that the experiment at Barking will be followed with interest by all designers and operating men in the power-generation field. Little information seems to be available at the moment to indicate how much exit-gas temperatures can be reduced safely. We will be looking forward to further reports in the future describing operating results with lower temperatures than are now considered practicable. Other installations would be most desirable to provide an opportunity to study operation with other troublesome fuels. The men responsible for the forward thinking that went into the development of this project are certainly to be congratulated.

E. F. Rothemich.[15] The authors have reviewed the basic concepts of the formation of troublesome deposits on air-preheater surfaces, and have explained their research program, starting with laboratory models, through pilot plant, to full-scale installation. They estimate that the periods between cleaning of the preheater surface can be extended, without increase in draft loss, by collecting the solids from the flue gas ahead of the air preheater. Thus, if these periods were a day with dirty gas, it would be reasonable to expect them to be one to three months with clean gas. Such results are indeed of significance.

In previous comments on papers discussing the effect of fine particles in flue gas on deposits on tubular air-heater surfaces, we have mentioned that our experience has indicated that locating the conventional mechanical dust collector ahead of the air heater results in greater deposits than with the dust collector following the air heater. Of course, the conventional mechanical dust collector removes only a small percentage of the medium fines and extreme fines (1.0 to 20 microns and 0.01 to 1.0 microns,

[15] Assistant Chief Service Engineer, Riley Stoker Corporation, Worcester, Mass. Mem. ASME.

respectively, as designated in the paper). When the conventional mechanical dust collector is located ahead of the air heater, the deposits on the air-heater surfaces are caused by these fines which have passed through the dust collector. This tends to confirm the general findings of the authors' paper.

In two existing installations with dust collectors preceding tubular air heaters, Illinois coal with 3 to 4 per cent sulphur is burned on traveling-grate spreader stokers. Daily cleaning of the air heater in service of one unit permits continuous full-load operation with expected efficiency. The air heater of the other unit is not cleaned between outages and the unit loses 15 per cent capacity in four to five months following the last cleaning. This unit operates with air heater exit-gas temperatures 25 to 50 deg F below expectations when clean (275 F gas temperature leaving the air heater has been recorded at full load when the air heater and boiler were clean).

As mentioned previously, our experience indicates that this cleaning problem probably would not exist if the dust collector had been located after the air heater. The mechanical collector located after the air heater has the added advantage of smaller design due to lower gas temperatures and lower gas volumes, and therefore represents a smaller capital investment. The installation of a high-efficiency electrostatic precipitator in conjunction with the present mechanical separator, both located between the boiler and the air heater, might eliminate the problem of these deposits, but the economics of the situation would not justify such an installation.

The foregoing results indicate the possibility of a different mechanism of deposits in tubular air heaters as compared to regenerative air heaters.

The relative size and shape of the gas passages through the regenerative air heater may be more conducive to deposit formation than round air-heater tubes. There has been some indication that small-diameter air-heater tubes are more prone to deposits and corrosion than larger diameter tubes.

It also has been found that the deposits occur in a few tubes around the periphery of the tube bundles or in the first few rows of tubes through which the air passes upon entering the air heater. Since a large majority of the tubes are unaffected by deposits, except in most severe cases, the increase in draft loss due to deposits is minor. On many tubular air heater installations, the first indication of difficulty is not an increase in draft loss on gas side resulting from deposits but the increased requirements on both the forced-draft and induced-draft fans as a result of the leakage from the air side to gas side through corroded tubes.

We would appreciate the authors' comments on the problem of disposing of the refuse collected in the high-efficiency electrostatic precipitator. Do the medium fines and extreme fines agglomerate sufficiently to permit convenient handling with present dust-unloading equipment? Collection of this fly ash at 650 F results in dry particles which facilitate collection, but may complicate unloading of the dust. Fly-ash disposal became a major problem at one plant justifying the installation of a slag-tap furnace for pulverized-coal firing with complete reinjection into furnace of all fly ash from dust collector, air heater, and boiler hoppers thus permitting removal in slag form. The increase in efficiency from the reinjection is insignificant due to the low-carbon content in the refuse. The prime consideration in choice of equipment was elimination of the disposal problem for fly ash. The fly-ash disposal problem is requiring an increasing amount of consideration throughout the entire power industry.

The authors mention that flue gas free of solids containing sulphurous vapors can continue to corrode cold-end elements of an air heater due to condensation of acid-bearing vapors and that this effect is being experimentally tested on a full-scale installation. It will be of interest to learn from the full-scale experiment at the Barking Steam Generating Station in England what reduction in deposits, formation of acid, and corrosion result from the removal of most of the solid particles ahead of the air heater.

W. P. Saunier.[16] The authors have given a presentation of the reasoning involved in the development of a dust precipitator which offers the prospect of improving boiler operating efficiency by some 2 per cent. At the same time it promises to increase the availability and life of air preheaters by a substantial factor and to decrease in a marked degree the air-preheater cleaning costs.

Considering that total boiler losses are today about 10 per cent of the heat input, an improvement of 2 per cent in efficiency should be looked at as a reduction of 20 per cent in the boiler losses. Viewed from this angle, as it properly may be, the advance in the art which the new dust precipitator promises to effect is indeed a real contribution to the field of steam generation. The authors who conceived the need for, and directed the development of, this new device are worthy of congratulations on their achievement.

A very interesting phase of the paper pertains to the problems of smog and the smoke plume which presently bedevil the power industry and other industries as well. The authors hint that the extremely fine particles of carbon, ash, and sulphur compounds are potent factors in producing smog and smoke plumes. When you have a smoke plume that is not only discernible at an airport a dozen or so miles from a plant but which is blamed for producing fog conditions at the airport, you are appreciative of even hints as to the reason a plume exists.

The paper brings out the interesting and useful fact that the maximum efficiency of the new precipitator occurs at a temperature between 600 and 700 F which is just about the temperature of the gases entering the air preheater in a modern boiler. Can the authors tell us whether it is a fortuitous circumstance?

Table 4 brings out quite sharply the effect of particle size on total surface area of the solids material in the flue gases. It is rather startling to note that the surface area of the dust particles in the gases from a unit fired by high-sulphur fuel oil may be three or more times as great as the surface area in the dust particles from a similar unit fired by Midwestern bituminous despite the fact that the total weight of particles in the case of oil firing may be considerably less than a tenth of the weight of particles resulting from coal firing. This works out to a surface ratio of about 40 lb for lb of oil ash versus coal ash.

Authors' Closure

In closing, the authors wish first to express their thanks to all of the discussers for their valuable contributions and to make the following comments:

The comments, discussions, guidance, and advice contributed throughout this project by Mr. J. F. Barkley have been of great value.

The authors agree with Mr. O. F. Campbell that on oil or gas improved combustion conditions will result in reduced solids in stack emissions, but believe further, that in certain localities with high sulphur-bearing fuels efficient removal of the remaining solids will be required to prevent, to the greatest possible extent, formation of haze and smog.

The authors agree with Mr. Martin Frisch that there would be more fouling of air-heater surface with stoker-fired and oil-fired installations than with powdered fuel of an equal sulphur content. In the case of oil firing, the expected degree of fouling may be indicated by the total number of particles and surface area of the particles as shown by Table 4 of the paper. It is also known

[16] Project Manager, Jackson & Moreland, Boston, Mass. Mem. ASME

that stoker firing creates a large number of fines (not percentagewise but in absolute numbers) much more so than do powdered fuels. It is also understandable that use of additives may reduce the fouling problem on stoker and oil-fired jobs. However, this depends upon the nature of the additive. If the additive is neutral and not particularly hygroscopic or if it is alkaline, help may be expected. However, if the additive is acid it could increase the problem. The authors wish to thank Mr. Frisch for his thoughts.

The authors are in agreement with Mr. W. B. Gurney that the dew point of the flue gas itself remains substantially the same whether solids are present or not. Condensation takes place on the fine solids at a considerably higher temperature than the dew point of the surrounding gas. The authors consider this as the effective dew point. This and previous discussions with Mr. Gurney have been very helpful to us.

Mr. S. I. Juhasz' comprehensive discussion is a valuable addition.

The authors agree with Mr. P. H. Koch that if certain additives are made to flue gases, such as dolomite, the fouling of air-heater surfaces might be reduced, since this is an alkaline material. In case of cyclone firing it is understandable that, even with a higher number of fines in the flue gas, less trouble would appear in the air preheater because the cyclone furnace reduces the sulphur content in the fly ash and in the flue gas, as indicated by Table 1.

Mr. Benjamin Linsky's comments are very constructive.

Mr. E. B. Powell's discussion and comments are greatly appreciated by the authors. The basis for the estimate of the particle surface area given in Tables 3 and 4 is as follows:

The surface area of the particles was figured assuming all to be spheres with a specific gravity of 2.0. It is then a simple matter to figure the weight and surface area of a particle of any size and from this the number and surface area of a given weight of any chosen micron diameter. For example, in the range less than 20 microns greater than 10 microns, the weight and surface area of a 15-micron particle are calculated. The total weight in this range was divided by the weight of one particle to get the number and this was multiplied by the surface area of one particle to get the total area in the range. The surface areas in the various ranges were added together to get total area for the complete dust and the percentages determined for each range.

The authors appreciate Mr. E. M. Powell's contribution.

Fly-ash handling mentioned by Mr. E. F. Rothemich is a problem, but is not unsurmountable, according to specialists in the field.

The authors appreciate Mr. W. P. Saunier's discussion. With reference to the question of the maximum precipitator efficiency occurring between 600 and 700 F, we did not know that an optimum would be reached at this level with the design used.

The authors are grateful for the comments and questions raised. Time and experience will answer many of these questions much more concretely. For instance, the recent experience of the Detroit Edison Company's installation at Connor's Creek Station, as reported by W. L. Wingert and R. J. Stanley in ASME Paper No. 55—A-143 entitled, "Design of a Large Coal-Fired Steam Generator for 200 F Exit Gas Temperature and Operating Experiences With Pilot Plant," presented during the 1955 Annual Meeting, substantiates the fact that reduced dust loading in the gases permits operating an air heater at very much lower temperatures than heretofore has been considered possible with sulphur-bearing coals, with no problem in the control of deposit build-up. However, corrosion is still an item to be considered. It is of interest that in the experiment reported, the air preheater has been operated with gas inlet temperatures of 275 F and lower and with gas exit temperatures down to 110 F with air-inlet temperature of 60 F.

Design Aspects of an Electrostatic Precipitator for the Collection of Small Solids Ahead of the Air Heater

By H. KLEMPERER[1] AND J. E. SAYERS[2]

The development of a novel electrostatic precipitator is described which operates in the temperature range between 500 and 750 F, at a gas velocity of 40 fps. The precipitator consists of twelve independent sectors, arranged in rotary symmetry. A stream of cleaning gas is continuously moving from one sector to the other to carry the deposited dust into a secondary cyclone-type collector. Each sector is connected to an individual power supply, controlled on the primary side by a system of saturable reactors. Design viewpoints are given that lead to the described system. A commercially sized test plant is described that is operated on a 150,000 lb of steam per hr pulverized-fuel-fired boiler, consisting of a mechanical precollector followed by the precipitator ahead of the regenerative-type air preheater. The efficiency of the electrostatic precipitator alone is of the order of 95 per cent.

Introduction

A PREVIOUS paper by Karlsson and Tigges[3] outlined the philosophy behind the experimental work done on a project to remove the "extreme" and "intermediate" fines from flue gas at high temperatures and high velocities.

The immediate problem was to utilize the relatively small-scale development work described in that paper for the design of a unit of commercial size.

In conjunction with James Howden & Company, Ltd., and with the aid of the British Electricity Authority, a boiler was selected for the experimental precipitator plant. It is located at the Barking Station near London and is a bin-and-feeder-fired pulverized-coal unit with a rating of 150,000 lb of steam per hr. The bin-and-feeder system assures a coal feed of relatively consistent particle size and moisture content, as well as giving a high percentage of extreme fines. An economizer by-pass was provided so that the normal-gas exit temperature from the economizer (400 F) could be regulated as desired to give a flue-gas temperature range of 400 to 700 F.

The Problem

The basic problem was to design a high-temperature precipitator for the collection of very small particles at high gas velocity and operating at a constant high efficiency. It was evident from the outset that the problem could not be solved by using traditional methods of design. The success of the new scheme would depend on the solution of the "cleaning problem." Efficient operation of a high-temperature precipitator at a gas velocity of 40 fps was possible only if re-entrainment of collected particles and back emission could be eliminated by keeping the depth of the dust deposit on the electrodes to a minimum. To achieve this and to keep the precipitator operating continuously, it was necessary periodically and at short intervals to clean a section of the collecting elements while other sections were kept in operation. If adequate cleaning means and their periodic application could be devised, it would be possible to keep in check such troubles as blowoff, back ionization, and flashover.

Cleaning Method

Cleaning methods like rapping or washing were found to be impractical. After some experimenting, the following cleaning method was resorted to: A high-velocity scavenging gas flow is applied periodically to carry off the dust deposit from the precipitator elements and is supplemented at longer time intervals by a soot blower. The blown-off dust is carried by the scavenging stream to a mechanical after-collector. The action of this collector depends on agglomeration of the small particles that have been deposited in the precipitator. After passing the mechanical collector, the scavenging stream is returned at the inlet side of the precipitator. Fortunately, at the higher operating temperatures, the dust is less corrosive and less adherent to the collector elements, and therefore can be blown off with relative ease.

Design Viewpoints

To meet the foregoing requirements, the design of the new precipitator was pursued along the following lines:

1 In order to reduce the growth of dust deposits on the electrodes, an efficient mechanical precollector was placed ahead of the electrostatic precipitator.

2 The precipitator was given rotary symmetry with groups of collecting electrodes combined into independent sectors. By means of rotating gas ducts, each sector passes through precipitating and cleaning periods in cyclic sequence.

3 The necessity of operating efficiently at unusually high gas velocities and high temperatures pointed toward the usage of long and closely spaced electrodes.

4 Mechanical considerations, especially the requirement of operation at high temperature, gave preference to the tubular type of electrodes.

5 To utilize intense ionization and high collecting field

[1] Electrical Engineer, The Air Preheater Corporation, Wellsville, N. Y.

[2] Electrical Engineer, James Howden & Company, Ltd., Glasgow, Scotland.

[3] "Lower Flue-Gas Exit Temperatures Through Removal of the Solids Ahead of the Air Preheater," by Alexander J. Tigges and Hilmer Karlsson, published in this issue, pp. 305–315.

Contributed by the Research Committee on Corrosion and Deposits from Combustion Gases and presented at a joint session of the Research Committee on Corrosion and Deposits from Combustion Gases and the Power Division, at the Annual Meeting, New York, N. Y., November 28–December 3, 1954, of THE AMERICAN SOCIETY OF MECHANICAL ENGINEERS.

NOTE: Statements and opinions advanced in papers are to be understood as individual expressions of their authors and not those of the Society. Manuscript received at ASME Headquarters, October 27, 1954. Paper No. 54—A-248.

strength at the surface of the collecting electrode, separate ionizing and collecting zones were provided in each tube. Once efficient cleaning was achieved, re-entrainment in the collecting zone and back emission in the ionizing zone should be of negligible proportions.

6 To obtain optimum field strength in the collector zone, the external cylinder should be matched by an internal cylinder of a diameter ratio 2.718 to 1. This ratio was increased somewhat because of dust conditions.

7 Under prevailing conditions the highest efficiencies were expected if smooth direct current was supplied to the precipitator elements.

8 Because the supply of power to every sector has to be interrupted during the cleaning periods, each sector was provided with its individual power-supply unit; all necessary switching was done on the low voltage a-c side in the excitation circuit of a system of saturable reactors. This avoids switching in the d-c high-voltage line.

9 Synchronization between the rotation of the gas streams in the precipitator and the operation of the power supplies was effected by an electrically synchronized rotary switch in which the power-supply units are represented by circumferentially spaced sets of contacts at regular intervals.

10 In a precipitator that is operated with a supply of smooth direct current, flashovers have a pronounced tendency to hang on and stay alive until the supply of power to the affected sector is interrupted. By combining electronic and magnetic means, a flashover interrupter was developed that clears flashovers without using moving parts, and restores full power to the affected sector within a small fraction of a second.

Theoretical Background

The precipitator-electrode system was designed after studying the characteristics of existing precipitators for low-temperature and low-velocity operation and then extrapolating, using the Deutsch formula[4] as a guide.

For best efficiency, the precipitating tubes should be as long as possible. Practical construction reasons limited that length to about 12 ft and divided this length into two independent sections each 6 ft long.

The collecting section consists of a concentric tube arrangement. The first test unit at Waltham used a tube about $2^1/_2$ in. diam, and this dimension has not been changed since. The ionizing elements consist of a number of disks mounted on a center rod. The operational voltage for this collector-ionizer combination at Barking, at 600 F and 40 fps gas velocity, is between 12 and 13 kv. The corresponding ionizing current in the ionizer is of the order of 0.5 to 0.7 milliamp. Fig. 1 shows the electrode used at Barking.

A check with the Deutsch formula may be applied as follows

$$\eta = 1 - e^{-\frac{2wr_eL}{v(r_e^2 - r_i^2)}}$$

where

η = dust-collecting efficiency
e = base of natural logarithms, 2.718
w = transverse velocity, calculated from Stoke's law for each particle size
v = longitudinal particle velocity or velocity of gas in collecting system
L = longitudinal extension of collecting system
r_e = radius of outer collecting tube
r_i = radius of inner collecting tube

Although high gas velocities in the precipitator make it more difficult to reach high efficiencies, it is possible to reconcile the opposing requirements by designing the collector system for a large $L/(r_e - r_i)$. The high operating temperature aggravates the difficulty because the increased viscosity slows down the transverse flow of the particles and the reduced density of the gas lowers the electrical breakdown field strength of the collector.

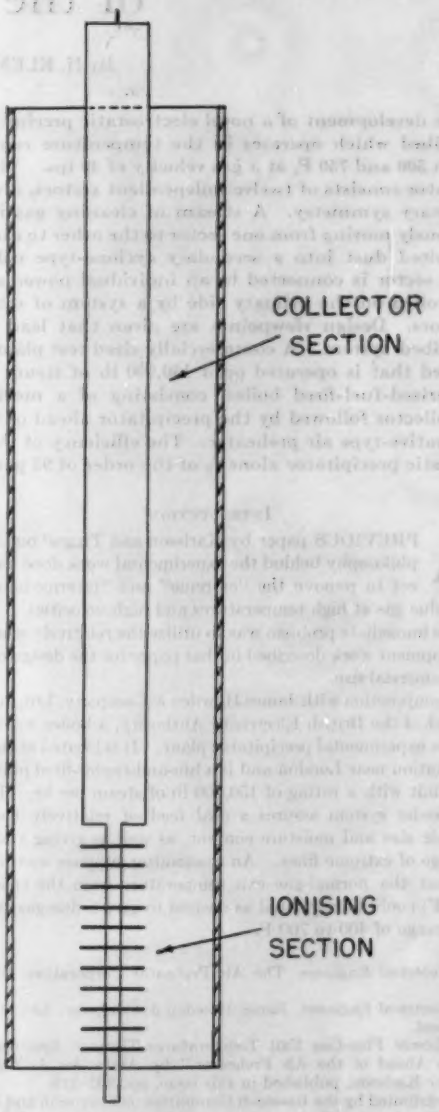

Fig. 1 Barking Electrode System

These effects are counteracted by dividing the precipitator into a high-intensity ionizing section followed by a collecting section which is designed to produce the highest collecting field strength obtainable under prevailing temperature conditions.

A general and accurate solution cannot be expected because the

[4] "Bewegung und Ladung der Elektrizitätsträger im Zylinder-kondensator," by W. Deutsch, *Annalen der Physik*, vol. 68, 1922, pp. 335–344.

transverse particle velocity varies with particle size. Furthermore, applying the formula to the collector zone only while taking the particle charge from the ionizing zone neglects among other factors the considerable precipitation in the ionizer zone.

Applying the mentioned design constants and operating conditions to the Deutsch formula for dust particles 1 micron in diameter, we obtain an expected efficiency of 85 per cent for a one-electrode system.

Using two of these systems in series and assuming the same precipitation efficiency for each system results for the 1 micron particles in an efficiency of 97.7 per cent, which is in fairly good agreement with operating experience at Barking.

General Design of Precipitator

Mechanical. As indicated in the section, The Problem, the necessity for frequent and efficient cleaning led to the design requirement of a precipitator with a continuous cleaning system. A general view of the design adopted is shown in Fig. 2 from which it will be seen that the nests of ionizing and collecting cells are arranged in two 360-deg banks, one above the other, in a vertical cylindrical stator shell, each bank being divided into twelve 30-deg sectors. Each sector is subdivided in two by a vertical radial sector division plate so that there are 24 sector-shaped tube nests in each 360-deg bank. This further subdivision is for economy in the scavenging gas flow required for cleaning purposes.

The grounded collecting tubes are hexagonal in shape, arranged in honeycomb formation to save space and the central combined ionizing/precipitating electrodes are supported by two grids mounted above and below each tube nest on high-temperature porcelain insulators. Fig. 3 shows top view of typical tube nest.

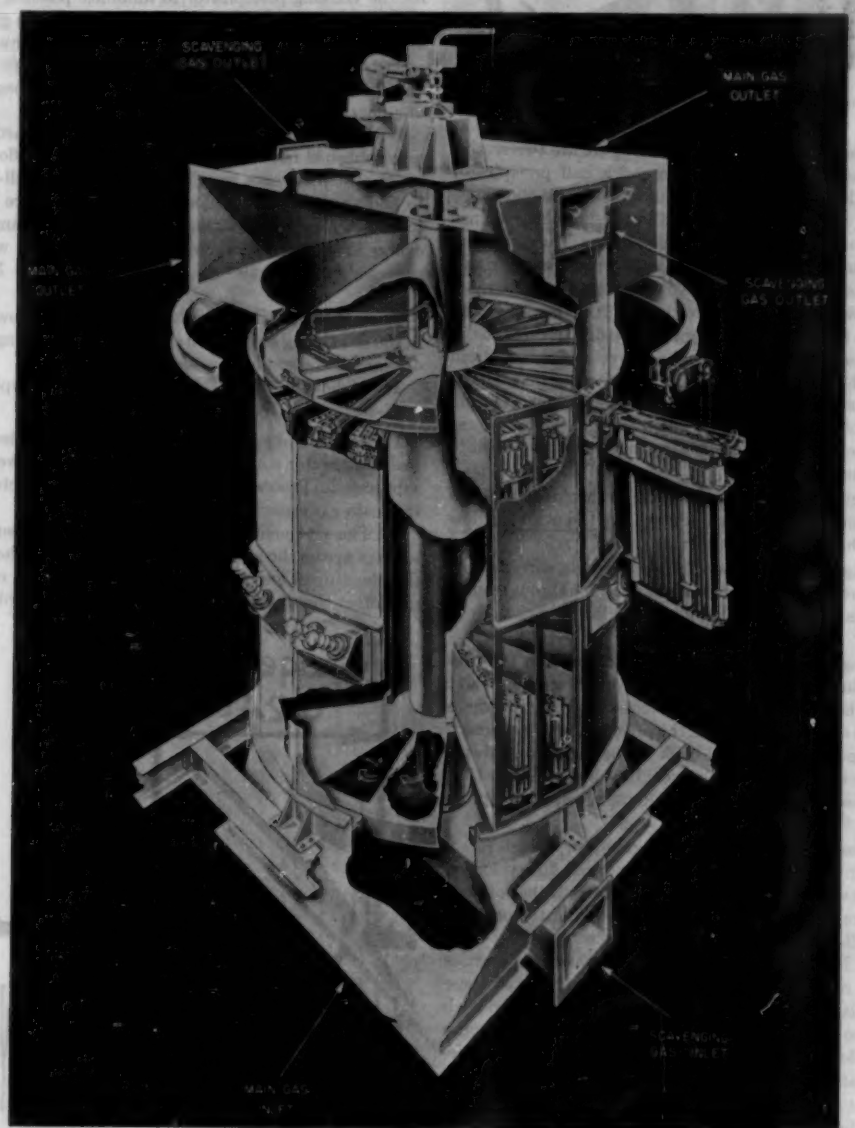

Fig. 2 General View, Barking Precipitator

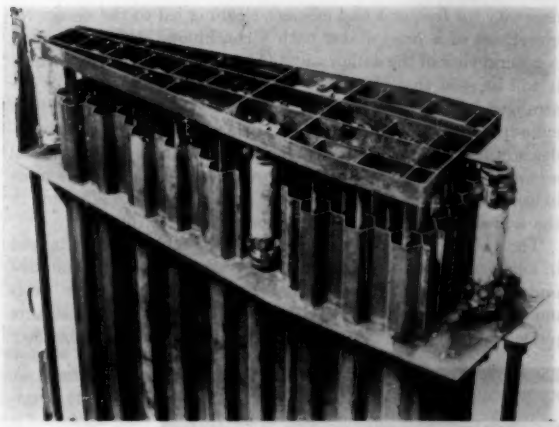

FIG. 3 TOP VIEW OF BARKING TUBE NEST

At the bottom and top of the precipitator there are two sector-shaped hoods, each covering about two and a half precipitator sectors and provided with slots approximately the size and shape of one half-sector, which are connected, through annular openings in the hoods, to inlet and outlet purge gas ducts. The hoods are mechanically coupled together and supported in bearings, mounted on the top and bottom purge ducts, and are provided with a drive unit which rotates the two hoods, in synchronism and in phase, so that a flow of scavenging gas can be drawn through the inlet duct and hood, upward through the two sets of cell nests in the particular half-sector opened to the scavenging gas through the slots in the hoods and out through the top hood and duct. During the scavenging of each sector the high-voltage electric-power supply to that sector is automatically suppressed to facilitate blowing off the dust.

Radial and circumferential seals bearing on machined surfaces of the hoods seal off the scavenging circuit from the main gas flow passing upward through the open sectors.

The high-voltage d-c power supply to the grids carrying the precipitator electrodes is led into each stator sector through bushing insulators located between the upper and lower banks of cell nests.

For the scavenging operation flue gas is drawn from the precipitator inlet, through the precipitator scavenging circuit and thence through a high-efficiency multicyclone-type collector where the agglomerated dust removed from the precipitator is extracted. The scavenging gas is then passed back to the main flow stream ahead of the precipitator, by the scavenging-circuit fan, so that any remaining gas-borne dust goes through the precipitation process again.

During the cleaning period the scavenging flow, which has a velocity of the order of two to three times normal flow velocity, moves across the whole tube nest in accordance with the rotation of the hood. The rotational speed of the hood is of the order of $^1/_2$ to 2 rpm. The scavenging action is supplemented by compressed-air soot blowing, delivered through traversing nozzles mounted in the rotating hoods. The rate of traverse of these nozzles, in a radial direction, and the number of nozzles in each hood is selected so that each cell nest is completely scanned by the traversing soot blowers in a period of the order of 30 to 60 min, depending on operational requirements.

It is of interest to observe the importance of high efficiency in the secondary collector. Assuming a relatively small flow volume in the scavenging circuit, it can be shown that the combined efficiency of the precipitator and its scavenging circuit is

$$\eta_s = \frac{\eta_p \eta_c}{(1 - \eta_p) + (\eta_p \eta_c)}$$

where

η_s = combined system efficiency
η_p = precipitator efficiency
η_c = secondary collector efficiency

For example, with a precipitator efficiency of 96 per cent measured from main gas inlet to outlet and excluding the purge system, and a secondary collector efficiency of 80 per cent the overall system efficiency would be 95.05 per cent.

Hot compressed air was selected as the soot-blowing medium for the Barking precipitator to minimize possible trouble due to condensation and impingement of moisture on the tube nests, and it was desirable to produce this compressed air with a minimum power expenditure. This implies keeping soot-blower nozzle-exit velocities below sonic speed to minimize shock losses, and the use of a nozzle-inlet pressure of 2 atm or less.

With this factor in mind and based on standard nozzle theory and published records of investigations into jet flow, a prolonged series of experiments were carried out with a full-scale tube nest to find the low-pressure nozzle sizes and pressure ratios required to produce in the Barking precipitator the same flow kinetic energy in the tube being soot-blown as obtained with the higher-pressure steam nozzles used successfully in the Hell Gate pilot plant.

The resulting figures all relating to the same flow kinetic energy in the tube being soot-blown show an energy-saving factor in favor of large-diameter low-pressure nozzles.

The following special features of the precipitator cleaning systems are worthy of emphasis:

1 Removal of collected dust from the electrodes is affected in a sealed-off sector with the supply of electrical power to that sector suppressed. Problems of re-entrainment of collected particles into the main gas stream are therefore minimized.

2 The scavenging circuit is operated under suction; any gas leakage across the seals in the precipitator has the direction from the clean main gas to the dirty scavenging gas circuit and does not affect the dust-collecting efficiency of the unit.

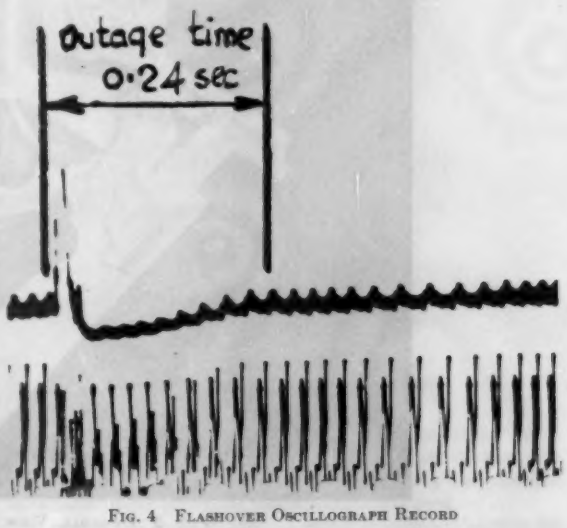

FIG. 4 FLASHOVER OSCILLOGRAPH RECORD

Electrical. Individual control of the electric-power supply to each sector of the precipitator is necessary for scavenging purposes so 12 separate high-voltage power-supply units are provided. Design criteria are that these units shall provide smooth direct current to obtain highest efficiency and shall each be easily, independently, and continuously controllable over an output range of 4 or 5 to 12 or 15 kv. Further, the output from each rectifier must be varied cyclically, of the order of once per minute (corresponding to the speed of rotation of the cleaning hoods), between the minimum and maximum, or near maximum, values and the control equipment must incorporate means for the automatic and fast suppression of flashovers occurring in the precipitator, followed by immediate restoration of normal operating conditions. The latter requirement of speed is dictated by the necessity for achieving the highest possible efficiency of performance.

To provide the smoothest practicable d-c supply, the 3-phase bridge circuit has been adopted and oil-immersed selenium rectifiers were selected for Barking, having in mind the advantages of cleanliness resulting from hermetic sealing, long life, and reliability. Control of the output voltage and flashover suppression is based on the use of saturable reactors connected in series and parallel with the primary lines to each high-voltage transformer. The purpose of the parallel reactors is to create a wattless load, and to increase speed of response of the system when the ionising load of the precipitator is removed from the rectifier. By this means cyclic switching of the high-voltage output from any rectifier and flashover suppression is affected by variation of comparatively small currents in the control windings of the saturable reactors and any mechanical switching of power lines, either a-c or high-voltage d-c, is obviated.

Under normal conditions the mode of operation is that as the precipitator cleaning hoods rotate, a 12-element electrically synchronized switch operates (1) to reduce the high voltage applied to each sector as the main gas flow is cut off by the approach of the cleaning hoods; (2) to suppress the voltage below ionization level as the sector is scavenged by the purge gas flow; (3) to restore the reduced voltage as the main gas flow is gradually admitted; and (4) to restore full voltage as the sector is fully opened to main gas flow.

For effective suppression of flashovers, automatic-control ap-

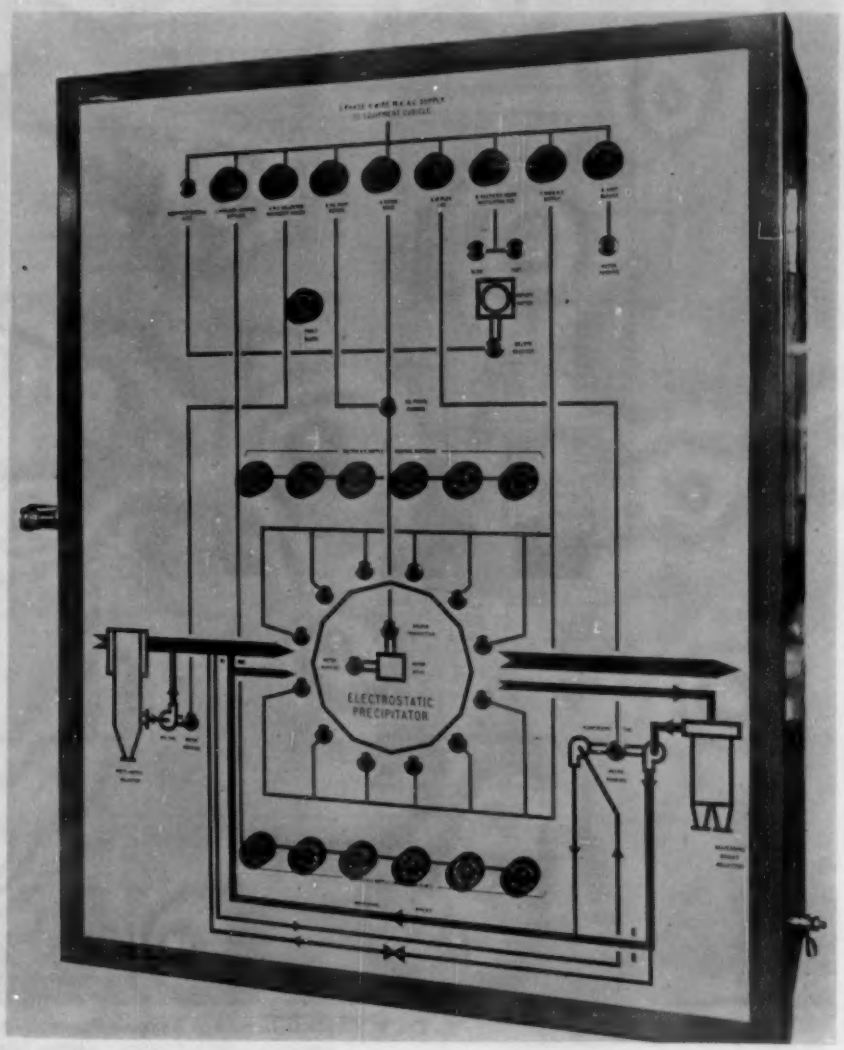

FIG. 5 (*right*) BARKING MASTER CONTROL PANEL

paratus is provided for each power supply, based on the use of a small thyratron and magnetic amplifier operating in conjunction with the saturable reactors previously referred to. Fig. 4 is a specimen oscillograph record showing outage times of flashover suppression of 0.3 sec or less.

In addition to the 12 power-supply units, the Barking precipitator installation incorporates a number of associated auxiliary motor drives and a certain measure of sequential starting and interlocking with the precipitator high-voltage supplies. On the control side there are thus some 20 items of equipment to be catered to and the controls for these are centralized with suitable indication equipment, on a precipitator master control panel. This may be mounted at some location remote from the various items of equipment controlled.

Fig. 5 shows the arrangement of the master control panel for the Barking precipitator and all its auxiliary equipment.

Description of Installation and First Test Results

The general layout of the plant is shown in Fig. 6 and the flow diagram in Fig. 7. The plant consists of the following components:

1 Cyclone-type precollector.

2 Electrostatic precipitator with scavenging circuit fan and secondary collector.

3 Main regenerative-type air preheater.

4 Regenerative-test preheater.

5 Main and auxiliary induced-draft fans.

The plant layout and ductwork is so arranged as to facilitate testing of the precollector and the precipitator for efficiency of dust extraction from the boiler flue gases before these pass to the main air preheater.

The precipitator is designed for a nominal gas volume of 120,000 cfm which corresponds to a calculated gas velocity of 40 fps in the tubes. The over-all diameter is 17 ft and over-all height about 30 ft, including ducts and cleaning hoods.

In laying out the installation, considerable attention was paid to the arrangement of the ductwork to obtain straight runs at the

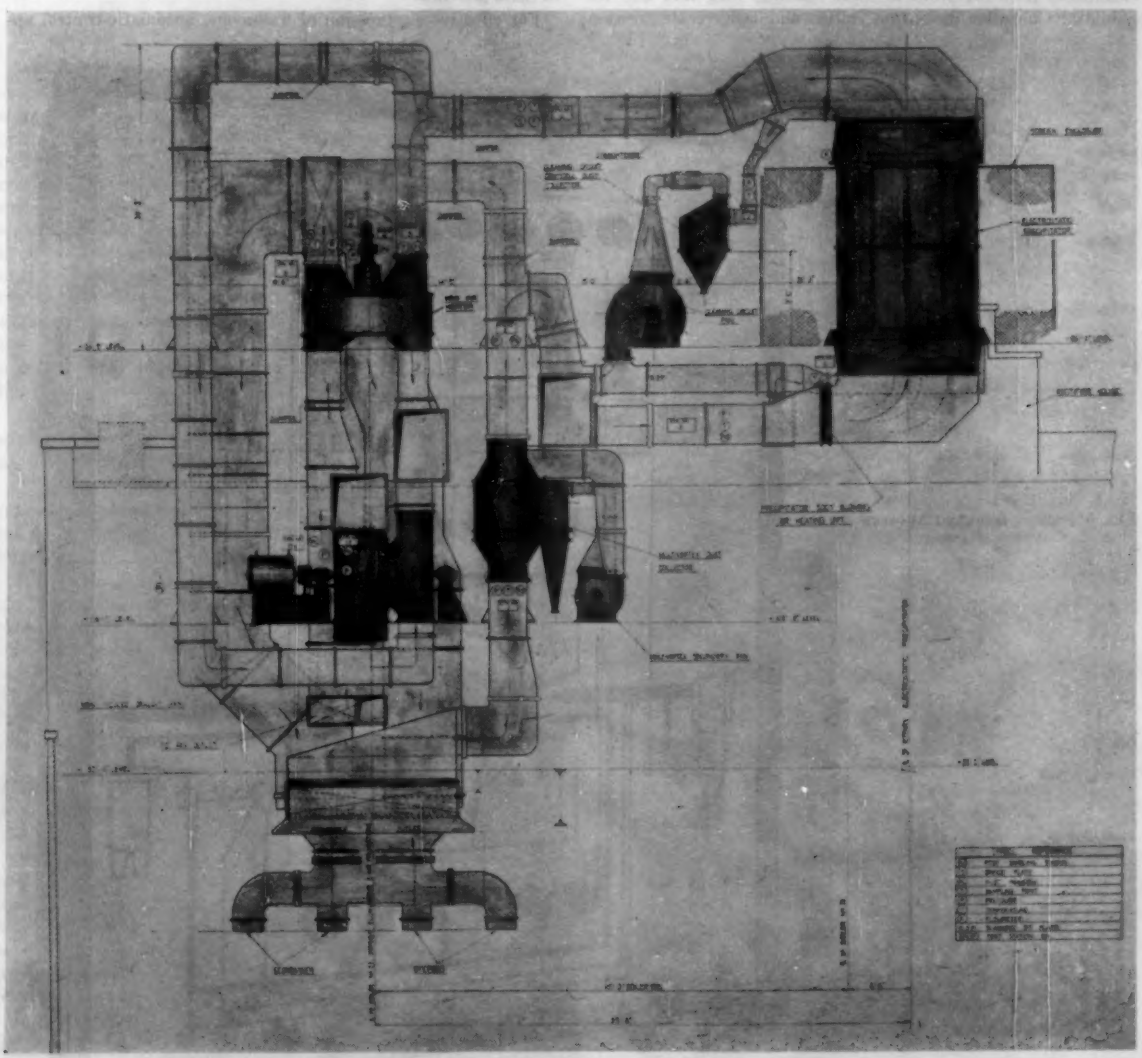

Fig. 6 General Layout of Barking Plant

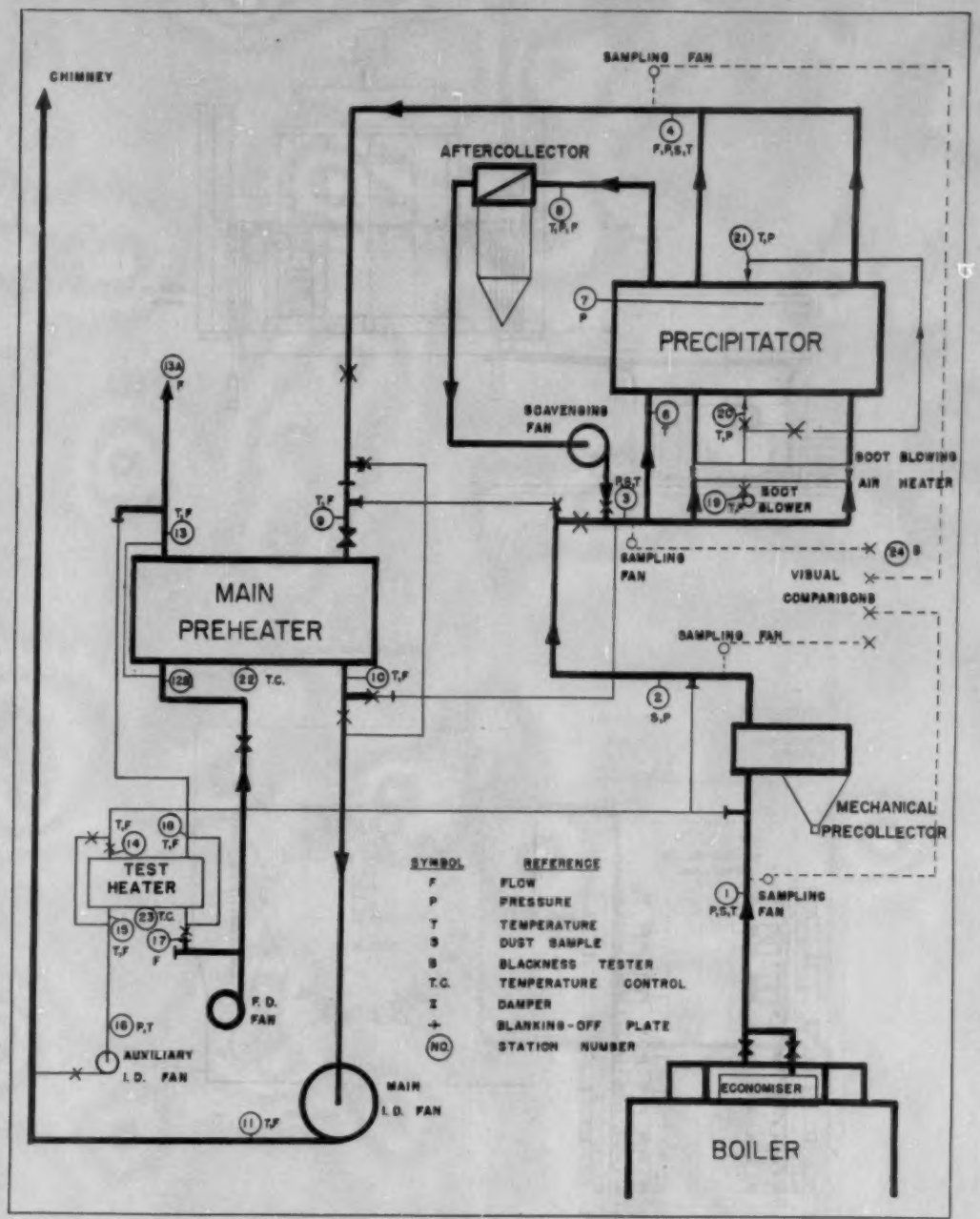

FIG. 7 FLOW DIAGRAM OF BARKING PLANT

points where dust-sampling traverses are required for assessment of performance. A comprehensive system of instrumentation is provided as indicated on the flow diagram, with all draft, flow, and pressure gages, recording and indicating thermometers, and the like, mounted on one centralized instrument panel to facilitate the keeping of full records of all test runs.

Facilities have also been included for dust sampling at both the precollector and precipitator inlets and outlets.

In addition, a discoloration-type efficiency indicator[5] has been provided to compare gas samples drawn from the precollector, or precipitator inlet, with precipitator outlet. Fairly close agreement between discoloration-test and weight-test results calculated from duct traverses has been maintained.

[5] "Evaluation of the Multiple Spot Discoloration Tester," by T. D. Price and H. Klemperer, *Air Repair*, vol. 4, no. 4, 1955, pp. 213–217.

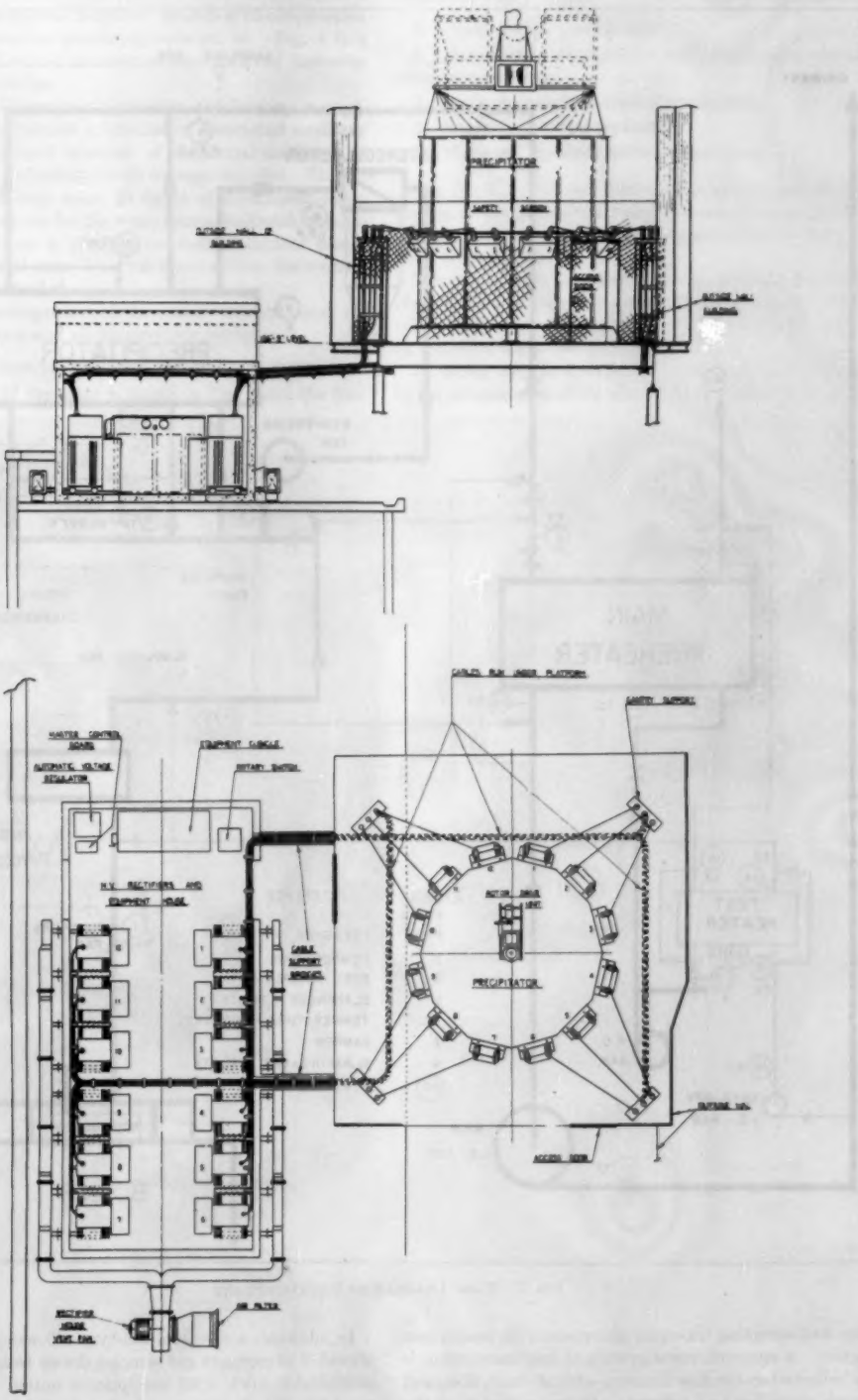

FIG. 8 POWER SUPPLIES, CONTROL EQUIPMENT, AND HIGH-VOLTAGE CABLE CONNECTIONS AT BARKING

To permit accurate assessment of the performance of the main preheater when supplied with cleaned gas from the precipitator, an auxiliary test heater is provided and supplied with a small quantity of raw gas taken direct from the precollector inlet. Gas by-pass ducts are arranged across each heater. For the preheater tests the gas by-pass flow will be continuously adjusted by dampers under automatic control to maintain the same preset, cold-end plate temperature in both heaters. Conditions will be such that air and gas volumes will be proportional to the sizes of the heaters so that flow velocities will be approximately equal in each case.

A direct comparison of the performances of the main heater, supplied with clean gas from the precipitator, and the test heater, supplied with raw gas from the precollector inlet, will therefore be possible—other factors being held constant during these tests.

Fig. 8 shows the physical layout of the power-supply and control equipment and the high-voltage cable connections to the precipitator. The power supplies and control equipment need not necessarily be accommodated together.

Operating Results

The plant went into operation in March, 1954, with the precipitator equipped for single-bank operation. The second bank of tube nests was installed in July, 1954, so that no long-term experience is yet available.

In the first series of tests, over-all system efficiencies of 97 per cent have been obtained, demonstrating the practicability of high-efficiency extraction of fly ash from flue gases at 40 fps in the high-temperature zone. The fly ash at this site is extremely fine in size; typical gradings of dust sampled at the main precollector inlet show over 80 per cent under 30 microns diameter and over 70 per cent under 20 microns.

Discussion

H. A. Bauman.[6] The authors are to be congratulated on having developed a new type of high-efficiency electrostatic precipitator for the extraction of fly ash from boiler flue gas moving at very high velocity and at high temperature.

The following information would be of interest:

1 What is the electric power required per 100,000 cfm of flue gas actually going through the precipitator?

2 What, if any, fouling or plugging difficulties have been encountered at the Barking Station? How much build-up of fly ash does take place before scavenging?

3 What is the effect on the efficiency of the precipitator of high electrical resistivity dusts?

4 What is the over-all draft drop through the collector system?

5 What is the efficiency of each mechanical collector used in this new system and what is the range of fly-ash dust concentrations and particle sizes leaving the boilers at the Barking Station?

O. F. Campbell.[7] This paper has presented some very interesting information concerning the removal of solids by this special equipment that may be useful in many fields other than boiler operations.

If this equipment so illustrated can be made to function efficiently at a temperature of approximately 1100 F, it would be a very useful tool to remove catalyst fines from exit flue gases of a fluid catalytic-cracking unit currently used in the petroleum industry.

At what maximum allowable temperature will the equipment function satisfactorily?

H. J. White.[8] The authors describe an interesting and rather unusual approach to the fly-ash-removal problem. The basic objective is to improve the operating efficiency of air preheaters through preremoval of suspended matter in the flue gases. Although inertial collectors have been used ahead of air preheaters for fly-ash removal, the work presented by the authors seems to be the first in which combination inertial-electrostatic collectors have been used for this purpose. Heretofore the disadvantages of higher gas temperature, higher gas flow, and low gas density which limits precipitator operating voltage have militated against the use of electrostatic collectors ahead of air preheaters.

The precipitator design described differs from presently accepted practice for fly-ash application particularly in the use of the two-stage type precipitator and in the use of relatively high gas velocities of the order of 40 fps. The principal application of two-stage precipitator has been in the air-cleaning field, with only limited use in industrial gas cleaning. Gas velocities for the collection of dry particles as a rule have been limited to about 5 to .15 fps because of re-entrainment of particles at higher velocities, although the effective collection and retention of liquid particles by electrostatic means has been demonstrated at gas velocities of over 100 fps.

The removal of precipitator electrode deposits by de-energizing and blanking off precipitator sections is an old principle. The methods of electrode cleaning covered in the paper represent an enlargement of this principle through very frequent cleaning before electrode deposits of any appreciable thickness can form. The authors indicate that this permits the successful use of high gas velocity in the precipitator.

Although the general description of the equipment is well covered in the paper, it would be valuable to have more specific data on certain parts of the equipment, particularly the design and arrangement of the primary and secondary inertial collectors. The inclusion of a consistent set of typical test results, together with the properties of the particular ash, would also be of interest. In this connection it is relevant to note that fly ash is an extremely heterogeneous and variable material. Long experience has shown that collector performance is strongly dependent on fly-ash characteristics. Therefore a natural question arises as to the extent to which the performance of the collector system described in the paper would be affected by these factors.

In conclusion, the authors are to be congratulated on their paper which covers a novel approach to the fly-ash-collection problem, and which should be of substantial interest in this field.

Authors' Closure

The authors wish to thank Mr. H. A. Bauman, Mr. O. F. Campbell, and Dr. H. J. White for their discussion and questions raised. They regret that limited operating experience at the time of presentation of this paper prevented them from including a consistent set of typical test results as appropriately asked for by Dr. White. We now have approximately 18 months of operating experience at Barking and have collected a considerable amount of data stressing the dependency of precipitator and combined system efficiency on the performance of the mechanical collectors. Even a summarized presentation of these re-

[6] Production Superintendent, Consolidated Edison Company of New York, Inc., New York, N. Y.

[7] Combustion Engineer, Sinclair Refining Company, East Chicago, Ind. Fellow ASME.

[8] Research Corporation, Bound Brook, N. J.

sults would go beyond the scope of this closure. We intend to hold it for a later occasion when results will be available from a number of new installations that are now being constructed or designed.

In answer to the specific questions of Mr. Bauman and Mr. Campbell: The electrical power input into the gas stream is of the order of 20 kw per 100,000 cfm. This figure comprises ionization and precipitation only and does not include the scavenging circuit, power-conversion losses, and auxiliaries.

No fouling or plugging difficulties have been encountered with the Barking precipitator in 18 months of operation under ordinary commercial conditions. The scavenging circuit is operated and timed to limit dust deposits at the collecting electrodes to a maximum thickness of the order of 0.03 in. No difficulties from high-resistivity dust have been encountered while dust deposits were kept below the limits mentioned.

The over-all draft loss through the electrostatic system at 40 fps gas velocity is under 1 in. water gage.

The efficiency of the mechanical precollector at Barking is of the order of 55 per cent; this low figure is due to fineness of the dust emitted from the boiler. The efficiency of the mechanical scavenging collector has been disappointing at times but has been considerably improved by installation of means to keep the dust-separating elements from plugging. An efficiency of 70 to 80 per cent for this scavenging collector is required for high over-all system efficiency; this has been obtained at Barking by returning the outlet of the scavenging circuit to the mechanical precollector inlet.

The fly-ash concentration at the Barking boiler outlet averages 5 to 6 grains/cu ft (at NTP) and a typical size analysis follows:

Microns	Per cent
0–10	45
10–20	27
20–30	11
30–40	7
Over 40	10

At Barking our experience is limited to temperatures between 500 and 700 F. Within this range there is no noticeable change in efficiency with temperature. In the laboratory our precipitator system was operated at temperatures up to 1100 F, but above 800 to 900 F the efficiency drops noticeably if we operate at atmospheric pressure.

Investigations Into Blade-Root Fixings of High-Temperature Steels

By W. SIEGFRIED,[1] WINTERTHUR, SWITZERLAND

The progress in mechanical engineering which has led in the past few years to much lighter designs of aircraft and land vehicles can be attributed to improvements in the materials used and to a much better adaptation of structural design to these materials. In cases where the temperature is low in aircraft and land conveyances, the engineer's main problem has been alternating stresses. In applications where steels are used at high temperatures similar problems exist, but our knowledge is here less firmly founded than in the domain of alternating stress at room temperature. The test results described in the paper, however, point to a similar line of advance as has been followed in automobile and aircraft engineering. Here, too, it is important not only to develop better materials but also to improve designs if the strength properties of these materials are to be utilized fully. It has developed that an improvement in creep properties at high temperatures can only be attained, as a rule, at the price of an increase in embrittlement and sensitivity to notching. These considerations are particularly important in the attachment of blade roots to turbine disks. A large number of tests have been made with the aim of throwing some light on these problems and obtaining a clearer idea of the basic connection between structural design and strength.

Introduction

THE investigations reported in the paper have comprised long-time tests on smooth and notched specimens and on various models of blade-root fixings. The results of the tests on smooth and notched specimens were explained on the basis of a working hypothesis which conforms to Ludwick's theory of the embrittlement of materials at room temperature. This made it possible to find at least a qualitative explanation of the relationship between materials and embrittlement and to clear up a number of points which hitherto have been rather obscure.

The tests carried out on models of blade-root fixings showed that, in assessing the strength of blade fixings, it is necessary to take account not only of the results of creep tests on smooth bars but also of embrittlement, which can be investigated only in tests on notched bars. It also was found that the design of the indentations in the blade root plays an important part in deciding the strength of a fixing, and that certain high-temperature metals which are subject to embrittlement can be used only if the indentations are given the most favorable form.

The results of the creep tests on smooth and notched specimens have been described in detail elsewhere.[2] The purpose of the present paper is primarily to describe the results of the creep tests on the blade-root fixings. But as these tests were conducted on the basis of the results obtained with the smooth and notched specimens, it is necessary first of all to give a brief outline of the latter results in so far as they have a bearing on the tests with blade-root fixings.

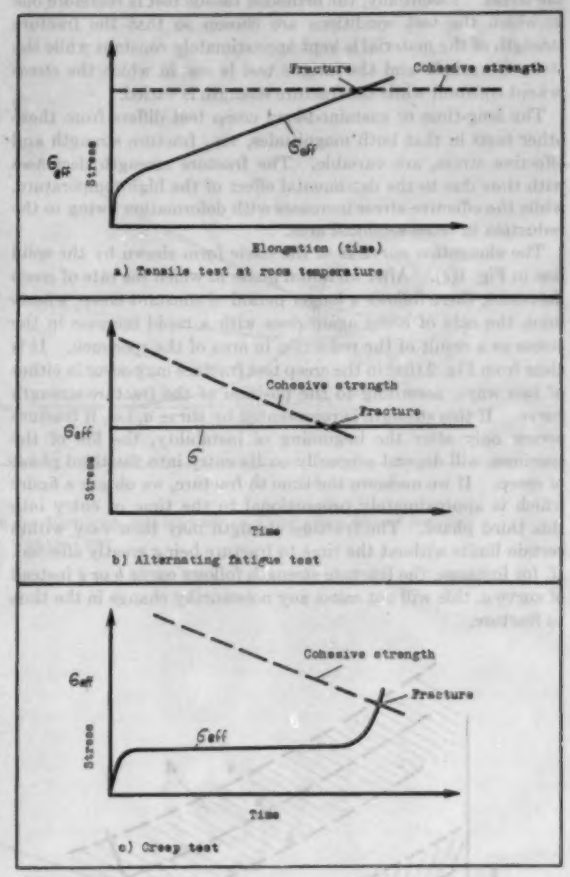

FIG. 1 BASIC DISTINCTION BETWEEN THE VARIOUS METHODS OF MATERIAL TESTING

Embrittlement in High-Temperature Materials

The conditions prevailing in the creep test are fundamentally different from those of the orthodox tensile test. In Fig. 1 the various types of tensile tests are compared. Fig. 1(a) illustrates

---

[1] Engineer, Sulzer Brothers, Ltd.; now with Battelle Memorial Institute, Geneva, Switzerland.

Contributed by the joint ASTM-ASME Committee on Effect of Temperature on the Properties of Metals and presented at the Annual Meeting, New York, N. Y., November 28–December 3, 1954, of THE AMERICAN SOCIETY OF MECHANICAL ENGINEERS.

NOTE: Statements and opinions advanced in papers are to be understood as individual expressions of their authors and not those of the Society. Manuscript received at ASME Headquarters, October 22, 1954. Paper No. 54—A-236.

[2] "Investigations Into the Development of Intercrystalline Fractures in Various Steels Under Triaxial Stress," Symposium on Creep and Fracture of Metals at High Temperatures, National Phys. Laboratory, May, 1954.

the conditions existing in the orthodox tensile test. The effective stress here rises as the test proceeds and fracture finally occurs when the effective stress equals the fracture strength of the material. For the purposes of a first approximation, we may assume that the fracture strength is constant during the test.

Fig. 1(*b*) illustrates the situation in the fatigue test. The stress is here constant, but the fracture strength decreases during the test and fracture occurs when it has dropped to the level of the stress. Essentially, the orthodox tensile test is therefore one in which the test conditions are chosen so that the fracture strength of the material is kept approximately constant while the stress is varied; and the fatigue test is one in which the stress is kept constant while the fracture strength is varied.

The long-time or sustained-load creep test differs from these other tests in that both magnitudes, viz., fracture strength and effective stress, are variable. The fracture strength decreases with time due to the detrimental effect of the high temperature, while the effective stress increases with deformation owing to the reduction in cross-sectional area.

The elongation curve is of the basic form shown by the solid line in Fig. 1(*c*). After an initial phase in which the rate of creep decreases, there follows a longer period of constant creep, whereupon the rate of creep again rises with a rapid increase in the stress as a result of the reduction in area of the specimen. It is clear from Fig. 2 that in the creep test fracture may occur in either of two ways, according to the position of the fracture-strength curve. If this strength is represented by curve *a*, i.e., if fracture occurs only after the beginning of instability, the life of the specimen will depend primarily on its entry into the third phase of creep. If we measure the time to fracture, we obtain a figure which is approximately proportional to the time of entry into this third phase. The fracture strength may then vary within certain limits without the time to fracture being greatly affected. If, for instance, the fracture strength follows curve *b* or *c* instead of curve *a*, this will not cause any noteworthy change in the time to fracture.

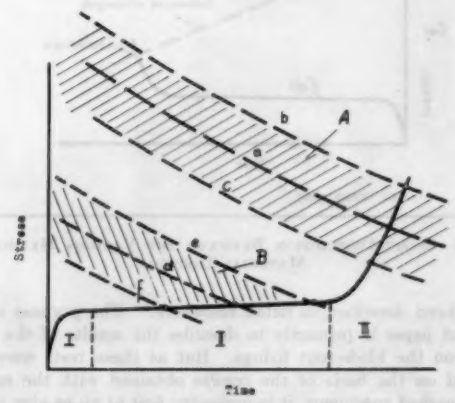

FIG. 2 INFLUENCE OF COHESIVE STRENGTH CURVE ON PROPERTIES OF A METAL IN CREEP TEST
(Curves *a*, *b*, *c*: high fracture strength; Curves *d*, *e*, *f*: low fracture strength)

The situation is different when the fracture strength of the material is lower, as illustrated by curve *d* in Fig. 2. Here fracture occurs before the third phase of creep is reached. As the intersection of the curves for the fracture strength and the true stress now lies in a much flatter range than in the previous case, a small change in the fracture strength will result in a big change in the time to fracture. What we are now measuring is accordingly the fracture or cohesive strength of the material.

In any creep test we are thus measuring either the instability or the fracture strength of the metal, without being able to tell in advance which of these two possibilities will apply. As a result there are considerable differences of opinion on the value of creep tests and on the conclusions to be drawn from them. In the first case, in which fracture takes place only after the point of instability, we shall be much better able to draw conclusions as to the time to fracture in the creep test from elongation measurements made after relatively short times than we should in the second case, in which the fracture strength of the metal is attained before the point of instability.

If we conduct creep tests with notched specimens, the conditions existing in smooth specimens will be modified in two ways: (1) A local stress concentration will appear at the root of the notch. (2) There will be a radial stress, mainly in the interior of the specimen, which, at a given axial stress, will result in a reduction of the deformation energy and will thus tend to prevent plastic flow. It is naturally much more difficult to indicate definite conditions of stress in notched specimens, as the stresses vary considerably during creep. At the beginning of the process an almost elastic stress distribution will prevail, while at a later period the distribution will be that resulting from the laws of creep. In addition, the radius of curvature of sharp notches will be greatly increased on account of the plastic flow, so that in the course of the creep test on a notched specimen there will be a very pronounced reduction of the peak stress.[8]

The conditions applying to notched specimens are illustrated in essentials in Fig. 3. The differences from tests on smooth specimens may be summed up by observing the effect of the notch on both the effective stress and the stress-concentration curves. The radial stress in the notch inhibits plastic flow, with the result that instability is reached only after longer periods. While the effective stress in the smooth specimen follows curve *a* in Fig. 3, the mean effective stress in the notched bar follows curve a_1. The transition point, *W*, of the smooth specimen is moved over to W_1 for the notched specimen. A stress concentration at the root of the notch is present in addition to the mean stress. It has the value of the elastic concentration factor at the beginning of the test and it decreases as the test proceeds. In essentials, it follows curve *b* in Fig. 3.

It is thus evident that in the notched specimen there are two tendencies, viz., a movement of the entry into the tertiary phase of creep toward longer times and the gradual reduction of a peak stress. These changes may have one of two effects, according to the position of the fracture-strength curve. If this curve follows *C* in Fig. 3, the smooth specimen will have a time to fracture of t_1 and the notched specimen one of t_1'; i.e., the notched bar will take longer to fracture than the smooth one. Exactly opposite results are obtained when the fracture strength follows curve *d*. The time to fracture of the smooth specimen is then t_2, that of the notched specimen t_2'; i.e., the notched bar breaks much more quickly than the smooth one at the same mean stress.

It appears, therefore, that if the times to fracture of notched specimens are shorter than those of smooth specimens, this is a sign that the material has a low fracture strength. When choosing our metals, it is thus necessary to select those which have a high fracture strength as well as a high resistance to deformation. This is not always a simple matter, as many measures which help to increase resistance to deformation at the same time reduce the fracture strength. The situation can be very well illustrated if we carry out creep tests on a series of sharp-notched specimens in which the notch is gradually made deeper while the radius of

[8] "Essais de résistance de longue durée, à la température ambiante, sur des éprouvettes entaillées en alliages d'étain," by W. Siegfried, *Revue de Métallurgie*, vol. 2, 1953, p. 50.

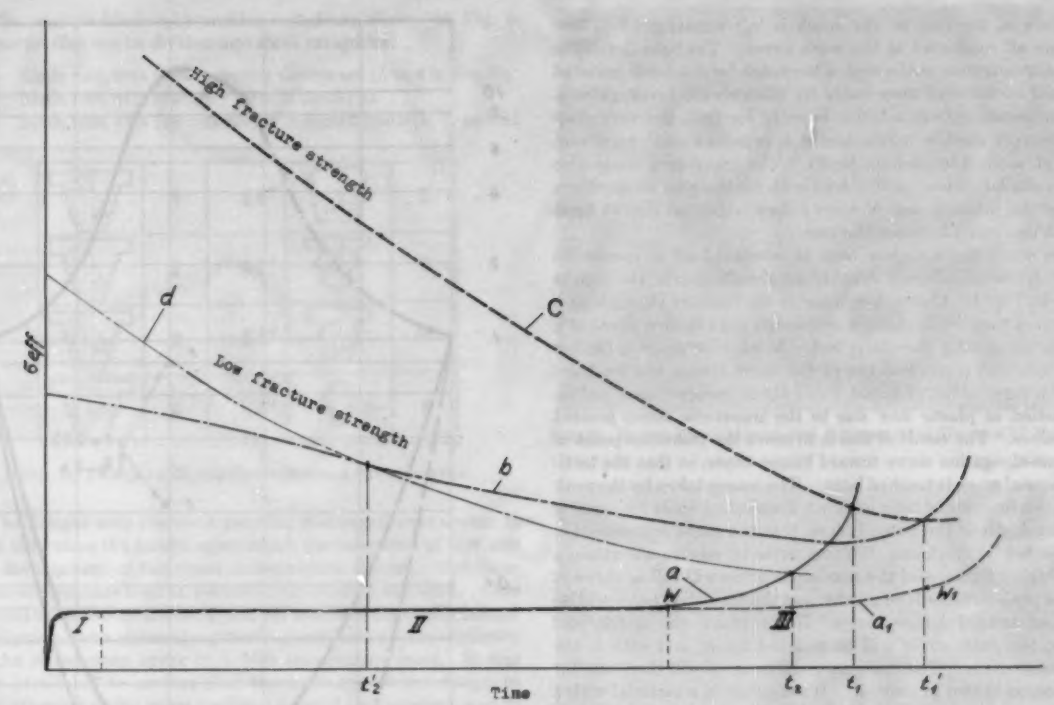

FIG. 3 INFLUENCE OF FRACTURE STRENGTH ON BEHAVIOR OF NOTCHED SPECIMENS AS COMPARED WITH SMOOTH SPECIMENS IN CREEP TEST

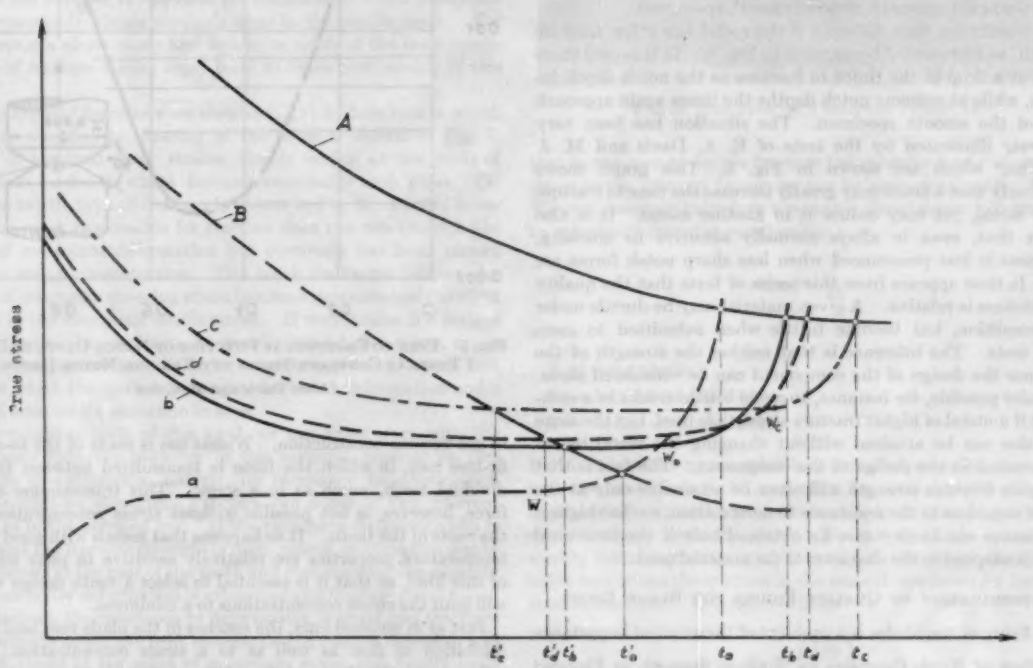

FIG. 4 EXPLANATION OF BEHAVIOR IN CREEP TESTS WITH NOTCHED SPECIMENS IN WHICH DEPTH OF THE NOTCH IS VARIED
(A, steel of high fracture strength; B, steel of low-fracture strength.)

curvature at the root of the notch is left unchanged.[4] These tests are all conducted at the same stress. The behavior of the stress concentration at the root of the notch for an elastic material can then be followed very easily by photoelastic investigations. The stress-concentration factor is unity for both the very deep and the very shallow notch, and it approaches some maximum value at some intermediate depth. The transverse stress also takes a similar course, as it is zero both for the smooth specimen and for the limiting case of a very deep notch, so that it must reach a maximum between the two.

If we now carry out creep tests at constant load on specimens with notches of different depths, we should obtain the results shown in Fig. 4. Curve A represents the fracture strength as a function of time while curve *a* represents the effective stress of a smooth bar during the creep test. If we now make a further creep test with a notched bar at the same stress, the fracture-strength curve is not changed, but a stress concentration and an obstruction of plastic flow due to the transverse stress present themselves. The result of this is to move the transition point in the time-elongation curve toward longer times, so that the tertiary phase of creep is reached later. The course taken by the peak stress as a function of time is shown diagrammatically by curve *b*.

If the depth of the notch is such that the stress concentration just reaches its maximum, the transverse stress also will attain a much higher figure, and the maximum stress will follow curve *c*; i.e., the peak stress will be greater and the transition point will be displaced toward longer times. If we make the notch still deeper, the peak stress will be reduced again, and with it the transverse stress. The maximum stress curve will then run, for instance, as shown in curve *d*. We see that in a material with a fracture strength corresponding to A in Fig. 4 there is an increase in the time to fracture of notched specimens at medium notch depths as compared with smooth specimens whereas at very large and very small notch depths the times to fracture of notched specimens again approach those of smooth specimens.

The results are very different if the metal has a low fracture strength, as represented by curve B in Fig. 4. In this case there is at first a drop in the times to fracture as the notch depth increases, while at extreme notch depths the times again approach those of the smooth specimen. The situation has been very effectively illustrated by the tests of E. A. Davis and M. J. Manjoine,[4] which are shown in Fig. 5. This graph shows very clearly that a notch may greatly increase the time to fracture in one metal, yet may reduce it in another metal. It is also evident that, even in alloys normally sensitive to notching, brittleness is less pronounced when less sharp notch forms are used. It thus appears from this series of tests that the quality of brittleness is relative. A given material may be ductile under some condition, but become brittle when submitted to more severe tests. The inference is that neither the strength of the metal nor the design of the component can be considered alone. It is quite possible, for instance, to avoid brittle cracks in a component if a metal of higher fracture strength is used, but the same effect also can be attained without changing the metal by an improvement in the design of the component. The fact is that the higher fracture strength will often be attainable only at the price of some loss in the resistance to deformation, so that highest performance can in any case be obtained only if the structural design is adapted to the character of the material used.

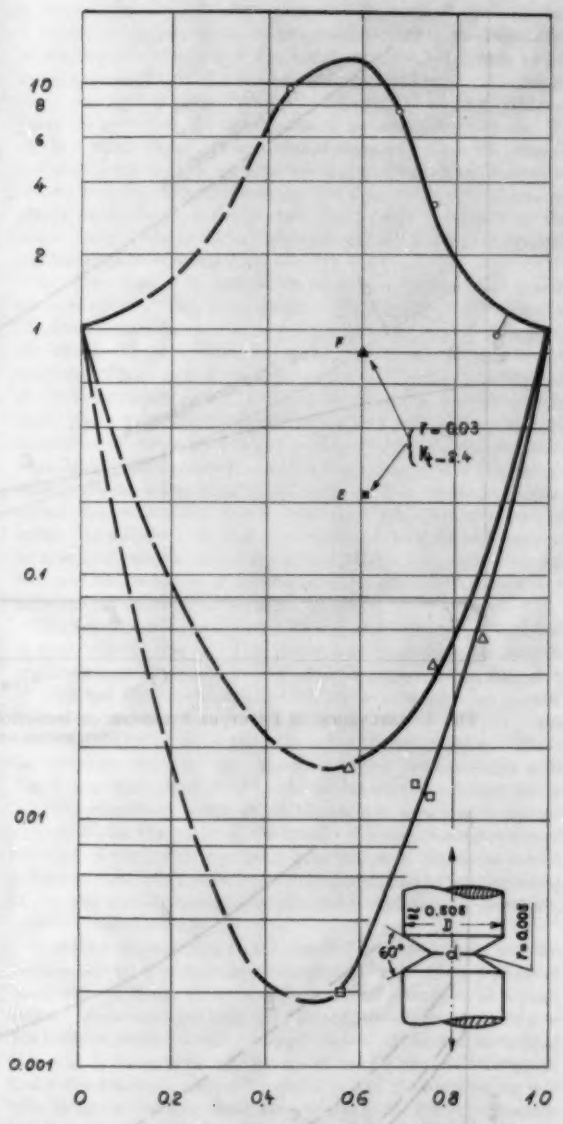

FIG. 5 TIME TO FRACTURE AS FUNCTION OF NOTCH DEPTH IN CREEP TESTS AT CONSTANT STRESS BUT VARYING NOTCH DEPTH
(After Davis and Manjoine.)

DETERMINATION OF QUALITY FIGURE FOR BLADE ROOTS

The fixing of the blades is a problem of the greatest importance in gas-turbine construction. Widest use is made of the so-called fir-tree root, in which the force is transmitted between the individual teeth, much as in a screw. This transmission of the force, however, is not possible without stress concentrations at the roots of the teeth. It so happens that metals with good high-temperature properties are relatively sensitive to peak stresses of this kind, so that it is essential to select a tooth design which will limit the stress concentrations to a minimum.

Just as in notched bars, the notches in the blade root lead to an inhibition of flow as well as to a stress concentration. The influence of the shape of the teeth on this obstruction to flow was therefore studied by conducting tensile tests at room temperature on the various designs of blade-root fixings.

[4] "Effect of Notch Geometry on Rupture Strength at Elevated Temperatures," by E. A. Davis and M. J. Manjoine, Symposium on Strength and Ductility of Metals at Elevated Temperatures, ASTM Special Technical Publications No. 128, 1953.

The various blade-root profiles tested are shown in Fig. 6. These profiles can be divided into three categories:

1 Blade root with teeth pointing downward (1 to 4 in Fig. 6).
2 Blade root with orthodox form of teeth (5).
3 Blade root with few but deeply indented teeth (6, 7, and 8).

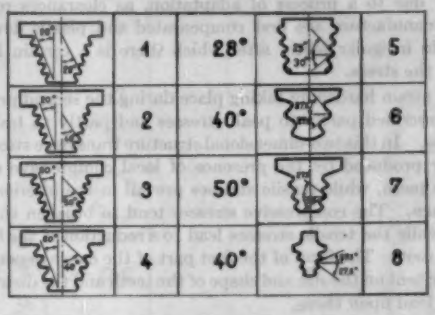

FIG. 6 TABLE OF BLADE-ROOT MODELS INVESTIGATED

The designs with the teeth pointing downward were chosen to help determine the factors upon which the inhibition of flow and the development of the stress concentration depend. For these room-temperature tests an austenitic Cr-Ni steel was used. Care was taken to choose a steel which did not have a sharply defined yield point, but a stress-elongation curve showing some similarity to the stress-creep curve in a high-temperature steel. It was thus justifiable to assume that the tendency of the design to strengthening under creep conditions would be measured, and in fact, this was confirmed by the creep tests carried out later. It was now necessary to select a method of evaluating the blade-fixing tests.

It is not possible to calculate the complicated stress conditions with reasonably simple methods even in the elastic range. For this reason a closer study had first to be made of the basic mechanism of fracture during creep tests on blade-root models of this kind.

Two types of fracture were observed: (1) A blade root in which fracture was due to shearing of the teeth is shown in Fig. 7. Areas of localized shear strains, clearly visible at the roots of the teeth, indicate where fracture eventually took place. (2) A more brittle type of fracture is shown in Fig. 8. In this latter test the crack responsible for fracture does not run through the zone of maximum deformation but obviously has been caused by the stress concentration. The crack no longer follows the plane of maximum shearing stress but runs approximately at right angles to the maximum tensile stress. If we examine the surface of fracture of the specimen, we can distinguish two zones, much as in a component broken under alternating stress, viz., a first zone in which the crack is propagated without deformation and a second zone with a reduction in area.

In evaluating tests of this kind, we can again work with the hypothesis that the behavior of the material depends on two strength characteristics, namely, its resistance to deformation and its fracture strength. Fracture can occur in two different ways, as in the notched bar. If the resistance to deformation is small and the fracture strength is high, plastic deformation due to shear occurs at the root of the tooth and continues till the capacity of the metal for deformation is exhausted and fracture results.

If, instead, the resistance to deformation is great and the fracture strength small, the peak stresses do not relax sufficiently, and a crack starts at the point of maximum stress and finally leads to fracture.

In evaluating our test results we set out with the consideration

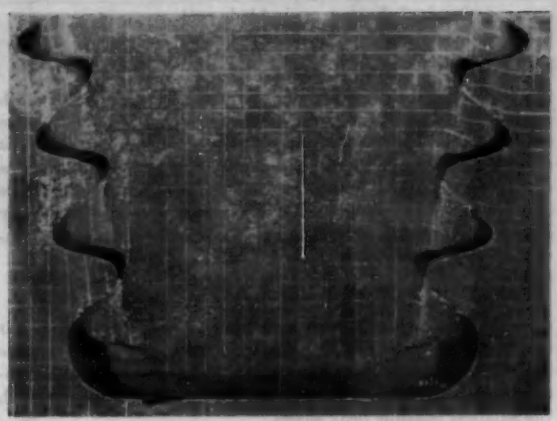

FIG. 7 BLADE-ROOT MODEL NO. 4 AFTER 8300 HR AT 4.77 KG/MM²

FIG. 8 EXAMPLE OF A BRITTLE FRACTURE

that in the case of ductile fracture the magnitude of the shearing stress is the primary factor, as can be seen clearly from Fig. 7. We can therefore introduce a nominal shear stress τ_{BN} that can be calculated from the relationship

$$\tau_{BN} = \frac{P}{bh} \quad \ldots\ldots [1]$$

where

P = force applied
b = breadth of blade root
h = height of blade root

If this calculated mean value has actually prevailed during the test, the same time to fracture must be obtained with the blade root as with a smooth bar in the tensile test, assuming the shear stress to have been the same. We can therefore introduce a quality figure in the form of the ratio of the shear stress in the blade root to the shear stress in the smooth specimen for the same time to fracture. This figure will be

$$\gamma_t = \left(\frac{\tau_{BN}}{\tau_0}\right)_t \quad \ldots\ldots [2]$$

where

τ_{BN} = nominal shear stress in blade root
τ_0 = shear stress in smooth specimen
t = time to fracture

if γ_k is greater than unity, there has been an increase of strength in the blade root as compared with the smooth specimen. The blade root is accordingly not sensitive to notching. If γ_k is smaller than unity, there has been a reduction of strength as compared with that of the smooth specimen, and this must be attributed to the notch effect. The factor γ_k depends not only on the form of the blade root but also on the metal, and this situation will now be discussed in more detail.

Test Results

As we noted when dealing with the results of the notched-bar tests, two conflicting tendencies are here at work, namely, the inhibition of plastic flow and the stress concentration. The problem is now to obtain the greatest possible inhibition of flow with the smallest possible peak stress.

The inhibition of flow was measured by pull-out tests at room temperature, while the influence of the stress concentration was determined in creep tests on various blade-root models of the same materials at elevated temperatures.

The influence of the metal was ascertained by carrying out creep tests with the same type of blade root but with different metals. At the same time the various metals also were submitted to sustained-load creep tests on smooth and notched bars.

Tensile Tests at Room Temperature

In Fig. 9 the elongation, in relation to the depth of the blade-root fixing, is plotted as a function of the nominal shear stress, Equation [1], for the various types of blade root. The elongation was measured after application of a preliminary load, which explains why the zero point of the elongation curve does not coincide with the zero point of the diagram. The curves all follow roughly the same course, consisting of a first section with decreasing rate of elongation, a second straight section, and a third section with increasing elongation. The first section is chiefly due to a process of adaptation, as clearances resulting from manufacture are first compensated and plastic flow takes place in irregular teeth, after which there is a certain leveling out of the stress.

The strain hardening taking place during the second process is to be ascribed partly to peak stresses and partly to transverse stresses. In this two-dimensional structure transverse stresses are mainly produced by the presence of local compressive stresses on the teeth, while tensile stresses prevail in the interior of the specimen. The compressive stresses tend to broaden the blade root, while the tensile stresses lead to a reduction of the breadth of the root. The form of the first part of the curve depends to a great extent on the size and shape of the teeth and the distribution of the load upon them.

The last part of the curve results from entry into a zone of instability in which the increase in the stress exceeds the capacity of the material for deformation in its present form. It may be stated in general that the gradient of the last part of the curve depends on the distribution of plastic deformation over a larger or smaller area and on the presence or absence of transverse stresses tending to inhibit plastic flow. The subsequent creep tests on models of blade roots showed that the beginning of this zone of instability is also a criterion for the capacity of a steel for hardening during the creep test, and that these two factors run parallel.

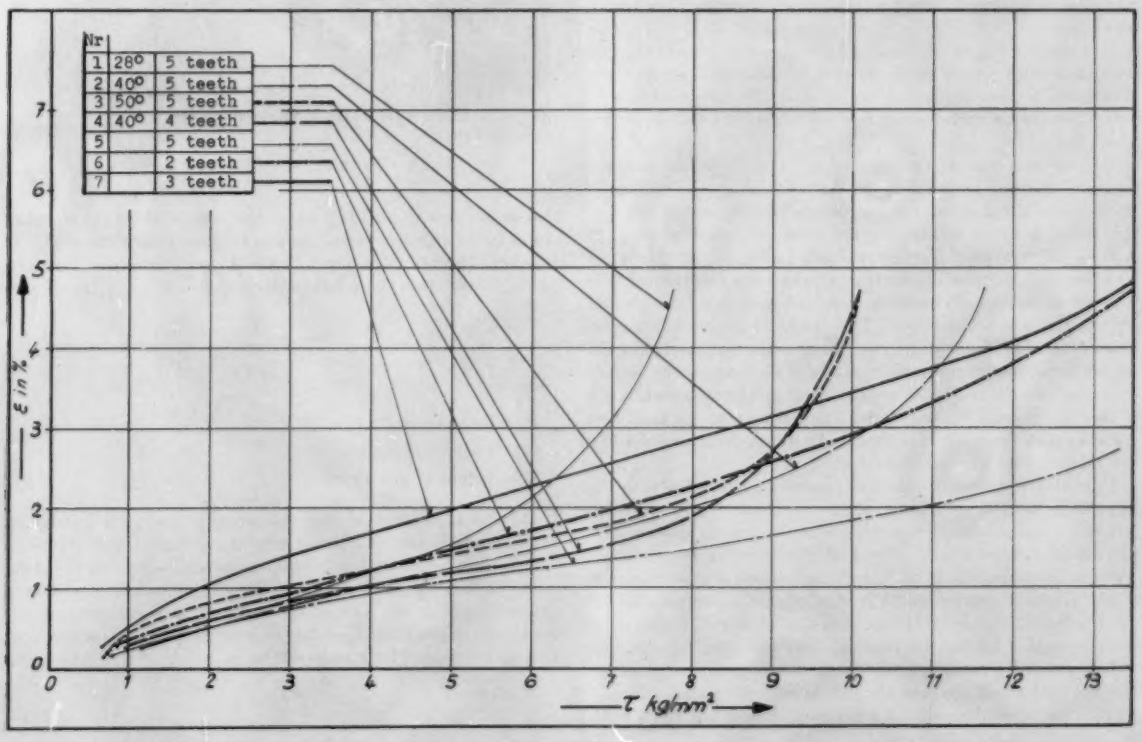

Fig. 9 Relationship Between Strain and Shear Stress in the Tensile Test at Room Temperature

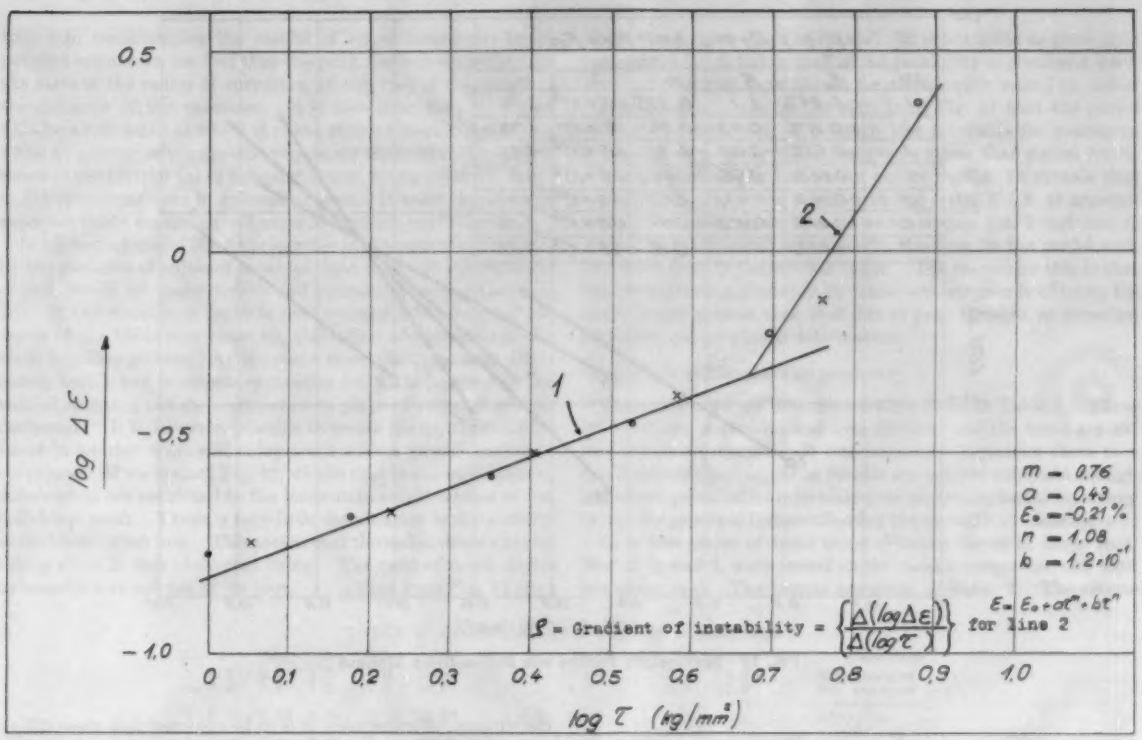

FIG. 10 STRESS-STRAIN CURVE FOR BLADE-ROOT MODEL NO. 2, PLOTTED BY DE LACOMBE'S METHOD

The method of De Lacombe was adopted for the further examination of these results.[5] This method consists in plotting the shear stress on a logarithmic scale along the abscissas and the logarithm of the differences in strain when the stress intervals increase in geometrical progression along the ordinates.

If the relationship between stress and strain can be given as a power function, the points lie on a straight line. It is an easy matter to determine the constants for the power function from the gradient and position of these straight lines. If we now plot the deformation curves of Fig. 9 by this method, we see that a new exponent appears for the strain curve at a definite shear stress. Fig. 10 illustrates the result of a pull-out test plotted in a diagram of this type. The entry into the zone of instability can now be very simply located. In addition, the exponent of the second section of the curve is a measure of the degree of instability. The second sections of the corresponding curves and the points of instability for the other blade roots are shown in Fig. 11. The number of the root model as indicated in Fig. 6 is shown near the instability point. The constants for the power-function relations are also shown in Fig. 11. With the aid of these curves the strengthening effect observed in the various blade roots can now be further discussed.

(*a*) *Blade Root With Teeth Pointing Downward* (*Forms Nos. 1 to 4*). Four forms of this type of blade root were investigated. The design was chosen to ascertain to what extent the distribution of stress affects the increase in strength. The considerations which led to this choice are summed up in Fig. 12 where the stressing of a tooth is shown with the methods of elementary stress analysis. The stressing in the root cross section is a combination of pressure, shearing, and bending. It is evident that the components of these three types of stress will change according to the form of the teeth.

The teeth in the first series of specimens are characterized by fairly high shear and pressure, while the bending stresses are relatively small. In tooth form No. 1 instability occurs at a low value of the stress as seen in Fig. 11. This is to be ascribed to the fact that the shear stresses in the critical sections are very high. An alteration of the tooth angle from 28 to 40 deg brings a marked improvement. It is the curve for this tooth form, No. 2, that is plotted in Fig. 10. The compressive stresses are now lower, the bending stresses are greater, and the maximum shearing stress in the critical section is reduced. A further increase in the tooth angle to 50 deg moves the point of instability back to lower shear-stress figures (point 3 in Fig. 11). The explanation of this is that the bending stresses have become still greater, so that the individual teeth are subjected to less favorable stressing.

(*b*) *Blade Root With Orthodox Form of Teeth* (*Form No. 5*). As compared with the first model, the compressive components are here reduced without any great rise in the bending stress. As Fig. 9 reveals, the new form leads to a considerable increase in the resistance to deformation. This is mainly due to a reduction in the compressive stresses with a consequent diminution of the shearing stress in the critical cross section. We see here the importance of the shearing stress in the blade root that we observed in the creep test, Fig. 7. Fig. 13 shows the blade-root fixing after a pull-out test at room temperature, while Fig. 14 shows the same fixing before the test. As can be seen from the distortions of the right-angled lines marked on the specimen, there is here a pronounced inhibition of plastic flow, which is also evident from the differences in height produced on

[5] "Un mode de représentation des Courbes de Fluage," by M. J. De Lacombe, *Revue de Métallurgie*, vol. 36, 1939, p. 178.

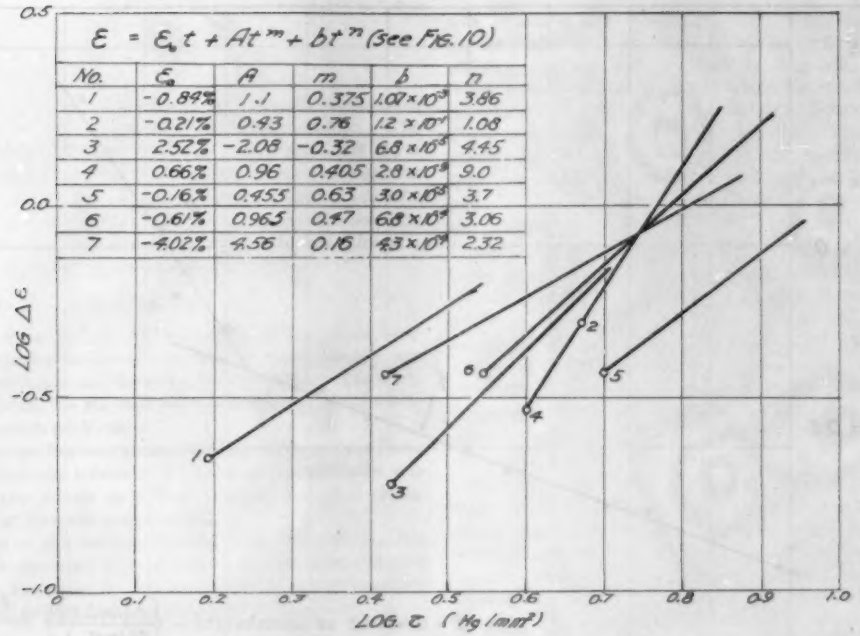

FIG. 11 INSTABILITY POINTS FOR BLADE-ROOT MODELS

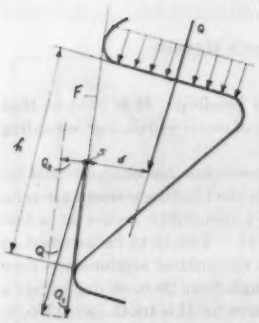

Shear stress ..... $\tau = \frac{Q_1}{F}$

Compressive Stress ..... $\sigma = \frac{Q_2}{F}$

Maximum bending stress ..... $\sigma_{B\max} = \frac{Qa6}{bh^3}$

Q = resultant
S = center of gravity of base
h = height of base section
b = width of base section

FIG. 12 STRESS AT ROOT OF A TOOTH ACCORDING TO ELEMENTARY BEAM THEORY

the surface. Furthermore, it is to be expected that these differences in height, which are restricted to a comparatively small area, will cause fairly high stress concentrations. The point of instability occurs at very high shear stresses in this model of blade root. In addition, the gradient of the curve after the point of instability is fairly gentle, which again points to strengthening. To sum up, it may be said that this type of root is very favorable in its deformation qualities, but that it involves certain stress concentrations which might lead to premature fracture in brittle materials.

(*c*) *Blade Root With Few but Deeply Indented Teeth (Forms Nos. 6, 7, and 8).* The question is now whether it is possible to obtain a similar inhibition of flow as in blade-root form No. 5 while at the same time reducing the peak stresses. The peak stresses depend to a large extent on the radius of curvature of the teeth. If we

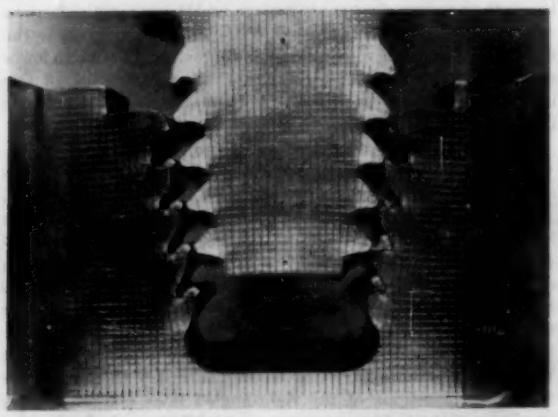

FIG. 13 PULL-OUT TEST AT ROOM TEMPERATURE ON BLADE-ROOT MODEL NO. 5

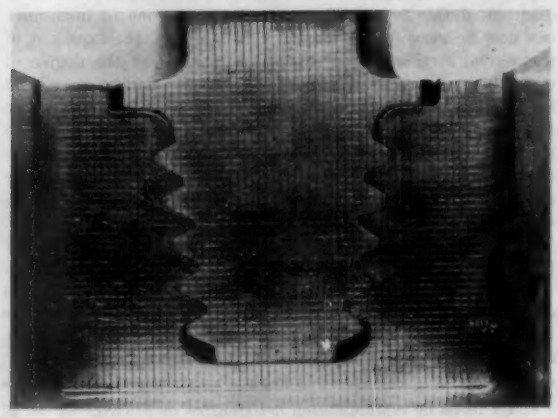

FIG. 14 BLADE-ROOT MODEL NO. 5 BEFORE TEST

take into consideration the results of stress investigations on notched specimens, we find that the peak stress is dependent on the ratio of the radius of curvature at the root of the notch to the diameter of the specimen. It is also clear that there is a definite notch depth at which the peak stresses reach a maximum, while at greater notch depths they again diminish. The radial stress in the interior takes a similar course, being naturally lower in flat specimens than in cylindrical ones. It must therefore be expected that a maximum will occur at medium notch depth.

In blade-root model No. 5 the increase in strength was produced by the presence of adjacent areas, at right angles to the direction of pull, which are under tensile and compressive stress (see Fig. 13). If the number of teeth is now reduced while keeping the depth of the blade root constant, the radius of curvature of the teeth becomes greater. At the same time, the areas with alternating tensile and compressive stresses are made larger, and the triaxial stressing and the obstruction to plastic flow are therefore decreased. It is, however, possible to secure the required triaxial stress in another way, still using teeth with a greater radius of curvature. If we inspect Fig. 13, we see that the areas of plastic deformation are restricted to the immediate neighborhood of the individual teeth. There is very little deformation in the vicinity of the blade center line. This means that the radial stress was not taking effect in this blade-root fixing. The ratio of notch depth to breadth was not yet at its best. It is clear from Fig. 11 that the strengthening effect of form No. 6 is not quite as good as in root model No. 5, but in view of the possibility of obtaining lower peak stresses this form should be much better suited to rather brittle materials. It can be seen from Fig. 11 that the model with three teeth, No. 7, is much less favorable for maximum hardening as a result of the transverse stress than model No. 6. A comparison of the instability points in Fig. 11 reveals that instability begins in the model with two teeth, No. 6, at approximately the same shear stresses as in models No. 2 and No. 4. Failure develops much more slowly, however, in the model with two teeth than in these latter types. The reason for this is that the strengthening produced by transverse stresses is effective for much longer periods than that due to peak stresses, as these are smoothed out by plastic deformation.

Creep Tests at Elevated Temperatures

The materials used in these tests are listed in Table 1. Three of them are austenitic and two ferritic. As the tests are extremely time-consuming, it was necessary to restrict them to a few important points. The results are not yet complete enough to furnish quantitative information on all details, but at least they reveal the principal factors affecting the strength of blade roots.

In a first series of tests three different forms of blade root, Nos. 2, 3, and 5, were tested at the same temperature and with the same steel. The results are given in Table 2. The results

TABLE 1 CHEMICAL ANALYSIS OF MATERIALS

No.	C	Mn	Si	Ni	Cr	W	V	Mo	Al	Nb	Co	Ti	Heat-treat
1	0.4	0.8	1.0	13.0	13.0	2.5	...	2.0	...	3.0	10.0	...	Sol. annealed
1a	0.4	0.8	1.0	13.0	13.0	2.5	...	2.0	...	3.0	10.0	...	Sol. annealed and warm-worked
2	0.23	0.43	0.54	0.14	12.07	...	0.34	0.58	...	0.12	...	...	1150 C/air 700 C/air
3	0.09	0.5	0.58	74	20.45	...	...	...	0.90	...	...	1.90	As received
4	0.35	0.69	1.36	9.5	19.6	1.3	...	1.18	0.3	0.55	...	0.57	As received
5	0.3	0.45	0.3	0.8	1	...	...	0.9	...	...	...	...	870 C/oil 680 C/air

TABLE 2 RESULTS OF TESTS

Shape of fir-tree (see Fig. 6)	Rupture tests at room temp on 18-8 Cr-Ni steel: Shear stress at point of instability, kg/mm²	ρ = gradient of instability for line 2, Fig. 10	Steel (see Table 1): Blade	Steel (see Table 1): Wheel rim	Creep tests on fir-tree models: Temperature °C / °F	Quality figure $\gamma_k = \frac{\tau_{BN}}{\tau_S}$ for duration of hours				Creep tests on smooth and notched bars: Comparison of smooth and notched bars: Notch-sensitivity figure γ_N = notched-bar strength / smooth-bar strength				Results of tests with smooth bars: Ratio of true rupture stress in tension to stress for 1% creep in 1000 hr $\eta = \frac{\sigma_k}{\sigma_{1\%/1000}}$				Temp deg C / deg F
						τ_{BN} = nominal shear stress for fracture of root; τ_S = nominal shear stress for fracture of smooth specimen												
2	4.7	3.04	1	1	650	Time h	1000	2000	—	Time h	50	2500	—	Time h	30	1000	4000	650
					1202	γ_k	0.72	0.72	—	γ_N	0.8	1.1	—	η	1.85	1.6	1.45	1202
3	2.63	1.96	1	1	650	Time h	40	1500	—	Time h	50	2500	—	Time h	30	1000	4000	650
					1202	γ_k	0.53	0.53	—	γ_N	0.8	1.1	—	η	1.85	1.6	1.45	1202
5	5.0	1.52	1	1	650	Time h	2500	30000	—	Time h	50	2500	—	Time h	30	1000	4000	650
					1202	γ_k	0.77	0.77	—	γ_N	0.8	1.1	—	η	1.85	1.6	1.45	1202
2	4.7	3.04	1a	1	710	Time h	550	30000	—	Time h	50	2000	—	Time h	5	100	1000	700
					1309	γ_k	0.49	0.54	—	γ_N[a]	0.8	0.8	—	η	1.6	1.3	1.0	1292
5	5.0	1.52	4	4	600	Time h	14500	—	—	Time h	3000	7000	—	Time h	100	1000	16500	600
					1112	γ_k	0.73	—	—	γ_N	1.05	0.95	—	η	3.0	2.1	0.72	1112
8	—	—	3	1	650	Time h	6600	—	—	Time h	50	2500	—	Time h	30	1000	4000	650
					1202	γ_k	0.625	—	—	γ_N[b]	0.8	1.1	—	η	1.85	1.6	1.45	1202
8	—	—	3	1	700	Time h	70	350	900	Time h	—	—	—	Time h	—	—	—	—
					1292	γ_k	0.67	0.67	0.69	γ_N	—	—	—	η	—	—	—	—
8	—	—	3	1	750	Time h	5	160	—	Time h	—	—	—	Time h	—	—	—	—
					1382	γ_k	0.62	0.74	—	γ_N	—	—	—	η	—	—	—	—
6	3.54	1.77	2	2	550	Time h	1.5	20	1000	Time h	—	—	—	Time h	1.5	20	1000	550
					1022	γ_k	1.08	1.03	1.0	γ_N	—	—	—	η	8.5	8.0	6.0	1022
7	2.5	1.12	5	5	550	Time h	680	1800	3300	Time h	60	300	2400	Time h	2	650	1800	550
					1022	γ_k	0.83	0.8	0.72	γ_N	1.2	1.1	1.05	η	13	2.9	1.25	1022

[a] Steel No. 1a.
[b] Steel No. 1.

of the pull-out tests at room temperature also have been entered in Table 2, where the shearing stress at the point of instability and the index ρ for the second phase of pull-out have been indicated. A comparison of columns 7, 8, and 9 with column 2 in Table 2 shows that the notch effect quality figures γ_k obtained in the creep test run parallel, in the main, with the instability stresses obtained in the tests at room temperature. Ductile fractures, i.e., the shearing-off of the blade teeth, were observed in all three cases, so that these tests do not supply any information on the quality of this fixing when used with a metal subject to embrittlement. The tests on smooth and notched specimens, which also are summarized in Table 2, show that the metal is not sensitive to notching in the range of about 1000 hr, the notch-sensitivity factor γ_N even taking on values above unity.

A further test with blade-root model No. 2 was next carried out, the metal again being No. 1, but with supplementary warm-working of the blade at 600 C. The test itself was carried out at 710 C. A first test lasting about 520 hr produced a brittle fracture, while the later tests, which were prolonged to times of as much as 30,000 hr, led to fractures by shearing-off of the teeth. However, the cracks did not run through the zone of maximum slip, but at an angle to the direction of pull, so that the fracture took up an intermediate position between pure slip and brittle fracture (compare Figs. 7 and 15). The creep tests on smooth and notched specimens show no embrittlement in steel No. 1 without warm working at times to fracture of about 2500 hr, while in the warm-worked steel some embrittlement was observed in a 2000-hr test, so that a 20 per cent reduction in the strength of the blade-root fixing was brought about by embrittlement.

The next test was made with blade-root model No. 5 and steel No. 4. It lasted 14,500 hr. The fixing had a quality figure of 0.73. This steel is one which becomes brittle after long periods, as sigma phase is formed. Unfortunately we have no test results with notched specimens of this duration. The available figures, however, clearly reveal a slight increase in embrittlement between 3000 and 7000 hours. The tendency to embrittlement can be distinctly observed in the capacity for elongation of the smooth bar, and it was found that these bars broke with very low elongation at about 16,000 hr.

These tests were followed by one with model No. 8 in which the rim piece was of steel No. 1 and the blade of steel No. 3. The tests were conducted at temperatures of 650, 700, and 750 C. The low-quality figures obtained with this model are explained in Fig. 16. The blade piece is of a steel which is considerably stronger at high temperature than that of the rim, so that much greater deformation occurred in the latter. It also proved that the bottom tooth was unfavorably stressed, as fracture occurred there at a time when there were no cracks in the other teeth. Fig. 16 refers to a test at 650 C with a shear stress of 7.6 kg per sq mm and a time to fracture of 6550 hr. The quality figure was 0.625. By comparison, Fig. 17 shows the blade fixing which was tested at a nominal stress of 6.2 kg per sq mm and 750 C. The test duration was 161 hr. In this case the metal of the rim piece was so soft that there was no further unfavorable stressing of the bottom tooth and the quality figure therefore rose to 0.74.

Two further tests were carried out with blade-root models Nos. 6 and 7, steel No. 2 being used with model No. 6 and steel No. 5 with model No. 7. The temperature was 550 C. Model No. 6 in conjunction with steel No. 2 proved to have extremely good, quality figures. The reason for this is that the steel is not at all sensitive to notching as appears from the high figures for reduction in area in the creep tests on smooth specimens. Model No. 7 is rather less good, but it must be mentioned that the steel used in this test is also less favorable. A comparison of the fractured blade roots showed very clearly the fundamental difference in their behavior under creep. Fig. 18 shows blade-root model No.

FIG. 15 CREEP TEST ON BLADE-ROOT MODEL NO. 1, STEEL NO. 1a "WARM WORKED," TEMPERATURE 710 DEG C, MEAN SHEAR STRESS = 4.28 KG PER SQ MM, TIME TO FRACTURE, 7677 HR

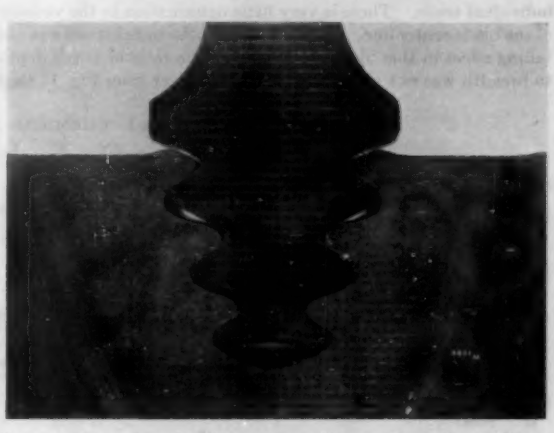

FIG. 16 CREEP TEST ON BLADE-ROOT MODEL NO. 8, BLADE PIECE OF STEEL NO. 3, RIM PIECE OF STEEL NO. 1, TEMPERATURE 650 DEG C, SHEAR STRESS 7.6 KG PER SQ MM, TEST DURATION UNTIL PHOTOGRAPH 6550 HR

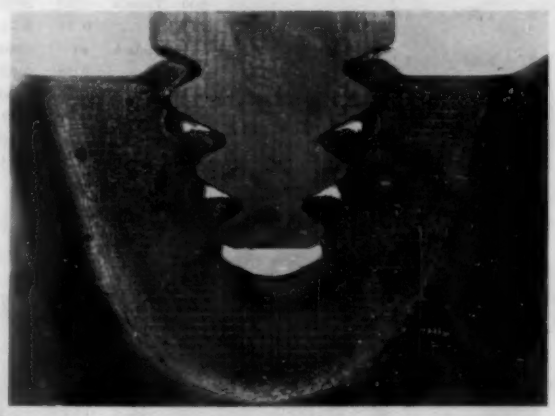

FIG. 17 CREEP TEST ON BLADE-ROOT MODEL NO. 8, BLADE PIECE OF STEEL NO. 3, RIM PIECE OF STEEL NO. 1, TEMPERATURE 750 DEG C, MEAN SHEAR STRESS 6.2 KG PER SQ MM, TIME TO FRACTURE 161 HR

FIG. 18 CREEP TEST ON BLADE-ROOT MODEL NO. 7, STEEL NO. 5, TEMPERATURE 550 DEG C, MEAN SHEAR STRESS 7.93 KG PER SQ MM, TIME TO FRACTURE 677 HR

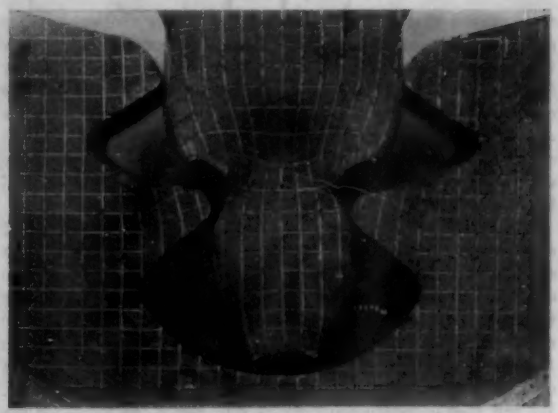

FIG. 19 CREEP TEST ON BLADE-ROOT MODEL NO. 6, STEEL NO. 2, TEMPERATURE 550 DEG C, MEAN SHEAR STRESS 12.4 KG PER SQ MM, TIME TO FRACTURE $20^1/_2$ HR

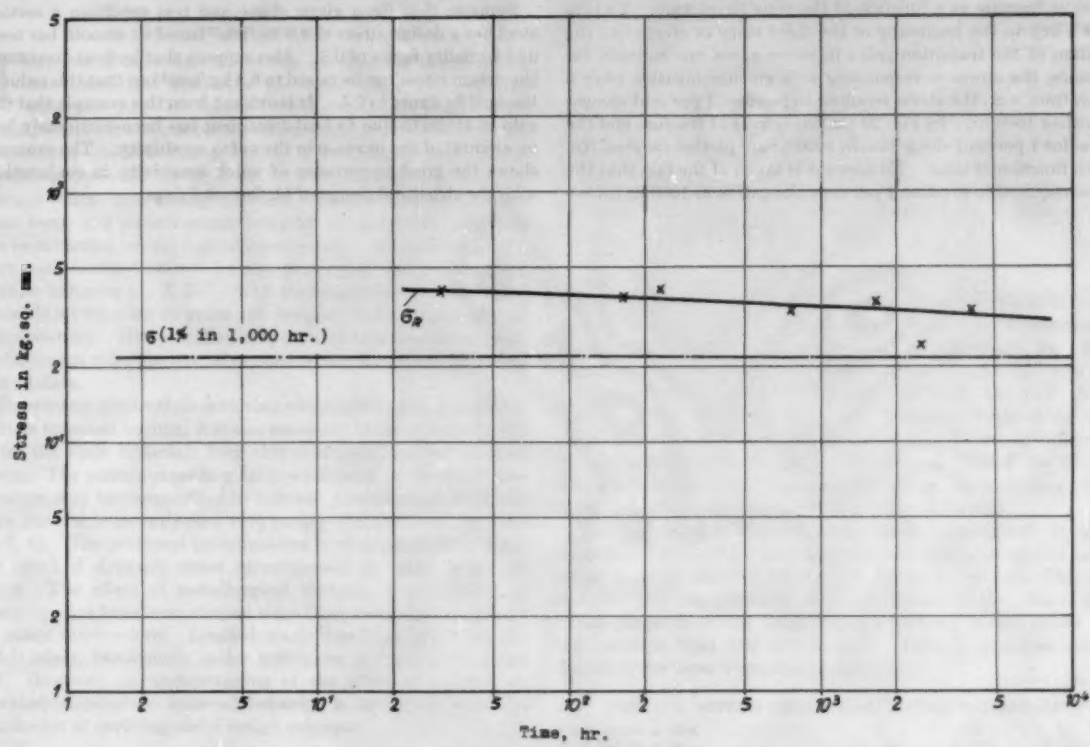

FIG. 20 TRUE STRESS AT FRACTURE AS A FUNCTION OF TEST DURATION AND STRESS FOR 1 PER CENT STRAIN IN 1000 HR FOR STEEL NO. 1 AT 650 DEG C

7 loaded with a nominal shear stress of 7.9 kg per sq mm for a duration of 2300 hr. Fig. 19 shows model No. 6, which broke under a shear stress of 12.4 kg per sq mm after $20^1/_2$ hr at 550 C. The quality figure of the model shown in Fig. 18 was 0.8, while that of the model in Fig. 19 was 1.03.

Creep Tests to Determine Notch Sensitivity of Steels Used

To determine the notch sensitivity of the steels, creep tests were conducted on smooth and notched specimens. The notched bars had a V-notch of 60 deg, the radius at the root of the notch being 0.1 mm. The ratio of the notch diameter to the bar diameter was 0.8. The notch sensitivity of the steel was taken to be the ratio of the stress for the notched specimen to that for the smooth specimen at the same time to fracture. It was not possible with the available equipment to carry out tests of this kind on notched bars of all the steels up to very long times to fracture. The notch-effect factors have therefore been indicated in Table 2 on the basis of the test results available. It must be

remembered that the notch sensitivity of a given steel is not generally constant, but varies in time. If we compare the quality figures γ_k of the blade-root fixings with the notch-sensitivity factors γ_N of the test bars at a given rupture time, we find that the quality figures of the fixings run approximately parallel with the notch-sensitivity factors, so that the determination of the notch sensitivity in smooth and notched specimens permits a fairly accurate estimate of the rupture-time behavior of the actual blade-root fixings.

With the aid of the working hypothesis set up in the first part of this paper, according to which the strength of a material at elevated temperatures is largely decided by the interaction of the resistance to deformation and the fracture strength, it is possible to draw conclusions from tests on smooth specimens as to the notch sensitivity of the material in question. According to Fig. 1(*c*), the true stress at the moment of fracture is one point on the curve giving the fracture strength as a function of time. We saw that embrittlement occurs if in Fig. 3 the curve for the fracture strength C is comparatively low in relation to curve a. If we now carry out creep tests at various nominal stresses, we can obtain curve C in a first approximation by plotting the true stress at fracture as a function of the time to fracture. To provide a key to the beginning of the third stage of creep, i.e., the position of the transition point in curve a, we can indicate, for instance, the stress corresponding to a given elongation after a given time, e.g., the stress required to produce 1 per cent elongation after 1000 hr. In Fig. 20 the true stress at fracture and the stress for 1 per cent elongation in 1000 hr are plotted for steel No. 1 as a function of time. No account is taken of the fact that the stress required to produce 1 per cent elongation in 1000 hr is likewise dependent on time, and probably very much so in precipitation-hardening metals and in ferritic steels. From curves of this type the ratio η of the true stress at fracture to the stress for 1 per cent elongation after 1000 hr can be determined for given times. Values for η for steels 1, 1(*a*), 2, 4, and 5 are listed in Table 2.

Conclusions

These tests show that the design stress figures obtained from creep tests are not the only important consideration in determining the strength of the blade-root fixings, but that they may be reduced by as much as 50 per cent ($\gamma_k = 0.5$) if the steel has not the ductility required by the structural design employed. These tests also show how important it is to select a suitable shape of root as well as a suitable metal with a view to insuring that no inadmissible stress concentrations will occur. The dimensions of the blade-root fixings must not be based on the smooth bar creep data alone, but these design stresses should be multiplied by the quality figures. If this is not done, the conclusions drawn may be quite wrong, as will appear from the following example:

Suppose that for a given shape and test condition a certain steel has a design stress of 4.0 kg/mm² based on smooth bar tests and a quality figure of 0.8. Also suppose that by heat-treatment the design stress can be raised to 6.4 kg/mm² but that this reduces the quality figure to 0.5. It is evident from this example that the gain in strength due to heat-treatment has been completely lost on account of the increase in the notch sensitivity. The example shows the great importance of notch sensitivity in conjunction with the structural design of blade-root fixings.

Factors Influencing the Notch Fatigue Strengthening of N-155 Alloy at Elevated Temperatures

By W. S. HYLER[1] and W. F. SIMMONS,[2] COLUMBUS, OHIO

Data are given to illustrate the effect of stress raisers on the elevated-temperature fatigue behavior of N-155 alloy. These data were obtained on specimens notched with V-grooves having various root radii and various notch severities. The experimental program was in direct-stress fatigue, and covered a range of alternating stress to mean stress from $A = 0.0$ to $A = \infty$ at temperatures of 1200 to 1500 F. The effect of surface finish also was studied to a limited extent. A metallographic study of fractured surfaces was carried out.

Introduction

THE use of materials for service at elevated temperatures has stimulated the need for data upon which design concepts may be based. Unlike ordinary-temperature design, where behavior is usually elastic, the problems at elevated temperature involve characterizing a time-temperature-stress-dependent behavior in addition to complicating metallurgical changes which occur during exposure. Considerable study of the basic creep and stress-rupture behavior of unnotched materials has been carried our for a great many years. More recent efforts have been directed toward a study of notched creep and stress-rupture behavior (1, 2, 3).[3] Such investigations have provided valuable information to guide the designer in the choice of specific materials. However, the integration of such information into useful design rules has not progressed as rapidly as has the collection of data.

Since many applications involving elevated-temperature service include repeated loading, it is also necessary to be able to characterize the basic materials from this standpoint as well as from creep. The picture regarding fatigue behavior at elevated temperature may be summarized as follows: Considerable work has been done fairly recently on a wide variety of unnotched materials (4, 5, 6). The pertinent investigations have attempted to assess the effect of dynamic stress superimposed on mean or steady stress. The effect of metallurgical changes, of creep and of damping, also have been studied since these factors are pertinent in many applications. Limited study has been given to the notch effect, particularly under conditions of high mean stress (7). However, an understanding of the effect of notches on elevated-temperature material behavior is necessary from the standpoint of evolving useful design concepts.

This investigation was initiated with the object of studying some of the important factors related to notched behavior in fatigue at elevated temperature. Although the basic material was considered one of the most important factors, it was decided to confine the investigation to N-155 alloy. This decision was based on: (*a*) Considerable available information describing the static and dynamic unnotched behavior of N-155, and (*b*) availability of several rods from the same heat of N-155 that had been used in previous investigations (8, 9). The factors studied in this investigation included alternating-stress to mean-stress ratio (load ratio A), temperature, and notch severity. Factors such as speed of cyclic stressing, rest periods at temperature, cyclic temperature, and others, although considered important, were beyond the scope of the present investigation.

Goodman-type diagrams were developed chiefly in the tension-tension region at 1200 and 1500 F. For certain notches, however, fatigue tests under completely reversed stressing ($A = \infty$) were made. Thus the entire Goodman diagram could be presented in those cases. Three 60-deg V-notches were employed to study notch severity. These ranged from a mild notch $K_t = 1.7$, to a severe notch $K_t = 5.1$.

Experimental Details

Test Material. The material used in this investigation consisted of 1-in. rounds of N-155 alloy that came from the same heat that was used on a number of NACA investigations (8, 9). The chemical composition of N-155 alloy, heat No. A-1726, was C, 0.13; Mn, 1.64; Si, 0.42; Cr, 21.22; Ni, 19.0; Co, 19.7; Mo, 2.90; W, 2.61; Cb, 0.84; N_2, 0.13. Heat-treatment of the bar stock was (*a*) solution heat-treatment at 2200 F for 1 hr followed by a water quench; (*b*) aging treatment at 1400 F for 16 hr. The solution treatment was carried out prior to machining; the aging treatment followed machining of the specimens.

Test Specimens. Three notches were investigated in this program. The notch dimensions were selected to achieve a large range in notch severity from $K_t = 1.7$ to $K_t = 5.1$. This afforded a range in triaxiality ratio (as defined by the ratio of the radial stress σ_3 to the longitudinal stress σ_1) at the center of the specimen from 0.62 to 0.81 (10). Table 1 compares notch details of the three V-grooves investigated.

TABLE 1 NOTCH DETAILS OF THREE V-GROOVES

Flank angle, ω, deg	60	60	60
Root radius, r, in.	0.005	0.010	0.050
Notch depth, t, in.	0.047	0.047	0.047
Minimum diameter, d, in.	0.225	0.225	0.225
Stress-concentration factor, K_t(11)	5.1	3.2	1.7
Triaxiality ratio, σ_3/σ_1	0.81	0.80	0.62

Notched specimens were machined following solution treatment, as shown in Fig. 1. Notches were lathe turned, using a special carbide tool and no subsequent polishing. Notch dimensions were checked with a 50 to 1 shadowgraph. This procedure resulted in fairly reproducible notches; however, it was thought some strain hardening of the notch root would occur. Therefore aging was done after machining to take advantage of any stress relief. It was found from microscopic examination

---

[1] Assistant Chief, Applied Mechanics Division, Battelle Memorial Institute. Assoc. Mem. ASME.

[2] Assistant Chief, High-Temperature Metals Research Division, Battelle Memorial Institute.

[3] Numbers in parentheses refer to the Bibliography at the end of the paper.

Contributed by the joint ASTM-ASME Committee on Effect of Temperature on the Properties of Metals and presented at the Annual Meeting, New York, N. Y., November 18–December 3, 1954, of The American Society of Mechanical Engineers.

Note: Statements and opinions advanced in papers are to be understood as individual expressions of their authors and not those of the Society. Manuscript received at ASME Headquarters, November 9, 1954. Paper No. 54—A-239.

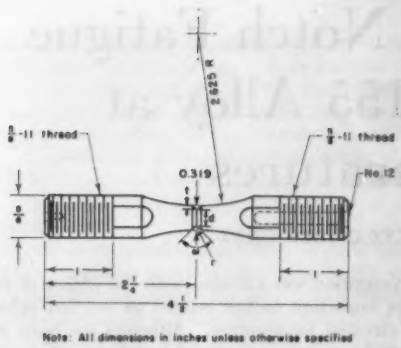

FIG. 1 NOTCHED-SPECIMEN DETAILS

that strain hardening did occur to a depth up to about 0.003 in.; therefore, during aging, some recrystallization occurred and precipitation was accelerated in this area. Several notched specimens of $R = 0.050$ in. root radius were lapped and electropolished to remove this worked and aged zone. These were used to investigate surface preparation in fatigue. Lapping of the notch root was accomplished with a rotating copper wire over which cutting oil and 600-grit emery dust were flowed continuously. This removed about 0.003 to 0.004 in. on the radius. Another 0.001 in. was removed by electropolishing. The process reduced the diameter of the specimen about 0.008 in.; its effect on K_t was negligible, however. Typical photomicrographs of the mild notch with and without the cold-worked and aged zone are shown in Fig. 2.

Equipment. Krouse direct-stress fatigue machines equipped with hydraulic load maintainers were used in this investigation. They operate at a frequency of about 1500 cycles per min (cpm). Sensitive electronic controls sense changes in load due to permanent deformation and actuate the hydraulic system for maintenance of the mean load.

Furnaces were resistance-wound with provision for balancing the temperature along the test section. Three thermocouples were wired to each specimen, one at the center for temperature control and one at each end. Each specimen was brought to temperature and stabilized over the test section to within 3 deg F in about 2 hrs. It was then soaked for 1 hr, after which the appropriate test load was applied.

Experimental Program. Originally, the program was to obtain sufficient data to construct Goodman-type diagrams in the tension-tension region for the three notched specimens. It was later decided to investigate on a limited scale the fatigue behavior under completely reversed axial loading and also the effect of surface preparation on the behavior of N-155.

With the exception of specimens notched with V-groove having $r = 0.010$ in., S-N curves were developed for constant load ratios A of 0.0, 0.25, and 0.80 at either 1200 or 1500 F or both. The data for the notch having $r = 0.010$ in. were obtained at various constant alternating-stress levels at 1200 F and for load ratios A of 0.0, 0.30, and 0.80 at 1500 F.

The limited study of completely reversed stressing was carried out on notches having $r = 0.005$ in. at 1200 and at 1500 F and having $r = 0.050$ in. at 1200 F. The study of the effect of surface finish was carried out at 1200 F on specimens having an 0.050-in-radius notch at load ratios A of 0.25 and of 0.80.

RESULTS

Stress-rupture and fatigue data obtained in this investigation were plotted on maximum-stress log-lifetime co-ordinates. A typical set of curves for specimens notched with $r = 0.005$ in. and

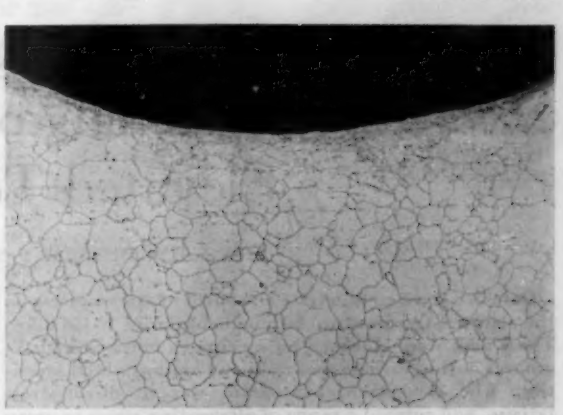

×100 As machined, aged N133949

×100 N15505

As machined, aged, lapped, and electropolished

FIG. 2 PHOTOMICROGRAPHS OF UNTESTED NOTCHED SPECIMENS OF N-155 ALLOY; $r = 0.05$ IN.

tested at 1200 F is shown in Fig. 3 (numbers associated with data points represent reduction-of-area values). In this figure, the stress-rupture curve ($A = 0.0$) intersects the $A = 0.25$ curve. This suggests that the superposition of an alternating stress on a mean stress may result in longer lifetimes to failure, in some cases. The same behavior was observed at each test temperature for notches with radii greater than 0.005 in.

The S-N curves were then used to construct the Goodman-type diagrams shown in Figs. 4 through 7 (for constant lifetimes of 1000, 500, 150, and 50 hrs). Also included on the diagrams are similar curves for unnotched data from an NACA investigation (8). A number of observations may be made in comparing the two sets of data:

1 Notch strengthening was observed to some extent for all notches.

2 The combinations of alternating stress, mean stress, and lifetime favoring notch strengthening became more extensive the greater the notch radius.

3 Notch strengthening was more pronounced at 1500 F than at 1200 F.

4 In general, at long lifetimes, it was observed that the mean stress to cause stress-rupture failure was less than

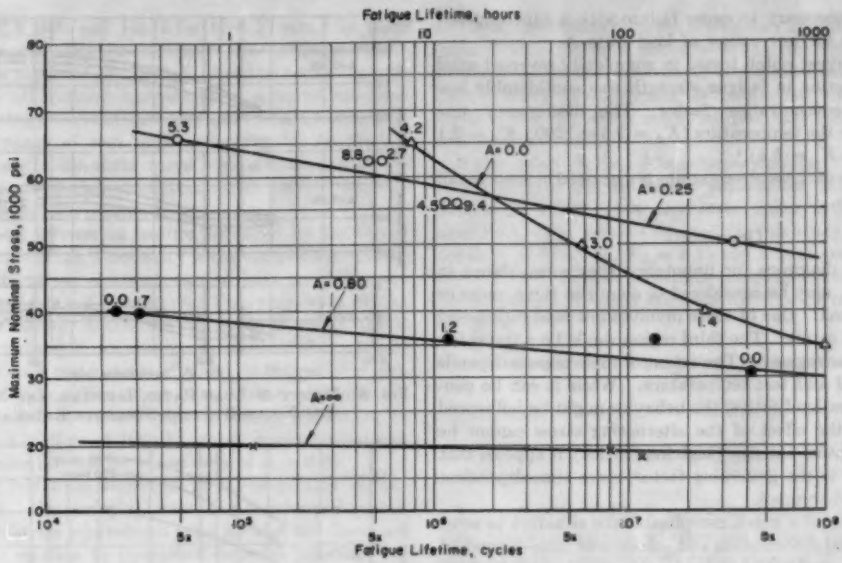

FIG. 3 AXIAL-LOAD FATIGUE-TEST RESULTS: N-155 at 1200 F, NOTCHED WITH r = 0.005-IN. GROOVE

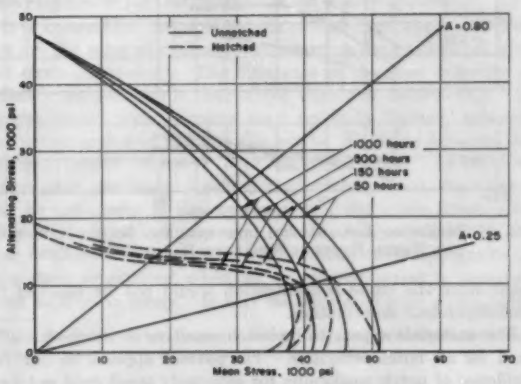

FIG. 4 GOODMAN DIAGRAM: N-155 at 1200 F, UNNOTCHED AND NOTCHED WITH 0.005-IN. GROOVE

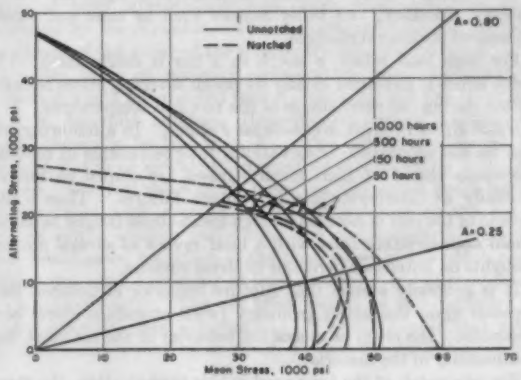

FIG. 6 GOODMAN DIAGRAM: N-155 AT 1200 F, UNNOTCHED AND NOTCHED WITH 0.05-IN. GROOVE

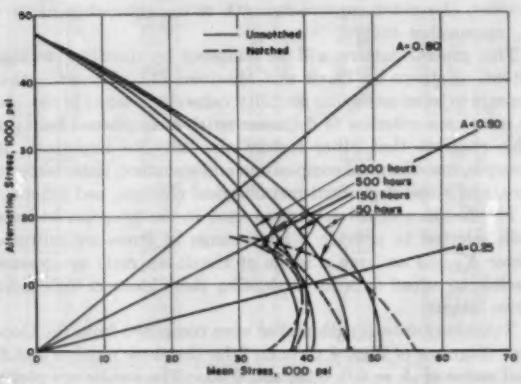

FIG. 5 GOODMAN DIAGRAM: N-155 AT 1200 F, UNNOTCHED AND NOTCHED WITH 0.010-IN. GROOVE

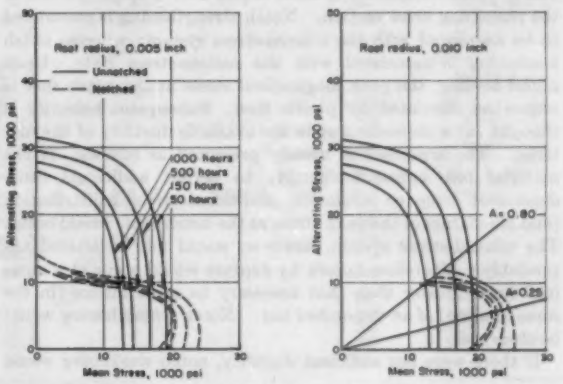

FIG. 7 GOODMAN DIAGRAM: N-155 AT 1500 F, UNNOTCHED AND NOTCHED SPECIMENS

the mean stress necessary to cause failure with a superimposed alternating stress for low values of load ratio A.

5 For the sharpest notch tested in completely reversed axial loading, the reduction in fatigue strength was considerably less than the stress-concentration factor. The discrepancy was greater the higher the temperature ($K_f = 2.6$ at 1200; $K_f = 2.1$ at 1500; whereas $K_t = 5.1$).[4]

The significance of these observations is discussed in some detail in the next section.

Discussion

Goodman-type diagrams for unnotched specimens, shown in Figs. 4 through 7, may be considered to comprise three, more or less distinct, regions. One of these involves low load ratios, and another high load ratios. The third region would be a transition between the former regions. The extent of these regions depends upon the material and test temperature. While it can be considered that, at low load ratios, the behavior might be influenced by mean stress, the effect of the alternating stress cannot be ignored. At the other extreme (high load ratios), it appears that alternating stress is the governing factor, since time-dependent deformation would be small.

The introduction of a notch complicates the situation to some extent. The initial deformation and subsequent time-dependent deformation associated with low load ratios would result in stress redistribution along the notch plane. Notch-bar strengthening or weakening might be observed depending upon the notch severity, ductility, and other factors such as time and stress-dependent structural changes.

For high load ratios, a notch in a bar is detrimental. The notch effect is governed chiefly by notch severity, stress redistribution during the early stages of the test and temperature.

Notch Effect in High Mean-Stress Fatigue. In a following section on metallographic observations, fatigue failures of notched specimens tested at high mean stresses are shown to initiate generally as intercrystalline or rupture failures. Thus a discussion of the role of notches on high mean-stress fatigue behavior would appropriately start with a brief review of several current thoughts on notch-bar behavior in stress rupture.

It is generally agreed that rupture behavior of notched bars depends upon the notch geometry (with attendant stress concentration), the creep or relaxation behavior of the material, and the ductility of the material.

For any notch of the type used in this investigation, the stress distribution is such that a biaxial-tensile-stress state appears at the surface of the notch root (with a high longitudinal stress), and a triaxial-tensile-stress state occurs over a major portion of the remaining cross section. Notch strengthening is considered to be associated with the triaxial-stress system; whereas notch weakening is associated with the surface-stress state. Upon initial loading, the peak longitudinal stress at the notch root is somewhat alleviated by plastic flow. Subsequent behavior is thought to be dependent upon the available ductility of the material. The argument is usually presented as follows: If the material has sufficient ductility to permit additional time-dependent creep or relaxation, additional stress redistribution (and alleviation of the peak stress at the notch root) would occur. The triaxial-stress system, however, would not be altered appreciably. Therefore failure by rupture would occur at a nominal stress greater than that necessary to cause failure (in the same lifetime) of an unnotched bar. Notch strengthening would be observed.

If there were not sufficient ductility, notch weakening would occur since the stress concentration would not be relieved by time-dependent deformation.

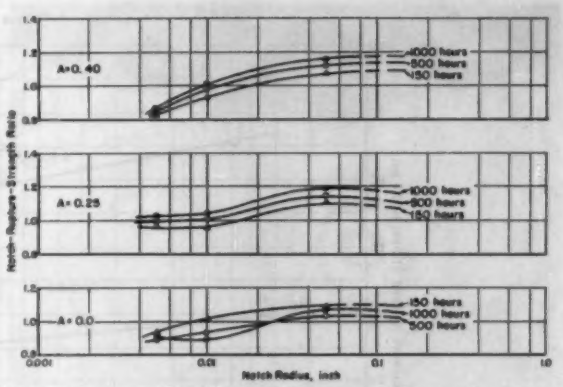

Fig. 8 Effect of Load Ratio, Lifetime, and Notch Radius on the Notch-Rupture-Strength Ratio at 1200 F

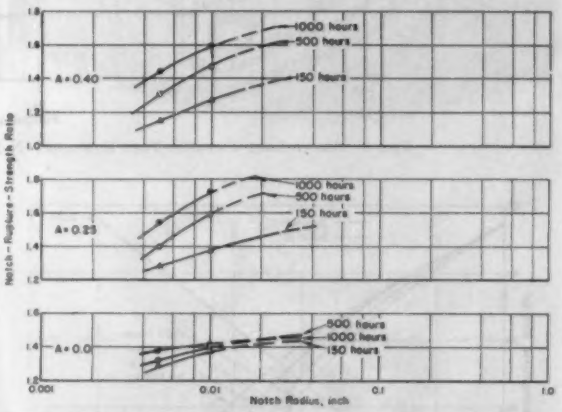

Fig. 9 Effect of Load Ratio, Lifetime, and Notch Radius on the Notch-Rupture-Strength Ratio at 1500 F

Few materials appear to be notch-sensitive or notch-strengthened for all notch severities. The pattern appears to be: (*a*) Evidence of notch weakening for extremely small radii notches; (*b*) with increasing notch radius, observance of notch strengthening as values of notch-rupture-strength ratio increase to some maximum value greater than 1; and (*c*) for even larger radii notches, the notch-rupture-strength ratio approaches unity as K_t approaches unity.

This general pattern will be tempered by ductility, to some extent, as shown by Davis and Manjoine (1). However, there appears to be no particular ductility value (unnotched or notched) to serve as a criterion to delineate notch-strengthened behavior. This suggests that other factors also may be important, for example, metallurgical composition and structure, time, temperature, and stress-dependent metallurgical changes, and others.

The N-155 notched specimens used in the program had root radii selected to provide a large range in stress-concentration factor K_t and as large a range of triaxiality ratio as appeared feasible to afford data for evaluating these ideas in high mean-stress fatigue.

Notch-rupture-strength ratios[5] were computed from the Goodman diagrams of Figs. 4 through 7 for the three notches and for load ratios of $A = 0.0$, 0.25, and 0.40. The results are plotted

[4] K_f is the ratio of the unnotched fatigue limit to the nominal notched fatigue limit at the same lifetime; K_t is the theoretical stress-concentration factor.

[5] This ratio is defined as the ratio of the notch-bar strength to the unnotched-bar strength at the same lifetime and load ratio.

in Fig. 8 for 1200 F data and Fig. 9 for 1500 F data. In these figures, the lower sets of curves represent stress-rupture results ($A = 0.0$). It is observed, at 1200 F, that the notch-rupture-strength ratio for all lifetimes increases from a value less than 1.0 (notch weakening) to a value greater than 1.0 (notch strengthening) over the range of root radii investigated. At 1500 F the notch-rupture-strength-ratio curve also increased with increasing root radius. Notch strengthening at 1500 F was observed for all notches investigated.

Perhaps the most interesting feature displayed by the Goodman-type diagrams of Figs. 4 through 7 is the marked strengthening effect that alternating stress appears to have on high mean stress at long lifetimes. For example, Fig. 6 ($r = 0.05$ in., 1200 F) shows a 1000-hr notch-rupture stress of about 41,000 psi. At a load ratio of 0.25, an alternating stress of about 11,000 psi superimposed on a mean stress of about 45,000 psi also produces a life of 1000 hr. The effect is such that, although the sharpest notch tested at 1200 F showed notch weakening in stress rupture at a lifetime of 1000 hr, notch strengthening was observed at the same lifetime for a load ratio of $A = 0.25$.

This behavior has been observed in investigations of unnotched materials. For example, Lazan (4) has defined the mean dynamic-to-static stress equivalence ratio E,[a] and has discussed its significance in relation to unnotched-material behavior. If E is greater than 1, the addition of an alternating stress to a mean stress would increase life or reduce creep. However, the mechanism responsible for this behavior is not clearly understood.

It is known that the mechanisms of static and cyclic deformation are the same at ordinary temperatures (fragmentation, slip, and strain hardening). The difference in observed behavior at ordinary temperature is that of the degree of deformation. In fatigue, small cyclic stresses may result in limited deformation within grains on discrete slip bands. In static deformation, slip may extend uniformly over the entire grain. At elevated temperature for static loading, uniform slip over the crystal may be expected. If the deformation under cyclic stress is localized as it is at ordinary temperature, it is not clear why the gross deformation associated with the mean stress appears to be suppressed or reduced when an alternating stress is superimposed on a mean stress. It may be associated with strain hardening at some temperatures; it also may be associated with other metallurgical changes accelerated by the cyclic stress. The presence of notches appears to accentuate this behavior (compare relative strengthening of unnotched and notched specimens in Fig. 4), which might suggest that these effects may be important factors.

Notch Effect in Low Mean-Stress Fatigue. The investigation of the effect of notches on low mean-stress fatigue of N-155 was limited in extent to a few tests under completely reversed axial load. The notches selected for this study included a severe notch ($r = 0.005$ in., $K_t = 5.1$) and a mild notch ($r = 0.05$ in., $K_t = 1.73$). Estimated fatigue limits and fatigue-notch factors for completely reversed stressing for 1000-hr behavior are given in Table 2.

TABLE 2 ESTIMATED FATIGUE LIMITS AND FATIGUE-NOTCH FACTORS

Notch radius, in.	Temp, deg F	Fatigue limit in 1000 hr, psi	K_f	K_t
0.005	1200	18000	2.6	5.1
0.005	1500	12500	2.1	5.1
0.050	1200	25500	1.8	1.7

The values in Table 2 apply to repeated stressing at 1500 cpm. It is not certain whether the fatigue limits would be the same were the frequency of cyclic stresses 10 or 100 times this value.

It will be observed that the strength reduction of the severe notch at both temperatures was considerably less than that predicted by the K_t-value. The strength reduction of the mild notch was of the order of the stress-concentration factor K_t.

On the basis of ordinary temperature notched-bar-fatigue studies, it would be expected that K_f would be not too dissimilar from K_t for mild notches. However, for severe notches, K_f would generally be less than K_t. The behavior observed on notched N-155 at elevated temperature is compatible with this picture. The low value of K_f noted for the severe notch would be associated with marked plastic deformation of the notch root on initial loading and during the early stages of fatigue. This would cause reduction of the peak stress at the notch root. Subsequent work hardening at least at 1200 F would strengthen the material locally. The net effect would be less reduction in fatigue strength than anticipated. It would appear that even the mild notch would be so affected, since the fatigue limit ap-

[a] E is the ratio of the mean dynamic stress to the static stress which causes the same creep or rupture behavior.

TABLE 3 RESULTS OF METALLURGICAL EXAMINATION OF FAILED NOTCHED SPECIMENS OF N-155 ALLOY

Specimen no.	Maximum stress, psi	Lifetime hr	Load ratio, A	Length of indicated fracture region, in., and type of fractures (Fig. 10) Region 1	Region 2	Region 3	Region 4	Specimen diam, in.	Remarks[b]
N-155-20A	50000	57.9	0.0	0.075, I	0.106, M	0.039, I	...	0.220	50% I
N-155-25A	35000	1201.5	0.0	... , I	... , M	... , I	...	...	...
N-155-1A	65625	0.53	0.25	0.185, T	...	...	...	0.185	...
N-155-3A	62500	6.04	0.25	0.071, T	0.142, M	...	...	0.213	10% I[c]
N-155-28A	56000	13.54	0.25	0.153, M	0.067, T	...	...	0.220	10% I[c]
N-155-30A	50000	384.0	0.25	0.028, I	0.071, T	0.118, M	...	0.217	10% I[c]
N-155-31A	31500	449.0	0.80	0.146, T	0.067, M	...	...	0.213	50% I
N-155-40A	19000	91.8	∞	0.019, T[d]	0.205, T	...	...	0.224	...
N-155-39A	18000	148.0	∞	0.024, T[d]	0.201, T	...	...	0.225	...
N-155-23A	20000	363.9	0.0	0.031, I	0.134, M	0.055, I	...	0.220	50% I
N-155-8A	28125	65.8	0.25	0.189, M	0.024, I	...	...	0.213	10% I[c]
N-155-10A	25200	43.4	0.80	0.122, T	0.083, M	...	...	0.205	10% I
N-155-5[e]	54500	66.4	0.16	0.022, I	0.064, T	0.058, M	0.072, I	0.216	...
N-155-4[e]	62000	7.4	0.32	0.068, T	0.042, M	0.104, I	...	0.214	...
N-155-25[e]	72000	0.23	0.53	0.068, T	0.068, M	0.070, I	...	0.206	...
N-155-19[e]	30500	30.3	0.33	0.140, T	0.053, M	0.026, I	...	0.218	...
N-155-23[e]	38000	1.07	0.65	0.128, T	0.086, M	...	...	0.214	...
N-155-24B	50000	149.1	0.0	0.031, I	0.134, M	0.055, I	...	0.220	50% I
N-155-30B	40000	1145.6	0.0	... , I	...	...	...	...	Did not fail
N-155-4B	75000	6.53	0.25	0.197, M	...	...	...	0.197	50% I[c]
N-155-2B	60000	155.0	0.25	0.008, I	0.075, T	0.130, M	...	0.213	50% I[c]
N-155-19B[f]	65000	10.8	0.25	0.153, M	0.052, T	...	...	0.205	20% I[c]
N-155-21B[f]	75000	0.7	0.25	0.185, M	0.020, T	...	...	0.205	80% I[c]

[a] I = intercrystalline, T = transcrystalline, and M = mixed.
[b] Values in this column represent estimated percentages of intercrystalline fracture in mixed region.
[c] The first few crystals appeared to fail by intercrystalline fracture although the defined region is mixed.
[d] A trace of intercrystalline fracture was observed in this region.
[e] These data were contributed by F. Ver Snyder of Thomson Laboratory, General Electric Company.
[f] The notch roots of Specimens 19B and 21B were lapped and electropolished.

pears to approximate the proportional limit (26,000 psi) of N-155 at 1500 F. Since the study was rather limited, this trend might not be observed in view of the slight slope to the *S-N* curve at $A = \infty$.

Metallographic Observations. A study of the fractures of a number of specimens was made to determine the fracture mechanisms for various conditions of alternating stress to mean stress.

Each specimen was examined macroscopically to determine the origin of failure. Photomacrographs were made of the fracture surface at ×10. Sections for metallographic study were cut from the specimen along a diameter through the fracture origin perpendicular to the fracture surface. These were prepared for microscopic examination by standard techniques. The etchant comprised four parts HCl and one part HNO_3. These sections were examined under the microscope to determine types of fracture mode along the fracture surface.

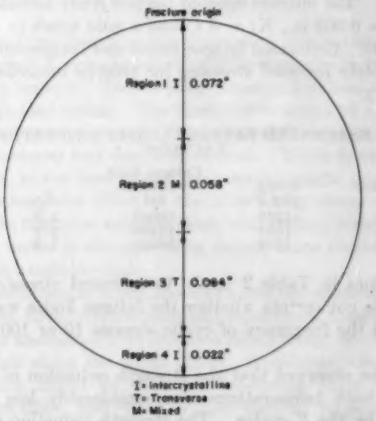

FIG. 10 SCHEMATIC DIAGRAM SHOWING THE RECOGNIZABLE REGIONS IN SPECIMEN N-155-5

Examination showed that the fractured surfaces contained regions where the fracture appeared to be intercrystalline, transcrystalline, or mixed inter and transcrystalline. Measurements were made of the extent of the distinct fracture regions along the fracture surfaces. These data are summarized in Table 3. Fig. 10 is a schematic diagram of a failed specimen surface showing the various regions and the length of each as given in Table 3. The specimen diagrammed in Fig. 10 had four distinct fracture regions, but the majority of the specimens had only two or three.

The examination also showed that specimens tested at zero mean stress failed with a transcrystalline failure over the entire surface. In stress rupture, failure was initiated as intercrystalline cracking, but the last-to-fail region at the center of the specimen was a mixture of inter and transcrystalline failure. The fracture mode at load ratios of 0.25 and 0.80 was not so clearly defined. In these specimens, failure appears to have initiated as intercrystalline cracking; however, generally within a few crystals, the fracture changed to a mixed fracture. The final failure was either intercrystalline or mixed.

It was difficult to be sure of the mode of cracking through the

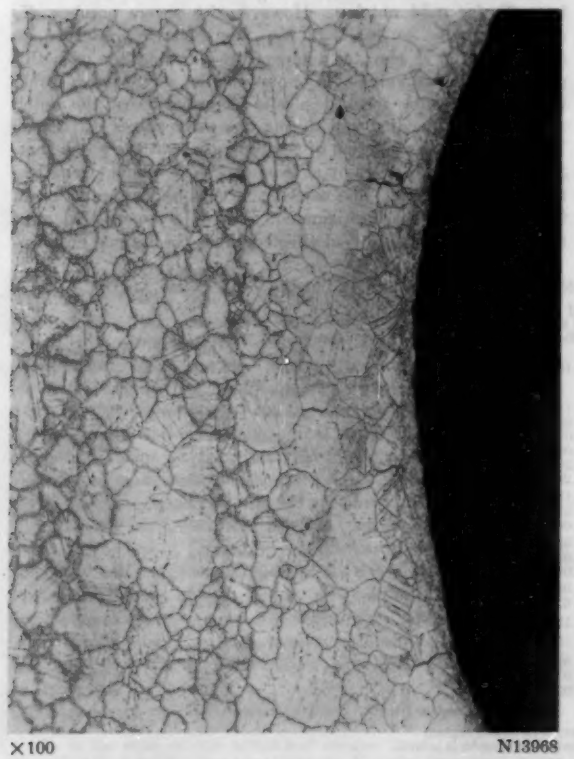

×100 N13968

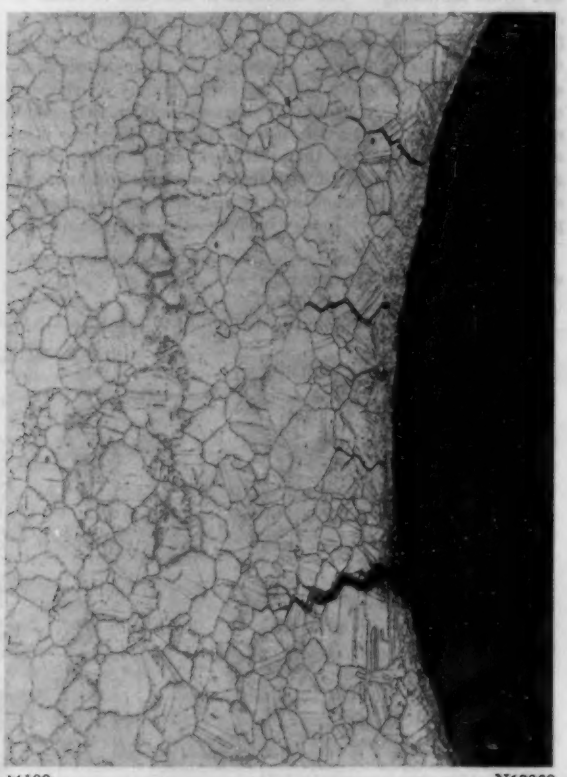

×100 N13969

FIG. 11 PHOTOMICROGRAPH OF STRESS-RUPTURE SPECIMEN N-155-30B; $r = 0.05$ IN.
(Stress, 40,000 psi; lifetime, 1145.6 hr—unruptured—1200F.)

thin recrystallized surface layer in these specimens because of its extremely fine grain size and lack of a well-defined structure. Therefore, for the specimens having a cold-worked surface, the cracks described are those observed below the recrystallized layer.

Representative photomacrographs and photomicrographs of the failures are shown in Figs. 11 through 14. Fig. 11 shows the 0.05-in-radius notched specimen tested in stress rupture at 1200 F. This specimen was unbroken but shows several incipient cracks, some of which appear to start in the cold-worked and aged zone just below the recrystallized surface layer. Similar cracks were observed in fatigue specimens N-155-2B and N-155-4B. These specimens also were tested at 1200 F and had the 0.05-in-radius notch. The appearance of cracks below the surface suggests that the cold-worked and aged surface zone might influence the observed results. This zone also can be seen in Figs. 12 and 13, which show fatigue failures of 0.005-in. notched specimens, tested at 1200 F at load ratios of $A = 0.25$ and $A = \infty$.

The effect of the cold-worked and aged zone on the fatigue results was studied to a limited extent at 1200 F with specimens having a 0.05-in. radius, notched-lapped and electropolished as described in a previous section. Tests were made at load ratios of 0.25 and 0.80. Fig. 14 shows the failure in lapped and electropolished specimen N-155-21B. Adjacent to the origin of failure, two incipient intercrystalline cracks can be seen which leave no doubt as to the mode of the initial cracking in this specimen. Similar intercrystalline cracking was also observed in the lapped and electropolished specimen N-155-19B.

S-N curves for the lapped and electropolished specimens are shown in Fig. 15, together with the curves for unpolished specimens. The data were not extensive enough for more than an estimate of the position of the curves to be made. However, it appears that elimination of the surface-worked zone tended to decrease the lifetime at high stress and increase the lifetime at lower stress levels. This infers that greater notch strengthening would have been observed with carefully lapped and electropolished notches in the lower stress levels which would be of engineering importance.

Conclusions

For the range of root radii and notch severity studied, the following conclusions appeared warranted on the basis of this investigation:

1 N-155 alloy is notch-strengthened to some extent in fatigue for low load ratios. The observed strengthening depends upon notch severity, load ratio, temperature, and time. It appears that greater strengthening is associated with larger radii notches, higher temperatures, and longer exposure times.

2 The effect of a notch on the fatigue behavior of N-155 at high load ratios is detrimental. The detrimental effect is influenced, particularly by notch severity, stress redistribution, which occurs during the early stages of fatigue, and temperature.

3 Some speculations with regard to the observed behavior of notched N-155 alloy have been made. It appears that a rational explanation of notch-bar strengthening in fatigue may be based on notch geometry, creep or relaxation behavior, and ductility; however, strain hardening and other metallurgical changes induced by cyclic stress also may be important factors. Studies of other materials might provide data upon which assessment of the effects of these factors could be made.

Acknowledgment

The material used in this program was manufactured by Universal-Cyclops Steel Corporation and was donated by the Cor-

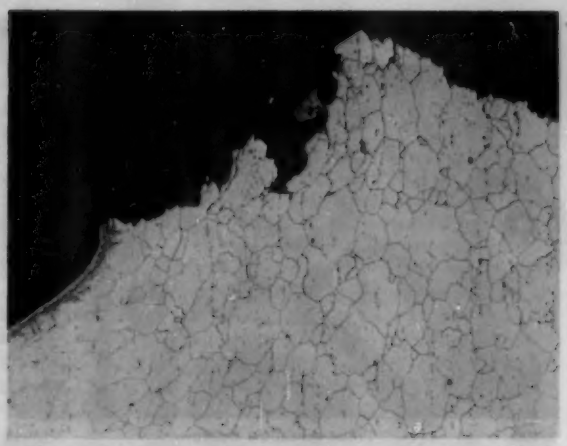

×100 Fracture origin N13942

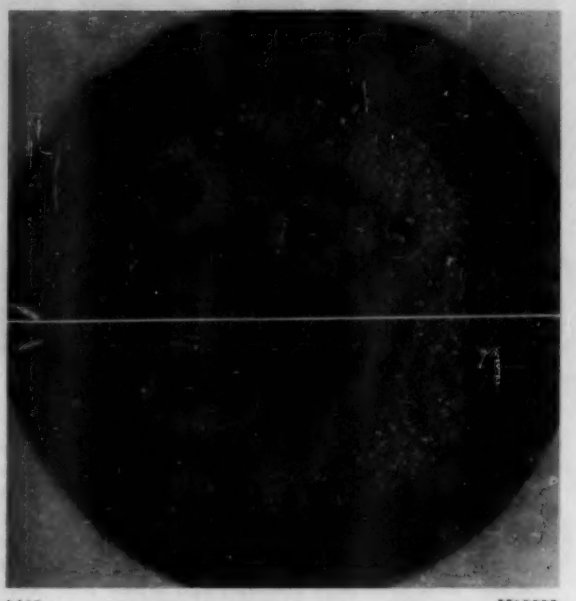

×10 N13538

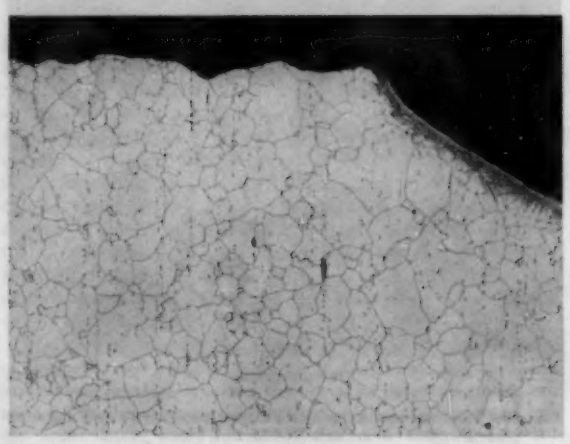

×100 Transcrystalline fracture N13943

Fig. 12 (*Right*) Photomacrograph and Photomicrographs of Fracture of Fatigue Specimen N-155-3A; $r = 0.005$ In. (Maximum stress, 62,500 psi; $A = 0.25$; lifetime, 543,100 cycles, 1200 F.)

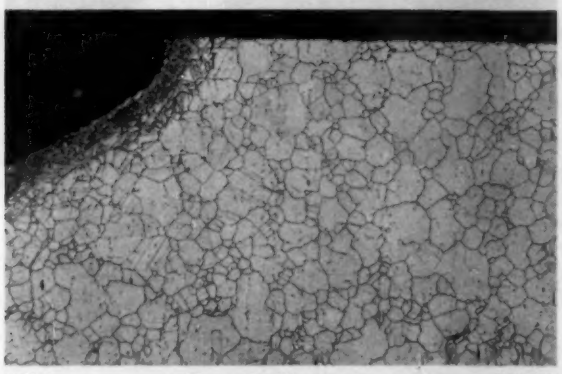

×100 Transcrystalline fracture N15946

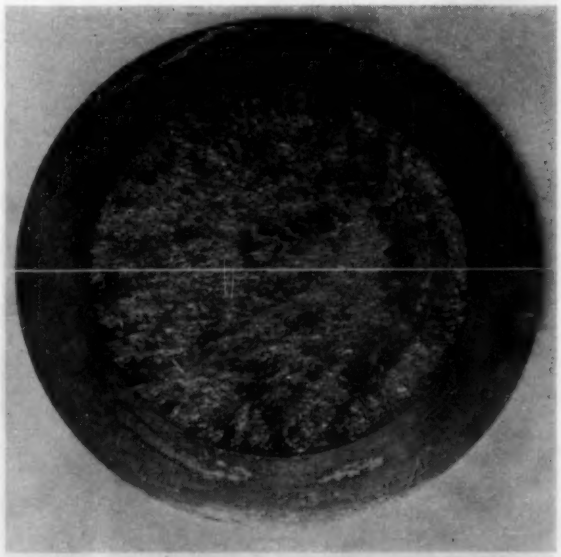

×10 N15772

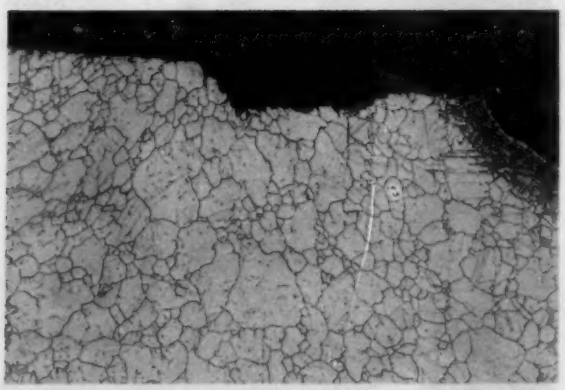

×100 Fracture origin N15945

FIG. 13 PHOTOMACROGRAPH AND PHOTOMICROGRAPHS OF FRACTURE OF FATIGUE SPECIMEN N-155-40A; r = 0.005 IN.
(Maximum stress, 19,000 psi; A = ∞; lifetime, 825,000 cycles; 1200 F.)

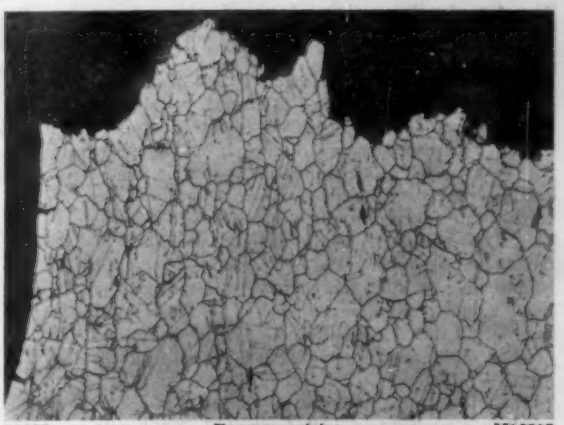

×100 Fracture origin N16313

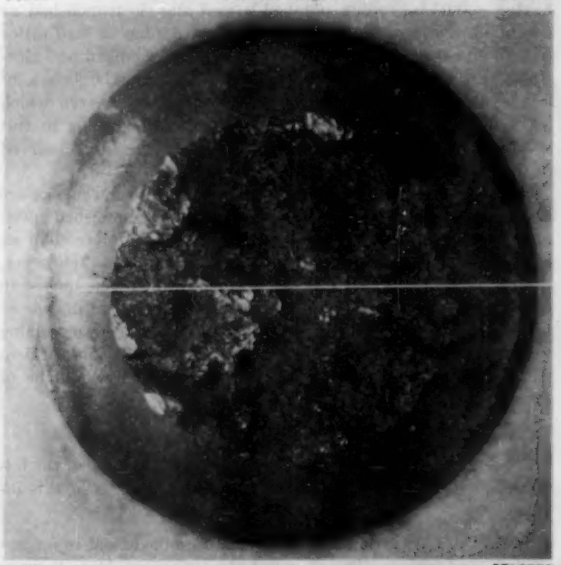

×10 N16235

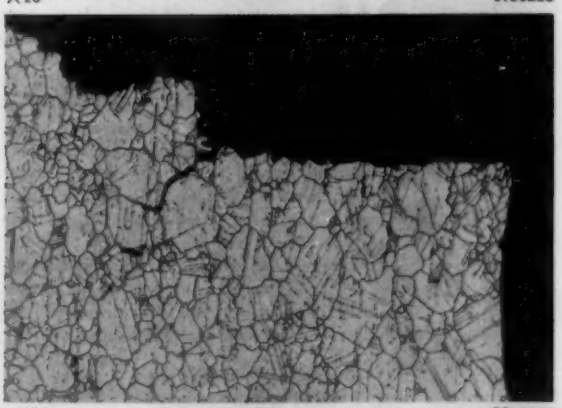

×100 Transcrystalline fracture N16312

FIG. 14 PHOTOMACROGRAPH AND PHOTOMICROGRAPHS OF FRACTURE OF FATIGUE SPECIMEN N-155-21B; r = 0.05 IN.; LAPPED AND ELECTROPOLISHED
(Maximum stress, 75,000 psi; A = 0.25; lifetime, 62,500 cycles; 1200 F.)

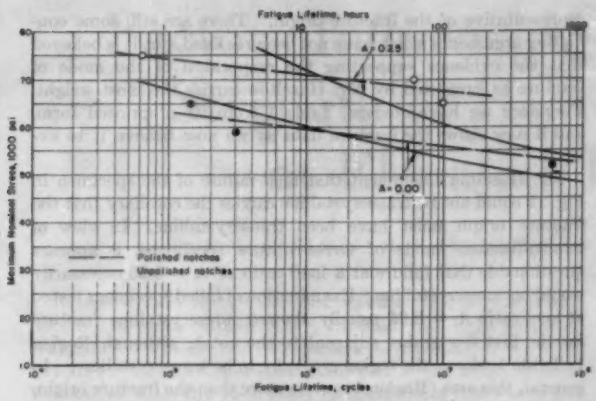

FIG. 15 EFFECT OF SURFACE PREPARATION ON BEHAVIOR OF NOTCHED SPECIMENS OF N-155 AT 1200 F

poration. The program was sponsored by the ASTM-ASME Joint Committee on the "Effect of Temperature on the Properties of Metals." It was initiated by a subgroup of the Gas-Turbine Panel of the Joint Committee. The authors wish to thank the various members of the Gas-Turbine Panel who contributed helpful suggestions on this investigation.

BIBLIOGRAPHY

1 "Effect of Notch Geometry on Rupture Strength at Elevated Temperatures," by E. A. Davis and M. J. Manjoine, Symposium on Strength and Ductility of Materials at Elevated Temperatures, American Society for Testing Materials, Special Technical Publication No. 128, 1952, pp. 67–87.

2 "Influence of Sharp Notches on the Stress-Rupture Characteristics of Heat-Resisting Alloys: Part II," by W. F. Brown, M. H. Jones, and D. P. Newman, Proceedings of the American Society for Testing Materials, vol. 53, 1953, pp. 661–677.

3 "Factors Influencing the Notch-Rupture Strength of Heat-Resistant Alloys at Elevated Temperatures," by R. L. Carlson, R. J. MacDonald, and W. F. Simmons, published in this issue, pp. 349–358.

4 "Dynamic Creep and Rupture Properties of Temperature-Resistant Materials to Tensile Fatigue Stress," by B. J. Lazan, Proceedings of the American Society for Testing Materials, vol. 49, 1949, pp. 757–787.

5 "Effect of Pulsating Loads on the Creep Characteristics of Aluminum Alloy 14S-T," by M. J. Manjoine, Proceedings of the American Society for Testing Materials, vol. 49, 1949, pp. 788–798.

6 "Effect of Tensile and Compressive Fatigue Stress on Creep, Rupture, and Ductility Properties of Temperature Resistant Materials," by B. J. Lazan and E. Westberg, Proceedings of the American Society for Testing Materials, vol. 52, 1952, pp. 837–854.

7 "Elevated-Temperature Fatigue Properties of SAE 4340 Steel," by W. J. Trapp and R. T. Schwartz, WADC TR 52-325, part 1, December, 1952.

8 "Cooperative Investigations of Relationship Between Static and Fatigue Properties of Heat-Resistant Alloys at Elevated Temperatures," NACA Subcommittee on Heat-Resisting Materials, NACA Research Memorandum 51AO4, March 7, 1951.

9 "Investigation of Torsion Creep to Rupture Properties of N-155 Alloy," by C. W. MacGregor and F. J. Walcott, Jr., NACA Research Memorandum 51EO4, August 21, 1951.

10 "Tension Properties of Aluminum Alloys in the Presence of Stress Raisers," by E. L. Aul, A. W. Dana, and G. Sachs, NACA Technical Notes Nos. 1830 and 1831, 1949.

11 "Theory of Notch Stresses," by H. Neuber, J. W. Edwards, Ann Arbor, Mich., 1946.

Discussion

W. S. HAZELTON.[7] Investigations of the behavior of materials similar to those reported in this paper are of great importance and, in particular, more attention should be paid to the study of fracture mechanisms.

In the analysis of the fractures reported here, there is some question about the determination of the fracture progression. For example, the writer is concerned about Fig. 12. It would seem that the failure might start either transcrystalline or intercrystalline, but at a stress ratio of 0.25 the final rupture could hardly have been transcrystalline. Therefore he raises the question whether in this case the fracture origin was not around the circumference in the transcrystalline zone, progressing more rapidly around the outside than toward the center. This would make the last section to fail the mixed torn zone shown in the paper by the photomicrograph N-13942, and labeled "fracture origin."

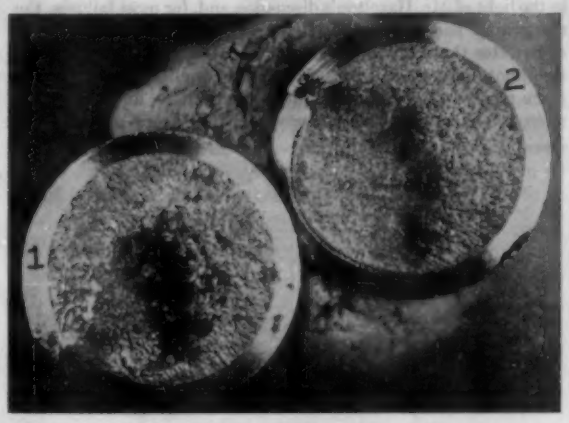

FIG. 16 PHOTOMACROGRAPH OF FRACTURED BOLTS

In this connection we have had some experience with bolt failures that show this fracture progression. In the macrograph shown in Fig. 16, herewith, are the fractures of two bolts from the same assembly. At reassembly of this part after engine running, one of the bolts failed during torquing. The rest of the bolts were inspected and found to be cracked. One of the cracked bolts was broken open to check on the appearance of the fracture. These bolts were of high-expansion steel, AMS 5624, were subjected to a rather high steady load from torquing and, in addition, were subject to an axial vibratory load. The temperature was rather low, however, not over 400 F. Because we had several bolts that had not failed, but which had cracks of varying severity, the mechanism of failure and mode of progression could be definitely established. The cracks started in several places around the circumference, at the root of the threads, and before they had progressed very far inward, had rapidly extended circumferentially to join in one crescent-shaped crack. This continued to progress around the outside and inward, until in the case of the failed bolt (No. 1) it extended almost completely around the outside. The bolt that was intentionally broken open (No. 2) was similar, although it seems to have progressed across the section relatively more rapidly than in the first case. The distinct crescent-shaped zone of transcrystalline failure is still clearly marked.

The marked similarity between the fractures shown in Fig. 12 of the paper and bolt No. 1 shown in Fig. 16 of this discussion makes one question whether the fracture progression was not similar. It also seems improbable that with a stress ratio of 0.25 the final rupture could be transcrystalline, as suggested by the authors. We are doing some similar work at the AGT Division

[7] Section Engr., Appl. & Dev. Section, Engineering Department, AGT Division, Westinghouse Electric Corporation, Kansas City, Mo.

of Westinghouse and are trying to determine the mechanism of fracture origination by studying specimens before they have been completely broken. By this approach we can tell with certainty where, and by what mechanism, the cracks initiate, and in what manner they progress. We feel this understanding is very important for the proper analysis of service failures.

Authors' Closure

The authors wish to thank Mr. Hazelton for his enlightening and appropriate discussion. The analysis of fractures, particularly those involving relatively large stress concentrations, as in in bolts or notched specimens, has not received attention commensurate with its importance; therefore Mr. Hazelton's comments regarding his experience are most welcome.

We have re-examined the fatigue failures reported in our paper, in the light of Mr. Hazelton's discussion and, for most failures, the reappraisal has resulted in a reversal of our concept of what constitutes the origin and final-failure areas. Thus, in Fig. 12, the photomicrograph marked fracture origin is now thought to be representative of the point of final failure, and the photomicrograph showing the transcrystalline fracture is considered representative of the fracture origin. There are still some conflicting arguments which have not been resolved, but it is believed that the evidence supporting the reappraisal of the mode of fracture as suggested by Mr. Hazelton carries the most weight. Therefore we have revised Table 1 from its preprinted form, and it now shows the fracture data as we now believe it to exist.

Mr. Hazelton's comment that final failure of the specimen in Fig. 12 could not be transcrystalline carries the corollary that the fracture origin must have been transcrystalline. In view of known-fracture mode of stress-rupture specimens, it appears questionable that failure at a load ratio of $A = 0.25$ necessarily would be transcrystalline. Examination of failed specimens tested at load ratio $A = 0.25$ usually showed intercrystalline fracture for the first few grains adjacent to the notch, although Region 1, Table 1, shows the region generally to be transcrystalline. In general, this area (Region 1) covers more than the fracture origin. It appears that the fracture mechanism, both initiation and propagation, are particularly complex. Additional studies of this nature certainly are needed, both from the standpoint of fatigue specimens as well as of parts which have failed in service.

Factors Influencing the Notch-Rupture Strength of Heat-Resistant Alloys at Elevated Temperatures

By R. L. CARLSON,[1] R. J. MACDONALD,[2] AND W. F. SIMMONS,[3] COLUMBUS, OHIO

Stress-rupture tests were conducted on notched and unnotched or plain bars of S-816, Inconel "X" Type 550, and Waspaloy alloys at test temperatures ranging from 1200 to 1600 F. The notched specimens had 50 per cent, 60-deg, V-notches with the root radii ranging from 0.005 to 0.100 in. In some tests, as many as three notches of different root radii were used. The test results indicated that S-816 alloy was notch-strengthened by all of the notches used in the temperature range from 1350 F to 1600 F. Inconel "X" Type 550 was always notch-strengthened by all of the notches only at the test temperature of 1600 F. Waspaloy was always notch-strengthened by all notches only at the temperature of 1500 F. Both Inconel "X" Type 550 and Waspaloy could be notch-strengthened for some test conditions (notch sharpness and time) at temperatures below 1600 and 1500 F, respectively. Factors considered to have an influence on stress-rupture behavior have been studied and the results are included. The factors investigated are notch geometry, notched and unnotched ductility, the modes of deformation and fracture, metallurgical changes, and surface condition. The influence of some of these factors can vary considerably from alloy to alloy. It does not appear possible, therefore, to evaluate completely the notch and unnotched stress-rupture behavior of a given alloy by any simple method. Rather, an evaluation should be based upon the combined consideration of those factors that are influential in each individual case.

Introduction

In recent years the use of metal parts at high operating temperatures has increased the number of problems confronting the designer. If he is to achieve efficient design, he must have a method of interpreting available data in such a fashion as to guide his design. The data that he will have often consist of stress-rupture tests on unnotched and, perhaps, notched bars. Although these tests reflect the creep behavior of the respective metals and, in some instances, their susceptibility to embrittlement, their relation to the information that the designer wants is not immediately obvious.

In the program summarized by this paper, three heat-resisting alloys were studied—S-816, Inconel "X" Type 550, and Waspaloy. One of the objectives was to learn under what test conditions these materials respond in a brittle manner, i.e., are notch-sensitive. A second objective was to study some of the factors that have an influence on notched and unnotched stress-rupture behavior.

The usual interpretation of notched-bar behavior is based on a consideration of the stress distribution resulting from the notch geometry and the available ductility of the bar material. If a notched bar of a given material ruptures at an average stress that is greater than the stress necessary to cause rupture in an unnotched bar of the same material, the material is said to be notch-strengthened.

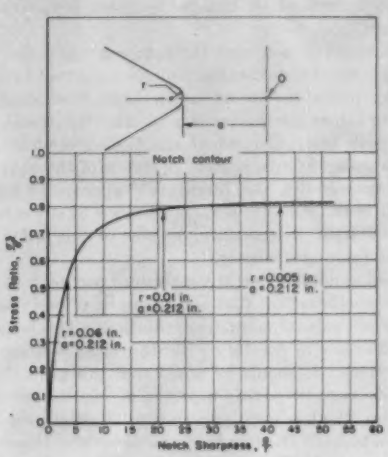

Fig. 1 Effect of Notch Sharpness on Triaxiality at Center (Point 0)

For notch strengthening to occur, it is necessary that sufficient ductility be available to relieve the stress concentration at the base of the notch. Strengthening can then result from the triaxial tensile-stress state retained. In the case of notched bars, a hydrostatic tension is only approached. How closely it is approached in a given specimen depends on the notch geometry. Fig. 1 (Fig. 11 in reference 1)[4] illustrates the variation of triaxiality at the center of infinitely deep notches with various notch sharpnesses. In the graph, the maximum and minimum normal stresses are designated as σ_1 and σ_3, respectively. The ratio σ_3/σ_1 is, therefore, an index of how closely a hydrostatic tension is approached, i.e., for a hydrostatic tension, $\sigma_3/\sigma_1 = 1$.

Although Neuber's equations, used to obtain the graph of Fig. 1, are not exactly applicable to the notches used in this investigation, they should describe the existing trends. For this reason, the notch-sharpness ratios for three of the notch radii

[1] Assistant Chief, Metallurgical Engineering Division, Battelle Memorial Institute.

[2] Principal Metallurgist, Metallurgical Engineering Division, Battelle Memorial Institute.

[3] Assistant Chief, High Temperature Metals Research Division, Battelle Memorial Institute.

Contributed by the joint ASTM-ASME Committee on Effect of Temperature on the Properties of Metals and presented at the Annual Meeting, New York, N. Y., November 28–December 3, 1954, of The American Society of Mechanical Engineers.

Note: Statements and opinions advanced in papers are to be understood as individual expressions of their authors and not those of the Society. Manuscript received at ASME Headquarters, November 9, 1954. Paper No. 54—A-240.

[4] Numbers in parentheses refer to the Bibliography at the end of the paper.

used have been indicated. As can be seen, the triaxial ratio σ_3/σ_1 changes markedly with changing a/r only for $a/r < 15$.

The foregoing discussion did not include a mention of the effects of creep. Creep is a time-dependent deformation, and it can be expected to help relieve local stress concentrations. In essence, the stress at the base of the notch can be expected to undergo relaxation. The maximum shear stress at each point in the neck of the notched bar will undergo readjustment. In order for each element of material to remain compatible or to "fit," it must be expected that the higher shear stresses will be decreased or relaxed (the external load remains constant), and the lower shear stresses will have a tendency to increase. The general tendency will be for a smoothing or leveling of the shear stresses governing flow. Since it would be expected that some of the initial triaxiality in the core of the notch would be retained, the maximum shear stresses in the core would tend to be less than those in an unnotched bar under the same average axial stress. This behavior presupposes the ability of the bar material to flow and to readjust as just described. In this investigation, the test bars of S-816 alloy were notch-strengthened at all test conditions, so it can be presumed that adequate flow was available. The two remaining alloys, Inconel "X" Type 550 and Waspaloy, were notch-sensitive for some test conditions and notch-strengthened for others. With regard to "available ductility," these alloys might be considered borderline cases. As such, they are strongly influenced by changes in notch geometry and test temperature.

It is of interest to note that the notch-strengthening index, as reflected by the notched-rupture-stress to unnotched-rupture-stress ratio, probably has an upper limit that would be approached for high notch sharpness in metals with enough available ductility (both time-independent and time-dependent ductility) to take advantage of triaxiality. A review of the data obtained and that available in the literature[2,3] appears to indicate an upper limit in the vicinity of 1.7. In terms of stress redistribution and retention of triaxiality, a value of this order probably represents a limiting efficiency.

In discussing notched-bar stress-rupture results, it is pertinent to consider another effect that appears to be of basic importance in so far as understanding fracture initiation. This behavior consists of a decrease in ductility with decreasing average stress or increasing time. It should be noted that this general tendency has been observed frequently in the past. In the results of this investigation, the tendency appeared to be most pronounced in what are considered the two least ductile of the three test materials—Inconel "X" Type 550 and Waspaloy. It was observed also that the amount of decrease in ductility for each material becomes larger with increasing test temperature. Although this tendency toward "embrittlement" might be attributed to a metallurgical change, this may be only a partial explanation. A discussion of metallurgical changes in the alloys studied is given in the section of the paper on Microstructure Studies.

Zener (4) has suggested an explanation for this behavior that is based on possible differences in the modes in which deformation can occur. He maintains that, during creep at elevated temperatures, shear stresses along grain boundaries are relaxed by slip along the boundaries. Because relative slip with respect to the corners at which three grains meet is not possible, there is a tendency for the relaxed load to shift to these sites. According to Zener, high hydrostatic tensions can be developed, and these can be responsible for the initiation of cracks. He then goes on to state that, at low-load conditions, for which large plastic deformation within the grains is not possible, the formation of cracks, according to the mechanism described, is responsible for low ductility at low-load creep conditions.

Perhaps the major importance of this explanation is the fact that it focuses attention on the importance of different possible modes of deformation. The role of the grain boundary need not, perhaps, be restricted to the interior as just indicated. It is conceivable, for example, that particular orientations of grain-boundary surfaces intersecting the specimen surface may create conditions favorable for the formation of a crack. (Figs. 14 and 15 of cracked notched bars suggest this possibility.)

It should be noted that Brown, et al. (2), have suggested that a precipitation mechanism is responsible for the reduction in ductility mentioned. Although this can be a contributing factor (see Microstructure Studies), the evidence supporting it is not complete. It is entirely possible, of course, that both of the foregoing explanations are influencing factors whose relative importance is determined by the material and test conditions.

Using either of these explanations, it is possible to describe cases in which the ratio of notched to unnotched strength decreases with increasing time as being instances in which the stress concentration at the base of the notch had not been relieved by flow. For a given average stress, the stress concentration in the notched bar makes it more susceptible to the formation of cracks resulting from the reduction in ductility. For materials that are weakened by such a loss of ductility, the notched-rupture test appears to be, for this reason, a more sensitive indicator than the unnotched-rupture test.

During the course of this investigation, it became apparent that the condition of the surface layer of material at the base of the notch might be an important factor in notched-bar behavior. Since multiple-notch specimens were used, it was possible in many instances to inspect cracks that were initiated in the unruptured notches. As all of the cracks inspected initiated at or near the surface, near the base of the notch, it was felt that the condition of the surface could be a factor of importance in notch behavior. An inspection of the notches indicated that, for all of the test materials, the cold-worked surface layer was subject to precipitation or recrystallization at some of the test temperatures.

Test Material

The three heat-resistant alloys selected for this investigation were S-816, Waspaloy, and Inconel "X" Type 550. S-816 and Waspaloy alloys were melted and processed by Allegheny Ludlum Steel Corporation, and Inconel "X" Type 550 was melted and processed by The International Nickel Company. The chemical compositions of the three alloys are given in Table 1.

Specimen blanks of the S-816 bar stock were heat-treated by heating at 2150 F for 1 hr and quenching in water, followed by aging at 1400 F for 12 hr and air-cooling.

The specimen blanks of Waspaloy were heat-treated by heating 4 hr at 1975 F and air-cooling, stabilizing 4 hr at 1550 F, and aging for 16 hr at 1400 F.

TABLE 1 CHEMICAL COMPOSITIONS OF ALLOYS TESTED

	Chemical composition, per cent		
Element	S-816 (Heat 03730)	Waspaloy (Heat 44036)	Inconel "X" Type 550 (Heat Y-7180-X)
C	0.38	0.08	0.05
Mn	1.22	0.80	0.73
Si	0.49	0.61	0.28
P	0.012	0.017	...
S	0.018	0.017	0.007
Cr	20.04	18.72	14.97
Ni	19.43	Bal	Bal
Mo	3.98	2.93	...
W	3.93	...	...
Cb	2.89	...	1.03[a]
Co	43.32	13.44	...
Fe	3.44	1.17	6.59
Al	...	1.29	1.16
Ta	0.85	...	...
Ti	...	2.29	2.5
Cu	...	0.10	0.03

[a] Cb + Ta.

Specimen blanks of Inconel "X" Type 550 bar stock were heat-treated by heating at 2150 F for 1 hr and air-cooling, followed by 4 hr at 1600 F and 4 hr at 1350 F.

Rupture Specimens and Test Procedure

Conventional creep-rupture tests were made on plain and notched bars to obtain data out to approximately 1000-hr rupture life. The types of test specimen used are shown in Fig. 2. The multiple-notch specimens were used to get a maximum of information from one test. All specimens had a constant shank diameter of 0.600 in. and a notch-root diameter of 0.424 in. ($d/D = 0.707$), giving a 50 per cent reduction of area. The plain specimen had a diameter of 0.424 in., the same as the notch-root diameter of the notched bars, and a 2-in. gage length. All notches were machined by grinding, and the root radii used in the various specimens are given in Table 2.

TABLE 2 ROOT RADII USED IN NOTCHED SPECIMENS, IN.

Alloy	Triple-notch specimen	Double-notch specimen	Single-notch specimen
S-816	0.005 0.010 0.060	...	...
Waspaloy	0.005 0.040 0.100	0.040 0.100	0.020 and 0.100
Inconel "X" Type 550	0.005 0.045 0.100	0.045 0.100	0.020 and 0.100

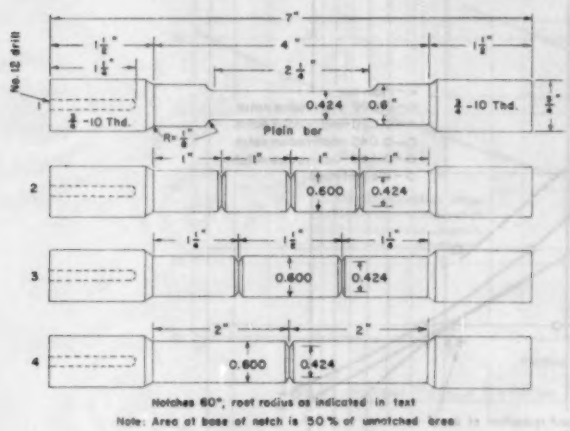

Fig. 2 Plain and Notched Test Specimens

Not all the test specimens were heat-treated and machined at one time, because it was not known at the beginning of the program what heat-treatments or notches would be desired before the program was completed. However, the specimens were quite uniform, with the exception of the last lot of Inconel "X" Type 550. Data from these specimens, shown as dashed lines in Figs. 4 and 5, in general, showed more scatter and lower notch-rupture strengths (at the shorter times) than for specimens from the first lot. Hardness measurements indicated that the second lot of specimens had a somewhat higher hardness than the first lot (108.1 and 101.2 Rockwell B). Since the machining procedure was the same for all specimens, it is probable that the difference between the two lots was the result of an undetected variation in the heat-treatment.

The procedure followed in carrying out the rupture-evaluation program was first to obtain plain-bar rupture data for times out to approximately 1000 hr as a basis for comparison. A series of notched-bar rupture tests was then made on all three alloys using the triple-notch specimen. The alloys that exhibited notch sensitivity in these tests were then tested at the temperatures where notch sensitivity was observed using the double-notch specimen with its coarser notches. These tests were followed by tests on single-notch specimens having the coarsest notch of 0.100 in. radius, or the intermediate notch of 0.020 in. radius.

Test Results

S-816 Alloys. Creep-rupture tests were made on plain and notched specimens of S-816 alloy at 1350, 1500, and 1600 F. Since rupture could occur in any one of the three notches, symbols were used in the figures to indicate which notch failed.

Fig. 3 shows the curves of stress versus rupture time for both the plain and the notched bars of S-816 alloy. Since S-816 alloy was relatively insensitive to the various notches, the rupture curves were drawn through the points of rupture, regardless of which notch ruptured. S-816 alloy was notch-strengthened at all temperatures, and most failures occurred in the less severe notches.

Since S-816 alloy exhibited notch strengthening in all three notches at all test temperatures, only the triple-notch specimen was used, and detailed data were not determined for each notch.

Hardness measurements were made on several of the tested specimens after exposure to the test temperature for times up to approximately 1000 hr. No significant changes in hardness were observed.

Inconel "X" Type 550. Creep-rupture tests were made at 1350, 1500, and 1600 F on plain and notched specimens of

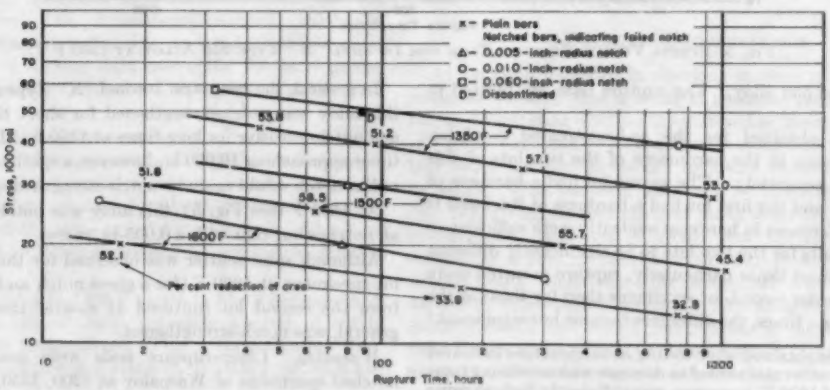

Fig. 3 Stress Versus Rupture-Time Curves for Plain and Notched Bars of S-816 Alloy

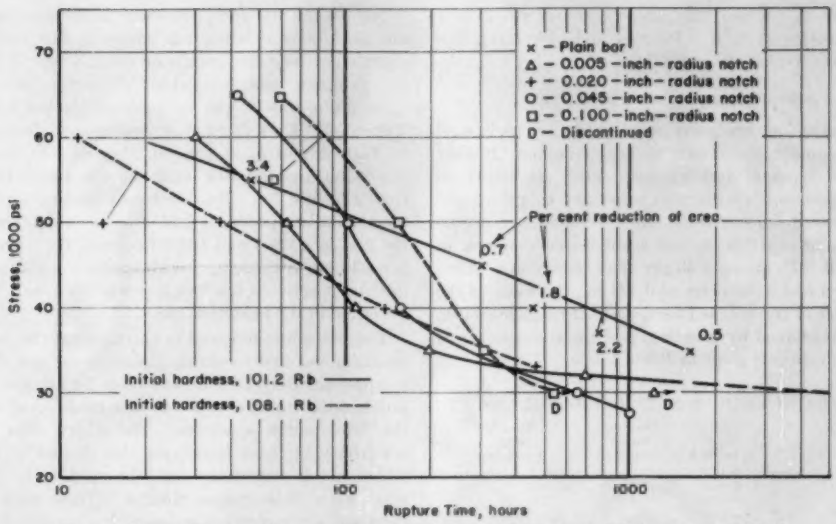
x – Plain bar
Δ – 0.005 – inch – radius notch
+ – 0.020 – inch – radius notch
○ – 0.045 – inch – radius notch
□ – 0.100 – inch – radius notch
D – Discontinued
Per cent reduction of area
Initial hardness, 101.2 Rb
Initial hardness, 108.1 Rb
Stress, 1000 psi
Rupture Time, hours

FIG. 4 STRESS VERSUS RUPTURE TIME FOR INCONEL "X" TYPE 550 ALLOY AT 1350 F

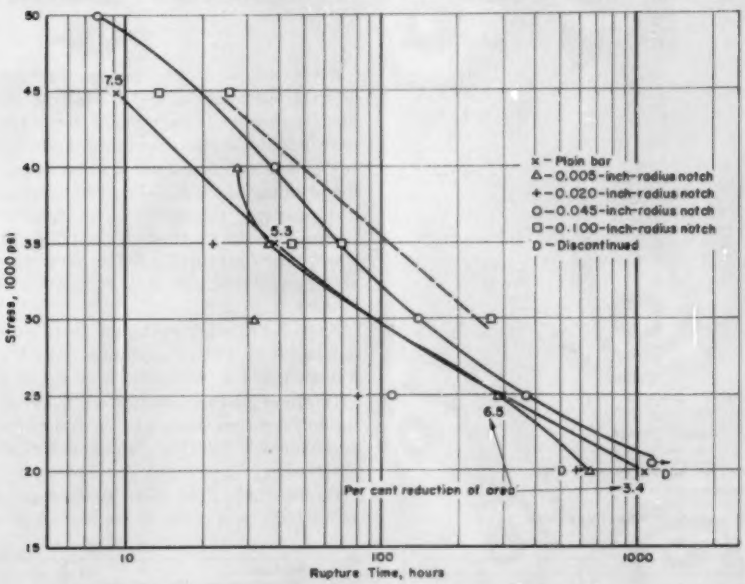
x – Plain bar
Δ – 0.005 – inch – radius notch
+ – 0.020 – inch – radius notch
○ – 0.045 – inch – radius notch
□ – 0.100 – inch – radius notch
D – Discontinued
Per cent reduction of area
Stress, 1000 psi
Rupture Time, hours

FIG. 5 STRESS VERSUS RUPTURE TIME FOR INCONEL "X" TYPE 550 ALLOY AT 1500 F

Inconel "X" Type 550 alloy. The rupture data are plotted in Figs. 4, 5, and 6.

Hardness data obtained for the as-heat-treated condition indicated a difference in the hardnesses of the two lots of this alloy heat-treated separately. The second lot had a hardness of Rockwell B 108.1 and the first lot had a hardness of Rockwell B 101.2. These differences in hardness evidently were sufficient to cause the test results for the two lots to be significantly different at 1350 F. For short times particularly, rupture occurred more quickly for the harder second-lot specimens than for those of the first lot. For longer times, the difference became less significant.[6]

[6] Hardness values obtained after testing at temperature indicated that hardness differences also tended to decrease with increasing time. The temperature of 1600 F, moreover, was sufficiently high to cause the hardness difference to decrease after only a short-time exposure.

In general, the results on Inconel "X" Type 550 indicated that this alloy was notch-strengthened for short times (see Fig. 4), and notch-sensitive for long times at 1350 F. It appears that, for times approaching 10,000 hr, however, a specimen with a 0.005-in-radius notch would again be notch-strengthened.

At 1500 F (see Fig. 5), this alloy was notch-strengthened for all notches but that with a 0.005-in. radius.

Although some scatter was observed for the first and second-lot specimens at 1600 F (for a given notch and stress, specimens from the second lot ruptured at shorter times), the alloy, in general, was notch-strengthened.

Waspaloy. Creep-rupture tests were made on plain and notched specimens of Waspaloy at 1200, 1350, and 1500 F, and the rupture data are plotted in Figs. 7, 8, and 9.

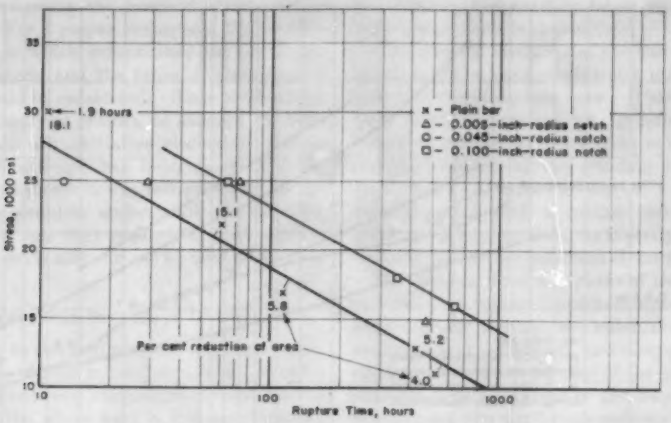

FIG. 6 STRESS VERSUS RUPTURE TIME FOR INCONEL "X" TYPE 550 ALLOY AT 1600 F

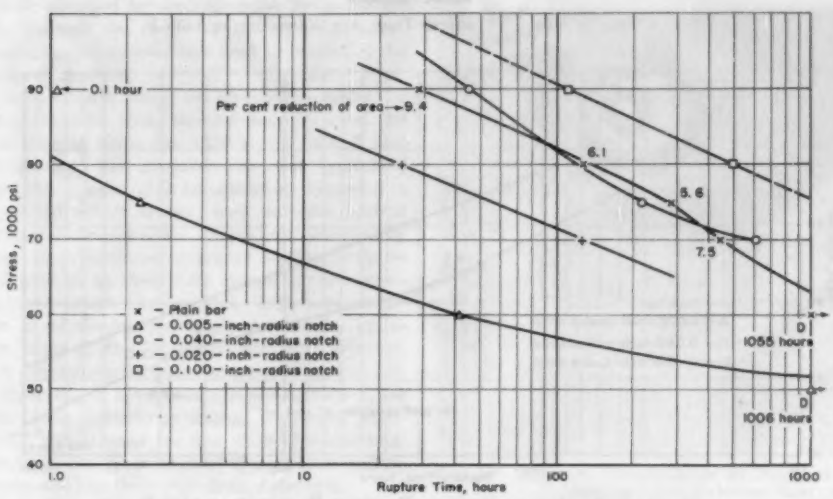

FIG. 7 STRESS VERSUS RUPTURE TIME FOR WASPALOY AT 1200 F

The plain and notched-bar rupture data for Waspaloy at 1200 F are shown in Fig. 7. The 0.005-in-radius-notch specimens were very notch-sensitive. The 0.020-in-radius-notch specimens were considerably less notch-sensitive, and the 0.040-in-radius-notch specimens gave rupture data essentially the same as the plain bars. The specimens with the 0.100-in-radius notch were notch-strengthened.

Fig. 8 shows the stress versus rupture-time curves for Waspaloy at 1350 F. At this temperature, the 0.005-in-radius notch was still producing notch-sensitive rupture results, but only slightly so, and the rupture data for the 0.020-in-radius-notch specimens were about the same as for the plain bars. The data for the 0.040 and 0.100-in-radius-notch specimens showed notch strengthening.

The data for Waspaloy at 1500 F shown in Fig. 9 indicate that all three notches produced about the same amount of notch strengthening at this temperature. This is an indication that Waspaloy is insensitive to notch severity, at 1500 F, at least for the notches studied.

It is apparent from the data obtained on Inconel "X" Type 500 and Waspaloy that notch-sensitivity is a function of notch geometry, temperature, and time.

DUCTILITY CONSIDERATIONS

As has been indicated in previous sections of this paper, the available ductility that a material possesses plays an important role in determining whether the material is "notch-strengthened" or "notch-sensitive." It is natural, then, that the question of how much ductility is enough to insure "notch-strengthening" be asked. This has been answered, at least, by Brown, et al. (2). They suggest that the best index is given by the notched-bar ductility (reduction of area). For the alloys which were studied as a part of their investigation, it was observed that notch-rupture sensitivity was associated with notch-rupture ductilities of less than 3 per cent. This value refers to the sharp notch utilized, and would not necessarily be expected to be valid for markedly different notches. Since, however, the sharp-notch ductility requirements are much greater than those of significantly less sharp notches, the use of sharp notches can be considered as a severe screening test.

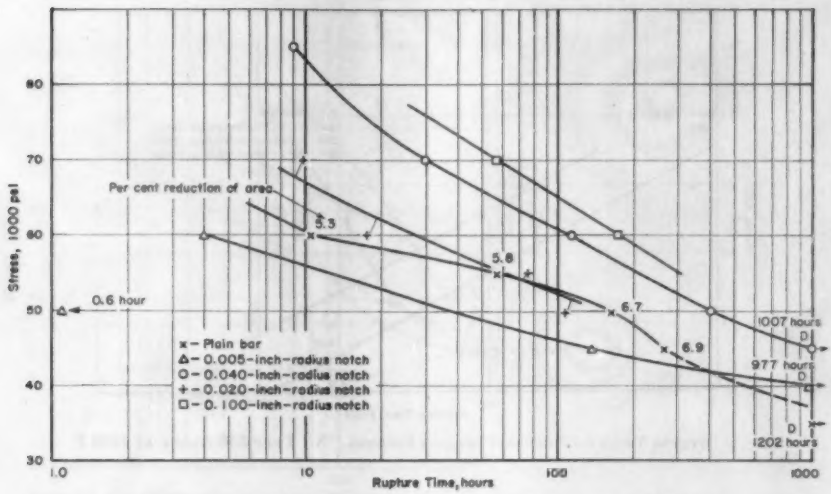

FIG. 8 STRESS VERSUS RUPTURE TIME FOR WASPALOY AT 1350 F

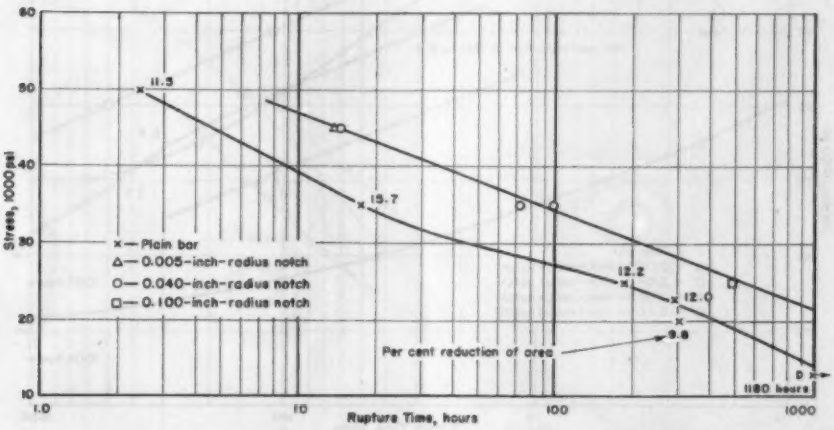

FIG. 9 STRESS VERSUS RUPTURE TIME FOR WASPALOY AT 1500 F

For design interests, it should be noted, however, that some value is to be derived from the use of notches of more than one sharpness. As has been indicated by Davis and Manjoine (3), the designation of an alloy as notch-sensitive is arbitrary when judged on the basis of results for only one notch sharpness. They observed that, for a given time, an alloy is strengthened (the ratio of notched to unnotched-rupture strength increases) with decreasing sharpness up to a maximum value. If this ratio can become greater than unity, it ultimately decreases to unity, since a bar of zero notch sharpness is an unnotched bar.

In this investigation, it has been found that all of the alloys tested had the ability to be notch-strengthened for some of the test temperatures and notch-sharpness values used. It is also of interest to note that, at some of the test temperatures, notch-strengthening was observed for the entire time range (approximately 1000 hr), in spite of the fact that the reduction in area of the notched bar was only slightly above 1 per cent at times. The reduction in area of the unnotched bars for these temperatures was as low as 5 per cent. Thus it appears that the ductility requirements for notch strengthening can vary significantly.

As has been noted previously in this report, the problem under study is complex, and it is probable that simple rules that apply always, without reservation, can be established only if one is satisfied with a rule that is excessively conservative in some instances.

An example of this is the use of the type of design rule which indicates that an alloy should be suspected of being notch-sensitive if the unnotched reduction in area is less than 30 per cent. If one considers S-816 and Waspaloy at 1500 F, however, this is seen to be a very rough gage of notch sensitivity. At 1500 F, both of these alloys are notch-strengthened by a factor of approximately 1.2, and they appear to be relatively insensitive to differences in notch sharpness. From these facts, one would be inclined to expect an unnotched ductility in excess of 30 per cent. For S-816, this is true, since the value is of the order of 50 per cent. The Waspaloy, however, ranges in value from 10 to 16 per cent. It is apparent that the internal response to loading must be different. Another example, found in the literature (2), cites the detection of notch sensitivity in Haynes Alloy 88 at 1350 F, in spite of the fact that unnotched-rupture ductilities were as high as 60 per cent.

It is apparent, then, that ductility, as such, is not a completely

satisfactory means of evaluating the notched stress-rupture characteristics of alloys. For a proper evaluation, the contributing effects of the modes in which deformation can occur, the characteristic type of fracture, and the types of metallurgical change that can occur should be considered. Since these effects are understood only imperfectly at present, no attempt has been made in this paper to make a quantitative evaluation of their contribution. Instead, an attempt has been made to focus attention on these effects whenever it was felt pertinent to the discussion. Until a more complete understanding is possible, however, it appears that a rule that requires a notch-rupture ductility of at least 3 per cent is safe and can be used as a useful design guide.

Microstructure Studies

With prolonged exposure to elevated temperatures, most heat-resistant alloys exhibit some change in microstructure. In order to establish a relationship between microstructure and testing conditions with respect to the alloys used in this investigation, metallographic analyses were made of rupture-bar specimens representing the range of temperatures studied. Characteristic microstructures were obtained by sectioning the stress-rupture bar longitudinally through the center of the notched region. Standard metallographic procedures were used in preparing the alloys for microscopic inspection.

With respect to the S-816 alloy, no observable change in microstructure was evident with rupture bars exposed for various periods of time at either the 1350 or the 1500 F test temperature. In general, the microstructure was typical of quenched and aged S-816 material (a carbide phase dispersed in a solid-solution alloyed cobalt matrix, with carbides present along the austenitic grain boundaries). It has been observed by some investigators that continued exposure to temperatures above 1600 F will produce an observable change in the characteristic aged microstructure. In general, high-temperature exposure initiates a solutioning process by which the grain-boundary carbide phase gradually enters into solid solution. The rate of such a process is both temperature and time-dependent. It can be observed, in specimens exposed to 1600 F, for example, that the grain boundaries appear somewhat intermittent or "spotty," indicative of the first stage of solutioning. At higher temperatures, the grain boundaries gradually become exhausted of carbides and lose their original aged strength.

Inconel "X" Type 550 is characterized by a marked tendency for precipitation hardening. Under the normal aging heat-treatment (4 hr at 1600 F, and 4 hr at 1350 F), matrix precipitation is not evident with standard microscopic techniques. With longer exposure times at temperatures of 1500 F or 1600 F, matrix precipitation occurs. For example, one specimen (1500 F, 110 hr) revealed a slight degree of matrix precipitation, whereas another (1600 F, 628 hr) indicated extremely heavy precipitation.

With the exception of the addition of cobalt, the composition of Waspaloy resembles, to some degree, that of Inconel "X" Type 550. With test temperatures of 1200 and 1350 F, no visible variation in microstructure was apparent. At the higher test temperature (1500 F), however, some matrix precipitation similar to that reported for Inconel "X" Type 550 was evident.

Essentially, this microscopic study has shown that the three heat-resistant alloys used in this investigation exhibit noticeable changes in microstructures at either 1500 or 1600 F. These observations of microstructural variations in the three different alloys with prolonged exposures to elevated temperature are intended to fix attention on one of the factors influencing the behavior of notched-rupture bars. They are presented to emphasize that metallurgical changes do occur with time and temperature, and must be taken into account when considering high-temperature behavior.

The physical condition of the surface layer at the root of the notch may also have considerable influence on the mode of fracture in notched-rupture bars. If structural damage does result from notch preparation, i.e., grinding, it is probable that the extent of damage will vary from notch to notch because of the unreproducibility of the grinding mechanism. This fact, by itself, might account for scatter within related testing data. Realizing that such a surface condition, if prevalent, could affect notch-rupture data, an investigation was initiated in order to study the surface condition of machined rupture bars.

The procedure for this phase of the investigation consisted of sectioning an untested notched-rupture specimen of each alloy longitudinally through the notch diameter. Then notch cross sections were examined metallographically for any surface cracks (especially at the root of the notch) that might have been introduced by machining or grinding. After completion of this examination, the notch cross sections were aged at a temperature of 1500 F for a period of 24 hr. The specimens were then re-examined microscopically.

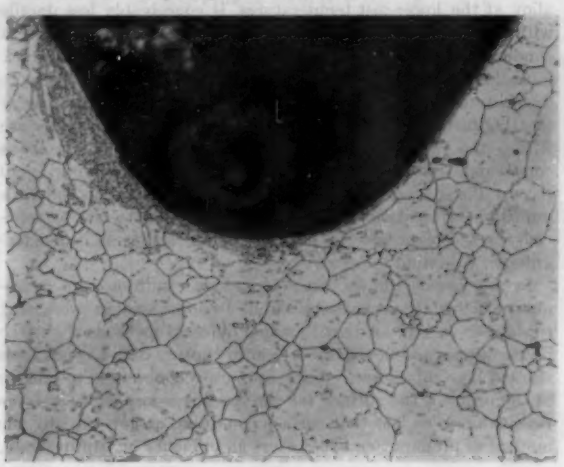

Fig. 10 Surface Deformation at Root of Notch (0.005-In. Radius) in S-816 Rupture Bar; ×250

Prior to aging, no evidence of surface cracking or grain deformation introduced by grinding was noted in any of the three notched (0.005-in-radius) rupture bars inspected. After aging, however, each alloy revealed some variation in surface microstructure, seemingly brought about by surface deformation. In the S-816 alloy, both the gage-length surface and the notch-contour surface revealed indications of massive carbide precipitation. This surface condition can be seen by examining the photomicrograph presented in Fig. 10. Fig. 10 shows evidence of deformation at the root of the 0.005-in-radius notch. It is interesting to note the uneven degree of carbide precipitation at the notch root, indicating that the grinding was not carried out evenly. On the left side of the notch, the deformed layer is almost 0.002 in. thick. It is apparent that the 1500 F aging temperature was not sufficient to promote recrystallization of the deformed surface layer. It was, however, capable of allowing carbide precipitation. In stressed bars of S-816 alloy, the effects of surface deformation also were present. At 1600 F, the deformed surface areas were completely recrystallized. Under very close inspection, and by slightly overetching the microstructure, a mass of small grains could be observed in these regions.

This recrystallized layer also was observed at the gage-length surface and notch-contour surface of the unstressed notch sections of both Inconel "X" Type 550 and Waspaloy. In these specimens, the aging temperature was adequate for recrystallization to occur. With the stressed rupture bars, a similar condition was present. In addition, it was noted that intergranular oxidation had occurred along the boundaries of the newly formed surface grains. As would be expected, the extent of oxidation increased with time and temperature. The photomicrograph in Fig. 11 clearly shows the surface region of recrystallization in a notched-rupture bar of Inconel "X" Type 550 stressed at 1600 F for a period of 628 hr. The lighter etching surface area represents the zone of recrystallization. Evidence of intergranular oxidation originating from the surface also can be seen. The matrix precipitation referred to in the foregoing discussion also is evident.

Microexamination, therefore, has indicated that the machining operations required to prepare a notched-rupture specimen for testing produce various surface conditions that might have considerable effect on the rupture properties of notched bars. A surface of massive carbide precipitation, as found in the S-816 alloy at the lower-test temperatures, is conceivably less ductile with reference to the unaffected interior material. Such a condition at the root of a notch would be ideally suited for crack initiation. Once the propagation of a crack reaches the more ductile interior, the original geometry of the notch changes, thereby creating further complications. When the test temperatures are within the range of recrystallization for the particular alloys considered, the deformed surface layers contain many small recrystallized grains. A surface layer of this nature offers a multitude of locations for intergranular rupture to begin, especially when exposure to elevated temperatures allows intergranular oxidation to occur.

In any event, the existence of surface condition as a consequence of surface preparation should be considered in evaluating rupture data. The extent to which different methods of surface preparation could be expected to alter rupture data has not been studied here, of course. Since fracture was observed to initiate at, or near to, the surface for the specimens inspected, it seems reasonable to expect that surface condition, as governed by the method of preparation, could exert an influence on rupture data.

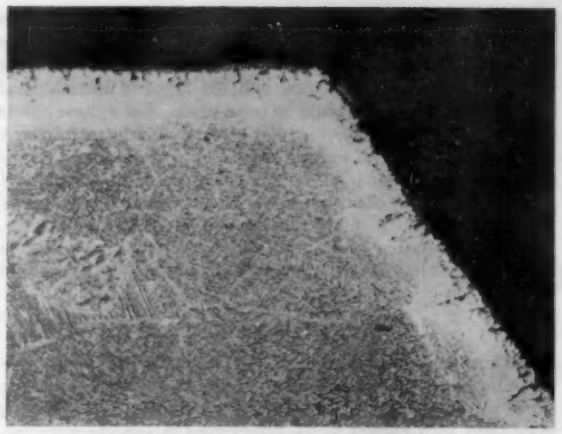

FIG. 11 SURFACE CONDITIONS AT NOTCH-GAGE LENGTH INTERFACE IN INCONEL "X" TYPE 550 RUPTURE BAR STRESSED AT 1600 F FOR 628 HR; ×250

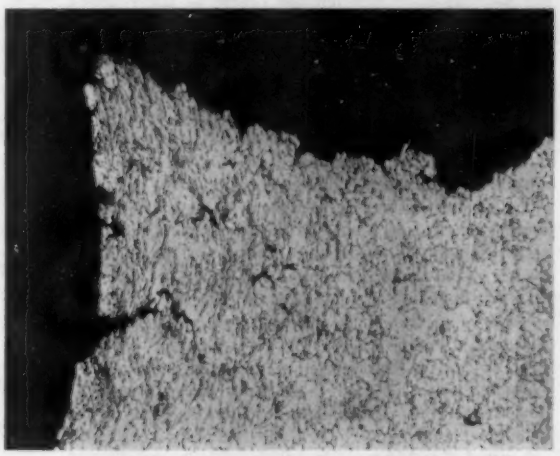

FIG. 12 FRACTURE OF S-816 (r = 0.06 IN.); ×75
(Fracture occurred in 32.1 hr at 1350 F and 58,000 psi.)

EXAMINATION OF CRACKS AND FRACTURES

The examination of cracks and fractures was facilitated by the preparation of photomicrographs. Those included in this section of the paper were selected as being representative of the specimens tested. The three alloys investigated, S-816, Inconel "X" Type 550, and Waspaloy, will be discussed separately.

S-816. The etchant used on the sectioned S-816 bars was a mixture of five parts HCL and two parts HNO_3. The test conditions are described beneath each figure.

The fracture surface in Fig. 12 is at the top of the figure and the notch contour is along the left edge. The photomicrograph reveals that severe deformation has occurred, and there is considerable evidence of intergranular cracking. This is typical of the S-816 fractures, with the exception that, at the higher temperatures, 1500 and 1600 F, the amount of deformation prior to fracture decreased. This was also evidenced in a decrease in the reduction-in-area values, and a shifting of fracture occurrence from the milder notches (r = 0.06 in. and 0.01 in.) to the sharper notches (r = 0.01 in. and 0.005 in.). This, of course, would be expected for a decrease in ductility.

The fracture surface of the specimen of Fig. 12 was inspected visually and, from the variation in darkness of the oxide film on the fracture surface, it appears that a circumferential crack formed at, or near, the root of the notch and progressed inward. The fractured surface has a fibrous appearance in the dark outer-oxide band, and tends toward a granular appearance in the central portion. From these observations, it might be concluded that the circumferential crack was initiated after considerable plastic deformation had occurred. After initiation, the crack propagated slowly until a critical condition was reached. Fracture then occurred abruptly.

Since most of the notched bars tested contained three notches, it was possible to examine the notch contour in the unruptured notches. Fig. 13 represents such a notch. Here, the structure at the base of the notch has deteriorated after severe local deformation.

From some of the previous observations, it might be concluded that, for the test conditions used, S-816 can tolerate the presence of cracks. This was also confirmed by the frequent occurrence of cracks in the unruptured notches.

To try to obtain a relative idea of the rates at which these cracks were propagating, several cracked but unruptured notches were broken, and the ends were inspected visually. In most instances, the cracks had penetrated to an approximately uniform

depth. Furthermore, it was found that the oxide film was very dark and of uniform intensity in the crack band. The transition from the dark cracked surface to the clean newly broken surface was very abrupt. This tends to indicate that the cracks had penetrated to a certain depth, and then either had ceased to grow or were growing very slowly.

The possibility of the cracks penetrating to a certain depth and then stopping is of interest for several reasons. This would indicate that, temporarily at least, an adjustment had occurred that made the crack stable. One possible explanation for such a behavior is that the crack moves through the cold-worked surface layer[4] and then stops in the more ductile interior. In some instances, the depths of the cracks appear to be of the approximate order of the cold-worked layer.

Cracks of the foregoing type, of course, could become unstable eventually by any of several means. Metallurgical change could bring about embrittlement, the grain-boundary mechanism discussed earlier might cause embrittlement, or corrosion of the material at the tip of the crack might occur. One important thing to note, however, is that a cracked bar has an essentially new notch geometry. This adds still another complication to those mentioned earlier, because any description of the fracture process should trace the formation and growth of such cracks.

Inconel "X" Type 550. Fractures of the Inconel "X" Type 550 specimens occurred after relatively small amounts of deformation. The fracture surfaces were quite distinctly intergranular, with very slight indication of deformation within the grains. It should be noted also that an observed absence of cracks in the unfractured notches tends to indicate that this alloy is more sensitive to the presence of cracks than S-816. It appears that cracks could be tolerated only a short time after initiation.

Fig. 14 illustrates the initiation of cracking in this alloy. This, incidentally, represents an instance in which cracking did occur in one of the unruptured notches, but was not detected visually. The test conditions are described beneath the figure. As can be seen, the crack has been initiated with very little deformation in the adjacent grains, and it is quite distinctly intergranular.

Waspaloy. As in the case of Inconel "X" Type 550, fracture in Waspaloy was not preceded by severe deformation. Also, fracture was intergranular in nature and appeared to initiate at, or near, the surface.

Fig. 15 illustrates the initiation of cracking in this alloy. The test conditions are described below the figure.

Although there is evidence of deformation within the grains, the distortion of grains is very slight. This is evidenced by the fact that the crack surfaces almost could be fitted together again because of the small amount of distortion that has occurred. It is of interest to note also that, at 1500 F, Waspaloy was notch-strengthened for all of the notches, in spite of the fact that the unnotched ductility ranged only from about 10 to 16 per cent. It should be noted further that Figs. 13 and 15 both represent deformation and cracking for notch-strengthened test conditions. In spite of the fact that the response to the external load resulted in notch strengthening for both alloys, it is apparent that the modes of deformation and cracking are markedly different.

Conclusions

The most significant points discussed in this paper are summarized as follows:

1 The unnotched-rupture ductility, although a rough index of available ductility, cannot be used as an efficient guide for in-

[4] The layer referred to here is that introduced in the grinding of the notch during the specimen preparation.

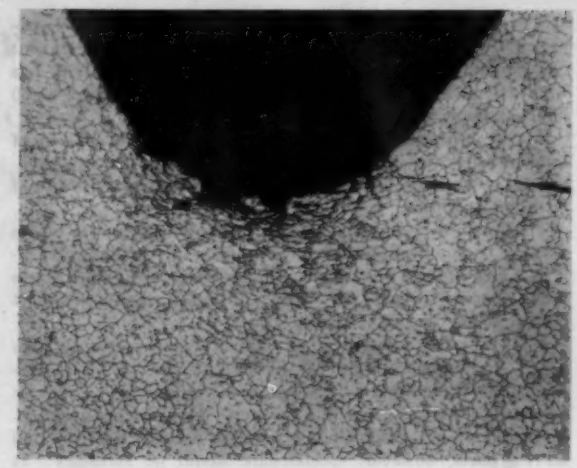

Fig. 13 Contour in S-816 (r = 0.01 In.); ×75
(Test discontinued after 89.1 hr at 1350 F and 50,000 psi.)

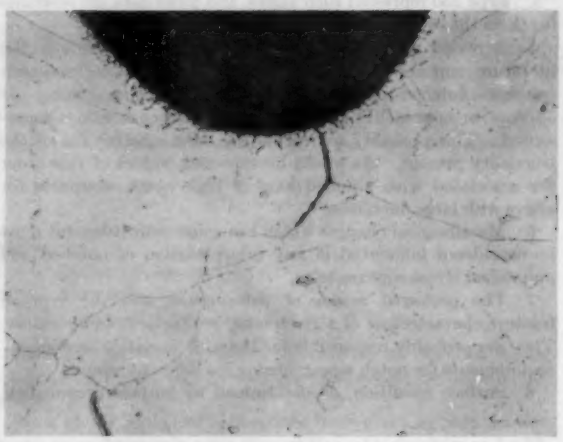

Fig. 14 Contour in Inconel "X" Type 550 (r = 0.005 In.); ×250
(Fracture occurred in r = 0.045-in. notch in 109.7 hr at 1500 F and 25,000 psi.)

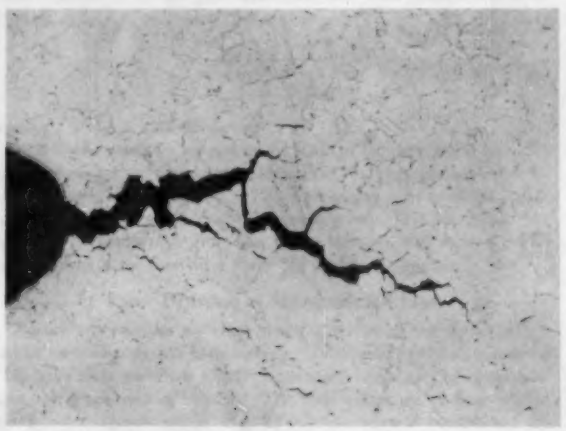

Fig. 15 Contour in Waspaloy (r = 0.005 In.)
(Fracture occurred in r = 0.040-in. notch in 72.5 hr at 1500 F and 35,000 psi.)

dicating notch sensitivity. Notch strengthening has been associated with unnotched-rupture ductilities as low as 10 per cent (Waspaloy at 1500 F). In other work, notch sensitivity has been detected with unnotched-rupture ductilities as high as 60 per cent, Haynes alloy 88 at 1350 F (2).

2 Notch-rupture ductility appears to be the simplest gage of notch sensitivity. As indicated by Brown, et al. (2), notch sensitivity seems to be associated with notch-rupture ductilities of less than 3 per cent.

3 The most desirable condition for design purposes is for an alloy to be notch-strengthened for a wide range of notch sharpness. S-816 fulfills this condition for all of the test temperatures used, whereas Inconel "X" Type 550 and Waspaloy satisfy it only at 1600 F and 1500 F, respectively.

4 It is probable that an alloy which is notch-sensitive for high notch sharpnesses can be used safely if it can be notch-strengthened for lower notch-sharpness values. This could be achieved primarily by avoiding the use of sharp notches in design. Since there is no direct relation between notched test bars and service parts, however, special care would be necessary. It would also be desirable to have more detailed data than for alloys satisfying the condition in item 3. Waspaloy and Inconel "X" Type 550 represent such alloys, and more data are desirable for them than for S-816.

5 A review of the data obtained and that available in the literature appears to indicate that there may be a maximum possible notched-rupture to unnotched-rupture value. It appears to approach 1.7 for the notch-sharpness values represented. This probably represents the most efficient use of the triaxiality present. As would be expected, values of this order are associated with notched bars of high notch sharpness for alloys with large ductilities.

6 Metallurgical changes which can cause embrittlement must be considered influential in any interpretation of notched and unnotched stress-rupture tests.

7 The preferred modes of deformation and the type of fracture characteristic of a given alloy are factors of importance. They are probably responsible for the wide variation in ductility requirements for notch strengthening for different alloys.

8 Surface condition, as determined by surface preparation, probably has an influence on stress-rupture results. It is possible that surface condition is quite important in service parts where the special procedures used to prepare test bars are not observed. This could result not only in lower strengths, but also in greater variation in strengths in cases where control is less rigid.

9 The abilities of different alloys to tolerate the presence of cracks initiated during a stress-rupture test apparently can be markedly different. Cracks were observed frequently at the base of unruptured notches in S-816, whereas cracks seldom were observed in unruptured notches of Inconel "X" Type 550 and Waspaloy. In these latter cases, failure evidently occurred shortly after crack initiation. Since cracking appears to be initiated during a test, the crack-propagation characteristics of a material are important.

Acknowledgment

The work upon which this paper was based was carried out under contract with the Materials Laboratory, Wright Air Development Center, Wright-Patterson Air Force Base, Ohio. The authors wish to thank the Wright Air Development Center for permission to publish this paper. The help and advice of Dr. A. Herzog of WADC and of Messrs. L. R. Jackson, Howard C. Cross, and G. K. Manning of the Battelle Staff are gratefully acknowledged.

BIBLIOGRAPHY

1 "Tension Properties of Aluminum Alloys in the Presence of Stress-Raisers," by E. L. Aul, A. W. Dana, and G. Sachs, NACA Technical Notes No. 1831, 44, 1949.

2 "Influence of Sharp Notches on the Stress-Rupture Characteristics of Several Heat-Resisting Alloys," by W. F. Brown, Jr., M. H. Jones, and D. P. Newman, Symposium on Strength and Ductility of Metals at Elevated Temperatures, ASM Special Technical Publication No. 128, 1952, pp. 25–45.

3 "Effect of Notch Geometry on Rupture Strength at Elevated Temperatures," by E. A. Davis and M. J. Manjoine, Symposium on Strength and Ductility of Metals at Elevated Temperatures, ASM Special Technical Publication No. 128, 1952, pp. 67–87.

4 "The Micromechanism of Fracture," by C. Zener; "Fracture of Metals," American Society for Metals, 1948.

5 "Notch Brittleness and Ductile Fracture in Metals," by E. Orowan, J. F. Nye, and W. J. Cairns; "Strength and Testing of Materials," Part 1, published by Her Majesty's Stationery Office, London, England, 1952, pp. 127–175.

Orifice Coefficients for Reynolds Numbers From 4 to 50,000

By H. W. IVERSEN,[1] BERKELEY, CALIF.

The sharp-edged orifice meter is standardized in shape and application by The American Society of Mechanical Engineers (1, 2)[2] and by the International Standards Association (3). With sufficient precision and care in fabrication of the orifice and metering section, and with standard techniques of use, the accepted coefficients as listed in the codes may be used within prescribed metering accuracy tolerance over the Reynolds number range of the standardization. Many applications arise for use of the orifices in the Reynolds-number range below that of the present standards. Calibration results in the "low" Reynolds-number range are available in the literature as obtained by numerous investigators. These were assembled to produce, if possible, standard coefficients for the Reynolds-number range of 4 to 50,000 (based on the pipe diameter) and for orifice-to-pipe diameter ratios of 0.1 to 0.8.

Standard Meters

STANDARD meter designs, with pressure-tap locations, are shown in Fig. 1. According to the ASME standards (2), "the upstream corner of the orifice plate shall be square and sharp, so that, when viewed without magnification a beam of light is not reflected by the corner." The designation of meter type as labeled will be used in the following discussion to classify the general shape of each meter for which calibrations were obtained, i.e., ISA for meters with a 30-deg beveled downstream edge, ASME for meters with a 45-deg beveled downstream edge, and Modified ASME for flat-plate meters with no beveled downstream edge.

The literature survey produced independent experimental calibrations of pipe-line orifices as listed in Table 1. Included in Table 1 are the major geometrical features of each meter, and the range of the test conditions in terms of the Reynolds-number range. The Reynolds number as given here is based on the flow conditions in the approach pipe upstream of the orifice

$$Re_D = \frac{VD}{\nu} = \frac{4Q}{\pi D\nu} \quad \ldots\ldots [1]$$

where

Q = volume flow rate, cfs
D = approach pipe diameter, ft
V = average velocity in approach pipe, fps
ν = fluid kinematic viscosity, ft²/sec

Meter coefficients were put in the form

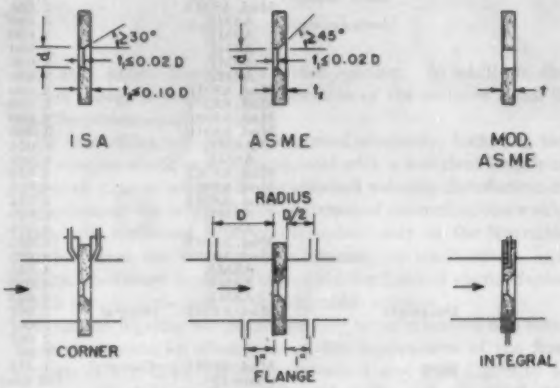

FIG. 1 STANDARD METER SHAPES AND PRESSURE-TAP LOCATIONS
Note: for ASME, from reference (2), $^1/_{16}$ in. $\leq t_2 \leq {}^1/_2$ in. for $D \leq 3$ in. $t_2 = {}^1/_2$ in. for 3 in. $< D \leq 6$ in., $t_2 \leq {}^1/_4$ in. for 6 in. $< D \leq 16$ in.; for Mod ASME $t = t_1 = t_2$ when $0.02D$ is equal to, or greater than, recommended t_2

$$K = \frac{Q}{A\sqrt{2gh}} \quad \ldots\ldots [2]$$

where

A = orifice opening area, sq ft
g = 32.17 ft/sec²
h = metering differential head, ft

Table 2 lists other pertinent information on the test fluids, conditions of operation, approach pipe surface, and approach pipe length.

Most of the published calibrations were given as reduced test results of coefficients as a function of Reynolds numbers and with a curve through the points from each meter. The reported correlations were given with Reynolds numbers based on the orifice diameter or the pipe diameter, and with coefficients as in Equation [2], or coefficients defined as

$$C = \frac{Q\sqrt{1-(d/D)^4}}{A\sqrt{2gh}} \quad \ldots\ldots [3]$$

where d is the orifice diameter.

Where the results were not in the form of Equations [1] and [2], points were taken from the published curves, changed into the desired values, and replotted. This technique was used to eliminate possible errors in selecting single points, and to obtain the best curve after changing the series of selected values. The calibrations were then in a form for direct comparison.

Flow Pattern in Metering Section

Before any comparisons are made, a review of the flow pattern in the metering section is necessary. Johansen (10) and Kowalke (17) give flow patterns from visual inspection and photographs through glass-walled tubing. The two extremes of flow conditions are diagrammed in Fig. 2; (*a*) the normal contracted jet with eddy formation in the downstream region adjacent to the orifice plate, and (*b*) completely laminar flow with no eddies.

[1] Associate Professor of Mechanical Engineering, University of California. Assoc. Mem. ASME.

[2] Numbers in parentheses refer to the Bibliography at the end of the paper.

Contributed by the Research Committee on Fluid Meters and presented at the Annual Meeting, New York, N. Y., November 28–December 3, 1954, of THE AMERICAN SOCIETY OF MECHANICAL ENGINEERS.

NOTE: Statements and opinions advanced in papers are to be understood as individual expressions of their authors and not those of the Society. Manuscript received at ASME Headquarters, November 29, 1954. This paper was not preprinted.

TABLE 1 RANGE OF TEST CONDITIONS

Ref. no.	Investigator(s)	Meter type	Pressure tap	Pipe diam, D, in.	Orifice diam, d, in.	Diam ratio, d/D	Thickness ratios, t_1/D	t_1/d	t_2/D	Reynolds number range
(4)	Ambrosius and Spink	ASME	Flange	2.056	0.240	0.117	0.008	0.067	0.07	5–1200
		ASME		2.056	0.540	0.263	0.031	0.114	...	10–2600
		ASME		2.067	0.688	0.333	0.035	0.102	0.12	500–3300
		ASME		2.056	0.832	0.405	0.043	0.103	0.12	16–4000
		ASME		2.056	1.068	0.520	0.047	0.088	0.13	20–5200
		Mod. ASME		2.056	1.2097	0.588	0.061	0.102	0.06	23–5900
		Mod. ASME		2.056	1.3702	0.666	0.063	0.092	0.06	27–6700
		ASME		2.067	1.446	0.700	0.050	0.069	0.12	220–7000
		Mod. ASME		2.056	1.5001	0.730	0.062	0.083	0.06	30–7300
		Mod. ASME		2.056	1.6305	0.793	0.062	0.075	0.06	80–8000
		Mod. ASME		2.056	1.720	0.834	0.063	0.074	0.06	50–8400
		ASME		3.080	0.460	0.149	0.019	0.122	0.08	6–1500
		ASME		3.080	0.460	0.149	0.021	0.133	0.08	6–1500
		ASME		3.080	1.022	0.332	0.031	0.092	0.08	13–5000
		ASME		3.080	1.022	0.332	0.017	0.052	0.08	13–5000
		ASME		3.080	1.585	0.515	0.020	0.037	0.08	20–5200
		Mod. ASME		3.080	1.585	0.515	0.037	0.070	0.04	20–5200
		Mod. ASME		3.080	1.8197	0.591	0.041	0.068	0.04	24–5900
		Mod. ASME		3.080	2.147	0.697	0.038	0.054	0.04	60–7000
		Mod. ASME		3.080	2.2702	0.737	0.041	0.054	0.04	74–7400
		ASME		4.024	0.603	0.150	0.015	0.100	0.06	6–1500
		ASME		4.025	1.208	0.300	0.019	0.065	0.06	12–3000
		Mod. ASME		4.025	1.208	0.300	0.026	0.088	0.026	12–3000
		Mod. ASME		4.024	1.610	0.400	0.027	0.066	0.027	16–4000
		Mod. ASME		4.025	2.013	0.500	0.027	0.054	0.027	20–5000
		ASME		4.025	2.013	0.500	0.019	0.038	0.06	20–5000
		ASME		4.025	2.416	0.600	0.019	0.032	0.06	24–6000
		Mod. ASME		4.025	2.416	0.600	0.027	0.045	0.027	24–6000
		Mod. ASME		4.025	2.818	0.700	0.027	0.038	0.027	70–7000
		ASME		4.025	2.818	0.700	0.027	0.038	0.06	70–7000
		ASME		4.025	3.0104	0.750	0.019	0.026	0.06	60–2200
		ASME		4.025	3.4107	0.847	0.019	0.0205	0.06	500–8400
(5)	Daugherty	Mod. ASME	Integral	2.067	1.00	0.483	0.156	0.312	0.156	380–1400
				2.067	1.25	0.604	0.156	0.250	0.156	700–4600
				2.067	1.50	0.725	0.156	0.210	0.156	6–140000
				7.98	6.00	0.753	0.039	0.055	0.039	60–590000
(6)	Giese	Mod. ASME	Corner	1.575	0.196	0.125	0.008	0.06	0.008	1–50
		Sharp 15°		(40 mm)	0.215	0.137	0	0	0.1	1–1400
		Sharp 15°			0.277	0.176	0	0	0.075	12–1700
		Mod. ASME			0.395	0.251	0.003	0.01	0.003	2–2500
		Mod. ASME			0.397	0.252	0.008	0.03	0.008	4–200
		Sharp 15°			0.406	0.258	0	0	0.1	2–2600
(7)	Grace and Lapple	Sharp 45°	Radius	1.049	0.0316	0.0301	0	0	0.065	3–600
					0.0320	0.0305	0	0	0.065	3–600
					0.0648	0.0618	0	0	0.065	18–1800
					0.0650	0.0620	0	0	0.065	18–1800
					0.0952	0.0908	0	0	0.065	27–2700
					0.0963	0.0918	0	0	0.065	27–2700
					0.1260	0.1201	0	0	0.065	50–4800
					0.1949	0.1858	0	0	0.065	100–19000
					0.750	0.715	0	0	0.065	3000–71000
					0.750	0.715	0	0	0.065	3000–71000
(8)	Hodgson	ASME	Corner	0.755	0.318	0.421	0.021	0.05	0.048	4–52000
				0.503	0.318	0.632	0.031	0.05	0.072	6–78000
				0.378	0.318	0.843	0.042	0.05	0.095	33–100000
(9)	Ippen	ASME	Radius	8.0	4.92	0.615	0.008	0.0126	0.047	370–1000000
(10)	Johansen	Sharp 45°	Corner	1.250	0.263	0.209	0	0	0.084	2–5300
					0.504	0.401	0	0	0.081	4–10000
					0.749	0.595	0	0	0.088	5–15000
					0.998	0.794	0	0	0.088	7–20000
(11)	Marchetti	ISA	Corner	6.09	1.34	0.220	0.013	0.059	0.065	870–25000
				(154.6 mm)	1.85	0.304	0.013	0.043	0.065	2000–66000
					2.64	0.434	0.013	0.030	0.065	2600–88000
					3.74	0.615	0.013	0.021	0.065	7000–89000
					4.36	0.717	0.013	0.018	0.065	11000–93000
					4.76	0.782	0.013	0.016	0.065	14500–87000
					5.11	0.840	0.013	0.015	0.065	20000–88000
(12)	Marchetti	ISA	Corner	5.88	1.34	0.228	0.007	0.029	0.065	530–38000
				(149.5 mm)	1.85	0.315	0.007	0.021	0.065	2100–71600
					2.64	0.448	0.007	0.015	0.065	3300–108000
					3.23	0.548	0.007	0.012	0.065	5170–114000
					3.54	0.602	0.007	0.011	0.065	6700–101000
					3.74	0.636	0.007	0.011	0.065	9400–93000
					3.98	0.675	0.007	0.010	0.065	8000–102000
					4.17	0.708	0.007	0.009	0.065	10700–108000
					4.36	0.742	0.007	0.009	0.065	13000–89000
					4.57	0.776	0.007	0.009	0.065	16500–101800
					4.76	0.810	0.007	0.008	0.065	19000–110000
					4.96	0.843	0.007	0.008	0.065	22000–95000
					5.11	0.870	0.007	0.007	0.065	22700–106000
					5.28	0.896	0.007	0.007	0.065	27000–120000
(13)	Peterson	Mod. ASME	Corner	0.703	0.39	0.555	0.09	0.16	0.09	33–1600
				0.703	0.461	0.656	0.09	0.134	0.09	50–2000
				1.00	0.400	0.400	0.06	0.156	0.06	16–1200
				1.00	0.500	0.500	0.06	0.126	0.06	45–1500
(14)	Tuve and Sprenkle	ASME	Corner	1.272	0.254	0.200	0.012	0.061	0.025	4–400
					0.382	0.300	0.012	0.041	0.025	3–18000
					0.509	0.400	0.012	0.031	0.025	2–16000
					0.636	0.500	0.012	0.025	0.025	30–20000
					0.763	0.600	0.012	0.020	0.025	120–36000
					0.890	0.700	0.012	0.018	0.025	140–42000
					0.954	0.750	0.012	0.016	0.025	160–60000
					1.018	0.800	0.012	0.015	0.025	64–64000
(15)	Witte	ASME	Corner	1.965	0.735	0.374	0.01	0.027	0.12	100–80000
				1.965	0.865	0.440	0.01	0.023	0.12	300–100000
				1.965	1.065	0.542	0.01	0.018	0.12	300–100000
				1.965	1.338	0.680	0.01	0.015	0.12	500–100000
				3.930	0.957	0.243	0.005	0.021	0.06	100–100000
				3.930	1.335	0.339	0.005	0.015	0.06	200–100000
				3.930	1.720	0.438	0.005	0.011	0.06	200–100000
(16)	Linden and Othmer	Mod. ASME	Radius	2.00	0.063	0.032	0.012	0.38	0.012	5–40
					0.064	0.032	0.019	0.58	0.019	5–43
					0.124	0.062	0.019	0.30	0.019	18–130
					0.189	0.094	0.019	0.20	0.019	40–260

TABLE 2 TEST CONDITIONS

Ref. no.	Investigator(s)	Fluids	Approach Pipe: Length (pipe diameters)	Approach Pipe: Type
(4)	Ambrosius and Spink	Oils, heated	19	Standard
(5)	Daugherty	Oil blends	...	Standard steel
(6)	Giese	Water, oils heated	30	...
(7)	Grace and Lapple	Air, water	15	Stainless steel
(8)	Hodgson	Water and glycerine mixture	...	...
(9)	Ippen	Oils	22	Standard steel
(10)	Johansen	Water and oils	46	...
(11)	Marchetti	Water	50	Seamless steel
(12)	Marchetti	Water	50	Seamless steel
(13)	Peterson	Oil, heated	6	Smooth
(14)	Tuve and Sprenkle	Oils, heated	100	Smooth brass
(15)	Witte	Water and oils	...	...
(16)	Linden and Othmer	Air	2¼	Stainless steel

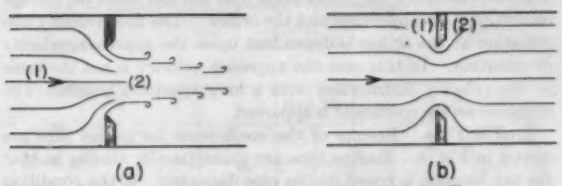

FIG. 2 DIAGRAMMATIC REPRESENTATION OF FLOW THROUGH AN ORIFICE; (a) CONTRACTED JET AT HIGH REYNOLDS NUMBERS, AND (b) LAMINAR FLOW AT LOW REYNOLDS NUMBERS

Johansen's flow patterns were obtained with a sharp-edged orifice of 0.502 diameter ratio in a glass tube of 1.06 in. ID. The straight-approach pipe length was approximately 100 tube diameters. The condition of Fig. 2(*b*) was observed at $Re_D = 5$. At $Re_D = 15$, the flow was still completely laminar but a jet began to form with a stagnant region adjacent to the downstream face of the orifice. As the Reynolds number was increased to 100 a laminar-flow back eddy was formed with a slight contraction of the jet issuing from the orifice. The laminar back eddy increased in length along the tube with the increase in Reynolds number until, at $Re_D = 125$ to 200, the jet issuing from the orifice became unstable with surface ripples indicating the tendency for ring vortex formations. The ring vortexes were accented as the flow increased to the conditions of Fig. 2(*a*)

The flow equation between sections 1 and 2 may be written, for an incompressible fluid in steady flow

$$\frac{p_1}{w} + z_1 + \alpha_1 \frac{V_1^2}{2g} = \frac{p_2}{w} + z_2 + \alpha_2 \frac{V_2^2}{2g} + C_f \frac{V_2^2}{2g} \quad [4]$$

where p is pressure, w is the fluid unit weight, z is the elevation, V is the average velocity, α is the velocity head correction factor to obtain the actual velocity head from the average velocity, and C_f is the friction head-loss coefficient.

With

$$Q = V_1 A_1 = C_c V_2 A \quad [5]$$

Equation [4] reduces to

$$Q = \frac{C_c A \sqrt{2gh}}{\sqrt{\alpha_2 + C_f - \alpha_1 \frac{C_c^2 A^2}{A_1^2}}} \quad [6]$$

where C_c is the contraction coefficient as defined in Equation [5] relating the velocity V_2 to the orifice area A and

$$h = \left(\frac{p_2}{w} + z_2\right) - \left(\frac{p_1}{w} + z_1\right)$$

The factors α_1, α_2, C_f, and C_c are not independent. In the approach pipe α_1 is known to be dependent on the Reynolds number, the pipe roughness, and the influence of upstream flow disturbances such as those originating from changes in flow direction. α_2, C_f, and C_c are dependent upon α_1, and on the relative magnitudes of the viscous and inertia forces which act on the fluid as it passes through the orifice opening. In addition, the factors change depending upon location of the sections 1 and 2, e.g., the pressure-tap location.

By prescribing complete geometrical similarity, including the pipe roughness and orifice shape, and with a sufficient length of approach pipe to produce an established velocity distribution in the approach pipe immediately upstream of the orifice, one would expect the coefficient K to be dependent only on the Reynolds number since the velocity distributions, jet contractions, and laminar shears are dependent upon the inertia and viscous forces which are characterized by the Reynolds number.

Equation [6] does not permit an easy transformation to a form more convenient for discussion of the implications of the flow pattern of Fig. 2(*b*). With the points 1 and 2 in Fig. 2(*b*) as shown, and with the assumption that the velocity head difference is small compared to the friction term, that is

$$\alpha_2 \frac{V_2^2}{2g} - \alpha_1 \frac{V_1^2}{2g} \ll C_f \frac{V_2^2}{2g} \quad [7]$$

and with a velocity $V = Q/A$ used instead of V_2 to define C_f, then Equation [4] is

$$C_f V^2 = 2gh \quad [8]$$

or

$$Q = \frac{A\sqrt{2gh}}{\sqrt{C_f}} \quad [9]$$

In complete laminar flow, such as that in conduits, or flow past objects such as spheres, analysis and experiment show friction coefficients inversely proportional to the Reynolds number. By analogy, one would expect a similar relationship for the orifice friction coefficient in complete laminar flow, or

$$C_f = \frac{B}{Re_D} \quad [10]$$

From Equations [2], [9], and [10]

$$K = \frac{\sqrt{Re_D}}{B} \quad [11]$$

The proportionality constant B of Equation [11] has not been determined analytically but may be determined experimentally.

LAMINAR-FLOW FRICTION

For the comparisons to be made, the implications of the laminar-flow friction are important. The meter coefficient becomes more a function of the laminar-flow pattern as the Reynolds number decreases; and the flow pattern becomes more a function of the exact geometry of the boundary, particularly the boundary in the vicinity of the orifice opening. Velocity gradients with corresponding shear stresses which, in turn, produce the differential head, will be different for orifices with thick throat sections as contrasted to thin orifice throat sections. The thickness of the orifice plate with the length and angle of the bev-

eled edge may produce discernible differences for small changes in these features.

As the Reynolds number becomes large, the laminar-flow considerations become small contrasted to the inertial influences (C_f is small compared to C, α_1, and α_2), and the exact geometry of the orifice opening becomes less important as long as the upstream edge is sharp and the thickness not overly long so that the jet remains free of the influence of the orifice throat boundary.

Complete geometrical similarity is not possible since a diameter ratio range is desired. But, at one diameter ratio, geometrical similarity can be specified with all other dimensions in terms of the approach pipe diameter or in terms of the orifice diameter.

Comparison of Orifices and Metering Systems

When the geometries of the orifices and metering systems of the various investigators, summarized in Tables 1 and 2, are compared, a number of features are apparent: (*a*) Seven of the twelve investigators used corner taps, three used radius taps, one used flange taps, and one used integral taps. (*b*) Most of the orifice cylindrical throat sections were standard in thickness ($t_1/D < 0.02$), but were not geometrically similar. (*c*) The approach-pipe straight length upstream of the orifice in most investigations was reasonable according to code recommendations. (*d*) The metering section pipe roughness ranged from standard steel pipe surfaces to smooth surfaces.

In view of the previous discussion on the nature of the flow through an orifice, particularly at low Reynolds numbers, each of the features listed in the foregoing will be discussed in terms of the calibration results of the correlation of the meter coefficient K of Equation [2], with the Reynolds number of Equation [1]. One assumption must be made, that all calibrations were accurate with no systematic instrumental error. The random variations of individual calibration points from each mean calibration curve reported by all investigators were within 1 per cent, except Linden and Othmar (16) who reported 2 per cent.

Corner Pressure Taps. Corner pressure taps are the only taps which can be considered geometrically similar for all pipe sizes and for which there are sufficient results for an extended comparison. Coefficients as a function of diameter ratio for selected Reynolds numbers from calibration with corner taps are shown in Fig. 3. Each point represents a co-ordinate from a calibration curve. The results of Daugherty with integral taps are also included in Fig. 3. Curves are shown that fit the majority of the points with three sets of points ignored, those of Daugherty with integral taps, those of Peterson, and those of Giese for the modified ASME meters. The curves are for reference only, and are not to be construed as recommended values of the coefficients. A 5 per cent deviation band from the mean curve is also shown.

At Reynolds numbers of 10,000 all points for the corner taps, except one, are within 1 per cent of the mean curve. There are no consistent deviation trends with respect to pipe diameter, pipe roughness, or variations in the relative shapes of the orifices. At lower Reynolds numbers the individual deviations from the mean increase percentagewise with maximum deviations of more than 5 per cent at Reynolds numbers of 8 and 10. These variations are too great to establish reliable code standards within desired tolerances for orifice-meter coefficients in the low Reynolds-number range.

The deviations of the coefficients in the low Reynolds-number range tend to substantiate the previous discussion of the influence of small orifice-shape variations on the laminar flow-velocity distribution, shear-stress pattern, and hence meter coefficient. The results of Giese are particularly impressive relative to the importance of the exact shape of the orifice. Giese calibrated two types of orifices, the ASME (beveled downstream corner shown as the open triangle points in Fig. 3), and the modified ASME (flat plate with no bevel shown as the filled-in triangles in Fig. 3). The coefficients of the two types of orifice plates at the same diameter ratio and the same Reynolds number differ by as much as 10 per cent.

No other definite comparisons on orifice shape are apparent from the corner-tap results since more than one shape factor is involved. However, Daugherty's modified ASME orifice calibrations for his orifices of diameter ratios 0.727 and 0.753 show the influence of orifice thickness.

The results of Peterson (the plus symbols in Fig. 3) were obtained with a short approach pipe length, approximately 6 pipe diameters between the inflow from four circular holes on the approach-pipe circumference and the orifice. The flow-velocity distribution at the orifice is dependent upon the approach-velocity distribution. In this case the approach velocity is not the same as the velocity distribution with a long approach length. The influence on the coefficient is apparent.

Radius Taps. Results of the coefficients for radius taps are shown in Fig. 4. Radius taps are geometrically similar in that the tap location is based on the pipe diameter. If the condition of complete laminar flow is present, then the friction coefficient should increase with the length between pressure taps and the meter coefficient should decrease. The results of Grace and Lapple show this trend as compared to the mean curve from the corner-tap results.

The coefficients of Linden and Othmer are not consistent within themselves, nor with the results of Grace and Lapple. The calibration system of Linden and Othmer consisted of an open-end approach pipe only $2^1/_4$ pipe diameters long. The orifices were relatively thick compared to the orifice diameter. Both of these nonstandard conditions contribute to the magnitude of the orifice coefficients and agreement with coefficients from other systems is not expected.

Flange Taps. The calibrations of Ambrosius and Spink with flange taps are not reproduced here. These are the only published calibrations with flange taps and correlation with corner taps, or radius taps, is not possible due to the differences in pressure-tap location. In view of the variations of coefficients for the corner taps for essentially standard orifices that differ slightly in geometry, and the variety of dimensions of the orifices of Ambrosius and Spink, their results should be used with caution in the low Reynolds-number range.

One further feature of the validity of Equation [11] should be noted. Meter coefficients as a function of Reynolds number on a log-log plot should result in a straight line with a slope of one half according to Equation [11] in the Reynolds-number range to which the equation applies. This relationship is shown in Fig. 5 for the few calibrations that extended to very low Reynolds numbers. The constant of Equation [11] depends upon the orifice-diameter ratio and other shape factors. (These features were pointed out by Johansen.)

Conclusion

The original intent of this survey of orifice-meter coefficients in the low Reynolds-number range was to establish standard coefficients. The calibration results which are available in the literature for corner taps do not correlate within desired tolerances for standards. In view of the variation of calibration results of seven investigators who used corner taps, the calibrations from one series of investigations are not sufficient to specify standards.

The essential requirement for the specification of standard coefficients for orifices in the low Reynolds-number range appears to be a complete specific standardization of the orifice shape, not merely upper limits of size of throat width and of plate thickness.

The program needed for experimental setups, instrumentation,

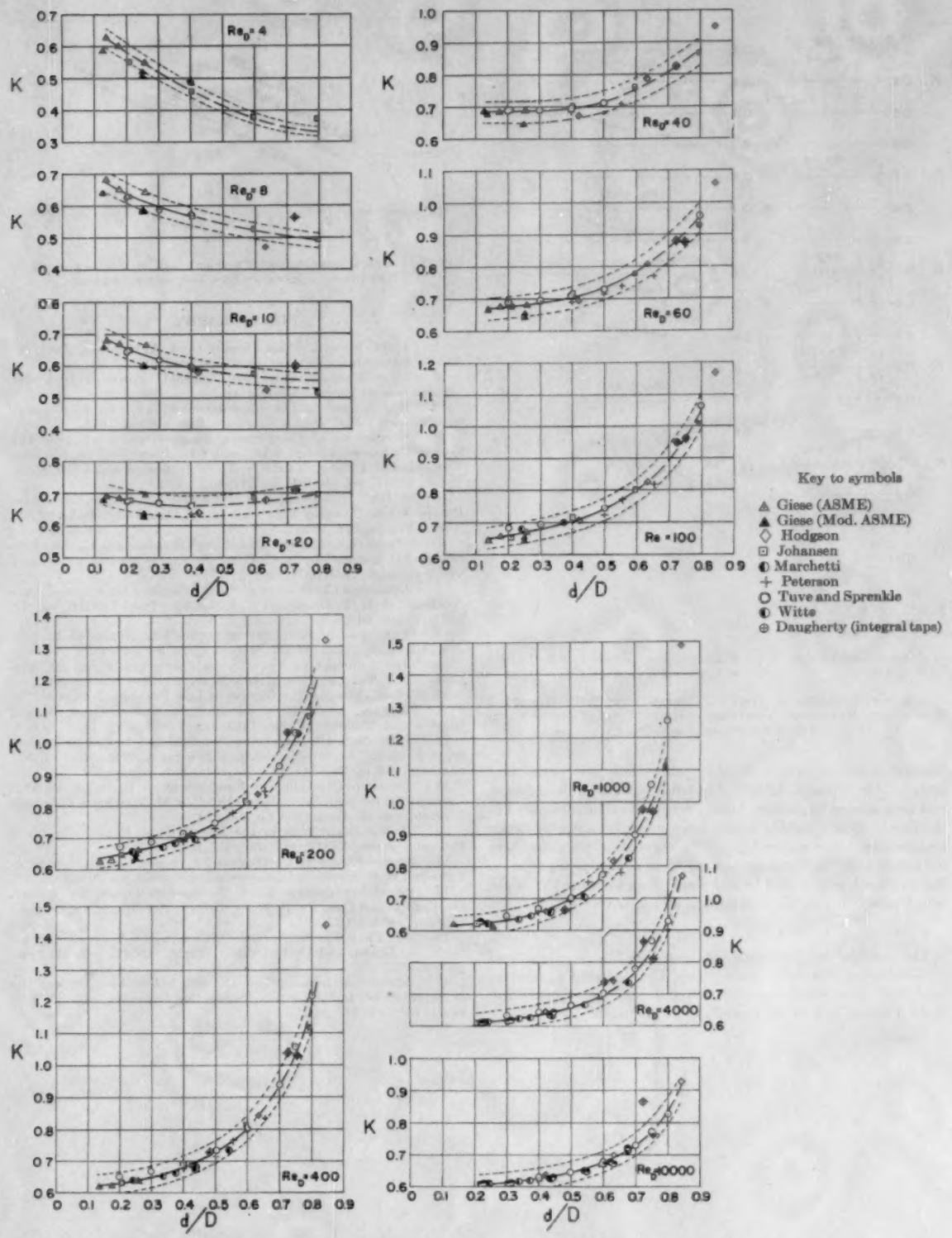

FIG. 3 CORRELATION OF ORIFICE COEFFICIENTS WITH DIAMETER RATIO AND REYNOLDS NUMBER; CORNER TAPS

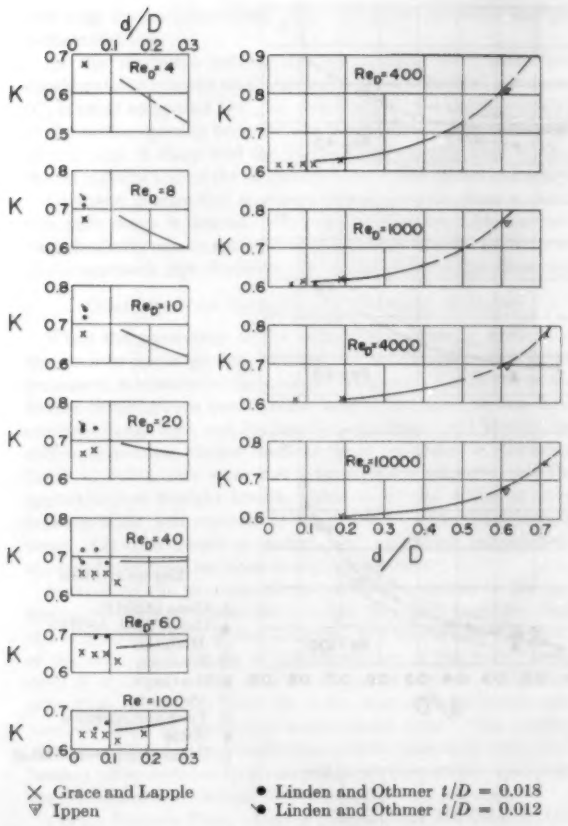

FIG. 4 CORRELATION OF ORIFICE COEFFICIENTS WITH DIAMETER RATIO AND REYNOLDS NUMBERS; RADIUS TAPS. CURVES FROM FIG. 3 FOR COMPARISON ONLY

and operation to obtain reliable calibrations is lengthy and costly. The present ASME standards include radius, flange, and vena contracta pressure taps. Any calibration attempted in the future should include results from pressure taps at all code locations including corner taps. The correlation presented here for corner taps may be used as a guide for comparison purposes. The approach pipe should be sufficiently long to insure the established pipe-line velocity distribution at the orifice.

ACKNOWLEDGMENTS

The material for this paper was assembled by W. Gross and A. Elvitsky, graduate students at the University of California, Berkeley. The program was started under the direction of Prof. R. G. Folsom, now at the University of Michigan.

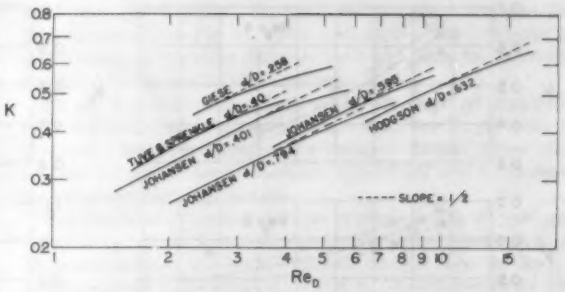

FIG. 5 ORIFICE COEFFICIENT PROPORTIONAL TO SQUARE ROOT OF REYNOLDS NUMBER AT LOW REYNOLDS NUMBER

BIBLIOGRAPHY

1 "Fluid Meters, Their Theory and Application, Part 1," ASME Research Publication, fourth edition, 1937.

2 "Flow Measurement, 1940," ASME Power Test Codes, Information on Instruments and Apparatus, Part 5.

3 "Regeln für die Durchflussmessung mit genormten Düsen und Blenden," VDI, Berlin, Germany, third edition, 1935.

4 "Coefficients of Discharge of Sharp-Edged Concentric Orifices in Commercial 2-In., 3-In., and 4-In. Pipes for Low Reynolds Numbers Using Flange Taps," by E. E. Ambrosius and L. K. Spink, Trans. ASME, vol. 69, 1947, pp. 805–812.

5 "A Further Investigation of the Performance of Centrifugal Pumps When Pumping Oils," by R. L. Daugherty, Bulletin 130, Goulds Pumps, Inc., 1926.

6 "Mengenmessung mit Düsen und Blenden dei Kleinen Reynolds-achen Zahlen," by H. G. Giese, *Forschung des Ingenieurwesens*, vol. 4, January, 1933, pp. 11–20.

7 "Discharge Coefficients of Small-Diameter Orifices and Flow Nozzles," by H. P. Grace and C. E. Lapple, Trans. ASME, vol. 73, 1951, pp. 639–647.

8 "The Laws of Similarity of Orifice and Nozzle Flows," by J. L. Hodgson, Trans. ASME, vol. 71, 1929, pp. 302–332.

9 "The Influence of Viscosity on Centrifugal-Pump Performance," by A. T. Ippen, Trans. ASME, vol. 68, 1946, pp. 823–848.

10 "Flow Through Pipe Orifices at Low Reynolds Numbers," by F. C. Johansen, Aeronautical Research Committee, Great Britain, Reports and Memoranda, No. 1252, June, 1929.

11 "I Boccagli EI Diaframmi Normalizzati Inserti nelle Condotte Forzate," by M. Marchetti, *L'Energia Elettrica*, vol. 12, November, 1935, pp. 789–811.

12 "Prove di Controllo sul Funzionamento Idraulico dei Diaframmi e dei Boccagli Normalizzati ISA," by M. Marchetti, *L'Energia Elettrica*, vol. 13, April, 1936, pp. 169–184.

13 "Orifice Coefficients in the Viscous-Flow Range," by G. S. Peterson, Trans. ASME, vol. 69, 1947, pp. 765–768.

14 "Orifice Discharge Coefficients for Viscous Liquids," by G. L. Tuve and R. E. Sprenkle, *Instruments*, vol. 6, 1933, pp. 201–206.

15 "Durchflussbeiwerte der I. G.-Messmündungen fur Wasser, Öl, Dampf, und Gas," by R. Witte, *Zeitschrift-VDI*, vol. 72, October, 1928, pp. 1493–1502.

16 "Air Flow Through Small Orifices in the Viscous Region," by H. R. Linden and D. F. Othmer, Trans. ASME, vol. 71, 1949, pp. 765–772.

17 "Manner of Liquid Flow Through a Pipe-Line Orifice," by O. L. Kowalke, *Industrial and Engineering Chemistry*, vol. 30, February, 1938, pp. 217–222.

Discharge Measurements at Low Reynolds Numbers—Special Devices

By A. L. JORISSEN,[1] ITHACA, N. Y.

Numerous investigators have attempted to develop a new type of differential fluid meter in which, by compensation of the effects of contraction and friction, a constant value of the coefficient of discharge can be maintained at low Reynolds numbers. As a result of the author's study of this problem, it is concluded that a number of devices offer distinct possibilities of maintaining a constant coefficient of discharge down to low values of Reynolds number. Particularly noteworthy, in the author's opinion, are the quadrant-edge orifice and the cylindrical nozzle with or without conical diffuser. For both, experimental evidence is available as proof of their satisfactory operation.

Introduction

THE utilization of constant-area differential types of fluid meters is in many cases limited to conditions for which the coefficient of discharge may be considered as practically independent of Reynolds number. This is true for orifices, nozzles, and venturi tubes. Under a certain value of Reynolds number, the coefficient of discharge exhibits a variable trend. The discharge may then only be computed by a method of successive approximations. Furthermore, experimental evidence shows that the accuracy of the device is generally lowered.

Since the accurate measurement of discharge at low Reynolds numbers is important in many cases (oils, various solutions, gases containing a large amount of hydrogen, hot gases, gases at low pressure), the twofold problem has arisen of investigating the behavior of standard devices at low Reynolds numbers and of studying new types of devices, more suitable for the measurement of fluid flow to Reynolds numbers as low as possible.

It is apparent from this discussion that by "low Reynolds numbers" we understand those flow conditions for which the flow Reynolds number is inferior to the lower limit to which the coefficient of discharge is maintained constant.

For incompressible fluids, the volumetric rate of flow through a constant-area differential type of fluid meter is expressed by the formula

$$q_v = \frac{Ca}{\sqrt{1-\beta^4}}\sqrt{2gh} \quad \ldots\ldots [1]$$

where

q_v = volumetric rate of flow
C = coefficient of discharge
a = orifice area = $\pi d^2/4$
d = orifice diameter
β = diameter ratio = d/D
D = pipe diameter
g = gravity
h = differential pressure head

Kretzschmer has shown (12)[2] that

$$K = \frac{C}{\sqrt{1-\beta^4}} = \frac{C_c}{\sqrt{1-C_c^2\beta^4+\dfrac{B}{f(\mathsf{R}_D)}}} \quad \ldots\ldots [2]$$

where

K = flow coefficient
C_c = coefficient of contraction
B = dimensionless form factor, a constant for a given device
R_D = pipe Reynolds number = $(4q_v)/(\pi D\nu)$
ν = coefficient of kinematic viscosity of fluid
$f(\mathsf{R}_D)$ = function of Reynolds number, increasing with its argument

According to Kretzschmer, $B/(f\mathsf{R}_D)$ represents, to a certain extent, the effect of frictional forces in the flow though the measuring device. The combined effect of this term and of the coefficient of contraction in Equation [2] explains to a certain extent the trend of the calibration curve—coefficient of discharge versus Reynolds number—for standard devices.

It appears that these devices should be used at low Reynolds numbers only with caution, that individual calibration is desirable, and that a lower measuring accuracy must generally be expected.

The foregoing considerations explain why numerous investigators have tried to develop new types of differential fluid meters in which, by an opportune compensation of the terms involving the effects of contraction and of friction in Equation [2], a constant value of the coefficient of discharge can be maintained at low Reynolds numbers.

Modifications of Standard Devices

Double-Bevel Orifice. Witte (18) attempted to modify the standard orifice in such a manner that the increase of C_c would be reduced but remain sufficient to combat the increase of the friction term when Reynolds number decreases. To this end, he used a new type of orifice, formed by two truncated cones separated by a cylindrical throat, Fig. 1. His tests showed not only that a suitable angle of convergence—approximately 15 deg—must be chosen, but also that the length of the converging cone must be sufficient; for $\beta = 0.4$, this length must at least be equal to $d/2$. Under these conditions the coefficient C remains constant within ± 0.5 per cent to $\mathsf{R}_D = 1000$ and within ± 2 per cent to $\mathsf{R}_D = 400$. A slight rounding of the entrance edge of the converging cone is generally favorable and permits a reduction in length.

Some of Witte's experiments have been repeated by Hansen (6) but no satisfactory check of the results was obtained. Hansen showed that C could not be maintained constant without omitting the cylindrical throat section.

Nevertheless, the double-bevel orifice with rounded entrance

[1] Head, Department of Hydraulics and Hydraulic Engineering, School of Civil Engineering, Cornell University. Mem. ASME.

Contributed by the Research Committee on Fluid Meters and presented at the Annual Meeting, New York, N. Y., November 28–December 3, 1954, of The American Society of Mechanical Engineers.

Note: Statements and opinions advanced in papers are to be understood as individual expressions of their authors and not those of the Society. Manuscript received at ASME Headquarters, September 29, 1954. Paper No. 54—A-190.

[2] Numbers in parentheses refer to the Bibliography at the end of the paper.

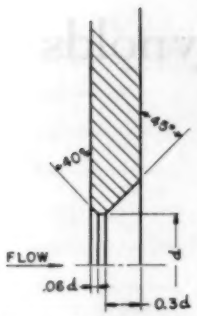

FIG. 1 DOUBLE-BEVEL ORIFICE

edge and sharp median edge was introduced in the 1935 edition of the VDI Code (1) for Reynolds numbers between 3000 and 100,000 and values of β between 0.4 and 0.5, with the stipulation that each orifice plate must be calibrated under conditions identical with its operating conditions.

The double-bevel orifice as studied by Witte with $\beta = 0.348$ was also retained by the Committee on Fluid Meters of the International Standards Association at a meeting in Helsinki in 1939. This device was declared suitable for Reynolds numbers between 50 and 30,000.

Double-bevel orifices with values of β ranging between 0.30 and 0.40 have also been tested by Ferroglio (4) but constant values of the coefficient of discharge could not be maintained in the useful range of Reynolds numbers (between 300 and 60,000). Witte (19) ascribes these irregularities to an insufficient length of the converging cone (0.02 d). With this value, he finds practically the same results. However, by increasing the length of the converging cone to 0.06 d, the results are much more satisfactory. This was checked to some extent by Ferroglio although toward $R_D = 10{,}000$, a sudden increase in the coefficient is observed. This increase is of the order of 1 per cent for $\beta = 0.346$.

A similar jump in the value of the coefficient was observed by Schlag (15).

Standard ISA Nozzle Without Cylindrical Throat. In another series of tests, Witte (17) tested a standard ISA nozzle without cylindrical throat. He succeeded in maintaining C constant to $R_D = 20{,}000$, instead of 80,000 for the nozzle with throat, for $\beta = 0.4$.

The standard nozzle without cylindrical throat was adopted by the VDI in 1935 for R_D between 4000 and 100,000 and β between 0.55 and 0.64. It was not retained in the international standardization.

Double Orifice—Orifices in Series. This type of flow-measuring device was developed by Wälzholz (16) who observed that it was possible to modify the curve of coefficient of discharge as a function of Reynolds number of an orifice by acting on the contraction of the fluid. This was evidenced in a series of experiments by Kretzschmer and Wälzholz (13) on the effects of a defective installation of an orifice. Wälzholz tried first to install, upstream of the orifice plate, a circular ring having a diameter between that of the pipe and that of the orifice. Such a device allowed maintaining a constant coefficient of discharge to low Reynolds numbers but it had a number of disadvantages, among which a great susceptibility to the roughness of the pipe, the difficulty of maintaining sharp edges, the necessity of using low values of β, and the fact that the orifice differential pressure was smaller than in the case of the orifice alone.

Wälzholz modified this system and replaced the ring by a second orifice, called auxiliary orifice, and installed a short distance upstream of the basic orifice. The differential pressure taps were located immediately upstream of the auxiliary orifice and downstream of the basic orifice.

Preliminary tests showed that, under certain conditions, it was possible to modify the curve of the coefficient of discharge of the orifice and even obtain a curve analogous to that of standard nozzles (coefficient of discharge decreasing with decreasing Reynolds number).

Wälzholz conducted a great number of experiments, trying to find optimum values for the distance between the two orifice plates and for their diameter ratios. His tests covered values of β as low as 0.3 and as high as 0.8.

Fig. 2(a) shows the modifications in the flow when the distance a between the two orifice plates is varied, the diameter ratios β of the basic orifice and $\beta' = d'/D$ of the auxiliary orifice remaining constant. Cases 3 and 5 exhibit a constant value of the coefficient over a wide range of Reynolds numbers. Fig. 2(b) describes the evolution of the phenomenon when β is changed, the spacing a and β' remaining constant. Wälzholz succeeded in maintaining the coefficient of discharge constant to values of Reynolds number of from 2000 for $\beta = 0.09$ to 29,000 for $\beta = 0.8$. These values are considerably lower than the corresponding values for standard orifices.

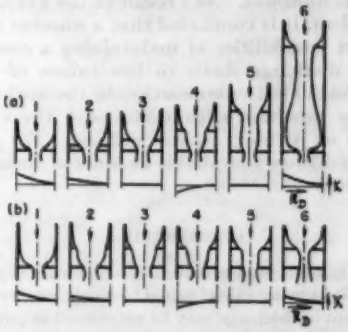

FIG. 2 FLOW CONDITIONS THROUGH TWO ORIFICES IN SERIES (After Wälzholz.)

The double orifice thus appears to constitute a statisfactory compromise between an orifice and a nozzle.

Some of Wälzholz's results have been verified by Koennecke (10). The agreement is reasonably satisfactory although the coefficient of discharge could not be maintained constant by Koennecke to Reynolds numbers quite as low.

NEW DEVICES

Schmidt's Nozzle. The double-bevel type of orifice, as developed by Witte, is characterized, not only by the value of β, but also by the angles and lengths of the two cones and eventually the length of the cylindrical throat. All edges are sharp and therefore likely to deteriorate when the cylindrical throat is omitted. The accurate measurement of d is difficult and has to be done optically.

For all these reasons, Schmidt suggested using a simpler shape, characterized by the diameter ratio β and one dimension only. The profile of this device, which was originally called the Schmidt nozzle, is formed by a half-circumference the diameter of which is equal to the thickness t of the orifice plate. According to Giese (5) the most favorable ratio d/t is equal to 4. For this value, the coefficient of discharge remains constant to $R_D = 150$ for $\beta = 0.25$ and to $R_D = 270$ for $\beta = 0.3$. It is difficult, however, to draw definite conclusions from Giese's experiments since for the low values of β considered the coefficient of discharge of other orifices is also reasonably constant. Furthermore, Giese's results are not confirmed by Koennecke (11). The latter observes a discrepancy of approximately 2 per cent in the value of C at $R_D = 5000$.

Richter's Nozzles. Richter (14) has developed several nozzle shapes in which he tries to guide the jet in such a manner that the position of the vena contracta does not change with Reynolds number. His results, although of interest, require confirmation.

Quadrant-Edge (Round-Edge, Quarter-Circle) Orifices. According to Koennecke (10, 11) this is one of the differential types

of fluid meters most suitable for discharge measurements at low Reynolds numbers. The radius of curvature r, Fig. 3, is equal to the thickness of the orifice plate. Optimum values of the ratio r/d, as given by Koennecke, are shown in Table 1. The quadrant-edge orifice may be used for values of β as low as 0.225, but the most suitable diameter ratios are between 0.5 and 0.7. The coefficient of discharge remains constant within ±0.5 per cent to values of Reynolds number as low as 700 for $\beta = 0.225$ and 250 for $\beta = 0.7$. The constancy of the coefficient is maintained to upper limits of 56,000 and 250,000, respectively.

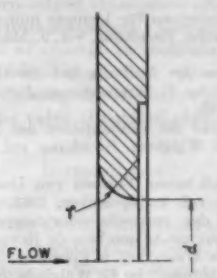

FIG. 3 QUADRANT-EDGE ORIFICE

When the diameter ratio β is larger than 0.628, the center of curvature falls outside of the inside wall of the pipe and the upstream face of the orifice plate must be machined again after the orifice opening has been cut.

TABLE 1 QUADRANT-EDGE ORIFICE. KOENNECKE'S DATA

			Limits of constant coefficient	
β	r/d	K	R_D min	R_D max
0.225	0.100	0.771	700	56000
0.400	0.114	0.792	650	140000
0.500	0.135	0.829	430	230000
0.600	0.209	0.902	350	250000
0.625	0.285	0.933	330	250000
0.656	0.380	0.985	270	250000
0.692	0.446	1.022	250	250000

Koennecke's results have been checked by Ferroglio (4). The latter observes that very small defects of manufacture affect the coefficient of discharge in a nonnegligible amount. The over-all pressure loss of these devices is between that of standard orifices and standard nozzles, under identical flow conditions.

Koennecke's results are also well substantiated by experiments by Beck (2) and Schlag (15), although the range of Reynolds numbers covered in those experiments is not as large as Koennecke's. Table 2 gives a comparison for $\beta = 0.500$.

TABLE 2 QUADRANT-EDGE ORIFICE. COMPARISON OF DATA FOR $\beta = 0.500$

			Limits of constant coefficient	
Author	r/d	K	R_D min	R_D max
Koennecke	0.135	0.829	430	230000
Beck	0.125	0.832	600	30000
Schlag	0.135	0.835	2000	100000

The quadrant-edge orifice has been retained for an international standardization by the International Standards Association since 1939, for values of β between 0.225 and 0.700 and Reynolds numbers between 500 and 300,000. Values of the coefficient of discharge, however, are not standardized; each device must be calibrated individually under conditions as close as possible to working conditions.

Recently, the quadrant-edge orifice has been studied by D. Brand in the Royal Dutch/Shell Laboratory in Delft, Holland, (3). It was found that the results obtained were valid for flange taps, as well as for corner taps.[2] Values of the expansion factor for quadrant-edge orifices were determined. Those values are slightly different from those for square-edged orifices.

Cylindrical Nozzle. The cylindrical nozzle was also originally studied by Koennecke (10, 11). He judged that although its field of utility was more restricted than that of quadrant-edge orifices its use was recommended at low values of β.

The cylindrical nozzle consists of a short cylinder with sharp upstream edge, Fig. 4; it is of simple manufacture and therefore of comparatively low price.

In an extensive series of experiments, Jorissen and Newton (7) first checked Koennecke's results, Table 3.

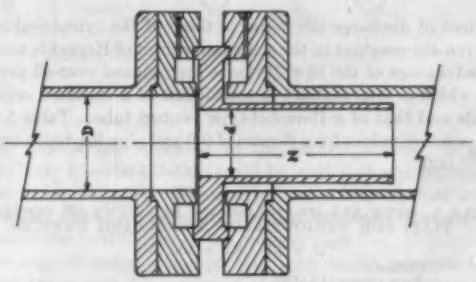

FIG. 4 CYLINDRICAL NOZZLE

However, owing to the fact that they used only water in their experiments, they could not obtain Reynolds numbers quite as low as those reached by Koennecke.

An attempt was then made to determine whether by cutting the nozzles, shorter devices could be obtained, still maintaining satisfactory constancy of the coefficient of discharge at low Reynolds numbers. The results are summarized in Table 4.

TABLE 4 CYLINDRICAL NOZZLES (JORISSEN AND NEWTON)

β	(z/d) optimum	C	R_D min
0.2224	1.5	0.798	2200
0.3709	1.7	0.803	7000
0.4944	2.0	0.811	15000
0.5934	1.5	0.808	25000

Cylindrical Nozzle With Rounded Entrance Edge. The optimum dimensions of this type of device, as studied by Koennecke (10, 11) may be obtained only for values of β larger than 0.7. It is recommended that the center of curvature of the rounded entrance be situated on the inner wall of the pipe, so that $r = (D - d)/2$. At best proportions, the values of β are between

[2] Beck (2) also used flange taps.

TABLE 3 CYLINDRICAL NOZZLES

	Koennecke $D = 4$ in.				Jorissen and Newton $D = 4.043$ in.			
			Limits of constant coefficient				Limits of constant coefficient	
z/d	β	C	R_D min	R_D max	β	C	R_D min	R_D max
1.547	0.2249	0.8000	600	30000	0.2224	0.798	2000	34000
1.750	0.3752	0.8029	1000	130000	0.3709	0.803	5000	100000
2.150	0.50	0.8075	1400	150000	0.4944	0.812	15000	190000
2.350	0.60	0.8117	1600	250000	0.5934	0.811	18000	260000
2.854	0.70	0.8037	1700	550000	0.6928	0.812	22000	300000

0.762 and 0.866. For $\beta = 0.80$, the coefficient of discharge remains constant between the limits of $R_D = 1500$ and $R_D = 250{,}000$. Best results are obtained with values of z/d larger than 0.5.

Cylindrical Nozzle With Conical Diffuser (Builders S. J. Flow Tube). A further modification of the cylindrical nozzle consists in the addition of a conical diffuser, thus transforming the nozzle into a venturi tube, Fig. 5 (ref. 8, 9). Values of the coefficient of discharge are equal to those of the cylindrical nozzle and remain constant to the same lower limit of Reynolds number. An advantage of the new device is the reduced over-all pressure loss which is intermediary between that of a standard orifice or nozzle and that of a Herschel-type venturi tube. Table 5 gives comparative values for a β-ratio of 0.6 and pipe Reynolds number of 150,000.

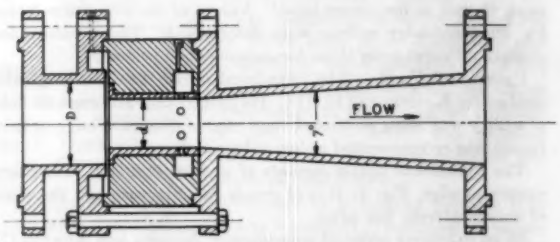

FIG. 5 CYLINDRICAL NOZZLE WITH CONICAL DIFFUSER

TABLE 5 OVER-ALL HEAD LOSS (IN PER CENT OF DIFFERENTIAL) FOR VARIOUS FLOW-MEASURING DEVICES

($\beta = 0.6$, $R_D = 150{,}000$)

Orifice	55
Flow nozzle (ASME)	54
Herschel venturi tube	11
Cylindrical nozzle	60
Cylindrical nozzle with conical diffuser	32

The over-all pressure loss of the cylindrical nozzle with conical diffuser can further be reduced by a slight beveling of the upstream edge of the nozzle; unfortunately, the lower limit of Reynolds number to which the coefficient of discharge remains constant is then increased.

CONCLUSIONS

It seems quite possible to maintain a constant coefficient of discharge down to low values of Reynolds number. A number of devices offer distinct possibilities in this field; particularly noteworthy, in the author's opinion, are the quadrant-edge orifice and the cylindrical nozzle with or without conical diffuser. For both, experimental evidence is available as proof of their satisfactory operation.

BIBLIOGRAPHY

1 "Regeln für die Durchflussmessung mit genormten Düsen und Blenden," DIN 1952, herausg. v. Strömungsmesserausschuss des Verein deutscher Ingenieure, Berlin, Germany, third edition, 1935.

2 "Measurement of Viscous Fluids—Tests Show Round-Edge Orifice May Be Used in the Flow," by H. V. Beck, *The Oil Weekly*, vol. 81, June 8, 1936, pp. 39–41.

3 "Quarter-Circle Orifices," by D. Brand, Delft Report 1312 M, Royal Dutch/Shell Laboratory, Delft, Holland, August, 1953.

4 "Boccagli e diaframmi per piccoli numeri di Reynolds," by L. Ferroglio, *L'Energia Elettrica*, vol. 19, 1942, pp. 413–421.

5 "Mengenmessung mit Düsen und Blenden bei kleinen Reynoldsschen Zahlen," by H. G. Giese, *Forschung auf dem Gebiete des Ingenieurwesens*, vol. 4, January-February, 1933, pp. 11–20.

6 "Dusen und Blenden bei kleinen Reynoldsschen Zahlen," by M. Hansen, *Forschung*, vol. 4, March-April, 1933, pp. 64–66.

7 "Discharge Measurements by Means of Cylindrical Nozzles," by A. L. Jorissen and H. T. Newton, Trans. ASME, vol. 74, 1952, pp. 825–835.

8 "Le debitmètre B.S.J. pour la mesure des débits de fluides aux faibles nombres de Reynolds," by A. L. Jorissen, *Revue Universelle des Mines*, vol. 9, March, 1953, pp. 144–151.

9 "Here's a New Flow Meter Design," by A. L. Jorissen, S. L. Wise, and J. M. Symons, *Petroleum Processing*, vol. 8, December, 1953, pp. 1870–1873.

10 "Messdüsenformen für kleinere und mittlere Reynoldszahlen," by W. Koennecke, *Zeitschrift VDI*, vol. 83, March 11, 1939, pp. 318–319.

11 "Neue Düsenformen für kleinere und mittlere Reynoldszahlen," by W. Koennecke, *Forschung*, vol. 9, May-June, 1938, pp. 109–125.

12 "Der Einfluss der Reibung auf den Durchflussbeiwert der Drosselmessgeräte," by F. Kretzschmer, *Forschung*, vol. 4, March-April, 1933, pp. 93–95.

13 "Versuche über die Einbaufehler der Normblenden," by F. Kretzschmer and G. Wälsholz, *Forschung*, vol. 5, January-February, 1934, pp. 25–35.

14 "Versuche mit neuen Formen von Durchflussdüsen," by H. Richter, *Forschung*, vol. 2, November, 1931, pp. 387–394.

15 "Essais sur des appareils déprimogenes proposés pour la mesure des débits aux petits nombres de Reynolds," by Alb. Schlag, *Revue Universelle des Mines*, vol. 6, February, 1950, pp. 45–47.

16 "Die Doppelblende," by G. Wälsholz, *Forschung*, vol. 7, July-August, 1936, pp. 191–201, and 226.

17 "Durchflussbeiwerte der IG-Messmündungen für Wasser, Öl, Dampf, und Gas," by R. Witte, *Zeitschrift VDI*, vol. 72, October 20, 1928, pp. 1493–1502.

18 "Durchflusszahlen von Düsen und Stauränderm," by R. Witte, *Technische Mechanik und Thermodynamik*, vol. 1, 1930, pp. 34–41, 72–85, 113–120.

19 "Die Durchflussmessung zäher Flussigkeiten nach dem Wirkdruckverfahren," by R. Witte, *Zeitschrift VDI*, vol. 87, May 15, 1943, pp. 289–290.

Discussion

W. A. GROSS.[4] The inconvenience of dealing with variable coefficients of discharge provides suitable motivation for papers such as this. Professor Jorissen's work, together with the analysis of other investigators' efforts, provides valuable information about this troublesome aspect of fluid metering.

It seems desirable to point out, as an addition to the author's remarks, that some applications may make a different meter property desirable. When one plans to use a constant area-differential-type flowmeter in the very low Reynolds-number range, it is convenient to utilize a meter which has, to the highest possible flow rate, a direct relationship between the coefficient and the square root of Reynolds number. Under these conditions, the discharge is directly proportional to the pressure drop across the meter.

The difficulties encountered when the coefficient of discharge is in the variable range can be overcome using a technique suggested by F. N. Connet.[5] He pointed out that the meter coefficient may be determined as a function of (over-all head loss)/(differential head). This technique uses the flowmeter as its own viscosimeter and removes the necessity of determining the Reynolds number.

An important difficulty which is always present in low Reynolds-number work is obtaining accurate pressure measurements. This provides a practical limit to the applicability of constant area-differential-type flowmeters at low discharges.

[4] Formerly Assistant Professor, Department of Theoretical and Applied Mechanics, Iowa State College, Ames, Iowa. Now at Bell Telephone Laboratories, Inc., Murray Hill, N. J. Assoc. Mem. ASME.

[5] Discussion, Trans. ASME, vol. 45, 1923, p. 74.

Effect of a Globe Valve in Approach Piping on Orifice-Meter Accuracy[1]

By J. W. MURDOCK,[2] C. J. FOLTZ,[3] and CLARENCE GREGORY, JR.,[4] PHILADELPHIA, PA.

This paper presents the results of a series of steam and water tests on sharp-edged thin-plate orifices preceded by a globe valve at various distances. Curves are given, showing the magnitude of change in indicated flow, when the approach piping is less than that recommended by the Joint AGA-ASME Committee on Orifice Meters. Comparative curves with the valve throttled also are given.

Introduction

THE tests described in this paper were conducted at the U. S. Naval Boiler and Turbine Laboratory (1)[5] as part of the co-operative program of the Joint AGA-ASME Committee on Orifice Meters. Tests with steam and water were made to supplement those with natural gas at Rockville, Md., and Refugio, Texas, and others with water at the National Bureau of Standards (2, 3).

A major requirement for the metering of fluid flow by means of an orifice is that the flow approaches the orifice in a normally turbulent pattern, a condition which can be obtained by providing adequate length of straight pipe preceding it. The Joint AGA-ASME Committee on Orifice Meters has established standards of piping requirements (4) delineating this length of pipe for the most common types of installations. These standards, however, only provide for the condition of no interference, and little information is available showing the magnitude of change in the indicated flow rate when less than the minimum straight pipe is used. Since space is often limited, and particularly so aboard ship, this problem of less than the minimum required straight pipe and the magnitude of error in flow measurement therefrom, is a recurring one. This paper presents the results of a series of steam and water tests on sharp-edged thin-plate orifices preceded by a globe valve at various distances.

Equipment and Operation

The test section, Fig. 1, consisted of a straight run of 4-in. pipe, 147 pipe diameters long, discharging into a condenser, thence to a weighing system. Either steam or water could be introduced into the system. Two orifice assemblies were used, designated "control" and "test" for the up and downstream locations, respectively. A straight run of pipe 60 diam in length, after the inlet

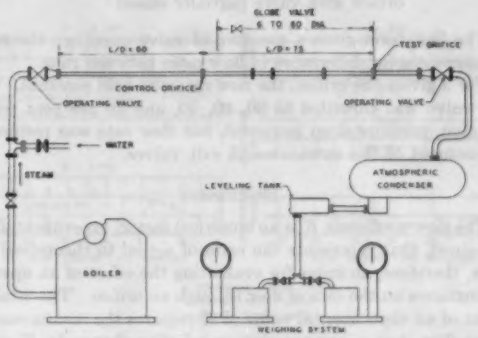

Fig. 1 Flow Diagram

flange, formed the approach to the control orifice. A globe valve (Navy Standard B-137) could be located at any multiple of 3 pipe diameters between 6 and 60 upstream from the test orifice. The valve was installed with its stem vertically upward and perpendicular to the plane of the pressure taps.

The control orifice was equipped with radius pressure taps; the test orifice with flange taps in addition thereto. Orifices were constructed in conformity with ASME standards (4) of $^1/_4$-in. 18-8 stainless steel, $6^3/_8$-in-OD holes beveled 45 deg on the downstream sides, and cylindrical edges $^5/_{64}$ in. thick. Care was exercised to make the upstream corners of the orifice plates sharp and square. Eight-inch centering pins—located 120 deg apart and flush with the upstream faces of the orifices but extending $^1/_4$ in. beyond their downstream faces—were installed in the plates to insure their accurate centering in the pipe. Nine pairs of orifices were used with the following β ratios: 0.30, 0.40, 0.50, 0.65, 0.74, 0.79, 0.80, 0.82, and 0.85.

Measurements of the variables were made as indicated in Table 1. All instruments were calibrated frequently.

TABLE 1 INSTRUMENTATION

Variable	Instrument system	Smallest increment
Pressure	Bourdon tube test gages, range 0–300 psi	0.5 psi
Differential	Manometers with various fluids so that a minimum of 30 in. was maintained for any flow rate	0.1 in.
Temperature	Iron-constantan thermocouples with junctions in total temperature wells (5) and ice bottles. Potentiometer range 0–40 mv	0.02 mv
Mass flow	Alternately into two weigh tanks, scale range of each 0–4000 lb	1 lb

Flow rates and line pressures were controlled by valves at the entrance and exit of test section. Data were recorded after a steady state had been established.

A 100-in. U-tube manometer, with mercury under water as the indicating fluid, was connected across the globe valve. Relative opening of the valve was calculated by means of the following relationship

$$\text{Relative valve opening} = \sqrt{\frac{H_o}{H_s}}\sqrt{\frac{h_s}{h_o}} \quad \ldots\ldots [1]$$

---

[1] The opinions and assertions in this paper are the private ones of the authors, and are not to be construed as official or reflecting the views of the Navy Department or the Naval Establishment at large.

[2] Superintendent, Instrument Division, Naval Boiler and Turbine Laboratory, Philadelphia Naval Base. Mem. ASME.

[3] Engineer-in-Charge, Scientific Branch, Naval Boiler and Turbine Laboratory, Philadelphia Naval Base. Assoc. Mem. ASME.

[4] Project Engineer, Scientific Branch, Instrument Division, Naval Boiler and Turbine Laboratory, Philadelphia Naval Base.

[5] Numbers in parentheses refer to the Bibliography at the end of the paper.

Contributed by the Research Committee on Fluid Meters and presented at the Annual Meeting, New York, N. Y., November 28–December 3, 1954, of The American Society of Mechanical Engineers.

Note: Statements and opinions advanced in papers are to be understood as individual expressions of their authors and not those of the Society. Manuscript received at ASME Headquarters, August 25, 1954. Paper No. 54—A-122.

where

H_o = inches of mercury differential across valve when wide open

H_x = inches of mercury differential across valve when partially closed

h_o = inches of manometer fluid differential across control orifice with valve wide open

h_x = inches of manometer fluid differential across control orifice with valve partially closed

The first term gives a measure of valve opening; the second compensates for differences in flow rates between runs.

For a given-size orifice, the flow rate was held constant. When the valve was throttled to 80, 60, 40, and 20 per cent relative opening, pressure drop increased, but flow rate was restored by adjustment of the entrance and exit valves.

Discussion

The flow coefficient K is an empirical factor, experimentally determined, that represents the ratio of actual to theoretical flow. It is, therefore, an index for evaluating the effect of an upstream disturbance on the rate of flow through an orifice. The establishment of an experimental value of K requires the measurement of mass flow, but a comparative or relative change in K can be measured by placing two nearly identical orifices in series, one with an approach of more than the minimum required straight pipe, the other with a disturbance-producing type of installation. Both methods were employed in these tests.

Comparison runs were made with water. The upstream orifice, Fig. 1, was free of any obstruction and designated control, the downstream orifice as test. Before and after each series of tests with the globe valve, base runs were made without the valve in the line. All of these were made with matched orifice plates having internal diameters within a few thousandths of an inch of each other. Mass flow and fluid density were the same at each orifice, so that the only variable was pressure differential. Letting the symbol Δp designate the differential pressure, and the subscripts C and R designate the radius taps of the control and test orifices, respectively, then the change in K is represented by $\sqrt{\Delta p_C/\Delta p_R}$. This value is used as the interference ratio for the plots shown in Fig. 8. For the flange taps of the test orifice a change in the value of K for comparison with the base runs is given by $\sqrt{\Delta p_C/\Delta p_F}$ where the subscript F denotes the flange taps of the test orifice.

Weighed water and steam runs were made under conditions described in reference (3). Base runs in this case established the flow coefficient of the test orifice without the valve. The values of interference ratio shown in Fig. 8 were obtained by dividing the coefficient obtained with the globe valve preceding the orifice by the coefficient established from the base runs.

As could be expected, the data from the largest orifice (β = 0.850) showed the greatest spread between the initial and final runs. The spread for the flange taps was 2 per cent, that for the radius taps, 4 per cent. This spread of data was seldom exceeded by either that due to valve location or opening. Results were similar for both the flange and radius taps. Fig. 2 shows radius-tap data for various valve locations and valve openings. The spread of data for the base runs is indicated on the curves by shading. Inspection of the curves shows no definite trend from which the effect of interference could be ascertained.

The difference between the initial and final base runs for the β = 0.822 orifice was approximately $1^1/_2$ per cent for both the radius and flange taps. Fig. 3 shows typical data for the radius taps. With the valve wide open there is some indication of change with valve location, but with the valve at 60 and 20 per cent of capacity, the trend disappears. It is likely that the reproducibility of this ratio orifice is less than that shown by the base runs. For all practical purposes interference cannot be determined from these data.

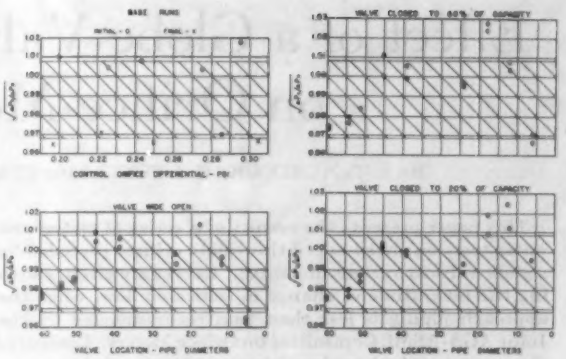

Fig. 2 Comparative Tests, β = 0.850 (Radius Taps)

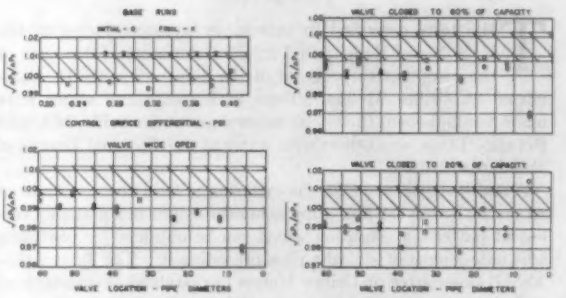

Fig. 3 Comparative Tests, β = 0.822 (Radius Taps)

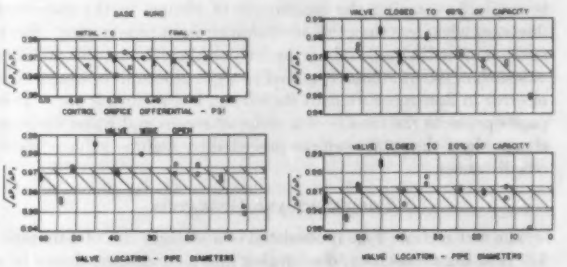

Fig. 4 Comparative Tests, β = 0.802 (Flange Taps)

The spread of data obtained from the base runs of the β = 0.802 orifice, unlike the larger sizes, is due more to the initial runs than to the difference between the initial and final. Typical flange-tap data are shown in Fig. 4. Data from the radius taps are similar in appearance. Here again, there is no trend to indicate the effect of either valve location or throttling.

The β = 0.742 orifice was the largest tested that showed definite interference. There was little spread of data between initial and final base runs for either set of taps. Fig. 5 shows typical radius-tap data (flange tap being similar). The curve was faired through data obtained with the valve wide open and then superimposed over that for various valve openings. As can be seen, relative valve opening has little discernible effect on interference. The

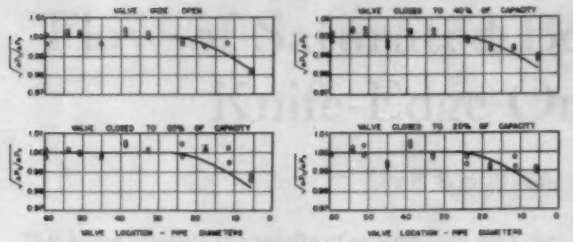

FIG. 5 COMPARATIVE TESTS, $\beta = 0.742$ (RADIUS TAPS)

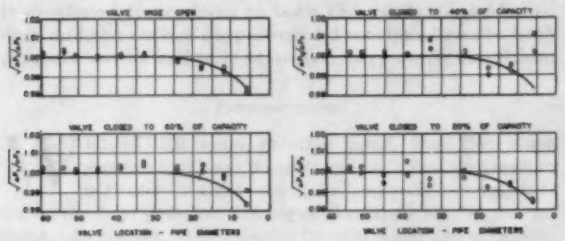

FIG. 6 COMPARATIVE TESTS, $\beta = 0.650$ (RADIUS TAPS)

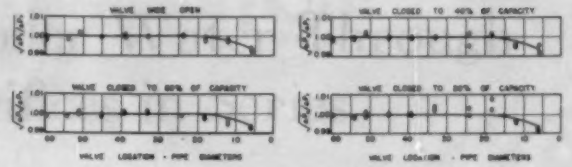

FIG. 7 COMPARATIVE TESTS, $\beta = 0.495$ (FLANGE TAPS)

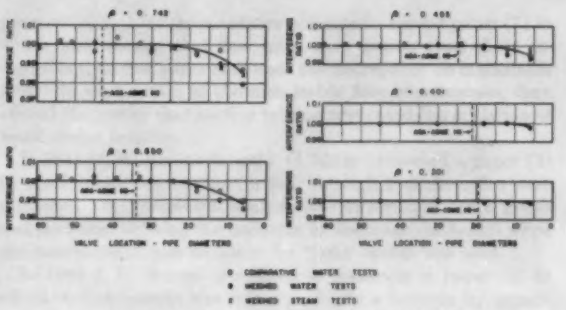

FIG. 8 SUMMARY (RADIUS TAPS)

effect of valve location is seen to begin at approximately 25 pipe diameters.

Base runs of the $\beta = 0.650$ orifice showed less than $^1/_2$ per cent variation for either set of taps. Fig. 6 shows typical results obtained with the valve wide open and closed to 60, 40, and 20 per cent capacity. The curve obtained from the data with the valve wide open, as for the $\beta = 0.742$ orifice, is superimposed over that for the various valve openings, illustrating the negligible effect of valve closure. The point of minimum straight pipe for no interference seems to begin at about 25 diam.

The smallest orifice tested using the comparison method was the $\beta = 0.495$. Base runs were nearly identical for both sets of taps. Again, a single curve represents data for the valve either wide open or closed to 20 per cent of capacity as shown in Fig. 7. Interference seems to begin at about 15 pipe diam.

Fig. 8 is a summary of typical test data. Orifice ratios above 0.742 have been omitted because of the irreproducibility of the data, and flange taps because of their similarity to the radius-tap data shown. Comparative tests show little difference in the weighed steam and water data conducted on the same orifice. Included in this figure are the AGA-ASME recommended straight minimum lengths (4) for the various orifices tested. A further comparison is given in Table 2.

It is of interest to note that minimum straight pipe did not increase for ratios greater than 0.650 although at 6 diam the magnitude of change was 2 per cent for the 0.742 as compared to half that for the 0.650 ratio. For ratios less than 0.650 the measured change was $^1/_2$ per cent or less at 6 diam, and it is questionable if any real interference was encountered with the smallest (0.301) even at 6 diam.

TABLE 2 COMPARISON OF MINIMUM PIPE FOR NO INTERFERENCE

Orifice beta ratio	Approximate straight pipe in diameters	
	AGA-ASME	Present tests
0.742	43	25
0.650	34	25
0.495	25	15
0.401	22	10
0.301	20	6 (or less)

CONCLUSIONS

The change of indicated flow rate due to a globe valve placed 6 diam before an orifice is 2 per cent or less for orifice ratios less than 0.75. For greater ratios the spread of data with or without the valve in the line is of such magnitude that valve disturbance cannot be distinguished from reproducibility, and no conclusions can be drawn from the data.

The exact location of the point of no interference is difficult to ascertain. General agreement of data was obtained between the comparative and weighed tests. Neither the use of steam or water, nor the location of the pressure differential taps at the flange or radius positions showed any significant influence on results obtained. The effect of globe-valve throttling down to 20 per cent relative opening was negligible.

The curves shown in Fig. 8 may be used to estimate the probable error of an installation for either flange or radius-tap assemblies. The use of orifice ratios greater than those shown in Fig. 8 should be avoided for accurate flow measurement.

ACKNOWLEDGMENTS

This work was made possible by the financial support and sponsorship of the Bureau of Ships, Navy Department, Washington, D. C. The guidance and assistance of the Joint AGA-ASME Committee on Orifice Meters was most helpful. The authors are grateful to the personnel of the U. S. Naval Boiler and Turbine Laboratory who assisted in these tests.

BIBLIOGRAPHY

1 "The Naval Boiler and Turbine Laboratory," by Capt. E. Kransfelder, USN, Trans. SNAME, vol. 55, 1947, pp. 341–358.

2 "Investigation of Orifice Meter Installation Requirements," Interim Research Report No. 2 of the Joint AGA-ASME, Committee on Orifice Meters, New York, N. Y., January, 1954.

3 "Experimental Evaluation of Expansion Factors for Steam," by J. W. Murdock and C. J. Foltz, Trans. ASME, vol. 75, 1953, pp. 953–959.

4 "History of Orifice Meters and the Calibration, Construction and Operation of Orifices for Metering," Report of the Joint AGA-ASME Committee on Orifice Coefficients, New York, N. Y., 1935.

5 "Measurement of Temperatures in High-Velocity Steam," by J. W. Murdock and E. F. Fiock, Trans. ASME, vol. 72, 1950, pp. 1155–1161.

Flow of Saturated Boiler Water Through Knife-Edge Orifices in Series

By E. S. MONROE, JR.,[1] ITHACA, N. Y.

This paper presents the results of experiments with the flow of saturated boiler water through from one to four knife-edge orifices arranged in series. A useful equation is developed to conform to both the available published data and the author's experimental results when the back pressure on the orifice is at or near barometric condition.

Introduction

WHENEVER water, or other liquid, flows from some pressure to a lower pressure and the initial temperature is greater than the saturation temperature corresponding to the final pressure, flashing of the liquid into vapor can occur. As a result, flow formulas for cold water are erroneous when applied to the flow of heated and compressed liquids.

This phenomenon has become of importance in engineering computations. Both in the United States (1)[2] and abroad (2, 3), engineers have proposed the substitution of orifices as regulators instead of traps for draining condensate from heaters. Several forms of traps utilizing the flashing phenomenon are available commercially today.

Orifices in series are sometimes used for control of continuous blowdown from high-pressure steam-generator drums and for recirculation of feedwater from the discharge side of boiler feed pumps in an effort to control erosion.

The flashing phenomenon also has been utilized in a calorimeter for the determination of the density and quality of steam-and-water mixtures in a steam generator (4, 5).

Because of the increasing use and importance of orifices passing heated and compressed liquids, several authors, in recent years, have attacked the problem both analytically and experimentally.

In 1937 W. T. Bottomley presented a very important paper (2) in which he derived theoretical expressions for the flow through an orifice at constant entropy and also gave experimental data for the flow through a single orifice. One important feature of this paper was the fact that the actual measured flow through the orifice was as much as five times the theoretical flow when using the formulas based on constant entropy expansion. Bottomley advanced the theory that surface tension was retarding the formation of vapor bubbles and, consequently, the density of the water-and-steam mixture was remaining greater than the theoretical value.

In 1936, M. C. Stuart and D. R. Yarnall published a paper (6) in which they analyzed the flow of fluids through two orifices in series. A graphical solution was presented based upon critical pressures. In 1944 these authors presented a second paper (7) in which they showed that flow rates were greater than those assumed in their first paper and based the discrepancy on metastable flow. In explanation of the metastable flow phenomenon, they offered the theory that surface tension prevented the initiation of small steam bubbles.

In 1941 M. W. Benjamin and J. G. Miller presented a paper (1) in which experimental data for flow through a single orifice were published. No theoretical analysis was undertaken but a graph was presented showing the variation in discharge coefficient when the conventional flow equation for "cold" water was used.

In 1946 J. G. Burnell published in Australia a paper (3) in which surface tension was introduced into a formula by experimental means. For a single orifice the results were in excellent agreement with experimental data. To the author's knowledge, this is the most significant contribution made to date in the field.

Test Equipment

Because of the lack of published data and prior to the author's knowledge of the Burnell work, experimental work was undertaken to study metastable flow. Variables selected for this study included (*a*) orifice size, (*b*) number of orifices in series, (*c*) presence of solids in the water, (*d*) spacing of orifices, (*e*) direction of flow, (*f*) variations in initial pressure, and (*g*) variations in final pressures.

The experimental setup was as illustrated in Fig. 1. Data were taken in 250 runs with this equipment over the following ranges: (*a*) Knife-edge orifice of $^1/_8$ in. thickness, beveled 45 deg from $^1/_4$ to $^5/_8$ in. diam; (*b*) one, two, three, or four orifices in series; (*c*) water flowing with methyl-orange alkalinities of 230 to 3320 ppm controlled by adding sodium carbonate to boiler feedwater; (*d*) orifice spacings of 6 in. to 4.7 ft; (*e*) both vertical and horizontal flow; (*f*) initial-pressure ranges of 31 to 155 psia; and (*g*) final-pressure ranges of 14.7 to 65 psia.

Pressures were measured by means of calibrated bourdon gages and temperatures by means of mercury-in-glass thermometers in oil-bath wells. Equilibrium conditions were obtained in each case with the level of the water steady in the gage glass on the water column. This level varied throughout the tests from 6 to 12 in. submergence on the first orifice. The orifices and their connecting piping were insulated heavily.

Correlation of Data

Three examples of typical data are shown in Fig. 2 for two, three, and four orifices in series, and in each case the largest pressure drop is across the last orifice. These expansions are shown plotted along constant-enthalpy lines. Test data showed that all temperatures corresponded to saturation pressures at points of measurement.

Numerous dimensional-analysis correlations were attempted without significant success. These included the use of surface tension. Finally, the pseudodimensional analysis shown in Fig. 3 was selected as the best obtainable from the various studies made. The term "pseudo" is used inasmuch as each group has the dimensions of the acceleration of gravity, g.

The relationship derived from Fig. 3 is

---

[1] Assistant Professor of Mechanical Engineering, Heat Power Department, East Mechanical Laboratory, Cornell University. Mem. ASME.

[2] Numbers in parentheses refer to the Bibliography at the end of the paper.

Contributed by the Research Committee on Fluid Meters and presented at the Annual Meeting, New York, N. Y., November 28–December 3, 1954, of The American Society of Mechanical Engineers.

Note: Statements and opinions advanced in papers are to be understood as individual expressions of their authors and not those of the Society. Manuscript received at ASME Headquarters, August 24, 1954. Paper No. 54—A-118.

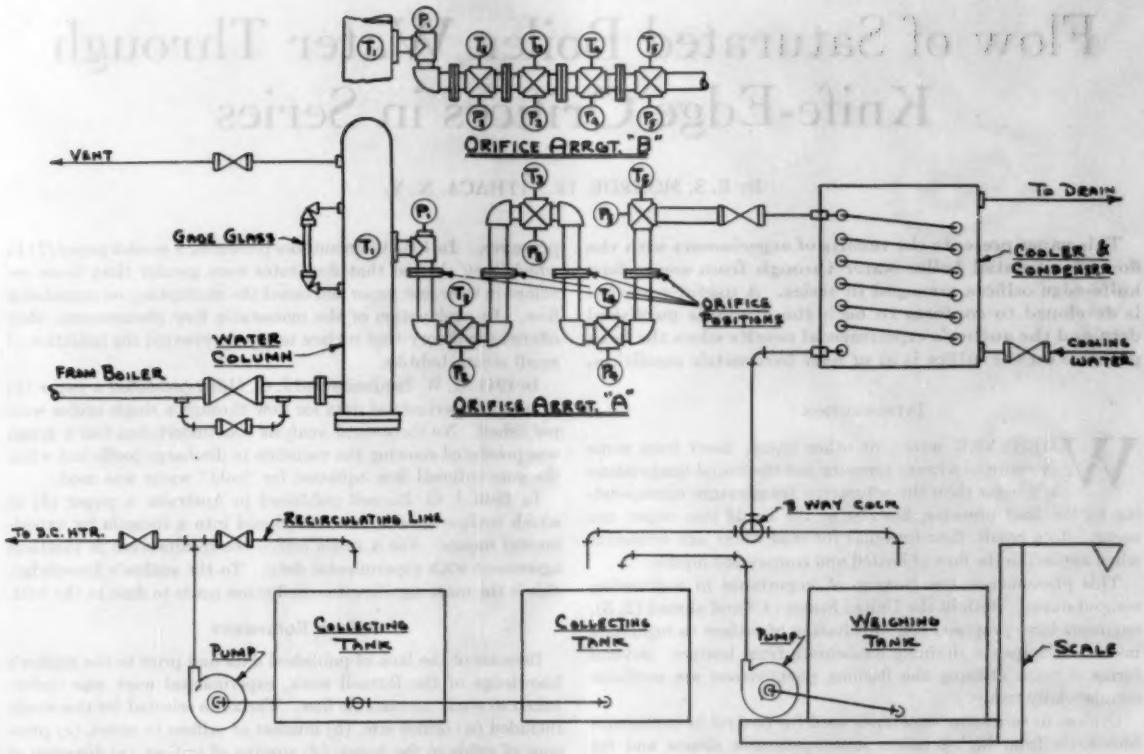

FIG. 1 DIAGRAM OF TEST SETUP

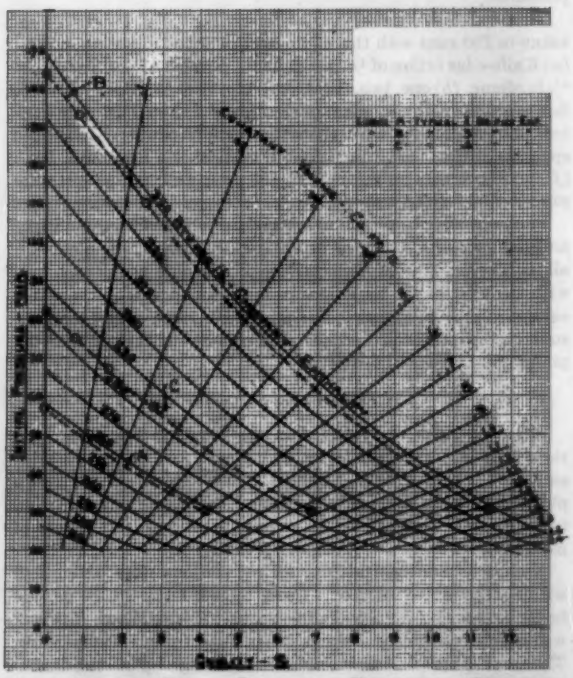

FIG. 2 PRESSURE-QUALITY DIAGRAM FOR EXPANSION OF SATURATED WATER

$$(N)^{0.75}\frac{G\mu}{(P_1-P_2)^2} = 36.4(10)^{10}\left[\frac{(P_1-P_2)T^2\rho}{\mu^2}\right]^{-1.133} \ldots [1]$$

where

N = number of orifices in series
G = mass flow (lb/sec-sq ft)
μ = initial absolute viscosity (lb/hr-ft)
$P_1 - P_2$ = pressure drop across all orifices (psi)
T = initial absolute temperature (deg R)
ρ = initial density (pcf)

For convenience this reduces to

$$G = \frac{25{,}300(P_1-P_2)^{0.9}(\mu)^{1.4}}{(N)^{0.75}\left(\frac{T}{1000}\right)^{2.4}(\rho)^{1.2}} \ldots [2]$$

This relationship satisfies the line drawn through the majority of the points plotted. Some of the deviation of the points not on the line may be due to experimental error but the author feels that it is caused by high back pressure and will discuss this point further. Since most of the test runs were at or near a back pressure of atmospheric pressure, the relationship is presented as valid only under that condition.

The derivation of the $(N)^{3/4}$ relationship may easily be seen from Figs. 4 and 5.

After determination of Equation [1] shown in Fig. 3, previously published data were analyzed to find out how they agreed or disagreed. Fig. 6 is a graphical comparison with data from three published sources compared with the straight line which represents Equation [1].

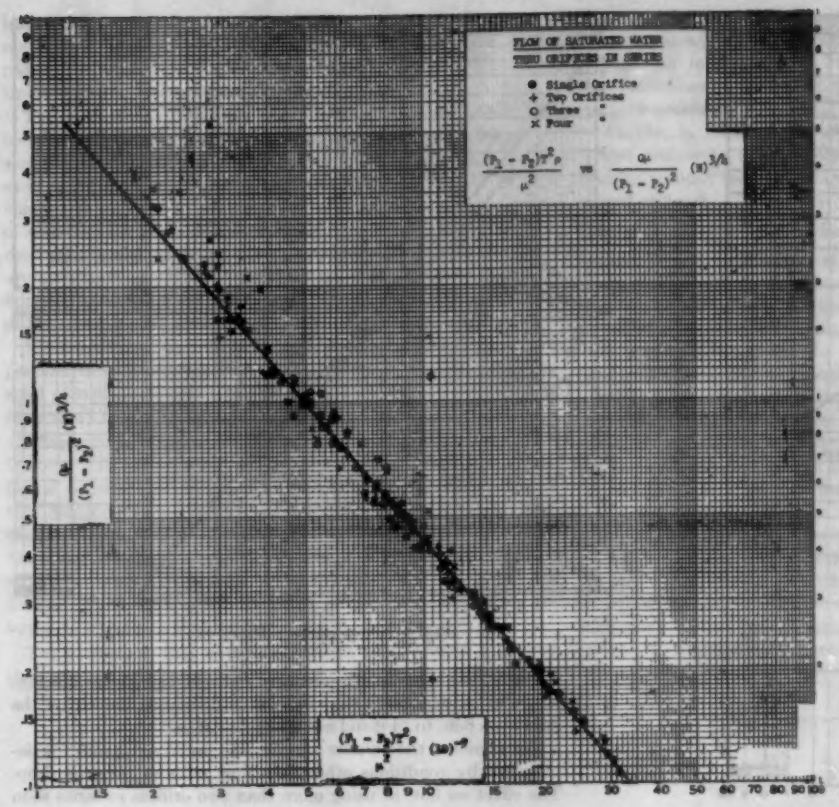

FIG. 3 FLOW OF SATURATED WATER THROUGH ORIFICES IN SERIES

The seven circular marked points are chosen from Fig. 2 of the Benjamin and Miller paper (1). They are for the flow of saturated distilled water from initial pressures of 40 psia to 200 psia to a final pressure of atmospheric. The orifices used were single knife-edged ones ranging in size from 1/4 to 7/8 in. diam. These points agree closely with the author's curve and the slight discrepancy easily may be traced to the large possible errors in reading values from a small graph.

The six points marked by squares and connected by a dotted line above the curve of Equation [1] are from Fig. 7 of the same paper (1). These points are for a single knife-edged orifice passing saturated distilled water with a constant initial pressure of 145 psia. The back pressure decreases from 120 psia on the left to 14.7 psia on the right. This dotted curve is typical of all the data presented in Fig. 7 of that paper.

The three points plotted and marked by triangles are from Fig. 15 of the discussion of the Benjamin and Miller paper and represent test data furnished by D. R. Yarnall. These points are for the flow of saturated distilled water through a single rounded-entrance orifice with initial pressures from 100 psia to 300 psia and a final pressure of atmospheric. These points agree precisely with the author's experimental curve although they extend into an initial-pressure region double that covered by his experiments.

The three points marked by crosses are from the English paper by Bottomley (2), and represent his test runs, Nos. 4, 5, and 6. Runs Nos. 1 to 3 were not plotted

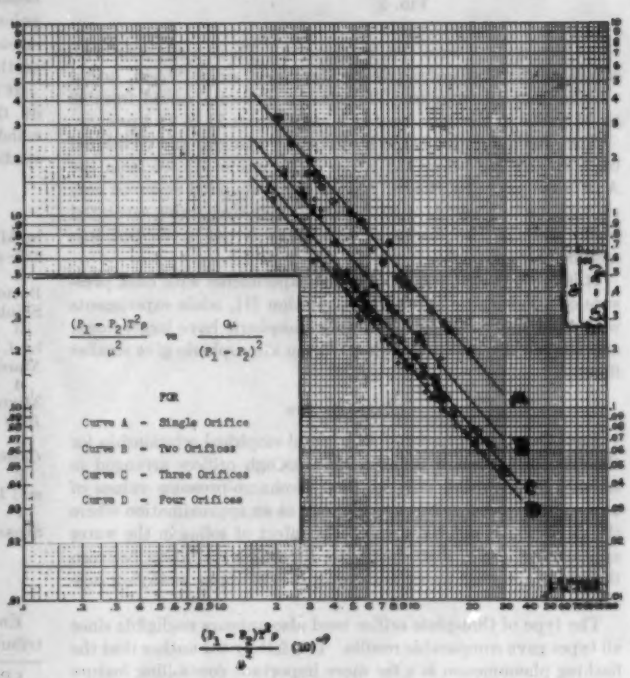

FIG. 4

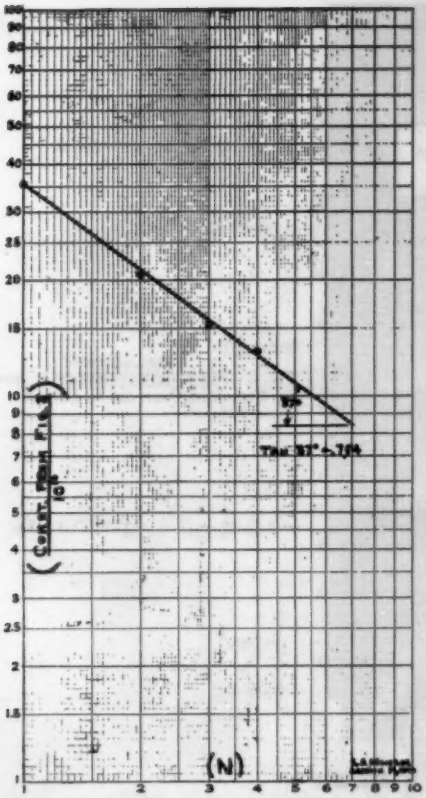

FIG. 5

since the orifices were not submerged. These runs were with saturated distilled water passing through a single $^{7}/_{16}$-in. orifice with a rounded entrance. The initial pressure varied from 48 to 64 psia and the final pressure varied from 21 to 28.4 psia.

The nine points indicated by inverted triangles and connected by a dotted line below the curve of Equation [1] are from the Australian paper by Burnell (3) for a well-rounded entrance nozzle with initial pressure of 10 to 180 psia and discharging saturated boiler water. The discharge pressure was not given but was assumed zero absolute.

It is obvious that other published experiments with back pressure of atmospheric agree with Equation [1], while experiments with final pressures greater than atmospheric have larger flows, and conversely final pressures less than atmospheric give smaller flows.

Conclusions

Equation [2] is presented as a useful empirical relationship for the flow of saturated boiler water through orifices arranged in series. It is correct only at final discharge-pressure values of atmospheric pressure but may be used as an approximation where the deviation is not too great. The effect of solids in the water appears negligible, there being no discernible variation between the use of distilled water and water of 3320 ppm methyl-orange alkalinity.

The type of thin-plate orifice used also appears negligible since all types gave comparable results. It is felt by the author that the flashing phenomenon is a far more important controlling feature than variations in the orifice discharge coefficient.

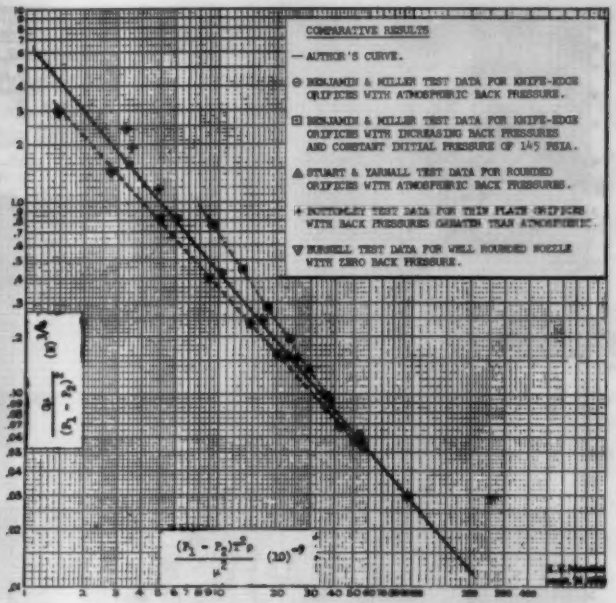
COMPARATIVE RESULTS
— AUTHOR'S CURVE.
⊖ BENJAMIN & MILLER TEST DATA FOR KNIFE-EDGE ORIFICES WITH ATMOSPHERIC BACK PRESSURE.
⊡ BENJAMIN & MILLER TEST DATA FOR KNIFE-EDGE ORIFICES WITH INCREASING BACK PRESSURES AND CONSTANT INITIAL PRESSURE OF 14.5 PSIA.
△ STUART & YARNALL TEST DATA FOR ROUNDED ORIFICES WITH ATMOSPHERIC BACK PRESSURE.
BOTTOMLEY TEST DATA FOR THIN PLATE ORIFICES WITH BACK PRESSURES GREATER THAN ATMOSPHERIC.
▽ BURNELL TEST DATA FOR WELL ROUNDED NOZZLE WITH ZERO BACK PRESSURE.

FIG. 6 COMPARATIVE RESULTS

Stable flow conditions are reached between expansions quickly. In the experimentation the variation of distance traveled by the fluid from 6 in. to 14 ft did not affect flow rate.

The choice of the number of orifices to use in series must be determined by conditions other than flow rates or pressure drop. The effect on flow of using more than two orifices in series soon becomes negligible as more orifices are added. From the viewpoint of flow control two orifices seem a practical maximum, but erosion studies should be made before any conclusions are reached on this point.

It appears that there is room for extensive research and analysis on the entire problem. Further attempts to derive equations which will satisfy any pressure range and, as mentioned, erosion studies are both much-needed objectives for the future.

BIBLIOGRAPHY

1 "The Flow of Saturated Water Through Throttling Orifices," by M. W. Benjamin and J. G. Miller, Trans. ASME, vol. 63, 1941, pp. 419–429.

2 "Flow of Boiling Water Through Orifices and Pipes," by W. T. Bottomley, Trans. North-East Coast Institution of Engineers and Shipbuilders, vol. 53, 1936–1937, pp. 65–100.

3 "Flow of Boiling Water Through Nozzles, Orifices and Pipes," by J. G. Burnell, *Journal of Institution of Engineers*, Australia, vol. 18, March, 1946, pp. 41–49.

4 "The Measurement of Density and Quality of Steam–Water Mixtures in Steam Generators," by Darfoon Du and R. A. Lorensini, *Heat Engineering*, vol. 21, January, 1946, pp. 7–9.

5 "The Flashing Calorimeter," by A. A. Markson and Y. A. Olson, *Combustion*, May, 1941, pp. 51–55.

6 "Fluid Flow Through Two Orifices in Series," by M. C. Stuart and D. R. Yarnall, Trans. ASME, vol. 58, 1936, pp. 479–489.

7 "Fluid Flow Through Two Orifices in Series—II," by M. C. Stuart and D. R. Yarnall, Trans. ASME, vol. 66, 1944, pp. 387–397.

Discussion

EDGAR W. WALES.[3] This paper represents a significant contribution to the growing list of investigations on the flow charac-

[3] Product Development and Application Engineer, Yarnall-Waring Company, Philadelphia, Pa. Assoc. Mem. ASME.

teristics of saturated water through pipes, nozzles, and orifices—a subject of great interest to engineers in the power field. The paper describes one of the few studies made on flow through multiple orifices in series.

The author has developed an empirical formula which will be helpful to those concerned with applications in which high concentrations of boiler water are a factor. His work is also significant from the standpoint that the resulting formula is only concerned with the initial condition of the fluid and the number of orifices in series. Although the present state of his work is confined to final discharge pressures of about atmospheric, there are numerous applications to which the working formula can be applied, and the author has noted a few of these. The simplicity of the formula will certainly lend itself to everyday usage.

It is significant to note that the solids in solution had no important bearing on results. It is assumed that reference to solid content is to solids in solution. The presence of solids in suspension might be expected to influence performance.

There are a few matters which seem to require further clarification. The first concerns the selection of a constant-enthalpy line to connect the test points as shown in Fig. 2. It is realized that the author is chiefly concerned with the state of the fluid at the initial and final points of measurement. However, it would add immeasurably to the value of his work if an analysis were made as to the manner of the change of state through each orifice. This would no doubt relate to the metastable state referred to by previous authors.

The statement that experiments with final pressures greater than atmospheric give larger flows and, conversely, final pressures less than atmospheric give smaller flows should be clarified. This apparently does not mean that actual flow of any one investigation increases with back pressure. Perhaps it reflects the limitations of the parameters of the formula as they pertain to back pressure.

Finally, in the author's comparison of his work with sharp-edged orifices to that of others using rounded-entrance orifices, did he account for the coefficient of contraction for the sharp-edged orifices?

Author's Closure

Mr. Wales' comments are both pertinent and appreciated. In general, they are self-explanatory. In reply to his last question relative to the variation in the coefficient of contraction between types of orifices in comparing the work of others, no correction was made. As stated in the paper: The type of thin-plate orifice used appeared to be a negligible factor.

Not to be taken lightly is Mr. Wales' request for the path of the fluid during its expansion. The author knows of no suitable set of co-ordinates to represent a transient phenomenon in thermodynamics but feels strongly that the parameter of time must be introduced. It is his opinion that the person who originates the first such diagram for the field of thermodynamics will make a significant and needed contribution.

A serious omission in acknowledgments was made in the original paper. This omission in no way should be construed as detracting from the author's sincere appreciation to the Yarnall-Waring Company for the loan of certain major pieces of equipment and to the Westinghouse Corporation for making funds available for the experimentation.

Notes on Some Recently Published Experiments on Orifice Meters

By EDGAR BUCKINGHAM[1]

Dr. Buckingham presents a procedure for plotting orifice coefficient data which results in straight lines over a considerable range of conditions. By relating the slopes and intercepts of these lines to size ratio and the Reynolds number parameters, it is possible to represent the coefficients for a wide range of sizes and rates by two linear equations. By applying this procedure to several available sets of data he has determined the limits of applicability of the equations. Furthermore, he shows that the mechanical finish of the orifice-plate surface and orifice edge affect both the slope and intercept of the lines resulting from the initial plottings.

Preface by H. S. Bean[2]

THIS paper was started and very nearly completed by the late Dr. Buckingham a year or two before his death. Just why the paper was not completed and presented for publication is not known. That he planned to do so is evidenced by his correspondence with Professor Marchetti. Also he discussed the paper and his intention to submit it for publication with the writer on several occasions.

There is today, as in the 1930 decade, a considerable and continuing interest in the thin-plate square-edged orifice and its use in fluid metering. Therefore it is believed that these notes by Dr. Buckingham will be a valuable addition to the literature, and that their value has not been lessened by the delayed publication.

It will be seen that in these notes Dr. Buckingham confined his attention to the analysis of coefficient data obtained with "corner taps." However, there is a close similarity among the coefficient data for the several different combinations of pressure-tap locations (with the exception of "pipe taps" or over-all loss taps). Therefore this analysis should be very helpful in the review of coefficient data for any set of pressure taps, with respect to both the data already on hand and any that may be derived from future tests.

1 Introduction

The International Standards Association (ISA) has issued two bulletins entitled, in English, "Rules for Measuring the Flow of Fluids by Means of Nozzles and Orifice Plates, Preliminary Recommendations." They are designated as "ISA Bulletin 9" and "ISA Bulletin 12" and are dated December, 1935, and August, 1936, respectively.[3]

These rules embody the recommendations of a committee set up by the Council of the ISA and were adopted after discussion at conferences held in Paris, May, 1930; Milan, June, 1932; and Stockholm, September, 1934. They are based upon, and in substance nearly identical with, the corresponding parts of the code adopted by the Society of German Engineers (VDI), which is entitled: "Regeln für die Durchflussmessung mit genormten Dusen und Blenden." The first edition of the VDI "Regeln, etc." was published in 1930, subsequent editions containing some additions and changes suggested by the further progress of research.

Several recently published sets of experiments on the flow of water through square-edged orifices have added considerably to our information on this phase of the subject, and their results suggest the desirability of certain modifications in those parts of the ISA Rules that refer to the use of orifice plates for metering liquids. Some of the conclusions to be drawn from these recent investigations are discussed in the following paper.

2 Nomenclature

The following notation will be employed: Where it differs materially from that of the ISA Bulletins, the ISA equivalents are given in parentheses. All quantities are understood to be measured in terms of normal units.

D = inside diameter of pipe in which orifice is installed concentrically

d = diameter of orifice

$\beta(\equiv\sqrt{m})$ = d/D = diameter ratio. As a specification of relative sizes of orifice and pipe, β is much to be preferred to area ratio m: it gives a clearer idea of the relation and is also more convenient in several respects.

$e(\equiv e')$ = length of cylindrical part of hole through plate, or width of cylindrical edge of orifice

$t(\equiv e)$ = thickness of orifice plate

V = volume of liquid discharged per unit time

g = acceleration of gravity

h = difference of head between upstream and downstream pressure taps, or difference of static pressure, expressed as a head of flowing liquid at its flowing temperature

$K(\equiv\alpha)$ = discharge coefficient of orifice with speed-of-approach factor included; it is defined by the equation

$$V = K\frac{\pi}{4}d^2\sqrt{2gh} \qquad [1]$$

ν = kinematic viscosity of liquid

R_D = Reynolds number referred to diameter of pipe; its definition is

$$\mathrm{R}_D = \frac{4V}{\pi D\nu} \qquad [2]$$

$X = 10^3/\sqrt{\mathrm{R}_D}$: this is a convenient independent variable for use in co-ordinating observed values of K

$C = K\sqrt{1-\beta^4}$ = discharge coefficient of orifice with speed-of-approach factor not included

---

[1] Deceased, April 29, 1940; formerly with the National Bureau of Standards, Washington, D. C.

[2] Physicist, Mechanics Division, National Bureau of Standards, Washington, D. C. Fellow ASME. The preface and abstract of the paper were prepared by Mr. Bean.

[3] Copies may be obtained by application to the American Standards Association, 70 East 45th Street, New York, N. Y.

Contributed by the Fluid Meters Research Committee and presented at the Annual Meeting, New York, N. Y., November 28–December 3, 1954, of The American Society of Mechanical Engineers.

Note: Statements and opinions advanced in papers are to be understood as individual expressions of their authors and not those of the Society. Manuscript received at ASME Headquarters, December 7, 1954. Paper No. 54—A-244.

$R_s = R_D/\beta$ = Reynolds number referred to diameter of orifice

3 Remarks on Graphical Representations

The discharge coefficient of an orifice meter depends, not only on the internal shape of the whole apparatus, but also on the rate of flow of the liquid and on its kinematic viscosity, both of which appear as factors in the Reynolds number along with the pipe diameter, which fixes the absolute size of the meter as distinguished from its shape.

The "shape," in the general sense of the term, may be specified by stating the ratio of each of the important dimensions of the whole installation to the diameter of the pipe, or the diameter ratio of the orifice may be omitted, to allow for the use of different orifice plates in the same meter. The ISA Rules contain such a set of specifications for the particular type of orifice meter that the ISA has adopted as its standard form.

When any adequate specifications have been adopted, but with β left as an independent variable, the discharge coefficient of any orifice meter that conforms to them is, for practical purposes, completely determined by the value of β for the orifice plate in question and the value of the Reynolds number R_D at which the meter happens to be working. It is known that no other circumstances have any appreciable effect on the value of K and, when this is true, it is readily shown by the method of dimensions that there is a general relation

$$K = f(\beta, R_D) \quad [3]$$

which holds in all cases, regardless of the absolute size of the meter, or the rate of flow of the liquid, or its kinematic viscosity, so long as the geometrical shape of the apparatus remains unchanged.

The detailed form of Equation [3] depends on the shape, and all we know, a priori, is that some such relation exists. The problem of determining it, for any specified shape, consists primarily in the experimental determination of values of K over a wide range of values of R_D, for a large number of orifices, of various diameter ratios and absolute sizes, all made and installed in the specified manner. But before the resulting mass of isolated values of K can be made generally useful for prediction in future cases, the separate observed values of K must be coordinated with those of β and R_D, so as to permit representing the Relation [3], either by a family of curves from which values of K may be read off, or by an equation in which the values of β and R_D may be substituted to give the value of K.

It is natural to start the attack on this second part of the problem by plotting the values of K obtained with each orifice over the values of R_D at which they were determined, and it is safe to assume that if all the measurements were exact, the resulting points would all lie on some smooth curve. But in practice they are, of course, distributed along a curved band, the width of the band, and the uncertainty in drawing the most representative curve through it, depending on the magnitude of the accidental errors of experiment. Such curves are known (1, 2, 3)[4] to be of the general shape illustrated in Fig. 1.

At high values of R_D, the values of K are slowly falling as R_D increases, as if approaching a final constant value K_0 and, in the practical employment of orifices as flowmeters, the values of R_D are nearly always in this region. The ISA Rules and the recent investigations that are to be discussed here are concerned only with these high values of R_D, and no further attention will be paid to the less simple parts of the curves nearer the origin.

It is customary to shorten the figure by using log R_D as the abscissa in place of R_D, and the part in which we are now interested then has the appearance illustrated in Fig. 2, each curve referring to a larger value of β than the one next below it. A set of curves of this sort, for various round values of $m = \beta^2$ (given as Fig. 17, on page 6 of ISA Bulletin 12) and the values of K recommended by the ISA for square-edged orifices, installed in smooth pipes in accordance with the Rules, may be found from these curves—by interpolation when necessary. The figure seems to be a copy of one in the VDI "Regeln etc.," which was made up as a systematic representation of results obtained by Dr. R. Witte in the course of his very extensive and careful investigations (4, 5, 6, 7) of orifices and flow nozzles.

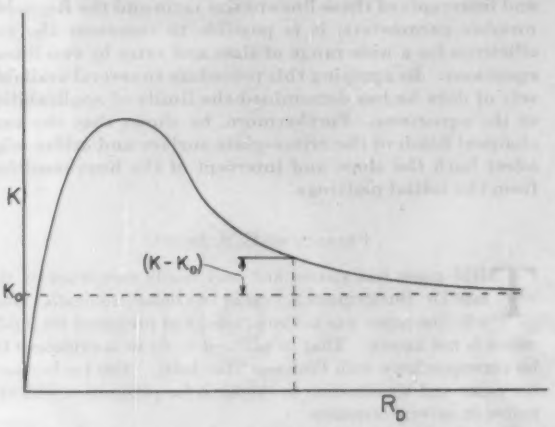

Fig. 1 General Form of Curve Obtained by Plotting K Against Corresponding Values of Log R_D

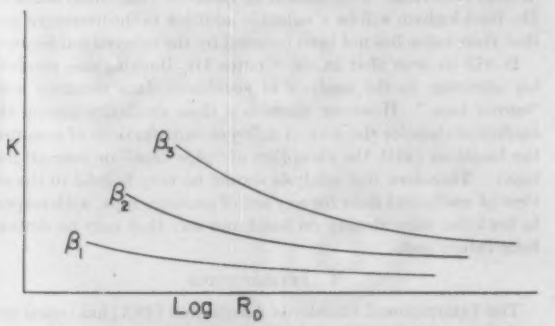

Fig. 2 Characteristic Curves of K Plotted Against Corresponding Values of Log R_D

Such a diagram or chart is convenient for reading off values of K for use in particular practical cases, but this method of plotting the results of determinations of K is not well adapted to analyzing a large mass of observed values for the purpose of discovering any general relations that may exist, and a little consideration of the physics of the subject suggests a better procedure.

The variation of K with R_D is due to the action of viscous forces. The effect of viscosity on the motion of the liquid toward and through the orifice is to diminish the contraction of the jet and so increase K above the value it would have in the absence of viscosity, and the difference $(K - K_0)$ in Fig. 1 represents this effect.

With a constant volume flow of liquid through a given orifice, that is, with V and D constant, if the kinematic viscosity is lowered, either by heating the liquid or by substituting another

[4] Numbers in parentheses refer to the Bibliography at the end of the paper.

with a lower value of ν, the value of $R_D = 4V/\pi D\nu$ is thereby increased. The plotted point moves along the curve toward the right and K decreases and, conversely, increasing ν increases K. This suggests that K might be expressed more simply in terms of ν than of $1/\nu$. In other words, it seems that instead of using R_D or $\log R_D$ as the abscissa we should be more likely to get a simple form of curve by using $1/R_D$ or some simple function of $1/R_D$.

When the value of this suggestion is tested by application to the best available experimental data, it turns out that if K is plotted over $\sqrt{1/R_D}$ each orifice gives a band of points that is not curved but straight; and for a series of orifices of different diameter ratios we get a sheaf of straight lines as illustrated in Fig. 3.

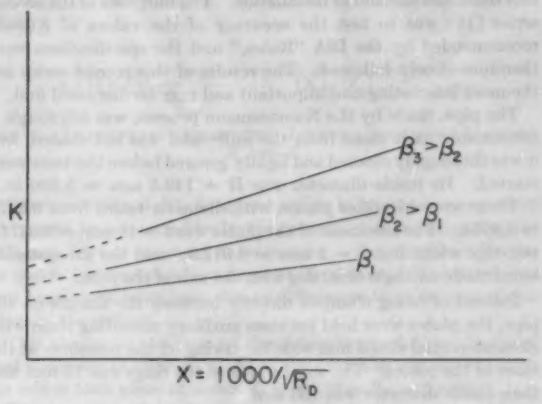

FIG. 3 RESULTS OF PLOTTING K VERSUS $1/\sqrt{R_D}$

For exceptionally low values of R_D—lower than would usually occur in practical metering, but still within the range to which the ISA Rules may be supposed to refer—the foregoing statements are no longer true, as will be shown later. But for all high values of R_D they are confirmed by all recent investigations of which the results have been published in sufficient detail to permit of any satisfactory analysis—by whatever graphical method.

This improvement in the graphical representation of experimental results is due to Prof. S. R. Beitler of Ohio State University. It is hardly necessary to insist on the superiority of a method of plotting that results in straight lines over one that results in curves, when there is no a priori knowledge of the form of equation that can be expected to fit the curves.

We may now give a very brief outline of a part of Beitler's investigation (8) published in May, 1935, after which the still more recently published experiments of Marchetti (9, 10) and Scimemi (11) will be discussed.

4 BEITLER'S EXPERIMENTS WITH WATER

The experiments now in question, which are only a small part of Professor Beitler's researches on flowmeters, were carried out on square-edged orifices, installed concentrically in clean commercial steel pipes of the inside diameters D = 1.033, 1.640, 2.039, 3.090, 6.067, 6.096, 10.117, and 14.14 in.

In most of the tests the differential head h was measured between five pairs of pressure taps, spaced at various distances from the orifice plate, and each pair gave a separate value of K for the one rate of flow during that test; but in this paper we shall be concerned only with the values of K obtained when the pressures were taken off immediately at the faces of the plates. This is the arrangement specified in the ISA Rules and generally adopted in Europe, and we continue our attention to these values of K for the sake of comparison with the results obtained by other observers with this same location of the pressure taps. Beitler (8) designates it by the term "German Standard"; it is also known, in America, as corner taps.

Nearly all the orifice plates were $^1/_8$ in. thick and, except in the case of the smallest pipe, the condition $t \leqq 0.1\ D$ was always satisfied, as required by the ISA Rules. Most of the plates, though not all, were beveled at 45 deg, on the downstream face, so as to reduce the width of the cylindrical edge of the orifice, and many were tested in two or more states, the edge width being successively reduced by increasing the depth of bevel without altering the square corner of the edge at the upstream face of the plate. A few of the plates were tested in two pipes of different diameters, and a few that were found to have slightly rounded edges were rebored to give perfectly square upstream corners and were tested in both states.

There were 79 plates in all but counting the separate edge widths and allowing for the tests of the same plate in different pipes and for the rebored plates, there was, in effect, a total of 164 different orifices. Corner taps were not used with all of them, but there are about 150 sets of values of K that are of present interest.

The differential head between corner taps was generally between 0.7 and 9.5 ft, and each orifice was tested at several rates of flow—usually five but occasionally on four or three, and in a few cases ten or twelve. The range of variation of R_D covered with each orifice was usually about 3.5 to 1, but for the whole collection the values of R_D ran from 310 to more than 1,500,000.

Beitler publishes his results as values of C and does not give the values of R_D at which they were measured, but he tabulates all the data needed for computing K and R_D. (See Table 1 for range of R_D covered in Beitler's tests.)

TABLE 1 RANGE OF R_D COVERED IN BEITLER'S TESTS

D	Range of $X = 10^3/\sqrt{R_D}$	Range of $R_D \times 10^{-3}$
1.033	24.52–3.47	1.66 – 83.1
1.640	31.02–3.16	1.04 – 100.
2.039	56.98–2.62	0.308– 146.
3.090	35.13–1.98	1.23 – 255.
6.067	22.61–1.334	1.96 – 562.
6.096	45.39–2.56	0.474– 153.
10.117	7.44–1.066	18.1 – 880.
14.14	5.11–0.806	38.3 –1540.

TABLE 2 CORRESPONDING VALUES OF R_D AND X

R_D	X
500	44.7
1000	31.6
1500	25.8
2000	22.4
2500	20.0
3000	18.3
4000	15.8
5000	14.1
7000	12.0
10000	10.0
15000	8.17
20000	7.08
100000	3.16
300000	1.83
600000	1.29
1000000	1.00

5 GENERAL CONCLUSIONS FROM BEITLER'S WORK

From August, 1932, onward, Professor Beitler's results were submitted to the Bureau of Standards for examination, as they accumulated and, in a first attempt to co-ordinate them, values of K were plotted over those of R_d. With a large number of points spaced over a wide range of values of R_D, this method of plotting gives pretty definite smooth curves, but with only a few points and no way of estimating which were the most trustworthy, it was not satisfactory. The elementary physical considerations mentioned in Section 3 then led to the use of $1/R_d$ as abscissa, and when plotted in this way the points for each orifice lay not very far from a straight line, except in some cases where

the points were too much scattered to suggest any sort of smooth curve. There were, however, clear indications that curves with a slight upward convexity would fit the points somewhat better, and Professor Beitler then took the final step of using $\sqrt{1/R_d}$ as abscissa instead of $1/R_d$.

It may be remarked here, parenthetically, that since $C = K\sqrt{1-\beta^4}$ and $R_D = \beta R_d$, either C or K may be used as ordinate with either $\sqrt{1/R_d}$ or $\sqrt{1/R_D}$ as abscissa, and that the four possible plots for each orifice will be interconvertible by mere changes of scale. For the future, it will be supposed that K is plotted over $10^3/\sqrt{R_D} = X$.

The accidental errors shown by the scattering of the points were evidently much greater for some of the orifices than for others, and if we had only the most irregular sets of values of K (or C)—say, 10 per cent of the whole number—it would be difficult to draw any definite conclusions from them. But in a much larger number of cases the plotted points lay surprisingly close to straight lines, and the values of K could be reproduced by equations of the form

$$K = K_0(1 + AX) \quad [4]$$

the values of the constant coefficients K_0 and A being different for different orifices.

When all the plots of C or K over X are examined together, there can be no possible doubt of what they indicate; it is that every square-edged orifice gives values of K that may be adequately represented by an equation of the form of Equation [4], over the range of values of R_D, within which the orifice would normally be used as a flowmeter. In particular, there is no indication that the sloping lines ever level off and become horizontal at high values of R_D, (low values of X), and extrapolation by means of equations of the form of Equation [4] to higher values of R_D than occurred in Beitler's experiments seems as well justified as any extrapolation ever is.

The constant K_0 appears in Equation [4] as a limiting value which K approaches when $R_D = \infty$. But whether it has any physical significance is a matter of no importance; for R_D cannot be increased indefinitely, since it is limited, for any one orifice by the available, or permissible, differential head h.

Aside from small irregularities of behavior caused by unavoidable mechanical imperfections in the edges of the orifices, K_0 increases with β and up to about $\beta = 0.7$ the increase is roughly proportional to the increase of β^4. When $\beta = 0.7$ the distance from the edge of the orifice to the wall of the pipe (Beitler calls it the "dam height") is only $0.15D$ and, as this distance is further diminished, K_0 increases faster than in proportion to β^4. In general, the slope coefficient A also increases with β, but it seems to be even more sensitive than K_0 to differences of finish of the entrance corner of the orifice.

One of the earliest conclusions from the results of the experiments related to the effect of changing the width of the cylindrical edge of an orifice. It was found that if $e = 0.02D$, making the edge still narrower had no measurable effect on the value of K at any given value of R_D. When e was as large as $0.03D$, K tended to be a little higher. And when $e = 0.04D$, K was always distinctly higher than when $e = 0.02D$, and it increases rapidly with any further increase of e/D. Later experiments by Ruppel (12) have confirmed these conclusions, except that at very high values of β, beyond the range of Beitler's experiments on this point, Ruppel found that e/D might be increased to 0.04 before K began to be appreciably affected.

In the earlier editions of the VDI "Regeln" the specification for edge width was $e \leq 0.04D$; but in the latest edition, and in the ISA Rules, this has been changed to $e \leq 0.02D$, in accordance with the latest information.

Beitler's experiments show that when $\beta \geq 0.1$—a very unusual case—this specification should be replaced by $e \geq 0.2d$. For when e is increased above $0.2d$, the orifice soon begins to act as a short tube and K increases rapidly with e/d.

6 Marchetti's Experiments

Prof. M. Marchetti, of Milan, has published the results of two series of experiments on the flow of water through square-edged orifices installed in commercial steel pipes of about 6 in. diam, and in both series the observations were extended to unusually low values of R_D. The first series (9) was designed to determine the effect on K of a certain small departure from the ISA Standard method of installation. The purposes of the second series (10) was to test the accuracy of the values of $K(\equiv\alpha)$ recommended by the ISA "Rules," and the specifications were therefore closely followed. The results of this second series are the more interesting and important and may be discussed first.

The pipe, made by the Namnesmann process, was left rough—presumably as it came from the mill—and was not coated, but it was thoroughly cleaned and lightly greased before the tests were started. Its inside diameter was $D = 149.5$ mm $= 5.886$ in.

There were 14 orifice plates, with diameter ratios from 0.2278 to 0.8964. The thickness of the plates was $t = 10$ mm $= 0.067D$; the edge width was $e = 2$ mm $= 0.013D$; and the downstream bevel made an angle of 30 deg with the axis of the pipe.

Instead of being clamped directly between the flanges on the pipe, the plates were held between auxiliary mounting rings with circumferential slits 3 mm wide for taking off the pressures at the faces of the plates. The axial width of the rings was 15 mm and their inside diameter was 150 mm.

If we omit a few values marked (?), there are 195 values of K, 25 for the smallest orifice and from 10 to 16 for each of the others. The values of R_D at which they were observed ran from 555 to 360,000, as compared with 485 to 190,000 in Beitler's experiments with his 6-in. pipes; but the range of values of R_D covered with each orifice was much wider than in Beitler's work, where it was seldom as great as 4 to 1. In Marchetti's experiments the range was 68 to 1 for the smallest orifice and 11 to 1 even for the largest.

When the values of K observed for any one orifice are plotted over the simultaneous values of X, the resulting points, for all the lower values of X lie along a straight line. But except in the case of the smallest orifice, which we disregard for the present but shall refer to later, the last few points, at the highest values of X (lowest values of R_D), depart from the line and lie along a curve that is strongly concave upward. The whole plot then has the appearance illustrated by either of the curves in Fig. 4, which also illustrates the further fact that the departure from the straight line starts at lower and lower values of X as the diameter ratio increases.

Since the straight line merges into the curve with no indication of a sudden change of direction, the point where the curvature starts is not well defined and estimates of its abscissa X_c are necessarily rather rough. The uncertainty is much greater in some cases than in others, in which the observed points happen to be more favorably distributed; but a cursory examination and comparison of the plots showed, at once, that the value of X_c was never very far from $4.3/\beta$.

Two independent sets of estimates of X_c were then made, and for one of the orifices the two estimates differed by 25 per cent; but the average difference for all 13 orifices was about 10 per cent and in six cases it was less than 6 per cent. Using the mean of the estimates of X_c for each orifice gave values of βX_c between 3.5 and 4.8. The average for all the orifices was $\beta X_c = 4.1$ and for the six least uncertain cases it was $\beta X_c = 4.2$.

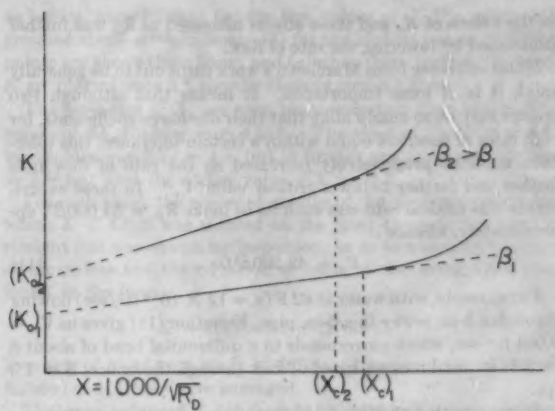

FIG. 4 DEPARTURES FROM THE LINEAR RELATION BETWEEN K AND X

The variations of βX_s from one orifice to another were greater than could be accounted for by the uncertainties in estimating the values of X_s, and appeared to be genuine. But they were irregular and not systematically related to the values of β, and it seems that they must have been due to differences in sharpness of the edges of the orifices.

This change in the form of the dependence of K on X shows that some sort of critical change in the nature of the flow through the orifice took place at about $X = 4.3/\beta$ or $R_D = 54000\beta^2$.

The detection of this limit to the validity of the linear relation already obtained from Beitler's observations which have been made possible by Marchetti's extension of his experiments to lower values of R_D, illustrates the desirability of publishing observed values of K and R_D in detailed numerical tables, instead of merely as points on small plots from which it is impossible to make accurate readings. It also illustrates the advantages of the new method of graphical representation for studying such a collection of observed data. For with the methods hitherto customary it would have been difficult to detect the critical changes in the relation of K to R_D, which the present method makes strikingly evident.

We shall return to the consideration of the form of the curves when $X > X_s$, but we may first discuss the values of K obtained when $X < 4.3/\beta$.

7 FORMULATION OF MARCHETTI'S RESULTS FOR HIGH VALUES OF R_D

The diameter ratios of plates Nos. 13 and 14 were $\beta = 0.8696$ and $\beta = 0.8964$, respectively; but plates with such high values of β are not commonly employed in practical metering when it can be avoided, because it is difficult to make satisfactory observations with them. Orifices with lower values of β are of more general interest and importance, and the following discussion refers only to plates Nos. 1 to 12, with diameter ratios from 0.2278 to 0.8431.

For these 12 plates, there are 118 observed values of K for $X < 4.3/\beta$. The whole collection can be fairly closely reproduced by computing values of K from the equations

$$K = K_o(1 + AX) \quad [4]$$

$$K_o = 0.6031 + 0.34\beta^4 + 0.62(\beta - 0.7)^{9/2} \quad [5]$$

$$A = (0.026\beta^4 + 0.002)K_o \quad [6]$$

the last term of Equation [5] being omitted when $\beta < 0.7$.

To illustrate the degree to which these equations represent the observations, let $\Delta = K(\text{obs}) - K(\text{calc}) =$ the excess of the observed value of K over the value found by substituting the values of β and X in the equations. Then the arithmetical-mean value of Δ for all the 118 cases is ± 0.15 per cent of K.

The algebraic-mean values of Δ for the separate plates are sometimes positive and sometimes negative; but they show no systematic variation with β, and so far as they are not due to accidental errors of observation, they are probably to be attributed to slight differences of finish between the edges of the orifices.

For one plate (No. 6, $\beta = 0.6354$) the observed values of K are consistently high, the algebraic mean Δ being $+0.29$ per cent, which suggests that the entrance corner of this orifice was probably not quite so sharp as the others. With the exception of this plate, the greatest values of Δ for the other 11 are -0.38 per cent and $+0.40$ per cent.

It is evident that the experimental work was extremely well done, and that the edges of the orifices were of unusually uniform quality. It also appears that Equations [4], [5], and [6] constitute a virtually perfect average representation of the values of K observed for $R_D > 54{,}000\beta^2$ and for diameter ratios between 0.22 and 0.85.

For a pipe of different roughness, or for orifices with less perfect edges, the numerical constants of the equations would doubtless need to be somewhat altered, and some small additional correction terms might be required; but it does not seem likely that the general form of Equations [5] and [6] would need any serious modifications. At all events, it seems beyond question that for each separate orifice an equation of the general form of Equation [4] is capable of representing the values of K observed at sufficiently high values of R_D, within the accidental errors of measurement. In this respect Marchetti's results are in perfect agreement with Beitler's; and it is highly probable that if Witte's very numerous observations were published in the same detail as Beitler's and Marchetti's have been they would be found to lead to this same conclusion.

8 RESULTS FOR LOWER VALUES OF R_D

We have next to consider the values of K obtained at such low rates of flow that $X > 4.3/\beta$ or $R_D < 54{,}000\beta^2$ and, as before, we shall confine our attention to the first 12 plates.

For plate No. 1, $\beta = 0.2278$, $54{,}000\beta^2 = 2800$, and there are 12 values of K, observed at values of R_D from 2295 down to 555. When they are plotted over the simultaneous values of X, the points are too much scattered to permit any other conclusion than that the motion of the stream ahead of the orifice must have been unstable. For plate No. 10 ($\beta = 0.7759$) there are five observed points, and they too are somewhat scattered, though much less than the points for plate No. 1.

For each of the remaining 10 plates there are either four or three observed values of K, and when they are plotted over X they lie on, or close to, curves of the shape illustrated in Fig. 4 for $X > X_s$. But if K is plotted over X^2 as abscissa, the curves are transformed into straight lines, each of which may be represented by an equation of the form

$$K = K_o'(1 + BX^2) \quad [7]$$

the constants K_o' and B varying somewhat irregularly from one plate to another but, on the whole, increasing with β.

The values of K for each plate were plotted over X^2; a straight line was drawn through the center of gravity of the points and as near them as could be done by simple inspection; and the equation of each line was determined in the form of Equation [7]. From these equations values of K were then computed for comparison with the observed values.

For the 10 plates now in question there were 36 observed values,

and the arithmetical mean of the departures, $K(\text{obs}) - K(\text{calc}) = \Delta$, was ± 0.13 per cent, the extremes being -0.37 and $+0.24$. When the five values of K for plate No. 10 were treated in the same way and included in the comparison, the arithmetical mean Δ for all 41 points was ± 0.15 per cent, with extremes of -0.68 and $+0.47$ per cent.

It appears from these figures, and still more clearly from the plots—which it is impracticable to reproduce here on an adequate scale—that somewhere in the vicinity of $\mathsf{R}_D = 54{,}000\beta^2$ the relation between K and R_D changed, rather abruptly, from the form of Equation [4], or

$$K = K_0\left(1 + A\,\frac{10^3}{\sqrt{\mathsf{R}_D}}\right) \quad [8]$$

to the form of Equation [7], or

$$K = K_0'\left(1 + B\,\frac{10^6}{\mathsf{R}_D}\right) \quad [9]$$

There is, however, a marked difference between the two cases. It was shown, in Section 7, that when $\mathsf{R}_D > 54{,}000\beta^2$ the coefficients K_0 and A of Equations [4] and [8] could be quite satisfactorily represented for all the plates, that is, for all the values of β from 0.228 to 0.843, by Equations [5] and [6]. But for the coefficients K_0' and B of Equations [7] and [9] no such general representation in terms of β was possible. It is true that the values of K_0', obtained from the separate plots of K over X^2 for $\mathsf{R}_D < 54{,}000\beta^2$, could be represented, rather roughly, by setting

$$K_0' = 0.604 + 0.38\beta^4 \quad [10]$$

the average value of $K_0'(\text{obs}) - K_0'(\text{calc})$ being ± 0.06 per cent, and the extremes -1.2 and $+1.4$ per cent, with no systematic run. But the slope coefficient B varied too irregularly and too much from one plate to another to permit any simple general formulation in terms of β.

In the former case there were from seven to twelve observed values of K for each plate, and their mean departure from the corresponding values computed from the general Equations [4], [5], and [6] was ± 0.15 per cent. In the latter case there are only three or four observed values (five for plate No. 10), and a serious error in any one value would have much more influence on the location of the straight line drawn by inspection, and on its equation as determined from the plot. Nevertheless, the mean departure of the observed values of K from the values computed from the individual equations is still only ± 0.15 per cent. This seems to indicate that the precision of measurement was about the same as these lower values of R_D as at the higher rates of flow which made $\mathsf{R}_D > 54{,}000\beta^2$; and that the irregular variations of K_0' and B from one plate to another were not accidental but due to real differences of behavior of the orifices which could not be attributed to the differences of β.

Now, aside from differences of diameter, the only other differences that may obviously have existed between the various orifices were in the perfection of finish of the edges. The values of K are known to be sensitive to small variations in the sharpness of the upstream corner of the cylindrical hole through the plate. And the fact that the whole collection of values of K observed at the higher values of R_D could be so well reproduced by a single set of general equations shows that, so long as the flow was rapid enough to make $\mathsf{R}_D > 54{,}000\beta^2$, the individual peculiarities of the separate orifices had only insignificant effects on the values of K. But during the second type of flow, which always developed when R_D fell much below $54{,}000\beta^2$, differences of finish that were of no importance during the first type of flow had appreciable effects on the values of K, and these effects increased as R_D was further diminished by lowering the rate of flow.

If this inference from Marchetti's work turns out to be generally valid, it is of some importance. It means that although two orifices may be so nearly alike that their discharge coefficients, for high rates of flow, are equal within a certain tolerance, this tolerance must be progressively increased as the rate of flow falls farther and farther below a critical value V_c.[5] In these experiments this critical rate was such as to make $\mathsf{R}_D = 54{,}000\beta^2$, approximately, whence

$$V_c = 42{,}500\beta^2 D\nu \quad [11]$$

For example, with water at 62 F ($\nu = 12 \times 10^{-6}$ ft²/sec) flowing through a 3-in. orifice in a 6-in. pipe, Equation [11] gives us $V_c = 0.064$ ft³/sec, which corresponds to a differential head of about $h = 0.84$ in., and a mean speed of flow through the orifice, $S = 1.3$ fps.

It appears that the transition from one regime to the other was due to some sort of critical change in the configuration of the fluid motion close to the edge of the orifice, but to determine the precise nature of this change would evidently require a good deal of difficult experimentation.

9 Remarks

We have seen that Beitler's experiments on a large number of orifices in eight different pipes, and Marchetti's less comprehensive but more concentrated experiments with a single pipe of medium size, are in complete agreement in showing that, at all sufficiently high values of R_D, the values of K for any square-edged orifice can be represented by an equation of the form

$$K = K_0(1 + AX) \quad [4]$$

where $X = 10^3/\sqrt{\mathsf{R}_D}$, and the values of K_0 and A depend primarily on the diameter ratio of the orifice, although they are also somewhat dependent on the mechanical perfection of the edge of the orifice.

Although the validity of this relation seems already sufficiently established, some further confirmatory evidence will be mentioned. But more interesting questions arise in connection with the critical change of regime. Do any other sets of observations reveal such a change? If so, is the critical value, $X = 4.3/\beta$ or $\mathsf{R}_D = 54{,}000\beta^2$, peculiar to the diameter $D = 150$ mm, or is it independent of the absolute size of the pipe? Does it depend on the sharpness of the orifice edges or on the degree of roughness of the pipe?

There is very little evidence on any of these questions, but what there is may be mentioned, beginning with Marchetti's first series of experiments (9).

10 Marchetti's First Series of Experiments

The seven orifice plates used in this series were members of the set of 14 used in the second series. They were held between mounting rings of 15-mm axial width and 150.0-mm ID, with circumferential slits 3-mm wide at the faces of the plate. But the diameter of the pipe was $D = 154.6$ mm, so that the installation differed from the ISA Standard form by having a square shoulder, 2.3 mm high, 15 mm from each face of the plate. The pipe was similar to the one used in the second investigation; it was free from rust and not coated. The diameter ratios of the orifices were from 0.2119 to 0.8409.

When the observed values of K are plotted over those of X, the somewhat greater scattering of the points shows that the precision of the measurements was not so high as in the later work. But the general conclusions to be drawn are qualitatively the same

[5] Here, as in Equation [11], V is volume rate.

as before, namely, that (*a*) for low values of X the points are grouped about straight lines; (*b*) for the highest values of X the points are above these lines; and (*c*) when these highest values of K are plotted over X^2, they lie close to straight lines.

The estimates of X_s are even more uncertain than before, the values of βX_s running from 4 to 6. The mean of the least uncertain values was $\beta X_s = 4.4$, but in further analyzing the data the author has used the earlier value, $\beta X_s = 4.3$.

For each plate, the center of gravity of the observed points for which $X < 4.3/\beta$ was entered on the plot; through this point a straight line was drawn by inspection, so as to represent the run of the points and the equation of each of the seven lines was found, in the form

$$K = K_0(\text{obs})[1 + A(\text{obs})X] \quad \ldots\ldots\ldots\ldots [12]$$

Two sets of plots were made at different times and the values of K_0(obs) and A(obs) were averaged.

The seven values of K_0 (obs) could be quite well represented by setting

$$K_0\,(\text{calc}) = 0.6007 + 0.37\beta^4 + 10.2\,(\beta - 0.63)^{10/3} \ldots [13]$$

omitting the last term when $\beta < 0.63$. The mean value of K_0 (obs) — K_0 (calc) was ± 0.08 per cent, the extremes being —0.13 and +0.18 per cent.

For the first four plates ($\beta \leq 0.6145$) the values of A (obs) are fairly well reproduced by setting

$$A\ (\text{calc}) = 0.015\beta^4 + 0.0013 \quad \ldots\ldots\ldots\ldots [14]$$

But for the other three plates this gave much too high values, and plotting A (obs) over β^4 showed that no one simple equation would be able to reproduce all seven values of A (obs) within their uncertainties.

Further attempts to represent K_0 and A by general expressions, as was found to be possible in the case of Marchetti's second series of experiments, were therefore abandoned, and the observed values of K were compared directly with the values of K found from the separate Equations [12]. There were 78 observed values of K for $X < 4.3/\beta$; the arithmetical mean value of K(obs) — K(calc) was ± 0.10 per cent and the extremes were —0.30 and +0.34 per cent.

Turning now to the experiments at lower rates of flow, there are 26 observed values of K for $X > 4.3/\beta$, but two of the three values for plate No. 1 and one of the six values for plate No. 2 were observed at values of R_D below 2000. In these three cases there was evidently a possibility that the motion of the approaching stream may have been unstable and since these three values of K did not agree with the indications of the others, they have been disregarded in what follows.

The remaining values of K—from three to five for each plate except No. 1—were plotted over X^2 as abscissa, straight lines were drawn by inspection as before, and the equations of the lines were determined. This was done on two separate occasions, and the values of K_0' and B were averaged, to give six equations of the form

$$K = K_0'(\text{obs})(1 + B(\text{obs})X^2) \quad \ldots\ldots\ldots\ldots [15]$$

From these equations values of $K = K$(calc) were computed for comparison with the values observed with each of the six orifices, and the arithmetical mean of the 22 resulting values of K(obs) — K(calc) was ± 0.10 per cent, the extremes being —0.36 and +0.35 per cent.

We find, then, that in spite of the slightly abnormal installation in Marchetti's first series of experiments the results agree with the general conclusions drawn from the more numerous and somewhat more precise experiments of the second series, as follows:

(*a*) For all high values of R_D, the relation

$$K = K_0\left(1 + A\,\frac{10^3}{\sqrt{\mathsf{R}_D}}\right) \quad \ldots\ldots\ldots\ldots [16]$$

first obtained from Beitler's work and then confirmed by Marchetti's second investigation is also confirmed by the first.

(*b*) For the lower values of R_D, as far as the experiments were carried, the relation

$$K = K_0'\left(1 + B\,\frac{10^6}{\mathsf{R}_D}\right) \quad \ldots\ldots\ldots\ldots [17]$$

is also confirmed, within the errors of experiment.

(*c*) The transition from one form of the relation to the other occurred at values of $10^3/\sqrt{\mathsf{R}_D} = X$ between $3/\beta$ and $6/\beta$ or, on the average, not far from $X = 4.3/\beta$. The corresponding values of R_D are $110{,}000\beta^2$, $28{,}000\beta^2$, and $54{,}000\beta^2$.

In view of the wide scope of Beitler's experiments as regards both pipe diameter and number of orifices used, and the wide range of values of R_D covered in Marchetti's two investigations, it appears that the relation described by Equation [16] may be accepted without further discussion as generally valid for all sufficiently high values of R_D that are encountered in commercial practice. But the conclusion that there is a critical value of R_D below which this relation ceases to hold rests, at present, only on Marchetti's experiments with one very uniform set of orifices in two pipes of about the same diameter and roughness. We have, therefore, to look for other evidence on this point, and we begin by re-examining Beitler's results.

11 Beitler's Values of K for Low Values of R_D

With the exception of the orifices used in the smallest pipe, the plots of K over X fail to show any evidence of systematic departure of the plotted points from straight lines and give no indication of a critical change. But the highest values of βX were usually much lower than in Marchetti's experiments, only a very few being as high as 4.3. For the four smallest of the orifices tested in the next to smallest pipe, the values of βX ran as high as 4.69 to 4.93, but although these are somewhat higher than the mean of my estimates of βX_s from Marchetti's work they are not outside the range of those estimates.

We next turn to the plots for the six orifices that were used in the smallest pipe ($D = 1.033$ in.). These plates were $^1/_8$ in. thick so that $t = 0.12D$, or a little more than the limit specified in the ISA Rules. The edge width was $e = {}^1/_{32}$ in. $= 0.03D$, which is also a little greater than permitted by the latest revision of the Rules.

For two of these orifices the highest values of βX were 5.96 and 7.26, respectively; but, unfortunately, the accidental errors happened to be unusually large in both cases and the plotted points are too much scattered to furnish any evidence.

On the other hand, two orifices gave very clear indications of the occurrence of a critical change, although they only fix its position within very wide limits. For each of these orifices, the first four points lie extremely close to a straight line while the fifth and last point lies far above it. For one of the orifices ($\beta = 0.7254$) the last point on the line is at $\beta X = 4.61$, and the fifth point is at $\beta X = 5.64$. For the other orifice ($\beta = 0.7742$) the last point on the line is at $\beta X = 4.10$, and the fifth point is at $\beta X = 5.50$.

For the remaining two orifices, the accidental errors of measurement were evidently somewhat larger, so that the straight line cannot be so precisely fixed and the evidence for a critical change of regime is not so striking. But in both cases, the last point is considerably above the best straight line that can be drawn to represent the run of the earlier points. For one of these orifices

($\beta = 0.2406$) the last point that lies close to the line is at $\beta X = 4.09$, and the final high point is at $\beta X = 5.89$. For the other orifice ($\beta = 0.6045$) the last point close to the line is at $\beta X = 4.20$ and the final high point is at $\beta X = 5.94$.

From the observations on these four orifices it appears that the linear relation of K to X persisted up to about $\beta X = 4.6$ but had ceased to hold at $\beta X = 5.5$, and that a critical change must have occurred somewhere between these values of βX. This is somewhat higher than the mean of the author's estimates of βX_c from Marchetti's work, but it is within the range of those estimates.

Now Beitler's smallest pipe, in which these orifices were tested, was only about $^1/_6$ as large as Marchetti's pipes and it was certainly much rougher relatively to its size, and yet the critical value of βX was about the same, as nearly as we can tell. It is, of course, possible that the differences of size and of roughness may have had approximately equal and opposite effects on the value of βX_c. But it seems more likely that the value of βX_c for each orifice is determined, mainly if not entirely, by the condition of the edge of the orifice—at all events, for diameter ratios up to about 0.85.

This surmise receives a little support from some of Scimemi's experiments, which may now be considered.

12 Scimemi's Experiments

Prof. E. Scimemi, of Padua, has published (11) results of experiments with water, on orifices installed in pipes of about 200 mm or 7.9 in. diam. They furnish a little confirmatory evidence on the subject now in hand, but need not be discussed at any great length.

There were, at the start, 14 commercial brass orifice plates. When they were tested, as received from the maker, it appeared that the edges of the orifices were slightly rounded, and the plates were therefore rebored and the upstream corners of the orifices made perfectly square and sharp. It is not clearly stated whether or not all the plates were tested in both conditions, but the published tables of results refer only to ten orifices with the original, slightly rounded edges, and six with sharp edges. The plates were 10 mm thick and the width of the cylindrical edge was 2 mm, except in one case where it was reduced to 1 mm by facing off the upstream side of the plate. The plates were held between mounting rings of 200-mm ID, provided with the usual circumferential slits for taking off the pressures at the faces of the plate.

Three pipes were employed. Pipe A, made by the Mannesmann process, had the "normal" tar coating; its diameter was 198.84 mm. Pipe B, of similar make, had a somewhat smoother tar coating; its diameter was 200.30 mm. Pipe C was of new cast iron and was, apparently, not coated; its diameter was 202.60 mm.

With diameters of nearly 8 in., the pipes cannot have behaved very differently from perfectly smooth pipes, except possibly for very high diameter ratios. But since no orifice was tested in more than one pipe, there is no evidence regarding possible effects of differences in roughness on the values of K. At present, however, we are not interested in the absolute values of K but only in the variations of K with X (or $\mathbf{R}_D$), and we proceed to summarize the results of plotting the observed values of K over those of X.

(*a*) *Results for Sharp-Edged Orifices.* These six orifices were used in pipe A. For the largest of them ($\beta = 0.9002$) the eight points up to $\beta X = 2.35$ show no systematic departure from a straight line, although the precision of the measurements was evidently inferior to that for the smaller orifices, as might be expected. But the ninth point, at $\beta X = 2.65$, lies distinctly above the best straight line through the earlier points and a final point, at $\beta X = 3.11$, fall still farther above the line. A change of regime seems to have occurred in the vicinity of $\beta X = 2.5$.

For the other five orifices ($\beta = 0.2414$ to 0.8192) the highest value of βX was 2.36, and the points all lie fairly close to straight lines.

(*b*) *Results for the Round-Edged Orifices.* Of these ten orifices six were used in pipe A, two in B, and two in C. We begin with the cast-iron pipe C, which was probably somewhat rougher than the others.

For orifice No. 8 ($\beta = 0.6663$) there are 19 values of K, observed at values of βX from 1.04 to 4.28. The plotted points all lie well along a straight line.

For orifice No. 11 ($\beta = 0.7655$) 18 points, over the range $\beta X = 1.14$ to 3.17, lie fairly close to a straight line, although the irregular departures are considerably larger than for No. 8. But three further points, at $\beta X = 3.44$, 4.05, and 4.81, are well above the line, and there seems to have been a change of regime somewhere between $\beta X = 3$ and $\beta X = 3.8$.

The eight orifices tested in the smoother pipes, A and B, may be discussed together. For each of the first five ($\beta = 0.2263$ to 0.7141) there are from 8 to 12 values of K, the highest value of βX being 3.16. In all five cases the plotted points lie fairly close to straight lines, the departures being irregular and not systematic.

For the next larger orifice ($\beta = 0.8147$) there are 19 values of K, observed over the range $\beta X = 1.16$ to 3.78, but the resulting points on the K, X-plane are too much scattered to permit drawing any conclusions from the plot. The two largest orifices do, however, supply a little evidence though not much.

For orifice No. 14 ($\beta = 0.8449$) the 14 points from $\beta X = 1.21$ to $\beta X = 3.21$ lie fairly well along a straight line, while the 15th and last point, at $\beta X = 3.91$, is distinctly higher. The change seems to come between $\beta X = 3$ and $\beta X = 3.4$.

For orifice No. 15 ($\beta = 0.8750$) and the 21 observed points are badly scattered, which is not surprising in view of the general experience with such high-diameter ratios; but there is no doubt that the final point, at $\beta X = 4.81$ is far above any line that could reasonably be drawn to represent the run of the other 20 points. The rather vague indication is that the change comes between $\beta X = 2.6$ and $\beta X = 3.4$.

13 Comparison With Marchetti's Values of βX_c

(*a*) *Sharp-Edged Orifices.* For comparison with the single one of Scimemi's sharp-edged orifices that gave evidence of a critical change in the relation of K to X (or $\mathbf{R}_D$) we may refer to the two largest of Marchetti's orifices used in his second series of experiments. These have not hitherto been discussed because their values of K_0 and A could not be represented by the same simple equations as for the smaller orifices, but they also gave clear evidence of the occurrences of a critical change. The data for comparison are summarized in Table 3.

TABLE 3 COMPARISON OF MARCHETTI'S AND SCIMEMI'S DATA

	β	βX_c
Marchetti	0.8696	3.9 to 4.2
Marchetti	0.8964	4.0 to 3.8
Scimemi	0.9002	2.35 to 2.65

The two values of βX_c for each of Marchetti's two plates are independent estimates made at different times and from different plates. The two values for Scimemi's plate are merely limits between which the critical change seems to have occurred.

Conclusion

Only one of the sharp-edged orifices showed any evidence of a critical change. It seems to show a critical change in the neighborhood of $\beta X = 2.5$ or much lower than would be expected from the results of Marchetti's work. But this orifice had the very large diameter ratio $\beta = 0.9002$ and there is nothing in Mar-

chetti's results to compare with. We may, therefore, leave it as an isolated case without further attempting to interpret it.

BIBLIOGRAPHY

1 "The Orifice as a Basis of Flow Measurement," by J. I. Hodgson, Inst. of C. E. Selected Engr. Papers No. 31, 1925.

2 "Flow Through Pipe Orifices at Low Reynolds Numbers," by F. C. Johansen, Reports and Memoranda No. 1252, Aeronautical Research Committee, London, England, January, 1929.

3 "Orifice Discharge Coefficients for Viscous Liquids," by G. L. Tuve and R. E. Sprenkle, *Instruments*, vol. 6, November, 1933, pp. 201–206.

4 "Durchflusbeiwerte der IG - Mymundungen für Wasser, Oil Dampf und Gas," by R. Witte, *Zeitschrift VDI*, vol. 72, 1928, p. 1493.

5 "Durchflusszahlen von Dusen und Staurädern," by R. Witte, *Tech., Mech., und Thermodgn.*, vol. 1, 1930, pp. 1–3.

6 "Die Stromung durch Dusen und Blenden," by R. Witte, *Forschung auf dem Gebiete des Ingenieurwesens*, vol. 2, 1931, pp. 245–251.

7 "Neuer Mengenstrommessungen zur Normung von Dusen und Blenden," by R. Witte, *Forschung auf dem Gebiete des Ingenieurwesens*, vol. 5, 1934, pp. 205–211.

8 "The Flow of Water Through Orifices," by S. R. Beitler, Ohio State University Engineering Exp. Station Bulletin 89, 1935.

9 "I Boccagli E I Diaframim Normalissati Inseriti Nelle Condotte Forzate," by M. Marchetti, *L'Energia Elettrica*, vol. 12, Nov., 1935, pp. 789–811.

10 "La Misura Delle Portate Fluide A. Mezzo Die Diaframmi," by M. Marchetti, *L'Energia Elettrica*, vol. 14, Jan., 1937, pp. 61–67.

11 "Prove su boccagli e diaframmi normalizzati inscrite in condotte da 200 mm," by E. Scimemi, *L'Energia Elettrica*, vol. 13, 1936, pp. 359–369.

12 "Die Durchflusszahlen von Normblenden und ihre Abhangigkeit von der Kantenlange," by G. Ruppel, *Zeitschrift VDI*, vol. 80, 1936, pp. 1381–1387.

13 "Coefficienti di effusso dei diaframmi unificati. Formule di coordinamento dei valori sperimentali per bassi numeri di Reynolds," by M. Marchetti, *L'Energia Elettrica*, vol. 15, April, 1938, pp. 229–244.

The Mechanism of Separation in the Louver-Type Dust Separator

By J. L. SMITH, JR.,[1] and M. J. GOGLIA[2]

The air-flow pattern through the separator was found to be the controlling factor in its performance. The most desirable pattern prevailed when the velocity of the blowdown portion of the inlet air stream was constant from inlet to blowdown. Particle-path studies showed that an effective louver blade shape separates the region of particle impacts with the blades from the region where the air is passing between the blades. An approximate analysis of the particle paths was developed, which is helpful in explaining the trends in the experimental data.

Nomenclature

The following nomenclature is used in the paper:

A = projected area of a dust particle
C_d = coefficient of drag
D = particle diameter
D_{mw} = mean weight diameter
m = mass of a particle
n = number of particles
t = time
V_x = x-velocity of a particle
V_{xa} = x-velocity of air
V_{xr} = x-velocity of a particle relative to air
V_y = y-velocity of a particle
V_{ya} = y-velocity of air
V_{yo} = y-velocity of a particle the instant after an impact
V_{yr} = y-velocity of a particle relative to air
x = distance down louver face
y = distance normal to x
ρ_a = density of air in separator
ρ_p = density of a dust particle
Σ = summation

Introduction

The louver dust separator, Fig. 1, is an inertial-type separator. It is characterized by a stream of dust-laden air incident upon a row of blades or vanes which form the louver face. The larger portion of the air stream, clean air, turns and passes through the blades and the smaller portion of the air stream, blowdown, continues in its original direction without passing through the louver face. The blades are so arranged that the dust because of its high inertia is unable to pass through the blades and is concentrated in the blowdown air stream.

Harwell (1)[3] and Matheson (2) presented analyses of performance data for a louver separator; neither of the two analyses provided an understanding of the separation process. A literature search by Matheson (2) showed there is very little in the literature that is helpful in understanding the mechanism of separation.

This investigation has had as its first object an understanding of the process of separation. This involves a knowledge of why the particles that are separated are not able to pass through the louver blades and of how some particles manage to escape separation. The second object of the investigation was to use this knowledge of the separation mechanism to design a separator with improved performance. The redesigned separator was to embody features which would maximize the forces and effects causing particle separation and minimize those causing particles to pass between the blades.

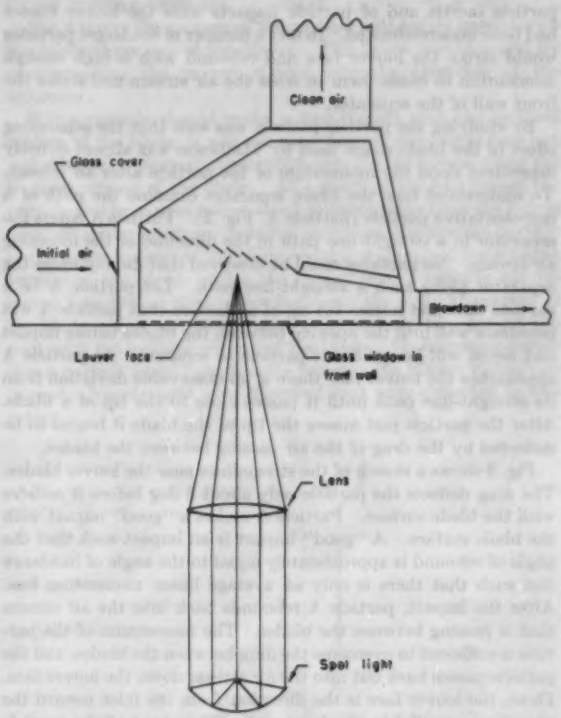

Fig. 1 Two-Dimensional Louver Separator With Modifications for Particle-Path Observations

Preliminary Studies

Method of Investigation. The investigation was conducted in two parts. For the preliminary studies the apparatus of Matheson (2) was modified and used to study the mechanism of separation. The second part of the investigation consisted of the design and construction of a new separator as well as an analysis of its performance.

Almost all that was learned in this investigation was the result of being able to follow the paths of the particles as they passed

[1] Second Lieutenant, U. S. Army, Albuquerque, N. M.

[2] Professor of Mechanical Engineering, Georgia Institute of Technology, Atlanta, Ga. Mem. ASME.

[3] Numbers in parentheses refer to Bibliography at end of paper.

Contributed by the Fuels Division and presented at a joint session of the Fuels and Power Divisions and Committee on Air Pollution Controls at the Annual Meeting, New York, N. Y., November 28–December 3, 1954, of The American Society of Mechanical Engineers.

Note: Statements and opinions advanced in papers are to be understood as individual expressions of their authors and not those of the Society. Manuscript received at ASME Headquarters, August 26, 1954. Paper No. 54—A-134.

through the separator. The particle paths were made visible by a system, Fig. 1, developed during the study. This system was suggested by the Tindall meter (3) and uses the same principle. Matheson's apparatus was modified, Fig. 1, so that this system could be used to follow the particle paths. With this arrangement the particles could be seen as thin threads of light as they passed through the high-intensity beam. Although this arrangement illuminated approximately a $^1/_2$-in. band through the separator, the entire pattern of particle paths could be determined by moving the beam to all parts of the separator.

Evaluation of Performance of Matheson's Separator. Immediately upon observing the paths of the particles in the separator it was evident that in the past the importance of the effects of particle inertia and of particle impacts with the louver blades had been underestimated. In fact a number of the larger particles would strike the louver face and rebound with a high enough momentum to cause them to cross the air stream and strike the front wall of the separator.

By studying the particle paths it was seen that the separating effect of the blade shape used by Matheson was almost entirely dependent upon the momentum of the particle after an impact. To understand how the blade separates examine the path of a representative particle (particle A. Fig. 2). Particle A enters the separator in a straight-line path in the direction of the incoming air stream. No particles could be observed that did not enter the separator along such a straight-line path. Let particle A be a particle that just misses the tip of a blade so that particle A will penetrate well into the opening between the blades before impact and hence will be a difficult particle to separate. As particle A approaches the louver face there is no observable deviation from its straight-line path until it passes close to the tip of a blade. After the particle just misses the tip of the blade it begins to be deflected by the drag of the air passing between the blades.

Fig. 3 shows a sketch of the streamlines near the louver blades. The drag deflects the particle only about 5 deg before it collides with the blade surface. Particle A makes a "good" impact with the blade surface. A "good" impact is an impact such that the angle of rebound is approximately equal to the angle of incidence and such that there is only an average linear momentum loss. After the impact, particle A rebounds back into the air stream that is passing between the blades. The momentum of the particle is sufficient to overcome the drag between the blades, and the particle passes back out into the air stream down the louver face. Down the louver face is the direction from the inlet toward the blowdown parallel to the front wall. The speed of the particle away from the louver face decreases and the speed down the face increases because of the drag of the air stream down the louver face. The particle A may move 6 to 8 in. down the louver face before the effect of the impact is no longer appreciable.

The pattern of the streamlines near the louver blades, Fig. 3, was estimated by observing the behavior of the very fine particles as they passed through the separator. These particles were all below 1 micron in diameter. The location of the air stagnation point on a blade was determined by the presence of a sharp-pointed build-up of fine dust. The build-ups were obviously at the stagnation point because they were fragile and fell off if the blade was tapped lightly.

The limit of the particle deflection before impact with the blade surface could be observed other than by particle paths. The blade face became brightly polished by the particle impacts. The end of the polished area of the blade was distinct and indicated the limit of particle deflection.

Particles were observed to pass between the blades because of "bad" impacts and because of too small an angle of incidence upon the louver face. A bad impact, used in contrast to a good impact, is an impact which is more inelastic than a good impact and which has an angle of rebound quite different from the angle of incidence. The bad impacts can be attributed to the irregular shape of the dust particles.

Particle B, Fig. 2, is a representative particle which makes a bad impact. Particle B enters the separator and proceeds to

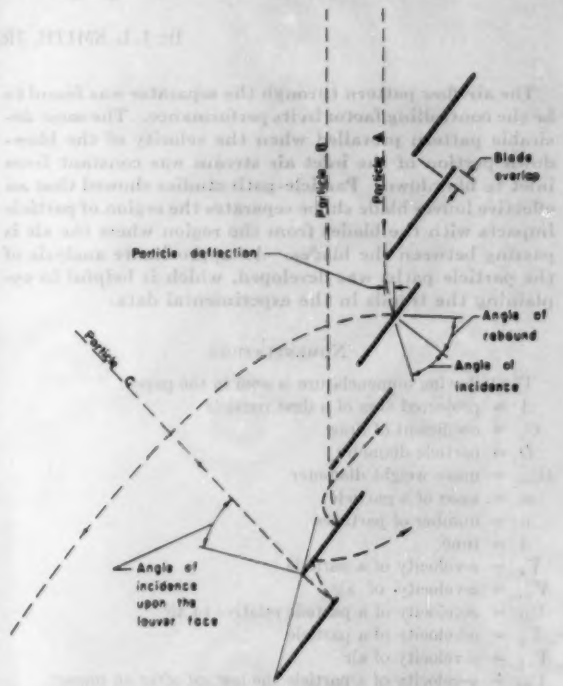

FIG. 2 SKETCH OF REPRESENTATIVE PARTICLE PATHS IN STRAIGHT-BLADE SEPARATOR

FIG. 3 SKETCH OF STREAMLINES NEAR STRAIGHT LOUVER BLADES

the point of impact as did particle A. However, the particle makes a bad impact and rebounds with a greatly reduced momentum and with an unfavorable angle of rebound. As the particle passes back into the air stream between the blades it does not have enough momentum to overcome the drag and it is carried between the blades.

Some particles were observed to pass between the blades because of too small an angle of incidence upon the louver face. Particle C, Fig. 2, is an example of a particle that is incident upon the louver face with too small an angle for separation. Particle C is incident upon the blade surface in such a manner that after impact there is no tendency for it to pass out from between the blades. The drag of the air stream passing between the blades then carries the particle through the louver face.

Conclusions From Preliminary Studies. The first conclusion was that any overlap (see Fig. 2) of the straight blades was unnecessary. Any particle that impacts the blade surface behind the point of zero overlap will rebound with a momentum directed through the louver face and hence cannot be separated. Therefore any overlapping portion of the blades does not aid separation but only restricts the flow of air between the blades.

The flat blade design does not develop the full capabilities of the louver separator. The blade design was poor in that the particles experienced the drag between the blades once before impact with the blade surface and again after impact. The drag after impact was especially bad because on impact the particles lose much of their momentum and, therefore, after impact their motion is strongly influenced by the drag. The drag after a bad impact was strong enough to carry the particles between the blades. Thus if the particles do not have sufficient momentum away from the louver face after impact they will pass through the louver.

The shape of the housing around the louver is of paramount importance. For good separator performance the housing must be so shaped that there will be the same air flow through each opening in the louver or possibly a decrease in air flow through the openings with distance down the louver face. In any case there should not be an increase in flow through the openings with distance down the louver face. In order to achieve this uniform flow through the louver face the velocity of the air stream in front of the louver face must be maintained constant from inlet to blowdown. The back wall and clean-air outlet of the separator must be arranged so that they will maintain a uniform back pressure on the louver.

Separator Design

Blade Design. To minimize the weaknesses of the flat blade design an effort was made to separate the region where the particles impact the blade from the opening between the blades. A more effective blade design would cause the particles to rebound into an air stream directed down the louver face and not between the blades. In this way if a particle made a bad impact it would not pass between the blades. This amounts to separating the action of the blade into two operations. First, because of impacts and resulting rebounds, the particles are moved across the air stream and away from the louver face. The second operation is to allow the air to pass between the blades without allowing any particles to pass. Apparently the second operation is all that is necessary to separate the particles. However if the particles were not moved away from the louver face a very concentrated dust band would develop in front of the face and a particle after first approaching the face would pass very close to all remaining openings between the blades. Hence the number of opportunities for a particle to pass through the louver face would be increased.

Several blade designs were mounted in the apparatus diagrammed in Fig. 1 and observed in operation. The blade shape which appeared to have the best performance is shown in Fig. 4; to understand the operation of this blade design examine the path of a representative particle. The particle enters the separator along a straight-line path in the direction of the inlet air stream. The particle is one that just misses the front tip of a blade. The particle does not deviate observably from its straight-line path until after it passes the tip of the blade which it just misses. After the particle passes the front tip of the blade, it passes into the air stream that is directed between the blades. The drag on the particle deflects the path, but the particle continues by virtue of its own inertia until it completely crosses the stream passing between the blades. The particle then passes into the air that is flowing down the straight portion of the blade. As the particle approaches the inclined portion of the blade it feels that effect of the air stream that has curved out along the inclined portion of the blade. The particle, affected only slightly by drag from this air stream, continues and impacts the inclined portion of the blade. The particle rebounds back into the air stream that has curved out along the inclined portion of the blade and then out into the main air stream down the louver face. The velocity of the particle away from the louver face decreases and the velocity down the face increases because of the drag of the main air stream. The particle may travel 6 to 8 in. after the impact before the effects of the impact are no longer observable.

The streamline pattern near the louver blades is sketched in Fig. 5. As before the stagnation points were determined by the location of fine dust build-ups.

Fig. 6 shows the pattern of the particle paths after impact with the inclined portion of the blades. The figure was obtained by photographing the pattern eroded into the glass top of the separator.

If the particle should make a bad impact with the inclined surface of the blade, it will not pass through the louver face but will rebound with small momentum into the air stream along the inclined portion of the blade. As a result of the bad impact the particle will be carried only a small distance away from the louver face. Particles which are deflected more than the average particle as they pass in front of the blade opening will impact the straight portion of the blade. After the impact such a particle will rebound into the air stream flowing down the straight portion of the blade. This air stream carries the particle to a second impact with the inclined portion of the blade. With enough deflection a particle could pass directly between the blades without an impact. No particles were observed that were deflected to this extent.

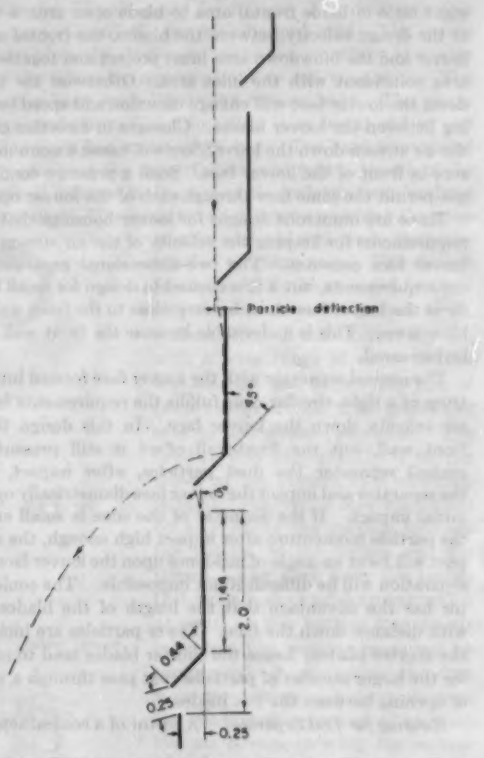

Fig. 4 Blade Design and Sketch of Typical Particle Path

The Louver-Housing Design. A louver housing was designed which, as nearly as possible, would give the same velocity between each of the louver blades and which, as nearly as possible, would keep the velocity of the main air stream down the louver face constant from inlet to blowdown. To explain the design of the louver housing it is necessary to define the variables which were the basis for its design. Inlet area is the cross-sectional area of the inlet to the separator. Blowdown area is the cross-sectional area of the passage in front of the end of the last blade in the louver. The frontal area of the louver face is the projected area of the louver face on a plane normal to the direction of the inlet-air stream. The open area of the louver face is the sum of the areas of all the openings through the face. The areas of the openings are measured in a plane that will give the maximum area. The frontal area of a blade is the portion of the frontal area of the louver that is the contribution of the blade. The open area of a blade is the area of the opening after the blade. The design velocity between the blades is the inlet velocity times the ratio of the blade frontal area to the blade open area. Thus if a louver of constant ratio of blade frontal area to blade open area is operating at the design velocity between the blades the air velocity through the louver face is constant.

The blades shown in Fig. 4 are designed so that the ratio of blade frontal area to blade open area is one for each blade. The object of the louver-housing design was to keep the velocity of the air stream down the louver face constant from inlet to blowdown. This requires first that the blowdown area must be selected to correspond to the blowdown flow desired. For example if a blowdown flow of 5 per cent is desired the blowdown area must be 5 per cent of the inlet area. The blowdown area must be located so that the blowdown portion of the inlet air stream can proceed to the blowdown without changing direction. If a louver of constant ratio of blade frontal area to blade open area is to operate at the design velocity between the blades, the frontal area of the louver and the blowdown area must project and together form an area coincident with the inlet area. Otherwise the air stream down the louver face will change direction and speed before passing between the louver blades. Changes in direction or speed of the air stream down the louver face will cause a nonuniform pressure in front of the louver face. Such a pressure condition does not permit the same flow through each of the louver openings.

There are numerous designs for louver housings that fulfill the requirements for keeping the velocity of the air stream down the louver face constant. The two-dimensional separator satisfies the requirements, but if it is desired to design for small blowdown flows the louver face must be very close to the front wall near the blowdown. This is undesirable because the front-wall effect will be increased.

The conical separator with the louver face formed into the frustrum of a right circular cone fulfills the requirements for uniform air velocity down the louver face. In this design there is no front wall, but the front-wall effect is still present. In the conical separator the dust particles, after impact, will cross the separator and impact the louver face diametrically opposite the initial impact. If the diameter of the cone is small enough and the particle momentum after impact high enough, the second impact will be at an angle of incidence upon the louver face such that separation will be difficult if not impossible. The conical separator has the advantage that the length of the blades decreases with distance down the face. Fewer particles are incident upon the shorter blades; hence the shorter blades tend to compensate for the larger number of particles that pass through a unit length of opening between the last blades.

Housing for Test Separator. A sector of a conical separator fulfills the requirements for uniform air velocity down the louver face and has the advantages of a conical separator. The housing for the test separator was designed to approximate a 30-deg sector of a conical separator. The separator was constructed with a trapezoidal cross section rather than a circular sector to facilitate fabrication.

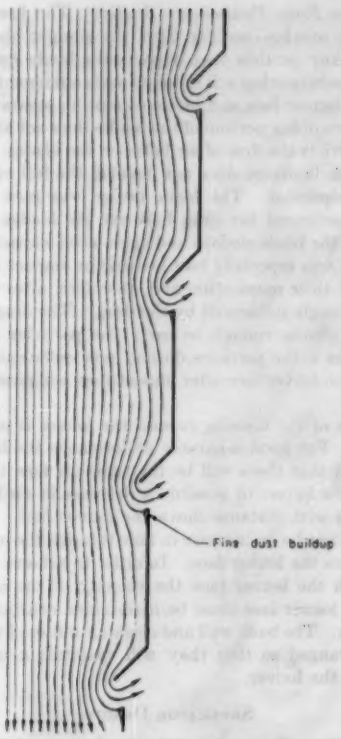

FIG. 5 SKETCH OF STREAMLINES NEAR LOUVER BLADES

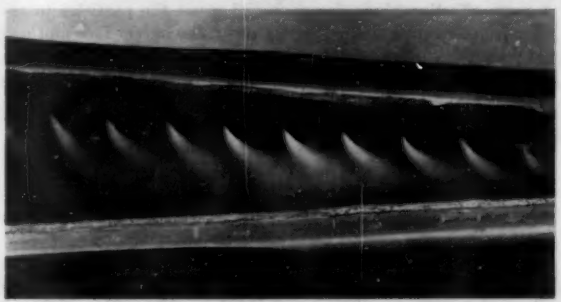

FIG. 6 PHOTOGRAPH OF PATTERN ERODED INTO GLASS TOP OF SEPARATOR

Simplified sketches of the separator are given in Fig. 7. A photograph of the separator is given in Fig. 8.

A detailed cross section showing the constructional features of the separator is given in Fig. 9. The top of the separator was plate glass, and glass windows were placed in the front wall so that the particle paths could be observed.

Apparatus

The Air System. Figs. 10 and 11 show the layout of the equipment. The clean air stream which made a 180-deg change of direction in passing through the separator passes from the separator through the trapezoidal outlet. The outlet cross section was changed by a transition section to a 2-in. × 4-in. rectangular duct. The air stream made a 90-deg turn in the horizontal plane, passed through a transition to a 2-in. × 3-in. duct, and made a 90-deg turn in the vertical plane before entering the dust-collecting chamber. For the outlet from the dust chamber, a length of standard 3-in. pipe provided with an orifice meter was fitted into the side of the dust chamber at the bottom.

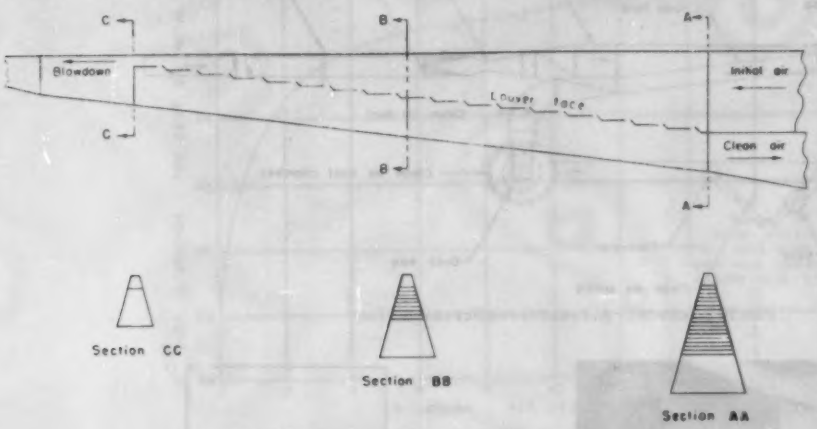

Fig. 7 Simplified Sketch of Separator

The blowdown air stream which flowed from the separator through a trapezoidal outlet passed through a transition to a 1-in. × 2-in. rectangular duct. The blowdown stream made a 90-deg turn in the vertical plane and passed into the blowdown dust-collecting chamber. The outlet from the blowdown dust chamber was a length of $1^1/_2$-in. standard pipe fitted with a metering orifice. For small blowdown flows a calibrated flowrator was attached to the outlet pipe.

The air flows were regulated by obstructing the blower inlet, by adjusting a globe valve in the outlet from the blowdown dust chamber, and by varying an obstruction in the inlet to the clean-air dust chamber.

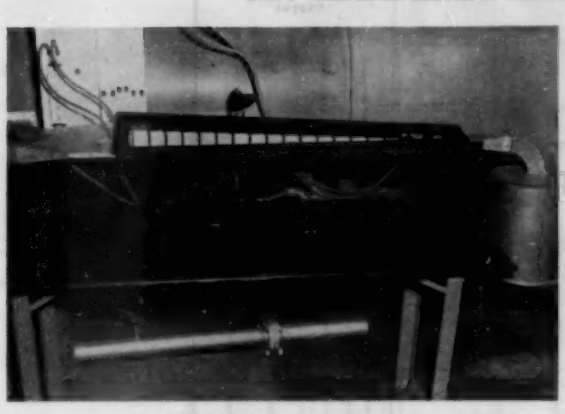

Fig. 8 Photograph of Separator

Dust-Collection Chambers and Dust Bags. The dust-collection chambers were cylindrical cans with flanged tops. The covers were connected to the ducts coming to the chambers and were secured to the flange by means of screws and wing nuts. The dust-collecting bags were Electrolux cleaner bags. The clean-air bag was made from four Electrolux bags sewed end to end and the blowdown bag was a single bag. The bags were sealed in place by clamping the flanged metal and rubber mouth of the bag between the flange on the top of the collecting can and the cover for the can. The wing nuts and screws provided the pressure for the seal and made disassembly for weighing easy. The outlets from the chambers were fastened into the sides near the bottom.

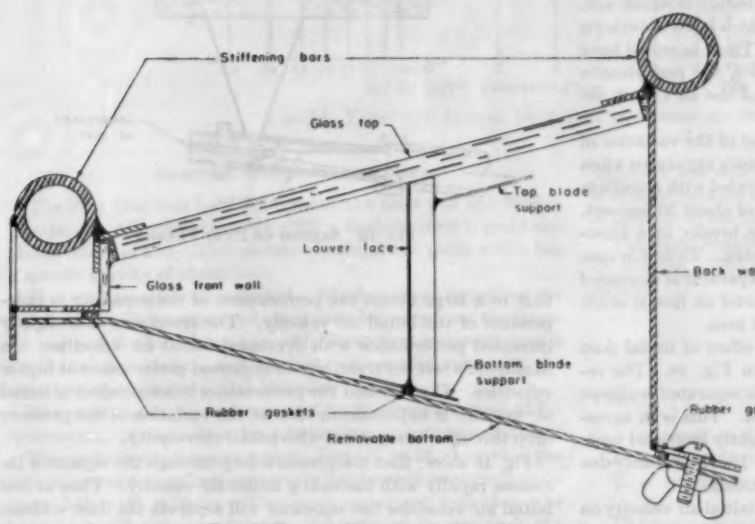

Fig. 9 Detail Cross Section of Separator

Dust Feed. A dust feeder, Fig. 12, with a wide range of rates of feed was designed and built. The rate of feed ranged from 2.72 grams per min to 255 grams per min. The feeder was essentially a hopper closed at the bottom by a vibrating trough. The rate of feed was varied by adjusting the opening between the bottom of the hopper and the trough. The dust from the trough fell into a second hopper which opened at the bottom into an air injector. The injector, operated by compressed air, picked up the dust from the trough and some air from the room and injected them into the air stream entering the separator.

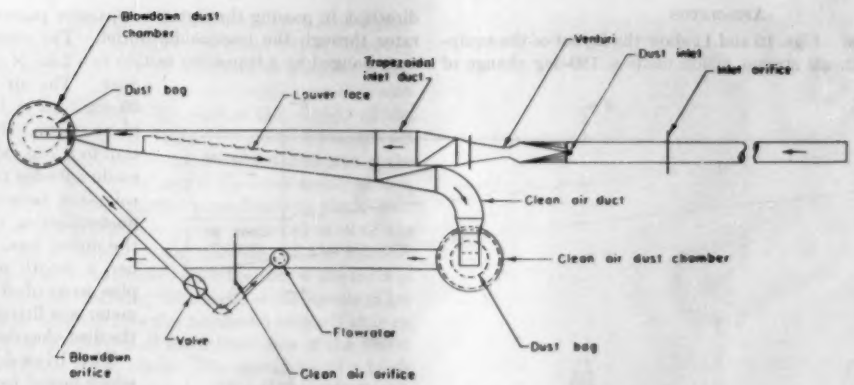

FIG. 10 SKETCH OF APPARATUS FOR SEPARATOR TEST

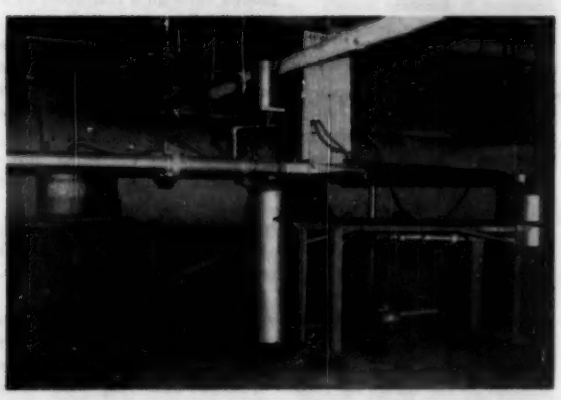

FIG. 11 PHOTOGRAPH OF APPARATUS FOR SEPARATOR TEST

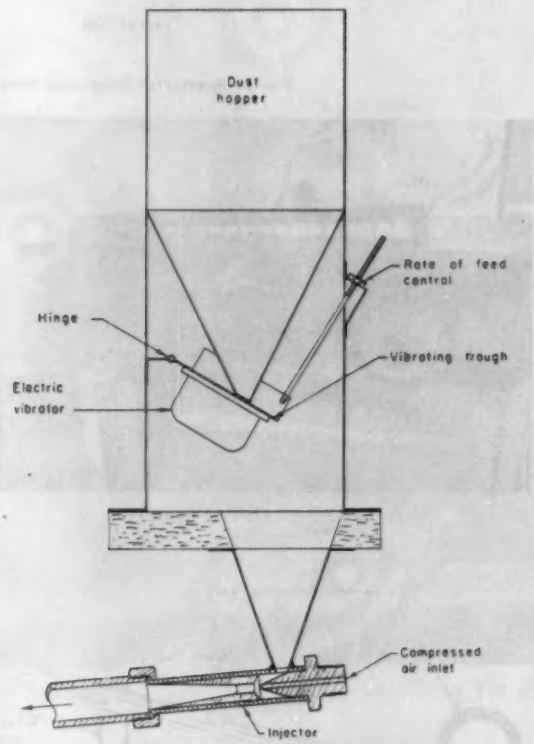

FIG. 12 SKETCH OF DUST FEEDER

DISCUSSION OF RESULTS

Effect of Blowdown. The effect of blowdown air flow on dust separation is shown in Fig. 13. The point at which the performance of the separator breaks and decreases sharply is significant. This point is at about 6 per cent blowdown which is the blowdown for uniform velocity down the louver face. Thus, as would have been predicted from the particle-path studies, the performance of the separator is decreased if the velocity of the air stream decreases as it passes down the louver face.

It is interesting to examine Matheson's plot of the variation of dust separation with blowdown (4). Matheson's apparatus when set for a 22.5-deg face angle would have operated with a uniform velocity down the louver face at a blowdown of about 30 per cent. Matheson's extrapolated performance curve breaks at a blowdown of about 30 per cent as would be predicted. Thus it is concluded that the performance of the louver separator is decreased sharply if the ratio of blowdown air flow to total air flow is much less than the ratio of blowdown area to inlet area.

Effect of Initial Dust Concentration. The effect of initial dust concentration on dust separation is shown in Fig. 14. The results show that the per cent of the dust that is separated is almost independent of the initial dust concentration. This is in agreement with Harwell (5). The trend is to a slightly increased separation with increasing initial concentrations. This is probably due to collisions between the particles in the air stream.

Effect of Initial Air Velocity. The effect of initial air velocity on dust separation is given in Fig. 15. This part of the test showed that to a large extent the performance of the separator is independent of the initial air velocity. The trend was to a slightly increased performance with decreased initial air velocities. In Matheson's test the trend was to improved performance at higher velocities. The fact that the performance is independent of initial air velocity is important in view of the variation of the pressure drop through the separator with initial air velocity.

Fig. 16 shows that the pressure drop through the separator increases rapidly with increasing initial air velocity. Thus at low initial air velocities the separator will separate the dust without absorbing the power that it would at high velocities.

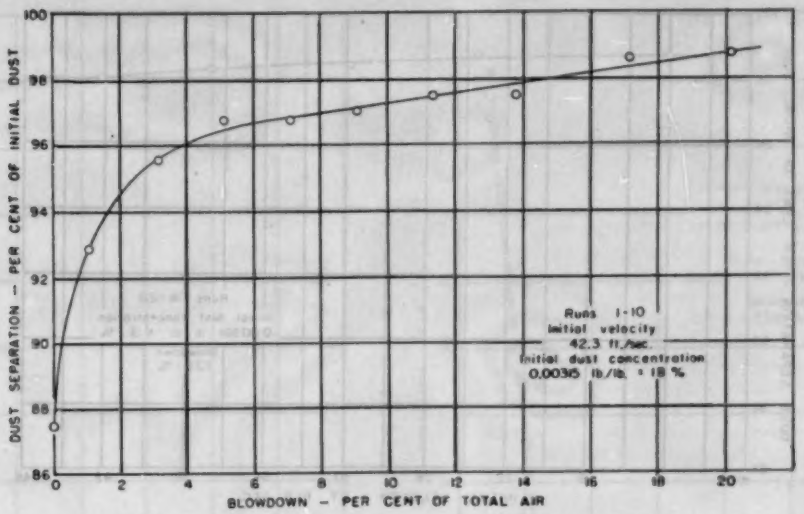

FIG. 13 EFFECT OF BLOWDOWN ON DUST SEPARATION

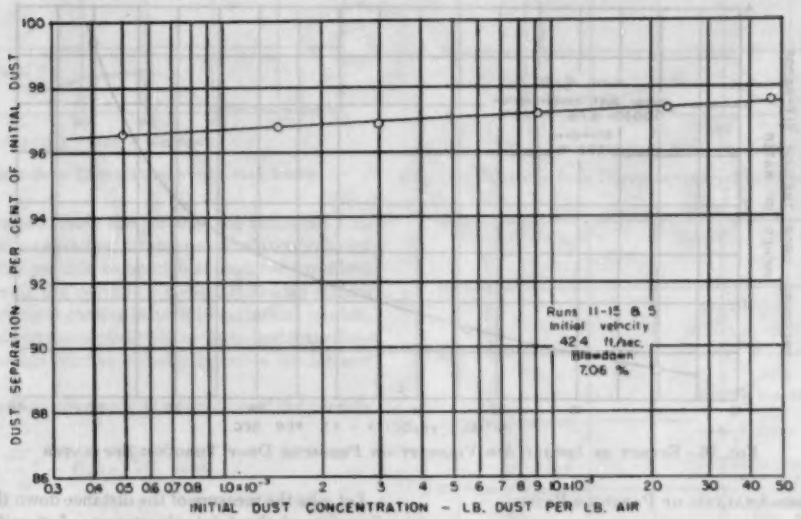

FIG. 14 EFFECT OF INITIAL DUST CONCENTRATION ON DUST SEPARATION

PARTICLE-SIZE DISTRIBUTIONS

The dust that was used throughout the tests was the Norton Company's Alundum abrasive with a manufacturer's grain-size classification of 240. This abrasive is aluminum oxide which has a specific gravity of about four.

Five dust samples were studied. The first was a sample of the input dust. The second and third samples were from the clean-air bag and the blowdown bag with the separator operating at a low initial air velocity, and the last two samples were with the separator operating at a high initial air velocity.

The particle sizes were determined by the standard method for determining particle sizes by microscopic measurements (6).

The particle-size frequency plots, Figs. 17 to 19, show that the separator was more effective on particles above 40 microns than on those below 40 microns. The most important fact that was brought out by the particle-size determinations was that the separator was effective on particles as small as 10 microns. This is evident because of the high frequency of occurrence of particles of this size in the blowdown dust.

The mean weight diameter for the input dust was found to be 49 microns. The mean weight diameter was computed by the formula (7)

$$D_{mw} = \left(\frac{\Sigma n D^3}{\Sigma n}\right)^{1/3}$$

where

n = number of particles in any size group
D = mean diameter of size group
Σ = summation

The mean diameter for the input dust sample was 25 microns

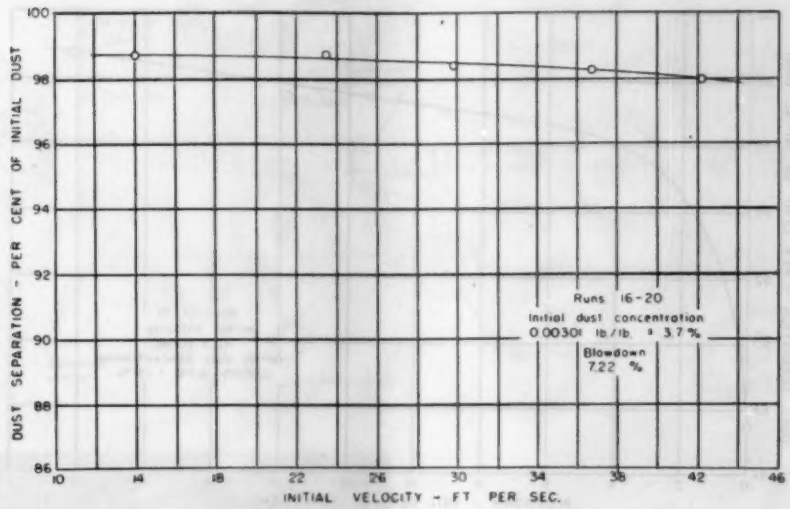

FIG. 15 EFFECT OF INITIAL AIR VELOCITY ON DUST SEPARATION

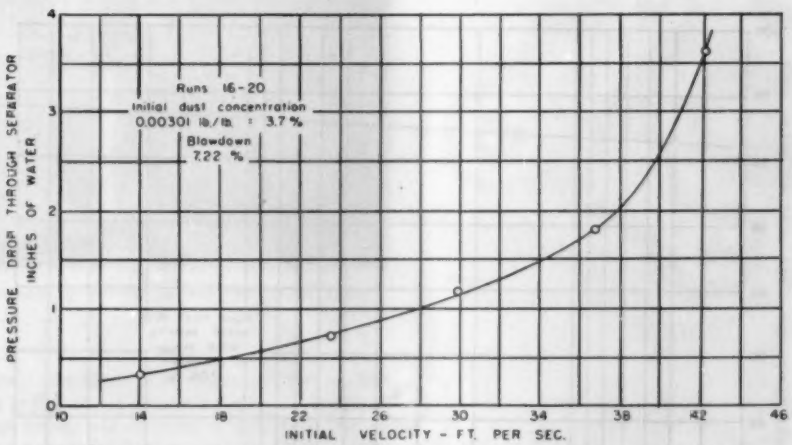

FIG. 16 EFFECT OF INITIAL AIR VELOCITY ON PRESSURE DROP THROUGH SEPARATOR

IDEALIZED ANALYSIS OF PARTICLE PATHS

Particle Paths Near an Opening Through Louver. In order to understand better the action of the separator, an idealized analysis of the particle paths has been developed. This analysis is helpful in understanding the results of the tests and it may prove helpful in predicting the effect of other variables not studied at this time. The analysis is in two parts, the first being an analysis of the drag effect on a particle as it passes an opening between the blades, and the second being an analysis of a particle path after an impact with the inclined portion of a louver blade.

It is assumed that the dust particles are smooth spheres. The dust particle that just misses the tip of a blade is analyzed and it is assumed that the particle passes the tip of the blade with a velocity equal to the velocity of the air stream down the louver face. It is also assumed that the particle is traveling in the direction of the inlet air stream. As the particle passes the blade tip it passes into the air stream that is flowing between the blades. It is assumed that this air stream is of uniform velocity directed between the blades and is perpendicular to the inlet air stream. The assumptions about the air flow are admittedly approximations.

Let x be the measure of the distance down the louver face in the direction of the inlet air stream. Let y be the measure of the distance through the louver face normal to x. Let the tip of the blade which the particle just misses be $x = 0, y = 0$. Let $t = 0$ be the time at which the particle in question passes through $x = 0, y = 0$.

The differential equation governing the x-motion of the particle is

$$m\frac{dV_x}{dt} + C_d A \rho_a \frac{V_x^2}{2} = 0$$

with the initial condition

$$V_x = V_{x0} \text{ at } t = 0$$

Because of the turbulence of the main air stream, the coefficient of drag for the particle is taken equal to 0.44, the value for fully developed turbulent motion of the air about the particle. This is in accordance with DallaValle (8). Although the average velocity of the particle relative to the air over some short-time interval may not be high enough to satisfy the criterin for fully developed

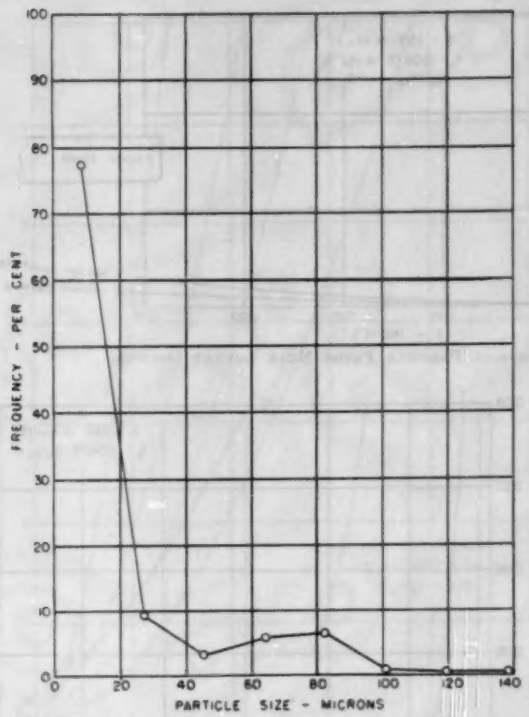

FIG. 17 PARTICLE-SIZE DISTRIBUTION—INITIAL DUST

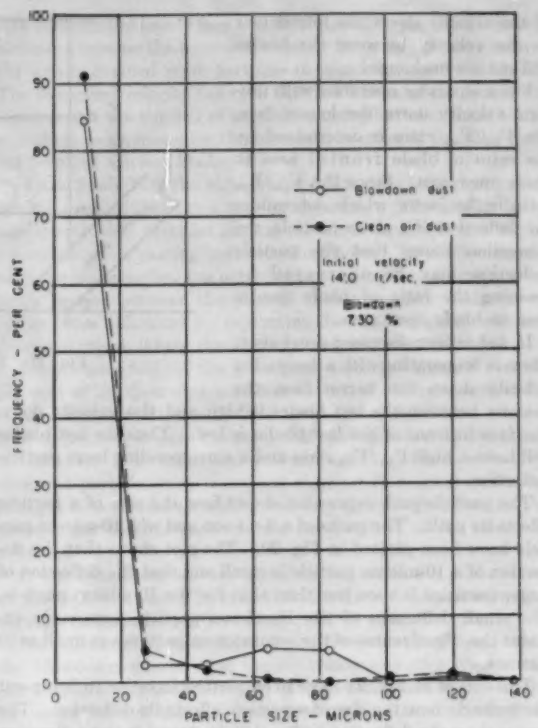

FIG. 18 PARTICLE-SIZE DISTRIBUTION—BLOWDOWN AND CLEAN AIR

turbulent motion of the air about the particle, the turbulent fluctuations of the air stream cause the instantaneous relative velocity between the air and the particle to be high enough for turbulent motion of the air about the particle. Hence, if the air stream through which the particle is passing is itself in turbulent motion, the motion of the air about the particle will be turbulent regardless of the value of the average relative velocity between the air and the particle.

The differential equation governing the y-motion of the particle after $t = 0$ is

$$m\frac{dV_y}{dt} - C_d A \rho_a \frac{V_{yr}^2}{2} = 0$$

with the initial condition

$$V_y = 0 \text{ at } y = 0$$

On solving the two differential equations and eliminating the parameter t, the equation of the particle path is

$$y = \frac{D\rho_p}{0.33\,\rho_a}\left\{\frac{V_{ya}}{V_{xa}}\left(e^{\frac{0.33\,\rho_a}{D\,\rho_p}x} - 1\right) - \ln\left[\frac{V_{ya}}{V_{xa}}\left(e^{\frac{0.33\,\rho_a}{D\,\rho_p}x} - 1\right) + 1\right]\right\}$$

The details of the solution are given in reference (9).

It is important to note that velocity appears in the expression only as the ratio V_{ya}/V_{xa} which is the ratio of the velocity of the air down the louver face to the velocity of the air between the louver blades. This shows that the particle paths near the openings between the blades are independent of the initial air velocity because if the initial air velocity is changed, the velocity between the blades will be changed by the same ratio, and the ratio

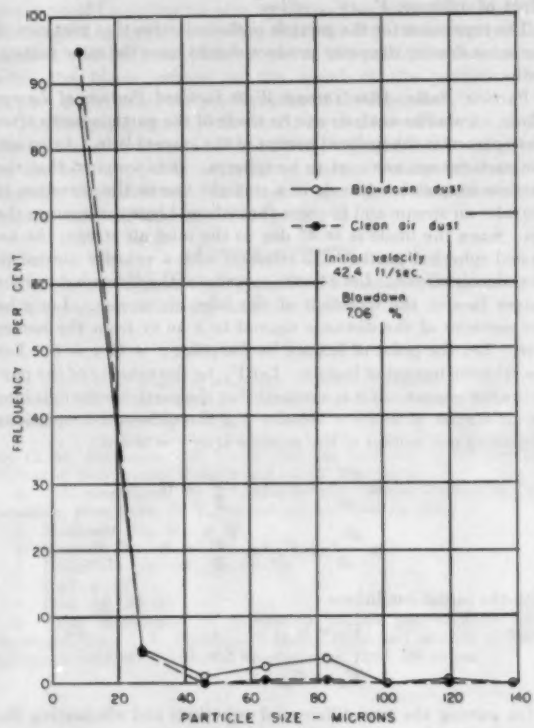

FIG. 19 PARTICLE-SIZE DISTRIBUTION—BLOWDOWN AND CLEAN AIR

of the velocity down the louver face to the velocity between the blades will remain unchanged.

For a separator operating with uniform velocity down the louver face, the V_{ya}/V_{xa} ratio is determined by the ratio of blade frontal area to blade open area. Since the V_{ya}/V_{xa} ratio is the factor which determines the deflection of a given particle, the expression shows that the particle deflection may be decreased by lowering the ratio of blade frontal area to blade open area.

If, as has been discussed previously, a louver is operating with a decreasing velocity down the louver face, the velocity between the last blades is high and the velocity down the face in front of the last blades is low. Thus the last blades will have a high V_{ya}/V_{xa} ratio and a corresponding large particle deflection.

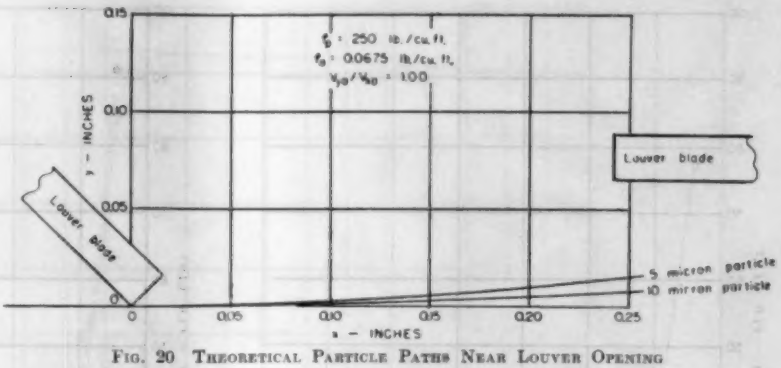

FIG. 20 THEORETICAL PARTICLE PATHS NEAR LOUVER OPENING

The particle-path expression shows how the size of a particle affects its path. The paths of a 5-micron and of a 10-micron particle have been plotted in Fig. 20. The plot shows that the deflection of a 10-micron particle is small and that the deflection of larger particles is even less than that for the 10-micron particle. The small deflection of the 10-micron particle apparently explains the effectiveness of the separator on particles as small as 10 microns.

The curves of Fig. 21 have been plotted in order to bring out more clearly how the size of a particle affects its deflection. The curves show the deflection y after 0.25-in. travel in the x-direction for different particle sizes. Curves also are plotted to show the effect of different V_{ya}/V_{xa} ratios.

The expression for the particle paths indicates that particles of the same density diameter product should have the same particle paths.

Particle Paths After Impact With Inclined Portion of Louver Blade. A similar analysis can be made of the particle paths after an impact with the inclined portion of the louver blade. As before, the particles are assumed to be spheres. It is assumed that the particle in question travels in a straight line in the direction of the inlet-air stream and impacts the inclined blade surface near the tip. Since the blade is at 45 deg to the inlet air stream the assumed spherical particle will rebound with a velocity normal to the inlet air stream. Let x be the measure of the distance down the louver face in the direction of the inlet air stream. Let y be the measure of the distance normal to x away from the louver face. Let the point of impact be the point $x = 0$, $y = 0$. Let $t = 0$ be the instant of impact. Let V_{yo} be the velocity of the particle after impact. If it is assumed that the particle rebounds into an air stream of uniform velocity V_{xa} the differential equations governing the motion of the particle after $t = 0$ are

$$m\frac{dV_x}{dt} - C_d A \rho_a \frac{V_{xr}^2}{2} = 0$$

$$m\frac{dV_y}{dt} + C_d A \rho_a \frac{V_{yr}^2}{2} = 0$$

with the initial conditions

$$V_x = 0 \qquad \text{at } t = 0$$

$$V_y = V_{yo}$$

On solving the two differential equations and eliminating the parameter t, the equation of the particle path is

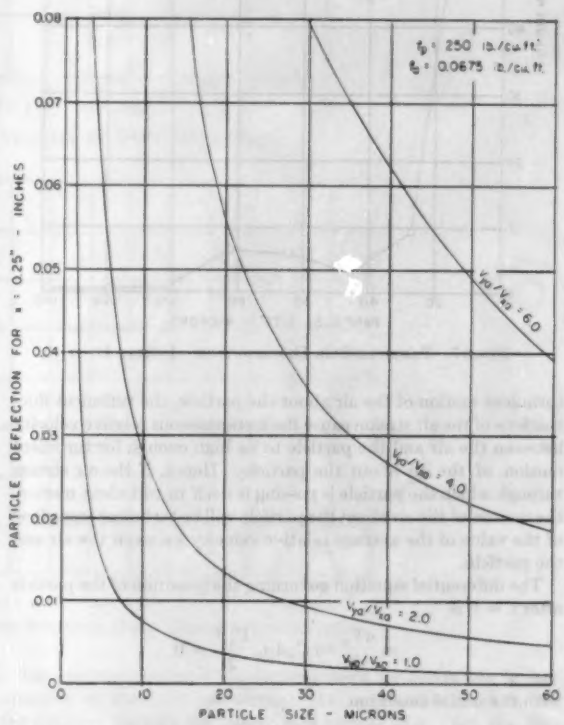

FIG. 21 THEORETICAL PARTICLE DEFLECTIONS FOR $x = 0.25$ IN.

$$x = \frac{D\rho_p}{0.33\rho_a}\left\{\frac{V_{xa}}{V_{yo}}\left(e^{\frac{0.33\rho_a}{D\rho_p}y} - 1\right) - \ln\left[\frac{V_{xa}}{V_{yo}}\left(e^{\frac{0.33\rho_a}{D\rho_p}y} - 1\right) + 1\right]\right\}$$

The details of the solution (9) are the same as for the solution of the paths near a louver opening.

In this expression for the particle paths the ratio V_{xa}/V_{yo} is important. If it is assumed that the particle before impact is traveling with the velocity of the air down the louver face, then the ratio V_{xa}/V_{yo} is the ratio of the speed of the particle before impact to the speed of the particle after impact. It seems reasonable that the ratio of the speed of the particle before impact to the speed of the particle after impact will be about the same regardless of the initial velocity. If this is true then the initial air

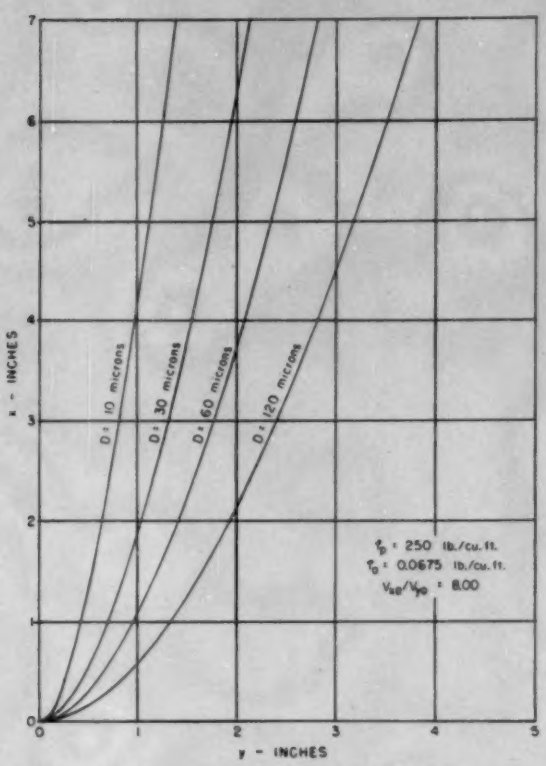

FIG. 22 THEORETICAL PARTICLE PATHS AFTER AN IMPACT

velocity will not affect the particle paths after impact. Observations of the particle paths after impact did not reveal a marked change of the paths with changes in the initial air velocity.

The paths for four different particle sizes are plotted in Fig. 22. A value of eight for the V_{xo}/V_{yo} ratio was arrived at for these curves. This value gave particle paths which closely resembled the particle paths observed in the separator.

The V_{xo}/V_{yo} ratio is undoubtedly dependent upon the nature of the particles. Since the V_{xo}/V_{yo} ratio is one of the factors which determines how effectively the particles are moved away from the louver face, it is a factor which must be considered when an attempt is made to predict the effectiveness of the separator on some other dust. If the particles have a low V_{xo}/V_{yo} ratio the front-wall effect will become important. If the particles have a high V_{xo}/V_{yo} ratio the particles will remain close to the louver face and have many opportunities to pass through a louver opening.

The limitations of this analysis of the particle paths must be kept in mind; the analysis is definitely only a first approximation.

CONCLUSIONS

The most important conclusion that can be drawn from this investigation is that the performance of the separator can be maintained at low blowdown flows if the louver housing is designed so that the velocity of the air stream down the louver face is constant from inlet to blowdown. It was found that the uniform velocity of the air stream down the louver face was necessary to insure a uniform flow through the louver face. A nonuniform flow through the louver face was detrimental to the separator performance because the increased velocity between the last blades of the louver enabled more particles to pass between these blades. The decreased velocity between the first blades of the louver did not decrease the number of particles passing between these blades enough to compensate for the increased number of particles passing between the last blades.

It was found that the straight flat-blade design did not develop the full capabilities of this type of separator. The flat-blade design is such that particles impact the blade surface in the region where the air is passing between the blades. Thus after impact with the blade surface the particles have a low momentum and are easily carried between the blades. The new blade design overcomes these difficulties by separating the region of particle impact from the region where the air is passing between the blades.

Performance tests of the redesigned separator showed that the per cent of the dust separated was essentially independent of the initial dust concentration. The tests also showed that the per cent of dust separated was essentially independent of the initial air velocity. This conclusion was supported by the fact that the observed particle paths were not changed to a great extent by changes in the initial air velocity and by the fact that the analysis showed the particle paths to be independent of the initial air velocity.

It was found that at low initial air velocities the performance of the separator could be maintained with a total pressure drop through the separator of less than $^1/_2$ in. of water.

Particle-size studies on dust samples from the clean air and from the blowdown showed that the separator was effective on dust particles as small as 10 microns. The effectiveness of the separator on particles of this size was supported by the analysis of the particle paths.

The approximate analysis of the particle paths also showed how the ratio of blade frontal area to blade open area, the size of the blade opening, the particle size, the ratio of particle density to air density, and the ratio of the speed of the particle before impact with the blade surface to the speed of the particle after impact might affect the performance of the separator.

The foregoing conclusions should be considered in view of the experimental observation that bottom, top, and front-wall effects in the test apparatus contributed to the passage of particles through the louver face. The use of a three-dimensional full conical unit will eliminate these problems.

ACKNOWLEDGMENT

The authors express their gratitude to Research Corporation in making funds available to conduct this study.

BIBLIOGRAPHY

1 "An Initial Study of a Louver-Type Dust Separator," by C. W. Harwell, MS thesis, Georgia Institute of Technology, School of Mechanical Engineering, 1950, 41 pages.

2 "A Two-Dimensional Study of a Louver-Type Dust Separator," by C. M. Matheson, MS thesis, Georgia Institute of Technology, School of Mechanical Engineering, 1952, 108 pages.

3 "Micromeritics," by J. M. DallaValle, Pitman Publishing Corporation, New York, N. Y., second edition, 1948, p. 201.

4 Matheson, Op. cit., p. 54.

5 Harwell, Op. cit., p. 28.

6 DallaValle, Op. cit., pp. 68–70.

7 Ibid., p. 47.

8 Ibid., pp. 39–40.

9 "The Mechanism of Separation in the Louver-Type Dust Separator," by J. L. Smith, MS thesis, Georgia Institute of Technology, School of Mechanical Engineering, 1953, 86 pages.

Plastic Working of Metals

By W. S. WAGNER,[1] CANTON, OHIO

The material presented in this paper is in itself a brief review of the art of plastic working of metals which has been compiled in order to stimulate discussion of the subject at the first annual meeting following the establishing of the ASME Research Subcommittee on the Plastic Working of Metals. The thermoplastic and crystoplastic states are presented as two distinct ranges of plastic working dependent on temperature. Basic laws governing these phenomena must be delineated. Work hardening and deformation strength are pointed out with one method of estimating deformation strength from true strain. The effect of aging after plastic working is introduced. The relationship between per cent reduction of area and true strain as measures of the extent of plastic working is presented. Further study of these fields and introduction of new problems along with definition of terms and development of both theory and practice are the responsibilities of the committee.

Nomenclature

The following nomenclature is used in the paper:

A_0 = original cross-section area, sq in.
A = final cross-section area, sq in.
X_0 = original length, in.
X = final length, in.
$\bar{\epsilon}$ = true deformation, dimensionless
ϵ = unit deformation, in. per in.
s_y = deformation stress, psi
s_e = stress at elastic limit, psi

Introduction

The ASME Research Subcommittee on the Plastic Working of Metals was organized a year ago to analyze the problems of this field and to gather and correlate usable material with the ultimate aim of compiling a handbook of metalworking for the industry. The objective of our initial panel discussion is to review the current status of the art in order to raise pertinent points for discussion and define the field to give a common starting ground for the many efforts which must be co-ordinated. The necessary development, interchange of knowledge, logical reasoning, and practical application cannot be embodied in any purely industrial, mathematical, or scientific approach. Information from all allied arts and sciences will be considered, interpreted, and translated with the application to industrial use as the final criterion of utility.

The field of plasticity is adjacent to that of elasticity. The two states for a given material are separated by the elastic limit of that material. In the elastic range the conditions and laws are fairly well fixed and understood, but in the plastic range they are much more complex and misunderstood. Plastic strain is a function of momentary stress and temperature, but it also is dependent on the past history of these phenomena, especially the past increases and decreases of stress. There are problems in which small plastic deformation is a vital factor but the stamping, forging, extruding, and other metalworking industries are interested primarily in the relatively large plastic changes which are required in the creation of new permanent forms. These changes in form may be accomplished either hot or cold with materials that are either isotropic or anisotropic.

Laws and Phenomena of Plasticity

It seems that there is a general misunderstanding, among engineers and designers, of the laws and phenomena of the plastic range. It is true that in the design of structures and machines the yield point may be used as the criterion of failure of a structural or mechanical member; however, a vast number of persons seem to believe that a material is utterly useless and destroyed if it has been stressed beyond its yield point. This belief, as we know, is definitely not true. On the contrary, for production purposes the opposite opinion is more nearly valid. Most metals after once having been stressed beyond their yield points have greater resistances to deformation than they had prior to such a treatment. The plastic phenomena make possible a vast number of methods and processes for producing specific forms and also specific physical properties of materials that could not be obtained with any other process.

There are two important states of plasticity in metals—the thermoplastic range and the crystoplastic range. The thermoplastic range occurs above the recrystallization temperature where crystal structure is not stable. It also is known as the forging range or the hot-work range. Interatomic stresses resulting from flow in this range may be more or less relieved by virtue of the rearrangement which takes place with time at these temperatures. The increased electron activity in this range offsets work-hardening effects and increases the extent to which the material can be worked. Lead and tin are in this range at room temperature and zinc, magnesium, and aluminum at slightly higher temperatures.

Time is also an important factor in thermoplastic working. Work hardening by slip-plane disturbance of interatomic spacing does take place and is useful, but it is subject to diminution by recrystallization depending on temperature and time. Residual work hardening is responsible for improved physicals in forged products.

The crystoplastic range is below the recrystallization temperature where the crystal structure is in a stable equilibrium. It is known as the cold-work range. In it plastic flow leaves permanently deformed crystals with their areas of relatively high energy at deformation planes. It is limited largely but not entirely to metals and alloys characterized by face-centered and body-centered cubic-crystal space lattices. Relatively small amounts of work may be performed upon the hexagonal lattice metals.

Within the crystoplastic range itself there are further subdivisions. They may be considered to be a lower range, a middle range, and an upper range, as shown in Fig. 1. The lower one does not have a sharply defined stress-strain relationship due to irregularities in plastic action in the region of the yield point. Some persons have expressed the belief that stress-relief occurs at room temperature after such small reductions. The middle range embodies the majority of commercial forming operations. Its true stress-strain relationship can be sharply defined, but these data

[1] Development Engineer, E. W. Bliss Company.

Contributed by the Research Committee on Metal Processing and presented at the Annual Meeting, New York, N. Y., November 28–December 3, 1954, of The American Society of Mechanical Engineers.

Note: Statements and opinions advanced in papers are to be understood as individual expressions of their authors and not those of the Society. Manuscript received at ASME Headquarters, June 30, 1954. Paper No. 54—A-64.

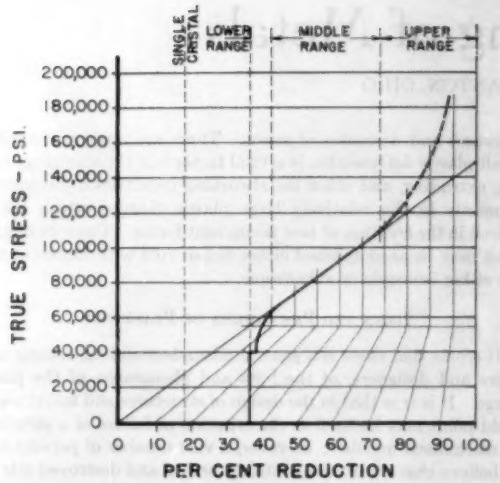

FIG. 1 CURVE OF STRAIN HARDENING OF LOW-CARBON STEEL IN THE CRYSTOPLASTIC RANGE
(The three subdivisions of crystoplastic working are shown.)

have not been compiled except in a few specific cases. In this middle range the increase in stress with strain is fairly constant, but at its limit the stress curve sweeps sharply upward into the upper range. This separating point has been roughly defined as the one at which all favorably oriented slip planes have been used up. This upper crystoplastic range should be of major interest, but it is difficult to investigate by current techniques. It develops exceptional strengths in wire drawing, Steckel rolling, and impact extrusion. Each of these is a compression working operation characterized by considerable work heat which seems to be an essential component. Bridgman's (1)[2] physical testing in a pressure zone offers promise as an investigating means providing that successive true stress readings may be obtained with respective areas.

Work hardening by slip-plane movement and interatomic strain involves the increasing of elastic limit, yield point, endurance limit, and resistance to deformation. In general these phenomena bear the same relationship to strain in tension as in compression. Hardness increases proportionately within the middle crystoplastic range but then appears not to increase even though the working may continue into the upper range.

Crane (2) has compiled a chart, Fig. 2, covering the middle crystoplastic range which helps to visualize the relative hardenability of various metals due to plastic working. It is also quite useful in determining the true stress in one or in a series of operations; however, it must have considerable explanation, partially illustrated in Fig. 3, in order to be understood thoroughly.

CHECKING ASSUMPTIONS AND APPROXIMATIONS

The basic laws of plasticity are more complex than those of elasticity and in some aspects our initial assumptions will bear careful re-examination. Thus far a wide latitude has been allowed both in assumption and approximation in order to obtain results in the theoretical approach. Of necessity, there has been a great dependence on accompanying experimental work. The validity of some of the commonly known physical laws has been questioned when applied to the plastic range and used as basic assumptions for development of theory. Hooke's law seems impossible in the plastic range with a metal that exhibits work hardening. Pascal's

[2] Numbers in parentheses refer to the Bibliography at the end of the paper.

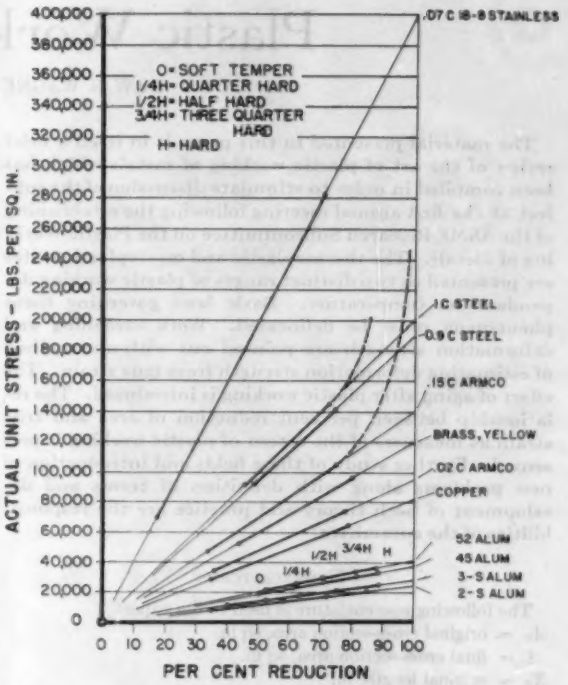

FIG. 2 TENTATIVE CURVES SHOWING COMMERCIAL COLD-WORKING RANGE AND RATE OF STRAIN HARDENING AT ROOM TEMPERATURE FOR SEVERAL METALS

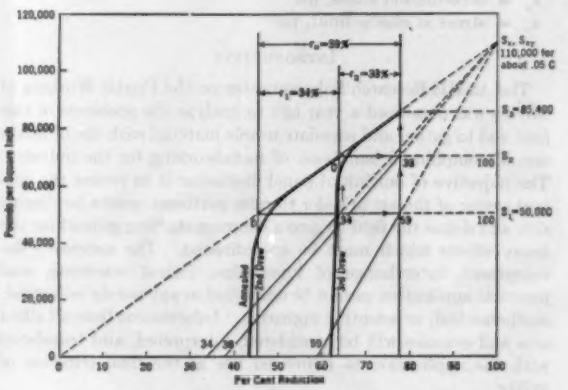

FIG. 3 STRAIN HARDENING DURING SUCCESSIVE REDRAWS OF STEEL SHELL, ILLUSTRATING USE OF CURVES OF FIG. 3

principle seems to be only approximate in the light of recent research investigating pressures during the extrusion of lead (3). Poisson's ratio changes in value in the plastic state. This change is natural, however, since certain investigations have pointed out that the more nearly the physical properties of a material approach those of a liquid, the more nearly its Poisson's ratio approaches 0.5. Another point of interest is that Kachonov (4) has shown that certain plastic-range problems may be treated the same as similar elastic-range problems provided the corresponding moduli of rigidity are reduced. There is a need for basic research thoroughly and accurately interpreted to clarify these issues and determine what laws apply to the plastic range and to

TABLE 1 DATA COMPILED TO CHECK SIEBER'S EQUATION FOR DEFORMATION STRENGTH

$$s_y = s_e + C\sqrt[n]{\ln(A_0/A)}$$

Material	s_e	n	C	Range of work	Data
Tobin bronze	17000	1.72	138000	$0.1 < \ln A_0/A < 0.7$	Experimental
C-1018 steel	32000	4.55	53000	$0.2 < \ln A_0/A < 1.5$	Experimental
Spheroidized cartridge-case steel	37800	2.23	81000	$0.15 < \ln A_0/A < 1.2$	Experimental
304 Stainless	35000	1.48	208000	$0.2 < \ln A_0/A < 0.9$	Published
321 Stainless	30000	1.60	154000	$0.2 < \ln A_0/A < 0.9$	Published
403 Stainless	40000	2.54	67000	$0.2 < \ln A_0/A < 0.9$	Published
2S Aluminum	4000	2.83	14000	$0.2 < \ln A_0/A < 1.6$	Published
3S Aluminum	5000	2.78	17000	$0.2 < \ln A_0/A < 1.6$	Published
4S Aluminum	10000	3	25200	$0.2 < \ln A_0/A < 1.6$	Published
52S Aluminum	14000	3.18	19600	$0.2 < \ln A_0/A < 1.6$	Published

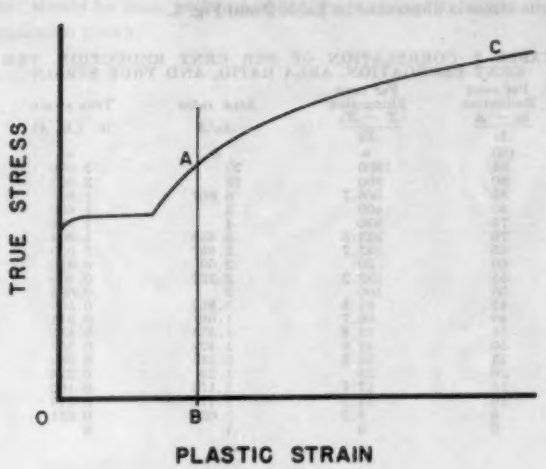

FIG. 4 A GENERAL CURVE OF TRUE STRESS AND PLASTIC STRAIN

what extent. The evaluation of the physical constants which are found applicable will also be an important contribution.

When the plastic strain increases beyond the greatest value that it has had previously, the true stress is a definite function of the plastic strain. A curve of stress and plastic strain may then be plotted as shown in Fig. 4.

When the true stress and the plastic strain have reached any point A on this curve, the material can be considered to be a new material. Point A then marks the elastic limit of this new material. If the stress drops below the value represented by A, the material is within its elastic range and obeys its original laws of elasticity with the original constants. If the stress A be again applied to the material, it again enters the plastic range. The new material will follow the stress-strain curve B-A-C where B replaces the original O.

The time rate of change is important under some instances. It introduces the idea that plastic action of metals may be considered somewhat as viscous flow of a fluid. Another fact contributing to this idea is that during a plastic action of large value "deformation theories" of plasticity give way to "flow theories." In deformation theories, displacements from points or planes are considered. However, in action there is considerable angular movement and warping of original planes so that the action must be considered from the standpoint of flow through definite points in space. Analysis of plasticity from the standpoint of viscous flow may present an invaluable aid to the understanding of the problem. Restrictions to flow and angular relationships have significance, however, not found in fluid problems.

DEFORMATION STRENGTH

Sieber has attempted to provide a method of calculating the deformation strength of a metal in terms of plastic strain. Using the expression for true deformation he may write

$$s_y = s_e + C\sqrt[n]{\ln(A_0/A)}$$

where

s_y = deformation strength, psi
s_e = elastic limit of commercially annealed material, psi
C = constant depending on material and determined experimentally
A_0 = original cross-section area, sq in.
A = final cross-section area, sq in.

Comparison of this equation with published and experimental physical data for various materials shows in Table 1 that the third root is not valid but the root varies approximately from 1.5 to 4. It is only fair to state, however, that the published data are not truly representative of the condition which Sieber (5) endeavored to define. His deformation strength is an instantaneous value existing during the actual working process. It changes somewhat during an aging period following the working. Aging is discussed later. Much more data are required to establish the values of the constant C and the necessary root, if in fact so simple a formula can be written for the full crystoplastic range.

THE PLASTIC CYCLE

In considering the structure of metals, basic theory demands that we consider a material not as a homogeneous mass, but as having properties which are the statistical average of the properties of the crystals and even more basically the atoms of which it is composed. The metallurgists have advanced well into this field and have provided much-needed scientific material on atomic and crystal structures. The whole story of plasticity is closely enfolded in slip-plane movements and the attractive forces between atoms as well as the changes in crystal structure with changes in temperature.

The changes of a metal specimen from the annealed state through work hardening and return to the original state by recrystallization at elevated temperatures have been referred to as the plastic cycle. This term does not denote a fixed amount of plasticity or of recrystallization, but merely indicates that the physical properties of a given metal may be altered in either direction by the proper use of mechanical or thermal treatment. It also connotes those thermal changes which do not alter crystal structure but allow relaxation and stress relief. The plastic cycle must be understood to plan mass-production operations adequately. In such cyclic processing, the metal is hardened by its being worked and then its plasticity is restored for further operations by the proper recrystallization or annealing. Grain-growth studies and grain-size effects, especially with respect to surface finish after forming, require study and presentation.

The effects of aging and work heat which result from crystoplastic working have not yet been investigated adequately and are an enigma to many in the field. Aging of a material which has been cold-worked allows it to build up an increased resistance to movement. For instance if one forming operation closely follows another the second will require a given load to perform. If, however, some period of time, say, more than 24 hr, is allowed to

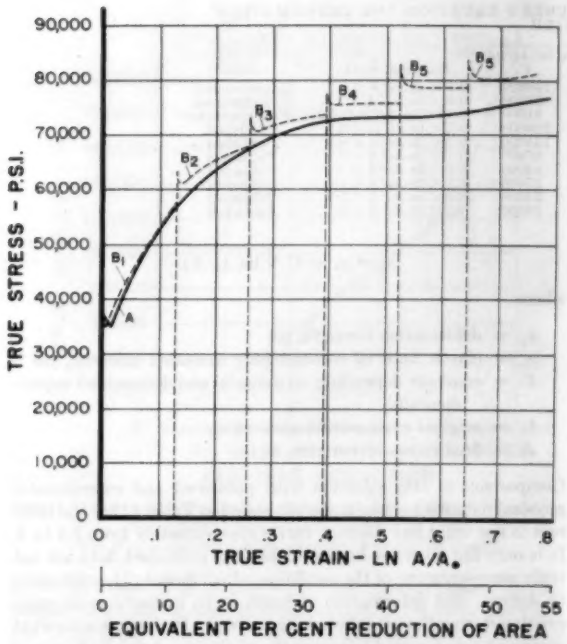

FIG. 5 COMPRESSION TESTS ON A FULLY ANNEALED C-1018 STEEL SPECIMEN TO SHOW EFFECT OF AGING

(A—Continuous compression in one stage. B_1, B_2, etc.—the same total amount of working on a similar specimen accomplished in five equal stages. Each stage performed on a successive day without annealing between stages.)

elapse between the operations the load to perform the second will be substantially increased. This phenomenon is illustrated in Fig. 5. The increase in some cases has been reported to be as high as 80 per cent of the original load. It has been pointed out that this particular effect is not due to internal heat since pieces may be allowed to cool thoroughly and still be worked at their original load if sufficient time had not elapsed to permit the aging process to occur. Work heat is an important factor in some operations. One particular job being cold-extruded came out of the dies at 500 to 700 F. Instantaneous localized temperatures in the work were evidently much higher than this. The actual effect of such work can thus far only be assumed.

MATHEMATICAL DERIVATIONS

Several investigators have offered mathematical derivations of physical phenomena assuming a perfect solid or one which deforms plastically under constant true stress. Results of these investigations must then be altered to account for work hardening. Such alteration is difficult and often questionable; consequently, the practical man regards them as irrelevant although they may present helpful information.

The term per cent reduction as a definition of extent of plastic work seems to be inadequate for some calculations and members of the trade should attempt to familiarize themselves with other designations. While it is widely used, and easily calculated itself, other expressions also are being used and should be understood. The determination of the per cent reduction for individual operations in a series is not easily calculated. We cannot speak of the per cent reduction in area in a simple compression test since the cross-section area is not reduced, but is increased. A better expression is that for true deformation

$$\bar{\epsilon} = \ln(1 + e) \text{ or } \bar{\epsilon} = \ln (A_o/A)$$

Using this expression, one notes that

$$\ln (A_o/A) = -\ln(A/A_o)$$

hence, it is evident the absolute value of the natural logarithm of the area ratio defines equally well a reduction or an increase in area. Each equal increment of true deformation represents a given amount of plastic working. Each successive increment of per cent reduction represents successively increasing amounts of plastic working. Correlation between per cent reduction and true stress is illustrated in Table 2 and Fig. 6.

TABLE 2 CORRELATION OF PER CENT REDUCTION, PER CENT ELONGATION, AREA RATIO, AND TRUE STRAIN

Per cent Reduction $\frac{A_o - A}{A_o}$	Per cent Elongation $\frac{X - X_o}{X_o}$	Area ratio A_o/A	True strain $\ln (A_o/A)$
100	∞	∞	∞
95	1900	20	2.996
90	900	10	2.303
85	566.7	6.667	1.897
80	400	5	1.609
75	300	4	1.386
70	233.3	3.333	1.204
65	185.7	2.857	1.050
60	150	2.50	0.916
55	122.2	2.222	0.800
50	100	2	0.693
45	81.8	1.818	0.598
40	66.7	1.667	0.511
35	53.8	1.538	0.431
30	42.9	1.429	0.357
25	33.3	1.333	0.289
20	25	1.25	0.223
15	17.7	1.176	0.162
10	11.1	1.111	0.115
5	5.3	1.053	0.051
0	0	1	0

CONCLUSION

The industry needs a wide range of information in order to operate on a firm scientific basis. It needs a definition of terms to

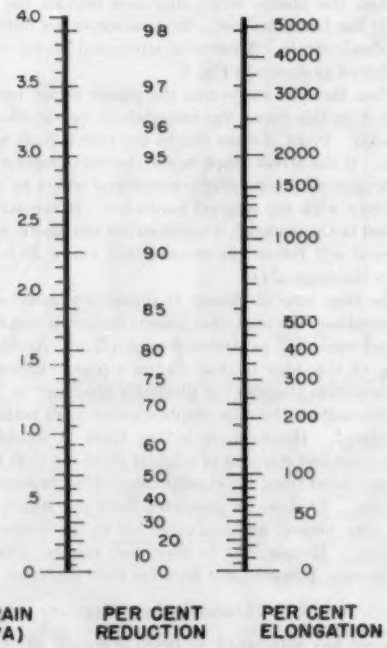

FIG. 6 CORRELATION OF TRUE STRAIN, PER CENT REDUCTION, AND PER CENT ELONGATION

aid understanding and communication of knowledge. It also needs specific true-stress physical data of the plastic-range properties of innumerable metals. These data should be made available for all work tempers furnished, for actually each is a new material. Stress-relieving, annealing, and thermal-treatment practice should be well defined and explained. The fields of external friction and lubrication under extreme pressures should be explored and pertinent data compiled. A classification of metalworking operations, e.g., rolling, extrusion, drawing, forging, punching, etc., should be made and each should be explained in a light of applicable theory.

BIBLIOGRAPHY

1 "Studies in Large Plastic Flow and Fracture," by P. W. Bridgman, McGraw-Hill Book Company, Inc., New York, N. Y., 1952.

2 "Plastic Working in Presses," by E. V. Crane, John Wiley & Sons, Inc., New York, N. Y., 1944, pp. 127–134.

3 "A New Approach to Metal-Forming Problems—Experimental Stress Analysis for a Tubular Extrusion," by E. G. Thomsen, Trans. ASME, vol. 77, 1955, pp. 515–522.

4 "The Elastoplastic Instability of a Bar Subjected to Combined Compression and Torsion" (in Russian), by L. N. Kachonov, *Dokladi Akad. Nauk*, USSR (N.S.), vol. 88, February, 1953, pp. 627–630.

5 "The Development and New Applications of Cold-Flow Pressing of Steel" (in German, translated to English for export trade), by Karl Sieber, Draht (Wire), July, 1952.

Plasticity Equations and Their Application to Working of Metals in the Work-Hardening Range[1]

By E. G. THOMSEN,[2] BERKELEY, CALIF.

A review of equations applicable to general states of stress in forming problems is presented. Theoretical solutions for the particular case of cold-extruding 2S-O aluminum in an inverted extrusion process with negligible external friction are compared with experimental results. It is shown that the solution obtained by the work-of-deformation method yields good estimates of extrusion pressures if a constant flow stress for the equivalent uniform strain in a compression test is used in the calculations, but that the solution gives an incorrect estimate of distribution of stress and metal movement. The slip-line method of solution for plane strain, on the other hand, yields good agreement for the specific case investigated for both extrusion pressure and stress distribution, if the flow stress for an equivalent uniform deformation in a compression or tension test is chosen. The solutions available using the latter method do not, however, fully account for the observed metal movement.

Nomenclature

The following nomenclature is used in the paper:

σ_i = true normal stress; subscript $i = x, y, z$ refers to planes normal to Cartesian co-ordinate directions on which stress acts, psi

τ_{ij} = shear stress; subscripts i, j refer to plane normal to direction of first subscript and in direction of second, psi

$\dot{\epsilon}_i, \dot{\gamma}_{ij}$ = plastic normal and shear strain rates; subscripts have same meaning as before

$d\epsilon_i, d\gamma_{ij}$ = infinitesimal plastic normal and infinitesimal shear strains; subscripts have same meaning as before

ϵ_i, γ_{ij} = true small plastic strains; subscripts have same meaning as before

$\dot{\lambda}$ = plasticity modulus, (psi × time)$^{-1}$

$\bar{\sigma}$ = effective stress, psi

$\dot{\bar{\epsilon}}, \bar{\epsilon}$ = effective plastic strain rate and true small effective plastic strain, respectively

p = mean pressure, psi

$\sigma_1, \sigma_2, \sigma_3$ = principal normal stress; subscripts 1, 2, and 3 refer to maximum, intermediate, and minimum values, respectively, psi

σ_0 = yield stress in tension or compression tests

W = plastic work of deformation, in-lb

L = load, lb

A_0, A = initial and instantaneous area of test bar, sq in.

D_0, D = initial and instantaneous diameter of test bar, in.

l_0, l = initial and instantaneous length of test bar, in.

p_{avg} = average extrusion pressure, psi

Introduction

The determination of the metal-forming variables, such as load, stress distribution, plastic strain and strain-rate distribution, metal flow direction, and others are of importance in practice in the design of forming equipment and in the selection of a suitable process for a given product design. While the data on forming loads are generally available from manufacturing practice for a given process and for some of the metals and alloys usually formed in practice, many of the important forming variables are not precisely known. The absence of precise knowledge of these forming variables is explained by the fact that the variables are not readily amenable to measurement whenever the forming operations involve nonuniform deformation. In such cases the initial and final dimensions of the formed part give no clue to the instantaneous configuration of the metal particles within the part and hence the instantaneous state of plastic deformation is generally unknown. Such incompletely understood production or experimental information concerning a particular forming operation, when extrapolated to a new situation, often results in expensive and time-consuming modifications of dies and equipment before a satisfactory product is obtained. However, even with the aid of simple plastic-deformation theories, in which a constant flow stress and uniform deformation are assumed, one can be led to predictions of forming loads and plastic strain or strain-rate distribution which are in error by a substantial amount. Hence the use of simple deformation theories as the basis for prediction of shape of die and capacity of forming equipment, whenever a new product and new metals or alloys are involved (like the use of extrapolated production data) can be used only as a rough first approximation. This lack of knowledge of the forming variables, furthermore, complicates the satisfactory elimination of forming defects in the finished part as, for example, tendency to cracking, poor surface finish, distortion, and others.

It is the purpose of this paper to summarize some important plasticity relationships applicable to metal-forming problems and to compare several available solutions for a given problem. The paper will deal only with the plastic-deformation aspects in the work-hardening range and it is assumed that the metal is homogeneous and isotropic. Defects and forming limits encountered in forming of metals, such as buckling, spring back or elastic recovery, necking, fracturing, and other metallurgical defects will not be treated here, but could well be the subject for discussions at a future symposium.

Stress-Strain Relationships

The stress-strain relationships applicable to metals during

[1] The investigation was supported jointly by the University of California and by The National Science Foundation under Grant G1002.

[2] Professor of Mechanical Engineering, University of California. Mem. ASME.

Contributed by the Research Committee on Metal Processing and presented at the Annual Meeting, New York, N. Y., November 28–December 3, 1954, of The American Society of Mechanical Engineers.

Note: Statements and opinions advanced in papers are to be understood as individual expressions of their authors and not those of the Society. Manuscript received at ASME Headquarters, November 3, 1954.

plastic deformation are generally believed to follow the Lévy-Mises equations. Lévy (1)[3] as early as 1871, based on Saint Venant's concept of an ideal plastic material, proposed equations in which the stresses are proportional to the rate of plastic strain or infinitesimal plastic strain. In 1913 von Mises (2) independently proposed similar equations which were interpreted to mean that plastic flow is initiated when the elastic shear distortion energy reaches a critical value. Lode (3) in 1926 confirmed, with tube experiments under biaxial stress conditions, that the Lévy-Mises equations are valid to a first approximation, but that some divergence existed. This divergence from ideality has been confirmed by Taylor and Quinney (4) and other investigators. Attempts to incorporate nonideal behavior of real metals into the plasticity equations have failed, however, to yield simple useful equations. Hence it is generally assumed that the Lévy-Mises equations hold and slight nonideal behavior of real metals and alloys is ignored.

The Lévy-Mises equations relating the six plastic strain-rate components at a point in the plastic metal in Cartesian co-ordinates, i.e., the normal $\dot{\epsilon}_x$, $\dot{\epsilon}_y$, $\dot{\epsilon}_z$ and the shear $\dot{\gamma}_{xy}$, $\dot{\gamma}_{yz}$, $\dot{\gamma}_{zx}$ to the stress components are given by

$$\left.\begin{aligned} \dot{\epsilon}_x &= \dot{\lambda}(\sigma_x + p), \quad \dot{\gamma}_{xy} = 2\dot{\lambda}\tau_{xy} \\ \dot{\epsilon}_y &= \dot{\lambda}(\sigma_y + p), \quad \dot{\gamma}_{yz} = 2\dot{\lambda}\tau_{yz} \\ \dot{\epsilon}_z &= \dot{\lambda}(\sigma_z + p), \quad \dot{\gamma}_{zx} = 2\dot{\lambda}\tau_{zx} \end{aligned}\right\} \quad \ldots\ldots\ldots [1]$$

where σ_x, σ_y, σ_z, and τ_{xy}, τ_{yz}, τ_{zx} are the true normal and shear-stress components, respectively

$$p = -1/3(\sigma_x + \sigma_y + \sigma_z)$$

is the mean pressure, and $\dot{\lambda}$ is a proportionality factor. These equations completely describe the state of stress and plastic-strain rate at a point within a plastic metal provided the elastic strains are small in comparison to the plastic strains and may, therefore, be neglected. While Equations [1] have the same form as those applicable to a viscous Newtonian fluid when $\dot{\lambda}$ is replaced by 2μ(μ = the viscosity of the fluid), they are different since $\dot{\lambda}$ is not a material constant but a scalar quantity given by

$$\dot{\lambda} = \frac{3}{2}\,\frac{\dot{\bar{\epsilon}}}{\bar{\sigma}} \quad \ldots\ldots\ldots [2]$$

also called the plasticity modulus, where

$$\dot{\bar{\epsilon}} = \frac{2}{3}\sqrt{\left\{\frac{1}{2}\,[(\dot{\epsilon}_x - \dot{\epsilon}_y)^2 + (\dot{\epsilon}_y - \dot{\epsilon}_z)^2 + (\dot{\epsilon}_z - \dot{\epsilon}_x)^2] + \frac{3}{4}\,[\dot{\gamma}_{xy}^2 + \dot{\gamma}_{yz}^2 + \dot{\gamma}_{zx}^2]\right\}} \quad \ldots\ldots [3]$$

and

$$\bar{\sigma} = \sqrt{\left\{\frac{1}{2}\,[(\sigma_x - \sigma_y)^2 + (\sigma_y - \sigma_z)^2 + (\sigma_z - \sigma_x)^2] + 3[\tau_{xy}^2 + \tau_{yz}^2 + \tau_{zx}^2]\right\}} \quad \ldots\ldots [4]$$

The complex quantities $\dot{\bar{\epsilon}}$ and $\bar{\sigma}$ are usually called effective strain rate and effective stress, respectively, and are proportional to Nadai's octahedral strain rate and stress, respectively. It is evident that $\dot{\bar{\epsilon}}$ and $\bar{\sigma}$ are variables; hence their ratio or $\dot{\lambda}$ is also a variable. $\bar{\sigma}$ and $\dot{\bar{\epsilon}}$, always taken as positive, are invariants of stress and strain-rate tensors, respectively, and hence are unvarying with respect to rotation of co-ordinate axes; their product is equal to the rate at which plastic work is being done, namely

$$\dot{W} = \bar{\sigma}\dot{\bar{\epsilon}} \quad \ldots\ldots\ldots [5]$$

When $\bar{\sigma}$ reaches a critical value, plastic deformation is initiated and it can be shown that this corresponds to a critical value in the elastic distortion energy. Hence $\dot{W}$ and $\dot{\bar{\epsilon}}$ are zero as long as $\bar{\sigma}$ is less than this critical value and the metal remains in a state of elastic deformation. The critical value for initiation of plastic deformation is known as the yield condition. If the co-ordinate axes correspond to principal directions, then the shear stresses are zero and $\bar{\sigma}$ in terms of the three principal stresses σ_1, σ_2, and σ_3 is given by

$$\bar{\sigma} = \sqrt{\frac{1}{2}\,[(\sigma_1 - \sigma_2)^2 + (\sigma_2 - \sigma_3)^2 + (\sigma_3 - \sigma_1)^2]} \quad \ldots [6]$$

Furthermore, if two of these principal stresses are zero, as, for example, in a compression or tension test, then $\bar{\sigma}$ reduces to

$$\bar{\sigma} = \sigma_1 = \sigma_0, \qquad \sigma_2 = \sigma_3 = 0 \quad \ldots\ldots\ldots [7]$$

where σ_1 is now the axial stress and σ_0 is the yield stress in tension or compression. Thus the effective stress $\bar{\sigma}$ gives the condition for yielding under conditions of general stressing as does σ_0 for simple stressing, providing the material is in the same initial state and the test conditions are comparable. Under these conditions the magnitude of $\bar{\sigma}$ is equal to the yield stress σ_0. It is of interest to note that Novozhilov (5)[4] has analyzed the state of stress at a point and in his derivation shows that $\bar{\sigma}$ is proportional to the root-mean-square shear stress at a point. Hence the effective stress $\bar{\sigma}$ takes on a relatively simple physical meaning. Similarly, it is possible to visualize that the effective strain rate can be interpreted to have a similar meaning since it is also composed of squares of plastic shear-strain rates under the square-root sign as may be seen by inspection of Equation [3].

Since Equation [4] shows $\bar{\sigma}$ to be that of a cylinder, which is inclined in space at equal angles to the three principal stress directions, a geometrical interpretation is also available. If the state of stress is such that a co-ordinate point lies within the cylinder, only elastic deformation occurs. A state of stress represented by a point on the axis of this cylinder is such a case and is one of equal triaxial tension or compression, depending on whether the stresses are positive or negative. It is an accepted fact that under these conditions no plastic flow occurs. This conclusion can be substantiated by examining the plasticity Equations [1] because if $\sigma_x = \sigma_y = \sigma_z$ are principal stresses, they are equal to $-p$ and the plastic strain rates consequently are zero. For plastic deformation to begin, the state of stress must lie on the surface of this cylinder; hence the surface of the cylinder is known as the yield surface. As deformation continues, however, $\bar{\sigma}$ increases in magnitude and it is required, therefore, that the diameter of the cylinder also increase. Hence the state of work hardening can be represented by the instantaneous diameter of the yield cylinder. As deformation continues, the expanding surface of the yield cylinder will finally be intercepted by a fracture surface and rupture takes place. Thus the useful deformations in forming processes must lie between the initial yield cylinder and that at which rupture takes place, and all intermediate cylinders between these two conditions can be thought of as instantaneous yield cylinders at any particular state of work hardening.

The work-hardening characteristics of a metal when deformed below the recrystallization temperature can be determined from a tension or compression test, provided strain-rate effects are absent. Hence, if L is the applied load and A is the instantaneous cross-sectional area of the specimen, $\bar{\sigma}$ is given by

$$\bar{\sigma} = \sigma_1 = L/A \quad \ldots\ldots\ldots [8]$$

[3] Numbers in parentheses refer to the Bibliography at the end of the paper.

[4] The author is indebted to Prof. G. A. Zisicas and Prof. Boris Bresler for bringing his hitherto untranslated material to his attention.

because only one principal stress is active. The plastic true strain $\bar{\epsilon}_n$, also sometimes called the natural or logarithmic plastic strain, is obtained by integration

$$\bar{\epsilon}_n = \ln(1 + \epsilon_1) = \int_{l_0}^{l} \frac{dl}{l} = \ln \frac{l}{l_0} \quad \ldots\ldots [9]$$

where l and l_0 are the instantaneous and original lengths between gage points during that portion of the test where uniform deformation prevails.[5] It should be noted that integration is difficult to perform if the deformation is not uniform. The validity of Equation [9] may be checked by substituting the constant volume or continuity relationship into Equation [3], namely

$$\left.\begin{aligned} &(a)\quad \dot{\epsilon}_x + \dot{\epsilon}_y + \dot{\epsilon}_z = \dot{\epsilon}_1 + \dot{\epsilon}_2 + \dot{\epsilon}_3 = 0 \\ &(b)\quad d\epsilon_x + d\epsilon_y + d\epsilon_z = d\epsilon_1 + d\epsilon_2 + d\epsilon_3 = 0 \\ &(c)\quad \epsilon_x + \epsilon_y + \epsilon_z = \epsilon_1 + \epsilon_2 + \epsilon_3 = 0 \end{aligned}\right\} \ldots [10]$$

where terms in (c) of Equations [10] are small plastic true strains. Equations [10] are believed to hold within a fraction of 1 per cent.

If the test is a tension test, the specimen will neck after the maximum load has been exceeded and the effective plastic strain $\bar{\epsilon}$ can be calculated from the original diameter D_0 of the test bar and the instantaneous diameter D in the neck by use of the constant-volume relationship

$$\frac{l_0 \pi D_0^2}{4} = \frac{l \pi D^2}{4} = \text{const}$$

or

$$l/l_0 = \left(\frac{D_0}{D}\right)^2$$

from which

$$\bar{\epsilon} = \ln \frac{l}{l_0} = 2 \ln \frac{D_0}{D} \quad \ldots\ldots [11]$$

Thus a tension test permits the evaluation of a $\bar{\sigma} - \bar{\epsilon}$ curve, which is usually called the true-stress true-strain curve. If it is required to refine the data to take into account the nonuniform stress distribution in the necked portion of the specimen, Bridgman's correction (6) may be applied. A simplified method of applying the Bridgman correction was recently given by Marshall and Shaw (7). It is understood, of course, that a compression test can be substituted for the tension test for the evaluation of the true-stress true-strain curve, provided the ends of the specimens are well lubricated to prevent barreling.

While Equations [1] together with the yield condition fully describe the state of stress and strain at a point, they give no information about the condition under which they are satisfied. This additional condition is that of equilibrium which must be satisfied at every point within the plastically moving metal. It is generally assumed that dynamic effects are small; this is true for most commercial forming operations (with the exception of those performed at high speed as, for example, impact extrusions) so that only statical equilibrium need be investigated. The equations describing statical equilibrium in Cartesian co-ordinates are given by

$$\left.\begin{aligned} \frac{\partial \sigma_x}{\partial x} + \frac{\partial \tau_{yx}}{\partial y} + \frac{\partial \tau_{zx}}{\partial z} = 0 \\ \frac{\partial \sigma_y}{\partial y} + \frac{\partial \tau_{zy}}{\partial z} + \frac{\partial \tau_{xy}}{\partial x} = 0 \\ \frac{\partial \sigma_z}{\partial z} + \frac{\partial \tau_{xz}}{\partial x} + \frac{\partial \tau_{yz}}{\partial y} = 0 \end{aligned}\right\} \ldots\ldots [12]$$

Examination of Equations [12] reveals that a solution for the general case, as represented by these equations, is difficult and that the success of an analysis depends on suitable simplification of these equations.

Solutions of Forming Problems

The solutions of forming problems are generally complicated by the fact that the deformation within the metal is difficult to determine accurately. The initial and final dimensions of a part, unless the deformation is uniform, will not give any clue to the actual state of deformation and work hardening. However, even in uniform deformation processes, the final state of work hardening cannot be determined unless the strain path is also known, which is to say that the state of work hardening is dependent on the strain path. A simple example will clarify this point. Assume that it were possible to deform a bar alternately by tension and compression so that the final dimensions of the bar were those of the original bar. In this case the net dimensional change is zero and the plastic strain calculated from the initial and final dimensions is zero. The metal, however, is not in a state of zero strain since it has been work-hardened during the stress cycling and hence it is necessary to sum up the strain between each known uniform deformation cycle in order to obtain the total strain imparted to the metal. Other examples in which the dimensions do not change and yet work hardening has been imparted are the reversal of bending or reversal of twisting of a rod or wire. In each case the final dimensions may be equal to the original dimensions of the rod or wire, but the state of work hardening or total strain is far from zero and may indeed reach a value so high as to cause rupture when small additional deformations are imparted.

It is evident from the foregoing that the strain path must be known in order to solve forming problems. Several techniques are used to obtain approximate solutions which will be applied to an extrusion problem. The extrusion problem was selected merely because a number of solutions are available and hence comparison of results between the several techniques is possible.

The extrusion is that of pressing a 4.3-in-diam-28-O aluminum billet into a 1.5-in-diam solid bar in an inverted extrusion process with substantially zero wall friction, the results of which have been recently reported (8). Three methods of analysis are presented and solutions are compared.

Work-of-Deformation Method (9, 10). The infinitesimal work-of-deformation per unit volume in a forming process, such as in an extrusion, is given by Equation [5] since during an increment of time dt

$$\left.\begin{aligned} dW &= \dot{W} dt \\ \text{and} \qquad dW &= \bar{\sigma} d\bar{\epsilon} dv \end{aligned}\right\} \ldots\ldots [13]$$

for each infinitesimal element of volume dv of the billet extruded. The total work in extruding a volume v then may be obtained by integration of Equation [13]

$$W = \int_0^v \int_0^{\bar{\epsilon}} \bar{\sigma} dv d\bar{\epsilon} \quad \ldots\ldots [14]$$

where $\bar{\sigma}$ is the effective flow stress and $d\bar{\epsilon}$ the infinitesimal effec-

[5] The maximum principal strain ϵ_1 is a conventional strain based on integral $\epsilon_1 = \int_{l_0}^{l} \frac{dl}{l_0}$ and hence is distinctly different from $(\epsilon_1)_n = \int_{l_0}^{l} \frac{dl}{l}$, when the strain becomes large. In subsequent sections all large strains are shown without subscript n but it is tacitly assumed that these strains are logarithmic strains.

tive strain. For the case of a billet of cross section A_0 and length l_0 extruded into a bar of cross section A_1 and length l_1, the total flow work during a steady-state extrusion is also given in terms of an average extrusion pressure p_{avg}, by

$$W = p_{avg} v = p_{avg} A_0 l_0 \quad [15]$$

which may be equated to the integral of Equation [14] since the external work done must equal the internal work, assuming no losses

$$W = p_{avg} A_0 l_0 = \int_0^v \int_0^{\bar{\epsilon}} \bar{\sigma} dv d\bar{\epsilon} \quad [16]$$

and the average extrusion pressure becomes

$$p_{avg} = \frac{1}{A_0 l_0} \int_0^v \int_0^{\bar{\epsilon}} \bar{\sigma} dv d\bar{\epsilon} \quad [17]$$

Equation [17] requires evaluation of the flow work for each elemental volume which may be assumed to have the form of an annulus in the billet and which transforms into another annulus having a reduced diameter and an increased length in the bar, by following its flow path. This can only be accomplished as will be shown later, if the complete strain paths of all elemental volumes are known. It is understood also that under steady-state conditions the billet is longer than the extruded length l_0 so that new undeformed metal continuously enters the region in which plastic deformation occurs as the deformed metal leaves the die opening, thus a constant extrusion pressure p_{avg} prevails. Since detailed information of the flow pattern is not readily available, an assumed simplification of the deformation mechanism is required to permit an analytical solution of Equation [17]. Such simplification may be obtained by assuming that no shear stresses exist, and that all elemental annuli continuously elongate without reversal of straining. Since it is known, however, that shear stresses exist and that reversal in straining occurs along the cylinder wall and near the die plate, the calculated pressure will be lower than the actual pressure and may be regarded as the minimum pressure for equivalent uniform deformation. Under these assumed conditions the following simplifications may be made:

The first integral of Equation [17] reduces to

$$\frac{1}{A_0 l_0} \int_0^{A_0 l_0} dv = 1 \quad [18]$$

and Equation [17] becomes

$$p_{avg} = \int_0^{\bar{\epsilon}} \bar{\sigma} d\bar{\epsilon} \quad [19]$$

The assumption that shearing stresses and strains are zero and that the maximum principal strain is in the x or axial direction of the extrusion gives the relation hips

$$\frac{1}{2} d\epsilon_x = -d\epsilon_y = -d\epsilon_z \quad [20]$$

for the axial symmetrical case, which satisfies the constant volume Equation [10]. Substituting these terms for the strain rates in Equation [3] results in

$$d\bar{\epsilon} = d\epsilon_z \quad [21]$$

hence the effective strain and the axial strain are identical. The integral of Equation [19] therefore is merely the equivalent plastic flow work in a compression or tension test for the same extent of deformation.

An examination of the equilibrium Equations [12] reveals that since all shear stresses are zero, the rate of change of the normal stresses in their respective co-ordinate directions are zero and hence the normal stresses σ_x, σ_y, σ_z must not vary with respect to these directions. This condition can only be visualized as existing when the billet is extruded uniformly over its whole length l_0 into a bar of length l_1 and not in successive stages of extension of each element into corresponding elements of the bar, as it actually occurs. Nevertheless it will be assumed that equilibrium exists and that the equilibrium equations are satisfied in this case.

In order to integrate Equation [19] it is necessary to introduce the functional relationship between $\bar{\sigma}$ and $\bar{\epsilon}$. For 2S-O aluminum it has been found that the approximate equation (11)

$$\bar{\sigma} = S_e + C(\bar{\epsilon})^{1/n} \quad [22]$$

reproduces the work-hardening characteristics of this metal, where $S_e = 4000$, $C = 14{,}000$, and $n = 2.83$. Substituting Equation [22] into Equation [19] and integrating, yields

$$p_{avg} = \int_0^{\bar{\epsilon}} (S_e + C\bar{\epsilon}^{1/n}) d\bar{\epsilon} = S_e \bar{\epsilon} + \frac{cn(\bar{\epsilon})^{\frac{1+n}{n}}}{1+n} \quad [23]$$

If $\bar{\epsilon}$ is now calculated in the same manner as that for a tension test, then

$$\bar{\epsilon} = \ln \frac{l_1}{l_0} = 2 \ln \frac{D_0}{D_1} \quad [24]$$

where $D_0 = 4.3$ in. and $D_1 = 1.5$ in., are the billet and bar diameters, respectively, and $\bar{\epsilon}$ becomes

$$\bar{\epsilon} = 2 \ln \frac{4.3}{1.5} = 2.1 \quad [25]$$

Substituting $\bar{\epsilon} = 2.1$ into Equation [23] yields

$$p_{avg} = 37{,}000 \text{ psi} \quad [26]$$

This value is appreciably below the actual load of 89,500 psi observed in the experiment. It was found, however, that the effective stress-effective strain curve determined for the actual material extruded as shown in Fig. 1, was given closely by

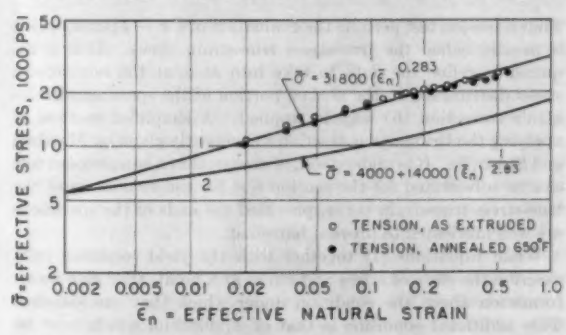

FIG. 1 EFFECTIVE STRESS-EFFECTIVE NATURAL STRAIN CURVES FOR 2S-O ALUMINUM (1100-0)

(Solid curve 1 shows results obtained from compression tests given in reference 8, upon which tensile data for the same material machined from the original 6-in-diam extrusions are superimposed.)

$$\bar{\sigma} = 31{,}800(\bar{\epsilon})^{0.283} \quad [27]$$

Hence, using $\bar{\sigma}$ of Equation [27] in Equation [19] results in

$$p_{avg} = \frac{31{,}800(2.1)^{1.283}}{1.283} = 64{,}000 \text{ psi} \quad [28]$$

It should be noted that the estimated pressure $p_{avg} = 64{,}000$ psi

is still appreciably below the observed pressure of 89,500 psi in spite of the fact that external friction was essentially absent in the experiment. It must be concluded therefore that the assumption of uniform deformation gives only a rough first approximation of the deformation mechanism actually occurring.

A close estimate of the actual extrusion pressure observed can be obtained by assuming a constant effective stress $\bar{\sigma} = 39{,}300$ psi which corresponds to the total strain $\bar{\epsilon} = 2.1$ in a property test

$$p_{avg} = \bar{\sigma} \int_0^{\bar{\epsilon}} d\bar{\epsilon} = 39{,}300 \times 2.1 = 82{,}500 \text{ psi} \quad \ldots [29]$$

This estimated pressure is close to the observed pressure of 89,500 psi.

Hencky's Plastic-Sector Method (12). The Hencky plastic-sector method of solving plasticity problems has been reported extensively by various investigators (13, 14, 15) and solutions for some forming problems, such as extrusions, made available. In most cases, however, these solutions are not in a form to be of direct practical utility to the design or production engineer because the solutions are given in terms of the so-called slip lines. Furthermore, no experimental method had been advanced previously to check the validity of the solutions, which in part accounts for the fact that they are not widely used in practice. The Hencky method, however, presents a powerful tool, because it is a purely analytical approach and hence requires only knowledge of the flow properties of the metal for a solution of forming problems. The solutions, however, are restricted to plane problems, since three-dimensional problems (for example, an axial symmetrical case as suggested by Hencky, reference 12) require the assumption of an unrealistic yield condition. The assumption of plane strain, however, does not necessarily involve large errors. The equations derived for statical equilibrium are

$$\left.\begin{aligned} p + 2k\phi &= \text{const along } \alpha \text{ slip line} \\ p - 2k\phi &= \text{const along } \beta \text{ slip line} \end{aligned}\right\} \quad \ldots [30]$$

where $k = \bar{\sigma}/\sqrt{3}$, p is the two-dimensional mean pressure $-\frac{1}{2}(\sigma_x + \sigma_y) = -\sigma_a$, and ϕ is the angle between the x-axis (or extrusion axis) and an α-slip line. These relationships can be proved by Mohr's stress-circle diagram, from which one can also get the expression for the axial stress, namely

$$\sigma_x = -p - k \sin 2\phi \quad \ldots [31]$$

The α and β slip lines are orthogonal lines of maximum shear. Similar equations referred to the α and β slip lines can also be derived in terms of particle velocities and must simultaneously be satisfied within the plastic metal together with the stress Equations [30]. Approximate solutions are obtained by assuming k to be a constant and by transforming Equations [30] to finite-difference equations. The resulting information is a plot of the α and β slip lines, from which the plastic zone can be obtained and the strain rates and stresses can be calculated. A complete description of the method is beyond the scope of this paper and reference should be made to the Bibliography appended.

Visioplasticity. The third method of solutions has been called "visioplasticity" and is an experimental method. It has been applied to extrusion problems of lead (16, 17) and more recently to the extrusion of 2S-O aluminum (8). It requires for the determination of strains and stresses a lengthy experimental procedure of obtaining particle velocities from incremental deformation steps made visible on split billets through displacements of grid-line intersections. The method employed has been fully described in the references cited. The natural effective strain distribution, in the die opening, as obtained from a graphical integration of the experimentally determined strain rates along the actual metal flow paths for the 2S-O aluminum, is shown in Fig. 2. The corresponding effective stress as calculated by use of Equation [27] is also shown in the same figure. These data permit solution of Equation [17] for each elemental volume by utilizing the following transformation

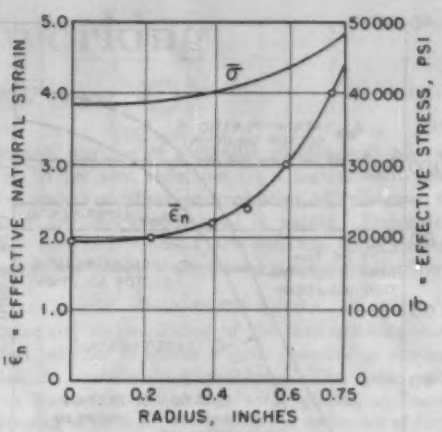

FIG. 2 EFFECTIVE STRESS AND EXPERIMENTAL EFFECTIVE NATURAL STRAIN DISTRIBUTION IN THE ORIFICE OF A 4.3-IN-DIAM SOLID CYLINDRICAL BILLET OF 2S-O ALUMINUM EXTRUDED INTO A 1.5-IN-DIAM BAR

(Effective stress was calculated by use of Equation [27].)

$$p_{avg} = \frac{1}{A_0 l_0} \int_0^{v} \int_0^{\bar{\epsilon}_n} \bar{\sigma} dv d\bar{\epsilon}_n = \frac{1}{A_1 l_1} \int_0^{A_1 l_1} \int_0^{\bar{\epsilon}_n} \bar{\sigma} l_1 dA_1 d\bar{\epsilon}_n$$

$$= \frac{1}{A_1} \sum_0^{A_1} \left[\int_0^{\bar{\epsilon}_n} \bar{\sigma} d\bar{\epsilon}_n \right] \Delta A_1 = \frac{1}{A_1} \sum_0^{A_1} \left[\frac{31{,}800}{1.283} (\bar{\epsilon}_n)^{1.283} \right] \Delta A_1 \quad \ldots [32]$$

where subscripts 0 and 1 indicate billet and extruded bar locations, respectively. Substituting the $\bar{\epsilon}_n$ values from Fig. 2 and carrying out the operation indicated by Equation [32], an average pressure $p_{avg} = 95{,}000$ psi results. This pressure is in excellent agreement with the average pressure of 89,500 psi measured in the experiment.

COMPARISON OF SOLUTIONS

The solutions for the 2S-O aluminum extrusion are given in Fig. 3. Both the measured average extrusion pressures (p_{avg}) and the calculated axial compressive stresses ($-\sigma_x$) have been plotted. The axial compressive stress distribution is given for a section in the billet approximately 0.8 in. upstream from the die or orifice.

The work-of-deformation method of solution for uniform deformation is given by curve 1 for both axial stress and extrusion pressure, when using a constant flow stress $\bar{\sigma} = 39{,}300$ psi. Comparing this result with the experimental extrusion pressure, as given by curve 3, it is seen that good agreement exists.

Hence, using the flow stress $\bar{\sigma}$ for the same uniform deformation as obtained in a compression test permits a close estimate of the extrusion pressure. It should be noted, however, that this solution gives no information about the actual distribution of axial stresses nor does it give any information about actual metal movement.

The Hencky plastic sector solution is given by curves 4 and 5. The flow stress again was assumed to be constant and in magnitude equal to 39,300 psi, the same as that used for the work-of-deformation solution. It is seen that the extrusion pressure is

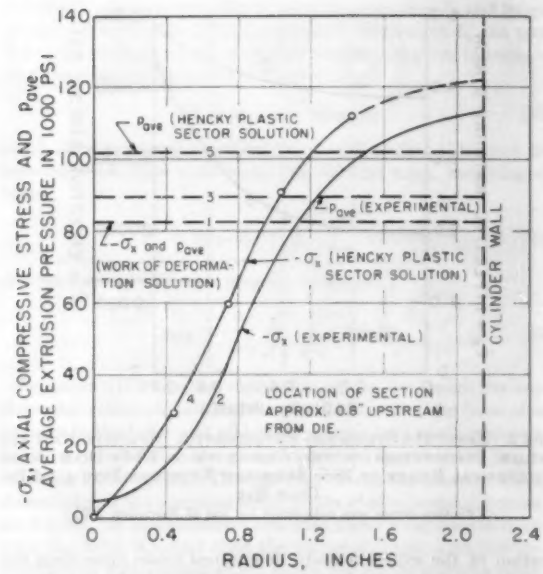

FIG. 3 COMPARISON OF SOLUTIONS FOR A 4.3-IN-DIAM SOLID CYLINDRICAL BILLET OF 2S-O ALUMINUM EXTRUDED INTO A 1.5-IN-DIAM SOLID CYLINDRICAL BAR AT ROOM TEMPERATURE WITH NEGLIGIBLE CYLINDER WALL AND DIE FRICTION

slightly higher than was observed in the experiment, but that the shape of the axial-stress curve is nearly identical with curve 2 which was obtained by using the visioplasticity method.

A comparison of average steady-state extrusion pressures as obtained by various methods is given in Table 1.

TABLE 1 COMPARISON OF SOLUTIONS

(Extrusion of 2S-O aluminum for 4.3-in-diam billet into 1.5-in-diam solid bar; frictionless and inverted process)

(*a*) Experimental	P_{avg} =	89500 psi
(*b*) Work of deformation (experimental strains)	P_{avg} =	95000 psi
(*c*) Work of deformation (uniform strain)	P_{avg} =	64000 psi
(*d*) Work of deformation (uniform strain, but effective stress = constant at equivalent uniform strain)	P_{avg} =	82500 psi
(*e*) Hencky's slip-line method (effective stress = constant at equivalent uniform strain)	P_{avg} =	102000 psi

CONCLUSIONS

Plasticity equations applicable to forming operations of metals in the work-hardening range were examined and three solutions for extruding 2S-O aluminum in a frictionless apparatus at room temperature were compared, from which the following conclusions may be drawn:

1 The visioplasticity method of solution gives a detailed picture of the nonuniform stress and strain distribution within the billet for a work-hardening metal. It requires for its solution the experimentally determined particle-velocity distribution during steady-state motion. It provides a workable means for comparison of analytical solutions.

2 The Hencky plastic sector or slip-line method of solution gives an axial stress distribution in the billet at a distance approximately 0.8 in. upstream from the die, which closely agrees with the distribution calculated by the visioplasticity method, if a constant flow stress for an equivalent uniform natural strain as determined from a compression test is substituted. It also gives a close estimate of the mean extrusion pressures. Present solutions, however, do not provide an accurate method for determining metal movement.

3 The work-of-deformation method of solution provides an incorrect estimate of the stress and strain distribution, since nonexisting uniform deformation is assumed in the calculations. It provides a close estimate of the mean extrusion pressure, however, if a constant flow stress for an equivalent uniform natural strain, as determined from a compression test, is used in the calculations.

BIBLIOGRAPHY

1 "Mémoires Présentés, Hydro-Dynamique—Mémoire sur les équations générales des mouvements intérieurs des corps solides ductiles au delà des limites où l'élasticité pourrait les ramener à leur premier état," by M. M. Lévy, Comptes Rendus, Académie des Sciences, Paris, France, vol. 70, 1870, pp. 1323–1325.

2 "Mechanik der festen Körper im plastisch-deformablen Zustand," by R. von Mises, Göttinger Nachrichten, *Mathematik und Physik*, vol. K1, 1913, pp. 582–592.

3 "Der Einfluss der mittleren Hauptspannung auf das Fliessen der Metalle—Forschungsarbeiten auf dem Gebiete des Ingenieurwesens," by W. Lode, *Verein deutscher Ingenieure*, Heft 303, 1928.

4 "The Plastic Distortion of Metals," by G. I. Taylor and H. Quinney, Philosophical Trans. of the Royal Society of London, series A, vol. 230, 1931, pp. 323–362.

5 "The Physical Meaning of the Stress Invariants of the Theory of Plasticity," by V. V. Novozhilov, *Applied Mathematics and Mechanics*, Acad. of Sciences of USSR Publication, vol. 16, 1952, pp. 617–619.

6 "The Stress Distribution at the Neck of a Tension Specimen," by P. W. Bridgman, Trans. ASM, vol. 32, 1944, pp. 553–574.

7 "The Determination of Flow Stress From a Tensile Specimen," by E. R. Marshall and M. C. Shaw, Trans. ASM, vol. 44, 1952, pp. 705–725.

8 "Stresses and Strains in Cold-Extruding 2S-O Aluminum," by E. G. Thomsen and J. Frisch, Trans. ASME, vol. 77, 1955, pp. 1343–1353.

9 "The Plastic Forming of Metals," by E. Siebel (translated by J. H. Hitchcock), *Steel*, November 13, 1933, and February 5, 1934.

10 "Practical Metallurgy," by G. Sachs and K. R. Van Horn, American Society for Metals, Cleveland, Ohio, 1946, pp. 301–314, and 375.

11 "Plastic Working of Metals," by W. S. Wagner, published in this issue pp. 401–406.

12 "Über einige statische bestimmte Fälle des Gleichgewichts in plastischen Körpern," by H. Hencky, *Zeitschrift für angewandte Mathematik und Mechanik*, vol. 3, 1923, pp. 241–251.

13 "A Theoretical Analysis of the Stresses and Strains in Extrusion and Piercing," by R. Hill, *Journal of the Iron and Steel Institute*, vol. 158, 1948, pp. 177–158.

14 "Theory of Perfectly Plastic Solids," by W. Prager and P. G. Hodge, John Wiley & Sons, Inc., New York, N. Y., 1951, pp. 175–193.

15 "The Mathematical Theory of Plasticity," by R. Hill, Clarendon Press, Oxford, England, 1950, pp. 181–186.

16 "An Experimental Investigation of the Mechanics of Plastic Deformation of Metals," by E. G. Thomsen, C. T. Yang, and J. B. Bierbower, University of California Publications in Engineering, vol. 5, no. 4, 1954, pp. 89–144.

17 "A New Approach to Metal-Forming Problems—Experimental Stress Analysis for a Tubular Extrusion," by E. G. Thomsen, Trans. ASME, vol. 77, 1955, pp. 515–522.

Plastic Metalworking

By E. V. CRANE,[1] CANTON, OHIO

Our prosaic objective is to stimulate analytical thinking, co-ordinate it with practice, and present it in usable form for the man in the field. Our assignment is in the art and science of forcing metals to flow into new shape, as distinguished from the whittling processes of metal cutting. More economical automobiles, better cooking utensils and refrigerators, faster planes, and even space ships are our field problems. We get exciting glimpses of new possibilities in the flowing of heat-treated steels at 150 tons per square inch and more. To obtain scientific basis for the advancement of the growing art, we must pursue the relationships of plastic flow, strain hardening, aging, residual stresses, and endurance characteristics back to the space-force relationships of the atom and the molecule. We face the sobering responsibility that our enthusiastic flights into higher mathematics, Greek letters, and coined terminologies must be brought back to a generally understandable and usable level.

Promise

THE work hardening or strain hardening of the common plastic metals seemed first a fault and then a virtue. The early hardware specialists of New England learned the economic advantages of using quarter-hard to hard tempers of "cold-rolled" steel. Modern industry makes some use of these assets but is restrained by confusion and misconception. Now we may progress from the pure metals to many alloys and may add work hardening in press operations to work hardening in rolled product. We may if we have adequate physical properties data and sufficiently simplified means of computing and controlling the cumulative work-hardening effects.

Dispersion hardening of alloyed metals by heat-treatment has been considered in a realm apart from the plastic working processes. But, that is no longer so. Practice and theory both show us now that we may pile the advantages of the one upon the gains of the other.

Aluminum alloys are now widely heat-treated; then aging is retarded by deep freezing, long enough to stretch form to shape. The old problems of distortion in heat-treatment after forming are eliminated. The work hardening must necessarily be additive. Engineers generally and even metallurgists do not yet have an adequate picture of the mechanisms of dispersion hardening, work hardening, and aging to take proper advantage of these possibilities.

Steel, like aluminum, is subject to similar phenomena. Its aging is not well understood, though quite apparent in many metalworking operations. Its heat-treated alloys may be worked plastically by large amounts. P. W. Bridgman[2] records experimental working of austenitic chrome-moly alloys by as much as 94 per cent reduction (in a high-pressure chamber). Industry reports of 60 per cent reduction of well-drawn martensitic steels are also experimental in nature. Problems of die materials and reinforcement are still the major restraint to application, but there is a stimulating promise for the future.

Back to the Atom

An adequate understanding of the distinguishing characteristics and behavior of atoms is quite essential to any scientific approach to metalworking problems. The space and force relations between atoms change with working and annealing. The grouping of different atoms into the molecules of the alloys, and their regrouping in heat-treatment and aging should be presented in reasonably simple form to help us understand the eccentricities of our processes.

The ASME Research Subcommittee on the Plastic Working of Metals went to an outstanding university research group and to the research laboratory of a leading metal-producing company in its efforts to obtain a paper on this subject. Much specialized research is available, but to obtain an over-all picture slanted to the viewpoint of plastic metalworking is not easy. We will keep at it, however; and with more time and collaboration, we should obtain it.

Plastic Flow

Long experience in the (old) art makes it possible to sense, after a fashion, where and how metal will flow. Our young science is helping to make the predictions more reliable. Even in tensile and compressive tests, flow and resultant work hardening are not uniformly distributed as Bridgman[2] has shown.

Figs. 1 to 6 will serve to illustrate some of the plastic-working problems. These are unrelated exhibits to illustrate a sequence in the compressive flowing of a cylindrical billet to a flattened disk or to a cold extruded cup.

Fig. 1 Homogeneous Cylindrical Test Slug

(Ends tend to grip pressing plates, restraining flow by surface friction, perhaps interatomic attraction. Slip-plane movement in many little crystals takes place at 45 deg to axis of load leaving material within conical areas undisturbed.)

The starting shape, Fig. 1, has been shaded to help visualize two conical shapes within which the metal seems to remain undisturbed until compression has progressed very far. It is argued that surface friction on the ends may amount to something of an interatomic attraction between the billet metal and the die steels. Effective lubricating separation is extremely difficult to maintain.

---

[1] Chief Development Engineer, E. W. Bliss Company. Mem. ASME.

[2] "Large Plastic Flow and Fracture," by P. W. Bridgman, McGraw-Hill Book Company, Inc., New York, N. Y., 1952.

Contributed by the Research Committee on Metal Processing and presented at a panel discussion of the Metal Processing Division at the Annual Meeting, New York, N. Y., November 28–December 3, 1954, of The American Society of Mechanical Engineers.

Note: Statements and opinions advanced in papers are to be understood as individual expressions of their authors and not those of the Society. Manuscript received at ASME Headquarters, November 3, 1954.

The slope of the conical walls appears to be the 45-deg angle at which slip is found to occur most easily in the atom-pattern relationship of steel. This is shown in Fig. 2. A cold-squeezed cylinder was cut vertically and etched. The acid attacks more deeply the area where the greatest metal movement has taken place. The most severe movement was a sliding along the surfaces of the locked-up cones and a squeezing between the points of the cones.

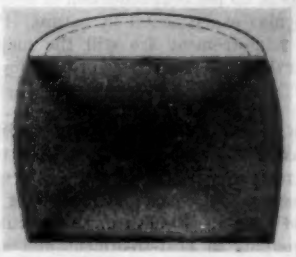

FIG. 2 MACROPHOTOGRAPH, BLISS

(Etchant attacks more deeply where metal movement is more severe. Note severe movement along the surfaces of static cones.)

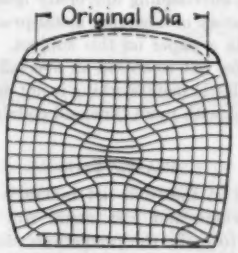

FIG. 3 BRIDGMAN'S[2] USE OF (VISIOPLASTICITY) SQUARE-MARKING METHOD SHOWS DISTRIBUTION OF METAL MOVEMENT

(He continued the process in a compression chamber, reducing austempered chrome-moly steel 94 per cent to 249,000 psi yield.)

Fig. 3 (after Bridgman,[2] Fig. 107) reproduces the distortion of an original square pattern marked upon the face of cylinder cut through its vertical axis. The change of shape of the squares permits measurement of the differences in per cent reduction in height in the areas of more and less severe flow. These percentages are noted in Fig. 4, together with typical hardness readings taken in about the same areas.

Here is something which we do not yet understand. We have found that the yield point of metal rises as we flow or work harden it. We have found that hardness readings rise with yield point, at least in the earlier stages of metal flowing. But, here we see that hardness has risen almost as much in an area where no flow is discernible as it has in an area where flow is relatively severe. This does not check with our general understanding of the results of slip-plane movement and casts some doubt upon the adequacy of that theory.

Fig. 5 illustrates continued squeezing to a flat disk. While the major forces are compressive, tensile failures have appeared as a result of continued stretching of the atomic bonds around the periphery. Bridgman's[2] use of a hydraulic medium under high pressure surrounding the part retarded such tensile failure.

The bowed surfaces of the disk suggest the much greater resistance to flow in the central area and hence greater deflection of the hardened die steels. The restraint of flow in squeezing large areas of thin metal and the consequent pyramiding of tonnage requirements has long been a problem to the mass-production press shops.

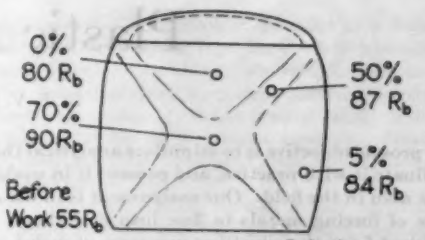

	Reduction in height	Hardness *Rb*
Undisturbed cones	Negligible	78–82
High slip on slopes	50% reduction	86–88
High slip core	70% reduction	89–90
Bulged metal	5% reduction	82–86
Hardness of metal before working		55

FIG. 4 PER CENT REDUCTION IN HEIGHT OF AREAS OF MORE OR LESS SEVERE FLOW

FIG. 5 IF CONTINUED TO A THIN DISK, THE HARDENED PRESSING BLOCKS DEFLECT SELECTIVELY BECAUSE OF PYRAMIDING LOAD IN THE LOCKED-UP CENTER AREA. LESS-WORKED MATERIAL AROUND THE EDGES FAILS IN TENSION AT OVER 100 PER CENT ELONGATION

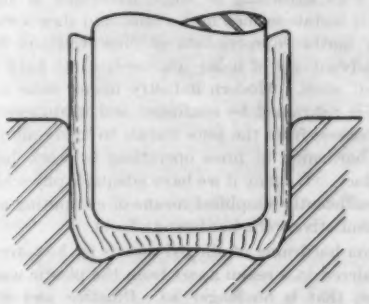

FIG. 6 WHEN 0.10-C STEEL SLUG (40,000 PSI YIELD POINT) IS IMPACT-EXTRUDED (SAY, 70 PER CENT REDUCTION), WORK HARDENING AND RESTRAINT OF FLOW TOGETHER RAISE PUNCH FACE LOAD TO 330,000 PSI OF WHICH 120,000 PSI SHOULD REPRESENT WORK HARDENING. THE BALANCE WOULD APPEAR TO BE DISTRIBUTABLE BETWEEN FRICTION, SPEED, AND RESTRAINT OF FLOW DUE TO SHAPE OR PROFILE WHICH IS PROBABLY THE MAJOR FACTOR

Fig. 6 illustrates the problem of metal flow in "backward extrusion" (flow backward with respect to punch travel). Here flow is complicated by the locking action of the right-angle turn and the orifice set up between punch and die, as well as by the ratio of area to thickness in the bottom. The net effect is an increase of resistance due to restraint of flow which is far beyond the normal increase in yield point due to work hardening.

Professors Thomsen and Frisch have brought out[3] in a series

[3] "A New Approach to Metal-Forming Problems, Experimental Stress Analysis for a Tubular Extrusion," by E. G. Thomsen, Trans. ASME, vol. 77, 1955, pp. 515–521.

"Contribution to the Knowledge of Pressure Measurements During Metal Deformation," by J. Frisch, Trans. ASME, vol. 77, 1955, pp. 509–512.

"An Experimental Study of Metal Extrusions at Various Strain Rates," by J. Frisch and E. G. Thomsen, Trans. ASME, vol. 76, 1954, pp. 599–606.

"Stresses and Strains in Cold Extruding 28-O Aluminum," by E. G. Thomsen and J. Frisch, Trans. ASME, vol. 77, 1955, pp. 1343–1353.

of papers the distribution of movement, of working, and of forces as in simple extrusion, together with means for mathematical analysis. It is now more clearly apparent how the metal stands stagnant in some areas and rushes by in adjacent areas. In the same containing tool, forces rise to destructive heights in some areas and fall away to zero in others near by.

To combine the increasing yield strength due to local work hardening, the changes of shape which restrain flow and require more pressure and the effects of speed, heat generation, lubrication, etc., are still a matter of approximation plus judgment.

Progress in Plastic Working of Metals

If the ASME research effort to promote progress in the plastic working of metals is to succeed, we must have three things:

1 A clearer co-ordination of the atomic-level relationships explaining our problems of work hardening, work limits, aging, stress relieving, and so on.

2 Much better plastic-range physical properties for the different metals. These form the starting point of any calculations of either crystoplastic or thermoplastic operations.

3 Improved but still simple and usable means of applying this better understanding and these basic data to surer solution of the almost infinite variety of problems in mass-production metal-flowing problems.

We must rely heavily upon the staffs of our technical schools and of industrial research centers and address our pleas to them.

The author begs indulgence for urging that our reputations will not be sullied by stooping to lower mathematics in presenting usable results of our efforts. The impressive use of Greek letters and calculus may be warranted in original analysis but, as Professor Thomsen wisely concluded in his review of formal theory, it is not practical for most purposes. If we emerge, however, with a clear understanding of our problems which we can transmit in usable form, we will have accomplished our assignment.

Performance Characteristics of Francis Type Pump-Turbines

By W. J. McCORMACK,[1] YORK, PA.

The object of this paper is to bring to the attention of operating companies and consulting engineers some general hydraulic characteristics of developed Francis type pump-turbines in order to assist them in designing and evaluating proposed installations. Complete performance and cavitation characteristics are presented together with an illustrative example showing how to select the optimum unit for a given set of operating conditions.

Introduction

THE advent of single reversible pump-turbines in recent years for utilization in pumped-storage projects has aroused considerable curiosity among operating companies and consulting engineers regarding the general hydraulic characteristics of these machines.

The roles played by pumped-storage projects in modern generating schemes as well as general descriptions of the projects have been presented in both the technical and nontechnical press (1 to 10).[2] Also, model test characteristics and expected performance curves of some individual machines have been published (11 to 13).

However, it does not appear that a study of the variation of performance characteristics versus specific speed for pump-turbines has been presented to this Society or published elsewhere, as has been done for hydraulic turbines (14 and 15) and pumps (16 and 17).

Limitation of Use of Curves

The author wishes to emphasize that the purpose of this paper is not to present a series of constants for the use of engineers in designing pump-turbine impellers, but rather to present a study of the variation of performance characteristics of some developed Francis type pump-turbines for the use of application engineers.

The number of reversible pump-turbines designed, model-tested, manufactured, and field-tested has not yet been sufficient to allow definite design or performance trends to be established. Therefore the data and curves presented herewith should be used only for preliminary studies of proposed projects. More specific information for final evaluation and writing of specifications should be obtained from the various pump-turbine manufacturers.

Source of Data

The data used in this study were obtained from some developed S. Morgan Smith units that have been model-tested, as well as from published information of other manufacturers. A discussion of these various units seems in order.

The unit designated Newport News was one of a series of pumps proposed for Grand Coulee (12), and had very respectable efficiencies both as a pump and as a turbine.

The Grand Coulee (18) and Granby (19) pump characteristics are plotted to show the similarity between good centrifugal pumps and the pumping performance of a centrifugal pump-turbine. These two pumps had suction elbows and full volute casings similar to those used on pump-turbines.

The two units designated Baldwin No. 115 and Baldwin No. 117 (20) have normal model turbine efficiencies with pump efficiencies about 5 points lower. This is the reverse of usual pump-turbine characteristics, indicating that these units may have been designed as turbines rather than pumps, which is also the reverse of modern pump-turbine design practice. Nevertheless, this type of design could find useful application where the monetary values placed upon the generating cycle of the machine outweigh the importance of higher pumping efficiency.

The Flatiron unit (13) has a relatively steep head-discharge curve for its specific speed. This was probably deemed necessary because of the large head range under which it must operate. This unit was not equipped with adjustable wicket gates, but the motor-generator was designed for two-speed operation.

The Sron Mor unit was designed and built by the Harland Engineering Company, Ltd., of Allon, Scotland, for pumping service but was tested both as pump and turbine.

The units designated S. Morgan Smith Pedreira, S. Morgan Smith No. 985, and S. Morgan Smith No. 946 are early S. Morgan Smith designs now considered obsolete, but presented to show the design improvements made in recent years.

S. Morgan Smith units Nos. 987 and 994 are two recently developed high specific speed pump-turbines.

Discussion of Curves

The data are presented in a form familiar to application engineers; that is, the usual units of specific speed, discharge, and horsepower are plotted so that the affinity (or similarity) laws may readily be used in sizing prototype units.

Fig. 1 is a plot of specific speed at the point of best efficiency for the pump duty cycle versus speed and discharge at 1 ft head for impellers having 12-in. throat diameters. Although the individual points indicate general trends, it must be remembered that the curves merely represent averages of the characteristics for the units considered and that they may be altered by future designs.

The individual points of best model efficiencies are plotted against specific speed together with a 2 per cent band that seems to represent a region of good pump duty cycle efficiencies. The reason for this band is that testing inaccuracies, sizes of models, and individual laboratory calibrations can easily vary maximum efficiencies by plus or minus 1 per cent among the models of the various manufacturers.

A distinction is made in the plotting of the individual points between units with and without adjustable wicket gates. It will be noted that for nongated units there are as many points above the speed and discharge curves as there are below, indicating that at the point of best efficiency adjustable wicket gates have little or no effect upon the performance of the unit.

---

[1] Hydraulic Engineer, S. Morgan Smith Company. Assoc. Mem. ASME.

[2] Numbers in parentheses refer to the Bibliography at the end of the paper.

Contributed by the Hydraulic Division and presented at the Diamond Jubilee Spring Meeting, Baltimore, Md., April 18–22, 1955, of The American Society of Mechanical Engineers.

Note: Statements and opinions advanced in papers are to be understood as individual expressions of their authors and not those of the Society. Manuscript received at ASME Headquarters, March 25, 1955. Paper No. 55—S-45.

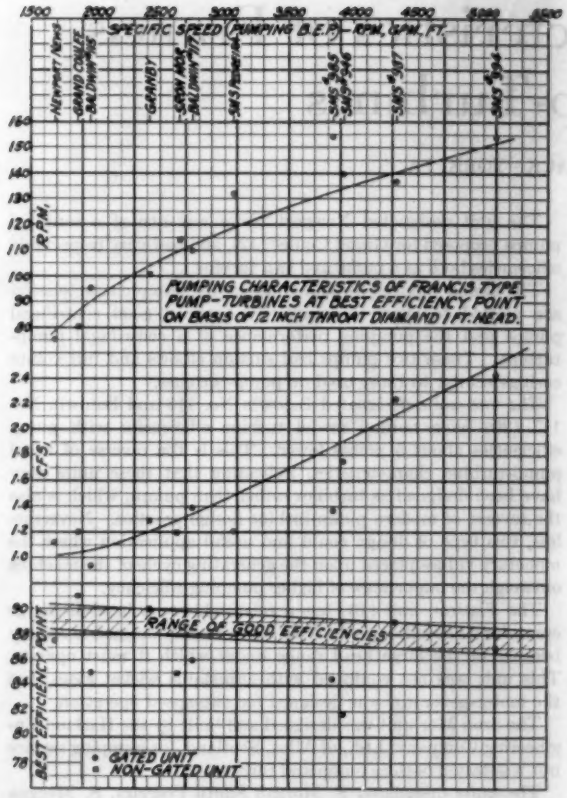
SPECIFIC SPEED (PUMPING B.E.P.) - RPM, GPM, FT.
PUMPING CHARACTERISTICS OF FRANCIS TYPE PUMP-TURBINES AT BEST EFFICIENCY POINT ON BASIS OF 12 INCH THROAT DIAM. AND 1 FT. HEAD.
RANGE OF GOOD EFFICIENCIES
R.P.M.
C.F.S.
BEST EFFICIENCY POINT
GATED UNIT
NON-GATED UNIT

FIG. 1 RELATION OF SPEED, DISCHARGE, AND EFFICIENCY TO SPECIFIC SPEED FOR PUMPING

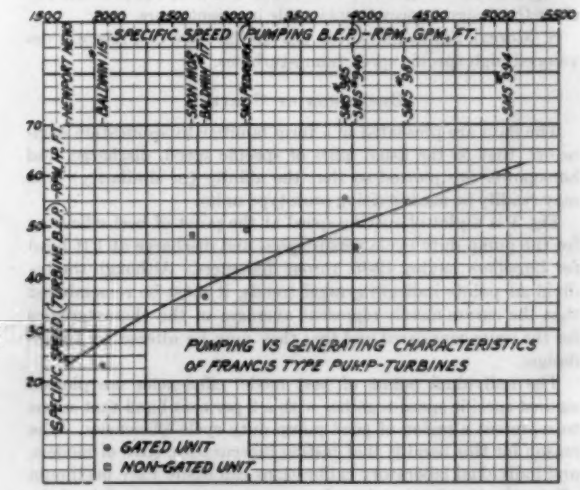
SPECIFIC SPEED (PUMPING B.E.P.) - RPM, GPM, FT.
SPECIFIC SPEED (TURBINE B.E.P.) - RPM, H.P., FT.
PUMPING VS GENERATING CHARACTERISTICS OF FRANCIS TYPE PUMP-TURBINES
GATED UNIT
NON-GATED UNIT

FIG. 2 RELATION OF PUMPING SPECIFIC SPEED TO GENERATING SPECIFIC SPEED

Fig. 2 is a plot of specific speed at the point of best efficiency for the pump duty cycle versus specific speed at the point of best efficiency for the turbine duty cycle. The points for the Newport News and S. Morgan Smith Nos. 987 and 994 units were followed in drawing this curve.

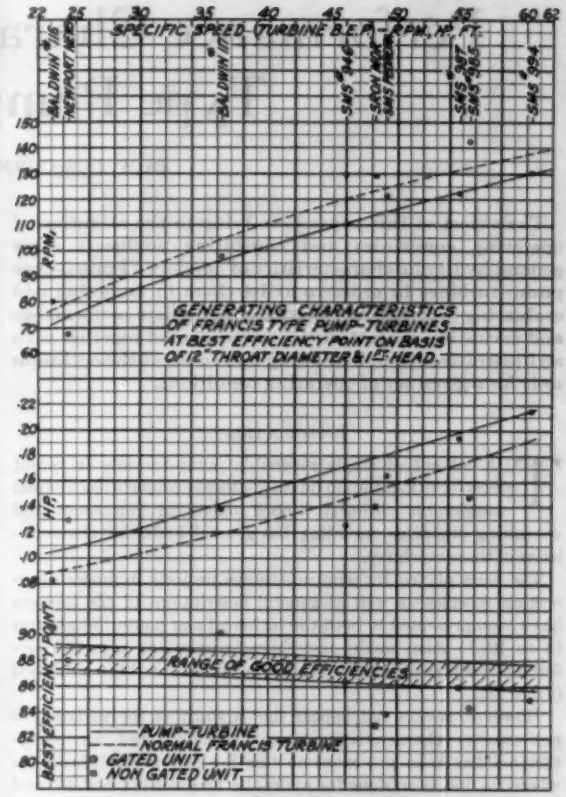
SPECIFIC SPEED (TURBINE B.E.P.) - RPM, H.P., FT.
GENERATING CHARACTERISTICS OF FRANCIS TYPE PUMP-TURBINES AT BEST EFFICIENCY POINT ON BASIS OF 12" THROAT DIAMETER & 1 FT. HEAD.
RANGE OF GOOD EFFICIENCIES
R.P.M.
H.P.
BEST EFFICIENCY POINT
PUMP-TURBINE
NORMAL FRANCIS TURBINE
GATED UNIT
NON GATED UNIT

FIG. 3 RELATION OF SPEED, HORSEPOWER, AND EFFICIENCY TO SPECIFIC SPEED FOR GENERATING

Fig. 3 shows specific speed at the point of best efficiency on the turbine duty cycle versus speed and horsepower at 1 ft head for impellers having 12-in. throat diameters. The solid lines show average characteristics for pump-turbines with the Newport News and S. Morgan Smith Nos. 987 and 994 units again receiving the most consideration.

For comparison normal Francis turbine practice as given by Sharp (14) is indicated by the dashed lines.

A 2 per cent band representing the range of good efficiencies for the turbine duty cycle is included as in the case of the pump duty cycle.

The curves of head and efficiency versus discharge for the pump duty cycle are plotted in Figs. 4 and 5 as percentages of the values at the best efficiency points. Note that the higher specific speed units have the steeper head-capacity curves, which is normal for centrifugal pumps.

The performance characteristics for the turbine duty cycle are plotted in Figs. 6 and 7 as percentages of the values at the best efficiency points (generating). For gated units the curves show the envelopes of best efficiencies for the complete rpm range. The reasons for the rather odd-shaped horsepower curves of the two S. Morgan Smith, high specific-speed, gated units is that the best efficiency of the unit occurs at a fairly low gate opening and, consequently, at a low unit power. At higher values of unit speed, the best efficiencies occur at larger gate openings with higher unit powers.

The envelopes of maximum power versus unit speed are not shown since pump-turbines are not used generally for regulating

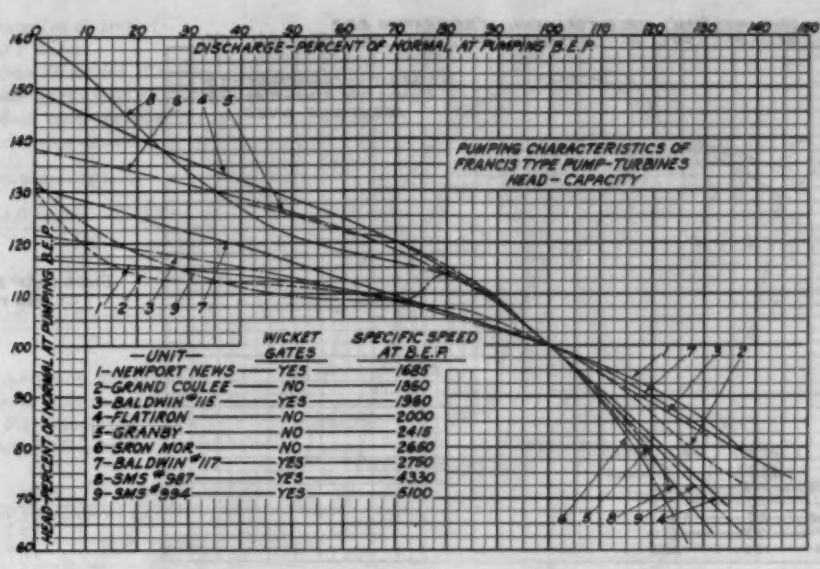
DISCHARGE-PERCENT OF NORMAL AT PUMPING B.E.P.
HEAD-PERCENT OF NORMAL AT PUMPING B.E.P.
PUMPING CHARACTERISTICS OF FRANCIS TYPE PUMP-TURBINES HEAD-CAPACITY
—UNIT— WICKET GATES SPECIFIC SPEED AT B.E.P.
1-NEWPORT NEWS YES 1685
2-GRAND COULEE NO 1860
3-BALDWIN @ 115 YES 1960
4-FLATIRON NO 2000
5-GRANBY NO 2415
6-SIRON MOR NO 2660
7-BALDWIN @ 117 YES 2750
8-SMS @ 987 YES 4330
9-SMS @ 994 YES 5100

Fig. 4 Head-Capacity Curves for Pumping

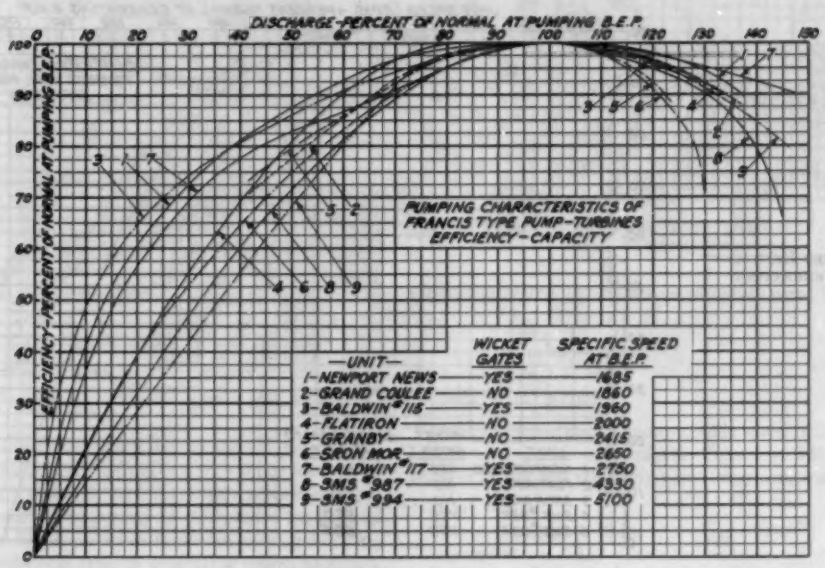
DISCHARGE-PERCENT OF NORMAL AT PUMPING B.E.P.
EFFICIENCY-PERCENT OF NORMAL AT PUMPING B.E.P.
PUMPING CHARACTERISTICS OF FRANCIS TYPE PUMP-TURBINES EFFICIENCY-CAPACITY
—UNIT— WICKET GATES SPECIFIC SPEED AT B.E.P.
1-NEWPORT NEWS YES 1685
2-GRAND COULEE NO 1860
3-BALDWIN @ 115 YES 1960
4-FLATIRON NO 2000
5-GRANBY NO 2415
6-SIRON MOR NO 2650
7-BALDWIN @ 117 YES 2750
8-SMS @ 987 YES 4330
9-SMS @ 994 YES 5100

Fig. 5 Efficiency Curves for Pumping

load but for supplying blocks of power to a system. Therefore they should be operated at the maximum efficiency for economical justification, as will be shown by an illustrative example.

Fig. 8 is a plot of critical sigma versus specific speed at best efficiency for the pump duty cycle. Also shown for comparison is the recommended upper limit of specific speeds for single-stage, single-suction pumps with shaft through impeller eye pumping clear water at sea level at 85 F from the Standards of Hydraulic Institute. Normally, the critical sigma value for the pump duty cycle will determine the setting with respect to suction level. However, on some Francis type pump-turbines, particularly those of high specific speeds, a runaway speed-sigma effect, similar to that obtained on Kaplan turbines (21), may restrict the use of the unit over a varying head range by limiting the minimum head at which the unit could operate.

Fig. 9 shows the variation of critical sigma versus discharge expressed as percentages of the values at the best efficiency points for the various units of different specific speeds. Because of the general similarity of the various data plotted, a curve of recommended safe values has been included for preliminary purposes.

Example of Use of Curves

To illustrate the use of the curves, assume that the following conditions are to be met:

1 An average of about 50,000 hp is desired during a daily 8-hr generating cycle, utilizing a single unit, if feasible.

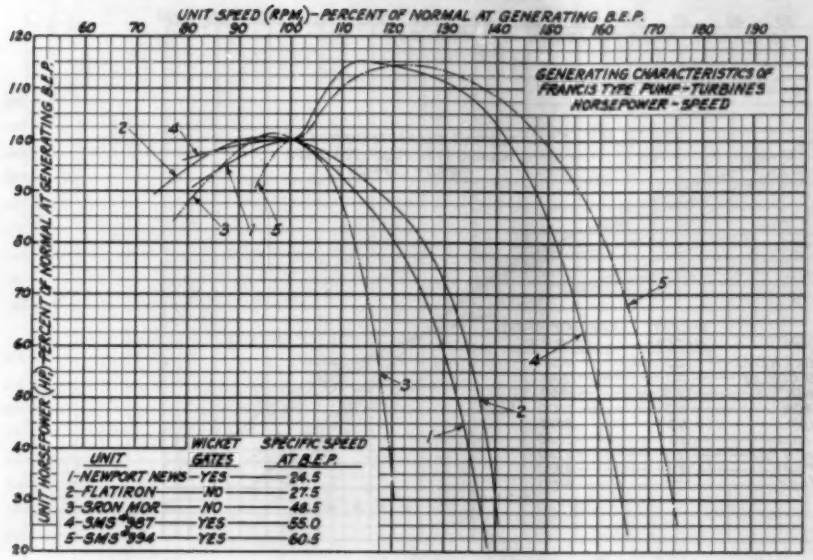
UNIT SPEED (RPM) – PERCENT OF NORMAL AT GENERATING B.E.P.
UNIT HORSEPOWER (HP) – PERCENT OF NORMAL AT GENERATING B.E.P.
GENERATING CHARACTERISTICS OF FRANCIS TYPE PUMP-TURBINES HORSEPOWER-SPEED
UNIT | WICKET GATES | SPECIFIC SPEED AT B.E.P.
1-NEWPORT NEWS – YES – 24.5
2-FLATIRON – NO – 27.5
3-SRON MOR – NO – 48.5
4-SMS #987 – YES – 55.0
5-SMS #994 – YES – 60.5

FIG. 6 (*left*) SPEED-HORSEPOWER CURVES FOR GENERATING

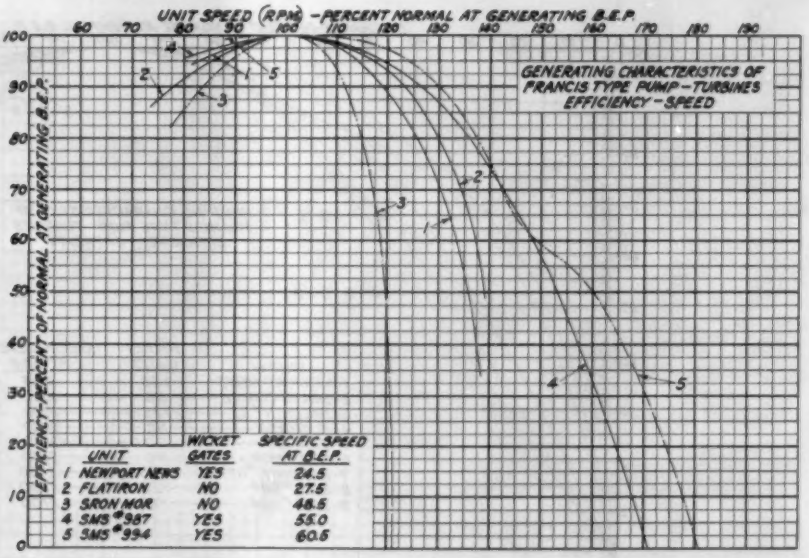
UNIT SPEED (RPM) – PERCENT NORMAL AT GENERATING B.E.P.
EFFICIENCY – PERCENT OF NORMAL AT GENERATING B.E.P.
GENERATING CHARACTERISTICS OF FRANCIS TYPE PUMP-TURBINES EFFICIENCY-SPEED
UNIT | WICKET GATES | SPECIFIC SPEED AT B.E.P.
1 NEWPORT NEWS – YES – 24.5
2 FLATIRON – NO – 27.5
3 SRON MOR – NO – 48.5
4 SMS #987 – YES – 55.0
5 SMS #994 – YES – 60.5

FIG. 7 (*right*) SPEED-EFFICIENCY CURVES FOR GENERATING

2 The approximate total volume of water required should be verified so that the reservoir capacity can be studied.

3 The unit will be operated at best efficiency continuously to supply block load to the system.

4 The elevation of the storage reservoir at the beginning of the generating cycle will be about 2180 ft.

5 The elevation of the storage reservoir at the end of the generating cycle will be about 2150 ft.

6 The estimated friction loss in the penstock for a flow of 2700 cfs is about 2 ft.

7 A maximum of 10 hr per day is available for pumping.

8 The elevation of the suction pool is 2000 ft with no appreciable drawdown.

9 The suction-pool level will never be less than 2000 ft.

10 The unit should be self-priming as a pump.

11 Generating power is worth 9 mils per kwhr and pumping power costs 3 mils per kwhr.

12 The pumped-storage plant will draw water from the forebay of an existing hydrogenerating plant and will pump into a reservoir that will be built nearby.

The normal head limits under which the unit must operate are as follows:

Maximum pumping head = 182 ft (el. 2180 ft — el. 2000 ft + 2 ft friction)
Minimum pumping head = 152 ft (el. 2150 ft — el. 2000 ft + 2 ft friction)
Maximum generating head = 178 ft (180 ft — 2 ft friction)
Minimum generating head = 148 ft (150 ft — 2 ft friction)

Compute plant sigma for the maximum and minimum pumping heads, assuming:

H_a = 31.6 ft of water (at el. 2000 ft)
H_{vp} = 0.6 ft for 60 F water
H_s = —8.0 ft ± (this dimension, the depth of the impeller eye below suction-pool level as required for self-priming, is dependent upon impeller proportions and should be cleared with a manufacturer)

Then, for maximum pumping head

$$\sigma = \frac{31.6 - 0.6 - (-8.0)}{182} = 0.215$$

and, for minimum pumping head

$$\sigma = \frac{31.6 - 0.6 - (-8.0)}{152} = 0.255$$

In order to avoid cavitation, the critical sigma of the unit at each head must be lower than the corresponding plant sigma.

A cursory look at Fig. 8 indicates that a unit with a specific speed between 2500 and 3500 is required.

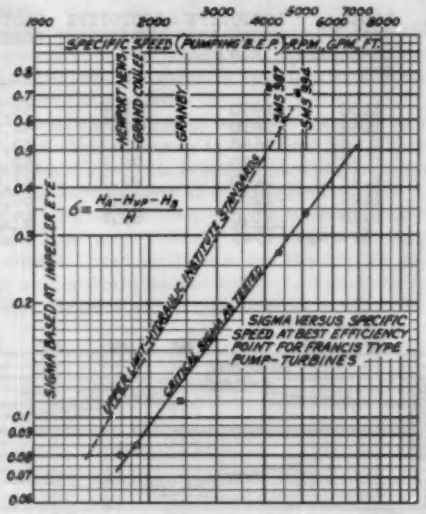
SPECIFIC SPEED (PUMPING B.E.P.) R.P.M. G.P.M. FT.
SIGMA BASED AT IMPELLER EYE
NEWPORT NEWS
GRAND COULEE
GRANBY
SMS 387
SMS 934
SIGMA VERSUS SPECIFIC SPEED AT BEST EFFICIENCY POINT FOR FRANCIS TYPE PUMP-TURBINES

FIG. 8 RELATION OF SIGMA TO SPECIFIC SPEED FOR PUMPING

The approximate head variation from the average head of 167 ft during the pump duty cycle is from —9 to +9 per cent, or 18 per cent total. It will generally be found that a greater percentage of the head variation for pumping must lie above the head at best efficiency point, Fig. 4, in order to obtain good generating efficiencies and the optimum ratio of generating return to pumping cost. Assume, therefore, 12 per cent head variation above the head at best efficiency point and 6 per cent below. Entering Fig. 4 with this assumption indicates that the pumping discharge will vary from approximately 80 per cent of normal to 110 per cent of normal.

From the "recommended safe sigma" curve of Fig. 9 it can be seen that the critical sigma will exceed normal by 25 per cent at 182 ft head and by 50 per cent at 152 ft head. Hence the critical sigma of the unit should not be less than either of the following at the pumping best efficiency point:

$$\frac{0.215}{1.25} = 0.172 \quad \text{or} \quad \frac{0.255}{1.50} = 0.170$$

Referring to Fig. 8, a unit with a specific speed of approximately 3000 is indicated for a critical sigma of 0.165. From Fig. 1 the

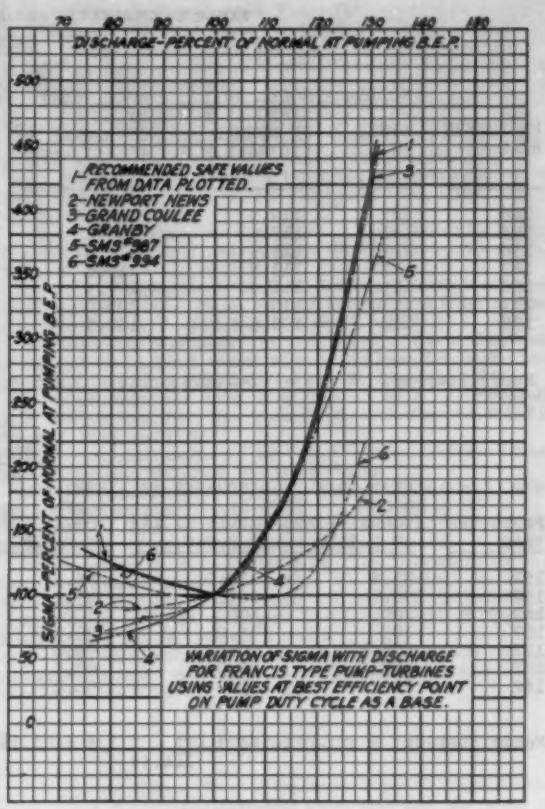
DISCHARGE—PERCENT OF NORMAL AT PUMPING B.E.P.
SIGMA—PERCENT OF NORMAL AT PUMPING B.E.P.
1—RECOMMENDED SAFE VALUES FROM DATA PLOTTED.
2—NEWPORT NEWS
3—GRAND COULEE
4—GRANBY
5—SMS 387
6—SMS 934
VARIATION OF SIGMA WITH DISCHARGE FOR FRANCIS TYPE PUMP-TURBINES USING VALUES AT BEST EFFICIENCY POINT ON PUMP DUTY CYCLE AS A BASE.

FIG. 9 VARIATION OF SIGMA WITH DISCHARGE FOR A CONSTANT SPECIFIC SPEED

model characteristics at the best efficiency point for pumping are:

Head = 1 ft
Throat diameter = 12 in.
Discharge = 1.45 cfs
Speed = 117.5 rpm

Fig. 2 indicates that a pump specific speed of 3000 corresponds to a turbine specific speed of 41. From Fig. 3 the model characteristics at the best efficiency point for generating are:

Head = 1 ft
Throat diameter = 12 in.
Horsepower = 0.157
Speed = 103 rpm

The prototype should be sized to generate approximately 50,000 hp at the average head of 163 ft. From the assumption that 12 per cent of the pumping-head variation will be above the head at the pumping best efficiency point and 6 per cent below, the model speed of 117.5 rpm corresponds to a prototype head of 182/1.12 = 162 ft. Therefore the average generating head of 163 ft corresponds to a model speed of approximately 117 rpm, which is 14 per cent above the normal generating speed at best efficiency.

By interpolation from Fig. 6, at 114 per cent of the best efficiency generating speed for a specific speed of 41, the model unit horsepower is about 110 per cent of that at the best efficiency point. The model characteristics corresponding to a generating head of 163 ft are, therefore, as follows:

Head = 1 ft

TABLE 1 ENGINEERING DATA FOR PERFORMANCE CURVES

GENERATING CYCLE

PROTOTYPE HEAD	MODEL UNIT SPEED N_1	MODEL UNIT SPEED AS % OF NORMAL (103) at B.E.P.	MODEL UNIT HP AS % OF NORMAL (0.157) at BEP	MODEL UNIT EFF. AS % OF NORMAL (87.5) at BEP	MODEL UNIT HP	MODEL UNIT EFF.	PROTOTYPE HP	PROTOTYPE EFF.	PROTOTYPE DISCHARGE, CFS
148	123	119.5	109.0	94.0	0.171	82.3	44,600	87.2	3050
153	121	117.5	109.5	95.0	0.172	83.1	47,200	88.0	3090
158	119	115.5	110.0	96.0	0.173	84.0	49,800	88.9	3125
163	117	113.5	110.0	97.0	0.173	84.9	52,200	89.8	3140
168	115	111.5	109.5	98.0	0.172	85.8	54,400	90.7	3150
173	113.5	110	109.0	98.5	0.171	86.2	56,400	91.1	3150
178	112	108.5	107.5	99.0	0.169	86.6	58,200	91.5	3150
						Average	51,900		3125

Moody Step-up: $E = 1 - (1-0.875)\left(\frac{12}{144.5}\right)^{1/5} = 92.4\%\ (+4.9\%)$

PUMPING CYCLE

PROTOTYPE HEAD	HEAD AS % OF NORMAL (162) AT B.E.P.	DISCHARGE AS % OF NORMAL (1.45) AT B.E.P.	EFF. AS % OF NORMAL (88.7) AT B.E.P.	MODEL UNIT EFF.	MODEL UNIT DISCHARGE, CFS	PROTOTYPE DISCHARGE, C.F.S.	PROTOTYPE EFFICIENCY	PROTOTYPE HORSEPOWER
152	93.8	110.0	98.5	87.4	1.60	2950	91.8	55,400
157	96.9	105.0	99.5	88.3	1.52	2810	92.7	54,000
162	100	100	100	88.7	1.45	2680	93.1	52,900
167	103	95.0	99.7	88.4	1.38	2550	92.8	52,000
172	106.1	90.0	99.0	87.8	1.31	2410	92.2	51,000
177	109.2	85.0	97.5	86.5	1.23	2280	90.9	50,400
182	112.3	80.0	96.0	85.2	1.16	2140	89.6	49,300
					Average	2545		52,100

Moody Step-up: $E = 1 - (1-0.887)\left(\frac{12}{144.5}\right)^{1/5} = 93.1\%\ (+4.4\%)$

Throat diameter = 12 in.
Horsepower = $1.10 \times 0.157 = 0.173$
Speed = 117 rpm

Using the well-known similarity laws for hydrodynamic machinery indicates that a prototype with a throat diameter of 144.5 in. would generate 52,000 hp at 163 ft net head while running at 124.1 rpm. Table 1 indicates the method used to arrive at the performance curves shown in Fig. 10. The model efficiencies used are the averages of the "good efficiency bands" for both pumping and generating. The Moody formula with an exponent of $^1/_5$ was used to "step up" model efficiencies to prototype efficiencies, the resulting differentials being added in accordance with the NEMA Standards (22).

Evaluation of Example

Certain basic assumptions, such as the portion of the pump head-capacity curve to be utilized, were made in arriving at the prototype size and speed to meet the specified requirements. The suitability of these assumptions can be demonstrated only by other selections and evaluations.

Rheingans, et al. (7) suggest a method of evaluation for comparing a unit having adjustable wicket gates with a fixed-gate unit. This same type of evaluation can be used to determine the optimum range of the characteristic curves to be utilized for a given set of conditions.

The evaluation of the preceding example is as follows:

Generating:

1 Generating cycle is 8 hr.

2 Use prototype performance curves shown in Fig. 10.

3 Assume 97 per cent motor-generator efficiency.

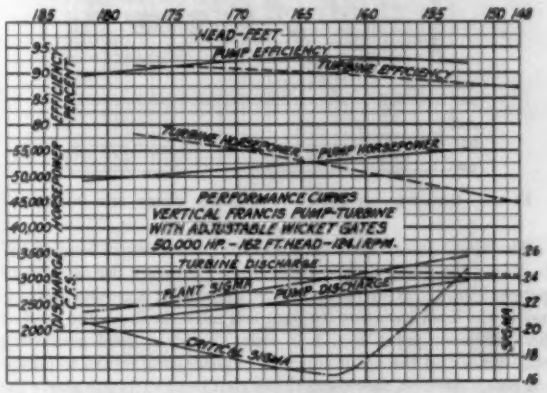

FIG. 10 PERFORMANCE CURVES FOR EXAMPLE

4 Over a generating head range of 178 to 148 ft, unit will develop an average of 51,900 hp, or $51,900 \times 0.97 \times 0.746 \times 8 = 300,000$ kwhr in 8 hr.

5 Average amount of water used over head range is 3125 cfs, or $3125 \times 3600 \times 8 = 90,000,000$ cu ft in 8 hr.

6 Generated power is worth \$0.009 per kwhr.

7 During generating cycle power returns $300,000 \times \$0.009 = \$2700$.

Pumping:

8 Average discharge during pumping cycle over head range of 152 to 182 ft is 2545 cfs, or $2545 \times 3600 = 9,160,000$ cfh.

9 Pumping time required is $\frac{90{,}000{,}000}{9{,}160{,}000} = 9.82$ hr.

10 Average power consumed during pumping cycle is 52,100 hp or $\frac{52{,}100 \times 0.746 \times 9.82}{0.97} = 394{,}000$ kwhr in 9.82 hr.

11 Pumping power costs \$0.003 per kwhr.

12 During pumping cycle, power costs $394{,}000 \times \$0.003 = \$1180$.

13 Ratio of generating return to pumping cost is

$$\frac{2700}{1180} = 2.29$$

This ratio is the criterion for selecting the most efficient unit for any particular application. Other selections should be similarly evaluated for the same specific speed but utilizing a different portion of the pumping head-capacity curve as well as for different specific speeds. The unit having the highest ratio of generating return to pumping cost will naturally be the most efficient hydraulically, but not necessarily the most economical installation.

Other factors, such as cost of the pump-turbine itself, cost of motor-generator, size of powerhouse, amount of excavation required, and so forth, will naturally enter into the final selection of the machine to be specified.

The hydraulic advantage of two-speed operation to allow the peaks of the efficiency curves to be utilized for both cycles may be economically justifiable in some instances, particularly where the unit must operate over an extreme head range or where the generating head is much lower than the pumping head.

Wicket gates may generally be justified. In applications where the total head variation is less than 10 per cent of the average head or where the unit will be used primarily for pumping service, the use of wicket gates may not be warranted.

Conclusion

No definite rules or standards can be given for the application of pump-turbines to various hydraulic conditions. Each application must be treated as a special problem, with the final selection of a particular design depending upon careful evaluation of the various factors involved.

Hence it becomes apparent that the size, speed, elevation of volute center line, and other hydraulic characteristics for specified conditions will vary from one manufacturer to another. These items should be left open in the customer's specifications. However, an approximate range of speeds and settings may be selected from information supplied in the preliminary stages by the various manufacturers or from the curves presented in this paper. The purchaser must then evaluate the various units offered to select the one best suited to his operating requirements.

BIBLIOGRAPHY

1 "Pumped Storage Hydro-Electric Plants," by F. A. Annett, *Power*, vol. 78, January, 1934, pp. 20–24.

2 "Pumped Storage Hydro-Electric Plants," by W. W. K. Freeman, Proceedings of the ASCE, vol. 54, 1928, pp. 2457–2475.

3 "Rocky River Hydro-Electric Development," by J. D. Justin, Proceedings of the ASCE, vol. 55, 1929, pp. 690–697.

4 "Pumped Storage Stations," by Arthur Koepchen, *Water Power*, vol. 1, November–December, 1949, pp. 232–234.

5 "Trend in Hydraulic Turbine Practice—a Symposium; Economic Principles in Design," by I. A. Winter, Proceedings of the ASCE, vol. 65, 1940, pp. 1554–1574.

6 "Pump Storage Systems," by A. Voska, *Water Power*, vol. 2, July–August, 1950, pp. 137–143; September–October, pp. 209–219.

7 "Pumped Storage," by W. J. Rheingans, Frank Jaski, and H. H. Roth, Proceedings of the Midwest Power Conference, vol. 13, 1951, pp. 153–162.

8 "TVA Installing Largest Pump-Turbine at Hiwassee," by D. H. Mattern, *Electrical World*, vol. 142, July 5, 1954, pp. 16–18, 20.

9 "Design Features of the Flatiron Power and Pumping Plant," by John Parmakian, to be published in *Mechanical Engineering*, vol. 77, August, 1955, pp. 677–680.

10 "Pumped Storage for Hydroelectric Power—A Selected List of References in English," TVA Technical Library, December, 1953.

11 "Hydraulic Turbine and Pump Combined in a Single Unit," by F. A. Allner, *Power*, vol. 76, November, 1932, pp. 266–267.

12 "Test Characteristics of a Combined Pump-Turbine Model With Wicket Gates," by R. V. Terry and F. E. Jaski, Trans. ASME, vol. 64, 1942, pp. 731–737.

13 "One Machine—Two Functions . . . New Reversible Pump-Turbine," by F. E. Jaski, *Allis Chalmers Electrical Review*, 4th quarter 1952, vol. 17, pp. 8–11.

14 "Hydraulic Turbines," by R. E. B. Sharp, "Kent's Mechanical Engineers' Handbook," *Power*, eleventh edition, John Wiley & Sons, Inc., New York, N. Y., 1936, Figs. 4, 9, 10, 12, and 22.

15 "Hydraulic Machinery," by L. F. Moody, "Davis' Handbook of Applied Hydraulics," second edition, McGraw-Hill Book Company, Inc., New York, N. Y., 1952, Figs. 26b, 31a, 31b, and 35.

16 "Centrifugal and Axial Flow Pumps," by A. J. Stepanoff, John Wiley & Sons, Inc., New York, N. Y., 1948, Figs. 5.1, 9.1, 9.2, 9.3, 9.16, 12.18, and 12.20.

17 "Stromungsmaschinen," by Carl Pfleiderer, Springer-Verlag, Berlin, Germany, 1952, Figs. 109, 110, and 110a.

18 "Development of the Hydraulic Design for the Grand Coulee Pumps," by Carl Blom, Trans. ASME, vol. 72, 1950, pp. 53–64.

19 "Model Tests of Granby Pumps," by B. L. Vanderboegh, Trans. ASME, vol. 69, 1947, pp. 535–538.

20 Discussion by R. E. B. Sharp on "Test Characteristics of a Combined Pump-Turbine Model With Wicket Gates," by R. V. Terry and F. E. Jaski, Trans. ASME, vol. 64, 1942, pp. 742–743.

21 "Runaway Speed of Kaplan Turbines," by G. H. Voaden, Trans. ASME, vol. 74, 1952, pp. 689–697.

22 "NEMA Specifying Hydraulic Turbines, Governors and Accessory Equipment," National Electrical Manufacturers Association, Publication No. HT2-1951, April, 1951.

Discussion

F. E. Jaski.[3] The abstract at the beginning of the paper makes a broad and all-inclusive statement which may lead the reader to some false conclusions. A paper such as this can only include data from a few actual samples of pump-turbines designed for a specific set of requirements.

It cannot include complete performance characteristics, or cavitation characteristics. For example, at a given specific speed, numerous designs are possible. For a pump, the specific speed is expressed by the formula N_s = RPM-1/$\sqrt{\text{gpm-1}}$. This means that a runner for each specific speed may have a high or low RPM-1, or a high or low gpm-1. It may have a flat Head—CFS curve, or a steep one depending upon the designer's selection of runner profile, ratio of D_2 to D_e (outside diameter to eye diameter), angles of the buckets at entrance and discharge, number of buckets, and so on.

Therefore, if an attempt is made to plot these values a scatter of points is obtained. While the shape of any curve drawn through such a group of points can show the general trend, it is not sufficiently correct to use these values for establishing dimensions of a unit. In fact it may be so far off that the size of motor required to drive the pump or generator to match the turbine output as obtained from these data may be entirely too small and may cause the estimate to be too low.

It is the writer's opinion that the paper will serve its purpose very well if it is used only as a guide to show the trends of some of the variables in the pumping characteristics or turbine characteristics of reversible pump-turbines.

For example, Fig. 1 of the paper shows that, in general, the RPM-1 and CFS-1 tend to increase with increase of specific speeds. It also shows that, in general, efficiency tends to be less

[3] Engineer in Charge Pump-Turbines, Hydraulic Section, Allis-Chalmers Manufacturing Company, Milwaukee, Wis. Mem. ASME.

at higher specific speeds. If we had data from a half-dozen designs for each of a whole series of specific speeds we would still obtain a scatter of points. This, of course, is true in all hydraulic machines whether they are centrifugal pumps, hydraulic turbines, or reversible pump-turbines. That is why in order to establish a size of unit for a given application, the consulting engineer must obtain this information from the manufacturer. In using data of the kind shown in this paper he may arrive at results that may or may not be optimum, but he may find that no such size is available. Each manufacturer has a series of designs already developed which are backed up by model tests, or field tests. These then are the preferred sizes or models which will be used for any given applications. Just as for hydraulic turbines there may be a variation in throat diameter for designs of different manufacturers. Each application usually has its own prescribed set of conditions so that the pump-turbine must be "tailor made" for these conditions. In one case, the maximum head may be as much as twice the minimum head, or even more. In another case, the head may vary only 10 per cent above or below the average head. Other differences in the requirements of various applications could be mentioned but to enumerate all of them would require the writing of another paper and it is probably impossible to enumerate all the peculiar conditions that are possible in pump-turbine applications. Therefore, in order to obtain a size for a given application, it will be better for the user to refer his inquiry directly to a manufacturer rather than to try to establish a size from a set of approximate curves.

The example worked out by means of the curves is an illustration of the mathematical process involved but does not mean that the results are to be used for establishing a size, nor can the curves of Head versus CFS, or horsepower or efficiency be plotted from these data for either the pump or the turbine. In stepping up efficiency from a model test of a hydraulic turbine the Moody formula is sometimes used. This must be used with caution because there have been applications in which the ratio of prototype to model resulted in stepped-up efficiency that was higher than obtained in a field test. For stepping up centrifugal-pump efficiency the Moody formula has not been adopted as yet by the industry because there also were applications with large pumps where the stepped-up efficiency came out higher than was obtained by field test.

There are many data in handbooks and textbooks about characteristics of centrifugal pumps and hydraulic turbines but nobody would use them to establish a size of unit required for a given set of requirements. A paper which would include complete characteristics of pump-turbines would have to contain all of the test data for all models built and tested by all manufacturers, and would then have to be revised from time to time to include all of the newest and latest developments.

The paper is a very good paper and the author should be complimented for his efforts because it represents a great deal of work in the preparation. However, it should be remembered that it does not have sufficient basis to enable the reader to establish a size of pump-turbine required for a given set of conditions.

C. R. Marks.[4] The author has presented a valuable compendium of information on this most timely subject. These data, together with the illustrative examples, provide what is believed to be the first published information which will permit the application engineer to make a preliminary selection of a pump-turbine to fit a given set of conditions in a manner comparable to that commonly followed for a conventional turbine installation.

The firm with which the writer is associated has just completed preliminary designs and a report on an extensive water-conservation and power development on the Brazos River in Texas. This development contemplates the installation of two pump-turbines in each of five new power plants, and the addition of one pump-turbine to an existing power plant. It is also planned to install a turbine of the conventional type in each of the five new powerhouses. The eleven pump-turbines will have a total combined output of 450,000 hp at their normal heads, which range from 55 to 130 ft.

The five new power plants will be essentially run-of-the-river plants, but the five reservoirs will be situated on a stretch of the river between two existing storage reservoirs, so that the complete development will consist of a chain of seven reservoirs. The pump-turbines will permit successive pumping from the lower-most reservoir to the uppermost.

A system of reservoirs such as planned for the Brazos River will generally permit the greatest advantages of the pump-turbine to be obtained, because with substantial storage at both ends of a chain of reservoirs, it is possible to use off-peak energy for pumping operations on week ends as well as at night, and at the same time to avoid undesirably large fluctuations of water levels with consequent reductions in the combined critical heads for the system.

The writer was much interested in the author's exposition of the process of selecting the most efficient unit for any particular application. However, it appears that fully as important as this determination will be the proper balance between pump-turbines and conventional turbines.

The data presented are of particular interest in demonstrating that it is feasible to design Francis type pump-turbines with relatively good efficiencies both as turbines and pumps over a wide range of specific speeds. It is the writer's observation that the loss of a few percentage points in efficiency is not of great importance in this type of a power installation, because in most applications of pump-turbines it will be either the pumping capacity or the generating capacity or some combination of these that will have the greatest value, and that obtaining maximum efficiency in generation or consumption of electric energy will not be of paramount importance.

C. L. Norris.[5] This paper on the selection and application of a pump-turbine is an indication of the interest in this type of machine not apparent a very few years ago.

The writer questions the use of the exponent $^1/_5$ in the Moody formula for determining the prototype-pump efficiency. We know of no pump manufacturer who uses this exponent. It appears that a great many model and prototype tests will have to be made before a realistic step-up value can be determined. The forthcoming salt-velocity test on the TVA's pump-turbine installation at Hiwassee should provide some concrete information in this respect.

The evaluation of the economics of the theoretical installations as given in the paper appears to the writer to be misleading because of the high benefit-cost ratio of 2.29. Our studies have shown that this ratio is usually much lower. However, as the author points out, this does not contain all of the factors involved and before an installation could be justified for any specific project a complete economic study should be made.

John Parmakian.[6] This excellent paper brings together many useful data on the hydraulic characteristics of single-unit pump-turbines. The data shown in the various curves of this paper for the Flatiron pump-turbine unit were obtained from data

[4] Vice-President, Ambursen Engineering Corporation, Houston, Texas.

[5] Mechanical Engineer, Tennessee Valley Authority, Knoxville, Tenn. Mem. ASME.

[6] Head, Technical Engineering Analysis Section, Design Division, U. S. Bureau of Reclamation, Denver, Colo. Mem. ASME.

which the manufacturer stepped up from model tests. At this installation the head on the unit varies from about 140 to 300 ft. The model tests for the particular impeller selected indicated that with these wide ranges in head, higher efficiencies could be obtained by running the turbine at 257 rpm and the pump at 300 rpm.

The field-performance data on the Flatiron pump-turbine unit have recently become available. Fig. 11 of this discussion shows the performance curves of the unit when operating as a turbine at 257 rpm. Although the head in the field can vary from 140 to 290 ft when operating as a turbine, the actual field tests were confined to heads from about 175 to 260 ft. In general, the prototype indicates better performance than the model throughout the entire head range tested.

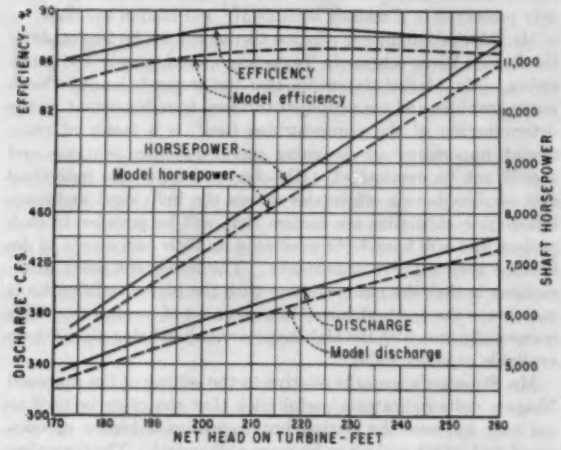

FIG. 11 PERFORMANCE CURVES—UNIT NO. 3 GENERATING, FLATIRON POWER AND PUMPING PLANT

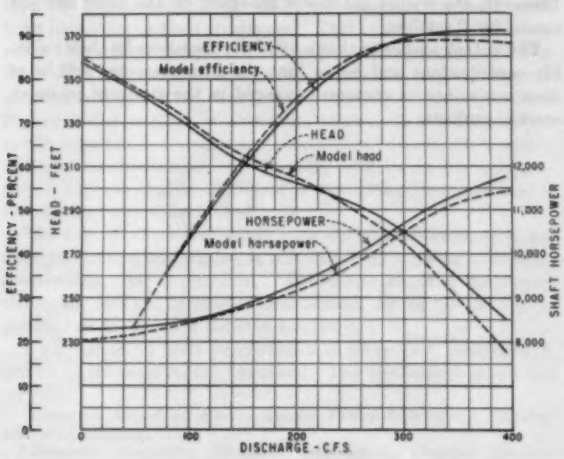

FIG. 12 PERFORMANCE CURVES—UNIT NO. 3 PUMPING, FLATIRON POWER AND PUMPING PLANT

Fig. 12 shows the performance curves of the unit when operating as a pump at 300 rpm. Although the head on the pump varies from 170 to 300 ft, the field tests were confined to heads above 240 ft. The model and prototype performance curves for pump operation are in close agreement throughout the range of heads tested. The flow measurements on which the performance curves were based when operating as a turbine or as a pump were determined by the salt-velocity method.

The primary use of the Flatiron pump-turbine is as a pump. As of April 1, 1955, it had operated 4326 hr as a pump and 226 hr as a turbine.

It is hoped that these specific performance data on the actual Flatiron pump-turbine unit will assist in establishing more definite performance trends and in evaluating stepped-up formulas between model and prototype for this type of machine.

E. B. STROWGER.[7] The author has presented data which will be useful to engineers engaged in the study or design of pumped storage projects.

The values of critical sigma presented are based upon operation at best efficiency. If there is a relatively large range in pumping head, conditions at low head may determine the pump setting and when this is true the value of sigma when operating beyond the best efficiency point is important. In this case the author's Fig. 9 comes into play.

Some of the pump turbines suggested for the Niagara Falls pump-storage project have a specific speed of 4500 at rating but may be called upon to operate at a specific speed of 7800. This comes about as follows: There will be available 50,000 cfs more at night in the tourist season than in the daytime so that pumping of water to the storage reservoir will take place at night for use the next day for generating. At the start of the pumping cycle, when the reservoir is empty and under certain river conditions, the dynamic pumping head will be down to about 57 ft. When pumping starts at the beginning of the night period, therefore, the head will be low, and at the end of the pumping cycle it will be up to about 82 ft. The quantity-head curve of the pump is steep at low heads and at 57 ft shows a discharge of 4000 cfs, while at 82 ft head the discharge is down to 3500 cfs. The high velocity at the eye of the pump when discharging 4000 cfs requires a low setting, the required elevation at center line of the distributor being for this condition approximately 520. However, the actual center line may be placed at elevation 530, because it is expensive to excavate

[7] Chief Hydraulic Engineer, Niagara Mohawk Power Corporation, Buffalo, N. Y. Mem. ASME.

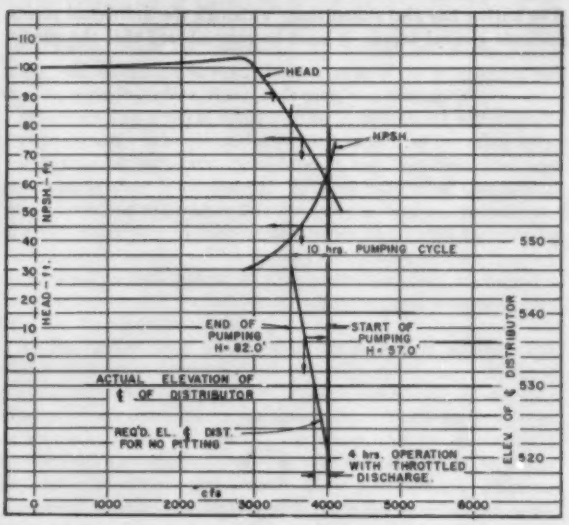

FIG. 13 HOW AUTHOR'S FIGS. 4 AND 9 WERE USED TO DETERMINE A REQUIRED PUMP SETTING

the rock an additional 10 ft for the whole area of the powerhouse. It is, therefore, proposed to throttle the pump discharge somewhat at the start of the pumping cycle until the head in the reservoir is built up sufficiently to obviate pitting. During the worst condition it is estimated that operation with throttled discharge will take place for about 4 hr at the start of the pumping cycle after which normal operation will take place. Fig. 13, herewith, shows how a combination of the author's Figs. 4 and 9 is used to determine pump setting in this case. Values of net positive suction head of the center line of the distributor are shown instead of values of sigma, the relation between the two being

$$\text{Sigma at pump eye} = \frac{\text{NPSH at center line—distance center-line runner to eye}}{\text{head}}$$

As the runners will of necessity be set below tail water in order to function properly as a pump, a tail water depressing compressed-air system will be required. The tail water will be depressed during the starting operation until the pumps have reached synchronous speed and are on the line.

Author's Closure

From the remarks made in the discussions by the engineers who represent consulting firms and operating companies, it appears that the avowed purpose of the paper has been achieved. Messrs. Marks, Parmakian, and Strowger indicate that the data contained in the paper will prove useful to application engineers engaged in the study of proposed pumped-storage projects "to make a preliminary selection of a pump-turbine to fit a given set of conditions in a manner comparable to that commonly followed for a conventional turbine installation."

The author naturally agrees with the arguments presented by Mr. Jaski showing how deviations in the design of the impeller can produce a variety of performance characteristics for a given specific speed. However, the intended purpose and use of the paper is amply covered in the paragraphs titled Limitation of Use of Curves and Conclusion, wherein it is clearly stated that the data presented should be used for preliminary purposes only and that the final selection of size, speed, setting, and other hydraulic characteristics should be left with the manufacturer. The author has also stated that "although the individual points indicate general trends, it must be remembered that the curves merely represent averages of the characteristics for the units considered and that they may be altered by future designs."

The late Mr. Norris and Mr. Jaski question the use of the Moody formula for determining the prototype pump efficiency. Mr. Parmakian has presented a comparison of the actual model and field tests on the Flatiron unit to assist in establishing and evaluating step-up formulas for pump-turbines. In the example given in the paper, the Moody formula with an exponent of 1/5 was used for the pump-duty cycle merely for illustrative purposes and not with the intention of advocating its use as an accepted "standard." This is a problem that has been argued in hydroelectric circles "from time immemorial," and the author did not intend to settle it in this paper. However, definite trends can only be established after many more units are completely model and field-tested and the data obtained are publicly presented in a manner such as Mr. Parmakian has done.

Mr. Marks' comments relative to the studies he has made of the Brazos River scheme in Texas are, indeed, timely and interesting. Mr. Marks' statement, that the proper balance between pump-turbines and conventional turbines is as important as the determination of the pump-turbine itself, is a factor of paramount importance in designing pumped-storage stations and should not be overlooked. His observations of the individual and combined-cycle efficiencies versus the individual and combined-cycle capacities are factors that will be peculiar to each project and will have to be evaluated on their own merits to determine their relative importance. The important point to remember is that the pump-turbine with the highest efficiencies is not always the one best suited to a given set of conditions. This is especially true with the high monetary values being placed upon available capacity today.

Mr. Strowger's remarks relative to the setting of the proposed Niagara units indicates a useful trick that can often be used to not only improve the setting but to utilize a higher specific-speed unit which will often be more economical. The throttling can be done with the wicket gates, or by the use of a butterfly valve in the penstock if the unit does not have wicket gates. However, the wicket gates will generally be the more efficient means for throttling.

The author wishes to thank all of the discussers for their valuable contributions and hopes that the data presented will be of some assistance to engineers engaged in the study of pumped-storage projects.

Zirconium-Fabrication Techniques and Alloy Development

By C. E. LACY[1] AND J. H. KEELER,[2] SCHENECTADY, N. Y.

The fabrication techniques by which zirconium and its alloys have been successfully made into various product forms are described. The neutron-absorption characteristics, mechanical properties, and corrosion resistance of zirconium and some zirconium alloys are discussed.

Introduction

DURING the past five to ten years, the technology and large-scale production of ductile zirconium metal has undergone a rapid development. This development has been due chiefly to interest in this metal for nuclear-reactor applications.

Zirconium has a combination of properties which particularly suit it for use as a structural material in nuclear reactors. These include a tendency to absorb relatively few neutrons, a high melting point, fair strength, and good corrosion resistance in water and liquid metals. A minimum tendency to react with and absorb neutrons is an additional characteristic required of metals to be used in the active core of reactors. It is desirable to minimize the number of neutrons absorbed parasitically in the structural components in order to conserve them for reaction with the nuclear fuel.

A measure of the suitability of a metal for use as a reactor structural material may be obtained by dividing its absorption tendency per unit volume by its yield strength per unit area. This ratio of volume absorption per unit strength should be as low as possible for reactor application. Values of this ratio for a few common alloys are given in Table 1. Zirconium is clearly better than the iron and aluminum alloys; other common metals would have higher ratios than aluminum. This comparison is based on room-temperature properties. The position of zirconium relative to the other metals will change at higher temperatures, depending on the relative variation of properties with temperature. However, the position of zirconium relative to the second-best metal, aluminum, becomes more favorable because the strength of aluminum diminishes more rapidly with increasing temperature. The use of alloy additions to strengthen zirconium makes its position even more favorable.

The cost of zirconium, even with the development of large-scale production techniques, is still rather high, being somewhat greater than that of titanium. For this reason it is considered chiefly for core use in reactor installations, where its cost can be justified on the basis of neutron economy.

With regard to both processing and properties, zirconium is similar to its sister metal, titanium. The mechanical properties of zirconium are intermediate to those of aluminum and mild steel; corrosionwise, zirconium is better than aluminum and iron, but not as good as stainless steel for certain reactor applications.

TABLE 1 COMPARISON OF VOLUME NEUTRON ABSORPTION PER UNIT STRENGTH OF ZIRCONIUM WITH OTHER COMMON ALLOYS

Material	Volume neutron absorption per unit strength ratio[c]	Value of ratio relative to zirconium
Type 347 stainless steel	7.70	29.6
1035 steel	5.25	20.2
28-O aluminum	2.66	10.2
248-T aluminum	0.42	1.6
Zirconium	0.26	1.0

[c] Ratio = $\dfrac{\text{thermal neutron cross section (barns)}^{b}}{\text{cc}} \Big/ \text{yield strength (psi) at 70 F} \times 10^{-19}$.

[b] The tendency of an element to absorb neutrons is expressed in terms of cross section (units are barns per atom = 10^{-24} cm^2) which is a measure of the probability that the atoms will capture neutrons.

The commercial sources of zirconium are zircon, a silicate found in beach sands and baddeleyite, an oxide found in lode and placer deposits. Zirconium metal, like titanium is produced by the Kroll process, in which the tetrachloride is reduced with magnesium. Hafnium, generally associated with zirconium, has a great tendency to absorb neutrons; hence this element must be removed from zirconium destined for reactor use. Separation of hafnium is done chemically prior to the reduction step. The sponge product of the reduction step may be vacuum-melted in graphite crucibles but it is generally arc-melted to ingot form to minimize contamination with carbon. Zirconium sponge can be purified further prior to melting by the iodide or hot-wire process which yields a product termed crystal bar, but for most uses the additional cost of this operation cannot be justified.

The fabrication of zirconium is not particularly difficult although certain precautions not encountered with the more common metals must be exercised. Arc-melted zirconium ingots have been fabricated successfully into most of the standard metal shapes, including plate, sheet, rod, wire, and tubing.

There are two areas in which further development will increase the usefulness of zirconium for reactor as well as for other uses; one is broader industrial know-how in handling zirconium and the other is alloy development. While a number of commercial firms have had experience in processing zirconium, broader industrial experience in fabricating shapes and forms by existing techniques is needed. This is particularly true of cold-finishing operations. Development of this know-how may of necessity be slow because the market for zirconium is small compared with that for the standard metals.

In the field of alloy development the objectives are improved high-temperature strength and corrosion resistance. This, of course, must be accomplished without sacrificing zirconium's chief attribute, its low neutron absorption. There are two types of corrosion media of interest, one water and the other liquid metals such as sodium. Resistance to corrosion in these media present two distinct problems in alloy development. The requirement of high-temperature strength is the same in both cases, although the strength is usually required at a higher temperature for applications with liquid metals.

[1] Research Associate, Knolls Atomic Power Laboratory, General Electric Company.

[2] Research Associate, Research Laboratory, General Electric Company.

Contributed by the Metals Engineering Division and presented at a joint session of the Metals Engineering and Nuclear Engineering Divisions at the Diamond Jubilee Spring Meeting, Baltimore, Md., April 18–21, 1955, of THE AMERICAN SOCIETY OF MECHANICAL ENGINEERS.

NOTE: Statements and opinions advanced in papers are to be understood as individual expressions of their authors and not those of the Society. Manuscript received at ASME Headquarters, March 24, 1955. Paper No. 55—S-43.

Fabrication of Zirconium

General. As already noted, zirconium is not difficult to fabricate; it has been processed successfully into a variety of shapes by standard metalworking techniques. However, there are some general considerations which must be taken into account in its fabrication. These include the purity or composition of the zirconium being fabricated, the tendency of zirconium to react with gases at elevated temperatures, its tendency to gall under sliding contact with other metals, and behavior related to crystal structure.

TABLE 2 TYPICAL ANALYSES AND HARDNESS VALUES FOR THREE TYPES OF ZIRCONIUM INGOT (1)

	Arc-melted crystal-bar	Arc-melted sponge	Graphite-melted sponge
Carbon, per cent.....	0.02	0.025	0.15
Oxygen, per cent.....	0.04	0.15	...
Nitrogen, per cent.....	0.001	0.004	0.005
Hydrogen, per cent.....	0.004	0.004	0.006
Ingot hardness, Bhn — 3000 kg.....	75–90	120–155	130–190

Three kinds of zirconium ingot are commonly prepared; arc-melted iodide or crystal-bar metal, arc-melted sponge, and graphite-melted sponge. These types of ingots exhibit differences in their fabrication behavior because variations in their purity result in differences in hardness and ductility. As shown in Table 2 (1),[3] arc-melted crystal-bar ingots contain the least impurities and have the lowest hardness, while sponge ingots induction-melted in graphite crucibles contain the most impurities and have the highest hardness. The variations in composition have only a minor effect on hot-working behavior, but they do affect the cold-working characteristics. In general, as hardness increases, cold-working operations become more limited and more frequent anneals are required. The addition of alloying elements tends to increase the strength of zirconium at all temperatures and to reduce ductility, particularly at room temperature. Thus alloy additions will restrict cold-working operations in the same manner as impurities and also necessitate changes in the hot-working conditions.

Zirconium reacts with the gases oxygen, nitrogen, and hydrogen at elevated temperatures and takes them into solution with resulting embrittlement. Knowledge of this behavior is important in hot-working and annealing operations. Zirconium in heavy sections may be heated in oil, gas, or muffle furnaces and hot-worked in air since, for moderate heating times, the contaminated layer will be only a few mils thick and can, if required, be removed later by machining. However, use of such practice for thin sections is impractical if the contaminated layer becomes an appreciable fraction of the cross section. Time at temperature for such operations must be kept to a minimum, especially at temperatures above 1550 F, where the rate of gas absorption becomes more rapid. Inert-gas furnace atmospheres, salt-bath or lead-bath heating, and copper or mild-steel jackets are used frequently to reduce contamination during hot-working. Heating in atmospheres containing hydrogen should be avoided since small amounts of hydrogen cause serious embrittlement under certain conditions of heat-treatment.

Short-cycle heating in air can be used for annealing zirconium during cold-working if the section thickness is such that a thin contaminated layer will not affect its usefulness or if the contaminated zone can be removed. However, the use of vacuum annealing is preferred for assuring good-quality cold-finished products, and it is essential for thin sections. Annealing temperatures range from 1000 to 1550 F, with the higher temperatures being used for shorter heating times and for alloys.

[3] Numbers in parentheses refers to the Bibliography at the end of the paper.

Zirconium has a tendency to gall when in sliding contact with other metals. This behavior creates lubrication problems in hot extrusion and in cold-working operations such as tube and wire-drawing. Techniques have been developed for minimizing this effect.

The crystal structure of zirconium is close-packed hexagonal like that of titanium and magnesium. For this reason, zirconium does not appear to be as ductile in some types of cold-forming operations as cubic metals such as iron and copper; however, it is generally much easier to fabricate than magnesium. A high degree of preferred orientation is also generated during cold-working because of the limited slip systems of the hexagonal structure. The degree of orientation can be minimized by reducing the amount of cold work between anneals. Zirconium transforms from the hexagonal to a body-centered cubic structure at 1585 F, but the transformation has no effect on the hot-working characteristics in this temperature range.

Hot-Working. Zirconium ingots are produced in sizes from $2^1/_2$ to 12 in. diam with ingot weights ranging from 10 to 500 lb. Initial hot-working of the larger ingots has been done by forging; the smaller ingots have been worked initially by forging, rolling, or extrusion.

Slabs or round billets can be forged readily from the ingots on either press or hammer-forging equipment. Center bursting is seldom encountered even when the round ingots are converted into round billets. Forging is done in the temperature range from 1100 to 1800 F, with the lower end of the range being used for crystal-bar ingots and the higher end of the range for alloys. Ingots usually are handled bare with the heating and forging time being kept as short as possible to minimize contamination. Small billets occasionally are jacketed in copper or mild steel to protect the zirconium from oxidation during forging. Higher-purity scrap is produced in the subsequent machining of such forgings; however, it is questionable whether this gain offsets the cost of jacketing. It would be impractical to attempt the jacketing of large ingots for forging. Strip and plate with thicknesses of $^3/_{16}$ in. and greater can be hot-rolled from both small ingots and forged slabs. If required, the starting slabs or ingots are surface-conditioned prior to rolling. Protective sheaths or jackets are sometimes used in hot-rolling strip; the sheath-rolling of slabs frequently can be accomplished in the jacket applied prior to forging. Although the thickness of the sheath-rolled metal will vary more than that of bare-rolled stock, the former generally requires less surface cleaning after rolling. The temperature range for rolling is similar to that for forging except that the top temperature normally is kept below the zirconium transformation temperature.

Small ingots and forged billets can be hot-rolled in grooved rolls. Slabs and bars have not been fabricated from large ingots by grooved rolling because the ingot length and quantities of material involved make forging more practicable. However, those familiar with the fabrication of zirconium believe that the breakdown of large ingots by rolling would be feasible.

Rod and tubing are widely produced by extrusion, and in a few cases special shapes have been extruded successfully. To date these products have been extruded from ingots and forged billets 2 to 7 in. diam using reduction ratios of 10 to 1 to 100 to 1 and billet temperatures ranging from 1300 to 1825 F. Billet temperatures generally are raised toward the high end of the range as the reduction ratio and the strength of the material being extruded are increased. Where dimensional control and surface quality are important, worked billets are preferred to the as-melted ingots.

Good surface quality in the extruded product is the principal problem in the extrusion of zirconium. Because zirconium tends to stick to the die with resultant galling, special lubricants are required to give a satisfactory surface. Both molten glass, i.e.,

the Ugine-Sejournet process, and copper jackets are used for this purpose; however, copper has been more widely applied than glass. The cost of jacketing extrusion billets in copper is readily justified since the jacket serves the dual purpose of lubrication and minimizing contamination of the zirconium during heating and working. By proper application of this technique, it is possible to produce rod and tubing with surfaces which require no conditioning prior to cold fabrication other than removal of the copper jacket by pickling; however, some mechanical surface conditioning is normally done. When extruding tubing by this technique, the center hole is machined in the billet, and this opening is also lined with copper. Sections of tubing and rod extruded from copper-jacketed billets are shown in Fig. 1.

FIG. 1 ZIRCONIUM SECTIONS EXTRUDED FROM COPPER-JACKETED BILLETS

The extrusion constant[4] for copper-jacketed zirconium billets varies from 20,000 to 30,000 psi for reduction ratios of 10 to 1 to 125 to 1 and for temperatures of 1300 to 1650 F as listed in Table 3. One disadvantage of copper jacketing is that the maximum billet temperature must be limited to about 1500 F because a copper-zirconium eutectic reaction results in melting at 1600 F. The maximum billet temperature can be increased by using a steel liner between the zirconium and the copper jacket.

Initial attempts to extrude zirconium with salt or glass lubricants yielded a product with a rough surface. With improvements in the process, good-quality extruded products have been made; however, the extruded surfaces require mechanical conditioning if the products are to be cold-finished. The glass, in addition to serving as a lubricant, also tends to prevent contamination of the zirconium although not as effectively as a copper jacket. In the glass extrusion of tubing to date, the center holes in the billets have been made by machining. Recently, zirconium cylinders have been pierced successfully in a closed-end die using glass lubrication. When perfected, piercing should result in considerable savings in the preparation of billets for the extrusion of tubing.

Cold Fabrication. Flat products, sheet, strip, and foil, are easily fabricated from zirconium by cold-rolling. One of the unusual characteristics of this hexagonal metal is the amount of reduction that can be made in flat-rolling without annealing. Crystal-bar zirconium and good-quality sponge zirconium plate can be cold-rolled from 1/4 to 0.001-in-thick foil without intermediate anneals. Although edge-cracking may occur after 50 to 70 per cent reduction, the cracks do not tend to propagate, and if the shearing losses at final size can be tolerated, rolling can be continued. However, to minimize edge-cracking and preferred orientation, intermediate anneals are used after each 40 to 50 per cent reduction in area for crystal-bar metal; more frequent anneals are required for sponge metal and for alloys.

[4] Extrusion constant $= \dfrac{\text{pressure on billet}}{\log_e\left(\dfrac{\text{original area}}{\text{final area}}\right)}$.

TABLE 3 EXTRUSION CONSTANTS FOR ARC-MELTED ZIRCONIUM

Type of zirconium	Extruded form	Billet temp, deg F	Extrusion ratio	Extrusion constant,[a] psi
Crystal bar..	3/8-in. rod	1292	22–1	21600
Sponge.....	3/8-in. rod	1472	22–1	20600
Zircaloy-2...	3/8-in. rod	1575	126–1	22800
Crystal bar..	1 1/2 × 1 1/2-in. tube	1472	23–1	25800
Sponge.....	2 × 1 1/2-in. tube	1472	7.5–1	22000
Zircaloy-2...	2 1/2 × 2 1/2-in. tube	1575	35–1	31000

[a] Extrusion constant $= \dfrac{\text{extrusion pressure, psi.}}{\left(\log_e \dfrac{\text{original area}}{\text{final area}}\right)}$

Cold-finished rods from 1/4 to about 3/4 in. diam are fabricated by cold-rolling or cold-swaging larger hot-worked rods. Reductions of 10 per cent or less per pass are used in rolling; 15 per cent reductions are used in swaging. If large cold reductions are made, the rods are annealed after each 30 to 50 per cent reduction. Zirconium crystal bars can be converted to round rod by cold-swaging or rolling; however, to prevent defects in the final rod the rough surface of the crystal bars must be conditioned before rolling. These bars exhibit remarkable ductility in that it is possible to cold-work them in excess of 99 per cent reduction in area without annealing. Occasionally, rods can be cold-finished by drawing but for small quantities swaging is preferred because the lubrication problem in drawing is avoided.

Wire can be prepared from zirconium by cold-swaging and by cold-drawing. In drawing zirconium, normal lubricants are inadequate for preventing die seizure and resultant galling; hence special lubrication techniques are needed. Either of two methods is used, special lubricants or a special base plus more conventional lubricants. A lacquer-molybdenum disulphide mixture or copper has served as the lubricant while an oxidized surface or phosphate coatings have been used as a base for conventional lubricants. To obtain good surface quality in the drawn wire frequently is a problem since removal of the lubricant bases or relatively thick lubricants may leave a rough, or, in the case of the oxide, a contaminated surface. Although swaging is a more tedious and expensive method, it produces wire with good surface quality and there is no lubrication problem. For this reason, swaging is preferred for small quantities of wire larger than 0.030 in. diam. In both cold-drawing and cold-swaging of wire, reductions are made in increments of 10 to 20 per cent per pass with intermediate anneals after total reductions of 30 to 50 per cent.

Seamless zirconium tubing can be cold-finished from extruded starting tubes by tube-reducing, drawing, and a combination of the two methods. Starting tubes from 7/8 to 2 1/2 in. diam can be tube-reduced successfully using conventional tooling. Tube reduction provides a simultaneous reduction in wall thickness and diameter as the metal is worked between oscillating taper-grooved rolls and a tapered mandrel. Maximum single-pass reductions range from 50 per cent for zirconium alloys to 85 per cent for crystal-bar zirconium. Zirconium tubes with internal ribs parallel to the tube axis can be fabricated by tube-reducing over a grooved mandrel; however, a ribbed starting tube is required to yield a sound product. Internally ribbed stainless and mild-steel tubing can be tube-reduced by this technique from uniform, heavy-walled starting tubes, but in tube-reducing a uniform-wall zirconium tube, cracking occurs as a result of the different flow rates between the rib and wall metal. Thus, in this particular operation, zirconium appears to be less ductile than mild steel, even though it exhibits the ductility of high-purity iron in other cold-fabrication operations.

Tubing as small as 0.080 in. diam × 0.010 in. wall can be cold-drawn from extruded and tube-reduced or extruded starting tubes. Tube-drawing of zirconium, like wire-drawing, is difficult because of the die-seizure problem. All of the lubricants used for wire-drawing have been applied to the drawing of tubes, but

the largest quantity of tubing has been drawn using a phosphate coating and conventional lubricants. Even with the special lubrication procedures, drawing is done principally with rod mandrels; most attempts to draw with plug mandrels have been unsuccessful. A combination sink and iron pass giving a 20 to 30 per cent reduction in cross-sectional area is commonly used with an anneal after each pass. Separate sinking and ironing passes also can be applied successfully. A few attempts have been made to draw large-diameter thin-walled tubing. With sponge zirconium, 20-mil wall is about the minimum that can be achieved at tubing diameters of 1 to $1^1/_2$ in.

Welded zirconium tubing can be produced from strip by roll-forming and inert-arc welding. Tubing $^1/_2$ to $1^1/_2$ in. diam can be fabricated on continuous mills of this type. If such material is to be used in high-temperature water, care must be exercised in welding to prevent air contamination of the weld metal with resultant loss in corrosion resistance and ductility.

Other types of cold-forming operations which have been applied to zirconium include deep-drawing, impact extrusion, bending, flanging, shearing, slitting, and blanking. Sponge zirconium cans 1 in. diam × 8 in. deep × 0.015 in. wall have been deep-drawn with conventional tooling (2). Intermediate annealing between draws was done in a salt bath, and it was found that the adherent oxide film formed in annealing served as an excellent base for the commercial wax lubricants.

In one group of experiments (3) on impact extrusion of crystal-bar zirconium, the best success was achieved by impacting copper or aluminum-clad pieces at 600 to 900 F. Cans 8 in. long with a $^1/_{16}$-in. wall were made with these conditions. Successful experimental impact extrusions at room temperature have been reported. For bending operations, the surface condition of the sheet or strip is of utmost importance since it affects markedly the minimum bend radius. A slight amount of surface contamination during annealing can raise the bend radius of 0.035-in. sheet from $^1/_{16}$ to $^1/_2$ in. or more, even though the tensile ductility remains essentially unchanged. Such contamination can occur by improper vacuum-annealing as well as in air-annealing. Cutting operations such as shearing present no particular problems.

Zirconium samples, cold-finished by several different techniques, are shown in Fig. 2.

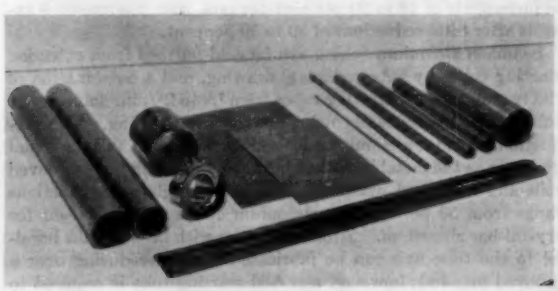

FIG. 2 COLD-FINISHED ZIRCONIUM PRODUCTS
(*Left to right*, deep-drawn thimble, tube-reduced tubing, flanged tube, roll-formed tube, 0.035-in. sheet, 0.0002-in. foil, six sizes of cold-drawn tubing.)

Machining. Zirconium may be machined by all of the standard operations. Its general machining characteristics are similar to those of titanium. It has a tendency to gall, which is analogous to aluminum for soft crystal-bar metal and to stainless for harder alloys. Therefore tools must be kept sharp, and light and interrupted cutting should be avoided. Since the oxide of zirconium is abrasive, it should be removed prior to machining to prevent rapid dulling of the tools.

Fine turnings of zirconium will burn if heated slightly. Under certain conditions the burning can be explosive. This is a further reason for using sharp tools and for not taking fine cuts. Water-soluble cutting oils are desirable to avoid the possibility of oil fires. Also, large quantities of chips should not be allowed to accumulate in the machines.

Zirconium tubing can be surface-conditioned by wet-belt grinding. Where lubricant coolants are used for this operation, it is essential that they be the water-soluble type.

Welding and Brazing. Zirconium is easily welded by the inert-arc technique; both helium and argon have been used successfully as the protective gases. Sound welds can be obtained by inert-arc welding in air, but to obtain welds with best ductility and optimum corrosion resistance, welding in a gastight box with a highly purified inert gas is desirable. This is particularly true for welds in plate. Most of the welding experience to date has been on material up to about $^1/_4$ in. thick.

Resistance spot and resistance seam welds can also be used successfully to join zirconium sheet.

Brazed joints may be made on zirconium with either copper or silver using a vacuum, an inert atmosphere, or special fluxes during heating. The amount of brazing alloy must be kept to a minimum to prevent excessive reaction with the zirconium.

Soft-soldering of zirconium by conventional methods has also been accomplished (4) after first applying an immersion coating of zinc from a molten zinc-chloride bath.

ALLOY DEVELOPMENT

Properties of Unalloyed Zirconium. High-purity or crystal-bar zirconium is considerably weaker, more ductile, and more corrosion-resistant than the early sponge product. However, the purity of sponge zirconium has increased significantly with improvements in processing and the difference in properties between crystal-bar and sponge-process material has greatly decreased. The tensile properties of the two kinds of zirconium are given in Table 4. The strength of zirconium has been shown to increase with decreasing grain size, increasing strain rate, increasing preferred orientation, and increasing strain (5).

TABLE 4 ROOM-TEMPERATURE MECHANICAL PROPERTIES OF ANNEALED ZIRCONIUM

Property	Crystal-bar zirconium	Sponge zirconium
Ult tens strength, psi	24000–43000	42000–62000
0.2% offset YS, psi	7700–26000	25000–38000
Elongation, per cent	24–54	23–40
Reduction in area, per cent	25–75	27–60
Modulus of elasticity, psi	$13.1–13.9 \times 10^6$	$13.6–14 \times 10^6$
Hardness (Vhn)	73–130	120–160
Charpy impact str (ft-lb)	2.5–75	14–16

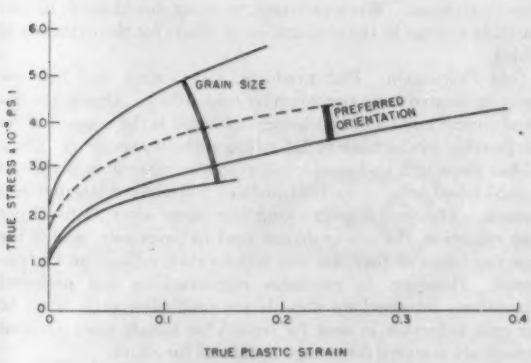

FIG. 3 TRUE-STRESS TRUE-STRAIN CURVES SHOWING RANGE OF VALUES RESULTING FROM CHANGES IN GRAIN SIZE AND IN PREFERRED ORIENTATION IN UNALLOYED ZIRCONIUM

Fig. 3 shows the spread in true-stress true-strain curves with varying grain size and preferred orientation. These values were obtained for crystal-bar zirconium at room temperature at a strain rate of 0.09 min^{-1}. Spreads of similar magnitude can be expected in curves for arc-melted crystal-bar and arc-melted sponge zirconium. It is of interest that 0.2 per cent offset yield strengths (approximately the strength at 0.002 true strain) can be changed by about a factor of 2 by varying the grain size or preferred orientation. The strength of unalloyed zirconium drops off rapidly with increasing temperature.

The impact strength of zirconium is influenced by impurities; when impurities are kept at a low level, zirconium remains ductile to very low temperatures. Resistance to impact also is affected by preferred orientation (6, 7). Mudge (6) has shown that the low-temperature impact strength is much lower if the notch of the test specimen is parallel to the original rolling plane than if the notch was perpendicular to the original rolling plane, as shown in Figs. 4 and 5.

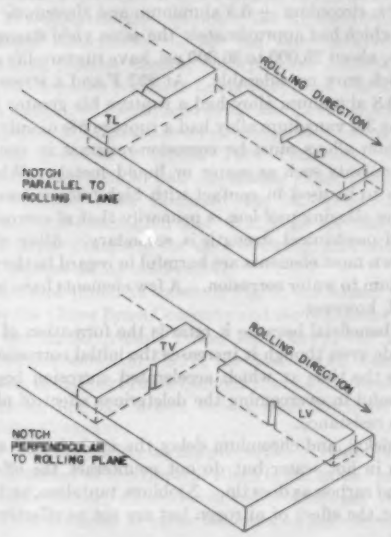

Fig. 4 Relation of Impact Specimen and Notch Orientation to Original Zirconium Sheet for Curves in Fig. 5

Unalloyed zirconium, either crystal-bar or sponge materials, is not very resistant to deformation by creep. A secondary creep rate of 1 per cent in 1000 hr is to be encountered for a stress of 49,900 psi at room temperature (8) and minimum creep rates of 8×10^{-6} to 4×10^{-3} hr^{-1} are obtained for stresses of 7000 to 10,000 psi at 932 F.

The most significant aspect of the creep behavior of unalloyed zirconium is the relatively large amount of "instantaneous" creep strain that occurs as the load is applied. Once the load is applied and this early strain is obtained, the strain-time curve flattens out and the rate of extension is very small. The creep behavior of unalloyed zirconium is also very sensitive to stress. A decrease of only a few thousand lb per sq in. increases the rupture life from a few hours to greater than a thousand hours.

The corrosion of unalloyed zirconium (9) is characterized by a period wherein the corrosion rate is low, followed by a period of more rapid corrosion. The kinetics of the reaction are a function of temperature, and the length of the initial period of low-corrosion rate depends strongly on impurities and surface condition. Cold-work and metallurgical structure do not affect the corrosion of pure zirconium markedly. Impurities in the water are much less important than impurities in the metal.

The initial period of the reaction between zirconium and water at elevated temperature can be described by the equation

$$\Delta m = kt^n$$

where Δm is the weight gain, t is the time, and k and n are constants. During the initial period when n is less than $1/2$, a thin adherent film, which is black or exhibits interference colors, forms on the zirconium, providing some protection. Later, a white, nonadherent corrosion product begins to form, and the new rate law is believed to be linear ($n = 1$).

Impurities such as nitrogen, carbon, and aluminum decrease the corrosion resistance, as do sufficiently large amounts of oxygen, calcium, magnesium, chlorine, and silicon.

Properties of Alloyed Zirconium. The purpose of alloying zirconium is to obtain improved elevated-temperature strength and corrosion resistance while maintaining low neutron absorption. Neutron absorption is predictable as this is a function of the atoms themselves and can be calculated from the composition of the

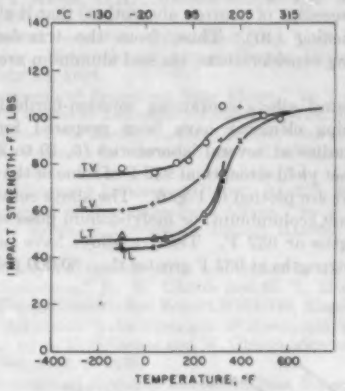

Fig. 5 Impact Strength Versus Temperature for Arc-Melted Crystal-Bar Zirconium—After Mudge (6)

alloy. To maintain low neutron absorption, it is only necessary to avoid alloying with elements having a high neutron absorption such as hafnium, tantalum, and tungsten. The thermal neutron-absorption cross sections of many of the possible alloying elements is shown in Table 5.

The problems of alloying zirconium to obtain increased high-temperature strength are somewhat analogous with those of titanium, except that there is less opportunity for solid-solution strengthening because zirconium has such a comparatively large atom size. This means that with the exception of a small number of elements (oxygen, nitrogen, titanium, hafnium, niobium, tin, and aluminum) strengthening is obtained through the presence of particles of a second phase, usually a compound of zirconium and the element added.

The design of zirconium alloys with high strength at elevated temperatures is complicated by the dimensional and mechanical instability associated with the transformation of zirconium from the hexagonal close-packed phase to a body-centered cubic structure at approximately 1585 F. This transformation limits the maximum useful temperature of zirconium and its alloys. Most elements either lower or do not affect appreciably the transformation temperature. The particle-forming elements which are only slightly soluble in the hexagonal close-packed phase compose most of this group. The solution-strengthening elements just listed, with the exceptions of titanium and niobium,

TABLE 5 NEUTRON CROSS SECTIONS OF ZIRCONIUM AND POSSIBLE ALLOYING ADDITIONS

Element	Barns	Element	Barns	Element	Barns
Low Cross Section (Less than 1.0 barn)					
Oxygen	0.0002	Silicon	0.13	Hydrogen	0.33
Carbon	0.0045	Lead	0.17	Calcium	0.43
Beryllium	0.009	Zirconium	0.18	Sodium	0.49
Bismuth	0.032	Phosphorus	0.19	Sulphur	0.49
Magnesium	0.059	Aluminum	0.22	Tin	0.65
Medium Cross Section (1.0 to 10.0 barns)					
Zinc	1.1	Iron	2.4	Copper	3.6
Niobium	1.1	Molybdenum	2.4	Nickel	4.5
Barium	1.2	Gallium	2.7	Tellurium	4.5
Strontium	1.2	Chromium	2.9	Vanadium	4.7
Nitrogen	1.8	Thallium	3.3	Titanium	5.6
Germanium	2.3			Antimony	6.4
Large Cross Section (Greater than 10 barns)					
Manganese	13	Silver	60	Iridium	440
Tungsten	19	Lithium	67	Boron	750
Tantalum	21	Gold	94	Cadmium	2400
Chlorine	32	Hafnium	115	Samarium	6500
Cobalt	35	Mercury	380	Gadolinium	44000

raise the temperature of this transformation, increasing the useful temperature range of the alloys. Oxygen and nitrogen do not greatly strengthen zirconium at temperatures much above 572 F and are not generally considered as useful strengthening elements for elevated temperatures. Hafnium is so much like zirconium (with the exception of neutron absorption) that it aids very little in strengthening (10). Thus, from the transformation and strengthening considerations, tin and aluminum are logical alloy additions.

Experimental alloys containing solution-hardening and particle-hardening elements have been prepared for mechanical property studies at several laboratories (6, 10 to 20). The 0.2 per cent offset yield strength at 932 F of some of the experimental binary alloys are plotted in Fig. 6. The alloys containing aluminum, niobium (columbium) or molybdenum possess the greatest yield strengths at 932 F. Ternary alloys have been produced with yield strengths at 932 F greater than 50,000 psi, all of which

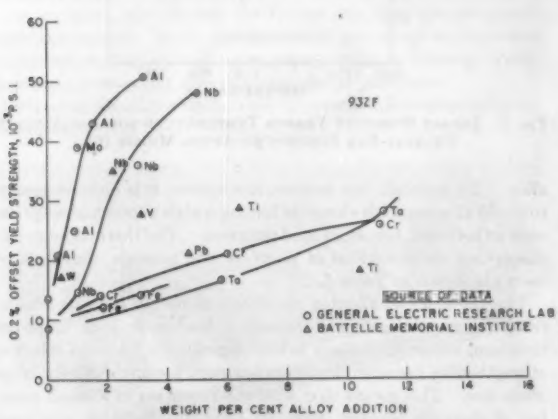
0.2% OFFSET YIELD STRENGTH, 10³ P.S.I.
WEIGHT PER CENT ALLOY ADDITION
932 F
SOURCE OF DATA
○ GENERAL ELECTRIC RESEARCH LAB
△ BATTELLE MEMORIAL INSTITUTE

FIG. 6 YIELD STRENGTH AT 932 F VERSUS ALLOY CONTENT FOR A NUMBER OF ZIRCONIUM-BASE ALLOYS

contain aluminum. Three of these, 92.6 zirconium–5.1 titanium–2.3 aluminum, 93.5 zirconium–3.3 titanium–3.2 aluminum, and 94.7 zirconium–3.5 titanium–1.8 aluminum, contain titanium (21, 22), and three, 93.7 zirconium–0.9 aluminum–5.4 molybdenum, 97.4 zirconium–1.5 aluminum–1.1 molybdenum, and 89.4 zirconium–0.9 aluminum–9.7 tantalum contain molybdenum or tantalum (23, 24). From these results it is apparent that strengthening zirconium at temperatures up to 932 F is not too difficult. Combining high strength with good corrosion resistance and low neutron absorption is considerably more complex.

Yield strengths are obtained from short-time tests and do not necessarily reflect the long-time (creep or creep-rupture) strength of the material. Evidence of this lack of correspondence has already been encountered (25) in experimental zirconium alloys. The alloys, zirconium + 0.8 aluminum and zirconium + 3.2 vanadium, which had approximately the same yield strength at 932 F, that is, about 25,000 to 30,000 psi, have rupture-life characteristics which vary considerably. At 932 F and a stress of 10,000 psi, the 0.8 aluminum alloy had a rupture life greater than 1170 hr and the 3.2 vanadium alloy had a rupture life of only 277 hr.

Zirconium alloys must be corrosion-resistant in contact with various coolants such as water or liquid metals. Where zirconium has to be used in contact with high-temperature water or steam, the alloying problem is primarily that of corrosion resistance, and mechanical strength is secondary. Alloy studies (9) have shown most elements are harmful in regard to the resistance of zirconium to water corrosion. A few elements have been found beneficial, however.

Tin is beneficial because it retards the formation of the white flaky oxide even though it increases the initial corrosion rate and decreases the time at which accelerated corrosion begins. Tin is also useful in overcoming the deleterious effect of nitrogen on corrosion resistance.

Iron, nickel, and chromium delay the initiation of accelerated corrosion in hot water but do not counteract the effects of nitrogen and carbon as does tin. Niobium, tantalum, and antimony also offset the effect of nitrogen but are not as effective as tin in doing so.

Most other alloying elements such as silicon, titanium, uranium, aluminum, cadmium, cerium, lanthanum, magnesium, manganese, neodymium, palladium, zinc, gallium, and vanadium, are harmful in respect to the corrosion resistance.

Zircaloy-2, a complex zirconium alloy containing tin, iron, nickel, and chromium (9) is used because of its ability to delay

TABLE 6 MECHANICAL PROPERTIES OF ZIRCALOY-2

	Room temperature	500 F
0.2% yield strength,[a] psi	44500	
Reduction in area,[a] per cent	28.4	
0.2% YS,[b] long, psi	49400	24400
0.2% YS,[b] trans, psi	70000	34100
Reduction in area,[b] long, per cent	28.3	42.2
Reduction in area,[b] trans, per cent	37.1	52.4

	−310 F	32 F	212 F	392 F	572 F
Impact strength (ft-lb)[c]	4	6	7	17	91

Creep properties at 650 F:

Stress, psi	Minimum creep rate, in/in/hr	Intercept strain, per cent
19000	1.95×10^{-4}	1.32
21000	5.86×10^{-4}	1.96
24600	2.96×10^{-3}	4.15
27200	6.1×10^{-3}	16.1
Endurance limit at 600 F		27500–28000 psi

[a] Annealed 20 hr at 1382 F and furnace-cooled.
[b] Annealed 10 min at 1550 F.
[c] Heat-treated 1 hr at 1850 F, water-quenched, and aged 3 hr at 600 F, followed by slow cooling.

the formation of flaky corrosion product. High-purity zirconium also may have an extended period before accelerated corrosion occurs, but because of its sensitivity to impurities, it is not as consistent in its corrosion behavior.

Zircaloy-2 combines good corrosion resistance, low neutron absorption, and improved mechanical strength. Its mechanical properties (13) are listed in Table 6.

Little or no impact data are available for many of the zirconium alloys. Mudge (6) has reported that zirconium-2.5 per cent tin alloys can remain ductile to very low temperatures, although hydrogen and its distribution can affect ductility adversely. Zircaloy-2 impact data are given in Table 6.

Acknowledgments

Much of the information on the fabrication of zirconium is based on experience at the Knolls Atomic Power Laboratory, operated for the Atomic Energy Commission by the General Electric Company under Contract No. W-21-109 Eng-52. However, the considerable experience of other similar laboratories also has been used in summarizing the status of the various forming techniques. These laboratories include the Westinghouse Atomic Power Division, Nuclear Metals, Incorporated, Battelle Memorial Institute, Argonne National Laboratory, and the Bureau of Mines. A number of commercial firms also have contributed to the development of information on zirconium fabrication. These firms include Babcock & Wilcox Tube Company, Allegheny Ludlum Steel Corporation, and the Chase Brass Company for extrusion; Superior Tube Company for tube-reducing, tube-drawing, and roll-forming; Yoder Company for roll-forming; Bridgeport Brass Company for deep-drawing; and Metals and Controls Corporation for cold-rolling.

Of the extruded products shown in Fig. 1, the largest tube was extruded by the Chase Brass Company and the remainder were extruded at the Knolls Atomic Power Laboratory. Of the cold-finished products shown in Fig. 2, the deep-drawn thimble was obtained from Bridgeport Brass Company, while the tube-reduced, the roll-formed, and the drawn tubing were fabricated by the Superior Tube Company.

Much of the information on the properties of zirconium and its alloys was obtained at the General Electric Research Laboratory for the Atomic Energy Commission under Contract W-31-109-Eng-52. Data obtained at other laboratories are referenced.

BIBLIOGRAPHY

1 Zirconium and Zirconium Alloys—"Fabrication of Zirconium," by R. B. Gordon and W. J. Hurford, American Society for Metals, Cleveland, Ohio, 1953, p. 133.

2 Private Communication by R. S. French. (Pertinent data may be obtained from authors.)

3 "The Forming of Zirconium by Impact Extrusion," by W. G. Rausch, Argonne National Laboratory Report ANL 5286, September 15, 1954.

4 "How to Braze and Solder Zirconium," by W. G. Schickner, J. G. Beach, and C. L. Faust, *Steel*, vol. 132, 1952, p. 118.

5 "The Tensile Characteristics of Unalloyed Zirconium at Low and Moderate Temperatures," by J. H. Keeler, Trans. ASM, vol. 47, 1954, Preprint No. 5.

6 Zirconium and Zirconium Alloys—"Effect of Hydrogen on the Embrittlement of Zirconium and Zirconium-Tin Alloys," by W. L. Mudge, Jr., American Society for Metals, Cleveland, Ohio, 1953.

7 "Zirconium Alloy Investigations," by S. M. Shelton, U. S. Bureau of Mines Report 11, Summary of Progress, March 15, 1950–March 15, 1952, BM11–33, Albany, Oregon.

8 "Creep Properties of Annealed Unalloyed Zirconium," by M. J. Manjoine and W. L. Mudge, Jr., American Society for Testing Materials, 1954, Preprint No. 106a.

9 "Corrosion of Zirconium and Its Alloys in High-Temperature Water," by D. E. Thomas, Westinghouse Atomic Power Division Report WAPD-T-186, June 17, 1954.

10 "Ten Zirconium Alloys Evaulated," by F. B. Litton, *Iron Age*, vol. 167, April 5, 1951, pp. 95–99.

11 "A Preliminary Survey of Zirconium Alloys," by C. T. Anderson, E. T. Hayes, A. H. Roberson, and W. J. Kroll, U. S. Bureau of Mines Report of Investigations 4658, U. S. Department of the Interior, March, 1950.

12 "Constitution and Mechanical Properties of Zirconium-Iron Alloys," by E. T. Hayes, A. H. Roberson, and W. L. O'Brien, Trans. ASM, vol. 43, 1951, pp. 888–904.

13 "Mechanical Properties of Zircaloy-2," by W. L. Mudge, Jr., and F. Forscher, Westinghouse Atomic Power Division Report WAPD-101, July 23, 1954.

14 "Development of Zirconium-Base Alloys," by J. H. Keeler, General Electric Research Laboratory Report RL-714, July 5, 1952.

15 "Development of Zirconium-Base Alloys," by J. H. Keeler, General Electric Research Laboratory Report RL-868, April 5, 1953.

16 "Development of Zirconium-Base Alloys," by J. H. Keeler, General Electric Research Laboratory Report RL-928, July 5, 1953.

17 "Development of Zirconium-Base Alloys," by J. H. Keeler, General Electric Research Laboratory Report RL-980, October 5, 1953.

18 "The Effects of Chromium, Iron and Nickel on the Mechanical Properties of Zirconium," by W. Chubb and G. T. Muehlenkamp, U. S. Atomic Energy Commission Report BMI-938, August 11, 1954.

19 "Small Additions Raise Strength of Zirconium at Elevated Temperatures," by A. D. Schwope and W. Chubb, *Journal of Metals*, vol. 4, November, 1952, p. 1138.

20 "The Strength of Wrought Zirconium-Base Binary Alloys at 1800° and 2200° F," by H. A. Saller, J. T. Stacy, and S. W. Porembka, Trans. ASM, vol. 47, 1955, Preprint 37.

21 "Development of Zirconium Alloys for High-Temperature Service," by W. Chubb, G. T. Muehlenkamp, and A. D. Schope, Battelle Memorial Institute Report BMI-885, November 1, 1953, unpublished.

22 "Mechanical Properties of Ternary Zirconium Alloys," by A. D. Schope and W. Chubb, Battelle Memorial Institute Report BMI-818, April 23, 1953, unpublished.

23 "Development of Zirconium-Base Alloys," by J. H. Keeler, General Electric Research Laboratory Report RL-1071, April 5, 1954.

24 "Development of Zirconium-Base Alloys," by J. H. Keeler, General Electric Research Laboratory Report RL-1124, July 5, 1954.

25 "Development of Zirconium Alloys for High-Temperature Use," by W. Chubb, G. T. Muehlenkamp, and A. D. Schope, Battelle Memorial Institute Report BMI-808, February 1, 1953, unpublished.

Laminar Free Convection From a Vertical Plate With Uniform Surface Heat Flux

By E. M. SPARROW[1] and J. L. GREGG,[1] CLEVELAND, OHIO

An exact solution of the laminar boundary-layer equations for free convection from a vertical plate having uniform surface heat flux has been obtained. Heat-transfer parameters have been calculated for Prandtl numbers in the range 0.1 to 100. The results have been extrapolated to a Prandtl number of 0.01.

Experimental results are compared with the theory and the agreement is found to be good. Heat-transfer results obtained from the von Kármán-Pohlhausen method also are shown to be in good agreement with those from the exact solution. It is demonstrated that when average Nusselt numbers are calculated for a plate with uniform surface heat flux using the temperature difference halfway along the height, the results are very close to those for a uniform temperature plate.

Nomenclature

The following nomenclature is used in the paper:

C_1 = dimensional constant, $\left(\frac{g\beta q}{5k\nu^2}\right)^{1/5} = \left(\frac{\mathrm{Gr}_x^*}{5x^4}\right)^{1/5}$, $\mathrm{ft}^{-1/5}$

C_2 = dimensional constant, $\left(\frac{5^4 g\beta q\nu^2}{k}\right)^{1/5} = \nu\left(\frac{5^4\mathrm{Gr}_x^*}{x^4}\right)^{1/5}$, $\frac{\mathrm{ft}^{4/5}}{\mathrm{sec}}$

c_p = specific heat at constant pressure, Btu/lb deg F

$F(\eta)$ = velocity function, dimensionless

g = acceleration of gravity, ft/sec^2

h_x = local heat-transfer coefficient, Btu/hr sq ft deg F

$\bar{h}$ = average heat-transfer coefficient, Btu/hr sq ft deg F

Gr_x^* = modified Grashof number based on x, $g\beta qx^4/k\nu^2$, dimensionless

Gr_L^* = modified Grashof number based on L

Gr_L = Grashof number based on L, $\frac{g\beta(t_w - t_\infty)L^3}{\nu^2}$, dimensionless

k = thermal conductivity, Btu/hr ft deg F

L = length of plate over which the flow is laminar, ft

Nu_x = local Nusselt number, $h_x x/k$, dimensionless

$\overline{\mathrm{Nu}}$ = average Nusselt number, $\bar{h}L/k$, dimensionless

Pr = Prandtl number, $\nu/\alpha = c_p\mu/k$, dimensionless

q = heat-flux rate, Btu/hr sq ft

q_{x_j} = heat-flux rate at x_j, Btu/hr sq ft

t = static temperature, deg F

t_w = wall temperature, deg F

t_∞ = ambient temperature, deg F

u = velocity component in x-direction, ft/sec

v = velocity component in y-direction, ft/sec

x = co-ordinate measuring distance along plate from leading edge, ft

y = co-ordinate measuring normal distance from plate, ft

α = thermal diffusivity, ft^2/sec

β = coefficient of thermal expansion, $-\frac{1}{\rho}\left(\frac{\partial\rho}{\partial t}\right)_p$, deg F^{-1}

η = similarity variable, $\frac{C_1 y}{x^{1/5}} = \frac{y}{x}\left(\frac{\mathrm{Gr}_x^*}{5}\right)^{1/5}$, dimensionless

θ = temperature variable, $\frac{C_2(t_\infty - t)}{\frac{x^{1/5}q}{k}}$, dimensionless

μ = absolute viscosity, lb/ft sec

ν = kinematic viscosity, ft^2/sec

ρ = density, lb/ft^3

ψ = stream function, ft^2/sec

Introduction

Laminar free convection from vertical surfaces (flat plates and cylinders) has been studied extensively when the temperature of the surface is uniform. The case of uniform heat-flux rate at the surface, which is sometimes approximated in practical applications, has received considerably less attention. Sparrow[2] presents an analysis for specific longitudinal variations of surface temperature and of surface heat-flux rate using the von Kármán-Pohlhausen method. Results for the case of uniform surface heat flux are given. Experimental data for free convection heat transfer to air from a vertical aluminum sheet through which an electric current is passing have been reported by Dotson.[3] Experiments on free convection to water and mercury from vertical plates heated by electrical resistance elements have been described by Saunders.[4]

In the present analysis, an exact solution of the differential equations of the laminar boundary layer is obtained for uniform heat-flux rate at the surface of a vertical flat plate. The partial differential equations expressing conservation of momentum, mass, and energy were transformed into ordinary differential equations, which were solved numerically for Prandtl numbers of 0.1, 1, 10, and 100. Heat-transfer parameters were derived and compared with those obtained by Sparrow,[2] by the less exact von Kármán-Pohlhausen method, as well as with experimental data. Temperature and velocity profiles are presented.

It is expected that results derived for a vertical flat plate should be applicable for vertical cylinders of large diameter.

Analysis

The equations expressing conservation of mass, momentum, and energy for laminar free convection in a boundary layer are

$$\frac{\partial u}{\partial x} + \frac{\partial v}{\partial y} = 0 \qquad [1]$$

$$u\frac{\partial u}{\partial x} + v\frac{\partial u}{\partial y} = g\beta(t - t_\infty) + \nu\frac{\partial^2 u}{\partial y^2} \qquad [2]$$

[1] Lewis Flight Propulsion Laboratory, National Advisory Committee for Aeronautics.

Contributed by the Heat Transfer Division and presented at the Diamond Jubilee Semi-Annual Meeting, Boston, Mass., June 19–23, 1955, of The American Society of Mechanical Engineers.

Note: Statements and opinions advanced in papers are to be understood as individual expressions of their authors and not those of the Society. Manuscript received at ASME Headquarters, February 24, 1955. Paper No. 55—SA-4.

[2] "Laminar Free Convection on a Vertical Plate With Prescribed Non-Uniform Wall Heat Flux or Prescribed Non-Uniform Wall Temperature," by E. M. Sparrow, NACA TN 3508.

[3] "Heat Transfer From a Vertical Plate by Free Convection," by J. P. Dotson, MS thesis, Purdue University, W. Lafayette, Ind., May, 1954.

[4] "Natural Convection in Liquids," by O. A. Saunders, Proceedings of the Royal Society of London, England, series A, vol. 172, 1939, pp. 55–71.

$$u\frac{\partial t}{\partial x} + v\frac{\partial t}{\partial y} = \alpha\frac{\partial^2 t}{\partial y^2} \quad [3]$$

In accord with the usual practice in free convection, the density has been considered a variable only in formulating the buoyancy term $g\beta(t - t_\infty)$. All other properties are taken as constant. Viscous dissipation and work against the gravity field have been neglected.

Equation [2] as written applies to the case of heat transfer from the plate to the fluid in the co-ordinate system shown in Fig. 1(a). When the heat transfer is from the fluid to the plate, Equation [2] will apply in the co-ordinate system shown in Fig. 1(b), providing that a minus sign is introduced before the buoyancy term. The distinction between these two problems vanishes when the variables in Equations [1], [2], and [3] are transformed. The analysis will be carried forward for the case of heat transfer from the wall to the fluid, but the results apply to either case.

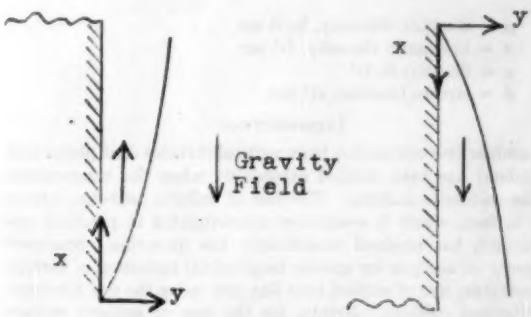

FIG. 1(a) HEAT TRANSFER FROM WALL

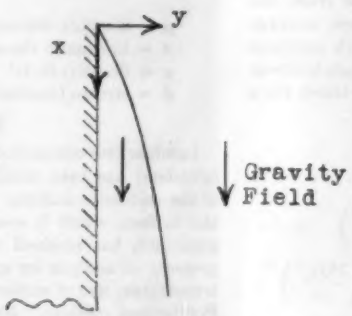

FIG. 1(b) HEAT TRANSFER TO WALL

The solution of Equation [1] can be written as usual in terms of a stream function ψ

$$u = \frac{\partial \psi}{\partial y}, \qquad v = -\frac{\partial \psi}{\partial x} \quad [4]$$

Next, the partial differential Equations [2] and [3] are transformed to ordinary differential equations by changing from the (x, y) co-ordinate system to the (x, η) system with the following substitutions

$$\eta = C_1\frac{y}{x^{1/5}} \quad [5]$$

$$F(\eta) = \frac{\psi}{C_2 x^{4/5}} \quad [6]$$

$$\theta(\eta) = \frac{C_1(t_\infty - t)}{\frac{x^{1/5}q}{k}} \quad [7]$$

where

$$C_1 = \left[\frac{g\beta q}{5k\nu^2}\right]^{1/5}, \quad C_2 = \left[\frac{5^4 g\beta q\nu^2}{k}\right]^{1/5} \quad [8]$$

Expressions for the velocity components can be derived using Equations [4], [5], and [6]

$$u = C_1 C_2 x^{3/5} F'(\eta) \quad [9]$$

$$v = \frac{C_2}{5x^{1/5}}[\eta F'(\eta) - 4F(\eta)] \quad [10]$$

where the primes indicate differentiation with respect to η. When the various terms of Equations [2] and [3] are evaluated it is found that all factors containing x cancel out, leaving only functions which depend upon η. The result is

$$F''' - 3(F')^2 + 4FF'' - \theta = 0 \quad [2a]$$

$$\theta'' + \Pr[4\theta' F - \theta F'] = 0 \quad [3a]$$

It is seen that the dependent variables F and θ appear in both equations. Simultaneous solution of the equations is thereby required. The coupling of the equations arises because the free-convection flow is due to differences in temperature which give rise to density differences.

The boundary conditions are derived by noting that at the plate surface ($y = 0$), it is required that $u = v = 0$; while at a great distance from the plate ($y = \infty$), it is required that $u = 0$. The condition of uniform heat-flux rate at the plate surface ($y = 0$) is imposed by taking

$$-k\left(\frac{\partial t}{\partial y}\right)_{y=0} = q, \text{ where } q \text{ is a given constant.}$$

At a great distance from the plate ($y = \infty$), the temperature will be equal to t_∞. By the use of Equations [5], [7], [9], and [10], the boundary conditions may be written as

$$\left.\begin{matrix} F = 0 \\ F' = 0 \\ \theta' = 1 \end{matrix}\right\} \text{ at } \eta = 0 \qquad \left.\begin{matrix} F' = 0 \\ \theta = 0 \end{matrix}\right\} \text{ at } \eta = \infty \quad [11]$$

It is to be noted that $\eta = \infty$ corresponds to $x = 0$ $(y > 0)$ as well as $y = \infty$. So, the conditions $t = t_\infty$ and $u = 0$ are automatically imposed at $x = 0$.

The solution to the differential Equations [2a] and [3a] subject to the Boundary Conditions [11] has been obtained numerically on the IBM Card Programmed Calculator. The fact that only three of the five boundary conditions are given at $\eta = 0$ required that guesses be made for $\theta(0)$ and $F''(0)$. Calculations were carried out for several pairs of $\theta(0)$ and $F''(0)$ until a solution was found which gave $F'(\infty) = 0$ and $\theta(\infty) = 0$. Results were obtained for Prandtl numbers of 0.1, 1, 10, and 100 and are listed in Appendix B.

HEAT-TRANSFER RESULTS

Surface-Temperature Variation. When the heat-flux rate at the surface is specified, the surface-temperature variation remains to be calculated. Equation [7] is evaluated at the surface ($\eta = 0$) and yields the following expression for the surface temperature

$$t_w - t_\infty = -5^{1/5}\theta(0)\frac{qx}{k}\left[\frac{g\beta q x^4}{\nu^2 k}\right]^{-1/5} \quad [12]$$

The dimensionless group in the bracket plays the role in this problem as does the Grashof number in the problem of free convection from a vertical plate having uniform wall temperature. For want of a better name, this group will be referred to here as a modified Grashof number and will be written as Gr_x^*. Then

$$\frac{(t_w - t_\infty)}{\frac{qx}{k}}\mathrm{Gr}_x^{*1/5} = -5^{1/5}\theta(0) \quad [12a]$$

This equation is plotted in Fig. 2, using the calculated values of $\theta(0)$. The resulting curve has been extrapolated to a Prandtl number of 0.01[8] to provide data for liquid metals. Also shown

[8] Calculations were not made for a Prandtl number of 0.01 because of the extensive time required to obtain a solution of Equations [2a] and [3a] for this case on the IBM Card Programmed Calculator.

in Fig. 2 are the results for the surface-temperature variation which were calculated by the von Kármán-Pohlhausen method[3] as

$$\frac{(t_w - t_\infty)}{\frac{qx}{k}} \mathrm{Gr}_x^{*1/5} = \frac{(360)^{1/5}}{2}\left[\frac{0.8 + \mathrm{Pr}}{\mathrm{Pr}^2}\right]^{1/5} \quad \ldots\ldots [13]$$

On any given surface, the solution indicates $(t_w - t_\infty)$ is proportional to $x^{1/5}$. So, the wall temperature t_w equals t_∞ at $x = 0$. The rate of increase of the wall temperature is greatest near $x = 0$ (the ambient temperature t_∞ is constant). The variation of the wall temperature with distance along the plate is seen graphically in Fig. 3 by plotting

$$\frac{t_w - t_\infty}{(t_w - t_\infty)_L} = \left(\frac{x}{L}\right)^{1/5}$$

where L is the length of surface for which the flow is laminar.

Local Nusselt Number. The local Nusselt number is obtained from its definition

$$\mathrm{Nu}_x = \frac{h_x x}{k} = \frac{q}{(t_w - t_\infty)}\frac{x}{k} \quad \ldots\ldots [14]$$

By rearrangement of Equation [12*a*], it follows that

$$\frac{\mathrm{Nu}_x}{\mathrm{Gr}_x^{*1/5}} = -\frac{1}{5^{1/5}\,\theta(0)} \quad \ldots\ldots [14a]$$

This equation is plotted in Fig. 4 along with the local Nusselt number calculated from the von Kármán-Pohlhausen method[3]

$$\frac{\mathrm{Nu}_x}{\mathrm{Gr}_x^{*1/5}} = \frac{2}{(360)^{1/5}}\left[\frac{\mathrm{Pr}^2}{0.8 + \mathrm{Pr}}\right]^{1/5} \quad \ldots\ldots [15]$$

Velocity and Temperature Distributions. At a fixed value of x, a plot of F' versus η gives the shape of the velocity distribution in the boundary layer, as may be seen by rearranging Equation [9].

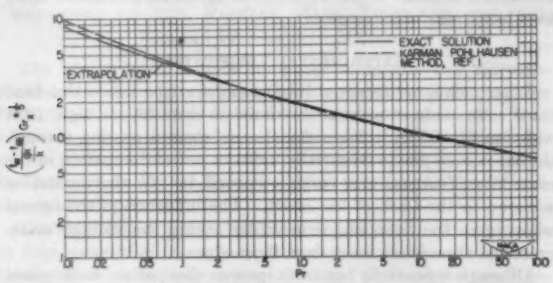

FIG. 2 VARIATION OF $\left(\frac{t_w - t_\infty}{qx/k}\right)\mathrm{Gr}_x^{*1/5}$ WITH PRANDTL NUMBER
($[t_w - t_\infty]$ is local temperature difference between wall and ambient. Gr_x^* is local value of modified Grashof number.)

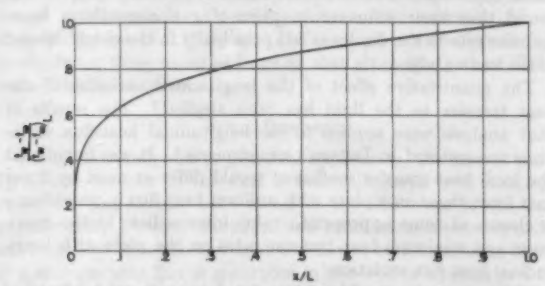

FIG. 3 VARIATION OF $(t_w - t_\infty)$ ALONG PLATE SURFACE
($x = 0$ is at leading edge; $x = L$ is length of plate for which flow is laminar)

$$F'(\eta) = \frac{u}{C_1 C_2 x^{2/5}} = \frac{\frac{ux}{\nu}}{5\left[\frac{\mathrm{Gr}_x^*}{5}\right]^{2/5}} \quad \ldots\ldots [9a]$$

The temperature distribution in the boundary layer is obtained from Equation [7]

$$\frac{t - t_\infty}{t_w - t_\infty} = \frac{\theta(\eta)}{\theta(0)} \quad \ldots\ldots [7a]$$

The velocity and temperature profiles are plotted in Figs. 5 and 6, respectively, for several Prandtl numbers.

Average Nusselt Numbers. Since there is no one temperature-difference characteristic of the problem, the choice of a temperature difference in defining an average heat-transfer coefficient (and hence an average Nusselt number) is purely arbitrary. In the literature of experimental work on uniform heat flux, average Nusselt numbers have been defined using the average plate temperature minus ambient (Dotson[2]) and also by using the temperature difference halfway along the plate (Saunders[4]). There has been a tendency to compare these average Nusselt numbers with those for uniform surface temperature. So, average Nusselt numbers will be derived here and compared with those derived by Ostrach[5] for a uniform temperature plate from an exact solution of the boundary-layer equations.

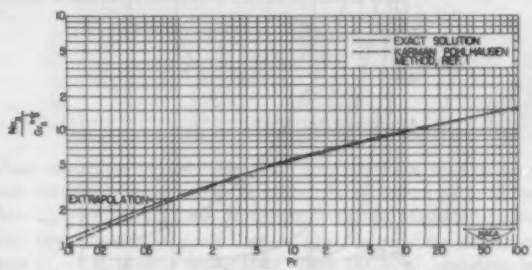

FIG. 4 VARIATION OF $(\mathrm{Nu}_x/\mathrm{Gr}_x^{*1/5})$ WITH PRANDTL NUMBER
(Nu_x is local Nusselt number. Gr_x^* is local value of modified Grashof number.)

(*a*) $\overline{\mathrm{Nu}}$ based on average temperature difference: The average temperature difference on a surface over which the flow is laminar for a length L is obtained by averaging Equation [12]

$$\overline{t_w - t_\infty} = \frac{1}{L}\int_0^L (t_w - t_\infty)dx = \frac{5}{6}(t_w - t_\infty)_L \ldots [16]$$

Using this temperature difference, an average heat-transfer coefficient is defined as

$$q = \bar{h}\,\overline{(t_w - t_\infty)} \quad \ldots\ldots [17]$$

When $(t_w - t_\infty)_L$ is evaluated from Equation [12*a*], and Equation [17] is used, there is obtained

$$\overline{\mathrm{Nu}} = \frac{\bar{h}L}{k} = -\frac{6}{5^{4/5}\,\theta(0)}\,\mathrm{Gr}_L^{*1/5} \quad \ldots\ldots [18]$$

But

$$\mathrm{Gr}_L^* = \left[\frac{g\beta q L^4}{k\nu^2}\right] = \left[g\beta\frac{\overline{(t_w - t_\infty)}}{\nu^2}L^3\right]\frac{\bar{h}L}{k} \quad \ldots\ldots [19]$$

So

$$\overline{\mathrm{Nu}} = \left[-\frac{6}{5^{4/5}\,\theta(0)}\right]^{5/4}\left[\frac{g\beta\,\overline{(t_w - t_\infty)}\,L^3}{\nu^2}\right]^{1/4} \quad \ldots\ldots [18a]$$

[5] "An Analysis of Laminar Free-Convection Flow and Heat Transfer About a Flat Plate Parallel to the Direction of the Generating Body Force," by Simon Ostrach, NACA TR 1111, 1953.

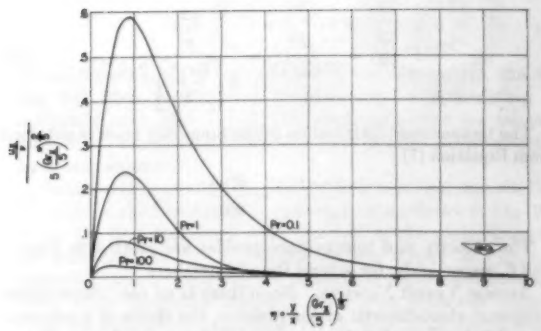

FIG. 5 DIMENSIONLESS VELOCITY DISTRIBUTIONS FOR SEVERAL PRANDTL NUMBERS

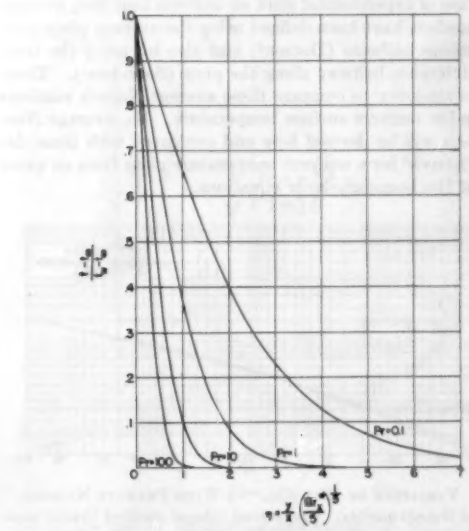

FIG. 6 DIMENSIONLESS TEMPERATURE DISTRIBUTIONS FOR SEVERAL PRANDTL NUMBERS

The second bracket on the right is the conventional Grashof number and will be denoted by Gr_L. Finally then

$$\frac{\overline{Nu}}{Gr_L^{1/4}} = \left[-\frac{6}{5^{3/4}\theta(0)}\right]^{1/4} \quad \ldots\ldots\ldots\ldots [18b]$$

The values of $\overline{Nu}/Gr_L^{1/4}$ for a flat plate having uniform surface temperature have been calculated from the results of Ostrach[4] and are tabulated in Table 1 with the value from Equation [18b].

TABLE 1 COMPARISON OF EQUATION [18b] WITH RESULTS FOR UNIFORM TEMPERATURE PLATE

Pr	$\frac{\overline{Nu}}{Gr_L^{1/4}}$ (Equation [18b])	$\frac{\overline{Nu}}{Gr_L^{1/4}}$ (Ostrach)
0.1	0.237	0.219
1	0.573	0.535
10	1.17	1.10
100	2.18	2.07

It is seen from the table that $\overline{Nu}/Gr_L^{1/4}$ evaluated at the average value of $(t_w - t_\infty)$ for a plate having uniform surface heat flux differs at most by 8 per cent from the value for a plate having uniform surface temperature. The deviation is often within the limits of experimental accuracy. Thus it is demonstrated why experimentally determined Nusselt numbers based on the average value of $(t_w - t_\infty)$ for a uniform heat-flux plate have correlated with results for a uniform wall-temperature plate.

(*b*) $\overline{Nu}$ based on temperature difference at $L/2$: The temperature difference between the plate and ambient at $L/2$ is

$$(t_w - t_\infty)_{L/2} = \left(\frac{1}{2}\right)^{1/4} (t_w - t_\infty)_L \quad \ldots\ldots\ldots [20]$$

An average heat-transfer coefficient can be defined using this temperature difference

$$q = \bar{h}\,(t_w - t_\infty)_{L/2} \quad \ldots\ldots\ldots\ldots [17a]$$

Proceeding in a fashion similar to that in the last paragraph, it is found that $\overline{Nu}/Gr_L^{1/4}$ based on the temperature difference $(t_w - t_\infty)_{L/2}$ is

$$\frac{\overline{Nu}}{Gr_L^{1/4}} = \left[-\frac{2^{1/4}}{5^{1/4}\theta(0)}\right]^{1/4} \quad \ldots\ldots\ldots\ldots [21]$$

Equation [21] is compared with the results for a uniform temperature plate in Table 2.

TABLE 2 COMPARISON OF EQUATION [21] WITH RESULTS FOR UNIFORM TEMPERATURE PLATE

Pr	$\frac{\overline{Nu}}{Gr_L^{1/4}}$ (Equation [21])	$\frac{\overline{Nu}}{Gr_L^{1/4}}$ (Ostrach)
0.1	0.224	0.219
1	0.543	0.535
10	1.11	1.10
100	2.07	2.07

The values of $\overline{Nu}/Gr_L^{1/4}$ evaluated using $(t_w - t_\infty)_{L/2}$ for the uniform heat-flux case are in excellent agreement with those for the uniform wall-temperature case. So, the agreement between experimental results for uniform surface heat flux with the results for uniform wall temperature is made plausible.

Comparison of Local Nusselt Numbers. Local Nusselt numbers for the cases of uniform heat flux and uniform wall temperature are compared in the Appendix A. By this comparison, there is obtained a measure of the influence of upstream conditions upon local heat-transfer parameters.

EXPERIMENTAL VERIFICATION

Experiments are reported by Dotson[3] for free convective heat transfer to air from a vertical aluminum sheet $2^3/_2$ ft high, 10 ft wide, and 0.005 in. thick. An electric current passing through the sheet gave rise to essentially uniform power dissipation in the material. Temperatures were recorded by 63 thermocouples soldered to the back of the sheet. The influence of the lateral edges upon the data was reduced by taking the voltage measurements at positions away from these edges.

Although essentially uniform power dissipation took place within the aluminum, the heat transferred to the air by free convection was made nonuniform by radiation, and by conduction out through the insulation at the rear surface of the sheet. When these conduction and radiation losses were computed, it was found that their influence in promoting a nonuniform heat-transfer rate to the fluid was felt principally in the neighborhood of the leading edge.

The quantitative effect of the longitudinal variation of the heat transfer to the fluid has been studied.[2] The results of that analysis were applied to the longitudinal heat-flux variations encountered in Dotson's experiments.[3] It was found that the local heat-transfer coefficient would differ at most by 2 per cent from those on a plate with uniform heat flux $\bar{q}$, providing $\bar{q}$ is chosen at some appropriate value intermediate to the maximum and minimum heat-transfer rates on the plate with longitudinal heat-flux variation.

The temperature and heat-transfer data reported by Dotson[3] have been used to calculate local Nusselt numbers defined accord-

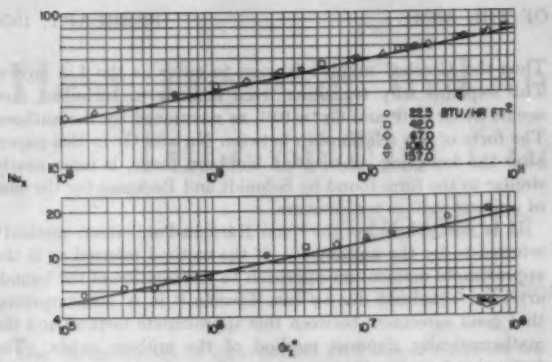

FIG. 7 COMPARISON OF PREDICTED NUSSELT NUMBERS WITH THOSE CALCULATED FROM DATA OF DOTSON[3]

ing to Equation [14]. Fluid properties were evaluated at ambient conditions. The experimental points as well as the theoretical line given by Equation [14a] are shown in Fig. 7. The agreement is good over the entire range $10^8 \leq Gr_x^* \leq 10^{11}$. The experimental points showing the greatest deviation from theory are for the lower heat-transfer rates. Dotson indicates that the experimental data become less accurate as the heat-transfer rate decreases.

It is to be noted that, although the value of the conventional Grashof number Gr at which transition from laminar to turbulent flow occurs is roughly 10^9 for air, it would appear that considerably higher values of Gr^* are associated with transition. This is borne out by the good agreement of the experimental data with the laminar theory up to $Gr^* = 10^{11}$, and also by Dotson's observations of the location at which thermocouple readings fluctuated with time.

Insufficient data are given by Saunders[4] to permit comparison of theory with experiment.

COMPARISON OF THE RESULTS WITH THOSE OF THE VON KÁRMÁN-POHLHAUSEN METHOD

The heat-transfer results computed from the von Kármán-Pohlhausen method are in good agreement with those derived here from the exact solution of the boundary-layer equations. It is interesting to note that the orientation of the Nusselt number curves in Fig. 4 relative to each other is identical to that found by Ostrach in a similar Nusselt-number plot for the case of uniform wall temperature.

The skin-friction results, which are of no practical importance in free convection, do not show such good agreement between those derived from the exact solution and those of the von Kármán-Pohlhausen method. For Prandtl numbers greater than 1, the von Kármán-Pohlhausen results are within 15 per cent of those of the exact solution. For Prandtl numbers less than 1, greater disagreement is noted, which becomes increasingly more severe with decreasing Prandtl number. For example, at a Prandtl number of 0.1, the exact solution gives a friction coefficient almost three times as large as that given by the von Kármán-Pohlhausen method.

FINAL REMARKS

From the standpoint of practical application, the case of uniform heat transfer to the fluid is best considered as a limiting case. As has already been noted in the discussion of the experiments by Dotson,[3] radiation and conduction inevitably will act to cause the convective heat transfer to be nonuniform, even if a uniform heat flux is generated in the wall or applied at the rear of the wall. The importance of the conduction and radiation relative to the convection is a function of the temperature and orientation of surrounding bodies, the thickness of the wall and the condition of its surface, and the nature of the structural supports of the wall.

Also, there may be considerable variation in conditions at the leading edge from one practical application to another. The leading edge may be free from obstructions, or else it may join to a horizontal surface, e.g., a floor. Another possibility is that the heated vertical surface is preceded by an unheated vertical surface. The influence of these various initial conditions requires further experimentation for clarification.

Appendix A

COMPARISON OF LOCAL NUSSELT NUMBERS FOR UNIFORM WALL TEMPERATURE AND UNIFORM SURFACE HEAT TRANSFER

This comparison is made to provide an insight into the influence of upstream thermal conditions on local heat-transfer parameters. Comparison is made for two separate conditions: (1) Local values of $(t_w - t_\infty)$ are equal; (2) local values of q are equal.

Case I. Consider a plate with uniform heat flux. It has already been shown (Fig. 3) that $(t_w - t_\infty)$ varies with x. At some position x_i, there is a temperature difference $(t_w - t_\infty)_{x_i}$. The local Nusselt number at x_i for this plate is to be compared with that at x_i on another plate having a uniform temperature difference $(t_w - t_\infty)_{x_i}$. Designating $Nu_{x,uh}$ and $Nu_{x,ut}$ as the local Nusselt numbers for the uniform heat-transfer and uniform-temperature cases, respectively, it is found that

Pr	$\frac{Nu_{x,uh}}{Nu_{x,ut}}$
0.1	1.15
1	1.14
10	1.13
100	1.12

These values are independent of x! For the plate with uniform heat transfer, the temperature difference upstream of x_i is less than $(t_w - t_\infty)_{x_i}$. It would appear from the tabulated values that these upstream deviations of the temperature difference from $(t_w - t_\infty)_{x_i}$ only moderately effect the local heat-transfer coefficient at x_i. It is to be noted that the Nusselt-number ratio in the tabulation is equal to the ratio of the local heat-transfer rates, since the comparison has been made for the same value of $(t_w - t_\infty)$ at x_i for the two cases.

Case II. Consider a plate with a uniform surface temperature. It is known that the local heat-flux rate q varies with x. At x_j, there is a local heat-flux rate q_{x_j}. The local Nusselt number at x_j for this plate is to be compared with that at x_j on another plate having a uniform heat flux q_{x_j}. The results are again independent of x

Pr	$\frac{Nu_{x,uh}}{Nu_{x,ut}}$
0.1	1.12
1	1.11
10	1.10
100	1.10

For the plate with uniform temperature, the heat-transfer rate upstream of x_j exceeds q_{x_j}. These upstream deviations from q_{x_j} only moderately affect the local heat-transfer coefficient at x_j. It is to be noted that the Nusselt-number ratio tabulated is the inverse of the temperature difference $(t_w - t_\infty)$ ratio, since the comparison has been made at the same value of q at x_j for the two cases.

Appendix B

The values of $\theta(0)$ and $f''(0)$ associated with a solution of the differential Equations [2a] and [3a] subject to the boundary con-

ditions, Equation [11], are listed below for Prandtl numbers of 0.1, 1, 10, and 100.

Pr	$\theta(0)$	$f''(0)$
0.1	−2.7507	1.6434
1	−1.3574	0.72196
10	−0.76746	0.30639
100	−0.46566	0.12620

Discussion

D. C. Hamilton.[7] This paper is most certainly a much-needed and useful contribution to the heat-transfer literature. The solution obtained, which the authors have called "exact solution," is more commonly called "numerical solution"; this is actually an abbreviation for the more precise definition "numerical approximation to the solution." In the discusser's opinion the authors' nomenclature will be misleading, particularly to the cursory reader.

A worth-while effort was expended by the authors in obtaining the solution of this same problem by the von Kármán method so that a comparison could be made. Since the von Kármán method is so useful in the more difficult boundary-layer problems that often occur in practice it is always gratifying to discover still another case where it gives a solution that is in satisfactory agreement with the more complete solution.

D. P. Timo.[8] The authors present an interesting, mathematically rigorous solution to the problem of the vertical heated plate with uniform surface heat flux. The term "mathematically rigorous" is perhaps preferable to the term "exact" in describing the solution, since the fluid properties other than the density were considered invariant. For this case of uniform surface heat flux, there is a longitudinal surface-temperature variation as well as a fluid-temperature variation normal to the plate. Thus, for large q, and hence large local values of $t_w - t_\infty$, the temperature at which to evaluate the fluid properties may present somewhat of a problem. However, for the laminar-flow region to which this analysis applies, the difficulty is relatively unimportant. The method of solution is analogous to that followed by Schmidt and Beckman,[9] in co-operation with Polhausen, in solving the problem of the vertical heated plate with uniform surface temperature.

The dimensionless group which the authors call the modified Grashof number is in reality the product of the conventional Grashof and Nusselt numbers. For example, the "modified Grashof number" based on x is

$$\mathrm{Gr}_x^* = \frac{g\beta x^4 q}{\nu^2 k} = \frac{g\beta x^4 [h_x(t_w - t_\infty)]}{\nu^2 k} = \left[\frac{g\beta x^3(t_w - t_\infty)}{\nu^2}\right]\left[\frac{h_x x}{k}\right] = \mathrm{Gr}_x \mathrm{Nu}_x$$

If this expression is substituted into Equation [14a], there results

$$\frac{\mathrm{Nu}_x}{\mathrm{Gr}_x^{1/4}} = -\frac{1}{5^{1/4}\theta(0)^{5/4}}$$

Thus the Grashof number is seen to enter as the 1/4 power. This explains why transition from laminar to turbulent flow occurs at $\mathrm{Gr} \approx 10^9$ and $\mathrm{Gr}^* \approx 10^{11}$, as mentioned by the authors. The form of the relationship between Nu and Gr in this paper, after the foregoing substitution has been made, is more nearly similar to the form found by Schmidt and Beckman for the case of uniform surface temperature.

It is not clear what the "von Kármán-Pohlhausen method" referred to by the authors is. If the method referred to is the approximate momentum approach to the solution of the boundary-layer equations due to von Kármán,[10] it is not surprising that good agreement between this approximate method and the mathematically rigorous method of the authors exists. The former has been justified experimentally and by comparison with the rigorous solution of Schmidt and Beckman. Eckert[11] has made this comparison.

The fact that the uniform surface heat-flux case and the uniform surface-temperature case are not greatly different is illustrated by Fig. 3 of the paper. It is seen that the surface-temperature variation for the uniform heat-flux case is not great over the major portion of the plate height. Hence, in practice, it seems hardly necessary to differentiate between the two cases.

For those not familiar with the solution of convection problems, it may be well to elaborate slightly on the origin of Equations [1], [2], and [3] of the paper. The rigorous solution of the free-convection problem requires the simultaneous solution of the fluid-flow equations (Navier-Stokes equations and continuity equation) and the equation of heat conduction in a moving fluid (energy equation). Equations [1], [2], and [3] are the remainders of the continuity equation, the Navier-Stokes equations, and the equation of heat conduction in a moving fluid, respectively,[12] after irrelevant terms have been discarded.

Authors' Closure

The authors wish to thank the discussers for their interest and for their comments.

The phrase "exact solution" was used to distinguish between solutions of: (a) the partial-differential equations expressing conservation of mass, momentum, and energy for the boundary layer, and (b) approximate forms of these conservation laws. It is regretted that this phrase conveyed other impressions.

The modified Grashof number, $\frac{g\beta x^4 q}{\nu^2 k}$, includes quantities which would all be known by a designer at the beginning of a calculation. For this reason the modified Grashof number, rather than the conventional Grashof number, was used in presenting the results of the analysis. It may be noted that the conventional Grashof number, $\frac{g\beta x^3(t_w - t_\infty)}{\nu^2}$, contains a temperature difference which would not be known at the beginning of a calculation.

The von Kármán-Pohlhausen method consists of the rather often-used integral formulation of the conservation laws due to von Kármán, coupled with the use of polynomial approximations for the velocity and temperature profiles due to K. Pohlhausen.

A rather careful exposition of the origin of Equations [1], [2], and [3] of the paper is given in *Modern Developments in Fluid Dynamics—High-Speed Flow*,[13] vol. II, pp. 766–769 and p. 801.

---

[7] Principal Development Engineer, Oak Ridge National Laboratory, Division of Carbide and Carbon Chemicals Company, Oak Ridge, Tenn. Mem. ASME.

[8] Engineer, Applied Research, Materials and Processes Laboratory, General Electric Company, Schenectady, N. Y. Assoc. Mem. ASME.

[9] "Das Temperatur- und Geschwindigkeitsfeld vor einer Wärme abgebenden senkrechten Platte bei natürlichen Konvektion," by E. Schmidt and W. Beckman, *Technische Mechanik und Thermodynamik*, vol. 1, 1930, pp. 1–24; the solution is also presented in "Heat Transfer," by M. Jakob, John Wiley & Sons, Inc., New York, N. Y., 1949, pp. 443–451.

[10] "Über laminare und turbulente Reibung," by T. von Kármán, *Zeitschrift für angewandte Mathematik und Mechanik*, vol. 1, 1921, pp. 235–252.

[11] "An Introduction to the Transfer of Heat and Mass," by E. R. G. Eckert, McGraw-Hill Book Company, Inc., New York, N. Y., 1950, pp. 158–164.

[12] See, for example, equations [3–14], [3–23], and [3–34] of "Heat Transfer," by M. Jakob, for these equations in their general form.

[13] L. Howarth, editor, Clarendon Press, Oxford, England, 1953.

Heat Transfer to Laminar Flow in a Round Tube or Flat Conduit—The Graetz Problem Extended

By J. R. SELLARS,[1] MYRON TRIBUS,[2] AND J. S. KLEIN[3]

The complete set of eigenvalues and eigenfunctions for the classical Graetz problem is presented and the solution is extended to cover arbitrary wall temperature or heat-flux variations.

Nomenclature

The following nomenclature is used in the paper:

A = coefficient occurring in Equation [10]
B = coefficient occurring in Equation [10]
b = half-width of flat duct, ft
C_n = coefficient in Equation [3]
C_p = unit heat capacity at constant pressure, Btu/lb deg F
D = coefficient occurring in Equation [18]
E = coefficient occurring in Equation [18]
F = $F(s, r^+)$, Laplace transform of Graetz solution
g = $g(x^+, r^+)$ integrating kernel for heat-flux problems, Equation [44]
G = $G(s, r^+)$ Laplace transform of g
h = $h(x^+)$ integrating kernel for heat-flux problems, Equation [34]
H = $H(s)$ Laplace transform of h
i = $\sqrt{-1}$
J_0 = Bessel function of first kind, zero order
$J_{1/3}$ = Bessel function of first kind, $^1/_3$ order
$J_{-1/3}$ = Bessel function of first kind, $-^1/_3$ order
k = thermal conductivity of fluid, Btu/sec-ft² (deg F/ft)
K_n = coefficient occurring in Equation [A-3]
Pr = Prandtl modulus, dimensionless, $(\mu C_p/k)(3600\ g_c)$
q = $q(x)$ heat flux per unit wall area, Btu/hr-ft²
Q = Laplace transform of (kq/r_0)
r = radius, ft
r_0 = tube radius, ft
r^+ = (r/r_0)
R = $R(r^+)$
Re = Reynolds modulus, dimensionless, $(2U_m r_0 \rho/\mu g_c)$ or $(4U_m b\rho/\mu g_c)$
s = transform variable
t = $t(x^+, r^+)$ temperature, deg F
T = $T(s, r^+)$, Laplace transform of t
u = velocity of fluid, fps
u_m = average fluid velocity in tube, fps
x = distance along tube, ft
x^+ = $(x/r_0)(\text{Re Pr})^{-1}$ or $(x/b)(\text{Re Pr})^{-1}$
y = distance from duct wall, ft
y^+ = (y/b)
z = distance from tube wall, ft
z^+ = (z/r_0)
γ_m = zero of $H(s)$
λ = eigenvalue
μ = viscosity of fluid, lb-sec/sq ft
ρ = fluid density, pcf
ξ = dummy variable
η = dummy variable
Γ = gamma function

Introduction

The problem considered here is posed by a system in which a fluid of constant properties flows in steady laminar motion in a round tube or flat duct. The velocity profile is fully established and parabolic. Up to a point ($x = 0$) the fluid is isothermal. After this point a prescribed heat flux or temperature is given at the wall of the conduit and the problem is to find the temperature distribution, as well as the connection between heat flux and wall temperature. The application of this solution to practical problems of heat exchange has already been so well established that further comment is unnecessary.

The problem has been considered in detail by a number of workers and an excellent review is contained in the book "Heat Transfer" by M. Jakob.[4] The problem readily reduces to the finding of eigenvalues and prior to this paper only the first three eigenfunctions and the first four eigenvalues have been known. A recent paper[5] has brought out the importance of obtaining more eigenvalues, and by using the complete set of eigenvalues and the methods of that paper the classical "Graetz Problem"[6] is extended to more complicated boundary conditions.

The problem can be stated in mathematical terms as follows:

Given

$$\left.\begin{aligned} t &= t(x, r) \\ u\rho C_p \frac{\partial t}{\partial x} &= \frac{k}{r}\frac{\partial}{\partial r}\left(r\frac{\partial t}{\partial r}\right) \\ u &= 2u_m\,[1 - (r/r_0)^2] \end{aligned}\right\} \quad \ldots\ldots\ldots [1]$$

and for

$$t = t_0 \qquad x < 0$$

with either

---

[1] Assistant Professor, Department of Aeronautical Engineering, University of Michigan, Ann Arbor, Mich.

[2] Associate Professor, Engineering Department, University of California, Los Angeles, Calif. Mem. ASME.

[3] Instructor in Mathematics, Oberlin College, Oberlin, Ohio.

Contributed by the Heat Transfer Division and presented at the Diamond Jubilee Semi-Annual Meeting, Boston, Mass., June 19–23, 1955, of The American Society of Mechanical Engineers.

Note: Statements and opinions advanced in papers are to be understood as individual expressions of their authors and not those of the Society. Manuscript received at ASME Headquarters, May 9, 1955. Paper No. 55—SA-66.

[4] "Heat Transfer," by Max Jakob, John Wiley & Sons, Inc., New York, N. Y., vol. 1, 1949.

[5] "Forced Convection From Nonisothermal Surfaces," by M. Tribus and J. Klein, "Heat Transfer: A Symposium," held at the University of Michigan during the summer of 1952, Engineering Research Institute, University of Michigan, 1953, pp. 211–235.

[6] "Über die Warmeleitungsfahigkeit von Flussigkeiten," by L. Graetz, Annalen der Physik Chem., vol. 25, 1885, pp. 337–357.

$$\left.\begin{aligned} t(x, r_0) &= t_w(x) \\ \text{or} \qquad kt_r(x, r_0) &= q(x) \end{aligned}\right\} \; x > 0$$

find $t(x, r)$ and the relation between $q(x)$ and $t_w(x)$.

The nondimensional form of the equations is

$$\frac{\partial t}{\partial x^+} = \frac{1}{1 - r^{+2}} \frac{1}{r^+} \frac{\partial}{\partial r^+} \left(r^+ \frac{\partial t}{\partial r^+} \right) \ldots\ldots\ldots\ldots [2]$$

The boundary conditions are

$$t = t_0 \qquad x^+ < 0$$

and either

$$\left.\begin{aligned} t(x^+, 1) &= t_w(x^+) \\ \text{or} \qquad t_{r^+}(x^+, 1) &= r_0 q(x^+)/k \end{aligned}\right\} \; x^+ > 0$$

In view of the linearity of Equation [2], it is necessary to have only the fundamental solution, known as the Graetz solution, to construct all other needed solutions. Therefore the initial step is the completion of the Graetz solution.

The Graetz Solution

The problem considered by Graetz and most other workers is Equation [2] with boundary conditions

$$t = 1 \qquad x^+ < 0$$
$$t_w = 0 \qquad x^+ > 0$$

Let θ be a solution of Equation [2], then

$$\theta = \sum_{n=0}^{\infty} C_n R_n(r^+) e^{-\lambda_n^2 x^+} \ldots\ldots\ldots\ldots [3]$$

where the λ_n are the eigenvalues required to make the solution to the following differential equation

$$r^+ R_n'' + R_n' + \lambda_n^2 r^+ (1 - r^{+2}) R_n = 0 \ldots\ldots [4]$$

satisfying the boundary conditions $R_n(1) = 0$, $R_n(0) = 1$. The coefficients C_n are determined from the relation

$$C_n = \frac{\int_0^1 r^+ (1 - r^{+2}) R_n \, dr^+}{\int_0^1 r^+ (1 - r^{+2}) R_n^2 \, dr^+} = \frac{-2}{\lambda_n \left(\dfrac{\partial R_n}{\partial \lambda} \right)_{\substack{r^+ = 1 \\ \lambda = \lambda_n}}} \ldots [5]$$

The eigenfunctions and eigenvalues have been given only for $n = 1, 2, 3$. The higher modes of Equation [4] are very difficult to calculate for large values of λ. Therefore, to obtain λ_n and C_n for $n > 3$, a solution is sought which will be valid as $\lambda_n \to \infty$. It will be found that the resulting formulas will provide good answers even when λ_n is small. First, look for a solution in the form

$$R = e^{g(r^+)}$$

and find that $g(r^+)$ satisfies

$$g'' + g'^2 + \frac{1}{r^+} g' + \lambda^2 (1 - r^{+2}) = 0 \ldots\ldots [6]$$

Now an asymptotic solution is sought in the form

$$g = \lambda g_0 + g_1 + \lambda^{-1} g_2 + \ldots\ldots\ldots\ldots [7]$$

Substitution in Equation [6] and equating powers of λ gives

$$g_0' = \pm i \sqrt{1 - r^{+2}} \ldots\ldots\ldots\ldots [8]$$

$$g_1 = -\ln \sqrt{g_0' r^+} \ldots\ldots\ldots\ldots [9]$$

Since λ is large, the remaining terms in Equation [7] are neglected. Substitution of Equations [8] and [9] in Equation [7] gives for R

$$R = \frac{A e^{\Omega \int_0^{r^+} \sqrt{1 - \xi^2} \, d\xi} + B e^{-\Omega \int_0^{r^+} \sqrt{1 - \xi^2} \, d\xi}}{\sqrt{r^+ (1 - r^{+2})^{1/4}}} \ldots [10]$$

Equation [10] is the so-called WKB approximation and is valid for $0 < r^+ < 1$ for sufficiently large λ. Now the coefficients A and B must be determined so that Equation [10] will correspond to the regular solution of Equation [4], where r^+ is small. For small r^+ Equation [10] is

$$R = \frac{A e^{\Omega r^+} + B e^{-\Omega r^+}}{\sqrt{r^+ (1 - r^{+2})^{1/4}}} \ldots\ldots\ldots\ldots [11]$$

Inspection of Equation [4] shows that when r^+ is small enough so that $\lambda^2 (1 - r^{+2}) \to \lambda^2$, the classical solution behaves as $J_0(\lambda r^+)$, since Equation [4] then becomes a Bessel equation. For large λr^+, even if r^+ is small, the asymptotic expression for $J_0(\lambda r^+)$ is

$$J_0(\lambda r^+) = \sqrt{\frac{2}{\pi \lambda r^+}} \cos (\lambda r^+ - \pi/4) \ldots\ldots [12]$$

and thus it is seen that to make Equations [11] and [12] equal for r^+ small, it is required that

$$A = \sqrt{\frac{2}{\lambda \pi}} e^{-i\pi/4} \qquad B = \sqrt{\frac{2}{\lambda \pi}} e^{i\pi/4} \ldots\ldots [13]$$

and for $0 < r^+ < 1$

$$R(r^+) = \sqrt{\frac{2}{\pi \lambda r^+}} \frac{\cos \left(\lambda \int_0^{r^+} \sqrt{1 - \xi^2} \, d\xi - \pi/4 \right)}{(1 - r^{+2})^{1/4}} \ldots [14]$$

Equation [14] is not a good approximation to the solution as $r^+ \to 1$, since it has a singularity there. Because a boundary condition is to be imposed at $r^+ = 1$, the development of an alternate solution, valid near $r^+ = 1$, is considered. By patching it onto Equation [14] the solution over the range $0 \leq r^+ \leq$ is obtained.

The following change of variable is made

$$z^+ = 1 - r^+$$

and Equation [4] becomes

$$\frac{d^2 R}{dz^{+2}} - \frac{1}{1 - z^+} \frac{dR}{dz^+} + \lambda^2 z^+ (2 - z^+) R = 0 \ldots [15]$$

Now consider $0 < z^+ \ll 1$ and define a new variable

$$\eta = \lambda^{2/3} z^+ \ldots\ldots\ldots\ldots [16]$$

Substitution of Equation [16] into Equation [14] yields for large λ

$$\frac{d^2 R}{d\eta^2} + 2\eta R = 0 \ldots\ldots\ldots\ldots [17]$$

which has the solution

$$R = D \sqrt{z^+} J_{1/3} \left(\frac{\lambda \sqrt{8}}{3} z^{+3/2} \right) + E \sqrt{z^+} J_{-1/3} \left(\frac{\lambda \sqrt{8}}{3} z^{+3/2} \right) \ldots [18]$$

The constants D and E are to be so chosen that for small z^+ Equations [18] and [14] are equivalent.

Change the variable from r^+ to z^+ in Equation [14] and perform the integration

$$\int_0^{r^+} \sqrt{1-\xi^2}\, d\xi = \int_0^1 \sqrt{1-\xi^2}\, d\xi + \int_1^{r^+} \sqrt{1-\xi^2}\, d\xi = \pi/4 - \int_0^{z^+} \sqrt{2\xi-\xi^2}\, d\xi \quad \ldots\ldots [19]$$

For small z^+ Equation [19] yields

$$\int_0^{r^+} \sqrt{1-\xi^2}\, d\xi = \pi/4 - \sqrt{8/3}\, z^{+3/2} \quad \ldots\ldots [20]$$

so that Equation [14] for small z^+ is

$$R(z^+) = \sqrt{\frac{2}{\pi\lambda}}\, \frac{\cos\left(\sqrt{8/3}\,\lambda z^{+3/2} - (\lambda-1)\pi/4\right)}{2^{1/4} z^{+1/4}} \quad \ldots [21]$$

For large λz^+, even if z^+ is small, Equation [18] becomes

$$R(z^+) = \sqrt{\frac{3}{\pi\lambda}}\, \frac{D\cos\left(\frac{\lambda\sqrt{8}}{3} z^{+3/2} - 5\pi/12\right) + E\cos\left(\frac{\lambda\sqrt{8}}{3} z^{+3/2} - \pi/12\right)}{2^{1/4} z^{+1/4}} \quad \ldots\ldots [22]$$

Expanding the cosines of differences of angle occurring in Equations [21] and [22] yields the simultaneous equation

$$D\cos 5\pi/12 + E\cos \pi/12 = \sqrt{2/3}\cos(\lambda-1)\pi/4$$

$$D\sin\frac{5\pi}{12} + E\sin\pi/12 = \sqrt{2/3}\sin(\lambda-1)\pi/4 \quad \ldots [23]$$

from which D and E are evaluated. Therefore Equation [18] is

$$R(z^+) = 2/3\sqrt{2z^+}\left[\sin\left(\frac{\lambda\pi}{4} - \frac{\pi}{3}\right) J_{1/3}\left(\frac{\lambda\sqrt{8}\, z^{+3/2}}{3}\right) - \sin\left(\frac{\lambda\pi}{4} - \frac{2\pi}{3}\right) J_{-1/3}\left(\frac{\lambda\sqrt{8}\, z^{+3/2}}{3}\right)\right] \quad \ldots\ldots [24]$$

As $z^+ \to 0$ the product

$$\sqrt{z^+}\, J_{1/3}\left[\lambda\sqrt{8/3}\, z^{+3/2}\right] \to 0$$

but the product involving $J_{-1/3}$ becomes constant. Therefore the coefficient of $J_{-1/3}$ must be zero if $R = 0$ at $z^+ = 0$. The values of λ_n must therefore be given by

$$\lambda_n = 4n + 8/3 \qquad n = 0, 1, 2, \ldots\ldots [25]$$

The equations for R_n are as follows:

For small r^+ (center of pipe)

$$R_n(r^+) = J_0(\lambda_n r^+) \quad \ldots\ldots [26]$$

For medium r^+

$$R_n(r^+) = \sqrt{\frac{2}{\pi\lambda_n r^+}}\, \frac{\cos\left[(\lambda_n/2)\, r^+\sqrt{1-r^{+2}} + (\lambda_n/2)\arcsin r^+ - \pi/4\right]}{(1-r^{+2})^{1/4}} \quad \ldots [27]$$

For small $z^+ = 1 - r^+$ (near the wall)

$$R_n(z^+) = \sqrt{\frac{2z^+}{3}}\,(-1)^n J_{1/3}\left(\frac{\lambda_n\sqrt{8}}{3} z^{+3/2}\right) \quad \ldots\ldots [28]$$

Equations [24] to [28] contain all the information essential to the problem solution. The coefficients C_n in Equation [3] are found from Equation [24] in accordance with Equation [5]. Thus it is found that

$$\left(\frac{\partial R}{\partial\lambda}\right)_{\substack{\lambda=\lambda_n \\ z^+=0}} = (-1)^{n+1}\frac{\pi\lambda_n^{-1/3}}{6^{2/3}\Gamma(2/3)} \qquad n = 0, 1, 2, \ldots\ldots [29]$$

and therefore

$$C_n = (-1)^n \frac{2\times 6^{1/3}\Gamma(2/3)}{\pi}\lambda_n^{-1/3}; \qquad n = 0, 1, 2, \ldots\ldots [30]$$

The derivative of R at the wall ($z^+ = 0$) which is

$$R_n'(1) = -\left(\frac{\partial R_n}{\partial z^+}\right)_{z^+=0} = \frac{(-1)^{n+1}\, 2^{3/2}\,\lambda_n^{1/3}}{\Gamma(4/3)3^{5/6}}; \qquad n = 0, 1, 2, \ldots\ldots [31]$$

will be required later.

Table 1 shows the first ten eigenvalues and the important constants for the case of flow in a round tube. Table 2 gives the same data for a flat duct with opposite walls at the same temperature. The development of the flat-duct system is similar to the

TABLE 1 FIRST TEN EIGENVALUES AND IMPORTANT CONSTANTS FOR CASE OF FLOW IN A ROUND TUBE

n	λ_n	λ_n^2	C_n	$-1/2 C_n R_n'(1)$
0	$2^3/_3$	7.1129	+1.47989	0.7303
1	$6^1/_3$	44.489	−0.80345	0.53810
2	$10^1/_3$	113.785	+0.58732	0.460074
3	$14^1/_3$	215.121	−0.474993	0.413743
4	$18^1/_3$	348.457	+0.404448	0.381785
5	$22^1/_3$	513.793	−0.355345	0.357853
6	$26^1/_3$	711.129	+0.318858	0.338988
7	$30^1/_3$	940.465	−0.290488	0.323555
8	$34^1/_3$	1201.8	+0.267691	0.310596
9	$38^1/_3$	1495.1	−0.248895	0.29950

$$C_n = (-1)^n \frac{2\times 6^{1/3}\Gamma(2/3)\lambda_n^{-1/3}}{\pi} = (-1)^n\, 2.84606\,\lambda_n^{-1/3}$$

$$-\frac{C_n}{2} R_n'(1) = \frac{6^{2/3}\Gamma(2/3)2^{1/3}\lambda_n^{-1/3}}{\pi\Gamma(4/3)3^{5/6}} = 1.01276\,\lambda_n^{-1/3}$$

$$\lambda_n = 4n + 8/3 \qquad n = 0, 1, 2, \ldots$$

$$\theta = \Sigma C_n R_n(r^+) e^{-\lambda_n^2 z^+}$$

$$q(z^+) = \frac{-4k}{d}\,\Sigma\frac{C_n}{2} R_n'(1) e^{-\lambda_n^2 z^+}(t_w - t_0)$$

TABLE 2 FIRST TEN EIGENVALUES AND THE IMPORTANT CONSTANTS FOR THE CASE OF FLOW IN A DUCT WITH OPPOSITE WALLS AT THE SAME TEMPERATURE

n	λ_n	λ_n^2	K_n	$-K_n Y_n'(1)$
0	1.667	2.779	+0.503	0.683
1	5.667	32.11	−0.121	0.454
2	9.667	93.45	+0.0648	0.380
3	13.67	186.9	−0.0431	0.338
4	17.67	312.2	+0.0319	0.311
5	21.67	469.6	−0.0253	0.291
6	25.67	658.9	+0.0207	0.274
7	29.67	880.3	−0.0174	0.262
8	33.67	1134	+0.0150	0.251
9	37.67	1419	−0.0131	0.242

$$K_n = (-1)^n \frac{3^{2/3}\Gamma(2/3)2^{10/3}}{\pi^{2/3}}\lambda_n^{-2/3} = (-1)^n\, 0.913\,\lambda_n^{-2/3}$$

$$-K_n Y_n'(1) = \frac{4\times 2^{1/3}\Gamma(2/3)\lambda_n^{-1/3}}{\pi\Gamma(4/3)3^{1/3}} = 0.810\,\lambda_n^{-1/3}$$

$$\lambda_n = 4n + 5/3 \qquad n = 0, 1, 2, \ldots \qquad \theta = \Sigma K_n Y_n(y^+) e^{-8/3\lambda_n^2 z^+}$$

$$q(z^+) = -\frac{k}{b}\,\Sigma K_n Y_n'(1) e^{-8/3\lambda_n^2 z^+}(t_w - t_0)$$

TABLE 3 COMPARISON WITH PREVIOUSLY KNOWN EIGENVALUES

	Sellars, Tribus, Klein			Jakob			Analog Computer		
n	λ_n	C_n	$\frac{-C_n R_n'(1)}{2}$	λ_n	C_n	$\frac{-C_n R_n'(1)}{2}$	λ_n	C_n	$\frac{-C_n R_n'(1)}{2}$
0	2.667	+1.47989	0.7303	2.705	+1.477	0.749	2.71	1.46	0.735
1	6.667	−0.80345	0.5381	6.66	−0.810	0.539	6.69	−0.809	0.533
2	10.667	+0.58732	0.4601	10.3	+0.385	0.179	10.62	+0.592	0.444
3	14.667	−0.47499	0.4137	14.67[a]	−0.479[a]	...	14.58	−0.51	0.398

[a] Attributed to Lee, Nelson, Cherry, and Boelter.

round duct and the equations are given in the Appendix, numbered to correspond with the text.

The previously known eigenvalues given by Jakob are shown in Table 3 for comparison. Since the solution presented here is valid for large λ_n and in view of the agreement even at moderate values of λ_n, it has been concluded that all the eigenvalues and functions are now sufficiently accurately known.

The heat flux at the wall is computed from the equation

$$q(x^+) = k\left(\frac{\partial t}{\partial r^+}\right)_{r^+=1} = \frac{-4k}{d}\sum\frac{C_n}{2}R_n'(1)\,e^{-\lambda_n x^+}(t_w - t_0) \quad [32]$$

Equation [32] is presented in the foregoing form to bring it into agreement with Jakob.[4]

Arbitrary Wall-Temperature Variations

If the wall-temperature variation is given by $t_w(x)$, then, as shown by Tribus and Klein,[5] the principle of superposition may be applied and the solution may be written in a Fourier-type Stieltjes integral

$$t - t_0 = \int_{\xi=0}^{x^+}[1 - \theta(x^+ - \xi, r^+)]dt_w(\xi) \quad [33]$$

where θ is the solution to Equation [2] defined by Equation [3]. The temperature of the wall and fluid for $x^+ < 0$ is t_0. The Stieltjes integral in Equation [33] is evaluated by substituting $(dt_w/d\xi)\,d\xi$ for dt_w wherever t_w is continuous and substituting

$$[1 - \theta(x^+ - \xi_1, r^+)][t_w(\xi_1^+) - t_w(\xi_1^-)]$$

as the contribution of the integral wherever $t_w(x^+)$ has a discontinuity. (See Tribus and Klein[5] for a more detailed discussion.) The heat flux is computed from

$$q(x^+) = k\left(\frac{\partial t}{\partial r^+}\right)_{r^+=1} = \frac{-k}{r_0}\int_0^{x^+}\theta_r(x^+ - \xi, 1)\,dt_w(\xi) \quad [34]$$

Heat Flux at the Wall Given

The inverse problem, namely, "Given the heat flux at the wall, what is the temperature?" may be solved with the aid of the Laplace-transform theory. Define the following transforms

$$T(s, r^+) = \int_0^\infty e^{-sx^+}(t - t_0)dx^+ \quad [35]$$

$$T_w(s) = T(s, 1) \quad [36]$$

$$F(s, r^+) = \int_0^\infty [1 - \theta(x^+, r^+)]e^{-sx^+}\,dx^+ \quad [37]$$

$$H(s) = -\int_0^\infty \theta_r(x^+, 1)e^{-sx^+}\,dx^+ \quad [38]$$

$$Q(s) = r_0/k\int_0^\infty e^{-sx^+}q(x^+)dx^+ \quad [39]$$

Applying the Faltung theorem to Equations [33] and [34] yields

$$T(s, r^+) = F(s, r^+)sT_w(s) \quad [40]$$

$$Q(s) = H(s)sT_w(s) \quad [41]$$

If the heat flux is finite, $t_w(x^+)$ will be continuous. Eliminating $T_w(s)$ from the foregoing equations

$$T(s, r^+) = \frac{F(s, r^+)}{H(s)}Q(s) \quad [42]$$

Now define

$$G(s, r^+) = \frac{F(s, r^+)}{H(s)} \quad [43]$$

and let $g(x^+, r^+)$ be the inverse transform of $G(s, r^+)$. Then, for arbitrary heat flux at the wall, the temperature is given by

$$t - t_0 = \frac{r_0}{k}\int_0^{x^+} g(x^+ - \xi, r^+)q(\xi)d\xi \quad [44]$$

Thus the problem is reduced to finding $g(x^+, r^+)$, which is given by

$$g(x^+, r^+) = \frac{1}{2\pi i}\int_{c-i\infty}^{c+i\infty} e^{sx^+}\frac{F(s, r^+)}{H(s)}\,ds \quad [45]$$

Returning to Equations [37], [38], and [3] it is found that

$$F(s, r^+) = \frac{1}{s} - \sum_{n=0}^{\infty}\frac{C_n R_n(r^+)}{s + \lambda_n^2} \quad [46]$$

$$H(s) = -\sum_{n=0}^{\infty}\frac{C_n R_n'(1)}{s + \lambda_n^2} \quad [47]$$

Because F and H have poles at $s = -\lambda_n^2$, the quotient F/H has no poles except at $S = 0$ and the zeros of $H(s)$. The zeros of $H(s)$ must be found numerically. Because $H'(s)$ is monotonic, it is found that the zeros of $H(s)$ occur between the $-\lambda_n^2$. Letting γ_m^2 be the values satisfying $H(-\gamma_m^2) = 0$, from the theory of residues

$$g(x, r^+) = \frac{1}{H(0)} - \sum_m^\infty\frac{e^{-\gamma_m^2 x^+}}{\gamma_m^2 H'(-\gamma_m^2)} - \sum_n^\infty C_n R_n(r^+)\sum_m^\infty\frac{e^{-\gamma_m^2 x^+}}{\lambda_n^2 - \gamma_m^2} \quad [48]$$

Table 4 gives the values of $\gamma_m^2\,H'(-\gamma_m^2)$ for the first three values of m. The term $H(0)$ has been shown by others[4] to be given by

$$H(0) = +1/4 \quad [49]$$

hence the wall temperature may be easily calculated with the aid of

$$g(x^+, 1) = 4 - \sum_m\frac{e^{-\gamma_m^2 x^+}}{\gamma_m^2 H'(-\gamma_m^2)} \quad [50]$$

A Sample Calculation for Constant Wall Heat Flux

By way of illustration consider the computation of the asymptotic value of the Nusselt modulus for the case of constant heat

TABLE 4 THE VALUES OF γ_m^2, $H'(-\gamma_m^2)$ FOR THE FIRST THREE VALUES OF m FOR A ROUND TUBE

Roots of $H(s) = 0$, Values of $H'(-\gamma_m^2)$

$$H(s) = -\sum_{n=0}^{\infty} \frac{C_n R_n'(1)}{s + \lambda_n^2}$$

$$C_n R_n'(1) = -2.02552\ \lambda_n^{-1/3}$$

$$\lambda_n = 4n + 8/3 \qquad n = 0, 1, 2, \ldots$$

$$H'(s) = \sum_n \frac{C_n R_n'(1)}{(s + \lambda_n^2)^2}$$

m	γ_m^2	$-H'(-\gamma_m^2)$	$\frac{-1}{\gamma_m^2 H'(-\gamma_m^2)}$
1	25.639	8.854×10^{-3}	4.405
2	84.624	2.062×10^{-3}	5.7308
3	176.40	9.435×10^{-4}	6.0084

TABLE 5 VALUES OF γ_m^2, $\bar{H}'(-\gamma_m^2)$ FOR THE FIRST THREE VALUES OF m FOR A FLAT DUCT

Roots of $\bar{H}(s) = 0$, Values of $\bar{H}'(-\gamma_m^2)$

$$\bar{H}(s) = -\Sigma \frac{K_n Y_n'(1)}{s + 8/3\lambda_n^2}$$

$$\bar{H}'(s) = \Sigma \frac{K_n Y_n'(1)}{(s + 8/3\ \lambda_n^2)^2}$$

$$\lambda_n = 4n + 5/3 \qquad n = 0, 1, 2, \ldots$$

m	γ_m^2	$-\bar{H}'(-\gamma_m^2)$	$\frac{-1}{\gamma_m^2 \bar{H}'(-\gamma_m^2)}$
1	49.345	7.45×10^{-4}	27.2
2	185.94	1.67×10^{-4}	32.1
3	409.45	6.89×10^{-5}	35.4

flux at the wall. Combining Equations [44] and [48] with $q(\xi) = q = \text{const}$, the following is obtained

$$t(x^+, r^+) - t_0 = \frac{qr_0}{k} \int_0^{x^+} \left[4 - \sum_m^{\infty} \frac{e^{-\gamma_m^2(x^+ - \xi^+)}}{\gamma_m^2 H'(-\gamma_m^2)} - \sum_n^{\infty} C_n R_n \sum_m^{\infty} \frac{e^{-\gamma_m^2(x^+ - \xi^+)}}{\lambda_n^2 - \gamma_m^2} \right] d\xi^+ \quad [51]$$

Letting $\beta x = x^+$, where $\beta = \pi k/2WC_p$, and integrating Equation [51] gives

$$t(x^+, r^+) - t_0 = \frac{qr_0}{k} \left\{ 4\beta x - \sum_m \frac{1 - e^{-\gamma_m^2 \beta x}}{\gamma_m^4 H'(-\gamma_m^2)} - \sum_n C_n R_n \sum_m \frac{1 - e^{-\gamma_m^2 \beta x}}{\gamma_m^2(\lambda_n^2 - \gamma_m^2)} \right\} \quad [52]$$

which may be rewritten as

$$t(x^+, r^+) - t_0 = \frac{qr_0}{k} \left[4\beta x - \sum_m \frac{1}{\gamma_m^4 H'(-\gamma_m^2)} + \sum_m \frac{e^{-\gamma_m^2 \beta x}}{\gamma_m^4 H'(-\gamma_m^2)} - \sum_n C_n R_n \sum_m \frac{1 - e^{-\gamma_m^2 \beta x}}{\gamma_m^2(\lambda_n^2 - \gamma_m^2)} \right] \quad [53]$$

Equation [53] shows that far down the pipe ($x^+ \to \infty$) the derivative of t with respect to x is independent of x or r^+, i.e.

$$\frac{\partial t}{\partial x} = \frac{4\beta q r_0}{k} \quad \text{for} \quad x^+ \to \infty \quad [54]$$

Substituting this quantity into Equation [2] leads to

$$\frac{4qr_0}{k} = \frac{1}{r^+(1 - r^{+4})} \frac{\partial}{\partial r^+} \left(r^+ \frac{\partial t}{\partial r^+} \right) \quad [55]$$

which may be integrated directly to give

$$t(x^+, r^+) - t(x^+, 0) = \frac{4r_0 q}{k} \left(\frac{r^{+2}}{4} - \frac{r^{+4}}{16} \right) \quad [56]$$

Now the mixed mean temperature along the pipe is given by

$$t_{mm}(x^+) - t_0 = \frac{2\pi r_0 q x}{WC_p} = \frac{4r_0 q}{k} \beta x \quad [57]$$

but the mixed mean temperature is also defined by

$$t_{mm}(x^+) = \frac{\int_0^1 u\rho C_p t(x^+, r^+)\, 2\pi r^+ dr^+}{WC_p} \quad [58]$$

Substituting Equation [56] into Equation [58] and integrating results in

$$t_{mm}(x^+) - t(x^+, 0) = 7/24 \frac{r_0 q}{k} \quad [59]$$

Combining Equations [59] and [56]

$$t(x^+, r^+) = \frac{4r_0 q}{k} \left(\frac{r^{+2}}{4} - \frac{r^{+4}}{16} \right) + t_{mm} - 7/24 \frac{r_0 q}{k} \quad [60]$$

and substituting Equation [57] into Equation [60]

$$t(x^+, r^+) - t_0 = \frac{r_0 q}{k} \left[4\beta x + r^{+2} - \frac{r^{+4}}{4} - 7/24 \right] \quad [61]$$

At $r^+ = 1$, this expression reduces to

$$t(x^+, 1) - t_0 = \frac{r_0 q}{k} [4\beta x + 11/24] \quad [62]$$

but from Equation [52], since $R_n(1) = 0$

$$t(x^+, 1) - t_0 = \frac{r_0 q}{k} \left[4\beta x - \sum_m \frac{1}{\gamma_m^4 H'(-\gamma_m^2)} \right] \quad [63]$$

Hence

$$\Sigma \frac{1}{\gamma_m^4 H'(-\gamma_m^2)} = -11/24 \cong -0.458 \quad [64]$$

(Note that the first three terms sum to approximately —0.27.) Now, the Nusselt modulus is given by

$$\text{Nu} = \frac{2r_0 q}{k(t_w - t_{mm})} \quad [65]$$

From Equation [60]

$$t(x^+, 1) - t_{mm} = 11/24\ r_0 q/k \quad [66]$$

which when substituted into Equation [65] gives

$$\text{Nu} = 48/11 \cong 4.36 \quad [67]$$

Substitution of Equations [64], [58], and [53] into [65] yields the local value of the Nusselt modulus for the case $q(x^+) = \text{const}$

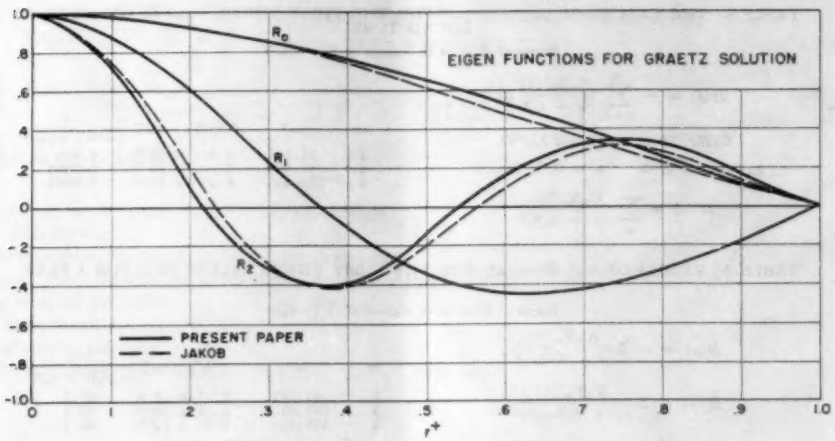

FIG. 1 EIGENFUNCTION FOR GRAETZ SOLUTION

$$\mathrm{Nu} = \frac{1}{\frac{11}{48} + \frac{1}{2}\sum_m \frac{e^{-\gamma_m^2 x^+}}{\gamma_m^4 H'(-\gamma_m^2)}} \quad \ldots\ldots [68]$$

CALCULATION FOR LINEARLY VARYING WALL TEMPERATURES

In similar fashion the use of the boundary condition $T_w(x^+) - T_0 = Ax^+$ where A = any constant, gives

$$q(x^+) = \frac{Ak}{4r_0} + \frac{2Ak}{r_0}\sum_n \frac{C_n}{2}\frac{R_n'(1)}{\lambda_n^2} e^{-\lambda_n^2 x^+} \quad \ldots\ldots [69]$$

$$T_{mm}(x^+) - T_0 = Ax^+ - \frac{88}{768}A - 8A\sum_n \frac{C_n}{2}\frac{R_n'(1)}{\lambda_n^4} e^{-\lambda_n^2 x^+} \quad \ldots\ldots [70]$$

$$\mathrm{Nu} = \frac{\frac{1}{2} + 4\sum_n \frac{C_n}{2}\frac{R_n'(1)}{\lambda_n^2} e^{-\lambda_n^2 x^+}}{\frac{88}{768} + 8\sum_n \frac{C_n}{2}\frac{R_n'(1)}{\lambda_n^4} e^{-\lambda_n^2 x^+}} \quad \ldots\ldots [71]$$

APPROXIMATIONS FOR SMALL x^+

Whenever x^+ is small, a large number of the terms in the series, Equation [3], must be taken. The Leveque solution is a good approximation for such cases. As shown by Tribus and Klein,[6] the wall temperature and heat flux for such a case are related by

$$q(x) = \frac{k\mathrm{Pr}^{1/3}}{3\Gamma(4/3)}\left(\frac{\rho}{9\mu}\right)^{1/3}\left(\frac{du}{dy}\right)_{y=0}^{1/3}\int_0^x (x-\xi)^{-1/3}\, dt_w(\xi) \quad \ldots [72]$$

and

$$t_w(x) - t_0 = \frac{2\mathrm{Pr}^{-1/3}}{3k\Gamma(5/3)}\left(\frac{\rho}{9\mu}\right)^{-1/3}\left(\frac{du}{dy}\right)_{y=0}^{-1/3}\int_0^x \frac{q(\xi)d\xi}{(x-\xi)^{2/3}} \quad \ldots\ldots [73]$$

For flat ducts

$$\left(\frac{du}{dy}\right)_{y=0} = 3u_m/b \quad \ldots\ldots [74]$$

For round ducts

$$\left(\frac{du}{dy}\right)_{y=0} = 4u_m/r_0 \quad \ldots\ldots [75]$$

Substitution of Equation [75] into Equations [72] or [73] (and noting that the mixed mean temperature of the fluid is essentially equal to its inlet value at small values of x^+) gives for the three cases under consideration:

For constant wall temperature

$$\mathrm{Nu} = \frac{2 \times 2^{1/3} x^{+-1/3}}{9^{1/3}\Gamma(4/3)} = 1.3565x^{+-1/3} \quad x^+ \leq 0.001 \ldots [76]$$

For constant heat flux

$$\mathrm{Nu} = \frac{2^{1/3} 9^{2/3}\Gamma(5/3)}{3} x^{+-1/3} = 1.6393\, x^{+-1/3} \quad \ldots\ldots [77]$$

For linearly varying wall temperature

$$\mathrm{Nu} = \frac{3 \times 2^{1/3} x^{+-1/3}}{9^{1/3}\Gamma(4/3)} = 2.0348\, x^{+-1/3} \quad \ldots\ldots [78]$$

Fig. 1 shows a graph of the functions R_0, R_1, and R_2 compared with solutions given by Jakob. Fig. 2 shows the variations in Nusselt modulus for three cases:

1 Wall-temperature constant.
2 Heat-flux constant.
3 Wall temperature increasing linearly along the pipe wall.

The Nusselt modulus is defined by the equation

$$\mathrm{Nu} = \frac{q(x)}{t_w(x) - t_{mm}}\frac{2r_0}{k} \quad \ldots\ldots [79]$$

The mixed mean temperature t_{mm} is determined by integrating the heat flux from the origin ($x^+ = 0$) to the position where $q(x)$ is known.

CONCLUSIONS

The methods used in this paper have a wide applicability. For example, the liquid-metals systems analyzed by Poppendiek[7] could be treated by the methods used here. The unsymmetrical boundary conditions treated by Yih and Cermak[8] can also be readily treated by these methods.

---

[7] "Forced Convection Heat Transfer in Thermal Entrance Regions, Part 1," by H. F. Poppendiek, Oak Ridge National Laboratory, Tenn., ORNL-913, Physics, series A, March, 1951.

[8] "Laminar Heat Convection in Pipes and Ducts," by C. S. Yih and J. E. Cermak, Civil Engineering Department, Colorado Agricultural and Mechanical College, Fort Collins, Colo., September, 1951. ONR Contract No. N90 nr 82401, NRO63-071/1-19-49.

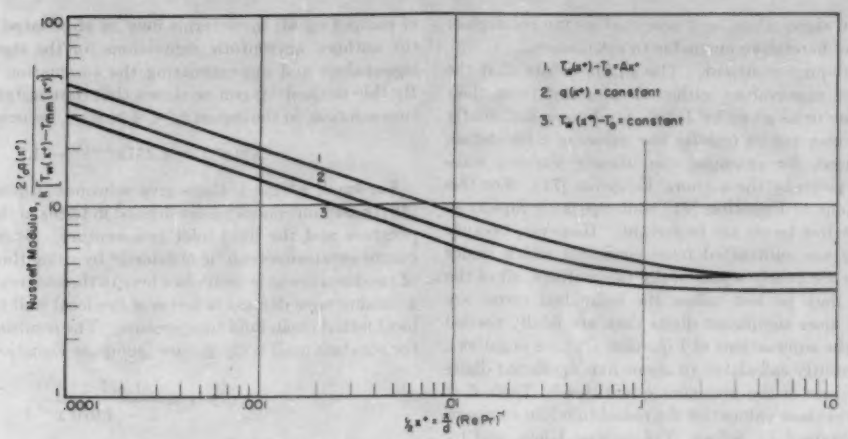

FIG. 2 LAMINAR FLOW OF A CONSTANT-PROPERTY FLUID IN A ROUND TUBE

The authors are somewhat surprised at the fact that whereas the asymptotic formulas are all supposed to be valid only for very large λ, in actuality values of n as small as 4 seem to give excellent results. The reasons for the good results are not now clear.

Appendix

The equations for a flat duct system with walls at

$$y = \pm b \qquad \text{[A-1]}$$

Defining

$$\mathrm{Re} = 4U_m\rho b/\mu, \quad x^+ = (x/b)(\mathrm{Re}\,\mathrm{Pr})^{-1}, \; y^+ = (y/b)$$

the equation to be solved is

$$\frac{3}{8}\frac{\partial t}{\partial x^+} = \frac{1}{1-y^{+2}}\frac{\partial^2 t}{\partial y^{+2}} \qquad \text{[A-2]}$$

which has a solution

$$\theta = \sum_{n=0}^{\infty} K_n Y_n(y^+)\, e^{-8/3\,\lambda_n^3 x^+} \qquad \text{[A-3]}$$

satisfying

$$\theta = 1 \text{ at } x^+ = 0, \; \theta \to 0, \; x^+ \to 0, \text{ if } Y(y^+)$$

satisfies

$$Y'' + \lambda^3(1-y^{+4})Y = 0 \qquad \text{[A-4]}$$

with $Y'(0) = Y(1) = 0$, λ_n is the value of λ to permit $Y_n(1) = 0$. The coefficients K_n are given by

$$K_n = \frac{-2}{\lambda_n\left(\dfrac{\partial Y_n}{\partial\lambda}\right)_{y^+=1 \;\; \lambda=\lambda_n}} \qquad \text{[A-5]}$$

By the methods in the text the WKB approximation is found to be

$$Y(y^+) = \frac{\cos\left\{\lambda\int_0^{y^+}(1-\xi^2)^{1/2}\,d\xi\right\}}{1-y^{+2}} \qquad \text{[A-14]}$$

for $0 \le y^+ < 1$.

Defining $z = 1 - y^+$, the solution of Equation [A-4] for $z \ll 1$ is found to be

$$Y(z) = \frac{1}{2}(\lambda\pi z)^{1/2}\left\{\sin\left(\frac{\pi\lambda}{4}-\frac{\pi}{12}\right)J_{1/3}\left(\frac{\lambda\sqrt{8}}{3}\,z^{3/2}\right) - \sin\left(\frac{\lambda\pi}{4}-\frac{5\pi}{12}\right)J_{-1/3}\left(\frac{\lambda\sqrt{8}}{3}\,z^{3/2}\right)\right\}$$

The eigenvalues are

$$\lambda_n = 4n + 5/3 \qquad \text{[A-25]}$$

$$\left(\frac{\partial Y_n}{\partial\lambda}\right)_{\substack{\lambda=\lambda_n \\ y^+=1}} = (-1)^{n+1}\frac{\pi^{3/2}\lambda_n^{1/2}}{3^{3/2}\,\Gamma(2/3)\,2^{7/2}} \qquad \text{[A-29]}$$

$$K_n = (-1)^n\frac{3^{3/2}\,\Gamma(2/3)\,2^{13/2}}{\pi^{3/2}}\,\lambda_n^{-7/2} \qquad \text{[A-30]}$$

$$\left(\frac{dY_n}{dy^+}\right)_{y^+=1} = (-1)^{n+1}\frac{\pi^{3/2}2^{1/2}\lambda_n^{3/2}}{3^{3/2}\,\Gamma(4/3)} \qquad \text{[A-31]}$$

$$q(x^+) = \frac{-k}{6}(t_w - t_0)\sum_n K_n Y_n'(1)\, e^{-8/3\lambda_n^3 x^+} \qquad \text{[A-32]}$$

To obtain the fluid temperature for a given heat flux use

$$t - t_0 = \frac{b}{k}\int_{\xi=0}^{x^+} \vartheta(x^+ - \xi, y^+) q(\xi)\,d\xi \qquad \text{[A-44]}$$

The integrating kernel ϑ is given by

$$\vartheta(x^+, y^+) = 2/3 - \sum_m \frac{e^{-\gamma_m^3 x^+}}{\gamma_m^2\, H'(-\gamma_m^2)} - \sum_n K_n Y_n(y^+)\sum_m \frac{e^{-\gamma_m^3 x^+}}{2/3\lambda_n^2 - \gamma_m^2} \qquad \text{[A-48]}$$

where the $-\gamma_m^2$ are the zeros of

$$H(s) = -\sum_n \frac{K_n Y_n'(1)}{s + 8/3\,\lambda_n^2} \qquad \text{[A-47]}$$

Discussion

R. P. LIPKIS.[9] The authors' valuable asymptotic solution of the Graetz problem has supplied accurate knowledge of the higher

[9] Department of Engineering, University of California, Los Angeles, Calif.

eigenfunctions and eigenvalues, and now enables the solution of many problems not heretofore amenable to calculation.

Several points require comment. The authors state that the eigenfunctions and eigenvalues, either as obtained from their asymptotic solution or as given by Jakob, are known sufficiently accurately. This may not be true for low values of n for certain boundary conditions, for example, the linearly varying wall-temperature case given by the authors' Equation [71]. For this case the summations of Equation [71] converge fairly rapidly so that only the first few terms are important. However, because these summations are subtracted from constants which under certain conditions are nearly equal to the summations, all of the significant digits may be lost unless the individual terms are known to several more significant digits than are finally needed (all the terms of the summations of Equation [71] are negative). The writer has recently calculated to about five significant digits the lowest five values of the pertinent quantities.[10] Table 6 of this discussion gives these values (for the round tube) for comparison with those obtained by Sellars, Tribus, and Klein, and by Jakob, as listed in the authors' Table 3.

TABLE 6 MORE ACCURATE VALUES OF THE EIGENFUNCTIONS AND EIGENVALUES OCCURRING IN THE GRAETZ PROBLEM[10,11]

n	λ_n	C_n	$-\frac{1}{2}C_nR'_n(1)$
0	2.7043644	+1.46622	0.74879
1	6.679032	−0.802476	0.54424
2	10.67338	+0.587094	0.46288
3	14.67108	−0.474897	0.41518
4	18.66987	+0.404402	0.38237

The writer employed a fairly rapidly converging series solution[11] of the Graetz equation (authors' Equation [4]) in making the calculations. These calculations appear to have sufficient internal checks to establish their correctness. The values are sufficiently accurate so that better and more complete solutions can now be obtained for the linearly varying wall-temperature case, the constant heat-input case, or for any other boundary condition where the solution involves the difference of nearly equal numbers. It is apparent from the table that the authors' asymptotic values are suitable for $n > 4$.

For some boundary conditions many terms of the series appearing in the solution may be needed. The burdensome problem of computing all these terms may be eliminated by substituting the authors' asymptotic expressions for the eigenfunctions and eigenvalues and approximating the summation by its integral. By this method[12] it can be shown that the constant wall-temperature solution, in the region $x^+ < 4 \times 10^{-3}$, becomes

$$\mathrm{Nu}(x^+) = 1.357x^{+-1/3} - 1.7$$

For small x^+ the authors give solutions (Equations [76], [77], [78]) based on conductances defined in terms of the local wall temperature and the fluid inlet temperature. Somewhat more accurate expressions can be obtained[10] by using the same definition of conductance as is used elsewhere in the authors' paper; namely a conductance defined in terms of the local wall temperature and local mixed mean fluid temperature. The resulting equations are, for constant wall temperature (compare Equation [76])

$$\mathrm{Nu}(x^+) = \frac{1.357\ x^{+-1/3}}{1 - 4.070\ x^{+2/3}}$$

and, for a linearly varying wall temperature (compare Equation [78])

$$\mathrm{Nu}(x^+) = \frac{2.035\ x^{+-1/3}}{1 - 2.442\ x^{+2/3}}$$

Regarding the suitability of the asymptotic formulas even for low values of n, such a result at least appears reasonable, in view of the following. With the values of λ_n given in Table 4 it can be seen that the eigenvalues reach, very closely, a constant difference; that is, they have reached their asymptotic state, even within the first few eigenvalues. Inasmuch as the other pertinent quantities are all functions of the eigenvalues (authors' Equations [29], [30], [31]), then these too will have reached their asymptotic state and thus be represented to a good degree of accuracy by the asymptotic formulas, even for low values of n.

It is difficult to read Fig. 2 quantitatively, but, as drawn, it appears to indicate that the entry length for the constant wall-temperature case (curve 3) is about as long, or longer, than that for the linearly varying wall-temperature case (curve 1). If the entry length is defined as the point at which the Nusselt modulus is within 1 per cent of its far downstream value, calculations employing the more accurately determined quantities of Table 4 show the interesting fact that the entry length for the constant wall-temperature case is only one fourth that for the linearly varying wall-temperature case.

[10] "Heat Transfer to an Incompressible Fluid in Laminar Motion," by R. P. Lipkis, MSc thesis, University of California, Los Angeles, Calif., August, 1954.

[11] "On Solution of Differential Equation Occurring in Problem of Heat Convection Laminar Flow in Tube," by M. Abramowitz, *Journal of Mathematics and Physics*, vol. 32, 1953, p. 184. The eigenvalues λ_n were given in this paper.

[12] Discussion by R. P. Lipkis of "Numerical Solutions for Laminar-Flow Heat Transfer in Circular Tubes," by W. M. Kays, Trans. ASME, vol. 77, 1955, pp. 1265–1274.